THESIS
4
2010

LIBRARY
Michigan State
University

This is to certify that the
dissertation entitled

Towards a Microscopic Energy Density Functional for Nuclei

presented by

Biruk B. Gebremariam

has been accepted towards fulfillment
of the requirements for the

Ph.D degree in Physics and Astronomy

Major Professor's Signature

02/12/2010

Date

MSU is an Affirmative Action/Equal Opportunity Employer

PLACE IN RETURN BOX to remove this checkout from your record.
TO AVOID FINES return on or before date due.
MAY BE RECALLED with earlier due date if requested.

DATE DUE	DATE DUE	DATE DUE

5/08 K:/Proj/Acc&Pres/CIRC/DateDue.indd

TOWARD

TOWARDS A MICROSCOPIC ENERGY DENSITY FUNCTIONAL FOR NUCLEI

By

Biruk B. Gebremariam

A DISSERTATION

Submitted to
Michigan State University
in partial fulfillment of the requirements
for the degree of

DOCTOR OF PHILOSOPHY

Physics and Astronomy

2010

TOWARD

ABSTRACT

TOWARDS A MICROSCOPIC ENERGY DENSITY FUNCTIONAL FOR NUCLEI

By

Biruk B. Gebremariam

In spite of their tremendous success, the limitations of current nuclear energy density functionals (EDFs), all parameterized empirically in the form of the local Skyrme, the nonlocal Gogny or relativistic functionals, have become apparent in the past several years. In order to address these deficiencies, a current objective of low-energy nuclear theory is to build non-empirical nuclear EDFs from underlying two-, three- and possibly four-nucleon interactions and many-body perturbation theory (MBPT). In this work, the first step towards that goal is taken by calculating the HF contribution from the chiral EFT two- and three-nucleon interaction at N^2LO. The density matrix expansion (DME) of Negele and Vautherin is a convenient method to map the highly non-local Hartree-Fock expression into the form of a quasi-local Skyrme-like functional with density dependent couplings. Reformulating the DME in terms of phase space averaging (PSA) techniques, we show that the resulting DME, PSA-DME, is more general and has a significantly better accuracy for spin-unsaturated systems than the original DME of Negele and Vautherin. This is achieved without compromising the accuracy of PSA-DME for spin-saturated ones. Imposing the assumption of time-reversal invariance, we apply PSA-DME to the HF energy from the chiral EFT two- and three-nucleon interaction (at N^2LO) and calculate the couplings of the emerging EDF analytically using a combination of analytical and symbolic approaches. Subsequently, we perform preliminary analysis of these couplings and show that their density dependence is driven by the long-range (pion-exchange) part of the interaction. Finally, we discuss the UNEDF semi-phenomenological approach that is attempting to utilize the results of this work.

DEDICATION

In loving memory of my aunt, ***Sebchiya Gebremariam***, whose love and support I still miss.

To my wife, ***Eden T. Elos***, whose love I cherish.

To my dearest friend, ***Misganaw A. Gashaw***, "guadea!" our time-like worldlines should cross soon!

ACKNOWLEDGMENT

I am indebted to my professors, Thomas Duguet and Scott Bogner, who provided me with all sorts of support in my research endeavor. I was lucky to tap into a much wider knowledge base than the typical graduate student. Besides helping me connect the major dots, the fact that they had the patience to let me explore problems in my own way has been a wonderful experience. I am deeply grateful for all of that. I would also like to thank the members of my guidance committee: Mark Dykman, Piotr Piecuch and Brad Sherrill for their helpful suggestions, comments and encouragements.

Next, I would like to show my gratitude to my fellow graduate students, officemates and friends. I should specially mention Jacob Clifford, Morewell Gaseller, Jeremy Armstrong, Ivan Brida, Angelo Signoracci, Liyuan Jia and Rhiannon Meharchand. Thanks for making me feel at home. Be it two of my three passions, science and soccer, we always had something to discuss. As to satisfying my third passion, literature and painting, Daniel Berhanemeskel, you played the main role there and I owe you a big thank you.

The perfect learning and research environment that the cyclotron and physics and astronomy department provided was one of the main ingredients for my successful completion of this PhD research project. Starting with the highly helpful administrative personnel and scientists to the availability of top-notch computer softwares, it is really a magnificent place to do one's research. In short, thanks! Talking of top-notch softwares, I should specially mention Wolfram Research's Mathematica. Here is my appreciation for powering my innovation. I also extend my gratitude to all members of the UNEDF collaboration, and the microscopic EDF group in particular, for letting me be a part of this wonderful collaboration.

My unique appreciation goes to my dearest wife Eden T. Elos. Her love, support and pragmatism have been and are very important in pulling me out of the often-romantic world that I create around myself. A friend in need is ... so goes the saying.

And I say, Mesge, you are indeed one true friend. I thank you for all the walks that we had in life, be it physically through the streets of Addis or telepathically when I am in East Lansing and you back home. Finally, thank you all my family members in Addis and Denver, especially my mom Belaynesh Seifu, Mulumebet Asfaw and Tekleab Hailu, and friends for all your love, good thoughts and understanding. Hey, mom! I have arrived now.

List of

List of

1 Low-er
1.1 L
1.2 C

2 Nuclea
2.1 H
2.2 S
2.3 R
2.4 C
2.4
2.4

3 The N
3.1 E
3.2 C
3

4 Phen
Func
4.1

4.2

TABLE OF CONTENTS

List of Tables xii

List of Figures xiii

1 Low-energy Nuclear Physics **1**
1.1 Introduction 1
1.2 Conventions and Notations 7

2 Nuclear Interactions **9**
2.1 Historical highlights 9
2.2 Symmetry Properties of Nuclear Interactions 10
2.3 Remarks on high-Precision Phenomenological Models 14
2.4 Chiral EFT Models 15
2.4.1 NN part at N^2LO 16
2.4.2 NNN part at N^2LO 19
The E-term 19
The D-term 19
The C-term 20
Low energy constants and parameters of the NNN interaction at N^2LO 20

3 The Nuclear Many-Body Problem **22**
3.1 Remark on ab-initio/MBPT-based methods 22
3.2 Goldstone-Brueckner formalism 23
3.2.1 Expansion of the ground-state wave-function and energy . . . 26
Hole-line expansion for non-perturbative potentials 26
Perturbative expansion 27
3.2.2 Choice of the one-body potential Γ 27

4 Phenomenological Energy Density Functionals **29**
4.1 Phenomenological Nuclear Energy Density Functionals 29
4.1.1 Motivation from density functional theory 29
4.1.2 Single- and multi-reference EDF formulations 33
4.2 Skyrme energy density functionals 35
4.2.1 Particle-hole functional 35
4.2.2 Particle-particle functional 37
4.2.3 Self-consistent solution 38

4.2

4.2

4.2

5 Constru

5.1 C

5.1

5.2 Th

5.2

5.2

5.3 PS

5.3

5.3

5.3

5.3

5.3

5.3

5.4 A

6 Non-

6.1

4.2.4 Existing parameterizations 39
4.2.5 Predictive power of empirical EDFs 39
4.2.6 Outlook 42

5 Constructing Non-Empirical Energy Density Functionals 45
5.1 Constructing Non-Empirical Energy Density Functional 45
5.1.1 Philosophy, Goals and Limitations 46
5.2 The Density Matrix Expansion (DME) 52
5.2.1 Basics of the DME 53
5.2.2 Existing variants of the DME 55
5.3 PSA-DME 56
5.3.1 Motivation for a PSA reformulation of the DME 56
5.3.2 Momentum phase-space of finite Fermi systems 58
5.3.3 PSA-DME for the scalar part of the OBDM of time-reversal invariant systems 62
5.3.4 PSA-DME for the vector part of the OBDM in time-reversal invariant systems 67
5.3.5 k_F^q and isospin invariance of the resulting EDF 71
5.3.6 Extension to non-time-reversal invariant systems 72
Constraints on the $\pi-$functions 76
5.3.7 Remarks on the DME of the local densities 80
5.3.8 Remarks on the DME of the anomalous densities 86
5.4 Accuracy of DME 91
5.4.1 Inputs to non-self-consistent tests 92
5.4.2 Fock contribution from V_C 93
5.4.3 Fock contribution from V_T 99
5.4.4 Fock contribution from V_{LS} 106
Basic analysis 106
Further investigation of the spin-orbit exchange 110
5.4.5 Hartree contribution from V_C, V_{LS} and V_T 115
5.4.6 Preliminary self-consistent tests 118

6 Non-Empirical Energy Density Functional from NN interaction 123
6.1 The HF energy from an NN interaction 123
6.1.1 HF contribution from a central interaction 126
6.1.2 HF contribution from the spin-orbit interaction 128
6.1.3 HF contribution from the tensor interaction 129
6.1.4 Additional contributions to the HF energy 131
6.1.5 The leading-order pairing contribution 133
6.2 Application of the DME to the NN-HF energy 133
6.2.1 Analytical couplings from the chiral EFT NN interaction at N^2LO 136
6.2.2 Single-particle fields and equations of motion 138

7 Non-
Intera
7.1 I
7.2 D
7.3 A
8 Semi-p
8.1 T
8.2 E
8.3 C
9 Appen
9.1 N

7 **Non-Empirical Energy Density Functional from Chiral EFT NNN Interaction at N^2LO** **140**
7.1 The Hartree-Fock energy from Chiral EFT NNN interaction at N^2LO 141
Basic form of the HF energy 142
HF energy from the E-term 147
HF energy from the D-term 147
HF energy from the C-term 148
7.2 DME for the HF energy from chiral EFT N^2LO 3NF in time-reversal invariant systems 149
7.2.1 Generic forms of the 3NF energy expressions 150
Generic-Form-1 151
Generic-Form-2 151
Generic-Form-3 152
7.2.2 The DME-coordinate system 152
7.2.3 Generalized PSA-DME 153
Infinite nuclear matter limit 155
7.2.4 The resulting EDF 155
Comments on the second-order truncation for spherical systems 158
7.3 Analytical Couplings from the chiral EFT NNN interaction at N^2LO for time-reversal invariant systems 160
Comparison of analytical and Monte-Carlo results 162

8 **Semi-phenomenological EDF, Future Extensions and Conclusions** **168**
8.1 The semi-phenomenological approach 168
8.2 Key future extensions 173
8.3 Conclusion 176

9 **Appendix** **178**
9.1 Mathematical Formulae 178
9.1.1 Miscellaneous elementary formulae 178
9.1.2 Clebsh-Gordon, Wigner 3-J and 6-J coefficients 180
9.1.3 A few special functions 182
Legendre polynomials 182
Laguerre polynomials 183
Gamma functions 184
Spherical harmonics 184
Bessel functions 185
9.1.4 Three-dimensional spherical harmonic oscillator eigenfunctions 186
9.1.5 Gegenbaur expansion 187
9.1.6 Functional derivatives 188
9.2 The one-body density matrix and densities 188
9.2.1 Properties of single particle states 189
9.2.2 One-body density matrix 190
9.2.3 Local densities 191

9.2.4 Properties under time reversal 192
9.2.5 Extension to anomalous contractions 193
9.2.6 Relations among the densities 195
9.3 Local Gauge transformation of the OBDM and local densities 197
9.3.1 Local Gauge transformation in many-body physics 198
Conventional formulation 198
Second quantization formulation 198
9.3.2 Local Gauge transformation of normal densities 200
9.3.3 Local Gauge transformation of anomalous densities 201
9.4 Densities in spherical systems 202
9.4.1 Expression for the normal densities in spherical symmetry . . 203
Scalar part of the density matrix - matter density 203
Kinetic density 204
The vector part of the density matrix - Spin density 205
Spin-orbit density 209
9.4.2 Expression for the anomalous densities in spherical symmetry 210
pairing density 211
Pairing kinetic density 211
Pairing spin-orbit density 211
9.5 Details on the density matrix expansion 212
9.5.1 Husimi distribution and the local anisotropy $P_2^q(\vec{r})$ 212
9.5.2 Wigner transform of the $\rho_q(\vec{r}_1, \vec{r}_2)$ up to $\hbar^2$ 214
9.5.3 Generalized PSA-DME 217
9.5.4 Generalized PSA-DME for the scalar part of the OBDM . . . 218
Recovering previous DMEs of the scalar part of the OBDM . . 223
Further approximation with respect to $\vec{X}$ 224
9.5.5 Generalized PSA-DME for the vector part of the OBDM . . . 225
9.5.6 Remarks on the generalized PSA-DME 228
9.5.7 The modified-Taylor series expansion 228
9.6 Derivation of EDF from HF energy of local NN interaction 232
9.6.1 Central contribution 232
9.6.2 Spin-orbit contribution 234
Spin-orbit contribution in time-reversal invariant systems . . . 235
9.6.3 Tensor contribution 236
9.6.4 Leading-order pairing contribution 237
9.6.5 The resulting EDF: EDF-NN-DME 237
9.6.6 Analytical couplings from chiral EFT NN interaction at N^{2}LO 240
9.7 HFB equations from EDF-NN-DME 243
9.7.1 The mean field from EDF-NN-DME 245
9.7.2 The Pairing field from EDF-NN-DME 247
9.8 Numerical solution of EDF-HF equations in spherical systems 248
9.8.1 Full-DME in spherical systems 249
9.8.2 Exchange-only-DME in spherical systems 250
9.8.3 Harmonic Oscillator basis expansion method 251

Matrix elements of the kinetic part 252
Matrix elements of the central potential part 253
Matrix elements of the spin-orbit part 253
9.8.4 Self-consistent iterations and convergence 254
9.9 The HF energy of chiral EFT NNN interaction at N^2LO 254
9.9.1 Remarks on the symbolic implementation 254
9.9.2 HF energy from the E-term 255
Direct part 255
Single-exchange part 255
Double-exchange part 255
E-term contribution for specific systems 256
9.9.3 HF energy from the D-term 256
Direct part 256
Single-exchange part 257
Double-exchange part 258
D-term contribution for specific systems 261
9.9.4 HF energy from the C-term 262
Direct part 262
Single-exchange part 263
Double-exchange part 265
C-term contribution for specific systems 274
9.10 Symbolic derivation of EDF-NNN-DME for time-reversal invariance . 275
9.10.1 Generic DME ansatz 276
Key points on the DME ansatz 278
Comments on the DME ansatz 280
9.10.2 The G-tensors and their analytical forms 280
9.10.3 Sample DME simplification 284
Angular integrations for spherical systems 285
9.10.4 Contributions to EDF-NNN-DME 288
Fourth order EDF from the D-term 288
Fourth order EDF from the single-exchange piece of the D-like part of the C-term 289
Fourth order EDF from the double-exchange piece of the D-like part of the C-term 289
Fourth order EDF from the R1-double-exchange piece of the C-term 290
Fourth order EDF from the R2-double-exchange piece of the C-term 291
Fourth order EDF from the R3-double-exchange piece of the C-term 292
Fourth order EDF from the R4-double-exchange piece of the C-term 292
9.10.5 Extension to deformed time-reversal invariant systems 293

An
N-
9.1
9.1
9.1
9.1
Bibliog

9.11 Analytical couplings for the EDF from chiral EFT NNN interaction at N^2LO . . . 295
  9.11.1 Functional form of the couplings . . . 295
    Couplings from Generic-Form-1 . . . 295
    Couplings from Generic-Form-2 . . . 296
    Couplings from Generic-Form-3 . . . 296
  9.11.2 Matching generalized PSA-DME against the DME-ansatz . . . 297
  9.11.3 Application of Gegenbaur's addition theorem . . . 298
  9.11.4 Analytical and symbolic integration . . . 301

Bibliography . . . 304

LIST OF TABLES

1.1 Acronyms used in this work. 7

1.2 Definitions and conventions used in this work. 8

2.1 Seven Decades of Struggle: The Theory of Nuclear Forces from Ref. [22]. 10

2.2 Parameters for chiral EFT NNN interaction at N^2LO, with Λ_x = 700 [MeV]. Note that the values for c_3 and c_4 are from Ref. [61]. . . . 21

4.1 INM properties of Skyrme functionals (from Ref. [81]): saturation density ρ_{sat}, bulk compressibility K_∞, isoscalar effective mass $(m^*/m)_s$, Thomas-Reiche-Kuhn enhancement factor κ_v and energy per particle at saturation E/A. 39

5.1 MBPT contributions from NN and NNN interactions up to second-order (Normal contractions) in Hugenholtz representation. 48

5.2 The first-order anomalous/pairing diagrams, otherwise called Bogoliubov contributions, from the NN and NNN interactions in Hugenholtz represenation. 48

5.3 The Brink-Boeker force(B1) 119

5.4 Full-DME and Exchange-only-DME for Brink-Boeker interaction and several DMEs 121

LIST OF FIGURES

Images in this dissertation are presented in color

1.1 (Color online) A selection of energy/length scales in physics. 2

1.2 (Color online) Low energy static and and dynamical nuclear properties. 3

1.3 (Color online) The chart of nuclide and the domains of applications of the standard nuclear structure method. The black region shows the stable nuclei, the green lines show the traditional magic numbers and the red curve delimits the experimentally known nuclei. From Ref. [81]. 5

2.1 Hierarchy of nuclear forces from Chiral Perturbation Theory, classified according to a power counting $(Q/\Lambda_{\chi})^{\nu}$, and restricted to $\nu \leq 3$ for simplicity. Three-body forces appears at next-to-next-to-leading order (N^2LO), but some of the associated low-energy constants are already constrained by the two-body domain (black symbols) while others (gray symbols) are to be adjusted on three-body observables. From ref. [81]. 17

4.1 Illustration of the asymptotic freedom of phenomenological EDF models in the case of two-neutron separation energies. In the major shell where empirical EDFs are adjusted on experimental data, the agreement between all relativistic and non-relativistic calculations is clearly seen. In the next major shell where no data exist, discrepancies between these models become more apparent (from J. Dobaczewski et al. [150]). 41

5.1 (Color online) Nuclear matter energy per particle as a function of Fermi momentum k_F at the Hartree-Fock level (left) and including second-order (middle) and particle-particle-ladder contributions (right), based on evolved N^3LO NN potentials and $3NF$ fit to E_{3_H} and $r_{4_{He}}$. Theoretical uncertainties are estimated by the NN (lines) and NNN (band) cutoff variations (from Bogner et. al. [28]). 47

5.2 (Color online) The S-wave solution of the Bethe-Goldsone equation and the uncorrelated S-wave function. 51

5.3 The quadrupole anisotropy $P_2^n(\vec{R})$ of the local neutron momentum distribution in a selected set of semi-magic nuclei. The black, red and blue vertical lines indicate the approximate half-radii (where the density becomes half of the density at the origin). 61

5.4 (Color online) k_F^p, k_F^n and the isoscalar k_F extracted from a converged self-consistent calculation of ^{214}Pb, a neutron rich nucleus. 72

5.5 (Color online) $\rho_n(r)$ for ^{48}Cr and ^{208}Pb from a converged self-consistent calculation using Sly4 EDF. 85

5.6 (Color online) The parameters for Cr and Pb isotopic chains obtained after fitting the neutron density, $\rho_n(\vec{r}_{1/2})$, with the $\pi-$functions as given in Eqs. (5.67)-(5.69). 85

5.7 (Color online) Coherence length $\xi(R)$ for ^{22}O, ^{60}Ca, ^{60}Ni, ^{104}Sn, ^{120}Sn, ^{212}Pb (From Pillet et. al. [187]). 89

5.8 (Color online) $|\tilde{\rho}_n(R,r)|^2$ calculated with HFB-D1S for ^{104}Sn, ^{120}Sn, ^{128}Sn. Scale has been multiplied by a factor of 10^6 (From Pillet et. al. [187]). 90

5.9 (Color online) Comparison of $C_{nn}^F(\vec{R},r)$ and $C_{nn}^{F,DME}(\vec{R},r)$ where the latter is computed from the $\pi-$functions of one of the three DMEs: NV-DME, PSA-DME or PSA-DME-II. Upper panels: two-dimensional integrands. Lower panels: ratios of $C_{nn}^{F,DME}(\vec{R},r)$ over $C_{nn}^F(\vec{R},r)$ for fixed values of R. Densities are obtained from a self-consistent EDF calculation of ^{208}Pb with the SLy4 Skyrme EDF in the particle-hole part and no pairing. 95

5.10 (Color online) Percentage error of $E_C^{DME}[nn]$ compared to $E_C^F[nn]$, where the former is computed from: NV-DME, PSA-DME or PSA-DME-II $\Pi-$functions. Densities are obtained from self-consistent EDF calculations using the SLy4 Skyrme EDF in the particle-hole channel and no pairing. 97

5.11 (Color online) The same as Figure 5.10 but for two different values of the range of the Gaussian interaction. 98

5.12 (Color online) Comparison of $T_{nn,1}^F(\vec{R},r)$ and $T_{nn,1}^{DME}(\vec{R},r)$ where the latter is computed from NV-DME, PSA-DME, PSA-DME-II or from PSA-DME with $P_2^n(\vec{R}) = 0$ which we denote as INM-DME. Upper panels: two-dimensional integrands. Lower panels: ratios of $T_{nn,1}^{DME}(\vec{R},r)$ over $T_{nn,1}^F(\vec{R},r)$ for fixed values of R. Densities are obtained from a converged self-consistent calculation of ^{208}Pb with the SLy4 Skyrme EDF in the particle-hole channel and no pairing. 101

5.13 (Color online) Percentage error of $E_T^{DME}[nn]$ compared to $E_T^F[nn]$ where the former is either computed from: NV-DME, from PSA-DME or PSA-DME-II. Densities are obtained from self-consistent EDF calculations using the SLy4 Skyrme EDF in the particle-hole channel and no pairing. Notice the different vertical scale compared to Fig. 5.10. . 103

5.14 (Color online) A few representative nuclei with diffuse $T_{nn,1}^F(\vec{R},r)$ together with absolute $E_T^F[nn]$ for the corresponding isotopic chains. Densities are obtained from a self-consistent EDF calculation using the SLy4 Skyrme functional in the particle-hole part and no pairing. . 105

5.15 (Color online) Comparison of $LS_{nn}^F(\vec{R},r)$ and $LS_{nn}^{F,DME}(\vec{R},r)$ where the latter is computed from either NV-DME or PSA-DME. Upper panels: two-dimensional integrands. Lower panels: ratios of $LS_{nn}^{DME}(\vec{R},r)$ over $LS_{nn}^F(\vec{R},r)$ for fixed values of R. Densities are obtained from a converged self-consistent calculation of ^{208}Pb with the SLy4 Skyrme EDF in the particle-hole channel and no pairing. 107

5.16 (Color online) Percentage error of $E_{LS}^{DME}[nn]$ compared to $E_{LS}^F[nn]$ where the latter is either computed from NV-DME or from PSA-DME. Densities are obtained from self-consistent EDF calculations using the SLy4 Skyrme EDF in the particle-hole channel and no pairing. Notice the different vertical scale compared to Figs. 5.10 and 5.13. 109

5.17 (Color online) Ratio of the DME (Eq.(5.101)) over the exact (Eq.(5.58)) expressions of the toy nonlocal matter density. 112

[illegible] C

[illegible] C

N

[illegible] C

M

[illegible] C

[illegible] C

[illegible] C

82 C

W

83 C

W

84

85

91

5.18 (Color online) $G_{ratio}(\vec{R},\vec{r})$ as a function of r for a selected set of ($\vec{R}$, A, N). 114

5.19 (Color online) Percentage error of $E_C^{H,DME}[nn]$ with respect to $E_C^{H}[nn]$ for Cr isotopic chain. The upper plots show C_{nn}^{H}, and $C_{nn}^{H,DME}$ for NV-DME and the parameterized $\pi-$function which we call PI-DME. 117

5.20 (Color online) LS_{nn}^{H}, and $LS_{nn}^{H,DME}$ for NV-DME, with densities obtaiend from a converged self-consistent calculation of ^{208}Pb with the SLy4 Skyrme EDF in the particle-hole channel and no pairing. 118

5.21 Comparison of Skyrme HFB and DME-based HFB codes. 119

7.1 (Color online) The percentage error of the truncated Gegenbaur expansion with respect to Monte-Carlo based calculation of the contribution to E/A in INM. Upper plots show the actual values for the calculation based on the truncated Gegenbaur expansion. 166

8.1 (Color online) $\mathcal{C}_0^{JJ}$ and $\mathcal{C}_1^{JJ}$ couplings from chiral EFT NN interaction at N^{2}LO. 170

8.2 (Color online) $\mathcal{C}_0^{JJ}$ couplings from the chiral NN interaction at N^{2}LO with error bands from naturalness requirement. 171

8.3 (Color online) $\mathcal{C}_1^{JJ}$ couplings from the chiral NN interaction at N^{2}LO with error bands from naturalness requirement. 172

8.4 The saturation curves, $W(\rho,I)$ of INM using the phenomenological SLY4 functional and semi-phenomenological DME-based functionals. Here, N^{2}LO includes the contribution from both NN and NNN interactions (From Ref. [164]). 174

8.5 The same as Fig. 8.4 but for PNM (From Ref. [164]). 174

9.1 (Color online) $R_5(k,x_2,x_3,\theta)$ for a set of angles. 300

Chap

Low-

1.1 I

[illegible]

Chapter 1

Low-energy Nuclear Physics

1.1 Introduction

Problems in physics are characterized by different energy or length scales as depicted in Fig. 1.1. Low-energy nuclear physics lies well below the energy scale for quantum chromodynamics (QCD), $\Lambda_{QCD} \backsim 1GeV$, and aims at describing nuclear phenomena that occur in the energy scale of a few tens of MeV, as characterized by the typical Fermi energy, $\mathcal{E}_F$. Even though QCD establishes that nucleons, viz, protons and neutrons have a complex structure in terms of quarks and gluons, low-energy nuclear physics never attempts to resolve their structure as justified by $\mathcal{E}_F/\Lambda_{QCD} \ll 1$. Its ultimate goal is the proper description of ground- and excited-state properties of nuclei and nuclear matter in terms of the interaction between and among the relevant low-energy degrees of freedom: protons and neutrons. Fig. 1.2 presents the diversity of nuclear properties one is looking after in the realm of low-energy nuclear physics.

There are several size-dependent and size-independent factors that complexify the coherent solution of the nuclear-many body problem. For infinite nuclear matter (INM) and finite-nuclei, the existence of the so-called Coester [[1]-[7]] and Tjon

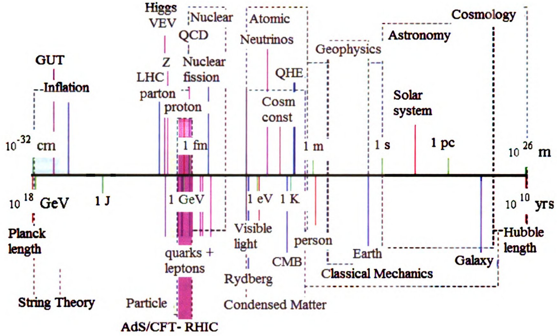
Higgs VEV
Nuclear
Atomic
Cosmology
QCD
Neutrinos
Astronomy
Geophysics
GUT
Z
Nuclear fission
LHC
QHE
Inflation
parton
Solar system
proton
Cosm const
10^{-32} cm
1 fm
1 m
1 s
1 pc
10^{26} m
10^{18} GeV
1 J
1 GeV
1 eV
1 K
10^{10} yrs
Planck length
Visible light
person
Hubble length
quarks + leptons
Earth
CMB
Galaxy
Rydberg
Classical Mechanics
String Theory
Particle
Condensed Matter
AdS/CFT- RHIC

Figure 1.1: (Color online) A selection of energy/length scales in physics.

lines [8] respectively, point to the fact that the nuclear-many body problem cannot be solved successfully without allowing for many-body forces. In addition, in a system of interacting nucleons, there exist both single-particle and collective excitations, such as sound waves in nuclear matter and rotational/vibrational modes in finite-nuclei, at about the same energy scale. At the same time, most nuclei (i.e. nuclei with masses typically between 40 and 350) are intermediate between few-body and statistical systems. This renders ab-initio techniques impractical due to computational complexity especially for systematic studies which involve hundreds of nuclei. It also prevents the application of statistical approaches due to the smallness of the number of constituents. Furthermore, the need to describe structure and reaction interfaces (fission, fusion, nucleon emission at the drip-line...), the existence of a large isospin asymmetry, and the essential role of superfluidity adds to the complexity of the problem.

Due to these factors, a coherent understanding and description of nuclear phe-

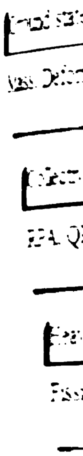

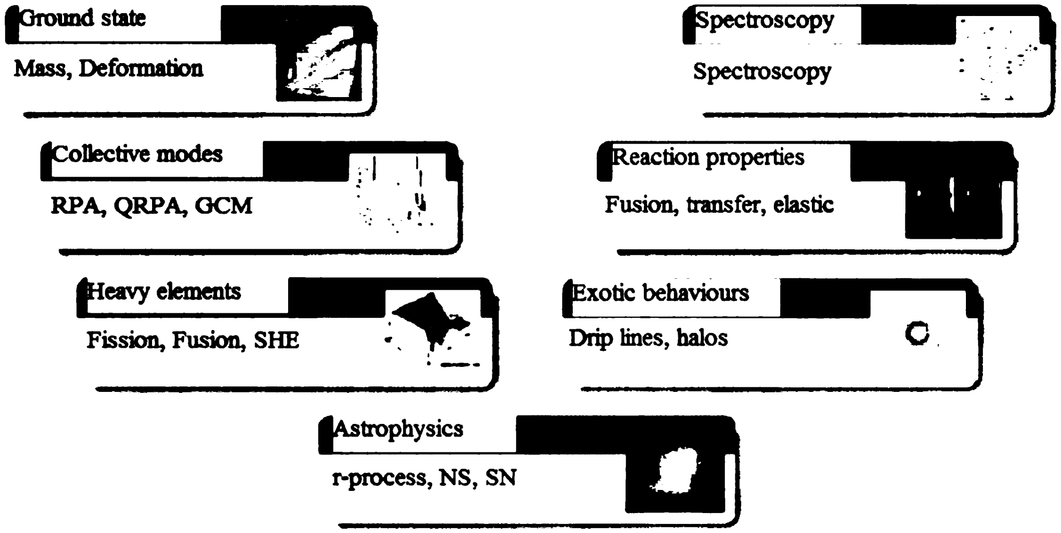
Ground state
Mass, Deformation
Spectroscopy
Spectroscopy
Collective modes
RPA, QRPA, GCM
Reaction properties
Fusion, transfer, elastic
Heavy elements
Fission, Fusion, SHE
Exotic behaviours
Drip lines, halos
Astrophysics
r-process, NS, SN

Figure 1.2: (Color online) Low energy static and and dynamical nuclear properties.

nomena remains elusive, in spite of several decades of theoretical and experimental investigations. Still, in the last decade, theoretical nuclear physics has seen significant progress from several fronts. Some of the main ones that are relevant to this work are the construction of nuclear interactions within the frame of chiral effective field theory (EFT) [9][[10]-[12]], the application of renormalization group techniques to soften two- and many-nucleon interactions [[13]-[15]], the use of ab-initio approaches to calculate the properties of increasingly heavier mass nuclei [23], and phenomenological energy density functional (EDF) approaches to computationally intensive calculations thanks to advances in computing power and numerical algorithms.

Although high-precision phenomenological two- (NN) and three-nucleon (NNN) interactions have existed for some time [[16]-[21]] and have been successfully used in nuclear structure and reaction calculations [23], they are inconvenient from both theoretical and practical points of view. These interactions lack a controlled expansion scheme that would provide a meaningful estimate of theoretical error bars, and there is no clear relation between their NN and NNN parts. Additionally, these phenomenological interactions lack a connection to the underlying low-energy QCD. As

a result, the role of chiral symmetry breaking of QCD which plays a crucial role in determining the long-range part of nuclear interactions is not consistently treated in such potential models [22].

From the viewpoint of nuclear structure calculations, phenomenological interactions contain a strong short-range repulsive core, thereby making the nuclear many-body problem highly non-perturbative. In general, the latter statement also holds for chiral EFT interactions which are built with a rather high intrinsic resolution scale, Λ, as this significantly couples low and high momenta [27]. Historically and in the context of infinite nuclear matter (INM) calculation, this necessitates an infinite re-summation of ladder diagrams, i.e. compute the Brueckner G-matrix, to obtain a meaningful starting point for more advanced calculations based on the hole-line expansion [[74],[30]]. The hole-line expansion method, usually at the lowest order, has been applied to closed-shell medium to heavy nuclei but with little success [38]. In the case of light nuclei with $A \leq 12$, state of the art Green's function Monte-Carlo (GFMC) and no-core shell model (NCSM) calculations can be performed with impressive results [23]. However, their large computational cost makes them inapplicable for beyond $A > 12$ region. Most recently, CC (coupled-cluster), IT-NCSM (importance-truncated no-core shell model) and IT-CI (importance-truncated configuration interaction) have been used to extend the applicability of ab-initio methods [24, 25].

Eventually, nuclear interactions necessarily depend on the resolution scale [27]. The realization of low-momentum interactions characterized by a low momentum cut-off, Λ, through renormalization group techniques results in the elimination of the non-perturbative aspects, viz, short-range repulsion and tensor forces of conventional nuclear interactions [27]. The analysis of Weinberg eigenvalues and the calculations of INM equation of state as well as the calculation of a selected set of finite nuclei confirm the perturbativeness of low-momentum interactions. As a matter of fact, INM

shows saturation already at the HF level, while the empirical saturation properties are reproduced satisfactorily at second-order in MBPT [28]. For finite nuclei, the energies and radii of a select set of nuclei seem to be remarkably converged at second order with good systematics and relatively small corrections coming from particle-hole states in the RPA [29]. Still, the application of these ab-initio methods for medium to heavy mass nuclei involves considerable numerical complexity. In addition, the accuracy of these methods is not on par with the current tool of choice for calculating ground- and excited-state properties of medium to heavy mass nuclei, namely, energy density functional (EDF) methods [26]. Fig. 1.3 shows the domains of application of the standard nuclear structure methods.

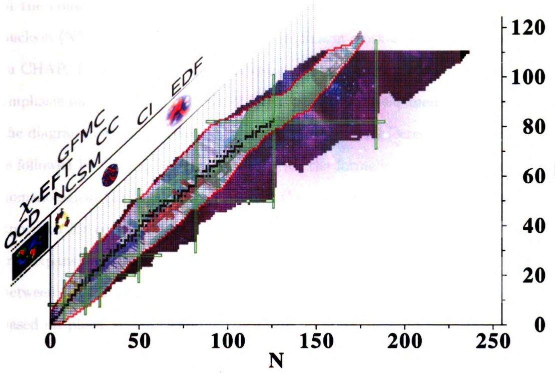

Figure 1.3: (Color online) The chart of nuclide and the domains of applications of the standard nuclear structure method. The black region shows the stable nuclei, the green lines show the traditional magic numbers and the red curve delimits the experimentally known nuclei. From Ref. [81].

Currently, EDFs are completely phenomenological by construction. Modern parameterizations of these empirical EDFs such as the Skyrme, Gogny and their relativistic counterparts provide a fair description of bulk properties and certain spectroscopic features of known nuclei [26]. However, such empirical EDFs lack predictive power away from the valley of stability or known data. In addition, the objective of having spectroscopic quality EDFs does not seem to be attainable with current energy functionals [26]. Consequently, an intense on-going effort is dedicated to empirically fitting EDFs possessing more complex analytical forms and/or enriched density dependent couplings [[31]-[36]].

Along with such phenomenological approach, the quest for predictive EDFs can be complemented by constraining the analytical form of the functional and the value of the couplings from MBPT and the underlying low-momentum two- and three-nucleon (NN and NNN) interactions. The present work is a step towards that goal. In CHAP. 1, we present a brief discussion of nuclear interaction models with special emphasis on chiral EFT. CHAP. 2 introduces the nuclear many-body problem and the diagrammatic approaches that rely on summing a selected set of diagrams. This is followed by CHAP. 3 where we deal with the formalism and performance of phenomenological EDFs. CHAP. 4 lays out the philosophy, goals and limitations of our approach for constructing a non-empirical EDF. After introducing the density matrix expansion (DME) as the mathematical technique to make an explicit connection between MBPT and quasi-local EDFs, we describe a new formulation of the DME based on phase space averaging (PSA). In addition, non-self-consistent and preliminary self-consistent performance tests of this newly formulated DME are given. In the subsequent chapter, CHAP. 5, we give details of the derivation of non-empirical EDF from a generic NN interaction, at the lowest order in MBPT (Hartree-Fock) and the application of the result to the chiral EFT NN interaction at N^2LO. CHAP. 6 discusses the contribution to the non-empirical EDF from chiral EFT NNN interactions at N^2LO at the HF level. In addition, an on-going effort to build a universal energy

1.2

EDF

DFT

NN

NNN

HF

HFB

INM

PNM

EFT

RG

RPA

density functional (UNEDF) that incorporates the results of this work, as well as possible extensions and conclusions are discussed in the last chapter, CHAP. 7. Finally, all relevant definitions, formulae and derivations, both analytical and symbolic, are presented in a set of detailed appendices.

1.2 Conventions and Notations

The acronyms, notations and definitions used throughout the thesis are listed below.

Table 1.1: Acronyms used in this work.

OBDM	One-body density matrix
EDF	Energy density functional
DFT	Density functional theory
NN interaction	two-nucleon interaction
NNN interaction	three-nucleon interaction
HF	Hartree-Fock
HFB	Hartree-Fock-Bogoliubov
INM	Symmetric and unpolarized infinite nuclear matter
PNM	Unpolarized pure neutron matter
EFT	Effective field theory
RG	Renormalization group
DME	Density matrix expansion
MBPT	Many-body perturbation theory
RPA	Random phase approximation

Table 1.2: Definitions and conventions used in this work.

$\otimes$	Denotes cross product
$\vec{\sigma}/\vec{\tau}$	Pauli vectors: $(\sigma_x, \sigma_y, \sigma_z)$, (τ_x, τ_y, τ_z)
$\hat{A}$	Unit vector along vector $\vec{A}$, or operator $\hat{A}$ in case A is an operator
$d\Omega_{\vec{A}}$	The differential solid angle with respect to $\vec{A}$
P^{σ}_{ij}	Exchanges the spin coordinates of the i^{th} and j^{th} particles. It is given by $P^{\sigma}_{ij} \; = \; 1/2\,(1 + \vec{\sigma}_1 \cdot \vec{\sigma}_2)$
P^{τ}_{ij}	Exchanges the iso-spin coordinates of the i^{th} and j^{th} particles. It is given by $P^{\tau}_{ij} \; = \; 1/2\,(1 + \vec{\tau}_1 \cdot \vec{\tau}_2)$
P^{r}_{ij}	Exchanges the spatial coordinates of the i^{th} and j^{th} particles
P_{ij}	The particle exchange operator given by $P_{ij} \; = \; P^{r}_{ij}\, P^{\sigma}_{ij}\, P^{\tau}_{ij}$
$\Pi_{\sigma i}$	The spin singlet $(i = 0)$ and triplet $(i = 1)$ projectors. These are given by $\Pi_{\sigma 0/1} \; = \; 1/2\,(1 \mp \vec{\sigma}_1 \cdot \vec{\sigma}_2)$
$\Pi_{\tau i}$	The isospin singlet $(i = 0)$ and triplet $(i = 1)$ projectors. These are given by $\Pi_{\tau 0/1} \; = \; 1/2\,(1 \mp \vec{\tau}_1 \cdot \vec{\tau}_2)$
V_I^{ST}	NN interaction vertex of type I where I can be C-central LS-spin orbit or T-tensor and ST can take the values $10, 01, 11, 00$ where the first $1/0$ refers to spin and the second $1/0$ refers to isospin triplet/singlet
$\pi_i^{\rho/\vec{s}/\vec{J}/\tilde{\rho}/\tilde{\vec{s}}}$	$i^{th}\,\pi-$function associated with local densities such as $\rho(\vec{R})\,/\,\vec{s}(\vec{R})\,/\,\vec{J}(\vec{R})$...
$\Pi_i^{\rho/\vec{s}/\tilde{\rho}/\tilde{\vec{s}}}$	$i^{th}\,\pi-$function associated with non-local densities $\rho(\vec{r}_1,\vec{r}_2)\,/\,\vec{s}(\vec{r}_1,\vec{r}_2)\,/\,\tilde{\rho}(\vec{r}_1,\vec{r}_2)\,/\,\tilde{\vec{s}}(\vec{r}_1,\vec{r}_2)$ ...
$a_1^{IST}[\pi_i^{\rho/\vec{s}}\,\pi_i^{\rho/\vec{s}}](\vec{R})$	$a_1^{IST}[\pi_i^{\rho/\vec{s}}\,\pi_i^{\rho/\vec{s}}](\vec{R}) \equiv 4\pi\,\int dr\, r^2\, V_I^{TS}(r)\,[\pi_i^{\rho/\vec{s}}\,\pi_i^{\rho/\vec{s}}]$
$a_2^{IST}[\pi_i^{\rho/\vec{s}}\,\pi_i^{\rho/\vec{s}}](\vec{R})$	$a_2^{IST}[\pi_i^{\rho/\vec{s}}\,\pi_i^{\rho/\vec{s}}](\vec{R}) \equiv \frac{4\pi}{3}\,\int dr\, r^4\, V_I^{TS}(r)\,[\pi_i^{\rho/\vec{s}}\,\pi_i^{\rho/\vec{s}}]$
$a_3^{IST}[\pi_i^{\rho/\vec{s}}\,\pi_i^{\rho/\vec{s}}](\vec{R})$	$a_3^{IST}[\pi_i^{\rho/\vec{s}}\,\pi_i^{\rho/\vec{s}}](\vec{R}) \equiv \int d\vec{r}\,\frac{x^2 y^2}{r^2}\, V_I^{TS}(r)\,[\pi_i^{\rho/\vec{s}}\,\pi_i^{\rho/\vec{s}}]$

Chapter 2

Nuclear Interactions

2.1 Historical highlights

The theory of nuclear forces started in the 1930s when Yukawa introduced the idea that the nuclear strong force is carried by a particle with a mass approximately 200 times that of an electron [37]. Table 2.1 summarizes the major developments of the past seven decades in the attempt to derive NN interactions from first principles.

With the conception of effective field theory (EFT)[9], it has become clear that pion-based theories of the fifties, this time with an explicit connection with low-energy quantum chromodynamics (QCD) [[10]-[12]], should be revived. In the last decade, EFT has been applied successfully to the consistent derivation of NN, NNN and many-nucleon interactions at various orders in the low-momentum expansion scale, Q/Λ_χ, where Q is the energy scale of the low-energy physics and $\Lambda_\chi \sim 1\,\mathrm{GeV}$ refers to the chiral symmetry breaking scale. Details relevant to the present work are given in section 2.4. In parallel with these efforts to derive nucleon-nucleon and many-nucleon interactions starting from field-theoretic approaches, various high-precision phenomenological NN and NNN interactions have been parameterized [[16]-[21]]. These efforts have been guided by requiring the interactions to satisfy a number

1

1

1

an

2.2

Table 2.1: Seven Decades of Struggle: The Theory of Nuclear Forces from Ref. [22].

1935	**Yukawa: Meson Theory**
1950's	*The "Pion Theories"* One-Pion Exchange: o.k. Multi-Pion Exchange: disaster
1960's	Many pions ≡ multi-pion resonances: $\boldsymbol{\sigma}$, $\boldsymbol{\rho}$, $\boldsymbol{\omega}$, ... The One-Boson-Exchange Model: success
1970's	Refined meson exchange models, including sophisticated $\mathbf{2\pi}$ exchange contributions (Stony Brook, Paris, Bonn)
1980's	Nuclear physicists discover **QCD** Quark Cluster Models
1990's **and beyond**	Nuclear physicists discover **EFT** Weinberg, van Kolck **Back to Pion Theory!** *But, constrained by Chiral Symmetry Breaking: success*

of symmetries. In the following, we discuss the symmetries that are used to constrain the form of NN interactions.

2.2 Symmetry Properties of Nuclear Interactions

While the derivation of the strong NN and many-nucleon interactions is an ongoing effort, there are a number of symmetries that a given nucleon-nucleon interaction should satisfy. Since one can denote the most general nucleon-nucleon interaction by its matrix element between two-body states, we use

$$v(\mathbf{1},\mathbf{2}) \equiv \langle\, \vec{r}_1'\sigma_1'q_1'\,\vec{r}_2'\sigma_2'q_2'\,|\hat{v}|\,\vec{r}_1\sigma_1q_1\,\vec{r}_2\sigma_2q_2\,\rangle \equiv v(\vec{r}_1\vec{k}_1\sigma_1q_1,\, \vec{r}_2\vec{k}_2\sigma_2q_2)\,, \qquad (2.1)$$

to discuss the action of the various symmetries. In Eq.(2.1), the dependence on the momentum of the interacting particles is to allow for nonlocality of the interaction. The following are the basic symmetry properties that a given NN interaction needs to satisfy [38].

- Hermiticity.
- Invariance under an exchange of coordinates

$$v(\mathbf{1},\mathbf{2}) = v(\mathbf{2},\mathbf{1})\,, \tag{2.2}$$

- Translational invariance

$$v(\mathbf{1},\mathbf{2}) = v(\vec{r},\, \vec{k}_1\,\sigma_1 q_1,\, \vec{k}_2\,\sigma_2 q_2)\,, \tag{2.3}$$

- Galilean invariance

$$v(\mathbf{1},\mathbf{2}) = v(\vec{r}\,\vec{k},\, \sigma_1 q_1,\, \sigma_2 q_2)\,, \tag{2.4}$$

- Invariance under space reflection

$$v(\vec{r}\,\vec{k},\, \sigma_1 q_1,\, \sigma_2 q_2) = v(-\vec{r}\, -\vec{k},\, \sigma_1 q_1,\, \sigma_2 q_2)\,, \tag{2.5}$$

- Time reversal invariance

$$v(\vec{r}\,\vec{k},\, \sigma_1 q_1,\, \sigma_2 q_2) = v(\vec{r}\, -\vec{k},\, -\sigma_1 q_1,\, -\sigma_2 q_2)\,, \tag{2.6}$$

- Rotational invariance in coordinate space implies that the interaction is a scalar. Additionally,

$$v(\vec{r}\,\vec{k},\, \sigma_1 q_1,\, \sigma_2 q_2) = v(-\vec{r}\, -\vec{k},\, \sigma_2 q_2,\, \sigma_1 q_2)\,, \tag{2.7}$$

which is due to Eqs. (2.2) and (2.5). Hence, terms in the interaction which are linear in σ_i and q_i depend only on $\sigma = (\sigma_1 + \sigma_2)/2$ and $q = (q_1 + q_2)/2$.

- Rotational invariance in isospin space which is an approximate symmetry broken by the coulomb interaction and other isospin-breaking effects. If assumed to hold, then

$$v(\vec{r}\vec{k},\, \sigma_1 q_1,\, \sigma_2 q_2) \;=\; v_0(\vec{r}\vec{k},\, \sigma_2,\, \sigma_1) \,+\, v_1(\vec{r}\vec{k},\, \sigma_2,\, \sigma_1)\, \tau_1 \cdot \tau_2\,. \qquad (2.8)$$

Even after correcting for electromagnetic effects, there is a strong experimental evidence that the nucleon-nucleon interaction breaks charge symmetry [39] and charge independence [[40], [41]]. The experimental evidence comes from the difference in the scattering lengths of *pp*, *nn* and *pn* systems. These values read $a_{pp} = -17.3 \pm 0.4$fm, $a_{nn} = -18.8 \pm 0.5$fm and $a_{pn} = -23.74 \pm 0.02$fm. In general, nucleon-nucleon interactions can be classified into four classes according allowed isospin operators [42], i.e.

- Class I forces have only dependencies on $[\mathbb{1}, (\tau_1 \cdot \tau_2)]$, and do not break either charge symmetry or independence,

- Class II forces maintain charge symmetry but are charge-independence-breaking (CIB). They are characterized by the isotensor T_{12} defined by analogy to the usual tensor S_{12} given in Eq. (2.10), and vanish for $T_z = \pm 1$ (nn or pp) systems,

- Class III forces are both charge-symmetry-breaking (CSB) and CIB, but remain invariant under the exchange of the two nucleons, and are thus proportional to $(\tau_{z1} + \tau_{z2})$. They do not cause isospin mixing since T_z commutes with T^2, and vanish for $T_z = 0$ (np) systems,

- Class IV forces are both CSB and CIB, and are antisymmetric under the ex-

change of the two nucleons, which causes isospin mixing. They are proportional to $(\tau_{z1} - \tau_{z2})$ or $(\tau_1 \otimes \tau_2)_z$, and vanish for $T_z = \pm 1$ systems.

The most general class-I two-body potential invariant under the fundamental symmetries recalled above can be decoupled into [43]

$$v(\mathbf{1}, \mathbf{2}) = \sum_p v_p(r) \begin{pmatrix} \mathbb{1} \begin{pmatrix} \mathbb{1} \\ (\sigma_1 \cdot \sigma_2) \end{pmatrix} \\ S_{12,\vec{r}} \\ (\vec{L} \cdot \vec{S}) \\ Q_{12} \\ S_{12,\vec{k}} \end{pmatrix} \begin{pmatrix} \mathbb{1} \\ (\tau_1 \cdot \tau_2) \end{pmatrix} ,$$

where the various operators are the so-called central $\mathbb{1}$, tensor $S_{12,\vec{r}}$, spin-orbit $(\vec{L} \cdot \vec{S})$, quadratic spin-orbit Q_{12}, and $S_{12,\vec{k}}$ components. The operators $S_{12,\vec{r}}$, $S_{12,\vec{k}}$ and Q_{12} are given by

$$S_{12,\vec{r}} = \frac{3}{r^2}(\sigma_1 \cdot \vec{r})(\sigma_2 \cdot \vec{r}) - \sigma_1 \cdot \sigma_2 \,, \tag{2.9}$$

$$S_{12,\vec{k}} = \frac{3}{k^2}(\sigma_1 \cdot \vec{k})(\sigma_2 \cdot \vec{k}) - \sigma_1 \cdot \sigma_2 \,, \tag{2.10}$$

$$Q_{12} = \frac{1}{2}[(\sigma_1 \cdot \vec{L})(\sigma_2 \cdot \vec{L}) + (\sigma_2 \cdot \vec{L})(\sigma_1 \cdot \vec{L})] \,, \tag{2.11}$$

where all operators in (2.2) have radial prefactors, $v_p(r)$, that can be constrained from microscopy or experimental data.

2.3

2.3 Remarks on high-Precision Phenomenological Models

The construction of phenomenological models for nucleon-nucleon interactions proceeds by parameterizing the radial prefactors $v_p(r)$. It is well known that the long-range ($r > 1/m_\pi$) part of the interaction is given by one-pion exchange, thereby fixing the radial form factor to the usual Yukawa form, $\frac{e^{-m_\pi r}}{r}$. The phenomenological models that have been parameterized in the last two decades [[16]-[21]] are said to be high-precision as they are able to fit low-energy ($\leq 350 MeV$) nucleon-nucleon scattering data with a chi square per degree of freedom, $\chi^2/N_{\mathbf{data}}$, close to one. Additionally, all currently available high-precision phenomenological models are charge dependent (CIB and CSB) and use about 40-50 parameters. The main difference among the various phenomenological models lies in the way they attempt to capture the intermediate- and short-range parts of the interaction.

The need to include many-body forces has been suggested by discrepancies between low-energy properties computed with two-body forces only and experimental data, such as differential nucleon-deuteron cross-sections [[44]-[46]], triton and other light nuclei binding energies [47], and the violation of the Koltun sum rule [48]. For instance, the binding energies of ^{3}H versus ^{4}He computed with all available NN models align on a so-called Tjon line that excludes the experimental point [8]. This is seen as a necessity to use consistent NNN forces to sneak away from this Tjon line. Likewise, the Coester line on which lies the saturation point of INM computed with NN forces only [[1]-[7]], is another indication that NNN forces are essential to reproduce bulk properties of nuclear matter[[49], [50]].

Phenomenological NNN potentials are available [[51]-[54]], based on mesons exchanges plus empirical short-range components. Using the same philosophy as phenomenological NN forces, they are adjusted on binding energies and scattering observables of three- (and four-) body systems such as proton/nucleon-deuteron diffusion data [[55]-[57]]. In the following section, it will be seen that chiral EFT, NNN interactions appear naturally which is one of the main advantages of the EFT approach.

2.4 Chiral EFT Models

Potentials based on chiral EFT [9] exploit the separation of scales between the chiral symmetry-breaking scale, $\Lambda_\chi \approx 1\,\mathrm{GeV}$, and typical momenta of low-energy processes at play in the nuclear structure context, Q, usually about $m_\pi \approx 140\,\mathrm{MeV}$ [[10]-[12]]. In that respect, few-nucleon processes can be treated using only nucleons and pions as degrees of freedom, the π−N interaction being governed by the spontaneously broken chiral symmetry of QCD. All other heavy mesons and nucleon resonances are integrated out of the theory, and their effects are contained inside scale-dependent couplings. The effective Lagrangian only depends, in this approximation, on a finite number of low-energy constants (LECs), and can be classified using a systematic expansion based on a power counting in terms of $(Q/\Lambda_\chi)^\nu$, where ν is called the chiral order. At a given accuracy $(Q/\Lambda_\chi)^\nu$, only a finite number of terms in the Lagrangian are needed in the low-momentum regime.

The leading order interaction corresponding to $\nu = 0$ is denoted by LO. There is no contribution for $\nu = 1$, and following terms $\nu > 1$ are called (next-to-)$^{\nu-1}$ leading-orders (N$^{\nu-1}$LO). This framework includes effects beyond the NN force, since three-, four-... body interactions appear naturally in the perturbative expansion, and the hierarchy $v_{NN} \gg v_{NNN} \gg v_{NNNN}$ is a direct consequence of the power counting, as shown in Fig. 2.1.

At this point, chiral interactions exist up to N^{3}LO [[58],[59]], where most of the NN and one-pion, two-pion and three-pion (OPE/2PE/3PE) diagrams have been computed using various approaches [58, 59]. Improvements of such approaches may consist in (i) increasing the chiral order ν of the perturbative expansion, although power counting implies that higher contributions will be substantially smaller, as already observed in the case of OPE/2PE [62], (ii) the introduction of four-nucleon forces arising naturally at N^{3}LO [63], (iii) treating extra degrees of freedom explicitly, such as nucleon Δ excitations that play a role in three-body forces [[66],[68]] and isospin breaking NN forces [68], or (iv) refining the short range phenomenological cutoff schemes. Finally, since chiral perturbation theory is a low-momentum expansion, its predictions are by essence only valid for momenta $Q \ll \Lambda_\chi$. Several families of chiral forces are defined depending on the values of the intrinsic high-momentum cutoff up to which they are defined, whose values typically range between 450 and 750 MeVs. This makes chiral potentials significantly softer than phenomenological hard-core interactions. In general, chiral EFT potentials have the general structure

$$V_{EFT} = V_{n\pi} + V_{ct}(\Lambda)\,, \tag{2.12}$$

where $V_{n\pi}$ are due to n pion-exchanges and $V_{ct}(\Lambda)$ refers to the contact parts which depend on the high-momentum cutoff scale, Λ.

In chapter 6 and 7, we calculate the HF energy from chiral EFT NN and NNN interactions at N^{2}LO, with emphasis on the contribution from the finite-range parts of the interaction $V_{n\pi}$. Hence, we now describe the chiral EFT interaction at N^{2}LO in some detail.

2.4.1 NN part at N^{2}LO

At N^{2}LO in the low-momentum expansion Q, the pion-exchange (finite-range) part of the NN interaction can be written as

$$V_{1\pi} = V_{1\pi}^{(0)} + V_{1\pi}^{(2)} + V_{1\pi}^{(3)}\,,$$

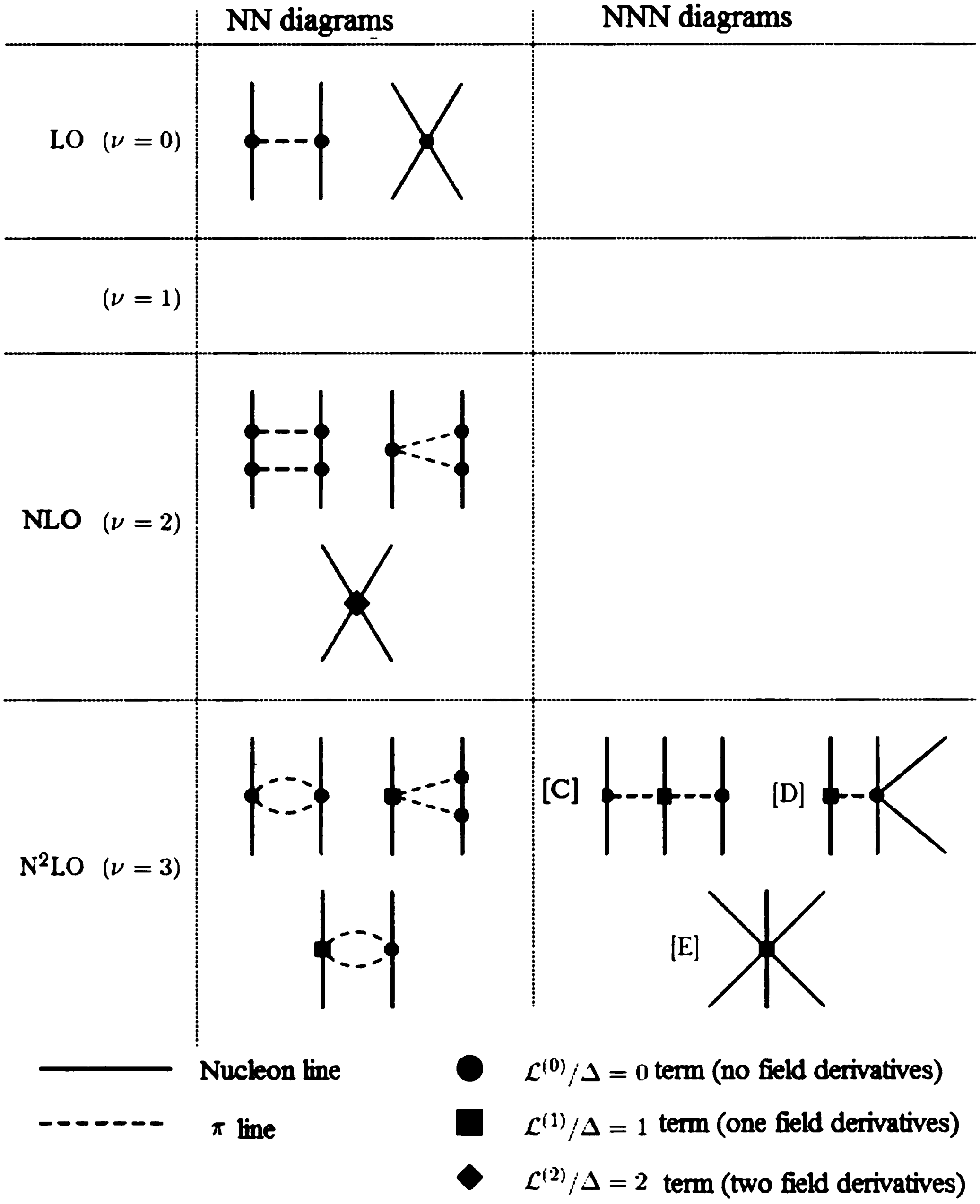
NN diagrams
NNN diagrams
LO $(\nu = 0)$
$(\nu = 1)$
NLO $(\nu = 2)$
N^{2}LO $(\nu = 3)$
[C]
[D]
[E]
Nucleon line
π line
$\mathcal{L}^{(0)}/\Delta = 0$ term (no field derivatives)
$\mathcal{L}^{(1)}/\Delta = 1$ term (one field derivatives)
$\mathcal{L}^{(2)}/\Delta = 2$ term (two field derivatives)

Figure 2.1: Hierarchy of nuclear forces from Chiral Perturbation Theory, classified according to a power counting $(Q/\Lambda_\chi)^\nu$, and restricted to $\nu \leq 3$ for simplicity. Three-body forces appears at next-to-next-to-leading order (N^{2}LO), but some of the associated low-energy constants are already constrained by the two-body domain (black symbols) while others (gray symbols) are to be adjusted on three-body observables. From ref. [81].

$$V_{2\pi} \;=\; V_{2\pi}^{(2)} + V_{2\pi}^{(3)} \,, \qquad (2.13)$$

Here the superscripts denote the corresponding chiral order and the ellipses refer to the Q^4-and higher order terms which are not considered in the present work. As can be seen, contributions due to the exchange of three-and more pions are further suppressed. In $|\vec{k}\rangle \otimes |\vec{\sigma}\rangle \otimes |\vec{\tau}\rangle$ space, the finite-range (pion-exchange) part of the chiral NN interaction through $\mathrm{N^2LO}$ takes the form[1]

$$\begin{aligned} \langle \vec{k}_1'\vec{k}_2' |V| \,\vec{k}_1\vec{k}_2 \rangle \;=\; & \Big(\big[V_C(q) + \vec{\tau}_1\cdot\vec{\tau}_2\, W_C(q)\big] + \big[\, V_S(q) + \vec{\tau}_1\cdot\vec{\tau}_2\, W_S(q)\,\big]\, \vec{\sigma}_1\cdot\vec{\sigma}_2 \\ & + \big[\, V_T(q) + \tau_1\cdot\tau_2\, W_T(q)\,\big]\, \vec{\sigma}_1\cdot\vec{q}\,\vec{\sigma}_2\cdot\vec{q} + \frac{i}{2}\big[V_{LS}(q) \\ & + \vec{\tau}_1\cdot\vec{\tau}_2\, W_{LS}(q)\big]\, (\vec{\sigma}_1+\vec{\sigma}_2)\cdot(\vec{q}\times\vec{k}'') \Big)\, \delta(\vec{K}-\vec{K}') \,, \qquad (2.14) \end{aligned}$$

where $\vec{q} = \vec{k}' - \vec{k}$ is the momentum transfer, with the relative momenta being $\vec{k} = \vec{k}_1 - \vec{k}_2$ and $\vec{k}' = \vec{k}_1' - \vec{k}_2'$. $\vec{K} = (\vec{k}_1 + \vec{k}_2)/2$ and $\vec{K}' = (\vec{k}_1' + \vec{k}_2')/2$ are center of mass momenta of incoming and outgoing interacting particles respectively. The requirement of Galilean invariance is enforced by $\delta(\vec{K} - \vec{K}')$. In passing, we remark that the the contact part of the interaction contains terms that depend on $\vec{p} = (\vec{k}' + \vec{k})/2$ and/or $\vec{q}$. The subscripts C, S, T, LS label the form factors of central, spin-spin, tensor and spin-orbit components of the interaction. The form factors are scalar functions of the momentum transfer q and are such that (i) only W_T gets contribution from one pion-exchange (ii) V_C, , W_C, , V_T , W_T , V_{LS} , W_{LS} get contribution from two-pion exchange. Actual expressions and details on the contact parts of the interaction are given in Ref. [59].

---

[1] The finite-range NN spin-orbit piece is actually zero-range up to $\mathrm{N^2LO}$.

2.4.2 NNN part at N^{2}LO

From a general standpoint, three-body forces can be characterized by

$$\langle \vec{k}_1\vec{k}_2\vec{k}_3 \,|\hat{V}_{3N}|\, \vec{k}'_1\vec{k}'_2\vec{k}'_3 \rangle \;=\; \frac{1}{\Omega^2}\,\delta_{\vec{k}_1+\vec{k}_2+\vec{k}_3,-\vec{k}'_1-\vec{k}'_2-\vec{k}'_3}\, \hat{V}_{3N}(\vec{k}_1\vec{k}_2\vec{k}_3|\vec{k}'_1\vec{k}'_2\vec{k}'_3)\,, \tag{2.15}$$

where Ω is the volume used in the box-normalization of the momentum basis states, $\delta_{\vec{k}_1+\vec{k}_2+\vec{k}_3,-\vec{k}'_1-\vec{k}'_2-\vec{k}'_3}$ is the Kronecker delta and $\hat{V}(\vec{k}_1\vec{k}_2\vec{k}_3|\vec{k}'_1\vec{k}'_2\vec{k}'_3)$ is a matrix element in momentum space and an operator in spin-isospin space whose dependence on spin and isospin degrees of freedom is not displayed. The NNN $\chi-$EFT interaction first appears at N^{2}LO where it is composed of three components [69] (i) the E-term (ii) the D-term and (iii) the C-term.

The E-term

The E-term, which is a three-nucleon contact interaction, is the simplest part of the $\chi-$EFT 3NF at N^{2}LO. Its expression reads

$$\hat{V}_E(\vec{k}_1\vec{k}_2\vec{k}_3|\vec{k}'_1\vec{k}'_2\vec{k}'_3) \;\equiv\; E\big(\,\vec{\tau}_1\cdot\vec{\tau}_2+\vec{\tau}_2\cdot\vec{\tau}_3+\vec{\tau}_3\cdot\vec{\tau}_1\,\big)\,, \tag{2.16}$$

where

$$E \;\equiv\; \frac{C_E}{f_\pi^4\Lambda_\chi}\,. \tag{2.17}$$

The D-term

The D-term involves one-pion exchange plus contact interaction. Its analytical reads

$$\begin{aligned} \hat{V}_D(\vec{k}_1\vec{k}_2\vec{k}_3|\vec{k}'_1\vec{k}'_2\vec{k}'_3) \;\;&\equiv\;\; -\frac{g_A}{4f_\pi^2}\frac{C_D}{f_\pi^2\Lambda_\chi}\Bigg(\frac{\sigma_1\cdot\vec{q}_2\,\sigma_2\cdot\vec{q}_2}{q_2^2+m_\pi^2}\tau_1\cdot\tau_2+\frac{\sigma_2\cdot\vec{q}_3\,\sigma_3\cdot\vec{q}_3}{q_3^2+m_\pi^2}\tau_2\cdot\tau_3 \\ &\qquad +\frac{\sigma_3\cdot\vec{q}_1\,\sigma_1\cdot\vec{q}_1}{q_1^2+m_\pi^2}\tau_3\cdot\tau_1\Bigg)\,, \end{aligned} \tag{2.18}$$

The C-t

Low er

where $\vec{q}_i \equiv \vec{k}_i - \vec{k}_i'$.

The C-term

The C-term of the interaction involves two-pion exchange. Its analytic form reads

$$\begin{aligned}\hat{V}_C(\vec{k}_1\vec{k}_2\vec{k}_3|\vec{k}_1'\vec{k}_2'\vec{k}_3') \equiv& \left(\frac{g_A}{2f_\pi}\right)^2 \left(\frac{\sigma_1 \cdot \vec{q}_1\, \sigma_2 \cdot \vec{q}_2}{(q_1^2 + m_\pi^2)(q_2^2 + m_\pi^2)} F_{123}^{\alpha\beta} \tau_1^\alpha \tau_2^\beta \right. \\ &+ \frac{\sigma_2 \cdot \vec{q}_2\, \sigma_3 \cdot \vec{q}_3}{(q_2^2 + m_\pi^2)(q_3^2 + m_\pi^2)} F_{231}^{\alpha\beta} \tau_2^\alpha \tau_3^\beta \\ &+ \left. \frac{\sigma_3 \cdot \vec{q}_3\, \sigma_1 \cdot \vec{q}_1}{(q_3^2 + m_\pi^2)(q_1^2 + m_\pi^2)} F_{312}^{\alpha\beta} \tau_3^\alpha \tau_1^\beta \right), \qquad (2.19)\end{aligned}$$

with

$$F_{ijk}^{\alpha\beta} \equiv \delta_{\alpha\beta} \left[-4 \frac{c_1 m_\pi^2}{f_\pi^2} + 2 \frac{c_3}{f_\pi^2} \vec{q}_i \cdot \vec{q}_j \right] + \frac{c_4}{f_\pi^2} \epsilon^{\alpha\beta\gamma} \tau_k^\gamma\, \vec{\sigma}_k \cdot (\vec{q}_i \times \vec{q}_j)\,. \qquad (2.20)$$

Low energy constants and parameters of the NNN interaction at N^{2}LO

Values of the various coupling constants appearing in Eqs.(2.16)-(2.20) can be found in Table 2.2. There are several ways to extract fix the C_D and C_E low-energy constants, one of which is adjusting these constants such that the binding energies of ^{3}H and ^{4}He from ab-initio calculations with NN and NNN interactions match experimental values. The above statements also hold for c_1. On the other hand, there is still some controversy over which set of values is "right" for c_3 and c_4 with extractions from $\pi-$N scattering and NN begin different with large uncertainties. Resolving these differences is important as many quantities are sensitive to the values of c_3 and c_4 [60].

Table 2.2: Parameters for chiral EFT NNN interaction at N^2LO, with $\Lambda_x = 700\,[\mathrm{MeV}]$. Note that the values for c_3 and c_4 are from Ref. [61].

g_A	1.29
f_π [MeV]	92.400
m_π [MeV]	138.040
c_1 [GeV^{-1}]	-0.760
c_3 [GeV^{-1}]	-4.780
c_4 [GeV^{-1}]	3.960
C_D	-2.062
E	-0.625

Chapter 3

The Nuclear Many-Body Problem

3.1 Remark on ab-initio/MBPT-based methods

Ab-initio methods for the nuclear many-body problem such as no-core shell model (NCSM) solve the A-body problem in a given model space while quantum Monte-Carlo methods such as Green's function Monte-Carlo (GFMC) rely on stochastic integration of the many-body Schrodinger equation [23]. Currently, they are able to incorporate both NN and NNN interactions. However such methods show exponential scaling with A, thus limiting their applicability to only $A \leq 12$ [23] due to their computation costs. In this regard, CC (coupled-cluster), IT-NCSM (importance-truncated no-core shell model) and IT-CI (importance-truncated configuration interaction) should be mentioned as ab-initio methods that solve the A-body problem approximately in the given model space. They have lower computational complexity and thus extend the applicability of ab-initio methods to heavier nuclei [24, 25].

In contrast, MBPT-based methods rely on partial finite/infinite-order summation of MBPT diagrams according to some organizing principle. Infinite-order summation may be necessitated by the non-perturbativeness of the starting interaction, and may not be necessary if one starts from perturbative low-momentum interactions [27]. The non-perturbative behavior of conventional phenomenological interaction models can be traced to [27] i.e. (i) the hard-core repulsion that makes nucleons scatter up to very high energies and requires large basis sets, (ii) the tensor force coming from OPE which is singular at short distances, and (iii) the presence or virtual (di-neutron) or bound (deuteron) states.

On the other hand, vacuum nuclear interactions are strongly renormalized in the nuclear medium. This suggests that expressing the many-body energy in terms of an unperturbed Slater determinant coupled to an **effective in-medium interaction** that already includes many-body correlations might be possible. That is, the minimal set of in-medium correlations that have to be included to reach a reasonable description of the system, i.e. infinite nuclear matter or finite nuclei, need to be incorporated in the definition of the in-medium interaction. This can be achieved for simple systems in the context of Goldstone-Brueckner theory [70].

3.2 Goldstone-Brueckner formalism

As long as pairing is not explicitly included, the Hamiltonian $H = t + v$ can be decomposed in terms of a one-body hamiltonian h_0 that has Slater determinants $|\Phi_i\rangle$ as eigenstates, and a perturbation h_1, i.e.

$$
\begin{aligned}
H &= h_0 + h_1 \,, && (3.1)\\
h_0 &\equiv t + \Gamma = \sum_i t_i + \sum_{ij} \Gamma_{ij}\, \hat{a}^\dagger_i\, \hat{a}_j = \sum_n \epsilon_n\, \hat{c}^\dagger_n\, \hat{c}_n \,, && (3.2)\\
h_1 &= v - \Gamma \,. && (3.3)
\end{aligned}
$$

The quantities ϵ_p are the eigenenergies of h_0 corresponding to single-particle states φ_p, whereas ε_i will denote many-body eigenenergies of h_0 associated with unperturbed

[illegible]

[illegible]

[illegible]

$= -\chi$

[illegible]

[illegible]

[illegible]

Slater determinants, i.e.

$$\varepsilon_i = \sum_{p=1}^{A} \epsilon_{i,p} \qquad\qquad |\Phi_i\rangle = \prod_{p=1}^{A} \hat{c}^{\dagger}_{i,p}|0\rangle \,. \tag{3.4}$$

According to Gell-Mann-Low's adiabatic theorem [71], the true ground state $|\Theta_0\rangle$ of H can be obtained from the adiabatic evolution of the ground state of h_0 from $t = -\infty$ to $t = 0$ by gradually turning on the residual interaction [72], i.e.

$$|\Theta_0\rangle = \lim_{\epsilon -> 0} \left(\frac{U_\epsilon(0, -\infty)|\Phi_0\rangle}{\langle\Phi_0|U_\epsilon(0, -\infty)|\Phi_0\rangle} \right) , \tag{3.5}$$

where the adiabatic evolution operator $U_\epsilon(t, t_0)$ from t to t_0 is defined in the interaction representation starting from the Hamiltonian in the Shrödinger representation $H(\epsilon, t - t_0)$ as

$$\begin{aligned} U(t, t_0) &\equiv \exp\left[\frac{i\,h_0\,t}{\hbar}\right] U_\epsilon(t, t_0) \exp\left[-\frac{i\,h_0\,t}{\hbar}\right] \qquad (3.6)\\ U_\epsilon(t, t_0) &\equiv \exp\left[-\frac{i}{\hbar}\int_{t_0}^{t} \tau\, H(\epsilon, \tau)\right] . \qquad (3.7) \end{aligned}$$

From an expansion of U_ϵ in powers of the residual interaction and integrations over time in Eq. (3.5), a series expansion of the ground state $|\Theta_0\rangle$ is obtained [73], i.e.

$$|\Theta_0\rangle = \sum_n \left(\frac{1}{\varepsilon_0 - h_0} h_1\right)^n |\Phi_0\rangle_{\text{linked}} \,, \tag{3.8}$$

where the sum runs only over linked diagrams, i.e. where $|\Phi_0\rangle$ does not appear as an intermediate state. The latter is enforced at the level of (3.5) where the denominator fixes the normalization of $|\Theta_0\rangle$ by eliminating disconnected vacuum-to-vacuum

diagrams [79]. Likewise, a similar expansion of the ground-state energy E_0 reads

$$E_0 = \varepsilon_0 + \sum_n \langle \Phi_0 | h_1 \left(\frac{1}{\varepsilon_0 - h_0} h_1 \right)^n | \Phi_0 \rangle_{\text{connected}} , \tag{3.9}$$

where the sums now only runs over connected diagrams.

However, if the expansions of Eqs. (3.8) and (3.9) are truncated at a given order, non-converging results arise if the vacuum interaction contains a non-perturbative hard core. On the other hand, it is possible to extract a series of ladder diagrams where a succession of interactions v scatters nucleons into particle states. This series can be replaced by a reaction matrix G which resums those Brueckner's particle-particle ladders and can be represented by the self-consistent Bethe-Goldstone equation [[75]-[78]]

$$G(\omega) \;=\; v \,+\, v \frac{Q}{\omega - h_0} G(\omega) , \tag{3.10}$$

where ω is the starting energy that corresponds to the in-medium energy of the nucleons at the location where G is inserted, whereas the Pauli operator Q excludes occupied states, i.e. those below the Fermi level ϵ_F associated with the unperturbed vacuum $|\Phi_0\rangle$, that is

$$Q = \sum_{\epsilon_p, \epsilon_{p'} > \epsilon_F} | p p' \rangle \langle p p' | . \tag{3.11}$$

The replacement of the initial interaction by the re-summed G-matrix modifies the short-range part of the in-medium two-body wave function, such that it is strongly suppressed over a distance of the order of the range of the repulsive core, that is the healing distance, or wound [70].

3.2.1

[illegible]

Hole-

[illegible]

E

[illegible]

3.2.1 Expansion of the ground-state wave-function and energy

The general idea consists in regrouping, if necessary, clusters of diagrams under G in such a way that a converging series is obtained, i.e. a truncation at a given order provides a result of a given precision [74]. Once the G-matrix has been computed, it replaces all instances of v in diagrams, excluding those where successive G-matrices are connected by a two-particle intermediate state, that is no particle-particle ladder connecting two G-matrices must be written.

Hole-line expansion for non-perturbative potentials

While the G-matrix regularizes the hard-core repulsion, an expansion in terms of G for the ground-state and single-particle energies remains non-perturbative, in such a way that the proper expansion parameter is the number of hole lines [80]. At lowest order in the hole-line expansion, the ground-state energy E is given by the Bruckener-Hartree-Fock (BHF) approximation. The BHF approximation consists of a self-consistent solution of the equations

$$\begin{aligned} E_0 \approx \langle ij \,|\, G(\omega) \,|\, ij \rangle &= \langle ij \,|\, v \,|\, ij \rangle + \frac{1}{2} \sum_{m,n > \epsilon_F} \langle ij \,|\, v \,|\, mn \rangle \frac{1}{\omega - \epsilon_m - \epsilon_n + i\eta} \\ &\quad \times \langle mn \,|\, G(\omega) \,|\, ij \rangle \,, \end{aligned} \tag{3.12}$$

where ϵ_i are the on-shell single-particle energies that are obtained by a functional derivative of the ground-state energy and the two-body matrix elements of $G(\omega)$ and v are anti-symmetrized. Thus, the lowest order in hole lines for E_0 (two hole lines) leads not only to a term with one line in the self energy but also to a rearrangement term containing two hole lines and coming from the functional derivative of the particle-particle ladder propagator.

3.2.2

Perturbative expansion

If the starting interaction is in fact perturbative, as it will be the case for low-momentum interactions, in-medium correlations can be treated through converging perturbative series in powers of v for E_0 and ϵ_i. Indeed, the ladder series from (3.10) becomes perturbative, such that it can be truncated at a given order in intermediate ladders. For instance, the ladder series for v_{low-k} is almost converged at second order in MBPT [81]. For the relevant diagrams that appear at second order from NN and NNN interactions, refer to Table 5.1 in section 5.1.1.

3.2.2 Choice of the one-body potential Γ

The proper choice of the unperturbed hamiltonian h_0 is crucial to have a rapidly convergent series [82]. Several choices for the one-body field Γ are possible, among which (i) a phenomenological expression that is fixed a priori, (ii) the Hartree-Fock approximation where ϵ_k are eigenenergies of the Schrödinger equation associated with the vacuum force, or (iii) a more involved approach necessary for non-perturbative potentials, e.g. where the one-body field Γ is constructed at lowest order in the on-shell G-matrix or includes rearrangement terms (extended Brueckner-Hartree-Fock calculations) [[83]-[86]].

Note that the truncation orders can be different in the series for the energy E_0 and the self-energy ϵ_i, e.g. E_0 can be computed at second order while single-particle energies are derived from a more simple (Woods-Saxon...) potential or only at first order in v. Still, adding more orders in the expansion of the single-particle energies adds extra diagrams in the series for E_0 such that it converges faster. Finally we remark that description of pairing within a diagrammatic framework is possible by defining anomalous propagators and allowing for anomalous contractions in addition to the normal contractions. Refer to [87] for details.

Cha

Phe
Fu

4.1

The

4.

Chapter 4

Phenomenological Energy Density Functionals

4.1 Phenomenological Nuclear Energy Density Functionals

The nuclear energy density functional (EDF) approach, due to its computational tractability, is the many-body method of choice to study medium- and heavy-mass nuclei in a systematic manner [26]. The central element of EDF approach is the energy density functional. Currently available realizations of the EDF approach, all empirically constructed, vary in the way they parameterize this energy density functional [26]. These include the quasi-local Skyrme, the nonlocal Gogny and relativistic models.

4.1.1 Motivation from density functional theory

Historically, nuclear EDF based approaches were motivated by starting from effective interactions in the particle-hole and particle-particle channels and solving the self-consistent mean-field equations [26]. Recently, the focus has shifted towards considering the energy density functional approach as motivated from effective field theory where the various densities of the system are the basic low-energy degrees of freedom [35].

In parallel, the development of density functional theory (DFT) [[88]-[91]] in quantum chemistry and condensed matter physics seems to have given nuclear energy density functional approaches a starting theoretical basis. DFT has been applied successfully to the structure of quantum many-body electronic systems (atoms, molecules, solids...). The comparatively small computational cost of the approach makes DFT the only feasible solution for systems with large number of electrons [92]. Instead of the many-body wave-function, DFT takes the fermion density as the "fundamental" variable.

The two building blocks of DFT are

- The Hohenberg-Kohn theorem [95], which states the existence of a functional $F[\rho]$ such that the ground-state energy of a system of N particles in a one-body external potential $u(r)$ can be written as

  $$E_u[\rho] = F[\rho] + \int d\vec{r}\, u(\vec{r})\, \rho(\vec{r}) \,, \tag{4.1}$$

  where $F[\rho]$ only depends on the Hamiltonian of the interacting system, thus is independent of the external potential $u(\vec{r})$. The ground- state density $\rho_0(\vec{r})$ and energy $E_0 = E_u[\rho_0]$ are then obtained by minimizing $E_u[\rho]$ with respect to a variation of the density $\rho(\vec{r})$ under the constraints that ρ is positive and $\int d\vec{r}\, \rho(\vec{r}) = N$. It should be noted that this existence theorem does not imply that all the information about the ground state is contained in the electron density $\rho(\vec{r})$ [93].

- Due to its practical difficulties, DFT is not implemented as a pure functional

of the density, a la Thomas-Fermi theory [94]. Rather, one makes use of the Kohn-Sham implementation [97], which asserts that for any interacting system, there exists a unique local single-particle potential $u_{KS}(\vec{r})$ such that the ground-state density of the interacting system equals the ground-state density of the auxiliary non-interacting system in the external potential $u_{KS}(\vec{r})$, that is

$$\rho(\vec{r}) \;=\; \rho_{KS}(\vec{r}) \;=\; \sum_{i=1}^{N} \left|\phi_i(\vec{r})\right|^2 , \tag{4.2}$$

expressed using the lowest N single-particle orbitals, $\phi_i(\vec{r})$, which are solutions of the one-body Kohn-Sham equation

$$\left[-\frac{\nabla^2}{2m} + u_{KS}(\vec{r})\right] \phi_i(\vec{r}) \;=\; \epsilon_i\, \phi_i(\vec{r}) , \tag{4.3}$$

where ϵ_i are the Kohn-Sham eigenvalues.

In the Kohn-Sham scheme, F is split into

$$F[\rho] \;=\; T[\rho] + U[\rho] + E_{xc}[\rho] , \tag{4.4}$$

where (i) $T[\rho]$ is the universal (kinetic) energy functional of the non-interacting system, (ii) $U[\rho]$ is the Hartree functional depending on the two-body interaction potential $V(|\vec{r}_i - \vec{r}_j|)$, and (iii) $E_{xc}[\rho]$ is the so-called exchange-correlation functional, including the Fock term and all remaining many-body correlations. When $E_{xc}[\rho]$ is neglected, the Kohn-Sham equations reduce to the standard self-consistent Hartree ones. Additionally, the Kohn-Sham potential is given through the condition that ground-state energies of the interacting and non-interacting problem ($U[\rho] = Exc[\rho] = 0$) are met for the same density $\rho(\vec{r})$, i.e.

$$u_{KS}(\vec{r}) \equiv u(\vec{r}) + \frac{\delta E_{xc}[\rho]}{\delta \rho(\vec{r})} . \tag{4.5}$$

While the Kohn-Sham potential is local/multiplicative, the exchange-correlation functional might be highly non-local. The main difficulty for DFT practitioners lies in the fact that no prescription is given to construct $F[\rho]$, i.e. the universal exchange-correlation part $E_{xc}[\rho]$. Several levels of realization exist to construct

$$E_{xc}[\rho] = \int d\vec{r}\, \varepsilon_{xc}(\vec{r}) \,, \tag{4.6}$$

and they correspond to adding more complex dependencies in the functional $E_{xc}[\rho]$. The standard classification separates, from the most simple to the most involved level of description [89]:

- The local density approximation (LDA), where $E_{xc}[\rho]$ only depends on the local density, $\rho(\vec{r})$ and is matched onto the energy per unit volume of the corresponding infinite homogenous system,

- The generalized gradient approximation (GGA), where additional specific dependencies on the gradient $\vec{\nabla}\rho(\vec{r})$ are added to $E_{xc}[\rho]$,

- The meta-GGA, which introduces as an additional degree of freedom the kinetic energy density of occupied Kohn-Sham orbitals

$$\tau(\vec{r}) = \sum_i \left| \vec{\nabla}\phi_i(\vec{r}) \right|^2 . \tag{4.7}$$

- The hyper-GGA, which takes also into account dependencies of $E_{xc}[\rho]$ on single-particle energies ϵ_i and occupations ρ_i ,

- The generalized random phase approximation (RPA) which involves unoccupied Kohn-Sham orbitals, and can be seen as the ultimate goal in terms of global accuracy.

However, in spite of several recent developments, a rigorous connection between nuclear EDF and DFT approaches is yet to be found [[98]-[103]]. The key aspect of this problem is the fact that unlike the systems that are studied in condensed matter physics and quantum chemistry (bound by external potentials), the nuclear many-body problem involves a self-bound system. In contrast to the standard Hohenberg-Kohn theorem which is symmetry-conserving, the nuclear Kohn-Sham potential implementation of EDF approaches breaks symmetries of the Hamiltonian such as translational and rotational symmetries. Even though projection techniques can be used to restore these symmetries, understanding its implications for DFT requires further theoretical development. Additionally, the presence of both spin and isospin degrees of freedom and the importance of pairing correlations need to be considered in nuclear EDF approaches. For a related formulation of pairing within the DFT framework, refer to Ref. [104] although the formulation corresponds to a system coupled to a particle reservoir.

4.1.2 Single- and multi-reference EDF formulations

As mentioned in section 1.1, the fact that nuclei are self-bound fermionic systems with both collective modes and individual excitations existing on the same energy scale make the nuclear many-body problem a complex one. In order to handle this problem, nuclear EDFs incorporate the assumption that these correlations can be divided into two different classes that can be incorporated in two different steps (i) short-range in-medium correlations which are recovered at the level of single-reference energy density functional (SR-EDF) calculations and commonly referred to as mean-field calculations (ii) long-range correlations that originate from collective modes and symmetry restoration. These are handled by multi-reference energy density functional (MR-EDF) calculations.

In SR-EDF calculations, the EDF is a functional of the normal, ρ_{ij}, and anoma-

lous, κ_{ij}, parts of the OBDM defined in appendix 9.2.2 and 9.2.5. In general, the energy density in SR-EDF is given by [105]

$$\begin{aligned}
\mathcal{E}_{SR}[\Phi_0] &\equiv \mathcal{E}_{SR}[\rho_{ij}, \kappa_{ij}, \kappa^*_{ij}] \\
&= t_{ij}\,\rho_{ji} + \frac{1}{2}\sum_{ijkl} v^{\rho\rho}_{ijkl}\,\rho_{ik}\,\rho_{lj} + \frac{1}{4}\sum_{ijkl} v^{\kappa\kappa}_{ijkl}\,\kappa{*}_{ik}\,\kappa_{lj} \\
&\quad + \frac{1}{6}\sum_{ijklmn} v^{\rho\rho\rho}_{ijklmn}\,\rho^*_{li}\,\rho_{mj}\,\rho_{nk} + \frac{1}{4}\sum_{ijklmn} v^{\rho\kappa\kappa}_{ijklmn}\,\rho_{li}\,\kappa^*_{jk}\,\kappa_{mn}\,,
\end{aligned} \tag{4.8}$$

where v denotes the effective interaction in the respective channel. Traditionally, SR-EDF calculations have been referred to as self-consistent mean-field theory where one starts from an effective two- and three-body interaction and calculates the Hartree-Fock (HF) or Hartree-Fock-Bogoliubov (HFB) energy density. However, SR-EDF calculations are distinctly different from mean-field calculations in that specific properties of the interaction vertices, e.g. $v^{\rho\rho}_{ijkl} = v^{\kappa\kappa}_{ijkl}$ are not satisfied [105].

SR-EDF calculations can reproduce static collective correlations such as pairing and deformation through the symmetry breaking of the auxiliary state $|\Phi_0\rangle$ with respect to which the OBDM is defined. This does not hold for collective modes and dynamical correlations, which require Multi-Reference (MR) calculations. Motivating from Hamiltonian-based generator coordinate method (GCM) calculations [105], MR-EDF is formulated as

$$\mathcal{E}_{MR} \equiv \frac{\sum_{0,1\epsilon MR} f_0^* f_1 \varepsilon_{MR}[\Phi_0, \Phi_1]\,\langle\Phi_0|\Phi_1\rangle}{\sum_{0,1\epsilon MR} f_0^* f_1\,\langle\Phi_0|\Phi_1\rangle}\,, \tag{4.9}$$

where $\mathcal{E}_{MR}[\Phi_0, \Phi_1]$ is the MR-EDF and the weight functions f_0, f_1 are determined by symmetry consideration and/or diagonalization. If one follows the Hamiltonian formalism, the most natural guidance for the construction of $\varepsilon_{MR}[\Phi_0, \Phi_1]$ is provided by the generalized Wick theorem (GWT) [105] which asserts that one obtains

$\mathcal{E}_{MR}[\Phi_0, \Phi_1]$ by replacing the SR density matrices by transition densities [105]. Nevertheless, the application of this prescription to currently available EDFs encounters several pathologies which have been traced to the occurrence of non-integer powers of the density matrix in the functional. One proposed solution [105] is the reparameterization of EDFs in terms of only integer-powers of the density matrix.

4.2 Skyrme energy density functionals

In the Skyrme-EDF model [26, 106], the energy density functional $\mathcal{E}$ is given as the sum of kinetic, particle-hole, particle-particle (pairing), Coulomb and center-of-mass correction terms, i.e.

$$\mathcal{E}[\rho, \kappa, \kappa^*] = \mathcal{E}_{\text{kin.}}[\rho] + \mathcal{E}_{\text{ph}}[\rho] + \mathcal{E}_{\text{pp}}[\rho, \kappa, \kappa^*] + \mathcal{E}_{\text{Coul.}}[\rho] + \mathcal{E}_{\text{c.o.m.}}[\rho]\,. \tag{4.10}$$

$\mathcal{E}$ is quasi-local and is expressed as the single integral in coordinate space of a local energy density. The expressions for $\mathcal{E}_{\text{kin.}}$, $\mathcal{E}_{\text{Coul.}}$, and $\mathcal{E}_{\text{c.o.m.}}$ can be found in the literature [26]. They are also discussed in section 6.1.4 in relation to the application of the density matrix expansion [[107],[170]] to the HF energy from a generic NN interaction.

4.2.1 Particle-hole functional

The particle-hole part of the Skyrme-EDF resembles meta-GGA functionals in a DFT context as it uses explicit dependencies on several local densities and currents, including spin-orbit densities. This is crucial for the proper treatment of finite nuclei. The functional is the most general bilinear combination of all local densities, built from the density matrix up to second order derivatives, in such a way that $\mathcal{E}$ remains invariant under the transformations associated with all symmetries of the nuclear

Hamiltonian, i.e. parity, time-reversal, rotation, translation, gauge and isospin transformations [126]. The functional reads

$$
\begin{aligned}
\mathcal{E}_{ph}[\rho] =& \mathcal{E}_{\text{Skyrme}}[\rho] \\
=& \sum_{q} \int d\vec{r}\, A^{\rho\rho}\, \rho^{q}\, \rho^{q} + A^{\rho\Delta\rho}\, \rho^{q} \Delta\rho^{q} + A^{\rho\tau} \left(\rho^{q}\tau^{q} - \vec{j}^{\,q} \cdot \vec{j}^{\,q}\right) \\
& + A^{ss}\, \vec{s}^{\,q} \cdot \vec{s}^{\,q} + A^{s\Delta s}\, \vec{s}^{\,q} \cdot \Delta\vec{s}^{\,q} + A^{\rho\nabla J} \left(\rho^{q}\vec{\nabla} \cdot \vec{J}^{\,q} + \vec{j}^{\,q} \cdot \vec{\nabla} \times \vec{s}^{\,q}\right) \\
& + A^{\nabla s\nabla s} (\nabla \cdot \vec{s}^{\,q})(\nabla \cdot \vec{s}^{\,q}) + A^{JJ} \Big(\sum_{\mu\nu} J^{q}_{\mu\nu} J^{q}_{q,\mu\nu} - \vec{s}^{\,q} q \cdot \vec{T}^{\,q} q\Big) \\
& + A^{J\bar{J}} \Big[\Big(\sum_{\mu} J^{q}_{\mu\mu}\Big)\Big(\sum_{\mu} J^{q}_{\mu\mu}\Big) + \sum_{\mu\nu} J^{q}_{\mu\nu} J^{q}_{\nu\mu} - 2\, \vec{s}^{\,q} \cdot \vec{F}^{\,q}\Big] \\
+& \sum_{q \neq q'} \int d\vec{r}\, B^{\rho\rho}\, \rho^{q} \rho^{q'} + B^{\rho\Delta\rho}\, \rho^{q} \Delta\rho^{q'} + B^{\rho\tau} \left(\rho^{q}\tau^{q'} - \vec{j}^{\,q} \cdot \vec{j}^{\,q'}\right) \\
& + B^{ss}\, \vec{s}^{\,q} \cdot \vec{s}^{\,q'} + B^{s\Delta s}\, \vec{s}^{\,q} \cdot \Delta\vec{s}^{\,q'} + B^{\rho\nabla J} \left(\rho^{q}\vec{\nabla} \cdot \vec{J}^{\,q'} + \vec{j}^{\,q} \cdot \vec{\nabla} \times \vec{s}^{\,q'}\right) \\
& + B^{\nabla s\nabla s} (\nabla \cdot \vec{s}^{\,q})(\nabla \cdot \vec{s}^{\,q'}) + B^{JJ} \Big(\sum_{\mu\nu} J^{q}_{\mu\nu} J^{q'}_{\mu\nu} - \vec{s}^{\,q} \cdot \vec{T}^{\,q'}\Big) \\
& + B^{J\bar{J}} \Big[\Big(\sum_{\mu} J^{q}_{\mu\mu}\Big)\Big(\sum_{\mu} J^{q'}_{\mu\mu}\Big) + \sum_{\mu\nu} J^{q}_{\mu\nu} J^{q'}_{\nu\mu} - 2\, \vec{s}^{\,q} \cdot \vec{F}^{\,q'}\Big],
\end{aligned}
\tag{4.11}
$$

where the coupling constants A^X/B^X refer to the interaction between particles with identical/different isospins, respectively. The densities that occur in Eq. (4.11) are given in appendix 9.2.3. The coupling constants A^X/B^X may further depend on densities that do not involve spatial derivatives. Historically, Eq. (4.11) was derived starting from the HF expectation value of a Skyrme interaction [108] which contains zero-range terms plus gradient corrections to encode finite-range effects, and is a sum of central, spin-orbit and tensor terms, i.e.

$$
v_{\text{Skyrme}}(\vec{R},\vec{r}) \;=\; v_{\text{cent.}}(\vec{R},\vec{r}) + v_{\text{LS}}(\vec{R},\vec{r}) + v_{\text{tens.}}(\vec{R},\vec{r}) \tag{4.12}
$$

$$\begin{aligned} v_{\text{cent}}(\vec{R},\vec{r}) &= t_0\,(1+x_0\hat{P}_\sigma)\,\delta(\vec{r}) + \frac{1}{6}\,t_3\,(1+x_3\hat{P}_\sigma) \\ &\quad + \frac{1}{2}\,t_1\,(1+x_1\hat{P}_\sigma)\big[\hat{\vec{k}}'^2\,\delta(\vec{r}) + \delta(\vec{r})\,\hat{\vec{k}}^{\,2}\big] + t_2\,(1+x_2\hat{P}_\sigma)\,\hat{\vec{k}}'\cdot\delta(\vec{r})\,\hat{\vec{k}} \\ &\quad + \rho^\gamma(\vec{r})\,\delta(\vec{r}) && (4.13) \\ v_{\text{LS}}(\vec{r}) &= iW_0\,(\hat{\vec{\sigma}}_1 + \hat{\vec{\sigma}}_2)\cdot\hat{\vec{k}}'\times\delta(\vec{r})\,\hat{\vec{k}} && (4.14) \\ v_{\text{tens.}}(\vec{r}) &= \frac{1}{2}\,t_e\Big\{\big[3\,(\vec{\sigma}_1\cdot\vec{k}')\,(\vec{\sigma}_2\cdot\vec{k}') - (\vec{\sigma}_1\cdot\vec{\sigma}_2)\,\vec{k}'^2\big]\,\delta(\vec{r}) \\ &\qquad + \delta(\vec{r})\,\Big[3\,(\vec{\sigma}_1\cdot\vec{k})\,(\vec{\sigma}_2\cdot\vec{k}) - (\vec{\sigma}_1\cdot\vec{\sigma}_2)\,\vec{k}^{\,2}\Big]\Big\} \\ &\quad + t_o\Big[3\,(\vec{\sigma}_1\cdot\vec{k}')\,\delta(\vec{r})\,(\vec{\sigma}_2\cdot\vec{k}) - (\vec{\sigma}_1\cdot\vec{\sigma}_2)\,\vec{k}'\cdot\,\delta(\vec{r})\,\vec{k}\Big]\,. && (4.15) \end{aligned}$$

In this context of viewing $\mathcal{E}_{ph}[\rho]$ as the HF energy from a zero-range Skyrme force, the time-even and time-odd terms of the coupling constants of the Skyrme energy functional are related through the underlying parameters of the Skyrme interaction [106]. However, in the general EDF formulation, the time-even and time-odd couplings are independent of each other, aside from relations dictated by local gauge invariance. Even though this most general second-order particle-hole functional has been known for quite some time, traditional studies concentrated only on those terms which were deemed most important. Recently, the impact of all couplings is being analyzed in various studies [[26], [159], [158]].

4.2.2 Particle-particle functional

Neutron-neutron and proton-proton pairing acts mostly in the spin-singlet channel $S = 0$ of the nuclear interaction, as shown by the properties of the bare NN force [117]. At the same time, it occurs mainly in the s wave, that is a local pairing functional. This is usually used to justify the expression of the particle-particle functional $\mathcal{E}_{pp}$ as

$$\mathcal{E}_{pp}[\rho,\kappa,\kappa^*] = \int d\vec{r}\,A^{\tilde{\rho}\tilde{\rho}}\sum_q |\tilde{\rho}^q|^2\;, \tag{4.16}$$

where usually

$$A^{\tilde{\rho}\tilde{\rho}} \equiv \frac{\tilde{t}_0}{4}\left[1-\eta\left(\frac{\rho_0}{\rho_{\mathrm{sat}}}\right)^{\alpha}\right]\,. \tag{4.17}$$

The latter expression derives from a density-dependent delta interaction (DDDI) [127, 128, 129, 130, 131]

$$v^{\tilde{\rho}\tilde{\rho}}(\vec{r},\vec{R}\,) \equiv v^{\tilde{\rho}\tilde{\rho}}(\vec{R}\,)\,\delta(\vec{r}\,) \equiv \tilde{t}_0\left(\frac{1-P_\sigma}{2}\right)\left[1-\eta\left(\frac{\rho_0(\vec{R}\,)}{\rho_{\mathrm{sat}}}\right)^{\alpha}\right]\delta(\vec{r}\,)\,. \tag{4.18}$$

It is bilinear in the pair density $\tilde{\rho}^q$, defined in Eq. (9.99), whereas the strength $\tilde{t}_0$ is taken to be the same for neutron-neutron and proton-proton pairing. $\mathcal{E}_{pp}[\rho,\tilde{\rho},\tilde{\rho}^*]$ enforces pairing correlations only in the $T = 1$ channel, as proton-neutron pairing is usually neglected. The introduction of $T = 0$ pairing requires a more involved formalism, since pairing correlations can now couple between superblocks of different signature in the HFB equations [118, 119]. Two parameters η and α control the spatial dependence of the coupling constant through the overall isoscalar density-dependent coupling. A zero value of η corresponds to a pairing strength that is uniform over the nuclear volume ("volume pairing") while $\eta = 1$ corresponds to pairing strength which is stronger in the vicinity of the nuclear surface ("surface pairing"). A value $\eta = 1/2$ corresponds to an intermediate situation ("mixed-type pairing"). Values $\alpha < 1$ correspond to stronger pairing correlations at low density.

4.2.3 Self-consistent solution

After the construction of the densities ρ_{ij} and κ_{ij} from an auxiliary $|\Phi\rangle$, the variation of the EDF (Skyrme-EDF) with respect to these densities results in Hartree-Fock Bogoliubov (HFB) equations. Refer to appendix 9.7 for a brief discussions of these equations. One solves these equations self-consistently. For detailed discussion on this, refer to Ref. [81].

	ρ_{sat} [fm^{-3}]	K_∞ [MeV]	$(m^*/m)_s$	κ_v	E/A [MeV]	Ref.
SLy4	0.160	229.9	0.70	0.25	−15.97	[135, 145]
SIII	0.145	355.4	0.76	0.53	−15.85	[146]
m^*1	0.162	230.0	1.00	0.25	−16.07	[144]
ρ^1_{sat}	0.145	230.0	0.70	0.25	−15.69	[144]
ρ^2_{sat}	0.160	230.0	0.70	0.25	−15.99	[144]
ρ^3_{sat}	0.175	230.0	0.70	0.25	−16.22	[144]
T6	0.161	235.6	1.00	0.00	−15.93	[147]
SKa	0.155	263.1	0.61	0.94	−15.99	[148]
T21-T26	0.161	230.0	0.70	0.25	−16.00	[142]

Table 4.1: INM properties of Skyrme functionals (from Ref. [81]): saturation density ρ_{sat}, bulk compressibility K_∞, isoscalar effective mass $(m^*/m)_s$, Thomas-Reiche-Kuhn enhancement factor κ_v and energy per particle at saturation E/A.

4.2.4 Existing parameterizations

About 150 parameterizations of the Skyrme EDF have been defined so far and adjusted for various purposes (see [120] and references therein for the most common parameterizations). Sample parameterizations and associated properties of INM are shown in Table 4.1. These functionals differ in what quantities were emphasized during the fits. For instance, T6 has an isoscalar effective nucleon mass $(m^*/m)_s = 1$, providing a denser single-particle spectrum, while SKa has a different isoscalar effective mass, but also a different density dependence (density-dependent term with an exponent of $\gamma = 1/3$ instead of $\gamma = 1/6$). T21 to T26 incorporate tensor terms that differ by their neutron-neutron couplings [142].

4.2.5 Predictive power of empirical EDFs

The discussions in the previous several sections were for the Skyrme EDF. Even though we have not discussed Gogny and relativistic [26] realizations of the EDF, the key points of this section regarding the predictive power of currently available EDFs holds for all three implementations. This is due to the fact that these EDFs generally provide comparable predictions, in spite of some variations for particular observables [[26], [106]].

The application of phenomenological EDFs for a broad range of nuclear structure problems has been a success story in the past few decades [26]. Recently, the growth of available computational power has allowed large-scale projects, such as deformed calculations of ground-state properties over the nuclear chart. Systematic calculations of ground-state properties, as well as some collective excitations, for all known and theoretically predicted nuclei, are now available. Mass residuals over about two thousand known nuclei obtained at the SR-EDF level are of the order of one MeV, which is an accuracy sufficient for a direct comparison with experimental data [[121] -[123]]. Such calculations also provide a reasonably good description of static properties beyond the ground-state energy, e.g. shell structure, pairing gaps, charge radii, individual excitations or deformation.

Likewise, MR-EDF calculations have already met a lot of success, in particular regarding the description of dynamical correlation energies, vibrational/rotational excitations and super-deformed bands or shape transitions [[124], [125]]. Among other challenging areas of interest, extensive studies have for instance been dedicated to [106] (i) (asymmetric) fission properties of heavy elements, (ii) the formation of superheavy nuclei, (iii) the application of dynamical approaches based on the time-dependent HF/HFB formalism to describe nuclear fission/fusion, and (iv) collective motions through the self-consistent (quasiparticle) random phase approximation ((Q)RPA).

However, many challenges are still ahead in order to (i) further increase the overall precision of EDF-based methods, e.g. decrease mass residuals, (ii) describe excited states with spectroscopic accuracy (of the order of 300 keVs), as it is achieved for sd-shell nuclei using the Shell Model [[132]-[134]], (iii) control spin and ferromagnetic instabilities and (iv) improve the predictive power of EDFs in the unknown region

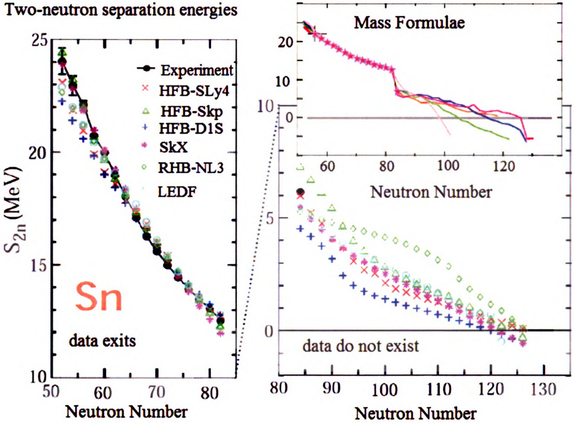

Figure 4.1: Illustration of the asymptotic freedom of phenomenological EDF models in the case of two-neutron separation energies. In the major shell where empirical EDFs are adjusted on experimental data, the agreement between all relativistic and non-relativistic calculations is clearly seen. In the next major shell where no data exist, discrepancies between these models become more apparent (from J. Dobaczewski et al. [150]).

of the nuclear chart. Indeed, while all empirical models constrained by experimental data mostly agree with each other within the major shell they are adjusted in, extrapolations towards the nucleon drip-line do not agree with each other. This divergence in the next major shell is seen for most standard observables such as the two-nucleon separation energy or the pairing gap and is exemplified by Fig. 4.1.

Furthermore, empirical EDF models give rise to spurious effects. For instance, the particle-hole effective vertex extracted from typical empirical functionals is rarely fully antisymmetric (e.g. fractional density-dependencies). This leads to a series of difficulties in SR- (self-interaction and self-pairing) and MR- (poles and spurious steps) EDF calculations. Some of these issues have been identified and practical cures have been proposed [105]. However further developments are required in order to develop a fully satisfactory theory.

4.2.6 Outlook

Various groups are pursuing different strategies to overcome the deficiencies of phenomenological EDFs and make them of spectroscopic quality. In this context, spectroscopic quality refers to the ability to describe and predict not only the bulk properties such as mass and radii but also low-energy spectroscopy and collective states of nuclear systems far below the MeV accuracy. On the one hand is the effort to empirically improve the analytical form and couplings of the EDFs [[31]-[36]]. This includes

- The construction of EDFs containing beyond second order derivatives [35]. Recently, the authors of Ref. [35] undertook the construction of nuclear EDF with up to sixth order in gradients. It is possible to reduce the large number of couplings significantly by the successive application of symmetry constraints such as Galilean (gauge) invariance. Further reduction can be accomplished due if one requires time-reversal and spherical symmetries. Furthermore, the number of couplings also depends on whether one incorporates density dependencies on all or some of the couplings.

- Approaches that rely on the pseudo-potential perspective, start by selectively enriching various parts of the effective interaction. There have been several suggestions to augment the traditional Skyrme interaction given in Eq. (4.12), e.g. adding a spin-density dependent term [33]

$$V = \frac{1}{6}\, t_3^s (1 + x_3^s P_\sigma [\vec{s}_0(\vec{R})]^{\gamma_s})\, \delta(\vec{r}) + \frac{1}{6}\, t_3^{st} (1 + x_3^{st} P_\sigma [\vec{s}_1(\vec{R})]^{\gamma_{st}})\, \delta(\vec{r}) , \qquad (4.19)$$

  where the exponents γ_s and γ_{st} are even integers in order for the EDF to remain time-even. The contribution of these terms vanish in even-even nuclei. These additions seem to remove spin and ferromagnetic instabilities [33] from conventional EDFs, an improvement that must be seen in light of the fact that the spin-isospin components of nuclear EDFs are less understood/constrained than their scalar/isoscalar counterparts.

- Systematic fitting of the nuclear EDF. This does not necessarily imply improving the form of the functional. Rather, it focuses on the application of advanced algorithms to explore the manifold of permissible parameterizations with the use of a large set of experimental data as a reference [106]. Traditionally, practitioners have taken the easier route of only using ground state properties of magic and semi-magic nuclei to constrain the couplings. The availability of data on nuclei far from the valley of stability have provided more stringent constraints on the couplings, with special emphasis on the isovector properties [106] that are less understood. The experimental data identified for this purpose include (i) bulk properties such as binding energy and charge radii (ii) spin-orbit splitting in nuclei for which accurate data exists such as ^{40}Ca, ^{48}Ca, ^{90}Zr or ^{132}Sn in addition to ^{16}O and ^{208}Pb which are usually employed (iii) neutron radii (iv) odd-even staggering of binding energies in medium to heavy nuclei (v) isotopic shifts, deformations, excitation properties and (vi) nuclear matter saturation properties and the equation of state of pure neutron matter. While no definite proof exists that one can not obtain significant improvement by following this method, recent results [109] indicate that the form of both the functional and couplings might be too limiting to obtain predictive EDFs.

A complementary approach is one that relies less on fitting empirical functionals to known data, but rather attempts to constrain the analytical form of the functional and that values of its couplings from many-body perturbation theory (MBPT), based on realistic two- and three-nucleon (NN and NNN) interactions [[110]-[154]]. This is the path followed in this work, which is similar in spirit to OEP (orbital-dependent energy potential or ab-initio DFT) [115, 116]. The main techniques, results, possible future extensions and outlooks are presented in the next several chapters.

Ch

Co

En

5.

Chapter 5

Constructing Non-Empirical Energy Density Functionals

5.1 Constructing Non-Empirical Energy Density Functional

It is commonly asserted that the nuclear many-body problem is intrinsically non-perturbative [38]. The strong short-range repulsion, the strong tensor force from iterated pion-exchange, and the presence of nearly bound states in the S-wave constitute the main reasons as to why the nuclear many-body problem is non-perturbative [27]. However, this argument relies on the assumption that the nuclear many-body problem is driven by an absolute, unique Hamiltonian, without making explicit reference to the intrinsic energy or resolution scale that underlies the modeling of such a Hamiltonian.

However, recent studies have shown that the above statements need qualification as the nuclear Hamiltonian depends on the energy resolution scale [27]. In this context, an important recent development is the construction of low-momentum interactions starting from chiral effective field theory (EFT) interactions and using renormalization group (RG) methods. Even though these methods can be applied to any interaction that originally couples low and high momentum states, chiral EFT interactions are preferable starting points because of the consistency that characterizes their many body-forces forces and operators as well as because of the possibility to systematically improve their precision by going to higher chiral orders. Refer to section 2.4 for details.

The use of low-momentum interactions simplifies the nuclear many-body problem as it eliminates, or at least weakens, the main origins of non-perturbativeness [27]. In particular, the consistent three-nucleon interactions become perturbative as one lowers the intrinsic momentum scale of the two-nucleon piece [28]. Calculations of infinite nuclear matter using MBPT in terms of low-momentum two- and three-nucleon interactions show convergence, at least in the particle-particle channel. As Fig. 5.1 shows, including the second-order contribution from the two- and three-nucleon interactions, one obtains reasonable saturation properties of infinite nuclear matter, with weak dependence on the resolution scale [28]. Moreover, the freedom to vary the order of the input EFT interactions and the cutoff via RG provide a powerful tool to assess theoretical errors arising from truncations in the Hamiltonian and the chosen many-body approximations.

All these features point to the fact that it may be possible to construct nonempirical energy density functionals. Indeed, Hartree-Fock becomes reasonable, if not quantitative, starting point [28], which suggests that the theoretical developments and phenomenological successes of EDF methods for Coulomb systems may be applicable to the nuclear case for low-momentum interactions.

5.1.1 Philosophy, Goals and Limitations

Calculations in INM [28] and the binding energies and radii of finite nuclei [29] show that at least second-order contributions from MBPT have to be incorporated to ob-

Energy/nucleon [MeV]

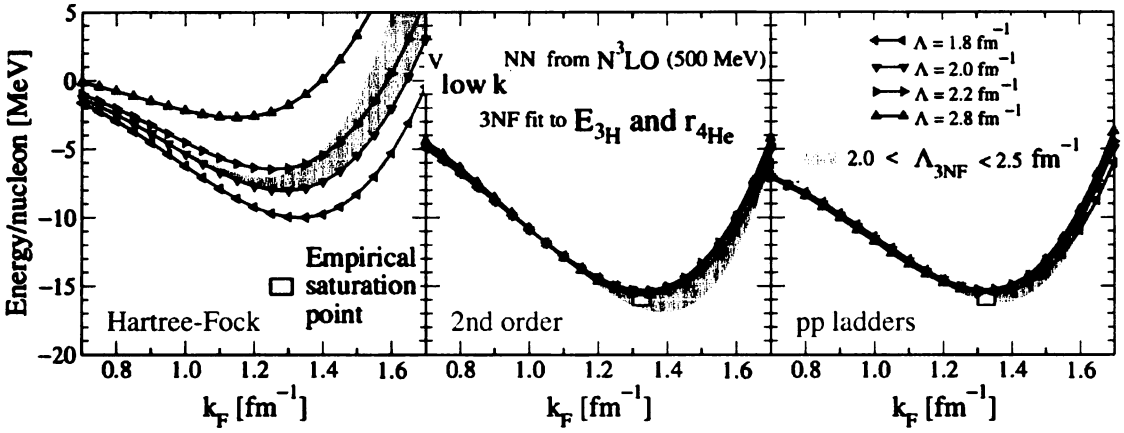

Figure 5.1: (Color online) Nuclear matter energy per particle as a function of Fermi momentum k_F at the Hartree-Fock level (left) and including second-order (middle) and particle-particle-ladder contributions (right), based on evolved N^3LO NN potentials and $3NF$ fit to E_{3_H} and $r_{4_{He}}$. Theoretical uncertainties are estimated by the NN (lines) and NNN (band) cutoff variations (from Bogner et. al. [28]).

tain quantitative success. Likewise, first-order treatment of pairing correlations using low-momentum two-nucleon interaction show good agreement with experimental results [112]. On the side of the interaction (chiral EFT interactions in this case), one needs to go up to N^{3}LO in the chiral expansion in order to describe elastic scattering phase shifts in the two-nucleon sector with χ^2/data close to one [12]. In addition, these interactions still contain significant coupling of low and high momentum modes which necessitates their consistent evolution to low-momentum to make HF a reasonable starting point and obtain a convergent MBPT. Hence, a microscopic/non-empirical calculation of the nuclear many-body problem should incorporate at least the contribution of the diagrams shown in table 5.1 for the normal and table 5.2 for the anomalous/pairing contributions, starting from low-momentum interactions.

Though the perturbativeness of the nuclear many-body problem when using low-momentum interactions is quite comforting, MBPT is still numerically too expensive for a systematic calculation of hundreds of heavy open-shell nuclei. Additionally, the accuracy of currently favored approaches such as empirical EDFs cannot be met, at this point, with completely non-empirical MBPT calculations. Hence, a method

Table 5.1: MBPT contributions from NN and NNN interactions up to second-order (Normal contractions) in Hugenholtz representation.

MBPT Order	NN-interaction	NNN-interaction
First Order in MBPT	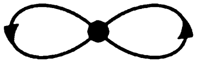	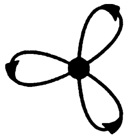
Second order in MBPT	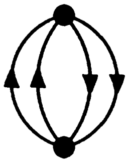 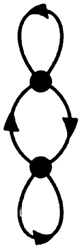	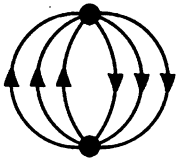 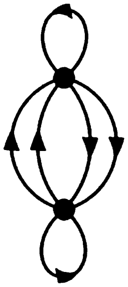 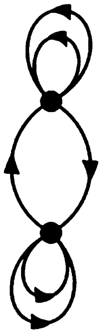

Table 5.2: The first-order anomalous/pairing diagrams, otherwise called Bogoliubov contributions, from the NN and NNN interactions in Hugenholtz represenation.

from NN: 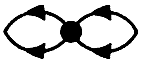

from NNN: 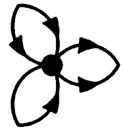

is sought to map MBPT contributions to numerically tractable forms, such as local EDFs, with the aim of refitting some parts of the functional in a controlled and theoretically motivated way.

In this work, we do not attempt to derive a completely non-empirical EDF. Rather, we have a more pragmatic goal of enriching and improving current phenomenological Skyrme EDFs by identifying and incorporating novel density dependencies arising from missing pion physics. We further restrict the work in that only the first-order (HF) contributions from the un-evolved chiral EFT NN + NNN interactions at N^2LO have been calculated. Subsequently, we apply the DME to the resulting nonlocal energy functional to obtain a quasi-local Skyrme-like EDF. In practical implementations, this is to be followed by refit of the couplings, which has the added benefit that the whole scheme can be implemented in existing codes with minimal modification. Refer to section 8.1 for more details. With the goals and limitations of the work in perspective, the justifications to concentrate only on the HF contribution from non-evolved chiral interactions and subsequent application of the DME are as follows:

- First, it is well known that RG evolution of interactions to low-momentum modifies only their short distance structure [15]. The input chiral interaction has both contact and finite-range pion exchange parts, as given by Eq. (2.12). The RG evolution modifies mostly $\hat{V}_{ct}(\Lambda)$. However, the energy contribution from $\hat{V}_{ct}(\Lambda)$, at least at the HF level, is of the same form as conventional Skyrme EDFs. Thus, refit of the Skyrme parameters should compensate for the RG evolution of this part of the interaction. As we are primarily interested in identifying the dominant density dependencies arising from finite-range physics, it is justifiable to apply the DME to the energy contribution from $\hat{V}_{\pi}$.

- Second, inclusion of second-order contributions necessitates the development of non-trivial extensions of the DME technique, as those expressions involve nonlocalities both in space and in time [166], while the currently available DMEs can only treat nonlocalities in space [[170],[107]]. This can be illustrated by contrasting the contributions to the energy from the HF and second-order diagrams. Discarding all spin and isospin coordinates for the sake of simplicity and considering only NN interaction, V^{NN},

$$
\begin{aligned}
\mathcal{E}^{HF} &\propto \int d\vec{r}_1\, d\vec{r}_1\, V^{NN}(|\vec{r}_1 - \vec{r}_2|)\, \rho(\vec{r}_1, \vec{r}_2)\, \rho(\vec{r}_2, \vec{r}_1)\,, \qquad (5.1)\\
\mathcal{E}^{2nd} &\propto \sum_{\alpha\beta\gamma\delta} \int d\vec{r}_1\, d\vec{r}_1\, d\vec{r}_3\, d\vec{r}_4 \Big[\phi^*_\alpha(\vec{r}_1)\, \phi^*_\beta(\vec{r}_2)\, V^{NN}(|\vec{r}_1 - \vec{r}_2|)\, \phi_\gamma(\vec{r}_1)\, \phi_\delta(\vec{r}_2)\\
&\quad \times \phi^*_\gamma(\vec{r}_3)\, \phi^*_\beta(\vec{r}_4)\, V^{NN}(|\vec{r}_3 - \vec{r}_4|)\, \phi_\alpha(\vec{r}_3)\, \phi_\beta(\vec{r}_4) \Big]\\
&\quad \times \frac{\rho_{\alpha\alpha}\, \rho_{\beta\beta}\, (1 - \rho_{\gamma\gamma})\, (1 - \rho_{\delta\delta})}{\epsilon_\alpha \,+\, \epsilon_\beta \,-\, \epsilon_\gamma \,-\, \epsilon_\delta}\,, \qquad (5.2)
\end{aligned}
$$

where $\rho_{\alpha\alpha}$ is the density matrix, defined in Eq. (9.70), in the canonical single-particle basis of the reference HF reference state and ϵ_α is the energy of the single-particle level. While the HF contribution, $\mathcal{E}^{HF}$, can be expressed as a functional of $\rho(\vec{r}_1, \vec{r}_2)$ only, the same cannot be said about the second-order contribution, $\mathcal{E}^{2^{nd}}$, or any beyond-HF contribution. This is due to the occurrence of energy-denominators. A satisfactory extension of the DME that can properly handle beyond-HF contributions and in particular the energy-denominators is yet to be invented [166].

- Third, it is well known that the dominant contributions to bulk nuclear properties are of Brueckner-Hartree-Fock (BHF) type [38]. Operationally, this amounts to replacing the vacuum interactions in the HF expression by a Brueckner G-matrix, which is discussed in section 3.2. But, the G-matrix "heals" to the bare interaction at long distances. This is usually demonstrated by studying the behavior of the $S-$wave in-medium pair wave-function (at zero center of mass momentum) of the Bethe-Goldstone equation in a repulsive hard-core spherical potential [38]

$$\begin{aligned}\phi(r) &= \frac{\sin(kr)}{kr} - \frac{\sin(kr_c)}{kr_c}\frac{g(r,r_c)}{g(r_c,r_c)}, \; r \geq r_c, & (5.3)\\ \phi(r) &= 0, \; r < r_c, & (5.4)\end{aligned}$$

where r_c is the radius of the hard-core, k is the relative momentum of the two-particles and

$$g(r,r') = \frac{1}{2\pi^2}\frac{1}{rr'}\int_{k_F}^{\infty} dk' \frac{\sin(k'r)\sin(k'r)}{k^2 - k'^2}. \qquad (5.5)$$

Figure 5.2 shows the solution of Bethe-Goldstone S-wave solution for relative momentum, $k = k_F/2$, and the uncorrelated two-body wavefunction, $\phi_0(r) = sin(kr)/(kr)$. Simple analysis shows that $g(r,r')$ decreases rapidly

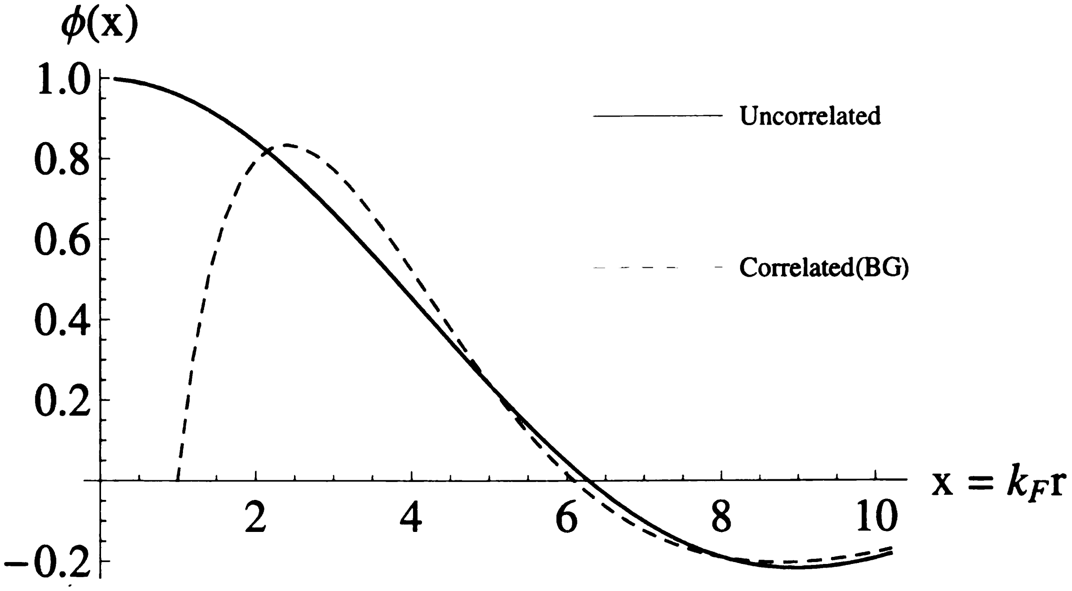

Figure 5.2: (Color online) The S-wave solution of the Bethe-Goldsone equation and the uncorrelated S-wave function.

with increasing r, with a distance scale of $1/k_F$. One defines the healing distance, r_h, which refers to the distance beyond which the the wave-function effectively attains the unperturbed value. This is given by the approximate relation $k_F r_h \approx 1.9$, more or less independent of the relative and center of mass momenta [38]. Then, one can use Eq. (3.10) to show that $G-$matrix heals to the bare interaction in the same manner. Hence, applying the DME to the finite-range part of the interaction, viz, $\hat{V}_\pi$ at the HF level will capture the same contributions to the density-dependent couplings as given by the finite-range part of the G-matrix in a more sophisticated BHF calculation. In this way, the dominant density-dependence that arises from the finite-range of the interactions is accounted for.

- Finally, the algebra required to obtain even the starting point for the DME (viz, DME on the HF energy from chiral EFT NN + NNN interactions at N^2LO) is so tremendous that most of the work can be done only using some form of automation [[156], [161]]. This is especially the case if one wants to have the complete form of the functional without any restricting assumptions regarding time-reversal invariance and/or spherical symmetry.

This work is just the first step in the long-term project of building non-empirical nuclear EDF. There are several possible extensions that can be made in the future. Refer to section 8.2 for a related discussion.

5.2 The Density Matrix Expansion (DME)

The DME was originally proposed by Negele and Vautherin [170] to derive an effective nuclear Hamiltonian. In the first paragraph of their paper [170], Negele and Vautherin note that *the purpose of the density matrix expansion is to relate the compu-*

tationally simple effective interactions of δ and Skyrme forces to the computationally cumbersome theory derived directly from the nucleon-nucleon force.

In deriving an effective nuclear Hamiltonian, Negele and Vautherin avoided following the moment based expansion which were considered in earlier works [167] in which one considers expansions of the fourier transform of a short-range interaction. Their rational for doing that was the fact that the long range part of the nuclear G-matrix heals to the bare one-pion-exchange-potential (OPEP), which causes convergence problems for moment based expansions. Hence, they invented an expansion, the density matrix expansion, that exactly includes the long-range OPEP tail for the nuclear density matrix [170].

5.2.1 Basics of the DME

The central idea of the DME is to factorize a local or nonlocal density obtained from the one-body density matrix (OBDM) by expanding it into a finite sum of terms that are separable, usually, in the relative and center of mass coordinates, $(\vec{r}, \vec{R})$. There are a few exceptions to the $(\vec{r}, \vec{R})$ choice as the DME-coordinates. These exceptions are mostly relevant to the the application of the DME to the HF energy from the chiral EFT NNN interaction at N^2LO. Refer to section 7.2 for details. Adopting $(\vec{r}, \vec{R})$ as our DME-coordinates and the notation introduced in Ref. [168], one writes the general DME formulae

$$\rho_q(\vec{r}_1, \vec{r}_2) \approx \sum_{l=0}^{l_{\max}} \Pi_l^{\rho}(k\,r)\, \mathcal{P}_l(\vec{R}) \; , \tag{5.6}$$

$$\vec{s}_q(\vec{r}_1, \vec{r}_2) \approx \sum_{m=0}^{m_{\max}} \Pi_m^{\vec{s}}(k\,r)\, \mathcal{Q}_m(\vec{R}) \; , \tag{5.7}$$

$$\tilde{\rho}_q(\vec{r}_1, \vec{r}_2) \approx \sum_{n=0}^{n_{\max}} \Pi_n^{\tilde{\rho}}(k\,r)\, \tilde{\mathcal{P}}_n(\vec{R}) \; , \tag{5.8}$$

$$\tilde{\vec{s}}_q(\vec{r}_1, \vec{r}_2) \approx \sum_{o=0}^{o_{\max}} \Pi_o^{\tilde{\vec{s}}}(k\,r)\ \tilde{\mathcal{Q}}_o(\vec{R}) \ , \tag{5.9}$$

$$\mathcal{G}_q(\vec{r}_{1/2}) \approx \sum_{u=0}^{u_{\max}} \pi_u^{\mathcal{G}}(k\,r)\ \mathcal{H}_u(\vec{R}) \ , \tag{5.10}$$

where k is a momentum scale to be determined that sets the scale for the decay in the direction of the relative coordinate $\vec{r}$, $\Pi_i^f(k\,r)$ are the so-called $\pi-$functions that remain to be specified, and

$$\begin{aligned}\{\mathcal{P}_l(\vec{R}), \mathcal{Q}_m(\vec{R})\} \in \quad & \{\rho_q(\vec{R}), \tau_q(\vec{R}), J_{q,\mu\nu}(\vec{R}), \vec{\nabla}\rho_q(\vec{R}), \Delta\rho_q(\vec{R}), \vec{s}_q(\vec{R}),\\ & \vec{F}_q(\vec{R}), \vec{T}_q(\vec{R})\}\,, \end{aligned} \tag{5.11}$$

denote the local normal densities

$$\begin{aligned}\{\tilde{\mathcal{P}}_n(\vec{R}), \tilde{\mathcal{Q}}_o(\vec{R})\} \in \quad & \{\tilde{\rho}_q(\vec{R}), \tilde{\tau}_q(\vec{R}), \tilde{J}_{q,\mu\nu}(\vec{R}), \vec{\nabla}\tilde{\rho}_q(\vec{R}), \Delta\tilde{\rho}_q(\vec{R}), \tilde{\vec{s}}_q(\vec{R}),\\ & \tilde{\vec{F}}_q(\vec{R}), \tilde{\vec{T}}_q(\vec{R})\}\,, \end{aligned} \tag{5.12}$$

refer to the local anomalous densities, while $\mathcal{G}_q(\vec{r}_{1/2})$ and $\mathcal{H}_u(\vec{R})$ are from the set of local normal or anomalous densities.

The DME emphasizes separability of the expansion in the relevant expansion-coordinates above the approximation of nonlocality. That is, even for local densities that depend on a single coordinate and hence with no nonlocality, one can talk about an expansion in terms of the DME-coordinates as stated by Eq. (5.10). In a sense, one is approximating the nonlocality in one of the DME-coordinates. For example, $\rho_q(\vec{r}_1) \equiv \rho_q(\vec{R} + \vec{r}/2)$ can be expanded in terms of quantities that depend on $\vec{R}$ and $\vec{r}$ separately. In practice, however, the emphasis on separability above the approximation of nonlocality is of limited use as most DME approaches rely on analytical techniques that fail to work when there is a long-range of nonlocality in the expansion-co

This work
components
The extensio
in constrain
The apparen
appear in th
why one sh
their possib
anomalous
enrich the p
densities, t
are discuss
DME app
preliminar

5.2.2

The main
mination
local de
DME to
band are
in a de
Parame
we have
while in
mations

expansion-coordinate.

This work concentrates mainly on the expansion of the nonlocal scalar and vector components of the normal part of the density matrix, viz, $\rho_q(\vec{r}_1, \vec{r}_2)$ and $\vec{s}_q(\vec{r}_1, \vec{r}_2)$. The extension of the approach to non time-reversal invariant systems is important for constraining the nuclear EDF for those systems. This is discussed in section 5.3.6. The apparent need for the DME of the local densities ($\rho_q(\vec{r}_{1/2})$ and $\vec{J}_q(\vec{r}_{1/2})$) that appear in the exact HF energy of time-reversal invariant systems, justifications for why one should avoid expanding these densities and related technical problems and their possible solutions are discussed in section 5.3.7. The expansion of the nonlocal anomalous densities, especially $\tilde{\rho}(\vec{r}_1, \vec{r}_2)$, has drawn some interest due to the need to enrich the pairing part of the nuclear EDF. Nevertheless, unlike the nonlocal normal densities, there are some conceptual and technical difficulties to be overcome. These are discussed in section 5.3.8. We gauge and compare the accuracy of the various DME approaches using non self-consistent measures. Finally, we augment this with preliminary self-consistent tests. These tests are discussed in section 5.4.

5.2.2 Existing variants of the DME

The main problem to be solved in constructing a viable DME technique is the determination and optimization of the various $\pi-$functions and the identification of which local densities occur in the expansion of the given density. The currently available DME techniques [[170]-[173]] approach this problem in two distinct ways. On the one hand are those methods that resum infinite order "Taylor-series" expansion terms in a clever way, while on the other are those that start with an inspired ansatz and paramterize and optimize the the $\pi-$functions phenomenologically. In the first group, we have the original DME of Negele and Vautherin and its variants [170, 171, 173], while in the second group we have those that are mostly based on gaussian approximations of the scalar part of the OBDM [172]. In the phenomenological optimization

of the π–fun
OBDM such
projector ide
In additi
approximate
While most
ones that ar
fall into the
regards to th
is a variant
that improv
optimizing
In app
the PSA-D
appendix
expansion

5.3

5.3.1

One of
mostly
acknow
of the
as the
of co
OBD

of the π−functions, the parameters are optimized to recover various properties of the OBDM such as the correct local semiclassical kinetic energy density and integrated projector identity of the OBDM (see Eq. (5.50)).

In addition, there is yet another classification based on whether the techniques approximate the full quantal or semi-classical approximations of the density matrix. While most of the existing DME techniques approximate the full quantal OBDM, the ones that are based on Wigner-Kirkwood expansion of the single-particle propagator fall into the second/semi-classical category [173]. Further differences appear with regards to the choice made to fix the momentum scale k. In fact, the DME of Ref. [171] is a variant of the original one proposed by Negele and Vautherin (NV-DME) [170] that improves the accuracy of the expansion obtained at first order ($n_{\text{max}} = 0$) by optimizing the momentum scale k.

In appendix 9.5.3, we recover the original DME of Negele and Vautherin using the PSA-DME discussed in the next section and the generalized PSA-DME, while appendix 9.5.2 contains the key points of the semi-classical Wigner-Kirkwood based expansion of the density matrix.

5.3 PSA-DME

5.3.1 Motivation for a PSA reformulation of the DME

One of the main shortcomings of all existing DME formulations is that they are mostly focused on the scalar part of the OBDM. For instance, Negele and Vautherin acknowledge in their seminal paper that they were not able to design an approximation of the vector part of the OBDM on the same level, and thus with the same accuracy, as the one they obtained for the scalar part. This is an essential problem in view of constraining the nuclear EDF non-empirically. Indeed, the vector part of the OBDM is non zero in spin-unsaturated nuclei, i.e. in almost all nuclei. Moreover,

all available D
apparent exte

These prob
qualities of
if not better
percentage er
small for var
dependence
of the OBD
for the DMH
of the OBD
their accura
time-revers

Hence,
stands for
not compl
approxim
averaging
Bessel-fun
developed
to both
weak an
in the o
Ref. [17
our PSA

In

Refer

all available DME techniques hold only for time-reversal invariant systems, with no apparent extension to non time-reversal invariant systems.

These problems convinced us to formulate a DME approach that has the following qualities: (i) the accuracy for the scalar part of the OBDM should be comparable to, if not better than, the existing DME techniques. It should be mentioned that the percentage error of existing DME techniques for the scalar part of the OBDM is quite small for various measures, which should be enough to capture the correct density dependence of the couplings in the resulting EDF. (ii) The DME of the vector part of the OBDM should have a comparable accuracy to that of the scalar part. Except for the DME of Negele and Vautherin [170] which performs badly for the vector part of the OBDM[1], the other techniques either do not refer to the vector part at all or their accuracies are not gauged properly. (iii) It should readily be extended to non time-reversal invariant systems.

Hence, we formulated a new DME technique which we call PSA-DME where PSA stands for phase space averaging. Note that the PSA formulation of the DME is not completely new. In fact, Negele and Vautherin start using the "local energy approximation" technique of Ref. [174] and mention the possibility of phase space averaging in infinite nuclear matter. For the actual derivation, they revert to a formal Bessel-function plane-wave expansion. From a formal point of view, the PSA approach developed below differs from that mentioned in Ref. [170] and is applied consistently to both the scalar and the vector parts of the OBDM. For instance, in spite of the weak angular dependence of the scalar part of the OBDM [176], the inconsistency in the order of application of the angle-averaging and series expansion that exists in Ref. [170] is not an issue in the present case. Still, it is shown in appendix 9.5.3 that our PSA-DME approach can be used to recover the original DME.

In the following, some of the key properties of the momentum phase space of nite Fermi s

---

[1] Refer to section 5.4 for actual percentage errors of the various DMEs.

the r-functio

temperatu

optimization

5.3.2 M

The momen

multitude o

Wigner dis

the local s

Fermi surf

of the mo

systems.

The W

space dis

logically

models in

monic os

a Woods

The a

the Wig

of spin-

potentia

ite Fermi systems are identified with the aim of incorporating these features into e π–functions with the PSA-DME approach. We implement two different strategies incorporate these phase space features: analytical derivation and phenomenological timization.

.3.2 Momentum phase-space of finite Fermi systems

he momentum phase-space distribution of quantum systems can be studied via a ultitude of quantum phase-space distribution functions [169]. Studies using the igner distribution in Ref. [177] and the Husimi distribution in Ref. [178] show that e local single-particle momentum distribution displays a diffuse and anisotropic rmi surface at the (spatial) surface of the finite system. These are peculiar features the momentum phase-space distribution that are not present for homogeneous stems.

The Wigner distribution function [175] is often used to approximate the phase ace distribution of nuclei. It has been studied both analytically and phenomeno-gically for various models applicable to nuclei (see Refs. [176], [179] , [180]). The odels include pure harmonic oscillator with sharp and smeared occupations, har-onic oscillator with orbital occupation from DDHF and meanfield calculations with Voods-Saxon potential.

The analytical calculations of the various models give the same general form for e Wigner distribution function. For the case of magic nuclei and in the absence spin-orbit interaction, the distribution function $\mathbf{f}_q(\vec{R},\vec{p})$ in a harmonic oscillator tential depends solely on the dimensionless parameter ε [180]

$$\mathcal{E} = \frac{\hbar}{m\omega}p^2 + \frac{m\omega}{\hbar}R^2\,, \tag{5.13}$$

and is given b

where $\hbar\omega$ =

number and

n_k is the oc

distribution

fermi-surfa

pronounced

The ab

show anis

authors so

with no sp

This has

INM. Th

tion can b

distributi

formation

where H

distribu

---

[4] As

multipole

and is given by

$$\mathbf{f}_q(\vec{R},\vec{p}) = \frac{4e^{\mathcal{E}}}{(\hbar\pi)^3}\sum_{K=0}^{\infty}(-1)^K L_K^2(2\mathcal{E})\,n_K\,, \tag{5.14}$$

where $\hbar\omega = 41A^{-1/3}$ is the oscillator size parameter, K is the principal quantum number and L_K^{α} is the associated Laguerre polynomial, given in appendix 9.1.1, and n_K is the occupation probability. In Ref. [177], the authors parameterize the Wigner distribution using the Fermi distribution function. All these studies indicate a diffuse fermi-surface for the local momentum distribution with the diffuseness being much pronounced around the nuclear surface.

The above model calculations are able to capture the diffuseness, but they do not show anisotropy/deformation of the local fermi surface. In Refs. [178] and [177], the authors solve for the single particle wave functions in spherical Woods-Saxon potential with no spin-orbit interaction and show that the local fermi surface is anisotropic. This has no counterpart in the phase space distribution of infinite-fermi systems (INM). The anisotropy of the local single particle momentum phase space distribution can be quantified with the lowest order deformation of a spherical phase space distribution, viz, quadrupolar deformation. In Ref. [178], the local quadrupolar deformation of the momentum Fermi surface (for a given isospin) is given by[2]

$$\begin{aligned} P_2^q(\vec{r}) &\equiv \frac{\int d\vec{p}\left[3(\vec{e}_r\cdot\vec{p})^2-\vec{p}^2\right]H_q(\vec{r},\vec{p})}{\int d\vec{p}\,\vec{p}^2 H_q(\vec{r},\vec{p})} \\ &= \left[\frac{3}{\tau_q(\vec{r})}\sum_i\left|(\vec{e}_r\cdot\vec{\nabla})\varphi_i(\vec{r}q)\right|^2\rho_{ii}^q-1\right]+\mathcal{O}((k_F^q r_0)^2)\,, \end{aligned} \tag{5.15}$$

where $H_q(\vec{r},\vec{p})$ is the Husimi distribution, r_0 is a length scale used in the Husimi distribution and k_F^q is a short-hand notation for the local Fermi momentum $k_F^q(\vec{R})$

---

[2] As the anisotropy is usually not large, it is not necessary (at least in this work) to go to higher multipoles to quantify the deformation.

defined in a

In subseque

for rotation.

dependence

as the has

distribution

semi-magn

Fig. 5.

defined in a local density approximation through

$$k_F^q(\vec{R}) \equiv k_F^q = \left[3\,\pi^2\,\rho_q(\vec{R})\right]^{1/3} . \tag{5.16}$$

In subsequent formulae, the $\vec{R}$ dependence of $k_F^q(\vec{R})$ is mostly not shown explicitly for notational simplicity, except in formulae/places where we have to remind its $\vec{R}$ dependence. Equation 5.15 is computed in the basis $\varphi_i(\vec{r}q)$ that diagonalizes ρ_{ij}, i.e. the basis from which the Slater determinant $|\Phi\rangle$ is built. Details on the Husimi distribution and simplified expression of $P_2^q(\vec{r})$ in spherical symmetry suitable for semi-magic nuclei is provided in the appendix 9.5.1.

Fig. 5.3 shows the quadrupole anisotropy of the local neutron momentum distribution calculated for a selection of semi-magic nuclei. Single-particle wave-functions are obtained from a Skyrme-EDF calculation performed with the BSLHFB code [181] using the SLy4 parametrization of the Skyrme EDF. The pairing terms in the EDF were switched off. Fig. 5.3 also displays the local neutron Fermi momentum (Eq. 5.16) in order to locate the position of the nuclear surface. In spite of pronounced shell fluctuations, the result corroborates the conclusions drawn in Ref. [178]; $P_2^n(\vec{R})$ becomes negative just inside the surface, denoting an oblate momentum Fermi surface while, outside this region, the local momentum Fermi surface becomes strongly prolate. In both cases, we have taken an axis normal to the nuclear surface as the reference axis. The next two sections show how we make use of these properties of the phase-space distribution of finite Fermi systems to design our PSA-DME of both the scalar and vector parts of the OBDM.

1.5
1.
0.
0
-0
1

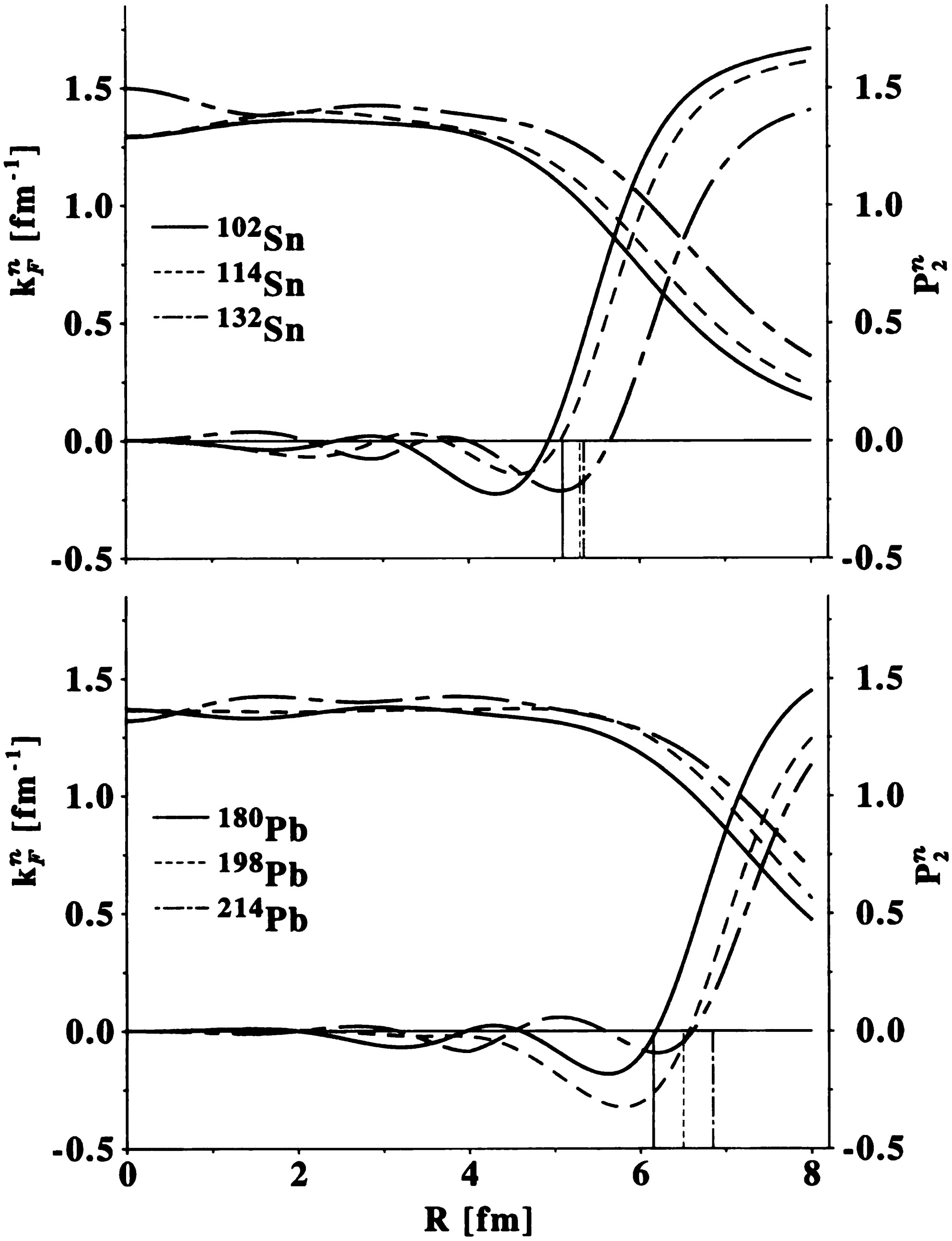

Figure 5.3: The quadrupole anisotropy $P_2^n(\vec{R})$ of the local neutron momentum distribution in a selected set of semi-magic nuclei. The black, red and blue vertical lines indicate the approximate half-radii (where the density becomes half of the density at the origin).

5.3.3

5.3.3 PSA-DME for the scalar part of the OBDM of time-reversal invariant systems

In PSA-DME, there are three key steps that are used to determine the local densities that occur in the expansion of the given nonlocal density and optimize the $\pi-$functions. These are: (i) Identifying of the nonlocality operator as an exponential derivative operator acting on the OBDM. (ii) Performing a Taylor series expansion of the operator about some momentum scale $\vec{k}$. This is the point at which a momentum scale is introduced in the DME, though the actual form of $\vec{k}$ is not fixed yet. (iii) Averaging the momentum scale over the local momentum distribution of the system of interest.

Applying the first step, viz, extraction of the exponential nonlocality operator of the scalar part of the OBDM, one writes

$$\begin{aligned}\rho_q(\vec{R}+\frac{\vec{r}}{2},\vec{R}-\frac{\vec{r}}{2}) &= \sum_{i\sigma} \varphi_i^*(\vec{r}_2\sigma q)\,\varphi_i(\vec{r}_1\sigma q)\,\rho_{ii}^q \\ &= e^{\vec{r}\cdot\left(\frac{\vec{\nabla}_1-\vec{\nabla}_2}{2}\right)} \sum_{i\sigma} \varphi_i^*(\vec{r}_2\sigma q)\,\varphi_i(\vec{r}_1\sigma q)\,\rho_{ii}^q\Big|_{\vec{r}_1=\vec{r}_2=\vec{R}} . \end{aligned} \tag{5.17}$$

In the next step, one extracts a phase factor $e^{i\vec{r}\cdot\vec{k}}$ in order to perform a Taylor series expansion of the non-locality about the momentum scale $\vec{k}$. Hence,

$$\begin{aligned}\rho_q(\vec{R}+\frac{\vec{r}}{2},\vec{R}-\frac{\vec{r}}{2}) &= e^{i\vec{r}\cdot\vec{k}}\, e^{\vec{r}\cdot\left(\frac{\vec{\nabla}_1-\vec{\nabla}_2}{2}-i\vec{k}\right)} \sum_{i\sigma} \varphi_i^*(\vec{r}_2\sigma q)\,\varphi_i(\vec{r}_1\sigma q)\,\rho_{ii}^q\Big|_{\vec{r}_1=\vec{r}_2=\vec{R}} , \\ &\simeq e^{i\vec{r}\cdot\vec{k}} \left\{1+\vec{r}\cdot\left(\frac{\vec{\nabla}_1-\vec{\nabla}_2}{2}-i\vec{k}\right)+\frac{1}{2}\left[\vec{r}\cdot\left(\frac{\vec{\nabla}_1-\vec{\nabla}_2}{2}-i\vec{k}\right)\right]^2\right\} \\ &\quad\times \sum_{i\sigma} \varphi_i^*(\vec{r}_2\sigma q)\,\varphi_i(\vec{r}_1\sigma q)\,\rho_{ii}^q\Big|_{\vec{r}_1=\vec{r}_2=\vec{R}} , \end{aligned} \tag{5.18}$$

where we truncated the expansion at second order. In principle, nothing prevents to one from including higher order terms. This is especially true in light of recent empha-

sis on the inclusion of beyond-second-order gradient terms in Skyrme like EDFs [35]. In that case, one needs to define additional local densities in addition to the ones given in section 9.2.3.

Noting that the derivation is restricted to time-reversal invariant systems, the next step consists of angle averaging over the orientation of $\vec{r}$, which is a reasonable step as the scalar part of the OBDM has negligible dependence on the orientation of $\vec{r}$ [176]. The final step involves averaging the dependence on the momentum scale $\vec{k}$ over a model phase space that characterizes the system under study. As mentioned in section 5.3.1, we make two different choices. First, we perform the PSA with the phase space of the locally-equivalent pure isospin infinite matter. Denoting the function to to be averaged as $g_q(\vec{k})$, this operation amounts to setting the local phase space distribution, $f_q(\vec{R}, \vec{k})$, as

$$f_q(\vec{R}, \vec{k}) \;=\; \Theta(k - k_F^q(\vec{R}))\,, \tag{5.19}$$

and thus

$$G_q(\vec{k}_F^q) \equiv \frac{3}{4\pi^3 k_F^{q3}} \int_{|\vec{k}|\leq k_F^q} d\vec{k}\, g_q(\vec{k})\,, \tag{5.20}$$

where $G_q(\vec{k}_F^q)$ is the final result of the PSA. Prior to the application of the PSA, Eq. (5.18) is angle averaged with respect the orientation of $\vec{r}$. This is a valid approximation as the scalar part of the normal component of the OBDM has a weak dependence on the orientation of $\vec{r}$ [176]. The subsequent application of the PSA as defined by Eqs. (5.19) and (5.20) on the resulting expression yields the DME of the scalar part of the OBDM as

$$\begin{aligned}\rho_q(\vec{R}+\frac{\vec{r}}{2}, \vec{R}-\frac{\vec{r}}{2}) \;\simeq\; & \Pi_0^{\rho}(k_F^q r)\,\rho_q(\vec{R}) + \frac{r^2}{6}\Pi_2^{\rho}(k_F^q r)\left[\frac{1}{4}\Delta\rho_q(\vec{R}) - \tau_q(\vec{R})\right.\\ & \left. + \frac{3}{5}k_F^{q2}\rho_q(\vec{R})\right],\end{aligned} \tag{5.21}$$

with

$$\Pi_0^{\rho}(k_F^q r) \equiv 3\,\frac{j_1(k_F^q(\vec{R})r)}{k_F^q(\vec{R})r}\,, \tag{5.22}$$

$$\Pi_2^{\rho}(k_F^q r) \equiv 3\,\frac{j_1(k_F^q(\vec{R})r)}{k_F^q(\vec{R})r}\,. \tag{5.23}$$

The details of the derivation can be found in appendix 9.5.3, where we perform the derivation in a more general context and recover specific cases. The reason why we do not have Π_1^{ρ} in the above expression is because the time-odd density, $\vec{j}_q(\vec{R})$, vanishes for time-reversal invariant systems. Note that the $\pi-$functions given in Eqs. (5.22)-(5.23) are completely analytical with no fit parameters.

However, the PSA did not invoke the diffuseness and anisotropy of the the phase space of finite Fermi systems discussed in the previous section. With the step of angle averaging over the orientation of $\vec{r}$, the orientations of $\vec{r}$ and $\vec{k}$ are decoupled, implying that the anisotropy is not going to play a key role in the subsequent approximations. Hence, we concentrate only on the incorporation of the diffuseness.

Unfortunately, we could not find completely analytical ways of characterizing the diffuseness. Thus, we parameterize $f_q(\vec{R},\vec{k})$. Inspired by the nature of the Wigner-distribution of the phase space distribution as discussed in the previous, we use the following ansatz to model the local momentum distribution

$$\mathbf{f}_q(\vec{R},\vec{k}) = C\left(1+\alpha\frac{k^2}{{k_F^q}^2}\right)e^{-\beta k^2/{k_F^q}^2}\,, \tag{5.24}$$

where α and β are parameters to be optimized, k_F^q is the local Fermi momentum and C is a constants determined from normalization i.e. volume integral of the momentum distribution should give $4/3\pi {k_F^q}^3$. Hence, C reads

$$C = \frac{8\,\beta^{5/2}}{3\sqrt{\pi}\,(3\alpha+2\beta)}\,. \tag{5.25}$$

Since it is of interest for later use, the average local RMS momentum is given by

$$\check{k}_F^q = \sqrt{\langle k^2 \rangle} = \sqrt{\frac{3\,(5\alpha + 2\beta)}{2\beta\,(3\alpha + 2\beta)}}\, k_F^q\,, \tag{5.26}$$

where the average is calculated taking Eq.(5.24) for the local momentum distribution. To finalize the determination of the scalar part π−functions, the following steps are applied to Eq. (5.18): (i) Average the leading term over the local momentum distribution given in Eq.(5.24). (ii) Since the next-to-leading order term is a small correction, it is simply evaluated at the RMS momentum given in Eq.(5.26). Applying the above prescription, one obtains the π−functions

$$\Pi_0^\rho = -\frac{\left(\alpha\, k_F^{q\,2} r^2 - 2\beta\,(2\beta + 3\alpha)\right)}{2\beta\,(3\alpha + 2\beta)}\, e^{-k_F^{q\,2} r^2/(4\beta)} \tag{5.27}$$

$$\Pi_2^\rho = \frac{3}{\check{k}_F^{q\,2}\, r}\, j_1(\check{k}_F^{q\,2} r)\,, \tag{5.28}$$

where the actual values of the parameters α and β are obtained from numerical fits to data obtained from converged self-consistent calculations of a selected set of isotopic chains. For the optimization of these parameters and the results on the accuracies of PSA-DME of the scalar part of the OBDM, refer to section 5.4.

Several comments are in order regarding the PSA-DME of the scalar part of the OBDME and the π−functions given in Eqs. (5.22)-(5.23) and (5.27)-(5.28). To start with, even though the phase space of finite nuclei has a marked difference from that of INM, the accuracy obtained using the two sets of π−functions is different at most by a few percentage points, with the π−functions given by Eqs.(5.27)-(5.28) being the better ones. This is apparent from the results of section 5.4. The reason being, unlike the vector part of the OBDM discussed below, the scalar part is a bulk quantity with most of its contribution coming from the interior of the nucleus where, to a good approximation, the momentum distribution resembles the one of INM [176]. Hence,

this is the main reason for the comparable accuracies obtained using the two sets of $\pi-$functions.

From the form of the $\pi-$functions, it can be seen that the DME is not a naive Taylor expansion of the OBDM with respect to the non-locality in $\vec{r}$. The $\pi-$functions resum dependencies on r to all orders in some of the leading terms, such that the long distance limit of the OBDM is reproduced. In the approach followed in Ref. [170], the truncation of the expansion about $\vec{k}$ to second order leaves Π_2^ρ indeteminate. Specifically, the values of the coefficients of terms beyond $k_F^q r$ in the Taylor series expansion of Π_2^ρ are undetermined. This indeterminateness gives one the freedom to optimize Π_2^ρ, which can be viewed as selecting a different rearrangement and truncation of the expansion [170].

Furthermore, the zeroth-order $\pi-$function $\Pi_0^\rho(k_F^q r)$ given in Eq. (5.22) is exactly the one found in the original NV-DME of Ref. [170]. Just as in the DME of Negele and Vautherin, this particular PSA reduces to the first term in symmetric INM, thereby reproducing the exact OBDM of INM. The second order $\pi-$function $\Pi_2^\rho(k_F^q r)$ given in Eq. (5.23) is different from

$$\Pi_2^\rho = 105\,\frac{j_3(k_F^q r)}{(k_F^q r)^3}\,, \tag{5.29}$$

which was obtained in Ref. [170]. However, this relates to the previous remark that emphasized the freedom in choosing the second-order π-function. In conclusion, our PSA-DME of the scalar part of the OBDM is essentially equivalent to the DME of Ref. [170] if we choose $f_q(\vec{R},\vec{k})$ to be the phase space of locally equivalent neutron or proton infinite matter. As a final remark, note that the phenomenological PSA whose $\pi-$functions are given in Eqs. (5.27) and (5.28) does not reproduce the exact OBDM of INM. This should not be surprising as the model $f_q(\vec{R},\vec{k})$ used in that case, Eq. (5.24), has a completely different analytical structure from that of the complet

5.3.4

Again r

same

can b

corresponding $f_q(\vec{R}, \vec{k})$ of INM (Eq. (5.19)).

5.3.4 PSA-DME for the vector part of the OBDM in time-reversal invariant systems

Again, restricting the discussion to time-reversal invariant systems and applying the same set of steps as for the scalar part of the OBDM, the vector part of the OBDM can be approximated by

$$\begin{aligned}
\vec{s}_q\left(\vec{R}+\frac{\vec{r}}{2}, \vec{R}-\frac{\vec{r}}{2}\right) &= \sum_{i\sigma_1\sigma_2} \varphi_i^*(\vec{r}_2\sigma_2 q)\, \langle\sigma_2|\vec{\sigma}|\sigma_1\rangle\, \varphi_i(\vec{r}_1\sigma_1 q)\, \rho_{ii}^q \\
&= e^{i\vec{r}\cdot\vec{k}}\, e^{\vec{r}\cdot\left(\frac{\vec{\nabla}_1-\vec{\nabla}_2}{2}-i\vec{k}\right)} \sum_{i\sigma_1\sigma_2} \varphi_i^*(\vec{r}_2\sigma_2 q) \\
&\quad \times \left.\langle\sigma_2|\vec{\sigma}|\sigma_1\rangle\, \varphi_i(\vec{r}_1\sigma_1 q)\, \rho_{ii}^q\right|_{\vec{r}_1=\vec{r}_2=\vec{R}} \\
&\simeq e^{i\vec{r}\cdot\vec{k}} \left\{1+\vec{r}\cdot\left(\frac{\vec{\nabla}_1-\vec{\nabla}_2}{2}-i\vec{k}\right)\right\} \sum_{i\sigma_1\sigma_2} \varphi_i^*(\vec{r}_2\sigma_2 q) \\
&\quad \times \left.\langle\sigma_2|\vec{\sigma}|\sigma_1\rangle\, \varphi_i(\vec{r}_1\sigma_1 q)\, \rho_{ii}^q\right|_{\vec{r}_1=\vec{r}_2=\vec{R}} ,
\end{aligned} \tag{5.30}$$

where only the first order term in the expansion of the non-locality operator is kept. The zero-order term in the above expansion provides the local spin density $\vec{s}_q(\vec{R})$ which is zero for the time-reversal invariant systems. In fact, for time-reversal invariant systems, the cartesian spin-current pseudotensor density $J_{q,\mu\nu}(\vec{R})$ and its gradients are the only standard local densities at hand to express the DME of the vector part of the OBDM. Consequently, we could not express the higher-order (beyond first-order) terms in the above expansion in a closed form in terms of the cartesian spin-current pseudotensor density and its gradients. Nevertheless, section 5.4 shows that PSA-DME attains a high accuracy even at this level of approximation. Still, there is a possibility of studying higher-order terms in the context of the generalized Skyrme

EDF discussed in Ref. [35].

Here also we carry out the two strategies of incorporating the phase space information: analytically and phenomenologically (parameterically). We start with the analytical procedure which was also discussed in Ref. [170], though with no reference to phase space of finite systems. Sticking with the first term, the authors in Ref. [170] argued that averaging over the orientation of $\vec{k}$ and setting $k = k_F^q$ should be sufficient to provide a reasonable account of the vector part of the exact OBDM. This gives

$$\vec{s}_{q,\nu}\left(\vec{R}+\frac{\vec{r}}{2},\vec{R}-\frac{\vec{r}}{2}\right) \simeq i\,\Pi_1^{\vec{s}}(k_F^q r)\sum_{\mu=x}^{z} r_\mu J_{q,\mu\nu}(\vec{R})\,, \tag{5.31}$$

where

$$\Pi_1^{\vec{s}}(k_F^q r) \;=\; j_0(k_F^q(\vec{R})r)\ . \tag{5.32}$$

If instead one applies the same procedure as for the scalar part of the OBDM, i.e. one performs the PSA over the locally-equivalent pure-isospin infinite matter phase-space, as given in Eq. (5.19), one rather obtains

$$\Pi_1^{\vec{s}}(k_F^q r) \;=\; 3\,\frac{j_1(k_F^q(\vec{R})r)}{k_F^q(\vec{R})r}\ . \tag{5.33}$$

However, and as mentioned in section 5.3.2, the local momentum phase-space distribution of finite nuclei has a markedly different behavior than that of INM around the nuclear (spatial) surface. Given that the vector part of the density matrix peaks around the nuclear surface, it seems more appropriate to perform the PSA over a diffuse and anisotropic phase space. Given that we do not have a parameter free way of introducing the diffuseness and the primary quantity to be averaged, $e^{i\vec{r}\cdot\vec{k}}$, couples the orientation of $\vec{r}$ and $\vec{k}$, we limit ourselves to invoking the anisotropy of the phase space. As a completely analytical approach, we perform the PSA over a deformed Fermi sphere that incorporates the information contained in the function $P_2^q(\vec{R})$ discussed in section 5.3.2. We do this by averaging over a spheroidal local momentum distribution given by

$$f_q(\vec{R},\vec{k}) = \Theta(k' - k_F^q) \tag{5.34}$$

where

$$k_q' = k_F^q \sqrt{\frac{k_x^2}{a(\vec{R})^2} + \frac{k_y^2}{a(\vec{R})^2} + \frac{k_z^2}{c(\vec{R})^2}}\,, \tag{5.35}$$

with $a(\vec{R})$ and $c(\vec{R})$ being position dependent quantities that relate to $P_2^q(\vec{R})$. The specific relations and various details of the derivation are given in appendix 9.5.3. The final result differs from that in Ref. [170] only in the analytical form of $\Pi_1^{\vec{s}}$. The result reads

$$\Pi_1^{\vec{s}}(\tilde{k}_F^q r) = 3\,\frac{j_1(\tilde{k}_F^q(\vec{R})r)}{\tilde{k}_F^q(\vec{R})r}\,, \tag{5.36}$$

where

$$\tilde{k}_F^q \equiv \left(\frac{2 + 2\,P_2^q(\vec{R})}{2 - P_2^q(\vec{R})}\right)^{1/3} k_F^q(\vec{R})\,. \tag{5.37}$$

The PSA over the locally-equivalent neutron or proton infinite matter modifies the analytical form of $\Pi_1^{\vec{s}}$ compared to NV-DME, i.e. compare Eqs. (5.32) against ((5.36) and (5.39)). In addition, and contrary to the scalar part of the OBDM for which it is unimportant, taking into account the deformation of the local momentum distribution of the finite system leads to a modification of the relevant momentum scale $\tilde{k}_F^q$. In view of isolating the significance of such an effect, while preserving the benefit of using PSA, one can set $P_2^q(\vec{R}) = 0$ in Eq. 5.37.

In the second strategy, we incorporate the phase space information by parameter-

izing the anisotropy of the Fermi surface. In leading order, one talks about quadrupolar deformation of the Fermi Surface. Thus, the PSA is performed in a phase space distribution with

$$f_q(\vec{R},\vec{k}) \;=\; \Theta(k-k_F^q)\left(1+a\,(3\,\mathrm{Cos}^2(\theta)-1)\right), \tag{5.38}$$

where a is a quadrupolar deformation parameter to be optimized, θ is the angle between $\vec{R}$ and $\vec{k}$ and Si is the SinIntegral function. Even though the deformation actually couples $\vec{R}$ and $\vec{k}$, we approximate this as a coupling between $\vec{r}$ and $\vec{k}$ to actually obtain the final form of the $\pi-$function. Thus, $\Pi_1^{\vec{s}}(\vec{R},r)$ reads

$$\Pi_1^{\vec{s}}(k_F^q r) \;=\; \frac{3\,j_1(k_F^q r)}{(k_F^q r)} + \frac{a}{(k_F^q r)^3}\left(-18\,\mathrm{Si}(k_F^q r) - 6k_F^q r\cos(k_F^q r) + 24\sin(k_F^q r)\right). \tag{5.39}$$

To parameterize the deformation parameter a, we take hint from Wigner-Kirkwood expansion of the scalar part of one-body density matrix. As explained in appendix 9.5.2, the $\hbar^2$ Wigner-Kirkwood expansion of the Wigner transform of the scalar part of one-body density matrix reads

$$\begin{aligned}\rho_{WK,q}(\vec{R},\vec{p}) \;&=\; \Theta(\lambda-h_W^q) - \frac{\hbar^2}{8m}\Delta V_q\delta'(\lambda-h_W^q) + \frac{\hbar^2}{24m}\left[(\nabla V_q)^2 + \frac{1}{m}(\vec{p}\cdot\nabla)^2 V_q\right]\\ &\quad\times\delta''(\lambda-h_W^q) + \mathcal{O}(\hbar^4),\end{aligned} \tag{5.40}$$

where $h_W^q \;=\; H_q \;=\; \frac{p^2}{2m} + V_q(R)$ is the single particle Hamiltonian and λ is the chemical potential. The origin of the deformation at this order is the $(\vec{p}\cdot\nabla)^2 V_q(R)$ term. It is well known that close to the nuclear surface, the self-consistent potential that acts on the nucleons, $V_q(R)$, and the density, $\rho_q(\vec{R})$, have similar profiles. Both are usually approximated by the Woods-Saxon shape, of course with opposite signs. Hence, we make the series of approximation $|\vec{\nabla}|^2 V_q(R) \approx \Delta V_q(\vec{R}) \propto \Delta\rho_q(\vec{R})$, with

5.3.5

our final parametrization being

$$a = m\,\Delta\rho_q(\vec{R}) + b \qquad (5.41)$$

where m and b are constants to be fit. If one sets $a = 0$, the $\Pi_1^{\bar{s}}(k_F^q r)$ given in Eq. (5.39) is recovered. In Sec. 5.4, we discuss and compare the accuracy obtained using all of the preceding DME variants for the vector part of the OBDM.

5.3.5 k_F^q and isospin invariance of the resulting EDF

Dealing separately with the neutron or proton OBDM in a finite nucleus, it is natural to perform the corresponding PSA over the phase space of neutrons or protons of the system. However, this provides π−functions with an explicit isospin dependence. Even though this does not have any implication at this point, it does when we apply the DME to the HF energy of two- and three-nucleon interactions as discussed in the next two chapters. This is because the EDF that results from the application of the DME breaks isospin invariance (but not its isospin symmetry). As mentioned in section 2.2, there are isospin-breaking parts of the nuclear interaction, still the fact that we get an EDF that breaks isospin invariance even when we start from one that has that symmetry might not be a welcome feature. A simple prescription to recover symmetry of isospin invariance is to replace all k_F^q with the isoscalar k_F which is defined through

$$k_F(\vec{R}) \equiv k_F = \left[\frac{3\pi^2}{2}\rho(\vec{R})\right]^{1/3} , \qquad (5.42)$$

where $\rho(\vec{R}) \equiv \rho_n(\vec{R}) + \rho_p(\vec{R})$. Fig. 5.4 shows k_F^p, k_F^n and the isoscalar k_F extracted from a converged self-consistent calculation of ^{214}Pb. This is a neutron rich nucleus and thus, the difference between the three momentum scales should be maximized. Considering the small difference between $k_F^p(\vec{R})$, $k_F^n(\vec{R})$ and the isoscalar $k_F(\vec{R})$ that

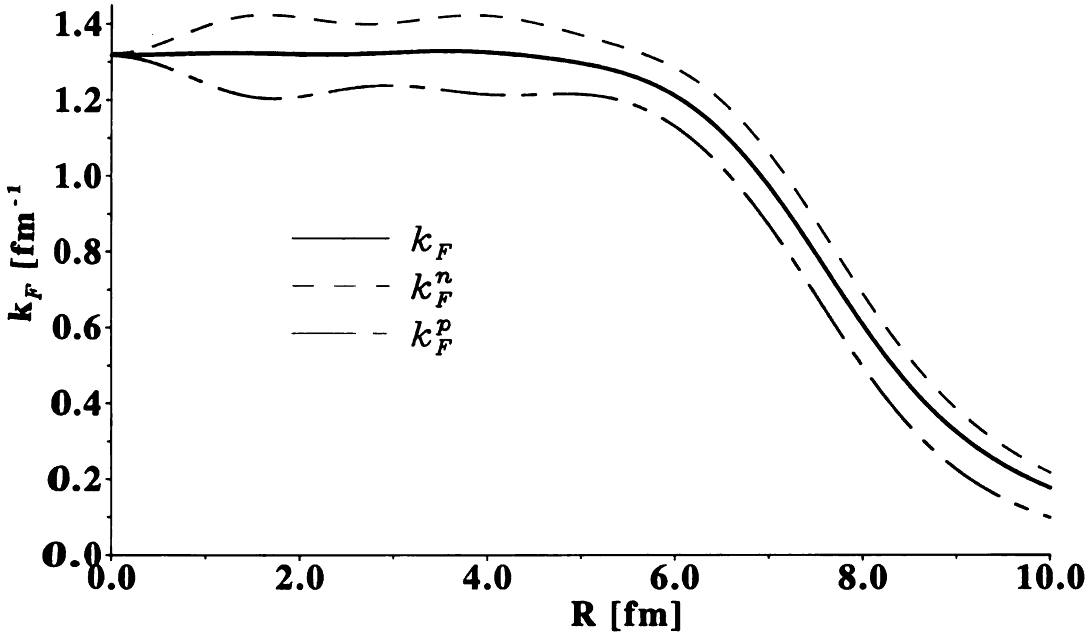

Figure 5.4: (Color online) k_F^p, k_F^n and the isoscalar k_F extracted from a converged self-consistent calculation of ^{214}Pb, a neutron rich nucleus.

we see in Fig. 5.4, the prescription of replacing k_F^q with k_F in the $\pi-$functions might be a satisfactory method to recover isospin invariance in the resulting EDF.

5.3.6 Extension to non-time-reversal invariant systems

The PSA-DME approach has enabled us to obtain both analytical and parametrized forms of the various $\pi-$functions that occur in the expansion of the scalar and vector parts of the OBDM in time-reversal invariant systems. However, from a formal point of view, PSA-DME uses the assumption of time-reversal invariance only to turn off the time-odd densities. Thus, one can envision direct extension of PSA-DME to non-time reversal invariant systems, where the time-odd densities such as $\vec{j}_q(\vec{R})$ in the case of $\rho_q(\vec{r}_1,\vec{r}_2)$ and $\vec{s}_q(\vec{R})$, $\vec{T}_q(\vec{R})$, $\vec{F}_q(\vec{R})$ in the case of $\vec{s}(\vec{r}_1,\vec{r}_2)$ start playing a vital role.

Nevertheless, it will be clear from the subsequent discussions that the appearance

of time-odd densities gives rise to various constraints that the π−functions have to satisfy in order for the EDF (that results from the application of the DME to the starting HF energy) to respect certain global and local symmetries. This requires a systematic study of the problem. We tackle this by formulating a generic DME, which we call the modified-Taylor series, and using it to perform a formal study of the issues related to the extension of the DME to non-time reversal invariant systems. The complete development of a DME for non-time reversal invariant systems with specific analytical/parameterical π−functions is outside the domain of this work.

The modified-Taylor series approach was introduced in Ref. [168] and expanded in this work. It consists of replacing the numerical coefficients in the Taylor series expansion of the density being expanded with π−functions which are yet to be determined. These π−functions can depend on one or several variables. Illustrating the expansion with the nonlocal scalar density and the nonlocal vector density, we have

$$\begin{aligned}\rho_q(\vec{r}_1\,,\vec{r}_2) \simeq& \Pi_0(\Omega)\,\rho_q\left(\vec{R}\right) + \Pi_1(\Omega)\frac{\vec{r}}{2}\cdot\left(\vec{\nabla}_1-\vec{\nabla}_2\right)\rho_q\left(\vec{r}_1\,,\vec{r}_2\right)\Big|_{\vec{r}_1=\vec{r}_2=\vec{R}}\\ &+\frac{1}{2}\Pi_2(\Omega)\left[\left(\frac{\vec{r}}{2}\cdot\vec{\nabla}_1\right)^2+\left(\frac{\vec{r}}{2}\cdot\vec{\nabla}_2\right)^2\right]\rho_q(\vec{r}_1\,,\vec{r}_2)\Big|_{\vec{r}_1=\vec{r}_2=\vec{R}}\\ &-\Pi_3(\Omega)\left(\frac{\vec{r}}{2}\cdot\vec{\nabla}_1\right)\left(\frac{\vec{r}}{2}\cdot\vec{\nabla}_2\right)\rho_q(\vec{r}_1\,,\vec{r}_2)\Big|_{\vec{r}_1=\vec{r}_2=\vec{R}}\,,\end{aligned}\tag{5.43}$$

and

$$\begin{aligned}\vec{s}_q(\vec{R}\pm\frac{\vec{r}}{2},\vec{R}\mp\frac{\vec{r}}{2}) =& \Pi_0^{\vec{s}}(\Omega)\vec{s}_q(\vec{R}) \pm \Pi_1^{\vec{s}}(\Omega)\frac{\vec{r}}{2}\cdot\left(\vec{\nabla}_1-\vec{\nabla}_2\right)\vec{s}_q(\vec{r}_1\,,\vec{r}_2)\Big|_{\vec{r}_1=\vec{r}_2=\vec{R}}\\ &+\frac{1}{2}\Pi_2^{\vec{s}}(\Omega)\left[\left(\frac{\vec{r}}{2}\cdot\vec{\nabla}_1\right)^2+\left(\frac{\vec{r}}{2}\cdot\vec{\nabla}_2\right)^2\right]\vec{s}_q(\vec{r}_1\,,\vec{r}_2)\Big|_{\vec{r}_1=\vec{r}_2=\vec{R}}\\ &-\Pi_3^{\vec{s}}(\Omega)\left(\frac{\vec{r}}{2}\cdot\vec{\nabla}_1\right)\left(\frac{\vec{r}}{2}\cdot\vec{\nabla}_2\right)\vec{s}_q(\vec{r}_1\,,\vec{r}_2)\Big|_{\vec{r}_1=\vec{r}_2=\vec{R}}\,,\end{aligned}\tag{5.44}$$

where the π−functions are to be found analytically or optimized phenomenologically.

Ω represents the variable on which the π functions depend. Requiring Ω to be scalar, dimensionless and depend on r implies that $\Omega = rk$. In case where Ω is assumed to depend on $\vec{r}$, then $\Omega = h(\vec{r}, \vec{k})$ for some scalar function h. Here, we assume the $\pi-$functions to be independent of the orientation of $\vec{r}$. The choice of having four $\pi-$functions instead of five in Eqs. (5.43) and (5.44) is motivated by the need to get a symmetric expansion in $\vec{R} + \frac{\vec{r}}{2}$ and $\vec{R} - \frac{\vec{r}}{2}$.

Even though a definite approach with which to constrain Ω and the $\pi-$functions is be discussed, it should be mentioned that the modified-Taylor series approach is formally applicable to all local/nonlocal and/or normal/anomalous densities in both time-reversal and non time-reversal invariant systems. In line with this, the modified-Taylor series expansion for all the densities defined in section 9.2.3 and 9.2.5 is given in appendix 9.5.7. In the construction of this expansion for the various densities, we have not made any reference to a constructive way of fixing the basic expansion variable, Ω, and the $\pi-$functions. This is where explicit connection is realized between the modified-Taylor series and PSA-DME (and/or other DME variants) discussed in the previous few sections. In other words, the modified-Taylor series can be seen as a template which can be adapted to various DMEs which in turn can be considered as as approaches to fix Ω and the $\pi-$functions. However, there is a technical problem in that one cannot, at this point, fully express the modified-Taylor series expansion in terms of standard local densities. Hence, we need one more layer of assumptions to realize the explicit connection.

Both problems are solved at once by realizing that the basic quantity that one is really interested in approximating is the energy density (or energy) at the Hartree-Fock-Bogoliubov level instead of the local densities. One starts from the exact expression for the energy, and approximates it by replacing the exact densities (local/nonlocal) with their counterparts as given by the modified-Taylor series expansion. Requiring the resulting expression to be a local EDF which fulfills various local and global sym-

metries results in several constraints relating the different $\pi-$functions. The required local or global symmetries can be rotational invariance, parity, particle number, time-reversal invariance, isospin invariance and local gauge invariance or its traditional counterpart, Galilean invariance. Naturally, the validity of some of the symmetries depends on the starting interaction.

In order to make the procedures clear, these steps are applied to typical terms from the central and tensor exchange parts of the Hartree-Fock energy (of two nucleon interaction). Since we are interested only in the form of the expression, numerical coefficients and spin-isospin labels of the interaction are dropped. As discussed in section 9.6.1, a typical term from the central part of the interaction takes the form

$$\langle\Phi|V_C|\Phi\rangle = \sum_q \int d\vec{R}\, d\vec{r}\; V_c(r)\, \rho_q(\vec{r}_1,\vec{r}_2)\, \rho_q(\vec{r}_2,\vec{r}_1)\,, \tag{5.45}$$

where $|\Phi\rangle$ is the slater determinant HF wave function. Next, we apply the modified Taylor series expansion of the densities, use our assumption that the $\pi-$functions are independent of the orientation of $\vec{r}$ and perform angle integration $\int d\Omega_r$, thereby obtaining

$$\begin{aligned}\langle\Phi|V_C|\Phi\rangle \;=\; & 4\pi \sum_q \int d\vec{R}\, dr\, V_c(r) \Big[\left(\Pi_0^\rho(\Omega)\right)^2 \rho_q^2(\vec{R}) + \frac{r^2}{3}\left(\Pi_1^\rho(\Omega)\right)^2 \vec{j}_q(\vec{R})\cdot\vec{j}_q(\vec{R}) \\ & + \frac{r^2}{12}\, \Pi_0^\rho(\Omega)\, \Pi_2^\rho(\Omega)\, \rho_q(\vec{R}) \left(\Delta\rho_q(\vec{R}) - 2\tau_q(\vec{R})\right) \\ & - \frac{r^2}{6}\, \Pi_0^\rho(\Omega)\, \Pi_3^\rho(\Omega)\, \rho_q(\vec{R})\, \tau_q(\vec{R}) \Big]\,,\end{aligned} \tag{5.46}$$

where we have truncated terms containing beyond-second order derivatives. Applying the same set of steps to a typical term from the tensor interaction, $\langle\Phi|V_T|\Phi\rangle$, we obtain

$$\langle\Phi|V_T|\Phi\rangle \;=\; \sum_q \int d\vec{R}\, d\vec{r}\; V_T(r)\, \vec{s}_q(\vec{r}_1,\vec{r}_2)\cdot\vec{s}_q(\vec{r}_2,\vec{r}_1)\,,$$

with si

In

and

in Eq

Con

ED

$$
\begin{aligned}
= \quad & 4\pi \sum_{q} \int d\vec{R}\, dr\, V_T(r) \Bigg[\left(\Pi_0^{\vec{s}}(\Omega)\right)^2 \vec{s}_q(\vec{R}) \cdot \vec{s}_q(\vec{R}) \\
& + \frac{r^2}{3} \left(\Pi_1^{\vec{s}}(\Omega)\right)^2 \sum_{\mu\nu\alpha} J_{q,\mu\nu}(\vec{R}) J_{q,\mu\alpha}(\vec{R}) \\
& + \frac{r^2}{12} \Pi_0^{\vec{s}}(r)\, \Pi_2^{\vec{s}}(r)\, \vec{s}_q(\vec{R}) \cdot \left(\Delta \vec{s}_q(\vec{R}) - 2\vec{T}_q(\vec{R}) \right) \\
& - \frac{r^2}{6} \Pi_0^{\vec{s}}(r)\, \Pi_3^{\vec{s}}(r)\, \vec{s}_q(\vec{R}) \cdot \vec{T}_q(\vec{R}) \Bigg], \qquad (5.47)
\end{aligned}
$$

with similar procedures being applicable to the remaining terms in the HFB energy.

In order to make the explicit connection between the modified-Taylor series expansion and PSA-DME (and/or other DME variants), we make use of the PSA-DME (and/or other DME variants) to approximate the Fock energy of time-reversal invariant systems and set it equal to the corresponding expression obtained from for the modified-Taylor series expansion. In this way, the $\pi-$functions and their arguments Ω in Eqs. (5.46) and (5.47) that multiply the time-even densities can be fixed. Still, the $\pi-$functions that multiply the time-odd, local and anomalous densities are not yet determined. This is where the relations between the $\pi-$functions through symmetry and other constraints come in to the picture.

Constraints on the $\pi-$functions

Requiring the $\pi-$functions to be independent of the orientation of $\vec{r}$ and the need to obtain gauge (Galilean) invariant bilinear combinations of densities in the resulting EDF impose strong constrains on the $\pi-$functions. The gauge transformation of the one-body local densities is discussed in appendix 9.3. These constraints are obtained by applying the modified Taylor series expansion to the various local and nonlocal densities that occur in the HFB energy of a finite-range two-body interaction and requiring the resulting EDF to be gauge invariant. Dropping the arguments of the $\pi-$functions for ease of notation, the resulting constraints read i I

[illegible]

[illegible]

i

[illegible]

On

[illegible]

[illegible]

[illegible]

[illegible]

whe

has

k

F

exp

as

Th

(i) $\Pi_0^\rho(\Pi_2^\rho + \Pi_3^\rho) = 2\left[\Pi_1^\rho\right]^2$ and $\Pi_0^{\vec{s}}(\Pi_2^{\vec{s}} + \Pi_3^{\vec{s}}) = 2\left[\Pi_1^{\vec{s}}\right]^2$

(ii) $\pi_0^\rho \pi_1^{\vec{J}} = \pi_0^{\vec{J}} \pi_1^{\vec{s}}$ and $\pi_1^\rho \pi_0^{\vec{J}} = \pi_0^{\vec{s}} \pi_1^{\vec{J}}$

(ii)$\Pi_0^\rho \Pi_1^{\vec{s}} = \Pi_1^\rho \Pi_0^{\vec{s}}$

(iv)$\Pi_3^v = \Pi_2^v$ where v is either $\tilde{\rho}_q(\vec{r}_1, \vec{r}_2)$ or $\tilde{\vec{s}}_q(\vec{r}_1, \vec{r}_2)$

(v) $\pi-$functions of the pairing densities have to be real-valued functions.

One of the most important qualities of the original DME of Negele and Vautherin is its exact treatment of unpolarized, symmetric INM at the Hartree-Fock level. Constraining the $\pi-$function DME to reproduce INM limit of the direct and exchange parts of the energy density separately, we obtain the following two constraints on the $\pi-$functions

$$\left(\pi_0^\rho\right)^2 = 1 \tag{5.48}$$

$$\left(\Pi_0^\rho\right)^2 - \frac{(rk)^2}{10}\Pi_0^\rho\left(\Pi_2^\rho + \Pi_3^\rho\right) = \left(3\frac{j_1(rk)}{rk}\right)^2, \tag{5.49}$$

where k must reduce to $k_F^q = \left[3\pi^2\rho_q\right]^{\frac{1}{3}}$ when one goes to INM. Thus either one has to use a fixed $k = k_F^q$ or the parameter k should be such that it evolves to $k \longrightarrow k_F^q = \left[3\pi^2\rho_q\right]^{\frac{1}{3}}$ as one goes to INM.

Further constraint is obtained using the idempotency of the density matrix to express the particle number. I.e. from $\rho_q = \rho_q^2$, the particle number can be expressed as

$$N_q = \mathrm{Tr}\,\rho_q = \int d\vec{R}\,d\vec{r}\,|\rho(\vec{R}, \vec{r})|^2 \tag{5.50}$$

Thus, a constraint on the $\pi-$functions can be obtained by inserting the DME expression for $\rho_q(\vec{R},\vec{r})$

$$\begin{aligned} N_q &= \int d\vec{R}\,d\vec{r} \Bigg| \Pi_0^\rho(\Omega)\,\rho_q(\vec{R}) + i\,\Pi_1^\rho(\Omega)\,\vec{r}\cdot\vec{j}_q(\vec{R}) + \frac{r^2}{24}\Pi_2^\rho(\Omega)\left(\Delta\rho_q(\vec{R}) - 2\tau_q(\vec{R})\right) \\ &\quad - \frac{r^2}{12}\Pi_3^\rho(\Omega)\,\tau_q(\vec{R}) \Bigg|^2 \\ &= 4\pi \int d\vec{R}\,dr \Bigg[\Pi_0^\rho(\Omega)^2\,\rho_q^2(\vec{R}) - \frac{r^2}{3}\Pi_1^\rho(\Omega)^2\,\vec{j}_q(\vec{R})\cdot\vec{j}_q(\vec{R}) \\ &\quad + \frac{r^2}{12}\,\Pi_0^\rho(\Omega)\,\Pi_2^\rho(\Omega)\,\rho_q(\vec{R})\left(\Delta\,\rho_q(\vec{R}) - 2\tau_q(\vec{R})\right) \\ &\quad - \frac{r^2}{6}\,\Pi_0^\rho(\Omega)\,\Pi_3^\rho(\Omega)\,\rho_q(\vec{R})\,\tau_q(\vec{R}) \Bigg], \end{aligned} \tag{5.51}$$

which is an integral constraint that can be utilized a posteriori to calculate some parameters. In the original DME and its variants, it can be shown that the number constraint is satisfied exactly [202], while the PSA-DME breaks this constraint slightly.

Finally, constraints on the π−function come from the large and small limits of r. The π—functions should go to zero for large r and for small r, the modified Taylor series has to reduce to ordinary Taylor series expansion. In addition, we require the π−functions to be such that the gradient, $\vec{\nabla}_{\vec{r}}$, and the gradient squared, $[\vec{\nabla}_{\vec{r}}]^2$, of the densities are reproduced exactly at $\vec{r} = 0$. The resulting constraints are

$$\begin{aligned} \Pi_0(0) &= \Pi_1(0) = \Pi_2(0) = \Pi_3(0) = 1, \\ \Pi_0'(0) &= \Pi_1'(0) = 0\,, \\ \Pi_0''(0) &= 0\,, \end{aligned} \tag{5.52}$$

$$\lim_{r\to\infty} \Pi_0(r) = \lim_{r\to\infty} \Pi_1(r) = \lim_{r\to\infty} \Pi_2(r) = \lim_{r\to\infty} \Pi_3(r) = 0\,, \tag{5.53}$$

where we have dropped the density label on the π−functions to denote that these constraints hold for the π−functions of any density. Additionally, we used only Π_i

which refers to the $i^{\rm th}$ π−function from nonlocal densities, even though the constraints are valid for π_i (from local densities). The only exception is there is no π_3 in the local case. In the DME of Ref. [172], the authors impose a local constraint

$$-\left[\Delta_r \rho_q(\vec{r}_1, \vec{r}_2)\right]\Big|_{\vec{r}=0} = \tau_q(\vec{R}) - \frac{1}{4}\rho_q(\vec{R}), \tag{5.54}$$

which is to be satisfied by the DME of $\rho_q(\vec{r}_1, \vec{r}_2)$. They refer to this constraint as the local imposition of the correct kinetic energy density. One recovers Eq. 5.54 by combining Eqs. (5.52), (9.108) and (9.109). It can easily be shown that π−functions satisfying the small r limits given in Eq. (5.52) satisfy this constraint. I.e. this particular constraint is a subset of the constraints listed in Eq. (5.52).

Concluding, the explicit relationship that we established between the modified-Taylor series expansion and PSA-DME (and/or other DME variants), together with the various constraints obtained through symmetry and other subsidiary conditions enable us to reduce the number of independent unknown π−functions significantly. Still, the number of unknown π−functions is larger than the number of constraint relations. Thus, the complete determination of all the π−functions requires further parametrization of some of the π−functions. In practice, it may not be possible to satisfy all the relations among the π−functions and at the same time obtain a reasonable accuracy. In that case, some of the less stringent constraints have to be relaxed. Since this work is confined to the development of non-empirical EDF for time-reversal invariant systems, most, if not all, of these constraints are satisfied by default as one can simply choose the π−functions of the time-odd densities in such a way that they satisfy the constraints.

5.3.7

The app

where

Eq.

with

5.3.7 Remarks on the DME of the local densities

The apparent need for the DME of local densities can be seen from the Hartree contribution to the energy originating from the central part of a two-nucleon interaction. Reproducing the expression derived and discussed in section 9.6.1

$$\langle V_{\rm Dir} \rangle = \int d\vec{r}_1 d\vec{r}_2 \, \rho_q(\vec{r}_1) \, \rho_{q'}(\vec{r}_2) \,, \tag{5.55}$$

where for simplicity, we have dropped the singlet-triplet label of the interaction and numerical coefficients. Thus, if one requires a local EDF, one needs to approximate Eq. (5.55) utilizing a suitable DME expansion for the local densities. Equivalently, one can approximate the energy density, $\mathcal{E}_{den}$, which is defined as

$$\mathcal{E}_{den} \equiv \frac{1}{4\pi} \int d\Omega_{\vec{r}} \, \rho_q(\vec{r}_1) \, \rho_{q'}(\vec{r}_2) \,, \tag{5.56}$$

with $\int d\Omega_{\vec{r}}$ referring to angular integration with respect to the orientation of $\vec{r}$.

In line with this, Negele and Vautherin, in Ref. [170], approximate the energy density given in Eq. (5.56) as

$$\begin{aligned} \mathcal{E}_{den} \approx & \ \rho_q(\vec{R})\rho_{q'}(\vec{R}) + \frac{35}{2rk_F^3} j_3(rk_F) \left[\frac{1}{4}\rho_{q'}(\vec{R})\Delta\rho_q(\vec{R}) + \frac{1}{4}\rho_q(\vec{R})\Delta\rho_{q'}(\vec{R}) \right. \\ & \left. - \frac{1}{2}\vec{\nabla}\rho_q(\vec{R}) \cdot \vec{\nabla}\rho_{q'}(\vec{R}) \right] , \end{aligned} \tag{5.57}$$

by applying the expansion technique they devised for the nonlocal density, $\rho(\vec{r}_1, \vec{r}_2)$, to the product of the local densities, $\rho_q(\vec{r}_1) \, \rho_{q'}(\vec{r}_2)$. However, subsequent numerical tests [[183],[184]] indicated that the expansion of local densities is at the root of most of the error propagation and enhancement in self-consistent tests of the DME. This is discussed in detail in section 5.4.6.

Even though the DME makes no direct reference to the range of nonlocality, as mentioned in section 5.2.1, the fact that the range of nonlocality with respect to $\vec{r}$ is very large for the local density, $\rho_q(\vec{r}_{1/2})$ (where $\vec{r}_{1/2}$ means the argument can be $\vec{r}_1$ or $\vec{r}_2$), is mentioned to be the main reason why the DME does not work as accurately as it does for the nonlocal density, $\rho_q(\vec{r}_1, \vec{r}_2)$. In Ref. Bhaduri78, using a one-dimensional harmonic oscillator model with partial occupation of the single-particle states, the authors show that the nonlocality with respect to $\vec{r}$ of the local nucleon density, $\rho_q(\vec{r}_{1/2})$, varies on the scale of the whole system, while the scale of the nonlocal nucleon density, $\rho_q(\vec{r}_1, \vec{r}_2)$, is set by the local Fermi momentum k_q^F. Even in the surface of nuclei, one can see that $\rho_q^2(\vec{r}_1, \vec{r}_2)$ falls off much faster than $\rho_q(\vec{r}_1)\rho_q(\vec{r}_2)$ in the relative coordinate, $\vec{r}$, by considering a one-dimensional surface with an exponential decay [183]. I.e. by modeling the local density with a schematic exponential decay function. Hence, the fact that both the local density and energy density involved in Eq. (5.57) have a large nonlocality scale with respect to $\vec{r}$ make the DME approximation inherently inaccurate, at least in one-dimensional problems.

Nonetheless, in problems with dimensions greater than one, the simple characterization of the failure of the the DME of $\rho_q(\vec{r}_{1/2})$ based on the scale of nonlocality needs refinement. This becomes obvious when one considers closed-form analytical expressions for $\rho_q(\vec{r}_1, \vec{r}_2)$ and $\rho_q(\vec{r}_{1/2})$ in various model systems. In Ref. [208], a closed form expression for $\rho_q(\vec{r}_1, \vec{r}_2)$ is given for the case of an isotropic harmonically trapped ideal Fermi gas in any dimension. The more relevant expression is the one given in Ref. [185] for a three-dimensional oscillator with a smeared occupancy

$$\rho_q(\vec{r}_1, \vec{r}_2) = \rho_q(\vec{R}) \exp\left[-\frac{1}{4}\alpha^2 r^2 \frac{1+t}{1-t}\right], \tag{5.58}$$

$$\rho_q(\vec{r}_{1/2}) = \frac{2\alpha^3}{\pi^{3/4}}(1-t^2)^{-3/2} \exp\left[-\alpha^2 r_{1/2}^2 \frac{1+t}{1-t}\right], \tag{5.59}$$

where $t = e^{-\beta\hbar\omega}$, β is the inverse temperature, $\alpha^2 = m\omega/\hbar$ with the energy $\mathcal{E} = (N + 3/2)\hbar\omega$. Thus, one can argue that both the local and nonlocal nucleon densities are

governed by comparable scales, relegating the supposed large scale of the nonlocality in $\vec{r}$ as an incomplete or limited explanation for the failure of the DME of $\rho_q(\vec{r}_{1/2})$.

The missing piece of the explanation can be identified once the DME-coordinates are replaced in Eq.(5.59), viz, $\vec{r}_{1/2} = \vec{R} \pm 1/2\,\vec{r}$. This makes the difference between the local and the nonlocal densities to be transparent. The nonlocal density falls-off exponentially (Gaussian fall-off) with respect to r independent of the orientation of $\vec{r}$, which is also the case for $\rho_q(\vec{r}_1, \vec{r}_2)$ extracted from a converged self-consistent calculation of nuclei as shown in section 5.4. In contrast, the local density shows maximally different behaviors depending on the orientation of $\vec{r}$. In short, sitting at a particular location in the nucleus, $\vec{R}$, one can go to the surface or deep into the interior of the nucleus with the same r but different directions of $\vec{r}$. Thus, the significant dependence of $\rho_q(\vec{r}_{1/2})$ on the orientation of $\vec{r}$ is partly responsible for the failure of the DME of $\rho_q(\vec{r}_{1/2})$ as DMEs invariably average over the orientation of $\vec{r}$.

In Ref. [183], it is argued that the DME of the Hartree contribution can be avoided by treating it exactly, especially as the exact Hartree treatment does not result in a significant increase in numerical complexity. In a related work, Ref. [184], the authors show that treating the Hartree contribution exactly removes most of the errors in the self-consistent numerical test of the DME. This and related issues are discussed in section 5.4.6. Our numerical tests include both expanded and exact Hartree treatments. In the expanded case, the $\pi-$functions of $\rho_q(\vec{r}_{1/2})$ are fixed by equating Eq. (5.57) with the expression obtained from replacing $\rho_q(\vec{r}_{1/2})$ in Eq. (5.56) with

$$\rho_q(\vec{r}_{1/2}) \to \pi_0^\rho(\Omega)\,\rho_q(\vec{R}) \pm \pi_1^\rho(\Omega)\,\frac{\vec{r}}{2}\cdot\vec{\nabla}_R\,\rho_q(\vec{R}) + \frac{1}{2}\,\pi_2^\rho(\Omega)\,\Big(\frac{\vec{r}}{2}\cdot\vec{\nabla}_R\Big)^2\rho_q(\vec{R})\,, \quad (5.60)$$

and truncating at second-order in the gradient

$$\begin{aligned}\mathcal{E}_{den} &\approx \left[\pi_0^\rho(\Omega)\right]^2 \rho_q(\vec{R})\rho_{q'}(\vec{R}) - \frac{r^2}{6}\left[\pi_1^\rho(\Omega)\right]^2 \vec{\nabla}\rho_q(\vec{R}) \cdot \vec{\nabla}\rho_{q'}(\vec{R}) \\ &+ \frac{r^2}{12}\,\pi_0^\rho(\Omega)\,\pi_2^\rho(\Omega)\left[\rho_q(\vec{R})\Delta\rho_{q'}(\vec{R}) + \rho_{q'}(\vec{R})\Delta\rho_q(\vec{R})\right], \qquad (5.61)\end{aligned}$$

which results in the $\pi-$functions

$$\pi_0^\rho(\Omega) = 1\,, \qquad (5.62)$$

$$\pi_1^\rho(\Omega) = \sqrt{\frac{105}{(rk_F^q)^3} j_3(rk_F^q)}\,, \qquad (5.63)$$

$$\pi_2^\rho(\Omega) = \frac{105}{(rk_F^q)^3} j_3(rk_F^q)\,, \qquad (5.64)$$

where $\Omega = rk_F^q$.

The parameterized version of the $\pi-$functions for $\rho_q(\vec{r}_{1/2})$ is inspired by the analytical form of $\rho_q(\vec{r}_{1/2})$ in the three-dimensional harmonic oscillator with a smeared occupancy [185] as given in Eq. (5.59). First, we fix the oscillator frequency ω and the oscillator length b according to the Blomqvist-Molinar formula [38]

$$\hbar\omega = 45A^{-1/3} - 25A^{-2/3}\,, \qquad (5.65)$$

$$b = \frac{197.33}{\sqrt{940\,\hbar\omega}}\,, \qquad (5.66)$$

where A is the mass number of the nucleon under consideration. The parameterized $\pi-$functions are given by

$$\pi_0^\rho(\Omega) = \left[a_0 + \left(\frac{a_2}{b}\right)^2 + \left(\frac{a_4}{b}\right)^4\right] e^{-r^2/b^2}\,, \qquad (5.67)$$

$$\pi_1^\rho(\Omega) = e^{-r^2/b^2}\,, \qquad (5.68)$$

$$\pi_2^\rho(\Omega) = e^{-r^2/b^2}\,, \qquad (5.69)$$

$$(5.70)$$

where the gradient corrections are damped with a gaussian of range b. From the short range limit of the $\pi-$functions as given in Eqs. (5.52), the leading parameter $a_0 = 1$. The rest of the parameters, viz, $\{a_2,\ a_4\}$ are fixed by fitting the exact $\mathcal{E}_{den}$ as given by Eq. (5.56) with Eq. (5.61), with densities extracted from a converged self-consistent calculation of a selection of nuclear chains.

A direct justification for the form of the $\pi-$functions given in Eqs. (5.67)-(5.69) comes from the fact that $\rho_q(x)$ of spherical nuclei can be fit to a very good accuracy with the ansatz

$$\rho_q(x) \;=\; \sum_{n=1}^{n=4} \rho_q(0)\, a_n \frac{x^n}{b^n}\, e^{-r^2/b^2} \;, \tag{5.71}$$

where $\rho_q(0)$ is the value of the central density and x stands for r_1, r_2, r or R. The fact that $\rho(0)$ is used instead of an additional free-parameter is due to there being local densities that play a similar role in the DME. Fig. 5.5 shows the neutron density obtained from a converged self-consistent calculations of ^{48}Cr and ^{208}Pb and their corresponding fit curves. Our extensive tests show that the $\rho_q(\vec{r}_{1/2})$ length scale b given in Eq. (5.66) remains uniformly valid and, perhaps not surprisingly, one can produce the same high-quality fits to almost all nuclei. However, the parameters show strong shell fluctuation, as can be seen from Fig. 5.6 which shows the parameters for Cr and Pb isotopic chains.

The above discussions consider only the local nucleon density, $\rho_q(\vec{r}_{1/2})$. The strong fluctuation of the other time-even local density, $\vec{J}_q(\vec{r}_{1/2})$, with respect to $\vec{r}$ due to its strong dependence on the shell structure of the particular nucleus under study, did not permit a systematic analytical study. Hence, for the numerical tests carried out in section 5.4.6, a simple Taylor series approximation is used to fix the $\pi-$functions of $\vec{J}_{1/2}$

$$\pi_0^J \;=\; \pi_1^J \;=\; \pi_2^J \;=\; 1\,, \tag{5.72}$$

where the arguments must be extended in non time-reversal invariant systems as the

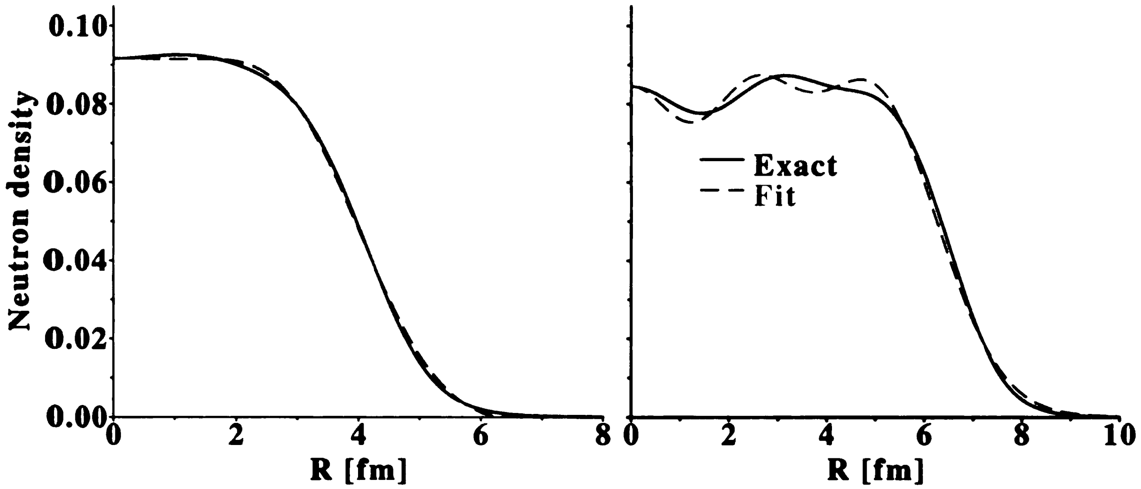

Figure 5.5: (Color online) $\rho_n(r)$ for ^{48}Cr and ^{208}Pb from a converged self-consistent calculation using Sly4 EDF.

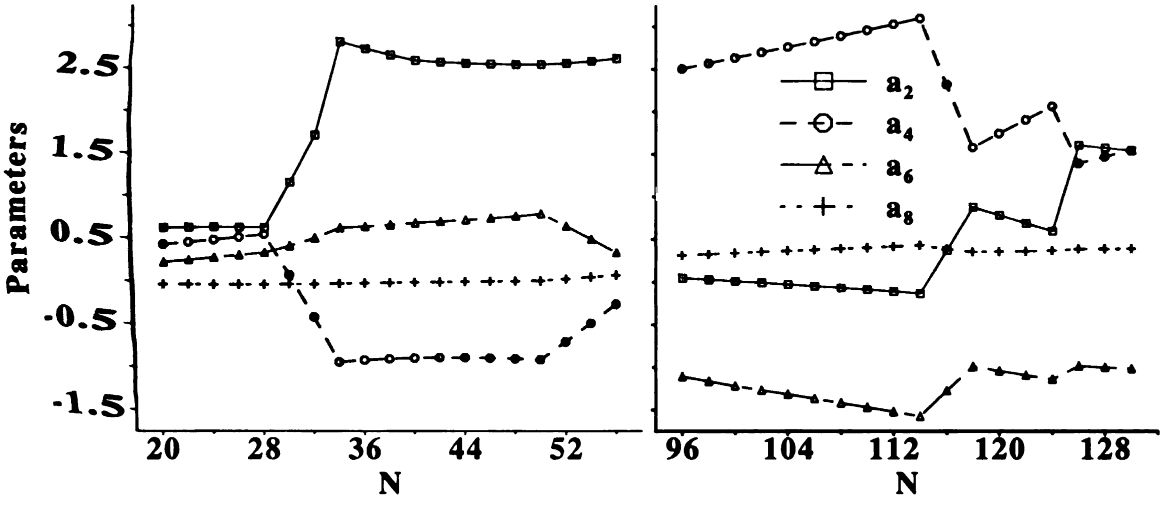

Figure 5.6: (Color online) The parameters for Cr and Pb isotopic chains obtained after fitting the neutron density, $\rho_n(\vec{r}_{1/2})$, with the $\pi-$functions as given in Eqs. (5.67)-(5.69).

time-odd local densities $j_q(\vec{r}_{1/2})$, $\vec{s}_q(\vec{r}_{1/2})$, $\vec{T}_q(\vec{r}_{1/2})$ and $\vec{F}_q(\vec{r}_{1/2})$ do not vanish. In this context, the discussion in section 5.3.6 is relevant. Finally, it should be mentioned that these expansions of the local densities can be avoided once the Hartree contribution to the HF energy from two-nucleon interaction is treated exactly. The situation is different and more complex for the HF contribution from the chiral EFT three-nucleon interaction at N^{2}LO. However, with a particular choice of DME-coordinates, we avoid the expansion of local densities altogether. This is discussed in section 7.2.

5.3.8 Remarks on the DME of the anomalous densities

Currently, there are several simple effective interactions that are being used in the pairing channel to perform HFB and related calculations. From a practical point of view, the simplicity of the effective interactions is necessitated by the numerical complexity that one would have to overcome in order to perform a 3D (deformed) HFB calculation for deformed nuclei. Still, the accuracy of current pairing part of current functionals calls for further improvements and constraints on the form and couplings of the functional [26].

Similar to what is being implemented in the case of particle-hole part, two complementary approaches, viz, phenomenological parameterizations and non-empirical construction of the functional are being undertaken [112]. The non-empirical approach tries to address the role of the the bare NN + NNN interaction and their finite-ranges by successive addition of MBPT contributions in the pairing channel. Recently, the first step towards non-empirical pairing functional for nuclei has been taken in Ref. [112] where the first systematic calculation of pairing gaps in semi-magic nuclei is carried out. By fixing the normal self-energy contributions with conventional Skyrme functionals, using low-momentum NN interaction and accounting only for the contribution of $^1S_0$ partial wave to the pairing gaps, the results show that it is indeed the leading order (Bogoliubov diagram) that contributes the bulk of the pairing gaps in finite nuclei. However, including NNN interaction in the treatment degrades the agreement between theoretical and experimental results leaving plenty of room for coupling to collective fluctuations.

One caveat of these works is the fact that they are limited to spherical nuclei, due to the aforementioned numerical complexity to perform 3D HFB calculations. The nonlocal contribution to the total energy from the pairing part can be seen from the form of the leading order (Bogoliubov diagram). Reproducing the expression given in Eq. (9.272) for the spin-singlet, isospin-triplet channel from the central part of the interaction,

$$\langle \Phi | V_C^{01} | \Phi \rangle_{pair} \propto \sum_q \int d\vec{r}_1 \, d\vec{r}_2 \, V_C^{01}(r) \, |\tilde{\rho}_q(\vec{r}_1, \vec{r}_2)|^2 \, , \tag{5.73}$$

where one notes that the nonlocal pairing density has the same role as the role of $\rho_q(\vec{r}_1, \vec{r}_2)$ in the particle-hole part of the functional.

From a formal point of view, the modified-Taylor series DME can be directly applied to the anomalous densities, thereby approximating the exact leading-order nonlocal pairing functional with a local one. For instance, the nonlocal pairing density can be expanded as

$$\begin{aligned}
\tilde{\rho}_q(\vec{R} \pm \frac{\vec{r}}{2}, \vec{R} \mp \frac{\vec{r}}{2}) \approx \; & \Pi_0^{\tilde{\rho}}(\Omega) \tilde{\rho}_q(\vec{R}) \pm \Pi_1^{\tilde{\rho}}(\Omega) \frac{\vec{r}}{2} \cdot \left(\vec{\nabla}_1 - \vec{\nabla}_2 \right) \tilde{\rho}_q(\vec{r}_1 \, , \vec{r}_2) \Big|_{\vec{r}_1 = \vec{r}_2 = \vec{R}} \\
& + \frac{1}{2} \Pi_2^{\tilde{\rho}}(\Omega) \left[\left(\frac{\vec{r}}{2} \cdot \vec{\nabla}_1 \right)^2 + \left(\frac{\vec{r}}{2} \cdot \vec{\nabla}_2 \right)^2 \right] \tilde{\rho}_q(\vec{r}_1 \, , \vec{r}_2) \Big|_{\vec{r}_1 = \vec{r}_2 = \vec{R}} \\
& - \Pi_3^{\tilde{\rho}}(\Omega) \left(\frac{\vec{r}}{2} \cdot \vec{\nabla}_1 \right) \left(\frac{\vec{r}}{2} \cdot \vec{\nabla}_2 \right) \tilde{\rho}_q(\vec{r}_1 \, , \vec{r}_2) \Big|_{\vec{r}_1 = \vec{r}_2 = \vec{R}} \, ,
\end{aligned} \tag{5.74}$$

where the $\pi-$functions are yet to be specified.

However, both the technical and conceptual problems that need to be settled in order to obtain accurate $\pi-$functions for the anomalous densities seem to be significantly harder than for the normal densities. To start with, the size of the nonlocality with r

is still

furth

the l

rela

is of

as

mak

on a

wish

who

to the

param

Pr

pretu

gest t

argu

of th

stud

whe

str

Fi

with regards to $\vec{r}$ of the nonlocal pairing density, $\tilde{\rho}_q(\vec{R} \pm \frac{\vec{r}}{2}, \vec{R} \mp \frac{\vec{r}}{2})$, in finite nuclei is still under discussion [[186],[187]]. It is commonly characterized by the coherence length, ξ, of nucleonic Cooper pairs. Arguments based on infinite nuclear matter and the local density approximation (LDA) seem to suggest that ξ as given by Pippard's relation [188]

$$\xi = \frac{\hbar^2 k_F}{\pi m^* \Delta}, \tag{5.75}$$

is of the size of the nucleus. In Eq. (5.75), m^* is the effective mass and Δ is the pairing gap. If the supposed large spatial extension of the nucleonic Cooper pairs in finite nuclei were to hold without any modification, a DME approach which does not rely on any assumed short-range nonlocality needs to be invented. In fact, the stronger versions of these arguments stipulate that the existence of a small parameter r_0/ξ, where r_0 is the interaction range, implies that pairing in nuclei should be insensitive to the details of the nuclear interaction. This is supposed to justify phenomenological parameterizations using a local functional with no derivative corrections [189].

Practical calculations in finite nuclei paint a moderately different and favorable picture. Indeed, results from the recent non-empirical pairing calculations [112] suggest that some details of the interaction may be important. Furthermore, the intuitive arguments that one builds starting from INM regarding such quantities as the size of the nucleon cooper pairs require precise qualification. In Ref. [187], the authors study the neutron correlation length, $\xi_n(R)$, having defined it as

$$\xi_n(R) = \sqrt{\frac{\int dr\, r^4 |\tilde{\rho}_n(\vec{R},\vec{r})|^2}{\int dr\, r^2 |\tilde{\rho}_n(\vec{R},\vec{r})|^2}}, \tag{5.76}$$

where the subscript n denotes that the quantities are extracted for neutrons. The strong position (density) dependence of the correlation length can be seen from Fig. 5.7. In addition, the authors extract $|\tilde{\rho}_n(\vec{R},\vec{r})|^2$ which is shown in Fig. 5.8.

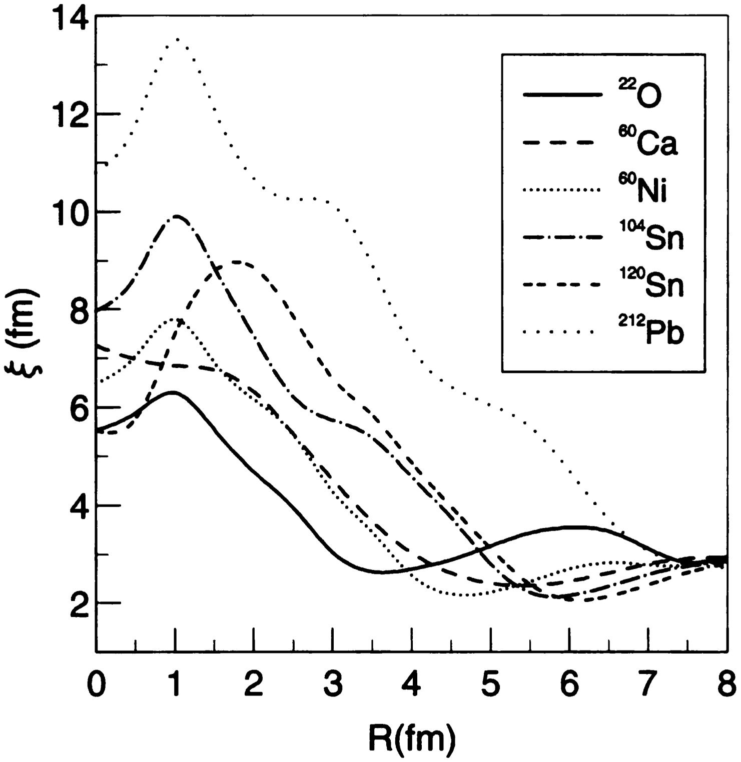

Figure 5.7: (Color online) Coherence length $\xi(R)$ for ^{22}O, ^{60}Ca, ^{60}Ni, ^{104}Sn, ^{120}Sn, ^{212}Pb (From Pillet et. al. [187]).

It can be seen that the nonlocality in $\vec{r}$ is in general in the range of $2-3fm$. In contrast, the correlation length is much larger except close to surface where it attains values in the range of $2-3fm$. Nonetheless, the basic quantity that is approximated by the DME is $|\tilde{\rho}_n(\vec{R},\vec{r})|^2$, which reduces the significance of the large values of the coherence length. In Ref. [190], the authors conduct a related study of a slab of infinite nuclear matter, confirming the smallness of the local correlation length at the surface and its largeness inside the slab.

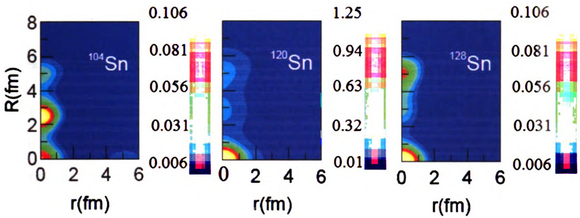

Figure 5.8: (Color online) $|\tilde{\rho}_n(R,r)|^2$ calculated with HFB-D1S for ^{104}Sn, ^{120}Sn, ^{128}Sn. Scale has been multiplied by a factor of 10^6 (From Pillet et. al. [187]).

Hence, these realistic studies of pairing in finite nuclei point to the possibility of developing a DME for the anomalous densities. In Ref. [191], a leading-order semi-classical expansion of the anomalous density based on the Thomas-Fermi approximation is given as

$$\tilde{\rho}_q(\vec{r}_1,\vec{r}_2) \approx C\, j_0(k_F^q(R)r)\, \rho_q(\vec{R})\,, \tag{5.77}$$

where j_0 denotes the spherical bessel function of order zero and C stands for constants characterizing the pairing field strength and the local Fermi momentum. In Ref. [187], it is shown that even at this level of approximation, there is a qualitative agreement between the exact and the corresponding DME approximation. In Ref. [38], the Wigner-Kirkwood $\hbar-$expansion of the Bloch propagator of a superfluid system is derived (up to $\hbar^2$). Leaving aside any further approximation that might be required, performing inverse laplace transform of the $\hbar-$expanded Bloch propagator should recover the gradient corrections to the leading-order expression given in Eq. (5.77). In relation to the DME of anomalous densities, further works along these lines include working out the analytical expressions for the inverse laplace transform, recovering the expressions for the $\pi-$functions and extensive systematic accuracy tests.

5.4 Accuracy of DME

The accuracy of a particular DME can be tested by comparing the exact density with its DME-approximation. But, our main objective is approximating the HF energy density and energy from two- and three-nucleon interactions. As discussed in section 6.1 for the two-nucleon case and section 7.1 for the three nucleon case, the HF energy expression involves a bilinear or trilinear combination of densities extracted from the OBDM. The numerical tests we conduct in this work concentrates on how well the DME approximates various contributions to the two-nucleon HF energy, in both non self-consistent and self-consistent HF calculations[3].

Prior to going in to the details, the following remarks are in order: (i) We consider only time-reversal invariant systems, (ii) Primarily, we concentrate on the DME of $\rho_q(\vec{r}_1,\vec{r}_2)$ and $\vec{s}_q(\vec{r}_1,\vec{r}_2)$. In the two-nucleon HF energy, these nonlocal densities occur in the Fock/exchange contribution from the central, tensor and spin-orbit pieces, while the picture is both different and significantly more complex in the case of three-nucleon interaction (refer to section 7.2). The fact that we concentrate mainly on the Fock contributions is because the DME is inherently inaccurate for the Hartree contribution from NN interactions [[183],[184]]. This is indeed confirmed in section 5.4.6, where we advocate treating the Hartree terms exactly. (iii) In a related note, the accuracy of the DME in reproducing the various contributions to the HF energy from three-nucleon interaction (chiral EFT three-nucleon interaction at N^{2}LO) has not been tested. However, we use analytical approaches that ensure that the approximations used in those calculations are exactly the same as the ones we use for the HF energy from NN interactions. (iv) Besides the two PSA-DMEs (the analytical and parameterized), we include the original DME of Ref. [170] for the accuracy test, as all the other DMEs [[171]- [173]] concentrate only on $\rho_q(\vec{r}_1, \vec{r}_2)$ and give comparable accuracy.

---

[3] In this section, we make repeated references to the HF energy from the generic two-nucleon interaction derived in the next chapter.

The three DMEs that we test in the following several sections are labeled as PSA-DME, PSA-DME-II and NV-DME. For PSA-DME, the $\pi-$functions are given in Eqs. (5.22), (5.23) and (5.36), PSA-DME-II (the parameterized version) is the one with $\pi-$functions as given in Eqs. (5.27), (5.28) and (5.39) and NV-DME refers to the original DME of Negele and Vautherin with $\pi-$functions as given in Eqs. (5.22) (the same as PSA), (5.29) and (5.32).

5.4.1 Inputs to non-self-consistent tests

The generic form of the central, spin-orbit and tensor interactions in the different spin-isospin channels are discussed in section 9.6.1, 9.6.2 and 9.6.3. The radial form factors in the present calculations are either a gaussian or a renormalized Yukawa (according to Ref. [192]). Specifically we use

$$v_I^{ST}(r) = \begin{cases} v_0\, e^{-r^2/a^2} \quad , \\ \\ \frac{v_0}{2r}\left[e^{-m_\pi r}\mathrm{erfc}\left(\frac{m_\pi}{\lambda} - r\lambda\right) - \left(r \to -r\right)\right] \quad , \end{cases} \tag{5.78}$$

independently of the spin/isospin-singlet/triplet channel, (S, T), and with $v_0 = 50$ MeV, $a = 1.5$ fm, $m_\pi = 0.7$ fm^{-1}. The momentum cut-off λ is set equal to 2.1 fm^{-1} while erfc is the complementary error function which is defined as

$$erfc(x) = \frac{2}{\sqrt{\pi}} \int_x^\infty dt\, e^{-t^2} . \tag{5.79}$$

It must be stressed that none of these interactions are realistic two-nucleon interactions, but rather schematic representatives. Still, they are reasonable form factors as the objective of this section is to gauge the accuracy of the DME variants against a reasonable reference point that is not itself meant to provide useful or realistic results. Finally, note that neutron density matrices and local densities used in the following sections have been obtained, for all semi-magic nuclei of interest, through spherical self-consistent EDF calculations employing the SLy4 EDF parameterizations with no pairing.

5.4.2 Fock contribution from V_C

In time-reversal invariant systems, the expression of the Fock contribution to the energy from the central part of the two-nucleon interaction contains a bilinear product of non-local matter densities as well as a bilinear product of non-local spin densities. Since the latter also appears as part of the tensor contribution to the Fock energy, we postpone the discussion regarding the spin-density product to section 5.4.3.

Before comparing the Fock energy to its DME counterpart, we first conduct a more stringent test on the energy density in which the integration over the angle of $\vec{r}$ has already been performed, i.e. we compare the integrand

$$C^F_{nn}(\vec{R}, r) \equiv \frac{1}{4\pi} \int d\Omega_r\, \rho_n(\vec{r}_1, \vec{r}_2)\, \rho_n(\vec{r}_2, \vec{r}_1) \ , \tag{5.80}$$

to its DME counterpart

$$\begin{aligned} C_{nn}^{F,DME}(\vec{R},r) \; \equiv \; & \left[\Pi_0^{\rho}(k_F^n r)\right]^2 \rho_n(\vec{R})\,\rho_n(\vec{R}) + \frac{r^2}{3}\Pi_0^{\rho}(k_F^n r)\,\Pi_2^{\rho}(k_F^n r)\,\rho_n(\vec{R})\bigg(\frac{1}{4}\Delta\rho_n(\vec{R}) \\ & - \tau_n(\vec{R}) + \frac{3}{5}{k_F^n}^2\rho_n(\vec{R})\bigg)\,, \end{aligned} \tag{5.81}$$

where the latter depends on which variant of the DME has been adopted. We denote such integrands as *energy densities* throughout this section. Strictly speaking, it is necessary to multiply them by the interaction to obtain the dimension of an energy density. Still, we postpone the folding with the interaction to the second measure introduced below. In the definition of $C_{nn}^{F,DME}(\vec{R},r)$, we have truncated terms with beyond-second order gradients, in line with current phenomenological implementations of Skyrme EDF. In addition, a consistent account of such fourth-order derivatives in the EDF would require to go also to fourth order in the DME itself, which is not addressed in this work. This is an important point that underlines our philosophy that the primary purpose of the DME method is not to reproduce the fine details of the OBDM, but rather to reproduce as best as possible the energy density and the total energy at a given order in the expansion. The latter two are precisely what are gauged in this work, whereas no tests dedicated to the reproduction of the OBDM by itself are performed.

The parameters of PSA-DME-II $\pi-$functions of the nonlocal matter density, as defined by Eq. (5.27), read

$$\alpha = -0.4130\,, \qquad \beta = 1.2430\,. \tag{5.82}$$

We obtained these values fitting Eq. (5.80) with Eq. (5.81) using densities extracted from a converged self-consistent calculations of a selected set of nuclei.

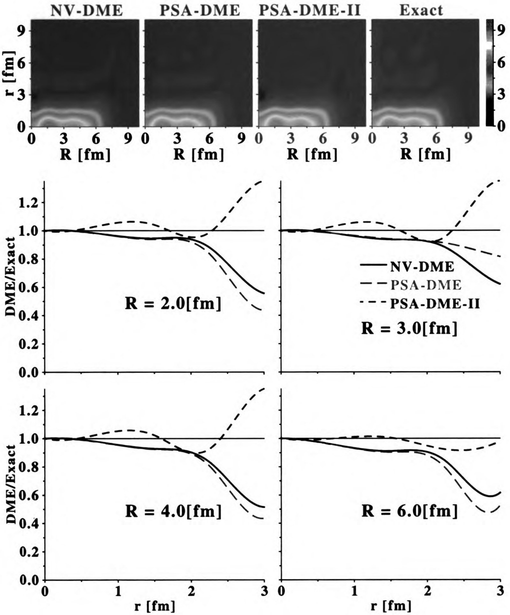

Figure 5.9: (Color online) Comparison of $C^{F}_{nn}(\vec{R},r)$ and $C^{F,DME}_{nn}(\vec{R},r)$ where the latter is computed from the $\pi-$functions of one of the three DMEs: NV-DME, PSA-DME or PSA-DME-II. Upper panels: two-dimensional integrands. Lower panels: ratios of $C^{F,DME}_{nn}(\vec{R},r)$ over $C^{F}_{nn}(\vec{R},r)$ for fixed values of R. Densities are obtained from a self-consistent EDF calculation of ^{208}Pb with the SLy4 Skyrme EDF in the particle-hole part and no pairing.

Figure 5.9 shows [4] that all the three DMEs provide comparably good profile-reproduction of the integrand $C^F_{nn}(\vec{R}, r)$ within the typical range of nuclear interactions ($r \sim 2$ fm). Beyond such a non locality, the quality of the reproduction deteriorates significantly, with that of PSA-DME deteriorating slightly faster. In addition, one sees from the lower panels of Fig. 5.9 that the quality of the reproduction decreases as one goes to the nuclear surface, i.e. for $R \gtrsim 4$ fm. This is slightly improved by taking into account the diffusivity of the local momentum distribution when designing the PSA-DME for the scalar part of the OBDM, as shown by the better accuracy of PSA-DME-II. In general, PSA-DME-II stays much more close to one than the other two DMEs, with slight overestimation in the range of nuclear interactions. Note also that, although the plots are provided for two sample nuclei, more systematic tests have been performed over several semi-magic isotonic and isotopic chains that support such conclusions.

Coming to the energy itself, i.e. to the integrated product of the interaction $v_C(r)$ with the central energy density, we compare

$$E^F_C[nn] = 4\pi \int d\vec{R}\, dr\, r^2\, v_C(r)\, C^F_{nn}(\vec{R}, r)\,, \tag{5.83}$$

$$E^{F,DME}_C[nn] = 4\pi \int d\vec{R}\, dr\, r^2\, v_C(r)\, C^{F,DME}_{nn}(\vec{R}, r). \tag{5.84}$$

Figure 5.10 shows the relative error obtained from the three DME variants compared to the exact Fock contribution for both the Gaussian and the renormalized-Yukawa radial form factors and for three semi-magic isotopic chains.

Let us start with Fig. 5.11 that shows that the dependence of the accuracy on the range of the (Gaussian) interaction used is significant, i.e. about a factor of 1.5 between $a = 1.0$ fm and $a = 1.5$ fm. As can be expected from the two-dimensional

---

[4] Note that for semi-magic spherical nuclei used in this work, the energy densities $C^F_{nn}(\vec{R}, r)$ and $C^{F,DME}_{nn}(\vec{R}, r)$ only depend on the magnitude of $\vec{R}$.

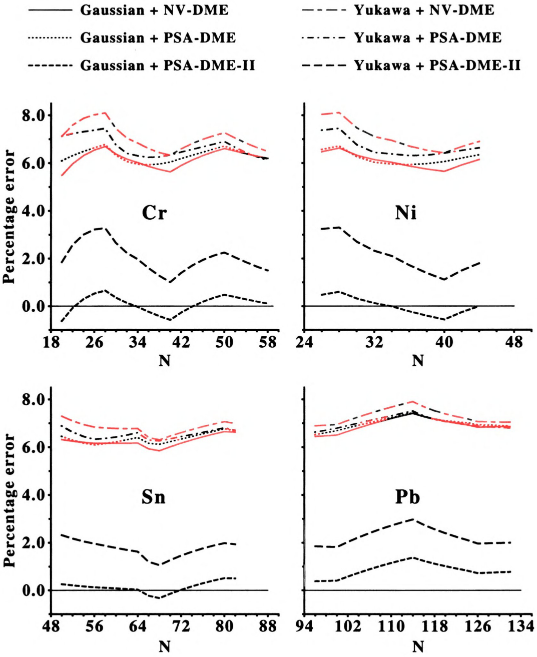

Figure 5.10: (Color online) Percentage error of $E_C^{DME}[nn]$ compared to $E_C^F[nn]$, where the former is computed from: NV-DME, PSA-DME or PSA-DME-II Π—functions. Densities are obtained from self-consistent EDF calculations using the SLy4 Skyrme EDF in the particle-hole channel and no pairing.

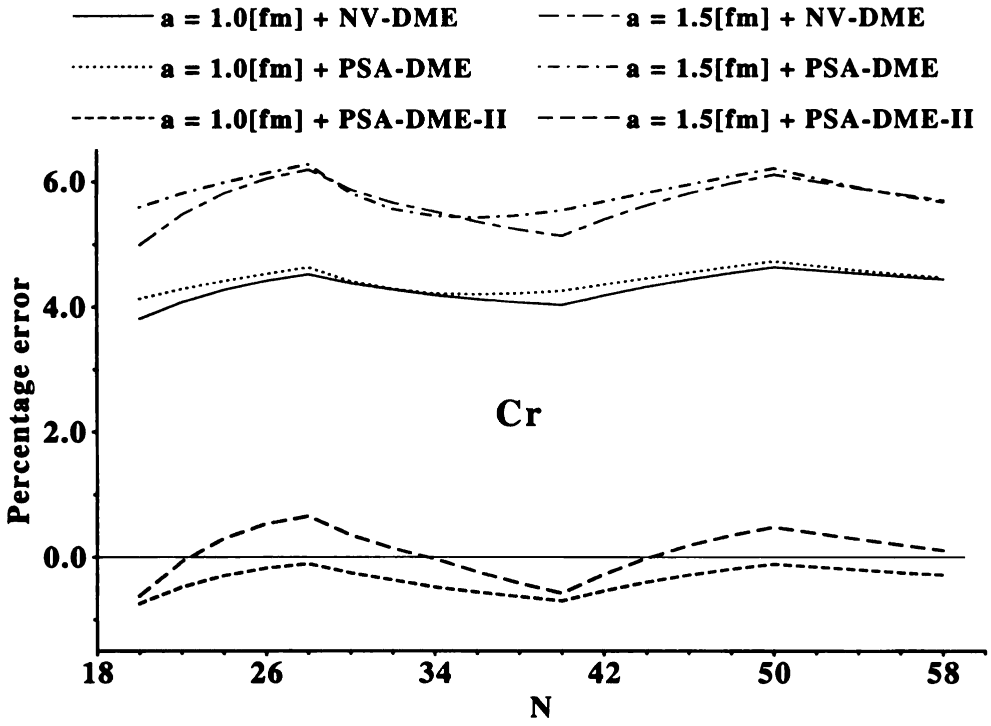

Figure 5.11: (Color online) The same as Figure 5.10 but for two different values of the range of the Gaussian interaction.

destr

which

phase

be wa

the lo

the D

On

be se

the G

better

over t

better

from

incre

5.4.

We

ar

a

ex

density profiles in Fig. 5.9, the accuracy decreases as the range of interaction increases. which holds for all available DME techniques [[170]-[173]]. This stresses that the local quasi-separability of the OBDM with respect to $\vec{r}$ and $\vec{R}$ underlining the DME, which is exact in INM, deteriorates with increasing non-locality r in finite nuclei. As long as the hypothesis of quasi-separability is well realized within the range of the interaction, the DME can be quantitatively successful.

On average, the error obtained with PSA-DME and NV-DME are similar as can be seen in Fig. 5.10, i.e. about $6-8\%$ for the three isotopic chains and for both for the Gaussian and the renormalized-Yukawa interactions. While PSA-DME-II gives a better accuracy with a percentage error between -0.5 and 2. Similar improvement over that of Ref. [170] is reported in Refs.[[171],[172]]. PSA-DME-II, while it is much better than PSA-DME and NV-DME, it shows a gradual drift of the sign of the error, from overestimation to underestimation of the exact value, as the interaction range increases.

5.4.3 Fock contribution from V_T

We now turn to the Fock contribution coming from the tensor part of the NN interaction. Such a contribution involves bilinear products of non-local spin densities. As a matter of fact, two terms with different analytical structures emerge such that the exchange tensor energy-density reads

$$\begin{aligned}
T^F_{nn}(\vec{R},r) &\equiv T^F_{nn,1}(\vec{R},r) + T^F_{nn,2}(\vec{R},r) \ , && (5.85)\\
T^F_{nn,1}(\vec{R},r) &\equiv \frac{1}{4\pi}\int d\Omega_r \, \vec{s}_n(\vec{r}_1,\vec{r}_2)\cdot\vec{s}_n(\vec{r}_2,\vec{r}_1) \ , && (5.86)\\
T^F_{nn,2}(\vec{R},r) &\equiv \frac{1}{4\pi}\int d\Omega_r \sum_{\mu\nu} \frac{r_\mu r_\nu}{r^2} s_{n,\mu}(\vec{r}_1,\vec{r}_2) \\
&\qquad \times s_{n,\nu}(\vec{r}_2,\vec{r}_1) \ , && (5.87)
\end{aligned}$$

wh

DN

ab

and

On

th

J

pro

ca

P

where $T^F_{nn,1}(\vec{R},r)$ also appear in the central contribution to the Fock energy. The two DME counterparts, which eventually depend on which variants of the DME is being adopted, read

$$
\begin{aligned}
T^{F,DME}_{nn,1}(\vec{R},r) &\equiv -\frac{r^2}{3}\left[\Pi^{\vec{s}}_1(\tilde{k}^n_F r)\right]^2 \sum_{\mu,\nu=x}^{z} J_{n,\mu\nu}(\vec{R})\, J_{n,\mu\nu}(\vec{R})\,, \\
T^{F,DME}_{nn,2}(\vec{R},r) &\equiv -\frac{r^2}{15}\left[\Pi^{\vec{s}}_1(\tilde{k}^n_F r)\right]^2 \sum_{\mu,\nu=x}^{z} \Big(J_{n,\mu\nu}(\vec{R})\, J_{n,\mu\nu}(\vec{R}) + J_{n,\mu\mu}(\vec{R}) J_{n,\nu\nu}(\vec{R}) \\
&\quad + J_{n,\mu\nu}(\vec{R}) J_{n,\nu\mu}(\vec{R}) \Big),
\end{aligned}
$$

and reduce for spherical systems to

$$T^{F,DME}_{nn,1}(\vec{R},r) \equiv -\frac{r^2}{6}\left[\Pi^{\vec{s}}_1(\tilde{k}^n_F r)\right]^2 \vec{J}_n(\vec{R}) \cdot \vec{J}_n(\vec{R})\,, \tag{5.88}$$

$$T^{F,DME}_{nn,2}(\vec{R},r) \equiv 0\,. \tag{5.89}$$

One recovers a pattern which is seen when deriving the empirical Skyrme EDF from an auxiliary Skyrme effective interaction. That is, the central part of the interaction only produces the so-called *symmetric* bilinear tensor terms proportional to $J_{n,\mu\nu}(\vec{R})\, J_{n,\mu\nu}(\vec{R})$ while $T^{F,DME}_{nn,2}(\vec{R},r)$ that contains *asymmetric* bilinear tensor terms proportional to $J_{n,\mu\nu}(\vec{R})\, J_{n,\nu\mu}(\vec{R})$ solely comes from the tensor interaction [196]. This can be easily traced back to the spin-space coupling that characterizes the tensor operator. Since the numerical tests are presently carried out for spherical systems, we are only concerned with $T^F_{nn,1}(\vec{R},r)$ and $T^{F,DME}_{nn,1}(\vec{R},r)$. For spin-unsaturated nuclei, $T^F_{nn,1}(\vec{R},r)$ is highly localized around the nuclear surface as seen in Fig. 5.12 for ^{208}Pb. The same figure shows the progressive and significant improvement that the PSA approach brings to the DME of the vector part of the OBDM. This is realized in both PSA-DME and PSA-DME-II. The optimal parameters that we obtained for

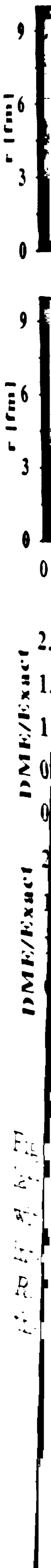
r [fm]
9
6
3
0
r [fm]
9
6
3
0
0
DME/Exact
DME/Exact

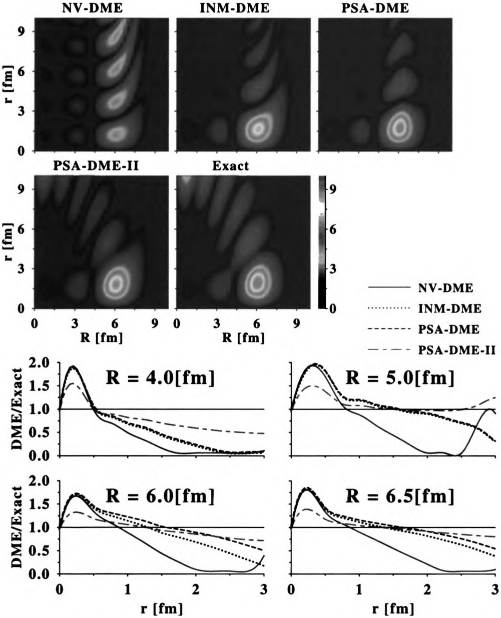

Figure 5.12: (Color online) Comparison of $T^{F}_{nn,1}(\vec{R},r)$ and $T^{DME}_{nn,1}(\vec{R},r)$ where the latter is computed from NV-DME, PSA-DME, PSA-DME-II or from PSA-DME with $P^{n}_{2}(\vec{R})=0$ which we denote as INM-DME. Upper panels: two-dimensional integrands. Lower panels: ratios of $T^{DME}_{nn,1}(\vec{R},r)$ over $T^{F}_{nn,1}(\vec{R},r)$ for fixed values of R. Densities are obtained from a converged self-consistent calculation of ^{208}Pb with the SLy4 Skyrme EDF in the particle-hole channel and no pairing.

PSA

Wh

he

ne

the

of

the

by

th

th

wh

th

wh

wh

sh

th

s

D

F

PSA-DME-II of $\vec{s}_q(\vec{r}_1, \vec{r}_2)$, as defined by Eq. (5.39), read

$$m = 2.543\,, \qquad b = -0.0799\,. \tag{5.90}$$

Within the typical range of nuclear-interactions, NV-DME falls off much faster than both PSA-DMEs. Less importantly, NV-DME also introduces artificial and pronounced structures in a region that corresponds to the tail of the interaction. Both of these drawbacks are rectified progressively by the PSA-DME approach. While most of the improvement is already brought by the spherical PSA ($P_2(\vec{R}) = 0$, which is the same for both PSA-DME and PSA-DME-II), an even better accuracy is obtained by incorporating the quadrupolar deformation $P_2(\vec{R})$ of the local momentum Fermi distribution. The overestimation of $T^F_{nn,1}(\vec{R}, r)$ at very small r seen for all DMEs in the lower panels of Fig. 5.12 corresponds to a region where the integrand is small and where its weight is further reduced in the integrated energy by the r^2 phase-space factor.

Coming to the energy itself, i.e. to the integrated product of the interaction $v_T(r)$ with the tensor energy density, we compare

$$E^F_T[nn] = 4\pi \int d\vec{R}\, dr\, r^2\, v_T(r)\, T^F_{nn}(\vec{R}, r)\,, \tag{5.91}$$

$$E^{F,DME}_T[nn] = 4\pi \int d\vec{R}\, dr\, r^2\, v_T(r)\, T^{DME}_{nn}(\vec{R}, r)\,, \tag{5.92}$$

which for spherical nuclei reduce to the contribution from $T^F_{nn,1}$ and $T^{F,DME}_{nn,1}$. Figure 5.13 shows the relative error of the three DMEs compared to the exact Fock contribution, for both the Gaussian and the renormalized-Yukawa radial form factors and for three semi-magic isotopic chains. For both types of interaction, the percentage error of NV-DME easily reaches 40%. This is in contrast to PSA-DME and PSA-DME-II whose percentage errors are typically within ±10% for most parts of the three isotopic

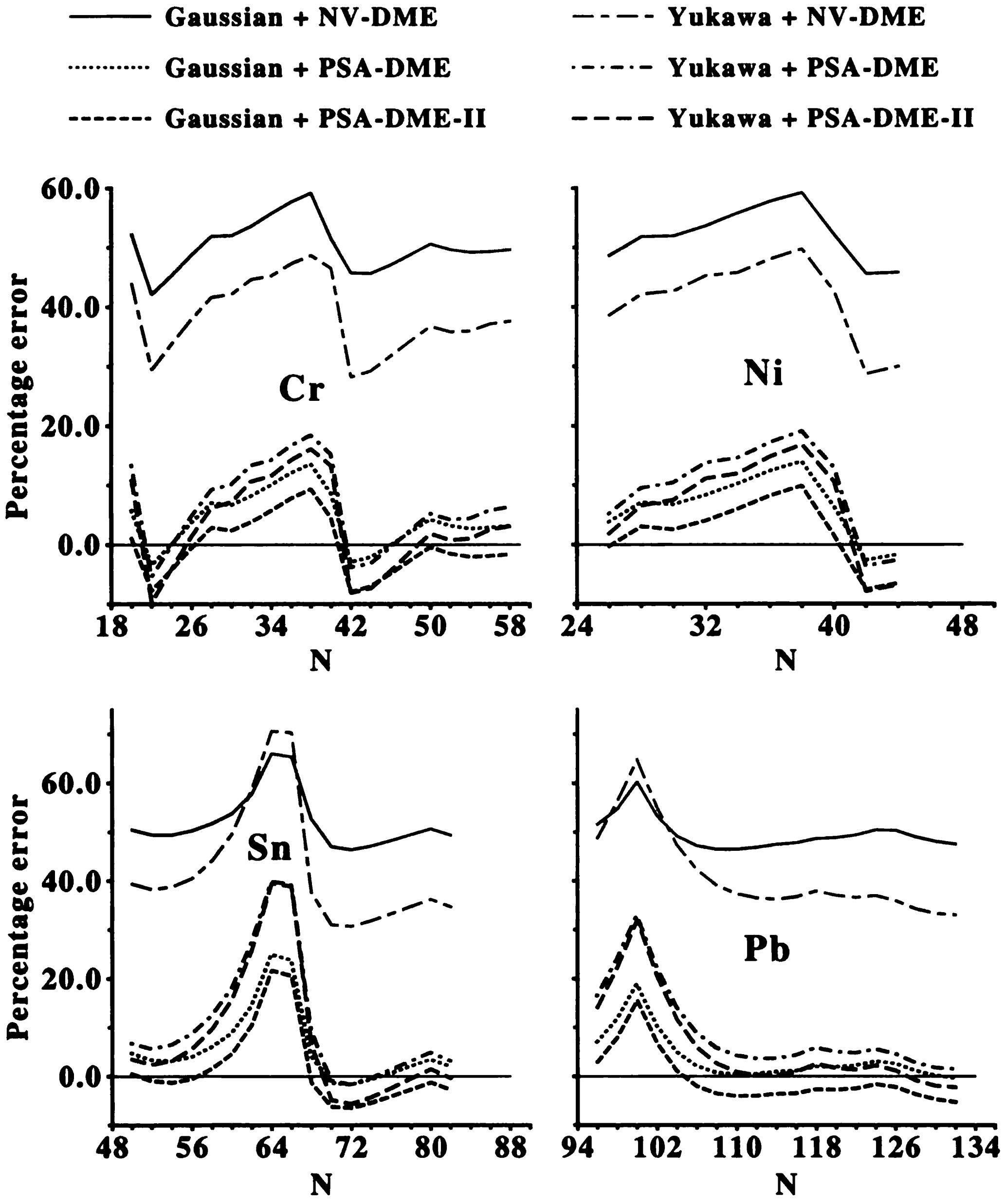

Figure 5.13: (Color online) Percentage error of $E_T^{DME}[nn]$ compared to $E_T^F[nn]$ where the former is either computed from: NV-DME, from PSA-DME or PSA-DME-II. Densities are obtained from self-consistent EDF calculations using the SLy4 Skyrme EDF in the particle-hole channel and no pairing. Notice the different vertical scale compared to Fig. 5.10.

chains. This can be traced to the fact that, while both NV-DME and PSA-DMEs overestimate the reference quantity for small r (typically less than 1 fm), NV-DME decreases much faster with r, thereby overcompensating for its initial overestimation. In contrast, PSA-DMEs stays close to the exact value for a much larger range of r values.

There exist short sequences of isotopes for which the percentage error shows a considerable increase. The fact that all three DMEs display such a feature suggests that the problem is independent of the specific form of the $\Pi_1^{\vec{s}}$ function used. To identify the source of the problem, Fig. 5.14 shows $T^F_{nn,1}(\vec{R},r)$ for three nuclei displaying a sudden loss of accuracy. One notices that $T^F_{nn,1}(\vec{R},r)$ extends over larger intervals in R and r than for ^{208}Pb (see Fig. 5.12). This corresponds to the fact that the selected nuclei are nearly spin-saturated and generate very small $E^F_T[nn]$ in absolute value, as seen from the lower panels of Fig. 5.14. As a result, the relative inaccuracy of any DME becomes large and the percentage error increases suddenly. Of course, the resulting error in the total EDF remains very small as the corresponding tensor contribution is anyway negligible, i.e. the local spin-orbit density $\vec{J}_q(\vec{R})$ is close to zero in nearly spin-saturated nuclei. Therefore the sudden losses of relative accuracy are not as worrying as Fig. 5.13 initially suggests.

In conclusion, the use of PSA techniques has allowed us to bring the DME applicable to the bilinear product of non-local spin densities on the same level of accuracy as for terms depending on the scalar part of the OBDM. One could certainly work even harder to bring down the overall DME percentage error. This could be achieved by (i) allowing for additional parameters in the $\Pi-$functions to be optimized on a set of reference calculations. However, our extensive optimization of the two-parameters of $\Pi_1^{\vec{s}}$ have convinced us that one cannot remove the sudden loss of relative accuracy discussed above for spin-saturated nuclei. As already stated, this is not a problem in the end as the corresponding contribution to the energy is negligible anyway. (ii) One

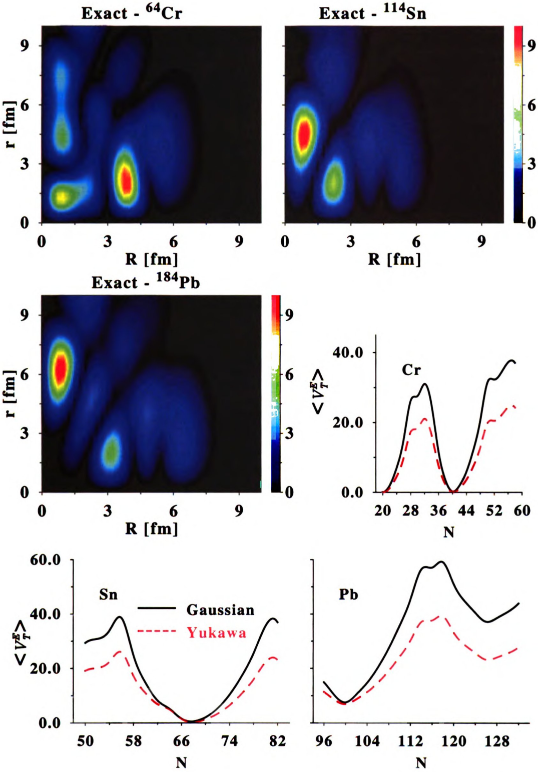

Figure 5.14: (Color online) A few representative nuclei with diffuse $T^F_{nn,1}(\vec{R}, r)$ together with absolute $E^F_T[nn]$ for the corresponding isotopic chains. Densities are obtained from a self-consistent EDF calculation using the SLy4 Skyrme functional in the particle-hole part and no pairing.

can go to higher orders in the DME, consistently for both the scalar and the vector parts of the OBDM. This should however be done within the frame of the generalized Skyrme EDF proposed in Ref. [35].

5.4.4 Fock contribution from V_{LS}

Basic analysis

We now turn to the spin-orbit contribution to the Fock energy. Unlike for the central and tensor forces, such a contribution involves both the scalar and the vector parts of the OBDM. In this case, we first compare the spin-orbit energy density

$$LS^{F}_{nn}(\vec{R},r) = \frac{i}{4\pi}\int d\Omega_r \, \vec{s}_n(\vec{r}_1,\vec{r}_2)\cdot\vec{r}\times\vec{\nabla}_2\rho_n(\vec{r}_2,\vec{r}_1) \ , \tag{5.93}$$

to its DME counterpart

$$LS^{F,DME}_{nn}(\vec{R},r) = \frac{1}{6}\,\Pi_1^{\vec{s}}(k_F^n r)\, r^2 \sum_{\mu,\nu,\beta=x}^{z} \epsilon^{\mu\nu\beta} J_{n,\mu\nu}(\vec{R})\, \nabla^{\beta}_{\vec{R}}\Big(\Pi_0^{\rho}(k_F^n r)\rho_n(\vec{R})\Big) \, ,$$

which eventually depends on which variants of the DME is being adopted and that reduces for spherical systems to

$$LS^{F,DME}_{nn}(\vec{R},r) = \frac{1}{6}\,\Pi_1^{\vec{s}}(k_F^n r)\, r^2 \vec{J}_n(\vec{R})\cdot\vec{\nabla}_{\vec{R}}\Big(\Pi_0^{\rho}(k_F^n r)\rho_n(\vec{R})\Big) \ . \tag{5.94}$$

Note that we have truncated terms with more than two gradients in $LS^{DME}_{nn}(\vec{R},r)$. The numerical tests shown in the present section actually use PSA-DME only (no PSA-DME-II) with the quadrupolar deformation parameter set to zero ($P_2^n(\vec{R}) = 0$). We still label the results as PSA-DME. It will be seen that these simplifying choices have no bearing on the discussion at hand.

Figure 5.15 shows that PSA-DME significantly overestimates (in absolute values)

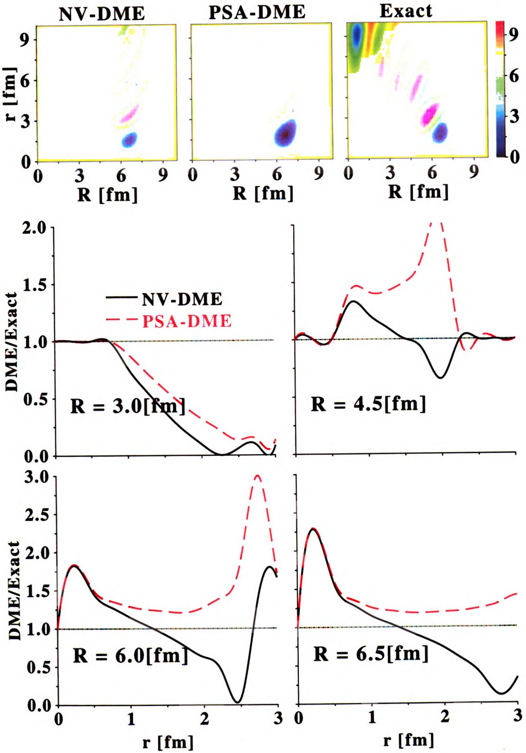

Figure 5.15: (Color online) Comparison of $LS^{F}_{nn}(\vec{R}, r)$ and $LS^{F,DME}_{nn}(\vec{R}, r)$ where the latter is computed from either NV-DME or PSA-DME. Upper panels: two-dimensional integrands. Lower panels: ratios of $LS^{DME}_{nn}(\vec{R}, r)$ over $LS^{F}_{nn}(\vec{R}, r)$ for fixed values of R. Densities are obtained from a converged self-consistent calculation of ^{208}Pb with the SLy4 Skyrme EDF in the particle-hole channel and no pairing.

the maximum peak of $LS^{F}_{nn}(\vec{R},r)$ at the nuclear surface. In addition, oscillations at larger r, i.e. in the tail of the two-nucleon interaction, are not captured by PSA-DME. In contrast, NV-DME reproduces relatively well the density profile $LS^{F}_{nn}(\vec{R},r)$, in particular as for the main peak at the nuclear surface. This suggests that the significant improvement for PSA-DME over NV-DME as to reproducing the tensor energy density does not carry over to the spin-orbit energy density. The previous assertions are supported by tests carried over several isotonic and isotopic chains. Looking for possible improvements, we tested that including truncated higher-order terms associated with the action of $\vec{\nabla}_{\vec{R}}$ on $(1/4\Delta\rho_n - \tau_n + 3/5k_F^{n\,2}\rho_n)$, when going from Eq. 5.93 to 5.94, does not improve the accuracy of PSA-DME.

Coming to the energy itself, i.e. to the integrated product of the interaction $v_{LS}(r)$ with the spin-orbit energy density, we compare

$$E^{F}_{LS}[nn] = 4\pi \int d\vec{R}\, dr\, r^2\, v_{LS}(r)\, LS^{F}_{nn}(\vec{R},r) \ , \tag{5.95}$$

$$E^{DME}_{LS}[nn] = 4\pi \int d\vec{R}\, dr\, r^2\, v_{LS}(r)\, r^2\, LS^{DME}_{nn}(\vec{R},r) \ . \tag{5.96}$$

Figure 5.16 shows the percentage error obtained for three isotopic chains. In agreement with the analysis done for the spin-orbit energy density, the percentage error of PSA-DME is impractically large and negative, in the range of -15% to -50% for the two schematic interactions used. In contrast, NV-DME provides a much better accuracy with percentage errors within ± 10% for most studied isotopes. Last but not least, one notes that the spikes in the percentage errors already discussed in section 5.4.3 arise for the same isotopes and relate to the vanishing non-local spin density in near spin-saturated nuclei.

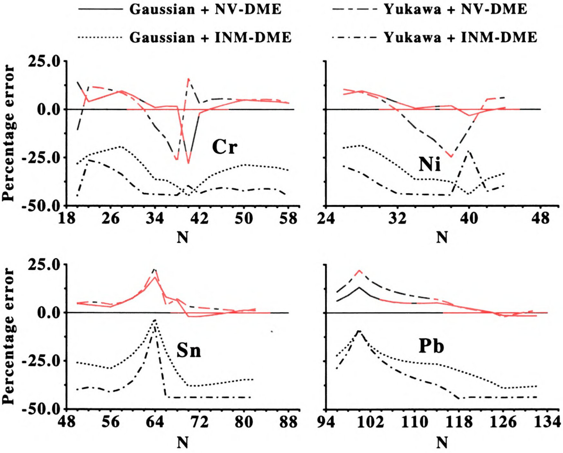

Figure 5.16: (Color online) Percentage error of $E_{LS}^{DME}[nn]$ compared to $E_{LS}^{F}[nn]$ where the latter is either computed from NV-DME or from PSA-DME. Densities are obtained from self-consistent EDF calculations using the SLy4 Skyrme EDF in the particle-hole channel and no pairing. Notice the different vertical scale compared to Figs. 5.10 and 5.13.

Further investigation of the spin-orbit exchange

The results of the previous section show that NV-DME is better suited than PSA-DME to reproduce the spin-orbit contribution to the Fock energy. This can be confounding in light of the better accuracy obtained using PSA-DME to reproduce the tensor contribution to the Fock energy. We can infer from Fig. 5.12 that NV-DME underestimates the main peak of the nonlocal spin density while the latter is well captured by PSA-DME. It is thus puzzling to find the opposite for the Fock spin-orbit energy density. In the following we employ a toy model of the OBDM of finite nuclei to show that this is due to a fortuitous cancelation of errors.

Having already a handle on the non-local spin density $\vec{s}_q(\vec{r}_1, \vec{r}_2)$, we focus on the term it multiplies in the spin-orbit energy density, i.e. $\vec{r} \times \vec{\nabla}_2 \rho_q(\vec{r}_1, \vec{r}_2)$, which we first approximate by $\vec{r} \times \vec{\nabla}_{\vec{R}}\, \rho_q(\vec{r}_1, \vec{r}_2)$ thanks to the weak dependence of the non-local matter density on the orientation of $\vec{r}$ [176]. Hence, and focusing arbitrarily on neutrons, we want to compare the two quantities

$$G_E = \vec{\nabla}_{\vec{R}}\, \rho_n(\vec{R}, \vec{r}) \ , \tag{5.97}$$

$$G_{DME} = \vec{\nabla}_{\vec{R}} \left(\Pi_0^{\rho}(k_F^n r)\, \rho_n(\vec{R}) \right) \ , \tag{5.98}$$

where the latter is independent of whether NV-DME or PSA-DME is used. To do so, we employ the toy model we discussed in section where the expressions for the local and nonlocal neutron densities are given by Eqs. (5.58) and (5.59). From these equations, one easily obtains

$$\vec{\nabla}_{\vec{R}} \rho_n(\vec{R} + \frac{\vec{r}}{2}, \vec{R} - \frac{\vec{r}}{2}) = \exp\left[-1/4\alpha^2 r^2 \frac{1+t}{1-t} \right] \left[\vec{\nabla}_R \rho_n(\vec{R}) \right] \ , \tag{5.99}$$

$$\vec{\nabla}_{\vec{R}} \rho_n(\vec{R}) = -\frac{4\alpha^5}{\pi^{3/2}} (1-t^2)^{-1/2} \frac{1-t}{1+t} R \ \exp\left[-\alpha^2 R^2 \frac{1-t}{1+t} \right] \tag{5.100}$$

The corresponding PSA-DME reads

$$\rho_n(\vec{R}+\frac{\vec{r}}{2},\vec{R}-\frac{\vec{r}}{2}) \approx 3\frac{j_1(k_F^n r)}{k_F^n r}\left[1+\frac{r^2}{4}\left(-\frac{1+t}{1-t}\alpha^2+\frac{2}{5}k_F^{n\,2}\right)\right]\rho_n(\vec{R})\,, \tag{5.101}$$

such that, given the definition of $k_F^q(\vec{R})$, one can easily obtain

$$\vec{\nabla}_{\vec{R}}\left[\Pi_0^\rho(k_F^n r)\rho(\vec{R})\right] = j_0(k_F^n r)\vec{\nabla}_{\vec{R}}\rho_n(\vec{R}) \tag{5.102}$$

and show that

$$G_{ratio}(\vec{R},\vec{r}) \equiv \frac{G_{DME}(\vec{R},\vec{r})}{G_E(\vec{R},\vec{r})} = j_0(k_F^n r)\exp\left[1/4\alpha^2 r^2\frac{1+t}{1-t}\right].$$

In order to study G_{ratio} quantitatively, we fix the inverse oscillator length, α, using the Blomqvist and Molinari formula, i.e. $\alpha = \left(0.90A^{1/3}+0.70\right)$. In subsequent discussions, we take reasonable combinations of A and N although we show that the conclusions of the present section are independent of the actual value of A.

Before analyzing the behavior of $G_{ratio}(\vec{R},\vec{r})$, it is worth noticing that the toy nonlocal matter density is exactly separable in relative and center-of-mass coordinates. Such a separability being one inherent, usually only approximate, aspect of the DME, we expect the latter to work well in the present case [185]. Computing the same ratio as in $G_{ratio}(\vec{R},\vec{r})$ *without* the gradient operators, we do indeed obtain the good performance of the DME as is visible in Fig. 5.17. Note in particular that the ratio is independent of the value of R. Such a result proves that the toy model provides a situation comparable to the one studied in Sec. 5.4.2, i.e. the DME of the scalar part of the density matrix performs well. Such a performance sets the stage in view of qualifying the results obtained below for $G_{ratio}(\vec{R},\vec{r})$.

In order to identify the short distance behavior of $G_{ratio}(\vec{R},\vec{r})$, we perform a Taylor

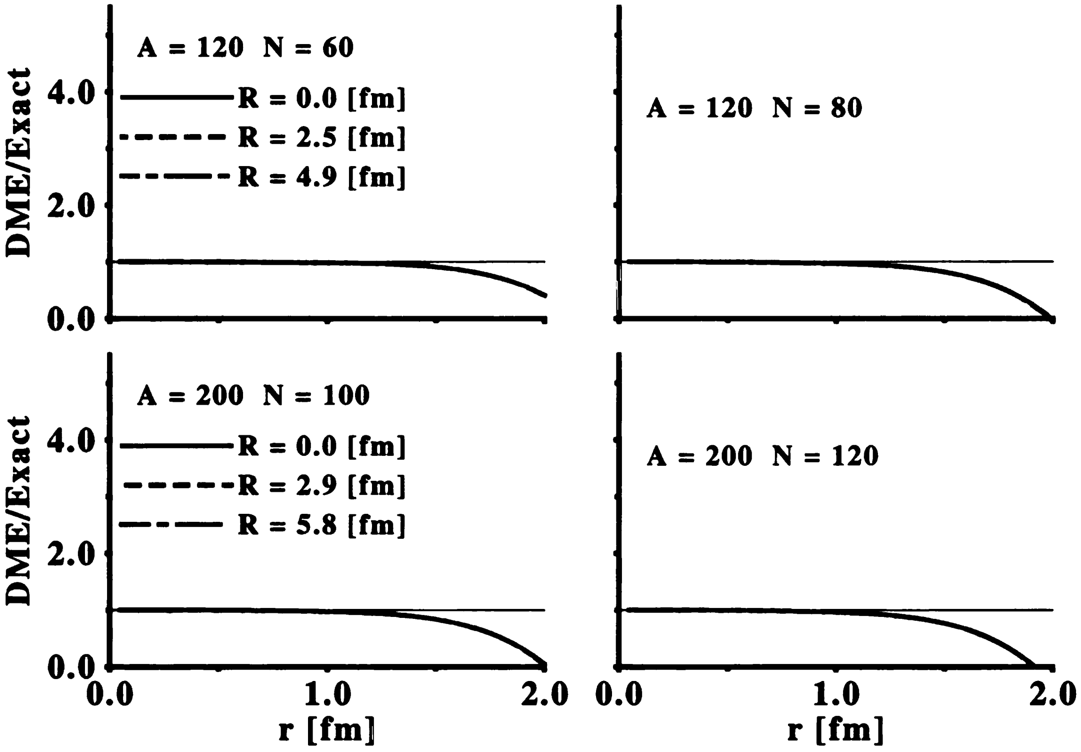

Figure 5.17: (Color online) Ratio of the DME (Eq.(5.101)) over the exact (Eq.(5.58)) expressions of the toy nonlocal matter density.

series expansion in r

$$G_{ratio}(\vec{R},\vec{r}) \approx 1 + \left(-\frac{k_F^{n\,2}}{6} + \frac{\alpha^2(1+t)}{4(1-t)}\right) r^2 . \tag{5.103}$$

Looking close to the surface of the nucleus, one can neglect $k_F^{n\,2}/6$ in comparison with the second term of Eq. (5.103). Defining $G_{error}(\vec{R},\vec{r}) \equiv G_{ratio}(\vec{R},\vec{r}) - 1$, one obtains

$$G_{error}(\vec{R},\vec{r}) \approx \left(0.326 - \frac{0.205}{n^{1/3}}\right) r^2 . \tag{5.104}$$

Equation 5.104 is valid around the nuclear surface. Inside the nucleus, one cannot neglect the first term $k_F^{n\,2}/6$ of Eq. (5.103). This is irrelevant as the spin-orbit energy density is concentrated around the nuclear surface. Figure 5.18 bears our expectation i.e. overestimation of G_E by G_{DME} around the nuclear surface for a wide range of R, A and N values. It can also be seen that there is a gradual and systematic shift from slight underestimation to overestimation as one moves from inside the nucleus to the nuclear surface.

Keeping the results shown in Fig. 5.17 as a reference, we conclude that the application of the gradient operator on the scalar part of the density matrix deteriorates the quality of the DME that overestimates the exact results, in particular as one goes to the surface of the nucleus where the exchange spin-orbit energy density is maximum. Combined with the good approximation of the vector part of the density matrix, such a semi-quantitative analysis explains the overall overestimation (in absolute value) of the exchange spin-orbit energy provided by PSA-DME (see Fig. 5.16). Contrarily, the underestimation of the vector part of the density matrix by NV-DME provides a fortuitous, but rather accurate, cancelation of errors such that the nonlocal spin-orbit energy density is much better reproduced overall (see Fig. 5.16). Even though we can be satisfied with such a situation in the short term future and advocate the use of the NV-DME variant for the spin-orbit contribution to the Fock energy, it would be

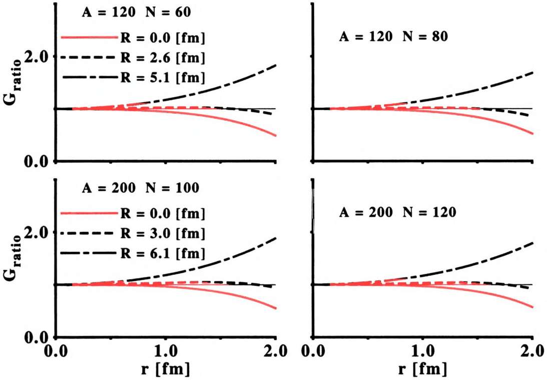

Figure 5.18: (Color online) $G_{ratio}(\vec{R}, \vec{r})$ as a function of r for a selected set of ($\vec{R}$, A, N).

more satisfying on the long run to design a suitable DME for the gradient of the scalar part of the density matrix that can be combined with the improved PSA-DME for the vector part.This loss of accuracy for the spin-orbit part does not have any impact on the application of the DME to the HF energy from chiral EFT NN + NNN interaction at N^{2}LO. This is due to the fact that the NN spin-orbit interaction that we have at N^{2}LO is zero-range/contact, thus does not require the application of the DME. In the NNN case, the problem does not seem to be relevant. Refer to section 7.2 for details.

5.4.5 Hartree contribution from V_C, V_{LS} and V_T

The numerical results given in section 5.4.6 confirm the view that the DME should be applied only to the Fock part of the HF energy. However, for the sake of completeness, we gauge the accuracy of the DME when applied to Hartree contributions. As shown in the next chapter, the Hartree contribution from the tensor part of the two-nucleon interaction vanishes for time-reversal invariant systems. For central and spin-orbit parts, the exact integrands for the profile comparison are

$$\begin{aligned} C^H_{nn}(\vec{R},r) &\equiv \frac{1}{4\pi}\int d\Omega_r\, \rho_n(\vec{r}_1)\, \rho_n(\vec{r}_2)\ , && (5.105)\\ LS^H_{nn}(\vec{R},r) &\equiv \frac{1}{4\pi}\int d\Omega_r\, \rho_n(\vec{r}_1)\, \vec{r}\cdot \vec{J}_n(\vec{r}_2)\ , && (5.106)\end{aligned}$$

while the corresponding DME expressions read

$$\begin{aligned} C^{H,DME}_{nn} &\approx \left[\pi^\rho_0(\Omega)\right]^2 \rho_q(\vec{R})\rho_{q'}(\vec{R}) - \frac{r^2}{6}\left[\pi^\rho_1(\Omega)\right]^2 \vec{\nabla}\rho_q(\vec{R})\cdot\vec{\nabla}\rho_{q'}(\vec{R}) \\ &\quad + \frac{r^2}{12}\,\pi^\rho_0(\Omega)\,\pi^\rho_2(\Omega)\left[\rho_q(\vec{R})\Delta\rho_{q'}(\vec{R}) + \rho_{q'}(\vec{R})\Delta\rho_q(\vec{R})\right], && (5.107)\\ LS^{H,DME}_{nn} &\approx \frac{1}{3}r^2\,\vec{J}_n(\vec{R})\cdot\vec{\nabla}\rho_n(\vec{R})\,, && (5.108)\end{aligned}$$

where the π−functions in Eq. (5.107) are fixed in two ways: (i) The first set (NV-DME) are given in Eqs. (5.62)-(5.64). (ii) The second set consists of the parameterized functions given in Eqs. (5.67)-(5.69) and whose optimized parameters are: $a_2 = 0.850$ and $a_4 = 0.3000$. Eq. (5.108) results after fixing the π−functions according to Eq. (5.72) (simple Taylor series expansion). The corresponding integrated energy contributions are given as

$$
\begin{aligned}
E_C^H[nn] &= 4\pi \int d\vec{R}\, dr r^2\, v_C(r)\, C_{nn}^H(\vec{R}, r)\,, && (5.109)\\
E_C^{H,DME}[nn] &= 4\pi \int d\vec{R}\, dr r^2\, v_C(r)\, C_{nn}^{H,DME}(\vec{R}, r)\,, && (5.110)\\
E_{LS}^H[nn] &= 4\pi \int d\vec{R}\, dr r^2\, v_C(r)\, LS_{nn}^H(\vec{R}, r)\,, && (5.111)\\
E_{LS}^{H,DME}[nn] &= 4\pi \int d\vec{R}\, dr r^2\, v_C(r)\, LS_{nn}^{H,DME}(\vec{R}, r)\,, && (5.112)
\end{aligned}
$$

Fig. 5.19 shows that for large r values, Eq. (5.107) does not reproduce the correct profile of Eq. (5.81) for both sets of π−functions. The two DMEs (sets of π−functions) have opposite effect in that region. In contrast, one can achieve an accurate reproduction of the integrated contribution, Eq. (5.109), with Eq. (5.110), when the range of the interaction is short. Furthermore, the plots contrast the accuracy of the two sets of π−functions, with the parameterized version performing significantly better as the range of the interaction increases, though with a decreasing overall accuracy. Even though this decrease in accuracy is a general trend for all DME approximated quantities, the deterioration is more significant in this case than the Fock contributions. Perhaps this is due to the wrong prediction of the exact profile (Eq. (5.81)) with Eq. (5.81). Fig. 5.20 compares the profile of the exact Hartree contribution from the spin-orbit part of the interaction to its DME approximation. One can see the DME fails to properly capture the profile, with a very large error resulting in the integrated contributions.

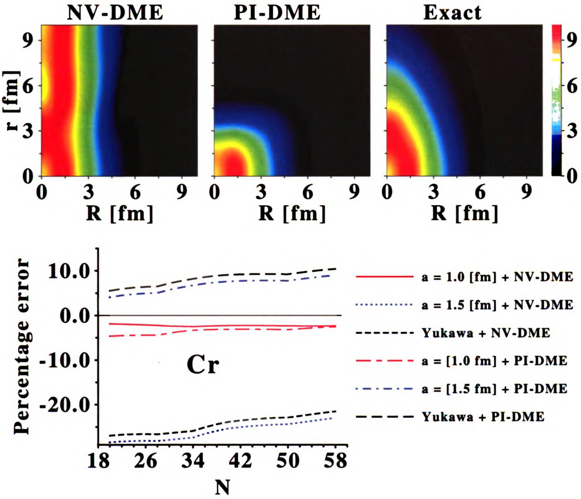

Figure 5.19: (Color online) Percentage error of $E_C^{H,DME}[nn]$ with respect to $E_C^{H}[nn]$ for Cr isotopic chain. The upper plots show C_{nn}^{H}, and $C_{nn}^{H,DME}$ for NV-DME and the parameterized $\pi-$function which we call PI-DME.

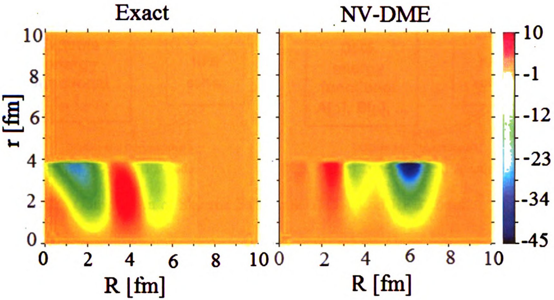

Figure 5.20: (Color online) LS^{H}_{nn}, and $LS^{H,DME}_{nn}$ for NV-DME, with densities obtaiend from a converged self-consistent calculation of ^{208}Pb with the SLy4 Skyrme EDF in the particle-hole channel and no pairing.

5.4.6 Preliminary self-consistent tests

In practical terms, one of the important benefits of the DME approximations is the fact that existing Skyrme HFB codes require minimal modifications to be used with EDFs obtained from the DME. Fig. 5.21 contrasts how a code is implemented for Skyrme HFB against one for the DME based functional. As can be seen the main change is in replacing the eventually constant Skyrme couplings, with density-dependent couplings obtained from the DME.

We carried out a limited set of self-consistent test to gauge the accuracy of the DME, in both full- and exchange-only-DME. In full-DME, both the Hartree and Fock contributions are approximated with the DME, while in exchange-only-DME, only the Fock contributions are approximated with the DME while the Hartree ones are treated exactly. In addition to confining the test to time-reversal invariant and spherically symmetric systems, there are several simplifying choices that we made.

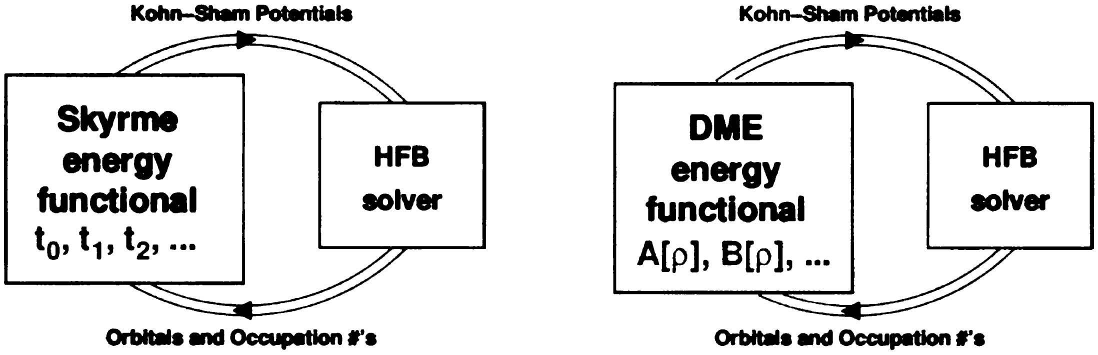
Kohn–Sham Potentials
Skyrme energy functional $t_0, t_1, t_2, \ldots$
HFB solver
Orbitals and Occupation #'s
Kohn–Sham Potentials
DME energy functional $A[\rho], B[\rho], \ldots$
HFB solver
Orbitals and Occupation #'s

(a) Skyrme-HFB code. (b) DME-based HFB code.

Figure 5.21: Comparison of Skyrme HFB and DME-based HFB codes.

These are

- We used the Brink-Boeker [193] force which has only a central component with gaussian form factors. The actual form and parameter values are

$$V_c(r) = \sum_{i=1}^{4} a_i \, e^{-(r_{12}/\mu_a)^2} + b_i \, e^{-(r_{12}/\mu_b)^2} , \tag{5.113}$$

  with $\mu_a = 0.7 fm$ and $\mu_b = 1.4 fm$. The magnitude and range parameters in the four spin-isospin channels read

Table 5.3: The Brink-Boeker force(B1)

	$\Pi_1^s\Pi_0^\tau$	$\Pi_0^s\Pi_1^\tau$	$\Pi_1^s\Pi_1^\tau$	$\Pi_0^s\Pi_0^\tau$
a_i	389.5	389.5	801.6	801.6
b_i	-140.6	-140.6	-3.82	-3.82

  Even though one usually adds a zero-range spin-orbit part to this interaction, this is not done in this work as our target is to compare the DME approximations, and a zero-range interaction is treated exactly in the DME. A complete self-consistent test of DME approximations should make use of modern NN interactions that have central, spin-orbit and tensor components. In this regard, building a local chiral interaction that has a low-momentum cutoff, and thus gives sensible HF results, will be useful.

- We calculate only the total energy, and its components such as kinetic, Hartree and Fock contributions of closed-shell nuclei: ^{16}O, ^{40}Ca, ^{48}Ca and ^{90}Zr. The fact that we do nOt resolve the single-particle spectra (such as spin-orbit splitting) prevents us from assessing the DME of $\vec{s}_q(\vec{r}_1, \vec{s}_2)$ for spin-unsaturated ^{48}Ca and ^{90}Zr. Specifically the impact of the significant improvement in the DME of $\vec{s}_q(\vec{r}_1, \vec{r}_2)$ brought by our PSA-DME is not yet gauged with self-consistent calculations. Additionally, we do not calculate the corresponding exact HF results. Rather, we use results from Ref. [184] when we need to refer to exact HF results.

Derivations related to the self-consistent numerical test are given in Appendix 9.8. For faster convergence of the calculations, we implemented both Broyden's [194] and imaginary-time methods. Table 5.4 lists the results of the self-consistent calculations. At this point, we remind the reader that there are four densities that appear in the exact HF energy of time-reversal invariant systems: $\rho_q(\vec{r}_1, \vec{r}_2)$, $\vec{s}_q(\vec{r}_1, \vec{r}_2)$, $\rho_q(\vec{r}_{1/2})$ and $\vec{J}_q(\vec{r}_{1/2})$ (which appears only if the given NN interaction has a finite-range spin-orbit part). The second column show how the $\pi-$functions of these densities are fixed. Obviously, $\rho_q(\vec{r}_{1/2})$ and $\vec{J}_q(\vec{r}_{1/2})$ are not expanded in exchange-only-DME calculations.

We start with the nonlocal densities. First, we have the labels NV-full and NV-exc-only. The full and exchange-only labels should be self-explanatory. NV refers to fixing the $\pi-$functions of $\rho_q(\vec{r}_1, \vec{r}_2)$ and $\vec{s}_q(\vec{r}_1, \vec{r}_2)$ according to the original DME of Negele and Vautherin (Ref. [170]). PSA-II-exc-only use the parameterized versions of the $\pi-$functions of $\rho_q(\vec{r}_1, \vec{r}_2)$ and $\vec{s}_q(\vec{r}_1, \vec{r}_2)$. The parameters that we used are the ones that we optimized for the non self-consistent test, while for $\rho_q(\vec{r}_{1/2})$, the parameters and $\pi-$functions are as discussed in the previous section (5.4.5). For the $\pi-$functions of $\vec{J}_q(\vec{r}_{1/2})$, we use Taylor series as was done in Ref. [170].

Table 5.4: Full-DME and Exchange-only-DME for Brink-Boeker interaction and several DMEs

		E_{tot}	kin	Dir	Exch
^{16}O	NV-full	-6.204	13.948	-	-
	NV-exc-only	-5.600	13.474	18.839	-37.914
	PSA-II-full	-7.932	15.417	-	-
	PSA-II-exc-only	-5.635	13.338	18.513	-37.487
^{40}Ca	NV-full	-8.526	16.822	-	-
	NV-exc-only	-7.516	15.793	22.567	-45.878
	PSA-II-full	-10.359	17.575	-	-
	PSA-II-exc-only	-7.539	15.583	22.075	-45.198
^{48}Ca	NV-full	-7.447	16.678	-	-
	NV-exc-only	-6.625	15.762	21.334	-43.803
	PSA-II-full	-9.304	17.57	-	-
	PSA-II-exc-only	-6.646	15.529	20.884	-43.062
^{90}Zr	NV-full	-9.339	18.778	-	-
	NV-exc-only	-8.388	17.320	24.322	-50.041
	PSA-II-full	-11.543	19.038	-	-
	PSA-II-exc-only	-8.389	17.040	23.700	-49.140

A complete self-consistent test should include the exact self-consistent HF calculation and the calculation of several other quantities such as matter, proton and neutron radii, proton and neutron densities. For the single-particle energies, the balance of Hartree to Fock contributions need to be assessed [184]. Still, our preliminary test is consistent with the main conclusion of Ref. [184], viz, the full-DME gives an excess of 1 MeV per particle binding energy compared to exchange-only-DME, irrespective of the performed DME. The exact HF calculations given in Ref. [184] show that the error in the exchange-only-DME (compared to the exact HF of Ref. [184]) are much smaller than that of the full-DME. Consequently, one can obtain a significant reduction of the error in DME approximations by treating the Hartree contribution exactly as exact treatment of the Hartree contribution does not add to the numerical complexity of the problem. Comparing the two DMEs, it can be seen that the difference between the exchange-only versions of NV-DME and PSA-DME-II is marginal, while for the case of the the full-DME version, there is a significant difference with NV-DME being much closer to the exact HF results reported in Ref. [184]. This must be due to the strong parameter dependence and self-consistent error enhancement as the non-self-consistent percentage error from PSA-DME-II (which we called PI-DME) of the Hartree contribution, given in section 5.4.5 is less than that of NV-DME. This requires further investigation.

Chapter 6

Non-Empirical Energy Density Functional from NN interaction

In this chapter, we calculate the HFB energy from a generic two-nucleon interaction that contains central, spin-orbit and tensor components. Furthermore, we apply the DME to the HFB energy to obtain a local EDF. Analytical couplings of the particle-hole (HF) part of the resulting EDF are calculated using the finite-range part of the chiral EFT two-nucleon interaction at N^2LO. Following the usual convention, we represent momentum transfers with q. To avoid ambiguity, the isospin coordinates of the particles are labeled with τ.

6.1 The HF energy from an NN interaction

Starting with a two-body interaction, the Hartree-Fock energy is given, in an arbitrary basis, by

$$E^{NN} = \frac{1}{2}\sum_{ijkl} \sum_{\tau\tau'\tau''\tau'''} \langle i\tau j\tau' | \hat{V} | k\tau'' l\tau''' \rangle \Big(\rho_{k\tau'' i\tau}\, \rho_{l\tau''' j\tau'} - \rho_{l\tau''' i\tau}\, \rho_{k\tau'' j\tau'} \Big), \qquad (6.1)$$

where $\langle i\tau j\tau'|\,\hat{V}\,|k\tau'' l\tau'''\rangle$ are non-antisymmetrized matrix elements of the two-body interaction and $\rho_{i\tau j\tau'}$ denote the one-body density matrix, as defined in Eq. (9.70). Because isospin is presently assumed to be a good quantum number, the density matrix is diagonal in isospin space, $\rho_{k\tau'' i\tau} = \rho^{\tau}_{ki}\,\delta_{\tau''\tau}$. Thus Eq. (6.1) becomes

$$E^{NN} = \frac{1}{2}\sum_{ijkl}\sum_{\tau\tau'}\langle i\tau j\tau'|\,\hat{V}\,|k\tau l\tau'\rangle\,\rho^{\tau}_{ki}\,\rho^{\tau'}_{lj} - \frac{1}{2}\sum_{ijkl}\sum_{\tau\tau'}\langle i\tau j\tau'|\,\hat{V}\,|k\tau' l\tau\rangle\,\rho^{\tau}_{li}\,\rho^{\tau'}_{kj}. \quad (6.2)$$

Using the completeness relationship in the two-body Hilbert space

$$\sum_{\sigma_1\sigma_2}\sum_{\tau_1\tau_2}\int |\,\vec{r}_1\sigma_1\tau_1;\vec{r}_2\sigma_2\tau_2\rangle\,\langle\vec{r}_1\sigma_1\tau_1;\vec{r}_2\sigma_2\tau_2\,|\,d\vec{r}_1 d\vec{r}_2 = \mathbb{1}\,, \quad (6.3)$$

and the definition of the density matrix in $|\vec{r}\rangle\otimes|\vec{\sigma}\rangle\otimes|\vec{\tau}\rangle$ space as given in Eqs. (9.70), the HF energy can also be written as

$$\begin{aligned} E^{NN} &= \frac{1}{2}\sum_{\sigma\tau}\int\prod_{i=1}^{4} d\vec{r}_i\,\langle\vec{r}_1\sigma_1\tau_1\vec{r}_2\sigma_2\tau_2|\hat{V}^{1\otimes 2}|\vec{r}_3\sigma_3\tau_3\vec{r}_4\sigma_4\tau_4\rangle \\ &\quad\times\rho(\vec{r}_3\sigma_3\tau_3,\vec{r}_1\sigma_1\tau_1)\rho(\vec{r}_4\sigma_4\tau_4,\vec{r}_2\sigma_2\tau_2) \\ &= \frac{1}{2}\mathrm{Tr}_1\mathrm{Tr}_2\int\prod_{i=1}^{4} d\vec{r}_i\,\langle\vec{r}_1\vec{r}_2|\hat{V}^{1\otimes 2}|\vec{r}_3\vec{r}_4\rangle\rho^{(1)}(\vec{r}_3,\vec{r}_1)\rho^{(2)}(\vec{r}_4,\vec{r}_2)\,, \end{aligned} \quad (6.4)$$

where $\hat{V}^{1\otimes 2} = \hat{V}(1 - P_{12})$, with P_{12} being the particle exchange operator defined in Table 1.2. A matrix notation is used in the second equation and the traces, denoted by Tr, denote summation over the spin and isospin indices of "particle 1" and "particle 2". The quantity $\rho^{(i)}(\vec{r}_j,\vec{r}_k)$ is defined in Eq. (7.12). As discussed in section 7.1 in relation to a similar calculation for the chiral three-nucleon interaction at N^{2}LO, this notation makes the direct Mathematica implementation of the equations transparent. Refer to that section for details on this notation [1].

In this chapter, we eventually qualify all results for the finite-range (pion-exchange) part of the chiral EFT two-nucleon interaction at N^{2}LO, which is discussed in section 2.4.1. As the HF energy from the contact part is already in a quasi-local (Skyrme-like) form, it does not require the application of the DME. Thus, we do not discuss it any further. The actual expression for the contribution to the EDF from the HF energy of the contact part can be found in Ref. [153].

---

[1] The calculations for the NN case are relatively much simpler than for the NNN case. Consequently, the complete HF + DME calculation was carried out manually in this case.

The application of the DME to the HF energy requires expressing the HF energy in terms of the scalar/vector-isoscalar/isovector components of the OBDM in $|\vec{r}\rangle \otimes |\vec{\sigma}\rangle \otimes |\vec{\tau}\rangle$ space. This is due to the fact that the DME, as formulated in section 5.2, is most intuitively expressed in that space. For its formulation in momentum space, consult Ref. [154]. Hence, we need to perform inverse-Fourier transformation of the chiral interaction given in Eq.(2.14). This results in

$$\begin{aligned}
\langle \vec{R}'\vec{r}'|V|\vec{R}\vec{r}\rangle &= \Big(\big[V_C(r) + \tau_1 \cdot \tau_2 W_C(r)\big] + \big[\, V_S(r) + \tau_1 \cdot \tau_2 W_S(r)\,\big]\, \vec{\sigma}_1 \cdot \sigma_2 \\
&\quad + \big[\, V_T(r) + \tau_1 \cdot \tau_2 W_T(r)\,\big]\, \vec{\sigma}_1 \cdot \vec{\Delta}_r\, \vec{\sigma}_2 \cdot \vec{\Delta}_r + \frac{i}{2}\big[V_{LS}(r) \\
&\quad + \tau_1 \cdot \tau_2 W_{LS}(r)\big]\, (\vec{\sigma}_1 + \vec{\sigma}_2) \cdot (\vec{\Delta}_r \otimes \vec{\Delta}_R) \Big)\, \delta(\vec{r} - \vec{r}')\, \delta(\vec{R} - \vec{R}')\ ,
\end{aligned} \tag{6.5}$$

where $\vec{R}'$, $\vec{R}$ denote the center of mass coordinates, $\vec{r}'$, $\vec{r}$ are the relative coordinates and $\vec{\nabla}_r$ and $\vec{\nabla}_R$ refer to gradients with respect to $\vec{r}$ and $\vec{R}$ respectively. The $\{V_c(r),\ W_c(r), ...\}$ denote the inverse-Fourier transform of the respective form factors given in momentum space [153]

$$V_i(r) = \int \frac{d\vec{q}}{(2\pi)^3}\, e^{i\vec{q}\cdot\vec{r}}\, V_i(q) \quad \text{for } i = C, S, T\ , \tag{6.6}$$

$$= \frac{i}{r^2} \int \frac{d\vec{q}}{(2\pi)^3}\, e^{i\vec{q}\cdot\vec{r}}\, (\vec{q} \cdot \vec{r})\, V_i(q) \quad \text{for } i = LS\ . \tag{6.7}$$

One should note that chiral interactions come with a regulator that cuts off high-momentum components. It should be noted that we have not included regulators in Eqs. (2.14), (2.16), (2.18) and (2.19). The commonly used regulators result in a non-local interaction since $\langle \vec{k}_1'\vec{k}_2' |V| \vec{k}_1\vec{k}_2 \rangle$ which can also be written as $\langle \vec{k}'|V|\vec{k}\rangle$ is replaced with $f(k'/\Lambda)\langle \vec{k}'|V|\vec{k}\rangle f(k/\Lambda)$ for some momentum scale Λ, where $f(k/\Lambda) \to 0$ for $k \gg \Lambda$ and $f(k/\Lambda) \approx 1$ for $k \ll \Lambda$. In contrast, Eq. (6.5) shows that the $|\vec{r}\rangle \otimes |\vec{\sigma}\rangle \otimes |\vec{\tau}\rangle$ space representation of the interaction given in Eq. (2.14), viz, without the regulator, is diagonal and depends on the gradient $\vec{\nabla}$ with respect to $\vec{r}$. The spin-orbit part in Eq. (2.14) is actually the only term that depends on $\vec{\nabla}_{\vec{R}}$. This dependence on $\vec{\nabla}_{\vec{R}}$ is usually remarked by referring to the interaction as quasi-local. In order to obtain a local interaction, one could use a regulator that suppresses large momentum transfers instead of large relative momenta. In any case, we neglect the regulator since we work at the HF level which samples only the low-momentum spectrum of the single-particle Hilbert space. This argument will remain valid as long as the local Fermi momentum $k_F \ll \Lambda$.

6.1.1 HF contribution from a central interaction

A local two-nucleon central interaction can be split into four different spin-isospin channels as

$$\hat{V}_c^{ij} = V_c^{ij}(r)\,\delta(\vec{r}_1 - \vec{r}_3)\,\delta(\vec{r}_2 - \vec{r}_4)\,\Pi_{\sigma_i}\,\Pi_{\tau_j}\,, \tag{6.8}$$

where $i,\, j \,\epsilon\, \{0, 1\}$ denote the singlet and triplet channels, $V_c^{ij}(r)$ is the form factor and Π_{σ_i} and Π_{τ_j} are the spin and isospin projection operators defined in Table 1.2. For the chiral interaction given in Eq. (6.5), the form factors of the central interaction in the different channels is given by

$$V_C^{10}(r) = V_c(r) - 3\,W_c(r) + V_s(r) - 3\,W_s(r)\,, \tag{6.9}$$

$$V_C^{01}(r) = V_c(r) + W_c(r) - 3\,V_s(r) - 3\,W_s(r)\,, \tag{6.10}$$

$$V_C^{11}(r) = V_c(r) + W_c(r) + V_s(r) + W_s(r) \,, \tag{6.11}$$

$$V_C^{00}(r) = V_c(r) - 3\,W_c(r) - 3\,V_s(r) + 9\,W_s(r) \,, \tag{6.12}$$

where $V_c(r)$, $W_c(r), \ldots$ are the coordinate space form factors given by Eq. (6.6)- (6.7).

Starting from Eq. (6.4), the HF energy in the four different channels can be derived by replacing $\hat{V}$ with the corresponding interaction given in Eq. (6.8). The details can be found in appendix 9.6.1. For the spin-triplet and isospin-singlet channel, one has

$$\begin{aligned} E_C^{NN}[10] = \; & \frac{1}{8}\sum_\tau \int d\vec{r}_1\, d\vec{r}_2\, V_C^{10}(\,r\,)\Big[\frac{3}{2}\,\rho_\tau(\vec{r}_1)\,\rho_{\bar{\tau}}(\vec{r}_2) + \frac{3}{2}\,\rho_\tau(\vec{r}_1,\vec{r}_2)\,\rho_{\bar{\tau}}(\vec{r}_2,\vec{r}_1) \\ & + \frac{1}{2}\,\vec{s}_\tau(\vec{r}_1) \cdot \vec{s}_{\bar{\tau}}(\vec{r}_2) + \frac{1}{2}\,\vec{s}_\tau(\vec{r}_1,\vec{r}_2) \cdot \vec{s}_{\bar{q}}(\vec{r}_2,\vec{r}_1)\Big] \,, \end{aligned} \tag{6.13}$$

while for the spin-singlet, isospin-triplet-channel

$$\begin{aligned} E_C^{NN}[01] = \; & \frac{1}{8}\sum_\tau \int d\vec{r}_1\, d\vec{r}_2\, V_C^{01}(\,r\,)\Big[\rho_\tau(\vec{r}_1)\,\rho_\tau(\vec{r}_2) + \rho_\tau(\vec{r}_1,\vec{r}_2)\,\rho_\tau(\vec{r}_2,\vec{r}_1) \\ & - \vec{s}_\tau(\vec{r}_1) \cdot \vec{s}_\tau(\vec{r}_2) - \vec{s}_\tau(\vec{r}_1,\vec{r}_2) \cdot \vec{s}_\tau(\vec{r}_2,\vec{r}_1)\Big] \\ + \; & \frac{1}{8}\sum_\tau \int d\vec{r}_1\, d\vec{r}_2\, V_C^{01}(r)\Big[\frac{1}{2}\,\rho_\tau(\vec{r}_1)\,\rho_{\bar{\tau}}(\vec{r}_2) + \frac{1}{2}\,\rho_\tau(\vec{r}_1,\vec{r}_2)\,\rho_{\bar{\tau}}(\vec{r}_2,\vec{r}_1) \\ & - \frac{1}{2}\,\vec{s}_\tau(\vec{r}_1) \cdot \vec{s}_{\bar{\tau}}(\vec{r}_2) - \frac{1}{2}\,\vec{s}_\tau(\vec{r}_1,\vec{r}_2) \cdot \vec{s}_{\bar{\tau}}(\vec{r}_2,\vec{r}_1)\Big] \,. \end{aligned} \tag{6.14}$$

The HF energy for the triplet-triplet and singlet-singlet channels read

$$\begin{aligned} E_C^{NN}[11] = \; & \frac{1}{8}\sum_\tau \int d\vec{r}_1\, d\vec{r}_2\, V_C^{11}(r)\Big[3\,\rho_\tau(\vec{r}_1)\,\rho_\tau(\vec{r}_2) - 3\,\rho_\tau(\vec{r}_1,\vec{r}_2)\,\rho_\tau(\vec{r}_2,\vec{r}_1) \\ & + \vec{s}_\tau(\vec{r}_1) \cdot \vec{s}_\tau(\vec{r}_2) - \vec{s}_\tau(\vec{r}_1,\vec{r}_2) \cdot \vec{s}_\tau(\vec{r}_2,\vec{r}_1)\Big] \\ + \; & \frac{1}{8}\sum_\tau \int d\vec{r}_1\, d\vec{r}_2\, V_C^{11}(r)\Big[\frac{3}{2}\,\rho_\tau(\vec{r}_1)\,\rho_{\bar{\tau}}(\vec{r}_2) - \frac{3}{2}\,\rho_\tau(\vec{r}_1,\vec{r}_2)\,\rho_{\bar{\tau}}(\vec{r}_2,\vec{r}_1) \\ & + \frac{1}{2}\,\vec{s}_\tau(\vec{r}_1) \cdot \vec{s}_{\bar{\tau}}(\vec{r}_2) - \frac{1}{2}\,\vec{s}_\tau(\vec{r}_1,\vec{r}_2) \cdot \vec{s}_{\bar{\tau}}(\vec{r}_2,\vec{r}_1)\Big] \,, \end{aligned} \tag{6.15}$$

and

$$
\begin{aligned}
E_C^{NN}[00] = \frac{1}{8} \sum_{\tau} \int d\vec{r}_1 \, d\vec{r}_2 \, V^{00}(r) \bigg[& \frac{1}{2} \rho_\tau(\vec{r}_1) \, \rho_{\bar{\tau}}(\vec{r}_2) \; - \; \frac{1}{2} \rho_\tau(\vec{r}_1, \vec{r}_2) \, \rho_{\bar{\tau}}(\vec{r}_2, \vec{r}_1) \\
& - \frac{1}{2} \vec{s}_\tau(\vec{r}_1) \cdot \vec{s}_{\bar{\tau}}(\vec{r}_2) + \frac{1}{2} \vec{s}_\tau(\vec{r}_1, \vec{r}_2) \cdot \vec{s}_{\bar{\tau}}(\vec{r}_2, \vec{r}_1) \bigg] .
\end{aligned}
\tag{6.16}
$$

The corresponding expressions for the finite-range part of the chiral NN interaction at N^2LO can be found by utilizing Eqs. (6.9)-(6.12) in the place of the generic form factors $V^{ij}(r)$. In time reversal invariant systems, the symmetry properties of the one-body density matrix discussed in section 9.2.4 can be used to simplify the expressions. In particular, those terms that depend on the local spin density vanish as $\vec{s}_q(\vec{r}) = 0$ in this case. Finally, it should be mentioned that the channel by channel expressions for the central interaction agree with the unpolarized and symmetric infinite nuclear matter limit of the same expression given in [170].

6.1.2 HF contribution from the spin-orbit interaction

A given quasi-local two-nucleon spin-orbit interaction can be split into its spin-isospin-singlet-triplet channels as

$$
\hat{V}_{LS}^{ij} = -\frac{i}{2} V_{LS}^{ij}(r) \, \delta(\vec{r}_1 - \vec{r}_3) \, \delta(\vec{r}_1 - \vec{r}_3) \, \vec{\nabla} \cdot (\vec{\sigma}_1 + \vec{\sigma}_2) \, \Pi_{\sigma_i} \Pi_{\tau_j} . \tag{6.17}
$$

The spin-orbit orbit interaction vanishes in the spin-singlet channels $|\chi_{singlet}\rangle = 1/\sqrt{2}\left(|\uparrow\downarrow\rangle - |\downarrow\uparrow\rangle\right)$ as $S^2 \, |\chi_{singlet}\rangle = 0$, with two-body spin operator $\vec{S} = (\vec{\sigma}_1 + \vec{\sigma}_2)/2$. For the chiral interaction given in Eq.(6.5), the spin-orbit form factors read

$$
\begin{aligned}
V_{LS}^{10}(r) &= 2 \, V_{LS}(r) - 6 \, W_{LS}(r) \, , \qquad (6.18) \\
V_{LS}^{11}(r) &= 2 \, V_{LS}(r) + 2 \, W_{LS}(r) \, . \qquad (6.19)
\end{aligned}
$$

The HF contribution from the spin-orbit interaction in the spin-triplet and isospin-singlet channel is given by

$$
\begin{aligned}
E_{LS}^{NN}[10] \;=\;& \frac{1}{4}\sum_{\tau}\int d\vec{r}_1\, d\vec{r}_2\, V_{LS}^{10}(r)\, \vec{r}\cdot \left[\vec{J}_\tau(\vec{r}_1)\, \rho_{\bar{\tau}}(\vec{r}_2) \,+\, \vec{s}_\tau(\vec{r}_1) \,\times\, \vec{j}_{\bar{\tau}}(\vec{r}_2)\right] \\
&+\frac{i}{4}\sum_{\tau}\int d\vec{r}_1\, d\vec{r}_2\, V_{LS}^{10}(r)\left[\vec{s}_\tau(\vec{r}_1,\vec{r}_2)\cdot \vec{r}\times \vec{\nabla}_2 \rho_{\bar{\tau}}(\vec{r}_2,\vec{r}_1)\right. \\
&\qquad \left. +\,\rho_\tau(\vec{r}_1,\vec{r}_2)\, \vec{r}\times \vec{\nabla}_2\cdot \vec{s}_{\bar{\tau}}(\vec{r}_2,\vec{r}_1)\right],
\end{aligned}
\tag{6.20}
$$

while in the spin-triplet and isospin-triplet channel, the result reads

$$
\begin{aligned}
E_{LS}^{NN}[11] \;=\;& \frac{1}{2}\sum_{\tau}\int d\vec{r}_1\, d\vec{r}_2\, V_{LS}^{11}(r)\, \vec{r}\cdot \left[\vec{J}_\tau(\vec{r}_1)\, \rho_\tau(\vec{r}_2) \,+\, \vec{s}_\tau(\vec{r}_1) \,\times\, \vec{j}_\tau(\vec{r}_2)\right] \\
&+\;\frac{i}{2}\sum_{\tau}\int d\vec{r}_1\, d\vec{r}_2\, V_{LS}^{11}(r)\left[\vec{s}_\tau(\vec{r}_1,\vec{r}_2)\cdot \vec{r}\times \vec{\nabla}_2 \rho_\tau(\vec{r}_2,\vec{r}_1)\right. \\
&\qquad\qquad \left. +\,\rho_\tau(\vec{r}_1,\vec{r}_2)\, \vec{r}\times \vec{\nabla}_2\cdot \vec{s}_\tau(\vec{r}_2,\vec{r}_1)\right] \\
&+\;\frac{1}{4}\sum_{\tau}\int d\vec{r}_1\, d\vec{r}_2\, V_{LS}^{11}(r)\, \vec{r}\cdot \left[\vec{J}_\tau(\vec{r}_1)\, \rho_{\bar{\tau}}(\vec{r}_2) \,+\, \vec{s}_\tau(\vec{r}_1) \,\times\, \vec{j}_{\bar{\tau}}(\vec{r}_2)\right] \\
&-\;\frac{i}{4}\sum_{\tau}\int d\vec{r}_1\, d\vec{r}_2\, V_{LS}^{11}(r)\left[\vec{s}_\tau(\vec{r}_1,\vec{r}_2)\cdot \vec{r}\times \vec{\nabla}_2 \rho_{\bar{\tau}}(\vec{r}_2,\vec{r}_1)\right. \\
&\qquad\qquad \left. +\,\rho_\tau(\vec{r}_1,\vec{r}_2)\, \vec{r}\times \vec{\nabla}_2\cdot \vec{s}_{\bar{\tau}}(\vec{r}_2,\vec{r}_1)\right].
\end{aligned}
\tag{6.21}
$$

The actual derivation is given in appendix 9.6.2.

6.1.3 HF contribution from the tensor interaction

A local two-nucleon tensor interaction in the four spin-isospin channels is given by

$$
\hat{V}_T^{ij} \;=\; V_T^{ij}(r)\, \delta(\vec{r}_1-\vec{r}_3)\, \delta(\vec{r}_2-\vec{r}_4)\, S_{12}\Pi_{\sigma_i}\, \Pi_{\tau_j}\,, \tag{6.22}
$$

where S_{12} is the tensor operator given in Eq. (2.10). The tensor interaction acts only in the spin-triplet channels. This becomes obvious once S_{12} is written as $S_{12} = 6\,(\vec{S}\cdot\hat{r})^2 - 2\,S^2$, where the total spin operator, $\vec{S}$, has zero expectation value in the spin-singlet state. Hence, concentrating on spin-triplet channels, the chiral NN interaction at N^{2}LO given in Eq.(6.5) has the following components

$$V_T^{10}(r) = \frac{1}{3}V_T(r) - W_T(r)\;, \tag{6.23}$$

$$V_T^{11}(r) = \frac{1}{3}V_T(r) + \frac{1}{3}W_T(r)\;. \tag{6.24}$$

The HF contribution to the energy in the spin-triplet and isospin-singlet channel is given by

$$\begin{aligned} E_T^{NN}[10] = \frac{1}{4}\sum_{\tau}\sum_{\mu\nu}\int d\vec{r}_1\,d\vec{r}_2\,V_T^{10}(r)\Bigg[&\frac{3\,r_\mu\,r_\nu}{r^2}\,s_{\tau,\mu}(\vec{r}_1)\,s_{\bar{\tau},\nu}(\vec{r}_2) - \vec{s}_\tau(\vec{r}_1)\cdot\vec{s}_{\bar{\tau}}(\vec{r}_2) \\ &+ \frac{3\,r_\nu\,r_\mu}{r^2}\,s_{\tau,\mu}(\vec{r}_1,\vec{r}_2)\,s_{\bar{\tau},\nu}(\vec{r}_2,\vec{r}_1) - \vec{s}_\tau(\vec{r}_1,\vec{r}_2)\cdot\vec{s}_{\bar{\tau}}(\vec{r}_2,\vec{r}_1)\Bigg]\;, \end{aligned} \tag{6.25}$$

while for the spin-triplet and isospin-triplet channel

$$\begin{aligned} E_T^{NN}[11] = \frac{1}{2}\sum_{\tau}\sum_{\mu\nu}\int d\vec{r}_1\,d\vec{r}_2\,V_T^{11}(r)\Bigg[&\frac{3\,r_\mu\,r_\nu}{r^2}\,s_{\tau,\mu}(\vec{r}_1)\,s_{\tau,\nu}(\vec{r}_2) - \vec{s}_\tau(\vec{r}_1)\cdot\vec{s}_\tau(\vec{r}_2) \\ &- \frac{3\,r_\mu\,r_\nu}{r^2}\,s_{\tau,\mu}(\vec{r}_1,\vec{r}_2)\,s_{\tau,\nu}(\vec{r}_2,\vec{r}_1) + \vec{s}_\tau(\vec{r}_1,\vec{r}_2)\cdot\vec{s}_\tau(\vec{r}_2,\vec{r}_1)\Bigg] \\ + \frac{1}{4}\sum_{\tau}\sum_{\mu\nu}\int d\vec{r}_1\,d\vec{r}_2\,V_T^{11}(\,r\,)\Bigg[&\frac{3\,r_\mu\,r_\nu}{r^2}\,s_{\tau,\mu}(\vec{r}_1)\,s_{\bar{\tau},\nu}(\vec{r}_2) - \vec{s}_\tau(\vec{r}_1)\cdot\vec{s}_{\bar{\tau}}(\vec{r}_2) \\ &- \frac{3\,r_\mu\,r_\nu}{r^2}\,s_{\tau,\mu}(\vec{r}_1,\vec{r}_2)\,s_{\bar{\tau},\nu}(\vec{r}_2,\vec{r}_1) + \vec{s}_\tau(\vec{r}_1,\vec{r}_2)\cdot\vec{s}_{\bar{\tau}}(\vec{r}_2,\vec{r}_1)\Bigg]. \end{aligned} \tag{6.26}$$

Once more, the relevant expressions for finite-range part tensor part of the chiral NN interaction at N^{2}LO can be obtained by making use of Eqs.(6.23)-(6.24). For time-reversal invariant systems, those terms that depend on the local spin density, $\vec{s}_q(\vec{r})$, vanish. This recovers the expression derived in Ref.[170]. Refer to appendix 9.6.3 for details.

6.1.4 Additional contributions to the HF energy

In addition to the contributions to the HF energy that come from the starting NN interaction, there are several additional terms that are due to the kinetic energy, the center of mass correction and the coulomb interaction. The simplest is the uncorrelated kinetic energy associated with the reference product (HF) state

$$E_{kin} = \frac{\hbar^2}{2m} \sum_{\tau} \int d\vec{r}\, \tau_\tau(\vec{r})\,. \tag{6.27}$$

Since (HF) meanfield solutions are localized in space, translational invariance of the actual nuclear hamiltonian is broken. Consequently, one needs to correct for the center of mass motion, which can be done by defining an intrinsic Hamiltonian [38]. In addition to the the starting Hamiltonian, the intrinsic Hamiltonian contains a correction term E_{CM} which reads

$$E_{CM} = -\frac{\langle\Phi|P^2_{CM}|\Phi\rangle}{2Am} = -\frac{\langle\Phi|(\sum_k \vec{p}_k)^2|\Phi\rangle}{2Am} \tag{6.28}$$

where $\vec{P}_{CM} = \sum_k \vec{p}_k$ is the sum of single-particle momentum operators and A is the number of nucleons and the $|\Phi\rangle$ is the reference independent particle or quasi-particle state. Expressing E_{CM} in terms of densities, one obtains

$$\begin{aligned} E_{CM} &= -\frac{\hbar^2}{2Am}\sum_{\tau}\int d\vec{r}\,\tau_{\tau}(\vec{r}) - \frac{\hbar^2}{2Am}\sum_{\tau\tau'}\int\int d\vec{r}\,d\vec{r}'\,\vec{j}_{\tau}(\vec{r})\cdot\vec{j}_{\tau'}(\vec{r}') \\ &+ \frac{\hbar^2}{2Am}\sum_{\tau\tau'}\int\int d\vec{r}\,d\vec{r}'\,\rho_{\tau}(\vec{r},\vec{r}')\,\tau_{\tau'}(\vec{r},\vec{r}') \\ &+ \frac{\hbar^2}{2Am}\sum_{\tau\tau'}\int\int d\vec{r}\,d\vec{r}'\,\kappa^{*}_{\tau}(\vec{r},\vec{r}')\,\varrho_{\tau}(\vec{r},\vec{r}'). \end{aligned} \qquad (6.29)$$

Several comments are at play concerning such a correction to the the HF energy (i) the first term is a one-body center of mass correction with an overall effect of rescaling the kinetic energy term, E_{kin} (ii) the second term is really local and is zero if the single-particle states have a good parity, which we assume to be the case (iii) the non-local third term is the so-called two-body center of mass correction and is often omitted; if single-particle states have a good parity, the two coupled densities are labeled with opposite parities (iv) the non-local fourth term contributes to the pairing energy appears if one considers a reference independent quasi-particle state. It has never been considered in practical calculations [26]. If the single particle states have a good parity, the two coupled densities are labelled with opposite parities. In its full generality, such a term generates neutron-proton pairing. These nonlocal (the third and fourth) terms will be neglected in our application of the DME.

The last correction arises from the Coulomb repulsion among the protons. It has both direct and exchange parts. The nonlocal exchange contribution is usually approximated with the slater approximation [155]. This is due to the fact that for the long-range Coulomb interaction, the simple slater approximation seems to perform at least as good as the DME techniques discussed in the previous section. Hence, we write the contribution from the Couloumb interaction as the HF energy reads

$$\mathcal{E}_{coul} = \frac{1}{2}e^2\int\int d\vec{r}\,d\vec{r}'\,\frac{\rho_p(\vec{r})\,\rho_p(\vec{r}')}{|\vec{r}-\vec{r}'|} - \frac{3}{4}e^2\left(\frac{3}{\pi}\right)^{1/3}\int d\vec{r}\,\rho_p^{4/3}(\vec{r})\,. \qquad (6.30)$$

6.1.5 The leading-order pairing contribution

The leading-order pairing contribution is obtained by calculating the expectation value of the interaction in a Bogoliubov quasi-particle vacuum. At this point, we enforce several restrictions: (i) we neglect proton-neutron pairing, hence no isospin-singlet contribution. This is justified in most cases as the Fermi energies of protons and neutrons are quite different for most nuclei [38]. (ii) only central interaction is considered, as it is the $^1S_0$ channel that exhausts most of the pairing contribution in nuclei, i.e. the contribution of other partial waves are negligible [117]. Leaving the details to appendix 9.6.4, the spin-singlet isospin-triplet contribution reads

$$\langle \Phi | V_C^{01} | \Phi \rangle_{pair} = \frac{1}{4} \sum_{\tau} \int d\vec{r}_1 \, d\vec{r}_2 \, V_C^{01}(r) \, |\tilde{\rho}_\tau(\vec{r}_1, \vec{r}_2)|^2 \, , \tag{6.31}$$

while for the spin-triplet and isospin-singlet channel, we have

$$\langle \Phi | V_C^{11} | \Phi \rangle_{pair} = \frac{1}{4} \sum_{\tau} \int d\vec{r}_1 \, d\vec{r}_2 \, V_C^{11}(r) \, \vec{\tilde{s}}^*_\tau(\vec{r}_1, \vec{r}_2) \cdot \vec{\tilde{s}}_\tau(\vec{r}_1, \vec{r}_2) \, . \tag{6.32}$$

The Coulomb interaction has an important effect on proton pairing gaps [110]. Specifically, its repulsive nature reduces proton pairing gaps (anti-pairing effect). To calculate these contributions, one simply replaces the form factors, $V_C^{11}(r)$ and $V_C^{01}(r)$, with the corresponding Coulomb interaction form factor.

6.2 Application of the DME to the NN-HF energy

In this section, we apply the DME to the HFB energy derived in the previous section to obtain a local EDF. In section 5.4.6, we have verified that the DME of the Hartree contribution is the main source of the descripancy between the DME-approximation and exact HF, thereby advocating the exact treatment of the Hartree contribution.

Still, for the sake of completeness, we apply the DME to all contributions of the HFB energy: Hartree, Fock and Bogoliubov. As the HFB energy is derived for a generic two-nucleon interaction, we perform the derivation of a local EDF using the modified-Taylor series detailed in appendix 9.5.7. As explained there, all available DMEs, including PSA-DME developed in this work, can be mapped in to this formal expansion.

Since, the starting point is the strict Hartree, Fock and Bogoliubov contributions (diagrams), the energy functional is intrinsically a bilinear functional of ρ and κ i.e.

$$\varepsilon\left[\rho, \kappa, \kappa^*\right] = \varepsilon_k^{\rho} + \varepsilon_{ph}^{\rho\rho} + \varepsilon_{pp}^{\kappa\kappa} + \varepsilon_{cm}^{\rho\rho} + \varepsilon_{coul}^{\rho\rho}, \tag{6.33}$$

where the right hand side corresponds to the uncorrelated kinetic energy, the particle-hole (HF), the particle-particle (Bogoliubov/B), the center of mass and Coulomb corrections. The ρ and κ exponents denote genuine, original dependence on the density matrices. To recap the steps for the application of the DME, first we replace the densities in the HFB energy with their formal expansion given in appendix 9.5.7. This is followed by the simplification of the expression using the angle independence of the $\pi-$ functions and the relations among the $\pi-$functions discussed in section 5.3.6. After neglecting terms with beyond second-order gradients, the particle-hole part of the EDF takes exactly the same form as given by Eq. (4.11), where in this case, the A/B couplings are functionals of the $\pi-$functions and the starting interaction.

Through the DME, finite-range contributions of the starting interactions are encoded into density-dependencies of the EDF couplings. For instance,

$$\begin{aligned} A^{\rho\rho} &= \frac{\pi}{2} \int dr\, r^2 \Big[V_C^{01}(r) \Big(\big(\pi_0^{\rho}(k_F r)\big)^2 + \big(\Pi_0^{\rho}(k_F r)\big)^2 \Big) + 3\, V_C^{11}(r) \Big(\big(\pi_0^{\rho}(k_F r)\big)^2 \\ &\quad - \big(\Pi_0^{\rho}(k_F r)\big)^2 \Big) \Big], \end{aligned} \tag{6.34}$$

where we used the isoscalar k_F as the DME length scale and suppressed the $\vec{R}$ dependence of k_F for brevity. It should be noted that due to the density dependence of the couplings, the usual integration by parts that is used in traditional Skyrme EDFs to reduce the number of independent terms can not be applied here. For instance, in conventional Skyrme EDFs, it is possible to convert the $\rho\Delta\rho$ term of the EDF into $\nabla\rho\nabla\rho$, thereby reducing the number of terms. Generally speaking, this is not possible in the previous case.

The couplings depend on the central, spin-orbit and tensor parts of the interaction as follows

$$\begin{aligned}
\text{Central} \quad &\rightarrow \quad \{ A^{\rho\rho}, A^{ss}, A^{\rho\tau}, A^{\rho\Delta\rho}, A^{\nabla\rho\nabla\rho}, A^{JJ}, A^{s\Delta s}, A^{\nabla s \circ \nabla s}, \\
&\qquad\quad B^{\rho\rho}, B^{ss}, B^{\rho\tau}, B^{\rho\Delta\rho}, B^{\nabla\rho\nabla\rho}, B^{JJ}, B^{s\Delta s}, B^{\nabla s \circ \nabla s} \} \\
\text{Spin-Orbit} \quad &\rightarrow \quad \{ A^{\rho\nabla J}, A^{\nabla\rho J}, B^{\rho\nabla J}, B^{\nabla\rho J} \} \\
\text{Tensor} \quad &\rightarrow \quad \{ A^{JJ}, A^{J\bar{J}}, A^{s\Delta s}, A^{\nabla s\nabla s}, A^{\nabla s \circ \nabla s}, \\
&\qquad\quad B^{JJ}, B^{J\bar{J}}, B^{s\Delta s}, B^{\nabla s\nabla s}, B^{\nabla s \circ \nabla s} \} .
\end{aligned}$$

The complete expression of the couplings is given in appendix 9.6.5.

In the particle-particle (pairing) channel, the application of the DME to the pairing contribution results in a functional that is more complex than the usual phenomenological forms, given in Eq. (4.16). It reads

$$\begin{aligned}
\mathcal{E}_{pp}\big[\rho, \kappa, \kappa^*\big] \;\; \equiv \;\; & \sum_{\tau} \int d\vec{R} \left[A^{\tilde{\rho}\tilde{\rho}} \, |\tilde{\rho}_\tau(\vec{R})|^2 \, + \, A^{\tilde{\rho}\tilde{\tau}} \, \tilde{\rho}_\tau(\vec{R}) \left(\Delta\tilde{\rho}^*_\tau(\vec{R}) - 4\tilde{\tau}^*_\tau(\vec{R}) \right) \right. \\
& + A^{\tilde{\rho}\tilde{\tau}} \, \tilde{\rho}^*_\tau(\vec{R}) \left(\Delta\tilde{\rho}_\tau(\vec{R}) - 4\tilde{\tau}_\tau(\vec{R}) \right) \\
& \left. + A^{\tilde{J}\tilde{J}} \sum_{\mu\nu} \tilde{J}^*_{\tau,\mu\nu}(\vec{R}) \, \tilde{J}_{\tau,\mu\nu}(\vec{R}) \right] ,
\end{aligned} \tag{6.35}$$

where the A^{jj} terms originate from spin-triplet pairing while the rest originate from spin-singlet pairing. The actual expressions for all couplings is given in appendix 9.6.5.

The EDF that results from the correction terms, namely, uncorrelated kinetic energy, center of mass and Coulomb corrections are simply given by

$$\begin{aligned}
\varepsilon_k^{\rho} &= \frac{\hbar^2}{2m}\sum_{\tau}\int d\vec{R}\,\tau_\tau(\vec{R})\ , \\
\varepsilon_{cm}^{\rho\rho} &= -\frac{\hbar^2}{2Am}\sum_{\tau}\int d\vec{R}\,\tau_\tau(\vec{R})\ , \\
\varepsilon_{coul}^{\rho\rho} &= \int d\vec{R}\,\left\{C^{\rho\rho}\,\rho_p\,\rho_p + C^{\rho\Delta\rho}\,\rho_p\,\Delta\,\rho_p + C^{\nabla\rho\nabla\rho}\,\vec{\nabla}\rho_p\cdot\vec{\nabla}\rho_p\right. \\
&\qquad -\frac{3}{4}e^2\left(\frac{3}{\pi}\right)^{1/3}\int d\vec{R}\,\rho_p^{4/3}(\vec{R})\ ,
\end{aligned} \tag{6.36}$$

where as noted in section 6.1.4, we have neglected the third and fourth terms of Eq. (6.29) while its second term vanishes due to the assumption of good parity for the single-particle states. For the Coulomb correction, we have applied the DME to the direct piece, while leaving intact the Slater approximation for the exchange part. The application of the DME to the Hartree contribution is given just for the sake of completeness. In fact, even the exchange contribution from the Coulomb interaction can not be treated accurately due to the long-rangedness of the Coulomb interaction. One can expect the DME of the direct part to be much worse. Still, we give the values for the C couplings in appendix 9.6.5.

6.2.1 Analytical couplings from the chiral EFT NN interaction at N^{2}LO

There are three steps necessary to obtain the analytical calculation of the couplings of the local EDF derived in the previous section. First, we have to restrict the discussion to time-reversal invariant systems as the analytical forms of the π−functions for time-odd densities are not completely determined yet. This is discussed in section 5.3.6 in detail. The next two steps involve (i) fixing the interaction which in this case is the finite-range part of the two-nucleon chiral EFT interaction at N^{2}LO. The respective use of the three-nucleon interaction is the subject of the next chapter. (ii) Specifying the $\pi-$functions. This can be PSA-DME, or any of the other available DMEs. In fact, using different DMEs results in different couplings, which is mentioned in section 8.2 as a way to estimate the error of the DME couplings. In our case, we calculate the couplings for PSA-DME. A similar calculation can easily be done for the original DME of Ref. [170].

The derivation is discussed in appendix 9.6.6. As the final expressions are too lengthy, we discuss only the skeleton expressions of the couplings. For the more on the couplings, consult section 8.1 for a relevant discussion. The lengthy analytic expressions for the DME couplings tend to obscure their underlying structural simplicity. Therefore, it is more illuminating to display the couplings in "skeleton form". Each coupling $C_t^{(i)}$ is given by the sum of the LO ($n = 0$), NLO ($n = 1$), and N^{2}LO ($n = 2$) contributions

$$C_t^{(i)}(u) = \sum_{n=0}^{2} C_{t,n}^{(i)}(u) \quad i \in \{\rho^2, \rho\tau, \rho\Delta\rho, \ldots\}, \tag{6.37}$$

where the dimensionless variable $u \equiv k_F/m_\pi$ and $t = \{0, 1\}$ is the isoscalar/isovector index. The fact that we express the couplings in terms of isoscalar/isovector notation instead of proton-neutron is for conformance with the notation used in the derivations related to the three-nucleon interaction. Refer to [156] as to why the isoscalar/isovector notation is more convenient in that case, and Eqs. (9.72)-(9.75) for the simple algebra relating isoscalar/isovector notation with that of proton-neutron notation. Now, each coupling can be written as

$$C_{t,n}^{(i)}(u) = \sum_j \alpha_j^{(i)}(n,t,u)\mathcal{F}_j(n,u) \tag{6.38}$$

where $\alpha_j^{(i)}(n,t,u)$ are rational polynomials in u and $\mathcal{F}_j(n,u)$ are functions which may exhibit non-analytic behavior in u due to the finite-range of the NN interaction. In the skeleton expressions listed below, we use a more compact notation where the dependence of the α's on u, t, and n is not explicitly shown:

- *LO couplings*

$$C^{(i)} = \alpha_0^{(i)} + \alpha_1^{(i)}\log\bigl(1+4u^2\bigr) + \alpha_2^{(i)}\arctan(2u) \tag{6.39}$$

- *NLO couplings*

$$\begin{aligned} C^{(i)} &= \alpha_0^{(i)} + \alpha_1^{(i)}\left[\log\bigl(1+2u^2+2u\sqrt{1+u^2}\bigr)\right]^2 \\ &\quad + \alpha_2^{(i)}\sqrt{1+u^2}\log\bigl(1+2u^2+2u\sqrt{1+u^2}\bigr) \end{aligned} \tag{6.40}$$

- *N^{2}LO couplings*

$$C^{(i)} = \alpha_0^{(i)} + \alpha_1^{(i)}\log\bigl(1+u^2\bigr) + \alpha_2^{(i)}\arctan(u) \tag{6.41}$$

6.2.2 Single-particle fields and equations of motion

In appendix 9.7, we give the derivation of the single-particle fields and HFB equations of motion that result from the variation of the Skyrme-like EDF given in

Eqs. (4.11),(6.35) and (6.36). Additionally, we give similar derivation for the case where the DME is applied only to the exchange part of the HF energy. As discussed in 5.4.6, all numerical tests are carried out for the case of spherical symmetry. Hence, we give the most simplified single-particle fields and equations of motion that result when spherical symmetry is imposed. Furthermore, the numerical methods used to solve the self-consistent spherical HF equations are also discussed. All this can be found in appendix 9.8.

Chapter 7

Non-Empirical Energy Density Functional from Chiral EFT NNN Interaction at N^{2}LO

In this chapter, we calculate the HF energy from the chiral EFT NNN interaction at N^{2}LO. Next, PSA-DME, formulated and discussed in chapter 4, is generalized in such a way that it becomes applicable to the N^{2}LO chiral EFT NNN HF energy. This is followed by the application of this generalized PSA-DME to obtain a local EDF and the analytical calculation of the couplings. Additionally, we make several references to the actual symbolic implementation of the calculation. Again, following the usual convention, we represent momentum transfers with q. To avoid ambiguity, the isospin coordinates of the particles are labelled with τ.

7.1 The Hartree-Fock energy from Chiral EFT NNN interaction at N^2LO

The consistent application of an MBPT calculation starting from a chiral EFT interaction, at a given order, requires utilizing all the components of the interaction: two- and many-nucleon interactions. As discussed in section 2.4.2, the leading three-nucleon interaction appears at N^2LO in the chiral expansion and it has three main pieces: the three-nucleon contact which is referred to as the E-term, the one-pion exchange plus contact (D-term) and the two-pion exchange which is called the C-term. In this section, we calculate the HF energy from these pieces of the NNN interaction and apply the DME to obtain a quasi-local EDF.

Unlike the NN case, the algebra required to arrive at our final target, namely, a quasi-local EDF, is so complicated that one can simply rule out a manual derivation. This is due to the tremendous size of the algebra required in both layers of the problem. Firstly, we have to derive the exact HF energy in terms of the scalar/vector-isoscalar/isovector parts of the OBDM. This has to be followed by the application of the DME to obtain the final quasi-local EDF.

However, the whole problem displays several features that make it amenable to symbolic automation [151]: (i) it involves many similar and repetitive algebraic steps (ii) most of it does not involve numerical computation, and (iii) the part of it that seems to require numerical computation, such as multidimensional integrals, can be performed using a combination of analytic expansion and symbolic integration. In the following section, the HF energy from chiral EFT NNN interaction at N^2LO is expressed in a form that makes the symbolic implementation transparent. The complete symbolic derivation is discussed in Ref. [156].

Basic form of the HF energy

A three-nucleon interaction can in general be decomposed as a sum of three terms

$$\hat{V}_{3N} \equiv \hat{V}_{12} + \hat{V}_{23} + \hat{V}_{13}\,, \tag{7.1}$$

where $\hat{V}_{ij}$ is symmetric in nucleon i and j. Specifically, for the chiral EFT three-nucleon interaction at N^{2}LO, V_{ij} depends on momentum transfers $\vec{q}_i$ and $\vec{q}_j$ and, in general, on the spin-isospin coordinates of the three nucleons. Refer to section 2.4.2 for details. Starting with the HF energy from a three-nucleon interaction

$$\langle \hat{V}_{3N}^{\rm HF} \rangle = \frac{1}{6} \sum_{ijk} \langle ijk | \hat{V}_{3N} (1 + P_{13}P_{12} + P_{23}P_{12})(1 - P_{12}) | ijk \rangle \,, \tag{7.2}$$

a few basic algebraic manipulations are in order to express the HF energy in terms of only one of the three $\hat{V}_{ij}$ operators, e.g. $\hat{V}_{23}$, as

$$\langle \hat{V}_{3N}^{\rm HF} \rangle = \frac{1}{2} \sum_{ijk} \langle ijk | \hat{V}_{23} (1 - 2\,P_{13} - P_{23} + 2\,P_{12}P_{23}) | ijk \rangle \,, \tag{7.3}$$

where P_{lm} denotes the exchange operator (of particles l and m) defined in Table 1.2 whereas i, j and k denote occupied HF single-particle states. Note that for ease of notation, we are using the single-particle basis that diagonalizes the one-body density matrix of the HF Slater determinant.

One can identify three groups of terms in Eq. (7.3): direct, single-exchange and double-exchange terms[1]. The direct term corresponds to the expectation value of $\hat{V}_{23}$, the single-exchange term to the expectation value of $\hat{V}_{23}(-2\,P_{13} - P_{23})$ and the double-exchange term to that of $2\,\hat{V}_{23}P_{12}P_{23}$

---

[1] This should not be confused with one- and two-pion exchanges contribution to the three-nucleon interaction.

$$\begin{aligned} \langle V_{3N}^{\mathrm{HF,dir}} \rangle &\equiv \frac{1}{2}\sum_{ijk} \langle ijk|\hat{V}_{23}|ijk\rangle\,, && (7.4)\\ \langle V_{3N}^{\mathrm{HF,1x}} \rangle &\equiv \frac{1}{2}\sum_{ijk} \langle ijk|\hat{V}_{23}(-2P_{13}-P_{23})|ijk\rangle\,, && (7.5)\\ \langle V_{3N}^{\mathrm{HF,2x}} \rangle &\equiv \sum_{ijk} \langle ijk|\hat{V}_{23}P_{12}P_{23}|ijk\rangle\,. && (7.6) \end{aligned}$$

As the derivation of the Skyrme-like quasi-local EDF from the exact HF energy requires the application of the DME, we need to express the HF energy in the $|\vec{r}\rangle \otimes |\vec{\sigma}\rangle \otimes |\vec{\tau}\rangle$ single-particle basis. Hence, we perform inverse-Fourier transformation of the interaction. This transformation leaves the spin-isospin dependencies untouched. Furthermore, just as in the case of the NN interaction, the fact that the calculation is confined to the HF contribution enables us to neglect the regulator so long as $k_F << \Lambda$, the momentum cutoff scale. The absence of the regulator makes the interaction local in coordinate space and simplifies the form of the interaction in $|\vec{r}\rangle \otimes |\sigma\rangle \otimes |\tau\rangle$ space. Confining the discussion to the spatial dependence, we have

$$\begin{aligned} \langle \vec{r}_1\vec{r}_2\vec{r}_3|\hat{V}_{23}|\vec{r}_1^{\,\prime}\vec{r}_2^{\,\prime}\vec{r}_3^{\,\prime}\rangle &= \delta(\vec{r}_1-\vec{r}_1^{\,\prime})\,\delta(\vec{r}_2-\vec{r}_2^{\,\prime})\,\delta(\vec{r}_3-\vec{r}_3^{\,\prime})\\ &\quad\times \mathbb{V}_{23}(\vec{r}_2-\vec{r}_1,\vec{r}_3-\vec{r}_1)\,, \qquad (7.7) \end{aligned}$$

where

$$\mathbb{V}_{23}(\vec{r}_2-\vec{r}_1,\vec{r}_3-\vec{r}_1) \equiv \frac{1}{(2\pi)^6}\int d\vec{q}_2 d\vec{q}_3\, e^{i\vec{q}_2\cdot(\vec{r}_2-\vec{r}_1)}\, e^{i\vec{q}_3\cdot(\vec{r}_3-\vec{r}_1)}\, V_{23}(\vec{q}_2,\vec{q}_3)\,. \qquad (7.8)$$

At this point, we do not actually perform the integrals over the momentum coordinates in Eq (7.8), except for the E-term of the interaction which is a trivial three-nucleon contact interaction, thereby yielding simple delta functions as shown in Eq. (9.347). Rather, Eq. (7.8) is used as it is, resulting in fifteen-dimensional integrals in Eqs. (7.13)-(7.15). As discussed in section 7.2, the application of the DME prior to the actual multi-dimensional integrations is crucial.

The next target is to rewrite Eqs. (7.4)-(7.6) in a form transparent for Mathematica implementation. We illustrate the steps required to achieve that with Eq. (7.6), for which we have

$$\begin{aligned}
\langle V_{3N}^{\mathrm{HF,2x}} \rangle &\equiv \sum_{ijk} \langle ijk|\hat{V}_{23} P_{12} P_{23}|ijk\rangle \\
&= \sum_{ijk} \sum_{\sigma'_1..\sigma_3} \sum_{\tau'_1..\tau_3} \int \prod_{m=1}^{3} d\vec{r}'_m \prod_{n=1}^{3} d\vec{r}'_n \, \langle ijk|\vec{r}'_1\sigma'_1\tau'_1 \, \vec{r}'_2\sigma'_2\tau'_2 \, \vec{r}'_3\sigma'_3\tau'_3\rangle \\
&\quad \times \langle \vec{r}'_1\sigma'_1\tau'_1 \, \vec{r}'_2\sigma'_2\tau'_2 \, \vec{r}'_3\sigma'_3\tau'_3|\hat{V}_{23} P_{12}^{\sigma\tau} P_{23}^{\sigma\tau}|\vec{r}_1\sigma_1\tau_1 \, \vec{r}_2\sigma_2\tau_2 \, \vec{r}_3\sigma_3\tau_3\rangle \\
&\quad \times \langle \vec{r}_1\sigma_1\tau_1 \, \vec{r}_2\sigma_2\tau_2 \, \vec{r}_3\sigma_3\tau_3|P_{12}^{\vec{r}} P_{23}^{\vec{r}}|ijk\rangle \,, \qquad (7.9)
\end{aligned}$$

where we used completeness relations in the three Hilbert space

$$\sum_{\sigma_1..\sigma_3} \sum_{\tau_1..\tau_3} \int \prod_{i=1}^{3} d\vec{r}_i \, |\vec{r}_1\sigma_1\tau_1 \, \vec{r}_2\sigma_2\tau_2 \, \vec{r}_3\sigma_3\tau_3\rangle \langle \vec{r}_1\sigma_1\tau_1 \, \vec{r}_2\sigma_2\tau_2 \, \vec{r}_3\sigma_3\tau_3| = \mathbb{1} \,, \qquad (7.10)$$

and $P_{lm}^{\sigma\tau} \equiv P_{lm}^{\sigma} P_{lm}^{\tau}$. We split the particle-exchange operator such that the coordinate part acts on the wave-functions while the spin-isospin piece is taken care of along with the interaction. Let $\vec{X}_i$ represent $(\vec{r}_i\sigma_i\tau_i)$ such that the one-body density matrix reads as

$$\varrho(\vec{X}_j, \vec{X}_k) \equiv \varrho(\vec{r}_j\sigma_j\tau_j, \vec{r}_k\sigma_k\tau_k) \equiv \sum_i \varphi_i^*(\vec{r}_k \, \sigma_k \, \tau_k) \, \varphi_i(\vec{r}_j \, \sigma_j \, \tau_j) \,, \qquad (7.11)$$

where the sums is over occupied single-particle HF states. Making use of this, we define another quantity, which we call the auxiliary density matrix, as

$$\varrho^i(\vec{X}_j, \vec{X}_k) \equiv \varrho\,(\vec{r}_j\sigma'_i\tau'_i, \vec{r}_k\sigma_i\tau_i) \,, \qquad (7.12)$$

where $i \in \{1, 2, 3\}$. Basically, the spin-isospin coordinates of this quantity are those of the i^{th} particle. Applying the steps demonstrated in Eq. (7.9) and using Eqs. (7.12), (7.7)-(7.8), one can express the direct, single-exchange and double-exchange parts of the three-nucleon interaction HF energy as

$$\begin{aligned}
\langle V_{3N}^{\text{HF,dir}} \rangle &= \frac{1}{2} \mathrm{Tr}_1 \mathrm{Tr}_2 \mathrm{Tr}_3 \Bigg[\int d\vec{r}_1 d\vec{r}_2 d\vec{r}_3 \, \varrho^1(\vec{X}_1) \, \varrho^2(\vec{X}_2) \, \varrho^3(\vec{X}_3) \\
&\qquad \times \mathbb{V}_{23}(\vec{r}_2 - \vec{r}_1, \vec{r}_3 - \vec{r}_1) \Bigg] \,, \qquad (7.13) \\
\langle V_{3N}^{\text{HF,1x}} \rangle &= - \mathrm{Tr}_1 \mathrm{Tr}_2 \mathrm{Tr}_3 \Bigg[\int d\vec{r}_1 d\vec{r}_2 d\vec{r}_3 \, \varrho^1(\vec{X}_3, \vec{X}_1) \, \varrho^2(\vec{X}_2) \, \varrho^3(\vec{X}_1, \vec{X}_3) \\
&\qquad \times \mathbb{V}_{23}(\vec{r}_2 - \vec{r}_1, \vec{r}_3 - \vec{r}_1) \, P_{13}^{\sigma\tau} \Bigg] \\
&\quad - \frac{1}{2} \mathrm{Tr}_1 \mathrm{Tr}_2 \mathrm{Tr}_3 \Bigg[\int d\vec{r}_1 d\vec{r}_2 d\vec{r}_3 \, \varrho^1(\vec{X}_1) \, \varrho^2(\vec{X}_3, \vec{X}_2) \, \varrho^3(\vec{X}_2, \vec{X}_3) \\
&\qquad \times \mathbb{V}_{23}(\vec{r}_2 - \vec{r}_1, \vec{r}_3 - \vec{r}_1) \, P_{23}^{\sigma\tau} \Bigg] \,, \qquad (7.14) \\
\langle V_{3N}^{\text{HF,2x}} \rangle &= \mathrm{Tr}_1 \mathrm{Tr}_2 \mathrm{Tr}_3 \int d\vec{r}_1 d\vec{r}_2 d\vec{r}_3 \Bigg[\varrho^1(\vec{X}_2, \vec{X}_1) \, \varrho^2(\vec{X}_3, \vec{X}_2) \, \varrho^3(\vec{X}_1, \vec{X}_3) \\
&\qquad \times \mathbb{V}_{23}(\vec{r}_2 - \vec{r}_1, \vec{r}_3 - \vec{r}_1) \, P_{23}^{\sigma\tau} P_{12}^{\sigma\tau} \Bigg] \,, \qquad (7.15)
\end{aligned}$$

where $\varrho^i(\vec{X}_j) \equiv \varrho^i(\vec{X}_j, \vec{X}_j)$ and Tr_i refers to tracing over spin and isospin coordinates of the i^{th} particle. The key to understand the form of these equations is the splitting of the particle exchange operator, performed in Eqs. (7.9), that results in the spin-isospin coordinates of each particle to be grouped in a single auxiliary density matrix. These are the basic equations that are implemented directly in Mathematica. In Ref. [156], it is shown that the implementation of these equations is transparent, viz, directly interpretable to the language that Mathematica understands. This would not have been the case without the trick used to group spin-isospin coordinates of each particle in a single auxiliary density matrix, Eq. (7.12).

The following sections state the contributions to the HF energy of time-reversal invariant systems from the E-, D- and C-terms of the chiral EFT NNN interaction at N^2LO. The complete expressions where the assumption of time-reversal invariance is relaxed are given in appendix 9.9. Even for time-reversal invariant systems, some of the expressions are too long. In those cases, the expressions are relegated to the same appendix, where we also give the corresponding results for INM and PNM (pure neutron matter).

Prior to delving in to the details of the expressions, the following observations can be made regarding the HF energy: (i) Each term in the energy expression should contain three local/nonlocal densities. (ii) As discussed in appendix 9.2.4, the various local and non-local densities that result from the one-body density matrix have specific time-reversal properties. Hence, considering that energy is a time-reversal invariant quantity, there can be no term that contains one/three time-odd densities. Note that at the level of exact HF, the only time-odd density that we have is the local spin density, $\vec{s}_q(\vec{r})$. Nonetheless, the application of the DME extends this set to include all the time-odd densities that are discussed in appendix 9.2.4. (iii) The fact that the starting interaction is isospin invariant makes the energy isospin invariant as well. Therefore, there can be no term in the energy expression that contains one/three isovector densities. (iv) For each part of the interaction, there are the direct, single- and double-exchange contributions as given by Eqs. (7.13)-(7.15).

Finally, we remark that the HF expressions and the resulting quasi-local EDF from the chiral EFT NNN interaction at N^2LO are given in terms of isoscalar-isovector notation instead of proton-neutron notation. In Ref. [156] where we discuss the Mathematica implementation, it is shown that the isovector-isoscalar notation is better suited to the implementation. Finally, keeping in mind that the NNN chiral EFT interaction at N^2LO does not have isospin invariance breaking terms, the isospin invariance of the energy expressions of both exact HF and quasi-local EDF become transparent in isoscalar-isovector notation.

HF energy from the E-term

The actual operator structure and analytical form of the E-term of the chiral EFT NNN interaction at N^{2}LO are given in Eq. (2.16). The HF energy that results from it for time-reversal invariant systems is given as

$$\langle V_{3N}^{\mathrm{HF},E,\mathrm{TRI}} \rangle = -\frac{3}{16} E \int d\vec{r} \left(\rho_0^3(\vec{r}) - \rho_0(\vec{r})\rho_1^2(\vec{r}) \right) . \qquad (7.16)$$

As expected due to its complete zero-range character, the HF energy from the E-term is already in the form of a local EDF. Consequently, it does not require the application of the DME. It should be noted that the E-term has a direct counterpart in the Skyrme interaction, Eq. (4.12). In most phenomenological Skyrme EDFs, the density dependence is in the form of $\rho_0^\gamma(\vec{r})$ where γ takes a fractional value [26], while the one that results from the E-term has $\gamma = 1$.

Three-nucleon contact interaction requires the three nucleons to have the same coordinate $\vec{r}$, which implies that three neutrons or three protons cannot interact via a contact interaction, due to Pauli's exclusion principle. Indeed, Eq. (9.346) shows that $V_{EN}^{\mathrm{HF},E,\mathrm{PNM}}$ vanishes for pure neutron matter and likewise for pure proton matter (though pure proton matter can not exist as it is not energetically stable).

HF energy from the D-term

The operator structure and analytical expression of the D-term of the chiral EFT NNN interaction at N^{2}LO are given in Eq. (2.18). Its contribution to the HF energy is nonlocal due to the finite-range pion-exchange part of the interaction. In time-reversal invariant systems, the HF energy contribution from the D-term takes the form

$$\langle V_{3N}^{\mathrm{HF},D,\mathrm{TRI}} \rangle = \frac{-g_A}{4f_\pi^2} \frac{C_D}{f_\pi^2 \Lambda_x} \frac{1}{16} \int d\vec{r}_2 d\vec{r}_3 \int \frac{1}{(2\pi)^3} d\vec{q}_3 \, e^{i\vec{q}_3 \cdot (\vec{r}_3 - \vec{r}_2)} \, \frac{q_3^\beta q_3^\gamma}{q_3^2 + m_\pi^2}$$

$$
\begin{aligned}
&\times \Big[-3\,\delta_{\beta\gamma}\,\rho_0(\vec{r}_2)\rho_0(\vec{r}_2,\vec{r}_3)\rho_0(\vec{r}_3,\vec{r}_2) \\
&+ 2\,\delta_{\beta\gamma}\,\rho_0(\vec{r}_2)\rho_1(\vec{r}_2,\vec{r}_3)\rho_1(\vec{r}_3,\vec{r}_2) \\
&+ \delta_{\beta\gamma}\,\rho_1(\vec{r}_2)\rho_0(\vec{r}_2,\vec{r}_3)\rho_1(\vec{r}_3,\vec{r}_2) \\
&- 3\,\rho_0(\vec{r}_2)s_0^{\beta}(\vec{r}_2,\vec{r}_3)s_0^{\gamma}(\vec{r}_3,\vec{r}_2) \\
&+ 3\,\epsilon^{\alpha\gamma\nu}\,\epsilon^{\omega\beta\nu}\,\rho_0(\vec{r}_2)s_0^{\alpha}(\vec{r}_2,\vec{r}_3)s_0^{\omega}(\vec{r}_3,\vec{r}_2) \\
&+ \rho_0(\vec{r}_2)s_1^{\beta}(\vec{r}_2,\vec{r}_3)s_1^{\gamma}(\vec{r}_3,\vec{r}_2) \\
&- \epsilon^{\alpha\gamma\nu}\,\epsilon^{\omega\beta\nu}\,\rho_0(\vec{r}_2)s_1^{\alpha}(\vec{r}_2,\vec{r}_3)s_1^{\omega}(\vec{r}_3,\vec{r}_2) \\
&+ 2\,\rho_1(\vec{r}_2)s_0^{\beta}(\vec{r}_2,\vec{r}_3)s_1^{\gamma}(\vec{r}_3,\vec{r}_2) \\
&- 2\,\epsilon^{\alpha\gamma\nu}\,\epsilon^{\omega\beta\nu}\,\rho_1(\vec{r}_2)s_0^{\alpha}(\vec{r}_2,\vec{r}_3)s_1^{\omega}(\vec{r}_3,\vec{r}_2) \Big] \,. \qquad (7.17)
\end{aligned}
$$

The multi-dimensional integrals that occur in the HF energy are tackled only after the application of the DME. As can be seen, each term in Eq. (7.17) is composed of one local and two nonlocal densities. This can be traced to the fact the D-term of the interaction combines a contact term and pion-exchange interaction.

HF energy from the C-term

The operator structure and analytical form of the C-term of the chiral EFT NNN interaction at $\mathrm{N}^2\mathrm{LO}$ are given in Eq. (2.19). The HF energy from the C-term can be grouped into two categories: a D-like term and remaining terms (which we call R-part). This grouping originates from the operator structure of $F_{ijk}^{\alpha\beta}$ given in Eq.(2.20). The D-like term is associated with $\delta_{\alpha\beta}\left[-4\frac{c_1 m_\pi^2}{f_\pi^2} + 2\frac{c_3}{f_\pi^2}\vec{q}_i \cdot \vec{q}_j\right]$ whereas the R-part relates to $\frac{c_4}{f_\pi^2}\epsilon^{\alpha\beta\gamma}\tau_k^{\gamma}\,\vec{\sigma}_k \cdot (\vec{q}_i + \vec{q}_j)$. For time-reversal invariant systems, the HF energy contribution from the C-term is relegated to appendix 9.9.4 due to its length. Rather, out of line with the previous sections, the contribution of the C-term to the HF energy in the particular case of symmetric INM is given by

$$\begin{aligned}\langle V_{3N}^{\mathrm{HF,C,INM}}\rangle &= \left(\frac{g_A}{2f_\pi}\right)^2 \frac{3}{16}\int d\vec{r}_1 d\vec{r}_2 d\vec{r}_3 \int \frac{1}{(2\pi)^6} d\vec{q}_2 d\vec{q}_3\, e^{i\vec{q}_2\cdot(\vec{r}_2-\vec{r}_1)}\, e^{i\vec{q}_3\cdot(\vec{r}_3-\vec{r}_1)} \\ &\times \frac{q_2^{\beta_1} q_3^{\gamma_1}}{(q_2^2+m_\pi^2)(q_3^2+m_\pi^2)} \Bigg[\left(-4\frac{c_1 m_\pi^2}{f_\pi^2} + 2\frac{c_3}{f_\pi^2}\vec{q}_2\cdot\vec{q}_3\right) \\ &\Big(-2\,\delta_{\beta_1\gamma_1}\,\rho_0(\vec{r}_1)\rho_0(\vec{r}_3,\vec{r}_2)\rho_0(\vec{r}_2,\vec{r}_3) \\ &\quad + \delta_{\beta_1\gamma_1}\,\rho_0(\vec{r}_1,\vec{r}_3)\rho_0(\vec{r}_2,\vec{r}_1)\rho_0(\vec{r}_3,\vec{r}_2)\Big) \\ &- 2\frac{c_4}{f_\pi^2}\,\epsilon^{\beta_1\gamma_1\nu}\epsilon^{\beta_2\gamma_2\nu}\, q_2^{\beta_2} q_3^{\gamma_2}\,\rho_0(\vec{r}_1,\vec{r}_3)\rho_0(\vec{r}_2,\vec{r}_1)\rho_0(\vec{r}_3,\vec{r}_2)\Bigg]. \qquad (7.18)\end{aligned}$$

Even though the full complexity of the expression for time-reversal finite systems, let alone non-time-reversal systems, cannot be appreciated by analyzing Eq.(7.18), one can still make a few observations. To start with, the complete reduction of the expression to a local EDF requires calculating twelve dimensional integrals, after the application of the DME. This is due to there being three position and two momentum coordinates, while a local EDF allows only one position coordinate in the energy density. This is in contrast to the E-term contribution which is already in a local EDF form and the D-term where one has to calculate five dimensional integrals. The details of the DME technique used that preceeds the multi-dimensional integrations and the specific analytical and symbolic approaches used for the multi-dimensional integration are discussed in the next several sections.

7.2 DME for the HF energy from chiral EFT N^{2}LO 3NF in time-reversal invariant systems

In this section, restricting the discussion to time-reversal invariant systems, we apply the DME to the HF energy from chiral EFT 3NF at N^{2}LO. In contrast to the application of the DME to the HF energy from NN interactions, the task at hand is complicated by several factors. Firstly, the usual choice of DME-coordinates as the relative and center of mass coordinates, of the three-nucleons in this case, turns out to be of little use. Secondly, the HF energy from local NNN interactions in general depend on three-coordinates. This is also the case for NNN chiral EFT interaction at N^2LO. Hence, there are two-nonlocality coordinates which should be integrated out in the final energy density. Finally, the complexity of the starting HF energy expression, even for the case of time-reversal invariant systems, renders manual derivation impractical. In order to mitigate these complexifying factors, it is imperative that we organize the HF energy expression in a systematic manner.

Even though one has a large number of seemingly different terms coming from HF contribution of the C and D-terms of the NNN chiral EFT interaction, it is possible to group these terms into three generic classes. Note that the E-term results in a local EDF without the application of the DME, and thus we do not refer to it in this section[2]. This systematic organization of the HF energy is done with the aim of identifying the optimal DME-coordinate system. What makes this systematic organization possible is the fact that, after the expansion of each local/nonlocal density, the DME requires only angle integrations irrespective of the nature of the densities involved. Certainly, each density has its own $\pi-$functions, but this does not undermine the previous statement.

7.2.1 Generic forms of the 3NF energy expressions

There are only three generic forms that appear in the HF energy from chiral EFT 3NF at N^2LO. These are listed in Eqs.(7.19), (7.20) and (7.21). In listing these expressions, the conventions used are that (i) all numerical and constant coefficients have been dropped, (ii) $\varsigma^{\mu}1, \varsigma^{\mu}2, \varsigma^{\mu}3$ can be any of the scalar/vector, isoscalar/isovector densities,

---

[2] Its contribution to the final contributions will be simply added at the end.

(iii) the tensors $T^{\mu_1\mu_2\mu_3}_{\beta_1\gamma_1\beta_2\gamma_2}$ and $T^{\mu_1\mu_2\mu_3}_{\beta\gamma}$ may not depend on μ_1, μ_2, or μ_3, then that particular index is dropped from T. This is the case when the corresponding density is a scalar density, $\rho_{0/1}$. For instance, if ς^{μ_2} is a scalar density, then the tensor T will not depend on μ_2. Hence, it will take the form $T^{\mu_1\mu_3}_{\beta_1\gamma_1\beta_2\gamma_2}$ or $T^{\mu_1\mu_3}_{\beta_1\gamma_1}$. This unconventional notation has been chosen to treat the scalar and vector densities with the same routine in Mathematica.

Generic-Form-1

The generic form of this group of terms is

$$\begin{aligned}\langle V_{3N}^{\mathrm{HF},G1}\rangle &= \int d\vec{r}_1 d\vec{r}_2 d\vec{r}_3 \int d\vec{q}_2 d\vec{q}_3\, e^{i\vec{q}_2\cdot(\vec{r}_2-\vec{r}_1)} e^{i\vec{q}_3\cdot(\vec{r}_3-\vec{r}_1)} \frac{q_2^{\beta_1} q_3^{\gamma_1}}{(q_2^2+m_\pi^2)(q_3^2+m_\pi^2)} \\ &\quad \times \left[c_1\, T^{\mu_1\mu_2\mu_3}_{\beta_1\gamma_1} + c_2\, \vec{q}_2\cdot\vec{q}_3\, T^{\mu_1\mu_2\mu_3}_{\beta_1\gamma_1} + c_3\, q_2^{\beta_2} q_3^{\gamma_2}\, T^{\mu_1\mu_2\mu_3}_{\beta_1\gamma_1\beta_2\gamma_2} \right] \\ &\quad \times \varsigma^{\mu_1}(\vec{r}_1,\vec{r}_3)\varsigma^{\mu_2}(\vec{r}_2,\vec{r}_1)\varsigma^{\mu_3}(\vec{r}_3,\vec{r}_2)\,, \qquad (7.19)\end{aligned}$$

where c_1, c_2 and c_3 are either zero or one. The double-exchange of the C-term (both D-like and R-part) is the sole origin of this type of terms.

Generic-Form-2

The generic form of this group of terms is

$$\begin{aligned}\langle V_{3N}^{\mathrm{HF},G2}\rangle &= \int d\vec{r}_1 d\vec{r}_2 d\vec{r}_3 \int d\vec{q}_2 d\vec{q}_3\, e^{i\vec{q}_2\cdot(\vec{r}_2-\vec{r}_1)} e^{i\vec{q}_3\cdot(\vec{r}_3-\vec{r}_1)} \frac{q_2^{\beta} q_3^{\gamma}(c_1 + c_2\,\vec{q}_2\cdot\vec{q}_3)}{(q_2^2+m_\pi^2)(q_3^2+m_\pi^2)} \\ &\quad \times T^{\mu_1\mu_2\mu_3}_{\beta\gamma} \left[\varsigma^{\mu_1}(\vec{r}_1)\varsigma^{\mu_2}(\vec{r}_2,\vec{r}_3)\varsigma^{\mu_3}(\vec{r}_3,\vec{r}_2) \right], \qquad (7.20)\end{aligned}$$

where c_1 and c_2 are either zero or one. The single-exchange of the C-term is the origin of this type of terms.

Generic-Form-3

The generic form of this group of terms is

$$\begin{aligned} \langle V_{3N}^{\mathrm{HF},G3} \rangle &= \int d\vec{r}_2 d\vec{r}_3 \int d\vec{q}_3\, e^{i\vec{q}_3\cdot(\vec{r}_3-\vec{r}_2)} \frac{q_3^\beta q_3^\gamma}{q_3^2+m_\pi^2} T_{\beta\gamma}^{\mu_1\mu_2\mu_3} \\ &\quad \times \left[\varsigma^{\mu_1}(\vec{r}_2)\varsigma^{\mu_2}(\vec{r}_2,\vec{r}_3)\varsigma^{\mu_3}(\vec{r}_3,\vec{r}_2) \right]. \end{aligned} \tag{7.21}$$

The D-term is the only origin of this type of terms.

7.2.2 The DME-coordinate system

Most of the complexifying factors in the application of DME to the HF energy from the chiral EFT NNN interaction at N^{2}LO can be mitigated by the proper choice of a DME-coordinate system. There are several qualities that we require from a viable DME-coordinate system. As discussed in section 5.3.7, the expansion of local densities is problematic. Hence, the DME-coordinate system should reduce the need for the expansion of the local densities. The other quality required of the coordinate system relates to the need to have analytical expressions for the couplings of the resulting EDF. This is a requirement in so far as there is no apparent reduction in the accuracy of the whole approximation. Finally, and related to the previous point, the coordinate system should be such that the amount of mathematical manipulation required to arrive at the final result is manageable.

These requirements rule out the usual relative and center of mass coordinates of the three-nucleon system. Likewise, the three-body Jacobi coordinates are found to be non-optimal. Rather, the coordinate system that we use is

$$\begin{aligned} \vec{x}_2 &= \vec{r}_2 - \vec{r}_1 \\ \vec{x}_3 &= \vec{r}_3 - \vec{r}_1 \end{aligned}$$

$$\vec{r}_1 = \vec{r}_1 , \tag{7.22}$$

which implies that we are expanding about the coordinate of the first particle, $\vec{r}_1$. While this choice is directly applicable to generic forms given in Eqs. (7.19) and (7.20), for that of Eq.(7.21), one simply sets $\vec{r}_1 = \vec{r}_2$ which results in $\vec{x}_2 = 0$. The main advantages of this coordinate system are:(i) It allows exact integration of the factors resulting from the interaction, with any approximation being confined to the expansion of the densities. This implies that this work can be modified and/or extended by simple modification of the expansion of the densities. This point is discussed in section 9.10.1. (ii) The chosen coordinate system enables one to apply the DME only to the nonlocal densities that occur in the HF energy expression.

7.2.3 Generalized PSA-DME

Using the coordinate system specified in Eq. (7.22), the non-local densities that appear in Eqs. (7.19)-(7.21) are of the form $\varsigma^{\mu 1}(\vec{r}_1, \vec{r}_1 + \vec{x}_3)$, $\varsigma^{\mu 2}(\vec{r}_1 + \vec{x}_2, \vec{r}_1)$ and $\varsigma^{\mu 3}(\vec{r}_1 + \vec{x}_3, \vec{r}_1 + \vec{x}_2)$. These non-local densities can be scalar/vector, isoscalar/isovector. The generalized PSA-DME aims at approximating each of these non-local densities in terms of local densities, dependent on $\vec{r}_1$, and $\pi-$functions which can depend on $\vec{x}_2$ and/or $\vec{x}_3$.

A detailed discussion on the generalized PSA-DME of these nonlocal densities is given in appendix 9.5.3. Reproducing the main results, the PSA-DME of the nonlocal densities that occur in the HF energy from chiral EFT three-nucleon interaction at N^{2}LO take the form

$$\begin{aligned}\rho_q(\vec{r}_1, \vec{r}_1 + \vec{x}_2) &= \Pi_0^\rho(k_F^q x_2)\,\rho_q(\vec{r}_1) + \frac{x_2^2}{6}\,\Pi_2^\rho(k_F^q x_2)\left(\frac{1}{2}\,\Delta\rho_q(\vec{r}_1) - \tau_q(\vec{r}_1)\right.\\ &\left. + \frac{3}{5} k_F^{q\,2}\,\rho_q(\vec{r}_1)\right),\end{aligned} \tag{7.23}$$

with the same form holding for $\rho_q(\vec{r}_1, \vec{r}_1 + \vec{x}_3)$. From the time-reversal property of the scalar part of the OBDM stated in Eq. (9.85), $\rho_q(\vec{r}_1 + \vec{x}_2, \vec{r}_1) = \rho_q(\vec{r}_1, \vec{r}_1 + \vec{x}_2)$. Hence, their DME can be obtained from Eq. (7.23). The DME of $\rho_q(\vec{r}_1 + \vec{x}_2, \vec{r}_1 + \vec{x}_3)$, which involves two nonlocality coordinates, $\vec{x}_2$ and $\vec{x}_3$, is given by

$$\begin{aligned}
\rho_q(\vec{r}_1 + \vec{x}_2, \vec{r}_1 + \vec{x}_3) &= \Pi_0^{\rho}(k_F^q x)\Big(\rho_q(\vec{r}_1) + \vec{X} \cdot \vec{\nabla}_1 \rho_q(\vec{r}_1) + \frac{1}{2}\big(\vec{X} \cdot \vec{\nabla}_1\big)^2 \rho_q(\vec{r}_1)\Big) \\
&\quad + \frac{x^2}{6}\,\Pi_2^{\rho}(k_F^q x)\Big((a^2 - a + \frac{1}{2})\Delta\rho_q(\vec{r}_1) - \tau_q(\vec{r}_1) \\
&\quad + \frac{3}{5} k_F^{q\,2} \rho_q(\vec{r}_1)\Big), \qquad (7.24)
\end{aligned}$$

where the coordinates $\vec{x}$ and $\vec{X}$ are given by $\vec{x} = \vec{x}_2 - \vec{x}_3$ and $\vec{X} = (1-a)\,\vec{x}_2 + a\vec{x}_3$. For a discussion on the DME-coordinate optimization parameter a, refer to appendix 9.5.3. The same form holds for its time-reversal counterpart $\rho_q(\vec{r}_1 + \vec{x}_3, \vec{r}_1 + \vec{x}_2)$. The π−functions that occur in both Eqs. (7.23) and (7.24) are given by

$$\Pi_0^{\rho}(k_F^q y) = 3\,\frac{j_1(k_F^q y)}{k_F^q y} = \Pi_2^{\rho}(k_F^q y)\,. \qquad (7.25)$$

The corresponding expansions for the vector part of the OBDM are given by

$$s_{q,\nu}\Big(\vec{r}_1, \vec{r} + \vec{x}_2\Big) \simeq i\,\Pi_1^{\tilde{s}}(k_F^q x_2) \sum_{\mu=x}^{z} x_{2,\mu}\, J_{q,\mu\nu}(\vec{r}_1)\,, \qquad (7.26)$$

$$s_{q,\nu}\Big(\vec{r}_1 + \vec{x}_2, \vec{r} + \vec{x}_3\Big) \simeq i\,\Pi_1^{\tilde{s}}(k_F^q x) \sum_{\mu=x}^{z} x_{\mu}\, J_{q,\mu\nu}(\vec{r}_1)\,, \qquad (7.27)$$

where the π−function occurring in Eqs. (7.26) and (7.27) is given by

$$\Pi_1^{\tilde{s}}(\tilde{k}_F^q y) \equiv 3\,\frac{j_1(\tilde{k}_F^q y)}{\tilde{k}_F^q y}\,. \qquad (7.28)$$

$\tilde{k}_F^q$ as given in Eq. (5.37). A similar expansion holds for $s_{q,\nu}(\vec{r}_1, \vec{r} + \vec{x}_3)$. Using the time-reversal property of the nonlocal vector density as given in Eq. (9.85), the expansions for $s_{q,\nu}(\vec{r}_1 + \vec{x}_2, \vec{r}_1)$, $s_{q,\nu}(\vec{r}_1 + \vec{x}_3, \vec{r}_1)$ and $s_{q,\nu}(\vec{r}_1 + \vec{x}_3, \vec{r}_1 + \vec{x}_2)$ can easily be generated from Eqs. (7.26) and (7.27).

Infinite nuclear matter limit

The generalized PSA-DME, just like the PSA-DME developed in section 5.3, is exact in INM. Since $\vec{s}_q(\vec{r}_1 + \vec{x}_2, \vec{r}_1 + \vec{x}_3) = 0.$ in spin-unpolarized INM, we consider only the scalar part of the density matrix. In INM, it is given by

$$\rho_q(\vec{r}_1, \vec{r}_1 + \vec{x}_2) = 3\,\frac{j_1(k_F^q x_2)}{k_F^q x_2}\,\rho_q(\vec{r}_1)\,, \tag{7.29}$$

$$\rho_q(\vec{r}_1 + \vec{x}_2, \vec{r}_1 + \vec{x}_3) = 3\,\frac{j_1(k_F^q |\vec{x}_3 - \vec{x}_2|)}{k_F^q |\vec{x}_3 - \vec{x}_2|}\,\rho_q(\vec{r}_1)\,, \tag{7.30}$$

which can be recovered exactly from Eqs. (7.23) and (7.24) by noting that $\vec{\nabla}\rho_q(\vec{r})$ and $\Delta\rho_q(\vec{r})$ vanish in INM and $\tau_q(\vec{r}) = \frac{3}{5}k_F^{q\,2}\rho_q(\vec{r})$. This implies that in the application of the DME to the HF energy from chiral EFT NNN interaction at N^{2}LO results in a local EDF which will reproduce the exact HF energy with no discrepancy. The previous statement holds as long as the DME is the only approximation in the whole set of steps followed to obtain a local EDF. As discussed in section 7.2.2, this is one of the benefits of the adopted DME-coordinate.

7.2.4 The resulting EDF

The application of the generalized PSA-DME given in the previous section to the exact HF energy from the chiral EFT three-nucleon interaction at N^{2}LO, followed by a set of mathematical steps that mostly involve angular integrations, results in a *local* EDF. Yet again, the complexity of the algebra required to arrive at the final simplified form of the EDF rules out manual derivation. Hence, we automate the derivation using Mathematica. The main ingredients of the symbolic derivation of the EDF are given in appendix 9.10, while the complete derivation can be found in

Ref. [161].

In the symbolic derivation of the EDF, the analytical PSA-DME expressions of the nonlocal densities given in Eqs. (7.23), (7.24), (7.26) and (7.27) are replaced with their symbolic counterparts. Even though this might seem an irrelevant technical detail of the actual implementation, it is important in the following respect. We have mentioned that, once nonlocal densities are approximated by their DME counterparts, the DME-coordinates $\vec{r}_1$, $\vec{x}_2$, $\vec{x}_3$ allow for the exact simplification of all components of the exact HF expression. This implies that any disagreement between the exact HF energy and the corresponding EDF can be reduced by further optimization of the DMEs of these nonlocal densities. In line with this, we develop a very general symbolic DME ansatz and one can consider the generalized PSA-DME discussed in the previous section as a specific realization of this symbolic DME ansatz. Refer to appendix 9.10.1 for detail. In this way, future improvements to the DME can be automatically implemented in the current approach.

There are several strong points about this symbolic derivation: (i) The couplings of the EDF are functionals of the $\pi-$functions. Consequently, by fixing the $\pi-$functions according to some analytical DME scheme, one can generate the corresponding couplings of the EDF. In the next section, we discuss how we obtain the analytical couplings for our choice of the $\pi-$functions according to the generalized PSA-DME. (ii) The automation of the whole task enables us to keep all the higher-order terms (up-to-sixth order) in the EDF. Note that only even orders occur in th EDF i.e. the occurrence of terms with one, three or five derivatives is precluded by the requirement of rotational invariance, as energy is a scalar quantity. The complete EDF, including all the higher-order terms, is reported in the Mathematica files accompanying Ref. [161]. The usual truncation of EDFs at second-order in gradients is mostly due to the complexity of numerical techniques to solve an equation of motion with beyond second-order gradient terms. Recently, there have been several efforts geared towards incorporating higher order terms in the EDF [35]. In appendix 9.10.4, we report the EDF by including terms up to fourth-order gradients.

At this point, the result of this work is being utilized along with phenomenological extensions. This is discussed in section 8.1. As terms with at most second-order gradients are the ones being used in the referred work, here, we report the form of the EDF by truncating it at second-order, with the added assumption of spherical symmetry,

$$\begin{aligned}
\mathcal{E}_{3NF,2} = \int d\vec{r} \Big\{ & C^{\rho_0^3}\, \rho_0^3(\vec{r}) + C^{\rho_0\rho_1^2}\, \rho_0(\vec{r})\, \rho_1^2(\vec{r}) + C^{\rho_0^2\tau_0}\, \rho_0^2(\vec{r})\, \tau_0(\vec{r}) \\
& + C^{\rho_1^2\tau_0}\, \rho_1^2(\vec{r})\, \tau_0(\vec{r}) + C^{\rho_0\rho_1\tau_1}\, \rho_0(\vec{r})\, \rho_1(\vec{r})\, \tau_1(\vec{r}) \\
& + C^{\rho_0\nabla\rho_0\nabla\rho_0}\, \rho_0(\vec{r})\, \vec{\nabla}\rho_0(\vec{r}) \cdot \vec{\nabla}\rho_0(\vec{r}) \\
& + C^{\rho_0\nabla\rho_1\nabla\rho_1}\, \rho_0(\vec{r})\, \vec{\nabla}\rho_1(\vec{r}) \cdot \vec{\nabla}\rho_1(\vec{r}) \\
& + C^{\rho_1\nabla\rho_0\nabla\rho_1}\, \rho_1(\vec{r})\, \vec{\nabla}\rho_0(\vec{r}) \cdot \vec{\nabla}\rho_1(\vec{r}) + C^{\rho_0^2\Delta\rho_0}\, \rho_0^2(\vec{r})\, \Delta\rho_0(\vec{r}) \\
& + C^{\rho_1^2\Delta\rho_0}\, \rho_1^2(\vec{r})\, \Delta\rho_0(\vec{r}) + C^{\rho_0\rho_1\Delta\rho_1}\, \rho_0(\vec{r})\, \rho_1(\vec{r})\, \Delta\rho_1(\vec{r}) \\
& + C^{\rho_0 J_0^2}\, \rho_0(\vec{r})\, \vec{J}_0(\vec{r}) \cdot \vec{J}_0(\vec{r}) + C^{\rho_0 J_1^2}\, \rho_0(\vec{r})\, \vec{J}_1(\vec{r}) \cdot \vec{J}_1(\vec{r}) \\
& + C^{\rho_1 J_0 J_1}\, \rho_1(\vec{r})\, \vec{J}_0(\vec{r}) \cdot \vec{J}_1(\vec{r}) + C^{\rho_0\nabla\rho_0 J_0}\, \rho_0(\vec{r})\, \vec{\nabla}\rho_0(\vec{r}) \cdot \vec{J}_0(\vec{r}) \\
& + C^{\rho_0\nabla\rho_1 J_1}\, \rho_0(\vec{r})\, \vec{\nabla}\rho_1(\vec{r}) \cdot \vec{J}_1(\vec{r}) + C^{\rho_1\nabla\rho_0 J_1}\, \rho_0(\vec{r})\, \vec{\nabla}\rho_0(\vec{r}) \cdot \vec{J}_1(\vec{r}) \\
& + C^{\rho_1\nabla\rho_1 J_0}\, \rho_0(\vec{r})\, \vec{\nabla}\rho_1(\vec{r}) \cdot \vec{J}_0(\vec{r}) + C^{\rho_0^2\nabla J_0}\, \rho_0^2(\vec{r})\, \vec{\nabla} \cdot \vec{J}_0(\vec{r}) \\
& + C^{\rho_1^2\nabla J_0}\, \rho_1^2(\vec{r})\, \vec{\nabla} \cdot \vec{J}_0(\vec{r}) + C^{\rho_0\rho_1\nabla J_1}\, \rho_0(\vec{r})\, \rho_1(\vec{r})\, \vec{\nabla} \cdot \vec{J}_1(\vec{r}) \Big\},
\end{aligned} \tag{7.31}$$

where $C^{\varsigma_1\varsigma_2\varsigma_3}$ are the couplings of the EDF. Note the explicit isotopic symmetry of the functional as each term contains an even number of isovector densities.

Comments on the second-order truncation for spherical systems

Even though all higher order terms in the resulting EDF (up to sixth order) can be used in the future, currently only up to second-order terms are being considered in the UNEDF implementation of this work as described in section 8.1. Numerical tests performed in section 5.4 confirm that the higher order terms generated by the DME are much smaller than the leading order terms. Still, it is important to ask which terms will be missing when truncating the resulting EDF at second-order. This is especially important for the tensor and spin-orbit pieces of the functional as current phenomenological EDFs show significant deficiencies in that respect [[109],[159],[158]]. It is also well known that the two-pion exchange part of the three-nucleon interaction plays a significant role in the spin-orbit splittings of atomic nuclei [154], further increasing the importance of reproducing the exact HF energy with the DME approximation.

Consequently, we analyze what the practical second-order truncation entails for terms in the exact HF energy that contain the nonlocal spin density, $\vec{s}_{0/1}(\vec{r}_i,\vec{r}_j)$, as these are the possible origins of tensor and spin-orbit terms in the resulting EDF. The assumption of time-reversal invariance sets $\vec{s}_{0/1}(\vec{r}) = 0$, meaning we have to consider only nonlocal spin densities. In addition, the analysis is done when the DME adopted is the generalized PSA-DME, instead of the more general symbolic DME ansatz described in appendix 9.10.1. The key difference between the two, for the purpose of the following analysis, is the fact that the DME of the nonlocal spin density does not involve the gradient, $\vec{\nabla}_\mu J_\nu$, and the laplacian, ΔJ_ν, corrections in the generalized PSA-DME while the symbolic DME ansatz contains such terms. Noting that the isoscalar/isovector label does not matter in the following analysis

- Generic-Form-1 (Eq. (9.406)) - here either one, two or all three of the nonlocal densities, viz, $\varsigma^{\mu 1}(\vec{r}_1,\vec{r}_3)$, $\varsigma^{\mu 2}(\vec{r}_2,\vec{r}_1)$, $\varsigma^{\mu 3}(\vec{r}_3,\vec{r}_2)$ can be nonlocal $\vec{s}_{0/1}$. Starting with one of them being nonlocal $\vec{s}_{0/1}$, the terms that are not considered during second-order truncation include fourth-order terms only such as $\nabla\rho_{0/1}\cdot\vec{J}_{0/1}\,\tau_{0/1}$. A similar analysis for the more general symbolic DME ansatz shows that there are neglected sixth-order terms in this case, as the DME of nonlocal $\vec{s}_{0/1}$ include corrections from gradient and laplacian of $\vec{J}_{0/1}$. When two of the nonlocal densities are nonlocal $\vec{s}_{0/1}$, there are again only fourth-order terms such as $\tau_{0/1}\,\vec{J}_{0/1}\cdot\vec{J}_{0/1}$. The case is much simpler when all the nonlocal densities are the nonlocal $\vec{s}_{0/1}$. The contribution of these terms to the EDF vanishes, as one cannot form a scalar by picking three spin-orbit densities from the set containing just two elements: $(\vec{J}_0,\ \vec{J}_1)$. Hence, the truncation does not introduce any missing terms when all the nonlocal densities are nonlocal $\vec{s}_{0/1}$. A similar, but more complex, analysis can be done for the case of the symbolic DME ansatz.

- Generic-Form-2 (Eq. (7.20)) - here either one or both of the two nonlocal densities, viz, $\varsigma^{\mu 2}(\vec{r}_2,\vec{r}_3)$, $\varsigma^{\mu 3}(\vec{r}_3,\vec{r}_2)$ can be nonlocal $\vec{s}_{0/1}$. Starting with one of the them being nonlocal $\vec{s}_{0/1}$, there are no terms that are not considered due to the second order truncation. This can be realized from the fact that the local density $\varsigma^{\mu 1}(\vec{r}_1)$ is not expanded and the only gradient terms come from the DME of the other nonlocal density. However, we have only up to second order gradients in the expansion of the other nonlocal density, of which only the first order term (along with $\vec{J}$ of the nonlocal $\vec{s}_{0/1}$) contributes to the EDF. This is due to the requirement of rotational invariance. Hence, there are no terms that contribute to the tensor/spin-orbit part of the EDF and are beyond second-order in gradients. When both nonlocal densities are nonlocal $\vec{s}_{0/1}$, the only EDF terms that result are of the form $\rho_{0/1}\,\vec{J}_{0/1}\cdot\vec{J}_{0/1}$, which contain only second-order gradients. Consequently, the second-order truncation does not result in any missing tensor/spin-orbit terms from terms of Generic-Form-2.

- Generic-Form-3 (Eq. (7.21)) - a similar analysis shows that the same conclusion as in the case of Generic-Form-2 holds. In other words, the second-order truncation does not result in any missing tensor/spin-orbit terms.

Concluding, the above analysis shows that, for the generalized PSA-DME, truncating at second-order keeps most, if not all, of the important spin-orbit/tensor terms of the resulting EDF. In fact, the few missing higher-order terms are fourth-order terms from Generic-Form-1. These terms can be expected to be absorbed in the part of the couplings that are phenomenologically fit. Refer to section 8.1 for detail. The above analysis can simply be extended to non spin-orbit/tensor terms of the EDF.

7.3 Analytical Couplings from the chiral EFT NNN interaction at N^{2}LO for time-reversal invariant systems

In this section, the general analytical structure of the couplings is discussed. As discussed in section 5.3.5, we use the isoscalar k_F instead of k_F^q in order to obtain isospin preserving EDF. Starting from Generic-Form-1, given in Eq. (9.406), it can be seen that the application of the DME to the nonlocal densities results in couplings of the form

$$C_{GF1}^{\varsigma 1\varsigma 2\varsigma 3} \sim \int d\vec{x}_2\, d\vec{x}_3\, d\vec{q}_2\, d\vec{q}_3\, F_1(k_F, \vec{x}_2, \vec{x}_3, \vec{q}_2, \vec{q}_3)\,, \tag{7.32}$$

where $C_{GF1}^{\varsigma 1\varsigma 2\varsigma 3}$ denotes the couplings obtained from the application of the DME to Generic-Form-1 type terms. In this equation, F_1 is in general separable in $\vec{q}_2$ and $\vec{q}_3$, but not in $\vec{x}_2$ and $\vec{x}_3$. This is due to the fact that the sole origin of the momentum transfer coordinates, $\vec{q}_2$ and $\vec{q}_3$, is the interaction where they already occur in separable form, while $\vec{x}_2$ and $\vec{x}_3$ remain coupled even after the application of the DME. This in turn is because of the $\pi-$functions associated with $\varsigma^{\mu}3(\vec{r}_1 + \vec{x}_2, \vec{r}_1 + \vec{x}_3)$, as given in Eqs. (7.25) and (7.28). A similar analysis shows that the couplings from Generic-Form-2 given in Eq. (7.20) take the same form as Eq. (7.32). The form of the couplings from Generic-Form-3 is simpler and it reads

$$C_{GF3}^{\varsigma_1\varsigma_2\varsigma_3} \sim \int d\vec{x}_3\, d\vec{q}_3\, F_3(k_F, \vec{x}_3, \vec{q}_3)\,. \tag{7.33}$$

In general, direct, exact and analytical integrations of couplings of the form Eq. (7.32) that require twelve-dimensional integration is a hopeless task. Even for couplings of the form given in Eq. (7.33) and a few other cases where there is a complete separation between terms dependent on $(\vec{x}_2, \vec{q}_2)$ and $(\vec{x}_3, \vec{q}_3)$, in general we have a product of three spherical Bessel functions in addition to exponential and polynomial prefactors for each group, i.e. for those dependent on $(\vec{x}_2, \vec{q}_2)$ and those that depend on $(\vec{x}_3, \vec{q}_3)$. In general there is no known analytical method to calculate these types of integrals, further complicating the problem. One can thus envision doing numerical Monte-Carlo integrations, thereby resulting in non-analytical/numerical couplings. However, the resulting lack of elegance and inconvenience for systematic study of the couplings convinced us to invent a combination of analytical and symbolic methods to integrate these couplings analytically. The symbolic and analytical procedures used for the analytical calculation of these couplings are discussed in appendix 9.11. In this regard, Gegenbaur's addition theorem which is detailed in appendix (9.1.5) and tested in appendix(9.11.3) plays a significant role.

The simple analytical structure that emerges for all the couplings of the EDF reads

$$C^{\varsigma_1\varsigma_2\varsigma_3}[u] = C_1^{\varsigma_1\varsigma_2\varsigma_3}[u] + C_2^{\varsigma_1\varsigma_2\varsigma_3}[u]\ln[4u^2+1] + C_3^{\varsigma_1\varsigma_2\varsigma_3}[u]\arctan[2u]\,, \tag{7.34}$$

where $C_i^{\varsigma 1 \varsigma 2 \varsigma 3}$ are polynomial functions of u. The variable u, which is also used in section 6.2.1, is a dimensionless quantity given by

$$u \equiv \frac{k_F(\vec{R})}{m_\pi}, \tag{7.35}$$

where we explicitly show the $\vec{R}$ dependence of $k_F(\vec{R})$ to emphasize that the couplings are functions of density/position. Note that in writing Eq. (7.34) for $C^{\varsigma 1 \varsigma 2 \varsigma 3}[u]$, we have dropped coefficients that appear in front of $C_i^{\varsigma 1 \varsigma 2 \varsigma 3}$. These coefficients are given in terms of the interaction parameter, m_π and $k_F(\vec{R})$. This can be seen from the requirements of the dimension of the couplings. For instance, $C^{\rho\rho\rho}$ needs to have $MeV\,(fm)^9$ dimension. Finally, we remark that the variable u stays predominantly within $u \epsilon [1.0, 2.0]$. For this, we used $k_F \approx 1.4\,fm^{-1}$ inside the nucleus and half that value out in the surface, while $m_\pi \approx 0.7\,fm^{-1}$. For the actual analytical forms of the couplings, consult Mathematica files of Ref. [161].

Comparison of analytical and Monte-Carlo results

We mentioned that the combination of analytical and symbolic approaches have enabled us to calculate the couplings of the EDF analytically. The calculation of the couplings from Generic-Form-1 and Generic-Form-2, given by the generic form Eq. (7.32), relies on Gegenbaur's addition theorem of Bessel functions followed by the symbolic approach that we invented for this purpose. In contrast, the integration of the couplings from Generic-Form-3, denoted by the generic form Eq. (7.32), do not require the use of Gegenbaur's addition theorem. Rather, they are calculated directly using the symbolic approach. Refer to section 9.11 for details.

Gegenbaur's addition theorem is exact only if it is not truncated at a finite order. Since we are forced to truncate the expansion at a finite order, this calls in to question the accuracy of the couplings which are calculated using this approach. In appendix 9.11.3, we discuss the accuracy of a truncated Gegenbaur's addition theorem, where we show that including at least the first five terms of the expansion gives a practically exact expansion. In this section, we test the impact of this truncation by comparing the local EDF that results after the application of the DME with the exact HF energy from chiral EFT NNN interaction at N^{2}LO. We perform the test for symmetric INM, where in principle we should have exact agrement.

The exact INM HF energy contribution from the chiral EFT NNN interaction, given in appendix 9.9, can be written in terms of Eqs. (7.29) and (7.30) as

$$\langle V_{3N}^{\mathrm{HF},E,\mathrm{INM}} \rangle = -\frac{3}{16} E \int d\vec{r}_1 \rho_0^3(\vec{r}_1) , \tag{7.36}$$

which is already in local form and does not need any DME. For the D-term, we have

$$\langle V_{3N}^{\mathrm{HF},D,\mathrm{INM}} \rangle = \int d\vec{r}_1 \, C^{\rho_0^3}_{D,INM} \, \rho_0^3(\vec{r}_1) , \tag{7.37}$$

where

$$C^{\rho_0^3}_{D,INM} \equiv \frac{27 \, g_A}{512 \, \pi^3} \frac{C_D}{f_\pi^4 \Lambda_x} \int d\vec{x}_3 \, d\vec{q}_3 \, e^{i\vec{q}_3 \cdot \vec{x}_3} \, \frac{q_3^2}{q_3^2 + m_\pi^2} \, \frac{j_1(k_F x_3)}{k_F x_3} \, \frac{j_1(k_F x_3)}{k_F x_3} . \tag{7.38}$$

Note that, in this formula $k_F = k_F(\vec{r}_1) = [3/2\pi^2 \rho_0(\vec{r}_1)]^{1/3}$, using the isoscalar density. This coupling can be integrated analytically without the application of Gegenbaur's addition theorem and thus we do not discuss it further. The C-term contributes

$$\begin{aligned} \langle V_{3N}^{\mathrm{HF},C,\mathrm{INM}} \rangle &= \langle V_{3N}^{\mathrm{HF},CD1X,\mathrm{INM}} \rangle + \langle V_{3N}^{\mathrm{HF},CD2X,\mathrm{INM}} \rangle \\ &\quad + \langle V_{3N}^{\mathrm{HF},R2X,\mathrm{INM}} \rangle \qquad (7.39) \\ &= \int d\vec{r}_1 \, C^{\rho_0^3}_{C,INM} \, \rho_0^3(\vec{r}_1) , \qquad (7.40) \end{aligned}$$

where

$$\mathcal{C}^{\rho_0^3}_{C,INM} \equiv \mathcal{C}^{\rho_0^3}_{CD1x,INM} + \mathcal{C}^{\rho_0^3}_{CD2x,INM} + \mathcal{C}^{\rho_0^3}_{R2x,INM} \,. \tag{7.41}$$

We have separated the three different contributions to the coupling in Eq. (7.41). As discussed in section 7.1, the C-term of the chiral EFT three-nucleon interaction at N^{2}LO has what we call the D-like and R pieces. In the coupling shown in Eq. (7.41), the first two terms of the couplings are from the single- and double-exchange parts of the D-like piece, while the last one is from the double-exchange part of the R-piece. These are given by

$$\begin{aligned}
\mathcal{C}^{\rho_0^3}_{CD1X,INM} \equiv& -\frac{54}{1024\,\pi^6}\left(\frac{g_A}{2f_\pi}\right)^2 \int d\vec{x}_2\, d\vec{x}_3\, d\vec{q}_2\, d\vec{q}_3\; e^{i\vec{q}_2\cdot\vec{x}_2}\, e^{i\vec{q}_3\cdot\vec{x}_3} \\
&\times \frac{\delta_{\beta_1\gamma_1}\, q_2^{\beta_1} q_3^{\gamma_1}}{(q_2^2+m_\pi^2)(q_3^2+m_\pi^2)} \left(-4\frac{c_1 m_\pi^2}{f_\pi^2} + 2\frac{c_3}{f_\pi^2}\vec{q}_2\cdot\vec{q}_3\right) \\
&\times \frac{j_1(k_F|\vec{x}_3-\vec{x}_2|)}{k_F|\vec{x}_3-\vec{x}_2|}\,\frac{j_1(k_F|\vec{x}_3-\vec{x}_2|)}{k_F|\vec{x}_3-\vec{x}_2|}\,. \qquad (7.42) \\
\mathcal{C}^{\rho_0^3}_{CD2X,INM} \equiv& \frac{81}{1024\,\pi^6}\left(\frac{g_A}{2f_\pi}\right)^2 \int d\vec{x}_2\, d\vec{x}_3\, d\vec{q}_2\, d\vec{q}_3\; e^{i\vec{q}_2\cdot\vec{x}_2}\, e^{i\vec{q}_3\cdot\vec{x}_3} \\
&\times \frac{\delta_{\beta_1\gamma_1}\, q_2^{\beta_1} q_3^{\gamma_1}}{(q_2^2+m_\pi^2)(q_3^2+m_\pi^2)} \left(-4\frac{c_1 m_\pi^2}{f_\pi^2} + 2\frac{c_3}{f_\pi^2}\vec{q}_2\cdot\vec{q}_3\right) \\
&\times \frac{j_1(k_F x_2)}{k_F x_2}\,\frac{j_1(k_F x_3)}{k_F x_3}\,\frac{j_1(k_F|\vec{x}_3-\vec{x}_2|)}{k_F|\vec{x}_3-\vec{x}_2|}\,, \qquad (7.43) \\
\mathcal{C}^{\rho_0^3}_{R2X,INM} \equiv& -\frac{243}{1024\,\pi^6}\left(\frac{g_A}{2f_\pi}\right)^2 \frac{c_4}{f_\pi^2} \int d\vec{x}_2\, d\vec{x}_3\, d\vec{q}_2\, d\vec{q}_3\; e^{i\vec{q}_2\cdot\vec{x}_2}\, e^{i\vec{q}_3\cdot\vec{x}_3} \\
&\times \frac{q_2^{\beta_1} q_3^{\gamma_1} q_2^{\beta_2} q_3^{\gamma_2}}{(q_2^2+m_\pi^2)(q_3^2+m_\pi^2)}\, \epsilon^{\beta_1\gamma_1\nu}\epsilon^{\beta_2\gamma_2\nu} \\
&\times \frac{j_1(k_F x_2)}{k_F x_2}\,\frac{j_1(k_F x_3)}{k_F x_3}\,\frac{j_1(k_F|\vec{x}_3-\vec{x}_2|)}{k_F|\vec{x}_3-\vec{x}_2|}\,. \qquad (7.44)
\end{aligned}$$

As can be seen from Eqs. (7.42), (7.43) and (7.44), all of them require the application of Gegenbaur's addition theorem. This is due to the occurrence of $j_1(k_F|\vec{x}_2 - \vec{x}_3|)/(k_F|\vec{x}_2 - \vec{x}_3|)$ in these terms that are not separable in $\vec{x}_2$ and $\vec{x}_3$. The numerical test discussed in appendix 9.11.3 shows that we can truncate the Gegenbaur expansion of this term at fifth order as

$$\begin{aligned}\frac{j_1(k_F|\vec{x}_3 - \vec{x}_2|)}{k_F|\vec{x}_3 - \vec{x}_2|} \approx & \sqrt{\frac{144}{\pi}} \frac{\Gamma(3/2)}{k_F^2\, x_3\, x_2} \sum_{\mu=0}^{5} (\mu + \frac{3}{2})\, j_{\mu+1}(k_F x_2)\, j_{\mu+1}(k_F x_3) \\ & \times C_\mu^{3/2}(\cos(\theta))\,, \end{aligned} \tag{7.45}$$

where θ is the angle between $\vec{x}_2$ and $\vec{x}_3$ This is followed by analytical integration of the couplings. Furthermore, one notes that Eq. (7.42) requires the application of two Gegenbaur expansions while Eq. (7.43) and (7.44) require the application of only one Gegenbaur expansion. To assess the accuracy of the couplings/EDF in Eq. (7.39) when calculated with the truncated Gegenbaur expansion, we compare the result with the case when the couplings are calculated with the essentially-exact Monte-Carlo integration (without Gegenbaur expansion).

In Fig. 7.1, we show the percentage error of the Gegenbaur-based calculation with respect to the Monte-Carlo ones, for the contribution of the three terms of Eq. (7.39) to the energy per particle of INM as a function k_F. For each of the three terms, we have two curves where the insets show the actual contribution to the energy per particle when the couplings (Eqs. (7.42)- (7.44)) are calculated analytically with the truncated Gegenbaur addition theorem, at fifth order, and the lower curves (main curves) represent the percentage errors. The constants of the chiral EFT three-nucleon interaction that are used in this particular calculation are specified in Table 2.2, with $\hbar c = 197.327$ [MeV fm].

The results show that, the percentage error resulting from truncating the Gegenbaur expansion is less than 0.5% over the range of physically interesting k_F values. In fact, for the double-exchange from the D-like and R pieces, the percentage error shows a strong fluctuation between 0 and 0.5%. For the single-exchange from the D-like term, the percentage error shows a steady increase from 0 to about 0.3%, which

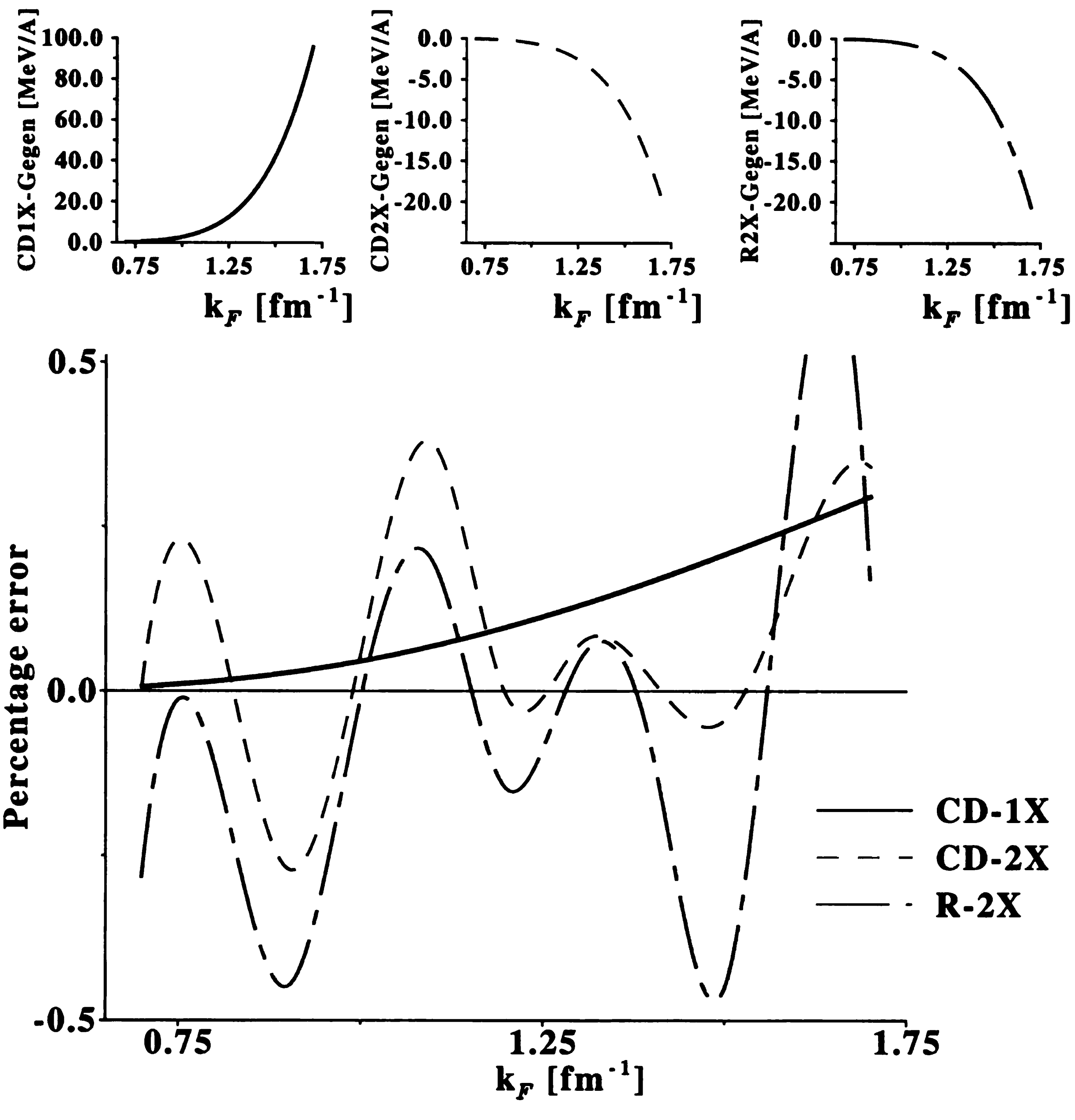

Figure 7.1: (Color online) The percentage error of the truncated Gegenbaur expansion with respect to Monte-Carlo based calculation of the contribution to E/A in INM. Upper plots show the actual values for the calculation based on the truncated Gegenbaur expansion.

is not surprising as we needed to apply Gegenbaur's addition theorem twice in that case. Considering the unavoidable numerical errors/flucuations in the Monte-Carlo calculation and the smallness of the percentage errors, obtained we can conclude that the truncation of Gegenbaur's addition theorem at fifth order provides a practically exact truncation. At this point, one should realize yet another reason for the need to automate the whole calculation. I.e. the application of Gegenbaur's addition theorem replaces each term in the couplings with about five terms when truncated at fifth order. For instance, in the integration of Eq. (7.42), the single Monte-Carlo integration is replaced with about 25 integrals due to the double-application of Gegenbaur's theorem. Hence, even though it enables us to obtain completely analytical couplings, Gegenbaur's addition theorem comes with a tricky overhead: about two orders of magnitude increase in the number of integrals to be calculated. Finally, we remark that the conclusion of this section, viz, the truncated Gegenbaur's addition theorem enables us to calculate the couplings in a practically exact manner, holds for all other couplings as the truncated Gegenbaur expansion is the only "approximation" that goes into the calculation of the couplings. In the next chapter, besides the possible future extensions and conclusions, we perform preliminary analysis of the couplings and the ongoing semi-phenomenological approach that is attempting to make use of this work.

Chapter 8

Semi-phenomenological EDF, Future Extensions and Conclusions

8.1 The semi-phenomenological approach

Based on the arguments discussed in section 5.1.1, we advocate a semi-phenomenological approach in which the phenomenological Skyrme functional is to be augmented with the DME-functional. Here, DME-functional refers to the EDF that we obtained from the application of the DME to the Fock energy contributions of finite-range NN and the complete HF of finite-range NNN chiral EFT interactions at N^{2}LO. In this scheme, the Hartree contributions from the NN part are to be treated exactly. Finally, the phenomenological Skyrme parameters are to be re-fit to INM and finite nuclei properties, leaving those couplings/terms that originate from the DME intact. Actually, the so-called phenomenological Skyrme parameters can also considered to have originated from the contact part of the chiral EFT NN and NNN interactions.

The generic structure of EFT interactions given in Eq. (2.12), $V_{EFT} = V_\pi + V_{ct}(\Lambda)$, shows a clean separation between long- and short-distance physics. Consequently, each DME coupling at the HF level can be decomposed as the sum of a density-independent, Λ-dependent piece, which are subsequently re-fit, coming from the contact terms of the EFT NN and NNN (E-term) interaction ($V_{ct}(\Lambda)$) and a density-dependent, Λ-independent piece coming from the finite-range pion exchanges

$$C_t^{\varsigma_1\varsigma_2} = C_t^{\varsigma_1\varsigma_2}(\Lambda; V_{ct}) + C_t^{\varsigma_1\varsigma_2}(\vec{R}; V_\pi)\,, \tag{8.1}$$

$$C_t^{\varsigma_1\varsigma_2\varsigma_3} = C_t^{\varsigma_1\varsigma_2\varsigma_3}(\Lambda; V_{ct}) + C_t^{\varsigma_1\varsigma_2\varsigma_3}(\vec{R}; V_\pi)\,, \tag{8.2}$$

where $\varsigma_1\varsigma_2$ and $\varsigma_1\varsigma_2\varsigma_3$ are bilinear and trilinear combinations of densities that occur in the EDF [[153], [160]].

In this sense, the re-fit parameters can be viewed as containing the effects of the HF contribution from the contact interactions, V_{ct}, plus higher order effects that would arise in a more sophisticated Brueckner-Hartree-Fock or 2nd-order MBPT calculations. In this regard, through the loose connection of the refit Skyrme parameters to the EFT contact terms, the EFT concept of naturalness might provide useful theoretical constraints for the fitting procedure [163].

The following several plots show sample $C_t^{\varsigma_1\varsigma_2}$. As can be seen from fig. 8.1, the novel density-dependence is controlled by the long-range parts of the NN interaction. Therefore, it is not surprising to see that the density profile of the couplings shown in the figures is driven by the LO term (one-pion exchange) since the NLO and N^{2}LO interactions are of shorter two-pion exchange range. Even though the couplings in fig. 8.1 seem to satisfy the hierarchy requirement, viz, LO > NLO > N^{2}LO, it is not guaranteed that this will always hold. This is because we are including only HF contributions to the couplings, with our focus being primarily on finite-range pieces. The fact that the hierarchy might not be maintained should not seem to be a big problem as HF amounts to comparing the LO, NLO, N^{2}LO potentials (which are not observables) and therefore are they not required to obey any hierarchy.

Fig. 8.2 and 8.3 show the C_0^{JJ} and C_1^{JJ} couplings with +/- error bands as de-

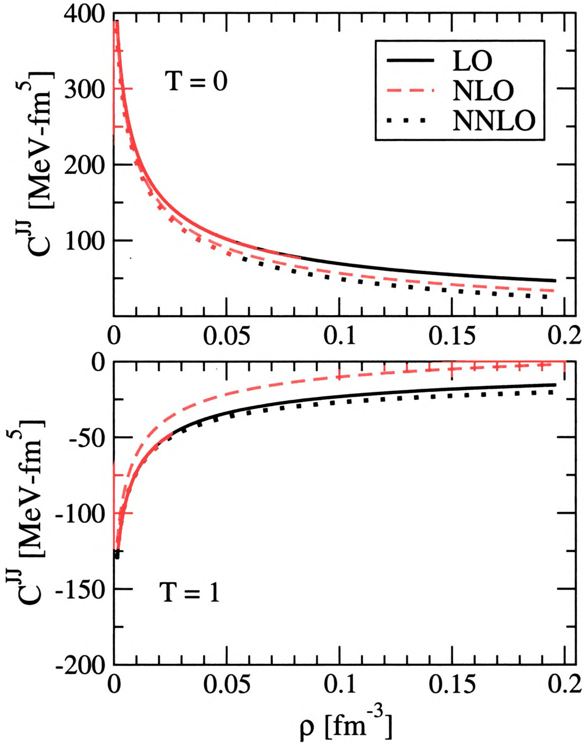

Figure 8.1: (Color online) $\mathcal{C}_0^{JJ}$ and $\mathcal{C}_1^{JJ}$ couplings from chiral EFT NN interaction at N^{2}LO.

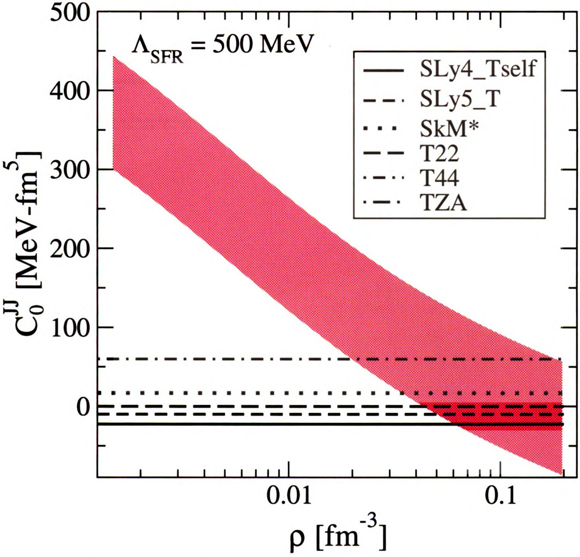

Figure 8.2: (Color online) $\mathcal{C}_0^{JJ}$ couplings from the chiral NN interaction at N^{2}LO with error bands from naturalness requirement.

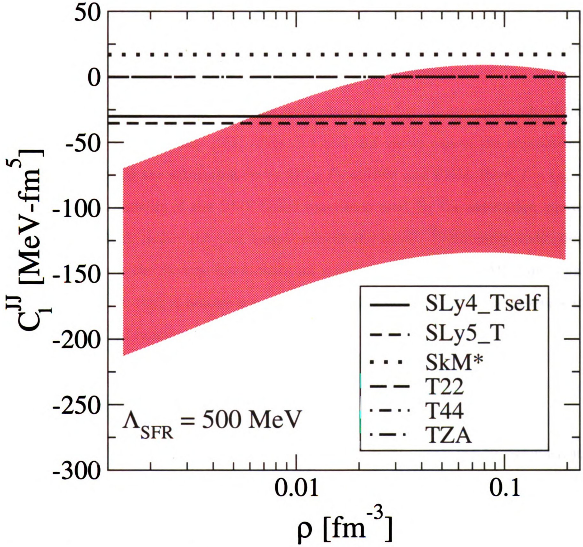

Figure 8.3: (Color online) $\mathcal{C}_1^{JJ}$ couplings from the chiral NN interaction at N^{2}LO with error bands from naturalness requirement.

termined from the naturalness requirement [163], compared with the corresponding phenomenological values. The error bands cover all phenomenological values in the density region of interest. Thus, the main conclusion that can be made at this stage is that the DME couplings are close to phenomenology, but with a novel density-dependence, as long as one allows for natural-sized contact terms. For a detailed discussion, refer to Ref. [153], while for the corresponding discussion on $C_t^{\varsigma_1\varsigma_2\varsigma_3}$, refer to Ref. [160].

The first calculations following the semi-phenomenological approach advocated in this section are underway [164]. Figs. 8.4 and 8.5 shows one of the exploratory "results" regarding the saturation curve, $W(\rho, I)$, of INM and PNM. Here, $I = (\rho_n - \rho_p)/\rho$. The parameters of the DME-based functional used for the saturation curves are not optimized, rather they are simple educated guesses. Preliminary indication from this study is the Skyrme functional that is augmented with the DME functional is more flexible in that it relaxes some of the interdependencies that one observes in phenomenological functionals [164].

8.2 Key future extensions

In this section, we revise the main directions in which this work can be extended in the future. These are

- Extensive self-consistent test of the PSA-DME. As discussed in section 5.4, our tests can be judged to be extensive only for non self-consistent ones. Along with the self-consistent test, the invention of a local NN and NNN chiral interaction that is soft enough to be used for these tests is important.

- Studying the impact of the different DMEs on the couplings of the resulting EDF. Note that the non-self consistent tests that we performed in this work are using schematic interactions and it will be beneficial to extend this and perform

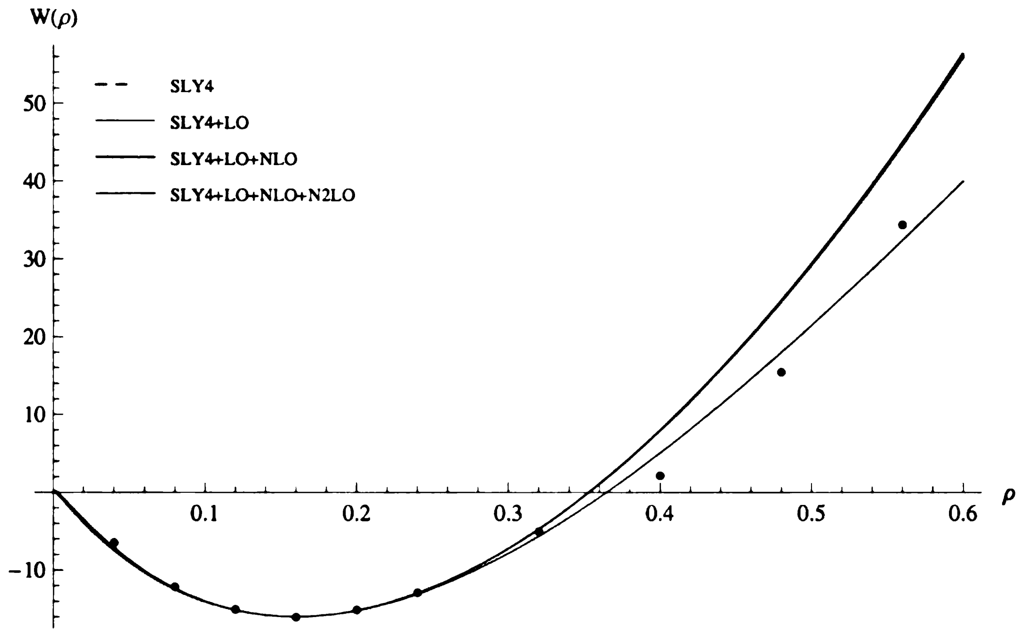

Figure 8.4: The saturation curves, $W(\rho, I)$ of INM using the phenomenological SLY4 functional and semi-phenomenological DME-based functionals. Here, $\mathrm{N}^2\mathrm{LO}$ includes the contribution from both NN and NNN interactions (From Ref. [164]).

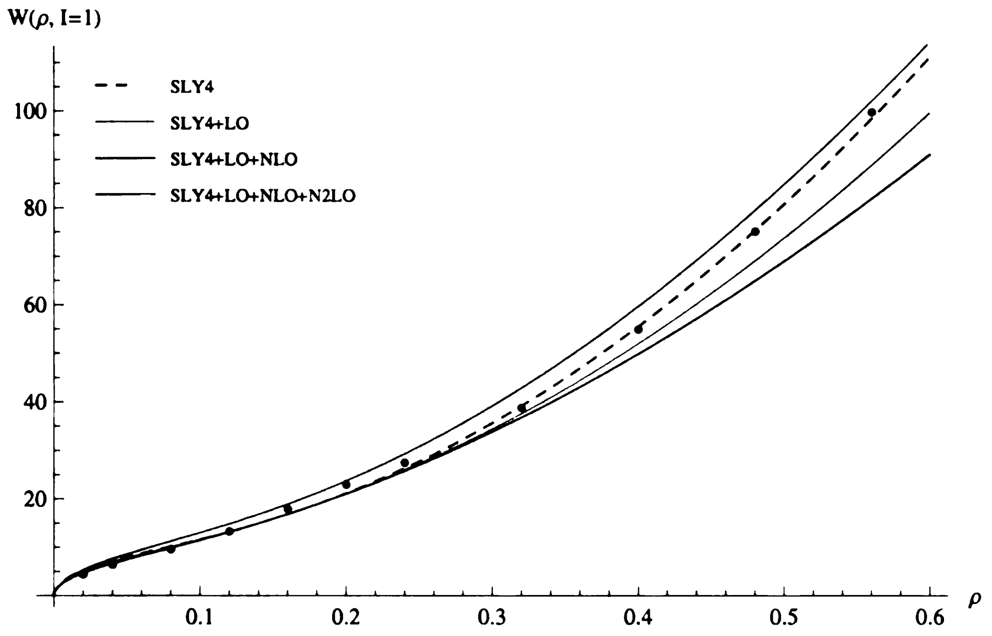

Figure 8.5: The same as Fig. 8.4 but for PNM (From Ref. [164]).

extensive comparison of the actual couplings that result from the application of different DMEs. This should provide a better estimate of the associated DME errors/uncertainities.

- Non-self-consistent and self-consistent tests of generalized PSA-DME. This is important to gauge the accuracy of the DME approximation that we made to the HF energy from the chiral EFT NNN interaction at N^2LO. Even though we have shown in appendix 9.5.3 that the approximations that we used to obtain the generalized PSA-DME are equivalent to the ones used for PSA-DME, the existence of more than one non-locality coordinate may change the relative accuracy of generalized PSA-DME with respect to PSA-DME. Furthermore, the effect of DME-coordinate optimization parameter a in Eq. (7.24) should be investigated.

- Calculation of Bogoliubov contribution from NN + NNN, extension of PSA-DME or its variants for pairing densities. Furthermore, the required renormalization should be designed along with the DME.

- From the interaction side, the extension should include the contributions from the N^3LO component of chiral EFT interactions. It should be noted that, even limiting the calculation at the HF level, the four-nucleon interaction which first appears at this order will make the extensions more complex. In principle, one needs to incorporate the contribution from the four-nucleon interaction. Nevertheless, current estimations of its effect on nuclei, at least in light-nuclei, suggest that it can be ignored safely. For instance, estimates in ^{4}He show that the additional binding energy it provides is of the order of a few hundred keV [165].

- Extension of the DME scheme to approximate higher-order contributions as discussed in section 5.1.1.

- Analysis of self-interaction and self-pairing issues that arise in the context of the DME [105].

8.3 Conclusion

This work is a part of a long-term project to develop nuclear EDFs starting from many-body perturbation theory and the underlying two- and three-nucleon interactions [[110]-[154]]. This is necessitated by the fact that empirical EDFs lack solid microscopic foundations and often result in uncontrolled (i.e., parameterization-dependent) predictions away from known data.

We used the DME as a tool to explicitly build microscopic physics associated with long-range pion-exchange interactions into existing Skyrme functionals in the form of novel density dependencies. An important component of this endeavor is the improved PSA-DME and its NNN counterpart, the generalized PSA-DME, which are crucial if we want to provide microscopic guidance to the description of spin-unsaturated nuclei. The rich spin/isovector dependence of pion-exchange interactions gives us hope that their inclusion via the DME will give valuable microscopic constraints on the isovector properties of the EDF. Moreover, it is comforting that these constraints are coming from the best-understood part of nuclear interactions.

The EDF obtained as a result of the present work contains only HF physics such that further correlations must be added to produce any reasonable description of nuclei. In the short term, such an addition is being implemented empirically by adding the DME couplings to empirical Skyrme functionals and performing a refit of the Skyrme constants to data [164]. While this is a purely empirical procedure, it is motivated by the well-known observation that a Brueckner G-matrix differs from the starting vacuum NN interaction only at short distances. Therefore, one can interpret the refit to data as approximating the short-distance part of the G-matrix with a zero-range expansion through second order in gradients. Eventually though, it is the goal of the UNEDF (universal energy density functional) project to design a generalized DME that is suited to higher orders in perturbation theory and move closer and closer to complete microscopy.

Chapter 9

Appendix

9.1 Mathematical Formulae

In this section, we list the Mathematical definitions, relations and formulae that have been used in the rest of the work. Only the relevant mathematical relations and formulae are listed, and for a more extensive list, refer to classic references such as [[152],[151]].

9.1.1 Miscellaneous elementary formulae

In various parts of this work, we use the following general linear coordinate transformation. Starting with two coordinates $(\vec{x}_1, \vec{x}_2)$, we define a new coordinate system $(\vec{x}, \vec{X})$ as

$$\vec{x} = \vec{x}_1 - \vec{x}_2 \qquad \vec{X} = (1-a)\,\vec{x}_1 + a\,\vec{x}_2\,, \tag{9.1}$$

where the unspecified parameter a is a real number satisfying $a \in [0,\, 1]$. The corresponding gradient operators are given by

$$\vec{\nabla}_x = a\,\vec{\nabla}_{x_1} - (1-a)\,\vec{\nabla}_{x_2}\,, \tag{9.2}$$

$$\vec{\nabla}_X = \vec{\nabla}_{x_1} + \vec{\nabla}_{x_2}, \tag{9.3}$$

with $a = 1/2$ recovering the usual center of mass and relative coordinates.

In the derivation of local densities, detailed in appendix 9.4 and other parts of the work, the following elementary results are important.

$$\vec{\nabla} \cdot \vec{\nabla}'(\hat{r}' \cdot \hat{r})\Big|_{\vec{r}'=\vec{r}} = \frac{2}{r^2}, \tag{9.4}$$

$$\partial_k(\hat{r} \cdot \hat{r}') = \sum_{ij} \frac{r'_j}{r'} \left(\frac{\delta_{ij} r'^2 - r_i r_j}{r^3} \right) \hat{k} \tag{9.5}$$

$$\frac{1}{4\pi} \int d\Omega_{\vec{r}} (\vec{r} \cdot \vec{A})(\vec{r} \cdot \vec{B}) = \frac{r^2}{3} \vec{A} \cdot \vec{B}. \tag{9.6}$$

The manual derivation of the HF energy from a generic two-nucleon interaction involves a modest amount of spin-isospin algebra. First, the Pauli matrices are given by

$$\sigma_x = \begin{pmatrix} 0 & 1 \\ 1 & 0 \end{pmatrix} \quad \sigma_y = \begin{pmatrix} 0 & -i \\ i & 0 \end{pmatrix} \quad \sigma_z = \begin{pmatrix} 1 & 0 \\ 0 & -1 \end{pmatrix} \tag{9.7}$$

They satisfy the commutation and anticommutation relations

$$\sigma_i \sigma_j - \sigma_j \sigma_i = i\, 2\epsilon_{ijk}\, \sigma_k, \tag{9.8}$$

$$\sigma_i \sigma_j + \sigma_j \sigma_i = 2\,\delta_{ij}\, I, \tag{9.9}$$

which can be used to prove

$$(\vec{A} \cdot \vec{\sigma})(\vec{B} \cdot \vec{\sigma}) = (\vec{A} \cdot \vec{B}) I + i \vec{\sigma} \cdot (\vec{A} \times \vec{B}), \tag{9.10}$$

$$e^{i\vec{A}\cdot\vec{\sigma}} = \cos(a) + i\,(\hat{n} \cdot \vec{\sigma}) \sin(a), \tag{9.11}$$

for any two vectors $\vec{A}$, $\vec{B}$ and $\vec{A} = a\hat{A}$. Additional, elementary relations are

$$\sum_{\sigma} \vec{\sigma}_{\sigma\sigma} = \vec{0}\,, \tag{9.12}$$

$$\sum_{\sigma\sigma'} (\vec{A} \cdot \vec{\sigma}_{\sigma\sigma'})\, \vec{\sigma}_{\sigma'\sigma} = 2\,\vec{A} \text{ for all } \vec{A}. \tag{9.13}$$

9.1.2 Clebsh-Gordon, Wigner 3-J and 6-J coefficients

Representing Clebsch-Gordon, Wigner 3-J and 6-J coefficients by

$$\langle\, jm \,|\, j_1 m_1 j_2 m_2 \rangle\,, \quad \begin{pmatrix} j_1 & j_2 & j \\ m_1 & m_2 & m \end{pmatrix}, \quad \begin{Bmatrix} j_1 & j_2 & j \\ m_1 & m_2 & m \end{Bmatrix}, \tag{9.14}$$

respectively, the following is a list of the relations that are important for different parts of this work.

$$\sum_{\sigma} \langle l m_l \tfrac{1}{2} \sigma | jm \rangle^2 \;=\; \frac{2j+1}{2l+1}\,, \tag{9.15}$$

for all m and m_l such that $m = m_l + \sigma$.

$$\langle j_1 m_1 j_2 m_2 | jm \rangle \;=\; (-1)^{m+j_1-j_2}\, \sqrt{2j+1} \begin{pmatrix} j_1 & j_2 & j \\ m_1 & m_2 & m \end{pmatrix} \tag{9.16}$$

$$\begin{aligned} \sum_{m_4 m_5 m_6} (-1)^{a} \begin{pmatrix} j_1 & j_5 & j_6 \\ m_1 & m_5 & m_6 \end{pmatrix} \begin{pmatrix} j_4 & j_2 & j_6 \\ -m_4 & m_2 & m_6 \end{pmatrix} \begin{pmatrix} j_4 & j_5 & j_6 \\ m_4 & -m_5 & m_6 \end{pmatrix} \\ = \begin{Bmatrix} j_1 & j_2 & j_3 \\ j_4 & j_5 & j_6 \end{Bmatrix} \begin{pmatrix} j_1 & j_2 & j_3 \\ m_1 & m_2 & m_3 \end{pmatrix}, \end{aligned} \tag{9.17}$$

where $a = j_4 + m_4 + j_5 + m_5 + j_6 + m_6\,.$

$$\begin{pmatrix} j_1 & j_2 & j \\ m_1 & m_2 & m \end{pmatrix} = (-1)^{j_1+j_2+j} \begin{pmatrix} j_1 & j & j_2 \\ m_1 & m & m_2 \end{pmatrix} \tag{9.18}$$

$$\sum_L (2L+1)\, f(l,L) \begin{Bmatrix} L & l & 1 \\ 1 & 1 & l \end{Bmatrix} \begin{pmatrix} l & L & 1 \\ 0 & 0 & 0 \end{pmatrix} = \frac{1}{\sqrt{6}} (-1)^l \sqrt{l(l+1)}. \tag{9.19}$$

where

$$f(l,L) = \begin{cases} -l\sqrt{\frac{l+1}{2l+3}} & \text{if } L = l+1; \\ -(l+1)\sqrt{\frac{l}{2l-1}} & \text{if } L = l-1; \\ 0 & \text{otherwise.} \end{cases}$$

$$\begin{pmatrix} l & l & 1 \\ m_l & m_l' & 0 \end{pmatrix} = (-1)^{l-m_l} \frac{m_l}{\sqrt{l(l+1)(2l+1)}} \delta_{m_l,-m_l'} \tag{9.20}$$

$$\begin{pmatrix} l & l & 1 \\ m_l & m_l' & 1 \end{pmatrix} = (-1)^{l-m_l} \sqrt{\frac{(l-m_l)(l+m_l+1)}{2l(l+1)(2l+1)}} \delta_{m_l,-m_l'-1} \tag{9.21}$$

$$\begin{pmatrix} l & l & 1 \\ m_l & m_l' & -1 \end{pmatrix} = (-1)^{l+m_l+1} \sqrt{\frac{(l+m_l)(l-m_l+1)}{2l(l+1)(2l+1)}} \delta_{m_l,-m_l'+1} \tag{9.22}$$

$$\begin{Bmatrix} l & l & 1 \\ \frac{1}{2} & \frac{1}{2} & j \end{Bmatrix} = \frac{1}{\sqrt{6}} (-1)^{l+j+3/2} \frac{3/4 + l(l+1) - j(j+1)}{\sqrt{l(l+1)(2l+1)}}. \tag{9.23}$$

9.1.3 A few special functions

Legendre polynomials

Starting with the associated Legendre differential equation, for integer l and m,

$$\frac{d}{dx}\left[(1-x^2)\,P_l^m(x)\right] + \left[l(l+1) - \frac{m^2}{1-x^2}\right]P_l^m(x) = 0\,, \tag{9.24}$$

where $x \in \mathrm{R}$ (the set of real numbers), $P_l^m(x)$ is the associated Legendre polynomial. The associated Legendre polynomials satisfy

$$P_l^{-m}(x) = (-1)^m \frac{(l-m)!}{(l+m)!}\,P_l^m(x)\,. \tag{9.25}$$

For $m = 0$, the differential equation given in Eq. (9.24) can be reduced to

$$(1-x^2)\frac{d^2P_l(x)}{dx^2} - 2x\frac{dP_l(x)}{dx} + l(l+1)\,P_l(x) = 0\,, \tag{9.26}$$

where $P_l(x)$ is Legendre polynomial of order l. The first few Legendre polynomials are

$$P_0(x) = 1\,, \tag{9.27}$$

$$P_1(x) = x\,, \tag{9.28}$$

$$P_2(x) = \frac{1}{2}(3x^2-1)\,, \tag{9.29}$$

The Legendre polynomials are orthogonal over the range $(-1,1)$ and satisfy

$$\int dx\,P_n(x)\,P_m(x) = \frac{2}{2n+1}\,\delta_{mn}\,. \tag{9.30}$$

Additionally, $P_l(1) = 1$ for any l. The derivative of Legendre polynomials satisfy the following properties

$$\left.\frac{dP_l(x)}{x}\right|_{x=1} = \frac{l(l+1)}{2}, \tag{9.31}$$

$$\frac{x^2-1}{n}\frac{dP_l(x)}{dx} = xP_l(x) - P_{l-1}(x). \tag{9.32}$$

Laguerre polynomials

The Laguerre polynomials are solutions of the Laguerre differential equation

$$x\frac{d^2 L_n(x)}{dx^2} + (1-x)\frac{dL_n(x)}{dx} + n\,L_n(x) = 0. \tag{9.33}$$

The can also be defined using Rodrigues formula

$$L_n^\alpha(x) = \frac{x^{-\alpha}\,e^x}{n!}\frac{d^n}{dx^n}\left(e^{-x}\,x^{n+\alpha}\right), \tag{9.34}$$

where $L_n^\alpha(x)$ is the associated Laguerre polynomial. The Laguerre polynomials are recovered by setting $\alpha = 0$

$$L_n(x) = L_n^0(x). \tag{9.35}$$

The first few associated Laguerre polynomials are given by

$$L_0^\alpha(x) = 1, \tag{9.36}$$

$$L_1^\alpha(x) = -x + \alpha + 1, \tag{9.37}$$

$$L_2^\alpha(x) = \frac{x^2}{2} - (\alpha+2)\,x + \frac{(\alpha+2)(\alpha+1)}{2}. \tag{9.38}$$

Gamma functions

The Gamma function, which appears from the extension of the factorial with a downward shift of the argument by 1, is given by

$$\Gamma(x) = \int_0^{\infty} dt\, t^{x-1}\, e^{-t}, \tag{9.39}$$

where x is a complex number with a positive real part. In this work, we need only the Gamma function for positive integer arguments, which is given by

$$\Gamma(n) = (n-1)!\,. \tag{9.40}$$

Spherical harmonics

Spherical Harmonics are eigenfunctions of angular momentum operators L^2 and L_z, and are given by

$$Y_l^m(\theta,\phi) = \sqrt{\frac{(2l+1)(l-m)!}{4\pi(l+m)!}}\, P_l^m(\cos(\theta))\, e^{im\phi}, \tag{9.41}$$

with their orthonormality relation being give by

$$\int_0^{\pi}\int_0^{2\pi} d\theta\, d\phi\, Y_l^{m'}(\theta,\phi)\, Y_{l'}^{m'}(\theta,\phi) = \delta_{ll'}\,\delta_{mm'}\,. \tag{9.42}$$

There are various relations satisfied by spherical harmonics, and which are of interest to this work. These are

$$\sum_{m_l} Y_l^{m_l *}(\hat{r}')Y_l^{m_l}(\hat{r}) = \frac{2l+1}{4\pi}\, P_l(\hat{r}'\cdot\hat{r}), \tag{9.43}$$

where the sum extends over all allowed values of m_l.

$$\vec{\nabla}\left[f(r)\,Y_l^m(\hat{r})\right] = \frac{\vec{r}}{r}\frac{\partial f(r)}{\partial r}\,Y_l^m(\hat{r}) + f(r)\,\vec{\nabla}\,Y_l^m(\hat{r})\,, \tag{9.44}$$

where $f(r)$ is any function dependent only on r.

$$\nabla_{\mu_1} Y_l^{m'}(\hat{r}) = \frac{1}{r}\sum_{LM} f(l,L)\,\langle l1m'\mu_1|LM\rangle\,Y_L^M(\hat{r})\,, \tag{9.45}$$

where

$$f(l,L) = \begin{cases} -l\sqrt{\frac{l+1}{2l+3}} & \text{if } L = l+1; \\ -(l+1)\sqrt{\frac{l}{2l-1}} & \text{if } L = l-1; \\ 0 & \text{otherwise.} \end{cases}$$

$$Y_l^m(\theta,\phi) = \sqrt{\frac{(2l+1)(l-m)!}{4\pi(l+m)!}}\,P_l^m(\cos\theta)\,e^{im\phi}\,, \tag{9.46}$$

$$\frac{\partial}{\partial\theta}Y_l^0(\theta,0) = \sqrt{\frac{\Gamma(l+1)}{\Gamma(l)}}\,Y_l^1(\theta,0)\,, \tag{9.47}$$

$$P_l^{-m}(x) = (-1)^m\,\frac{(l-m)!}{(l+m)!}\,P_l^m(x)\,. \tag{9.48}$$

Bessel functions

Bessel functions are solutions of Bessel's differential equation

$$x^2\frac{d^2J_\alpha(x)}{dx^2} + x\frac{dJ_\alpha(x)}{dx} + (x^2-\alpha^2)\,J_\alpha(x) = 0\,, \tag{9.49}$$

where α is a complex number and $J_\alpha(x)$ is Bessel function of order α. In most physical problems with spherical symmetry, α takes half-integer values, $\alpha = n+1/2$.

Consequently, one defines the spherical Bessel functions of integer order, n, as

$$j_n(x) \equiv \sqrt{\frac{\pi}{2x}}\, J_{n+1/2}(x) \equiv (-x)^n \left(\frac{1}{x}\frac{d}{dx}\right)^n \frac{\sin(x)}{x}. \tag{9.50}$$

The first few spherical Bessel functions are

$$\begin{aligned}
j_0(x) &= \frac{\sin(x)}{x}, && (9.51)\\
j_1(x) &= \frac{1}{x}\frac{\sin(x)}{x} - \frac{\cos(x)}{x}, && (9.52)\\
j_2(x) &= \left(\frac{3}{x^2} - 1\right)\frac{\sin(x)}{x} - \frac{3}{x}\frac{\cos(x)}{x}, && (9.53)\\
j_3(x) &= \left(\frac{15}{x^3} - \frac{6}{x}\right)\frac{\sin(x)}{x} - \left(\frac{15}{x^2} - 1\right)\frac{\cos(x)}{x}, && (9.54)\\
j_4(x) &= \left(\frac{105}{x^4} - \frac{45}{x^2} + 1\right)\frac{\sin(x)}{x} - \left(\frac{105}{x^3} - \frac{10}{x}\right)\frac{\cos(x)}{x}. && (9.55)
\end{aligned}$$

9.1.4 Three-dimensional spherical harmonic oscillator eigenfunctions

The isotropic three-dimensional harmonic oscillator is described by Schrodinger's equation

$$\left[-\frac{\hbar}{2m}\Delta + \frac{1}{2} m\,\omega^2 r^2\right] \phi_{nlm}(r,\theta,\phi) = \epsilon_{n\,l}\, \phi_{nlm}(r,\theta,\phi). \tag{9.56}$$

The wave-function is separable in the radial and polar coordinates as

$$\phi_{nlm}(r,\theta,\phi) = \frac{R_{nl}(r)}{r} Y_l^m(\theta,\phi), \tag{9.57}$$

where

$$\begin{aligned}
R_{nl}(r) &= \frac{1}{r}\left[\frac{2(n-1)!}{\sqrt{\beta}\Gamma(n+l+1/2)^3}\right]^{1/2} \sqrt{x}^{l+1}\, e^{-x/2}\, L_{n-1}^{l+1/2}(x)\\
x &= \beta r^2
\end{aligned}$$

$$
\begin{aligned}
\beta &= \frac{m\omega}{\hbar} \\
\epsilon_{nl} &= \hbar\omega(2n+l-1/2)\,.
\end{aligned}
\tag{9.58}
$$

Note that there are two conventions in use regarding the possible values of integer n: $n \geq 0$ and $n \geq 1$. The latter is used in this work.

9.1.5 Gegenbaur expansion

Gegenbaur's addition theorem of bessel functions of the first kind reads

$$
\frac{J_\nu(r)}{r^\nu} = \frac{2^\nu\,\Gamma(\nu)}{x^\nu y^\nu} \sum_{\mu=0}^{\infty} (\nu+\mu)\, J_{\nu+\mu}(x)\, J_{\nu+\mu}(y)\, C_\mu^\nu(\cos(\theta))\,, \tag{9.59}
$$

where $\nu > 0$ and for all values of x, y and θ (the angle between $\vec{x}$ and $\vec{y}$). The variable r is given by $r = \sqrt{x^2+y^2-2xy\cos(\theta)}$. $\Gamma(\nu)$ is the Gamma function and C_μ^ν refers to Gegenbaur polynomials. The first few Gegenbaur polynomials are given by

$$
\begin{aligned}
C_0^\nu &= 0\,, \\
C_1^{3/2} &= 3\cos(\theta)\,, \\
C_2^{3/2} &= -\frac{3}{2} + \frac{15\cos^2(\theta)}{2}\,, \\
C_3^{3/2} &= -\frac{15\cos(\theta)}{2} + \frac{35\cos^3(\theta)}{2}\,.
\end{aligned}
\tag{9.60}
$$

A formula related to Eq. (9.59) is

$$
\frac{J_{-\nu}(r)}{r^\nu} = \frac{2^\nu\,\Gamma(\nu)}{x^\nu y^\nu} \sum_{\mu=0}^{\infty} (-1)^\mu\,(\nu+\mu)\, J_{-\nu-\mu}(x)\, J_{\nu+\mu}(y)\, C_\mu^\nu(\cos(\theta))\,, \tag{9.61}
$$

and it holds only when $|ye^{\pm i\theta}| < |x|$. Combining Eqs. (9.59) and (9.61), one obtains the relevant expansion for Bessel functions of the second kind and those of the modified Bessel functions. For details, refer to [195]. Gegenbaur's addition theorem is a key ingredient for the analytical calculation of the EDF couplings obtained from the application of the DME to the HF of chiral EFT three-nucleon interaction at N^{2}LO. Refer to section 9.11 for details.

9.1.6 Functional derivatives

A functional maps functions into a number. Analogous to the derivative of functions, one defines the functional derivative of a functional, $F[f(x)]$, with respect to $f(x)$ as

$$\frac{\delta F}{\delta f(x)} = lim_{\varepsilon \to 0} \frac{F\left[f(y) + \varepsilon\, \delta\,(y-x)\right] - F\left[f(y)\right]}{\varepsilon} \,. \tag{9.62}$$

The functional derivative satisfies several relations which are analogous to the ones satisfied by the derivatives of functions. For instance, if F and G are two functional of $f(x)$,

$$\frac{\delta(FG)}{\delta f(x)} = G\frac{\delta(F)}{\delta f(x)} + F\frac{\delta(G)}{\delta f(x)} \,, \tag{9.63}$$

while for $F[f(x)] = \int_a^b dx\, [f(x)]^n$,

$$\frac{\delta(F)}{\delta f(x)} = n\, [f(x)]^{n-1} \,. \tag{9.64}$$

9.2 The one-body density matrix and densities

The basic quantity in the EDF approach for nuclei is the OBDM and the various nonlocal and local densities that can be extracted from it. An extensive discussion of these basic quantities is given in this section.

9.2.1 Properties of single particle states

The wave function of a particle having spin S is a spinor of rank $2S$, i.e. is composed of $2S + 1$ components. The particles constituting the nucleus are protons and neutrons which have spin, $S = \frac{1}{2}$. The single particle states are assumed to have a good isospin projection, but mix spin states. We use $\sigma = \pm\frac{1}{2}$, $q = \pm\frac{1}{2}$ to designate the spin, isospin and i, j, k... the remaining quantum numbers of the single-particle states respectively. Thus the single-particle states can be designated as

$$\mid iq\rangle = \sum_{\sigma} \mid i\sigma q\rangle \,. \tag{9.65}$$

In spinor notation, the single particle spinors are given by four real functions φ_1 , ..., φ_4

$$\langle\vec{r}|iq\rangle = \varphi_i(\vec{r}q) = \begin{pmatrix} \varphi_i(\vec{r}\,\sigma = +\frac{1}{2}\,q) \\ \varphi_i(\vec{r}\,\sigma = -\frac{1}{2}\,q) \end{pmatrix} = \begin{pmatrix} \varphi_{1,i}(\vec{r}q) \;+\; i\,\varphi_{2,i}(\vec{r}q) \\ \varphi_{3,i}(\vec{r}q) \;+\; i\,\varphi_{4,i}(\vec{r}q) \end{pmatrix} . \tag{9.66}$$

The orthonormality and closure relationships are given as

$$\int d\vec{r}\,\varphi_i^\dagger(\vec{r}q)\,\varphi_j(\vec{r}q') \;=\; \delta_{ij}\delta_{qq'}\,, \tag{9.67}$$

$$\sum_i \varphi_i^\dagger(\vec{r}\sigma q)\,\varphi_j(\vec{r}'\sigma' q') \;=\; \delta(\vec{r}-\vec{r}')\,\delta_{\sigma\sigma'}\,\delta_{qq'}\,. \tag{9.68}$$

It is important to characterize the single-particle properties under time reversal. The time-reversal operator is given by $T = i\sigma_y K_0$ where K_0 denotes the complex conjugation operator and σ_y is a pauli spin matrix. Thus the time-reverse of the single-particle states is

$$(T\varphi)_i\,(\vec{r}\sigma q) = 2\sigma\varphi_i^*(\vec{r}\bar{\sigma}q)\,, \tag{9.69}$$

where $\bar{\sigma} = -\sigma$. For an extensive discussion, refer to Ref. [81].

9.2.2 One-body density matrix

The one-body density matrix can be written in $(\vec{r}\sigma q)$ space as

$$\rho_q(\vec{r}\,\sigma,\vec{r}\,'\,\sigma') \;=\; \langle\,\Phi\,|\,c^\dagger(\vec{r}\,'\,\sigma'\,q)\,c\,(\vec{r}\,\sigma\,q)\,|\,\Phi\rangle = \sum_{ij}\;\varphi_i^*(\vec{r}\,'\sigma' q)\;\varphi_j(\vec{r}\sigma q)\;\rho_{ji}^q\,, \qquad (9.70)$$

where $|\Phi\rangle$ defines the many-body wave function and $\rho_{ji}^q = \langle\,\Phi\,|\,c_i^\dagger\,c_j\,|\,\Phi\rangle$ defines the density matrix in the basis $\{c_i/\varphi_i\}$. Since the single-particle states have definite isospin quantum number, the density matrix is diagonal in isospin subspace. The density matrix can be separated in its scalar/vector-isoscalar/isovector parts

$$\begin{aligned}\rho_q(\vec{r}\,\sigma,\vec{r}\,'\,\sigma') \;&=\; \frac{1}{4}\Bigg[\rho_0(\vec{r},\vec{r}\,')\;\delta_{\sigma\sigma'} + \vec{s}_0(\vec{r},\vec{r}\,').\vec{\sigma}_{\sigma\sigma'} \\ &\qquad + (-1)^{1/2-q}\Big(\rho_1(\vec{r},\vec{r}\,')\;\delta_{\sigma\sigma'} + \vec{s}_1(\vec{r},\vec{r}\,').\vec{\sigma}_{\sigma\sigma'}\Big)\Bigg]\,, \qquad (9.71)\end{aligned}$$

where the scalar-isoscalar, scalar-isovector, vector-isoscalar and vector-isovector parts are respectively

$$\begin{aligned}\rho_0(\vec{r},\vec{r}\,') \;&=\; \sum_{\sigma\sigma' q}\;\rho_q(\vec{r}\,\sigma,\vec{r}\,'\,\sigma')\,\delta_{\sigma\sigma'} = \sum_{\sigma q}\sum_{ij}\varphi_i^*(\vec{r}\,'\sigma q)\;\varphi_j(\vec{r}\sigma q)\;\rho_{ji}^q \\ &=\; \sum_q \rho_q(\vec{r},\vec{r}\,'), \qquad (9.72)\\ \rho_1(\vec{r},\vec{r}\,') \;&=\; \sum_{\sigma\sigma' q}\;\rho_q(\vec{r}\,\sigma,\vec{r}\,'\,\sigma')\,\delta_{\sigma\sigma'}\,\Lambda(q) \;=\; \sum_{\sigma q}\Lambda(q)\,\sum_{ij}\,\varphi_i^*(\vec{r}\,'\sigma q)\,\varphi_j(\vec{r}\sigma q)\,\rho_{ji}^q \\ &=\; \sum_q\;\rho_q(\vec{r},\vec{r}\,'), \qquad (9.73)\\ \vec{s}_0(\vec{r},\vec{r}\,') \;&=\; \sum_{\sigma\sigma' q}\;\rho_q(\vec{r}\,\sigma,\vec{r}\,'\,\sigma')\,\vec{\sigma}_{\sigma'\sigma} = \sum_{\sigma\sigma' q}\sum_{ij}\varphi_i^*(\vec{r}\,'\sigma' q)\;\varphi_j(\vec{r}\sigma q)\,\vec{\sigma}_{\sigma'\sigma}\,\rho_{ji}^q \\ &=\; \sum_q \vec{s}_q(\vec{r},\vec{r}\,'), \qquad (9.74)\\ \vec{s}_1(\vec{r},\vec{r}\,') \;&=\; \sum_{\sigma\sigma' q}\rho_q(\vec{r}\sigma,\vec{r}\,'\,\sigma')\vec{\sigma}_{\sigma'\sigma}\,\Lambda(q) \;=\; \sum_{\sigma\sigma' q}\Lambda(q)\,\sum_{ij}\,\varphi_i^*(\vec{r}\,'\sigma' q)\;\varphi_j(\vec{r}\sigma q)\,\vec{\sigma}_{\sigma'\sigma}\,\rho_{ji}^q\end{aligned}$$

$$= \sum_{q} \Lambda(q)\, \vec{s}_q(\vec{r}, \vec{r}')\,, \tag{9.75}$$

where $\Lambda(q) = (-1)^{\frac{1}{2}-q}$. The extraction of the scalar/vector-isoscalar/isovector parts from Eq.(9.71) can be done easily using properties of the Pauli matrices given in Eqs. (9.12)-(9.13).

9.2.3 Local densities

Working in neutron/proton representation and taking derivatives up to second order, the following local densities that can be formed from $\rho_q(\vec{r}, \vec{r}')$ and $\vec{s}_q(\vec{r}, \vec{r}')$

$$\begin{aligned}
\rho_q(\vec{r}) &= \sum_{ji} \varphi_j^\dagger(\vec{r}q)\, \varphi_i(\vec{r}q)\, \rho_{ij}^q\,, && (9.76)\\
\tau_q(\vec{r}) &= \sum_{ji} \vec{\nabla}\varphi_j^\dagger(\vec{r}q) \cdot \vec{\nabla}\varphi_i(\vec{r}q)\, \rho_{ij}^q\,, && (9.77)\\
s_{q,\mu}(\vec{r}) &= \sum_{ji} \varphi_j^\dagger(\vec{r}q)\, \sigma_\mu\, \varphi_i(\vec{r}q)\, \rho_{ij}^q\,, && (9.78)\\
j_{q,\mu}(\vec{r}) &= -\frac{i}{2} \sum_{ji} \Big(\varphi_j^\dagger(\vec{r}q)\, \nabla_\mu\, \varphi_i(\vec{r}q) - \nabla_\mu \varphi_j^\dagger(\vec{r}q)\, \varphi_i(\vec{r}q) \Big)\, \rho_{ij}^q\,, && (9.79)\\
J'_{q,\mu}(\vec{r}) &= -i \sum_{\nu\alpha} \sum_{ji} \varepsilon_{\mu\nu\alpha}\, \varphi_j^\dagger(\vec{r}q) \left[\nabla_\nu\, \sigma_\alpha\, \varphi_i(\vec{r}q) \right] \rho_{ij}^q && (9.80)\\
T_{q,\mu}(\vec{r}) &= \sum_{ij} \vec{\nabla}\varphi_j^\dagger(\vec{r}q) \left[\sigma_\mu \cdot \vec{\nabla}\varphi_i(\vec{r}q) \right] \rho_{ij}^q && (9.81)\\
J_{q,\mu}(\vec{r}) &= -\frac{i}{2} \sum_{\nu\alpha} \sum_{ji} \varepsilon_{\mu\nu\alpha} \Bigg(\varphi_j^\dagger(\vec{r}q) \left[\nabla_\nu\, \sigma_\alpha\, \varphi_i(\vec{r}q) \right] \\
&\qquad - \left[\nabla_\nu\, \varphi_j^\dagger(\vec{r}'q) \right] \sigma_\alpha\, \varphi_i(\vec{r}q) \Bigg)\, \rho_{ij}^q && (9.82)\\
J_{q,\mu\nu}(\vec{r}) &= -\frac{i}{2} \sum_{ij} \Bigg(\varphi_j^\dagger(\vec{r}q) \left[\sigma_\nu \nabla_\mu \varphi_i(\vec{r}q) \right] - \left[\nabla_\mu\, \varphi_j^\dagger(\vec{r}q) \right] \sigma_\nu\, \varphi_i(\vec{r}q) \Bigg)\, \rho_{ij}^q && (9.83)\\
F_{q,\mu}(\vec{r}) &= \frac{1}{2} \sum_{ij} \Bigg(\left[\vec{\nabla} \cdot \vec{\sigma}\varphi_j^\dagger(\vec{r}q) \right] \nabla_\mu \varphi_i(\vec{r}q) + \left[\nabla_\mu\, \varphi_j^\dagger(\vec{r}q) \right] \vec{\nabla} \cdot \vec{\sigma}\varphi_i(\vec{r}q) \Bigg)\, \rho_{ij}^q\,. && (9.84)
\end{aligned}$$

These are the matter density, kinetic density, spin density, current density, spin-orbit density, the spin kinetic density, the cartesian spin-orbit tensor density and the tensor kinetic density. These local densities, except $\vec{J}'_q$ are all real. It can easily be shown that in the case of time-reversal invariant systems, $\vec{J}'_q$ and $\vec{J}_q$ are equal to each other.

9.2.4 Properties under time reversal

According to Eq.(9.69), the scalar $\rho^T(\vec{r},\vec{r}')$ and vector $\vec{s}^T(\vec{r},\vec{r}')$ parts of the time reversed density matrix $\rho^T(\vec{r}\sigma,\vec{r}'\sigma')$ are [196]

$$\rho_q^T(\vec{r},\vec{r}') = \rho_q^*(\vec{r},\vec{r}') = \rho_q(\vec{r}',\vec{r}) \tag{9.85}$$

$$\vec{s}_q^T(\vec{r},\vec{r}') = -\vec{s}_q^*(\vec{r},\vec{r}') = -\vec{s}_q(\vec{r}',\vec{r}) \tag{9.86}$$

Thus, under time reversal, the transformation of the local densities is

$$\rho_q^T(\vec{r}) = \rho_q(\vec{r}), \quad \tau_q^T(\vec{r}) = \tau_q(\vec{r}), \quad \vec{s}_q^T(\vec{r}) = -\vec{s}(\vec{r}), \quad \vec{j}_q^T(\vec{r}) = -\vec{j}_q(\vec{r}) \tag{9.87}$$

$$\vec{J}_q^T(\vec{r}) = \vec{J}_q(\vec{r}), \qquad \vec{T}_q^T(\vec{r}) = -\vec{T}_q(\vec{r}), \qquad \vec{F}_q^T(\vec{r}) = -\vec{F}(\vec{r}), \tag{9.88}$$

where one can simply count the number of time-odd operators used to define the density to obtain its transformation property under time-reversal. For time-reversal invariant systems, one sets all the densities equal to their time-reversed counterparts

$$\rho_q^T(\vec{r},\vec{r}') = \rho_q(\vec{r},\vec{r}') = \rho(\vec{r}',\vec{r}) \tag{9.89}$$

$$\vec{s}_q^T(\vec{r},\vec{r}') = \vec{s}_q(\vec{r},\vec{r}') = -\vec{s}_q(\vec{r}',\vec{r}), \tag{9.90}$$

and the time-odd densities vanish. I.e.

$$\vec{s}_q(\vec{r}) = 0, \qquad \vec{j}_q(\vec{r}) = 0,$$

$$\vec{T}_q(\vec{r}) = 0 \qquad \vec{F}_q(\vec{r}) = 0. \tag{9.91}$$

The rest $\rho_q(\vec{r})$, $\tau_q(\vec{r})$, and $\vec{J}_q(\vec{r})$ are time-even densities.

9.2.5 Extension to anomalous contractions

The normal density is insufficient for the explicit treatment of pairing correlations. Thus in addition to the normal density, $\hat{\rho}_{l'l} = c^{\dagger}_{l'}c_l$, , one introduces pairing tensor, referred to as the anomalous density, $\hat{\kappa}_{l'l} = c_{l'}c_l$. The generalized one-body density matrix is defined as

$$\mathcal{R} = \begin{pmatrix} \langle\Phi|\hat{\rho}|\Phi\rangle & \langle\Phi|\hat{\kappa}|\Phi\rangle \\ -\langle\Phi|\hat{\kappa}|\Phi\rangle^{*} & 1-\langle\Phi|\hat{\rho}|\Phi\rangle^{*} \end{pmatrix} = \begin{pmatrix} \langle\Phi|c^{\dagger}_{l'}c_l|\Phi\rangle & \langle\Phi|c_{l'}c_l|\Phi\rangle \\ \langle\Phi|c^{\dagger}_{l'}c^{\dagger}_l|\Phi\rangle & \langle\Phi|c_{l'}c^{\dagger}_l|\Phi\rangle \end{pmatrix} \tag{9.92}$$

where l' and l are elements of the single particle configuration space and $|\Phi\rangle$ is a quasi-particle vacuum [38]. The operator $\hat{\rho}$ is hermitean $(\hat{\rho}^{\dagger} = \hat{\rho})$ and $\hat{\kappa}$ is skew (anti) symmetric $\hat{\kappa}^{T} = -\hat{\kappa}$. Here $\hat{\kappa}^{T}$ refers to the transpose of $\hat{\kappa}$, not the time reverse of $\hat{\kappa}$. Two important relations hold for $\hat{\rho}$ and $\hat{\kappa}$. These are

$$\hat{\rho}^{2} - \hat{\rho} = -\hat{\kappa}\hat{\kappa}^{\dagger}, \qquad \hat{\rho}\hat{\kappa} = \hat{\kappa}\hat{\rho}^{*}. \tag{9.93}$$

Using the above two relations, it can be easily seen that the generalized matrix $\mathcal{R}$ is idempotent i.e. $\mathcal{R}^{2} = \mathcal{R}$. In fact, $\mathcal{R}$ is also Hermitean. The pairing tensor can be transformed into the pairing density matrix, $\tilde{\rho}$. This is given in $(\vec{r}\sigma q)$ space as

$$\tilde{\rho}(\vec{r}\sigma q, \vec{r}'\sigma' q') \equiv 2\bar{\sigma}' \langle\Phi|\, c_{\vec{r}'\bar{\sigma}'q'}\, c_{\vec{r}\sigma q}\,|\Phi\rangle = 2\bar{\sigma}'\, \kappa(\vec{r}\sigma q, \vec{r}'\bar{\sigma}' q'). \tag{9.94}$$

We still assume that the density matrix is diagonal in isospin subspace. In pairing terms, this assumption means that there is no proton-neutron pairing. This implies that the pairing density $\tilde{\rho}(\vec{r}\sigma q, \vec{r}'\sigma' q')$ can be written in the form $\tilde{\rho}_q(\vec{r}\sigma, \vec{r}'\sigma')\,\delta_{qq'}$. The pairing density matrix can be resolved into its scalar/isoscalar, vector/isovector parts in exactly the same way as the normal density matrix. Thus, appropriate contractions in spin and isospin space yield

$$\begin{aligned}
\tilde{\rho}_0(\vec{r},\vec{r}') &= \sum_{\sigma\sigma' q} \tilde{\rho}_q(\vec{r}\,\sigma,\vec{r}'\,\sigma')\,\delta_{\sigma\sigma'} = \sum_{\sigma q}\sum_{ij} 2\bar{\sigma}\,\varphi_i(\vec{r}'\bar{\sigma}q)\;\varphi_j(\vec{r}\sigma q)\,\kappa^q_{ji}\,,\\
&= \sum_q \tilde{\rho}_q(\vec{r},\vec{r}')\,, \qquad (9.95)\\
\tilde{\rho}_1(\vec{r},\vec{r}') &= \sum_{\sigma\sigma' q} \tilde{\rho}_q(\vec{r}\,\sigma,\vec{r}'\,\sigma')\,\delta_{\sigma\sigma'}\,\Lambda(q) = \sum_{\sigma q}\Lambda(q)\sum_{ij} 2\bar{\sigma}\,\varphi_i(\vec{r}'\bar{\sigma}q)\,\varphi_j(\vec{r}\sigma q)\,\kappa^q_{ji}\,,\\
&= \sum_q \Lambda(q)\,\tilde{\rho}_q(\vec{r},\vec{r}')\,, \qquad (9.96)\\
\tilde{\vec{s}}_0(\vec{r},\vec{r}') &= \sum_{\sigma\sigma' q} \tilde{\rho}_q(\vec{r}\,\sigma,\vec{r}'\,\sigma')\,\vec{\sigma}_{\sigma'\sigma} = \sum_{\sigma\sigma' q}\sum_{ij} 2\bar{\sigma}'\,\varphi_i(\vec{r}'\bar{\sigma}'q)\;\varphi_j(\vec{r}\sigma q)\,\vec{\sigma}_{\sigma'\sigma}\,\kappa^q_{ji}\,,\\
&= \sum_q \tilde{\vec{s}}_q(\vec{r},\vec{r}')\,, \qquad (9.97)\\
\tilde{\vec{s}}_1(\vec{r},\vec{r}') &= \sum_{\sigma\sigma' q} \tilde{\rho}_q(\vec{r}\,\sigma,\vec{r}'\,\sigma')\;\vec{\sigma}_{\sigma'\sigma}\,\Lambda(q)\\
&= \sum_{\sigma\sigma' q}\Lambda(q)\sum_{ij} 2\bar{\sigma}'\,\varphi_i(\vec{r}'\bar{\sigma}'q)\;\varphi_j(\vec{r}\sigma q)\,\vec{\sigma}_{\sigma'\sigma}\,\kappa^q_{ji}\,,\\
&= \sum_q \tilde{\vec{s}}_q(\vec{r},\vec{r}')\,, \qquad (9.98)
\end{aligned}$$

Working in neutron/proton representations, and going directly to the local densities, the following is the list of the local pairing densities that can be formed by taking derivatives up to second order

$$\begin{aligned}
\tilde{\rho}_q(\vec{r}) &= \sum_{\sigma}\sum_{ij} 2\bar{\sigma}\,\varphi_i(\vec{r}\bar{\sigma}q)\;\varphi_j(\vec{r}\sigma q)\,\kappa^q_{ji}\,, \qquad (9.99)\\
\tilde{\tau}_q(\vec{r}) &= \sum_{\sigma}\sum_{ij} 2\bar{\sigma}\,\vec{\nabla}\varphi_i(\vec{r}\bar{\sigma}q)\,\cdot\,\vec{\nabla}\varphi_j(\vec{r}\sigma q)\,\kappa^q_{ji}\,, \qquad (9.100)\\
\tilde{s}_{q,\mu}(\vec{r}) &= \sum_{\sigma\sigma'}\sum_{ij} 2\bar{\sigma}'\,\varphi_i(\vec{r}\,\bar{\sigma}'q)\,\langle\sigma'|\sigma_\mu|\sigma\rangle\,\varphi_j(\vec{r}\sigma q)\,\kappa^q_{ji} = 0\,, \qquad (9.101)
\end{aligned}$$

$$
\begin{aligned}
\tilde{j}_{q,\mu}(\vec{r}) &= \sum_{\sigma ij} 2\bar{\sigma} \Big(\varphi_i(\vec{r}\bar{\sigma}q)\nabla_\mu \varphi_j(\vec{r}\sigma q) - \nabla_\mu \varphi_i(\vec{r}\bar{\sigma}q)\varphi_j(\vec{r}\sigma q) \Big) \kappa^q_{ji}, && (9.102) \\
\tilde{T}_{q,\mu}(\vec{r}) &= \sum_{\sigma\sigma'} \sum_{ij} 2\bar{\sigma}' \vec{\nabla} \varphi_i(\vec{r}\bar{\sigma}q) \cdot \langle \sigma' | \sigma_\mu | \sigma \rangle \vec{\nabla} \varphi_j(\vec{r}\sigma q)\, \kappa^q_{ji}\,, && (9.103) \\
\tilde{J}_{q,\mu}(\vec{r}) &= -\frac{i}{2} \sum_{\nu\alpha} \sum_{\sigma\sigma'} \sum_{ij} 2\bar{\sigma}'\varepsilon_{\mu\nu\alpha} \Big(\varphi_i(\vec{r}'\bar{\sigma}'q)\nabla_\nu \langle \sigma' | \sigma_\alpha | \sigma \rangle \varphi_j(\vec{r}\sigma q) \\
&\qquad - \nabla_\nu \varphi_i(\vec{r}\bar{\sigma}'q) \langle \sigma' | \sigma_\alpha | \sigma \rangle \varphi_j(\vec{r}'\sigma q) \Big) \kappa^q_{ji}, && (9.104) \\
\tilde{J}_{q,\mu\nu}(\vec{r}) &= -\frac{i}{2} \sum_{\sigma\sigma'} \sum_{ij} 2\bar{\sigma}' \Big(\varphi_i(\vec{r}\bar{\sigma}'q)\, \nabla_\mu \langle \sigma' | \sigma_\nu | \sigma \rangle \varphi_j(\vec{r}\sigma q) \\
&\qquad - \nabla_\mu \varphi_i(\vec{r}\bar{\sigma}'q) \langle \sigma' | \sigma_\nu | \sigma \rangle \varphi_j(\vec{r}\sigma q) \Big) \kappa^q_{ji}\,, && (9.105) \\
\tilde{F}_{q,\mu}(\vec{r}) &= \frac{1}{2} \sum_{\sigma\sigma'} \sum_{ij} 2\bar{\sigma}' \Big(\vec{\nabla} \cdot \langle \sigma' | \vec{\sigma} | \sigma \rangle \varphi_j(\vec{r}\bar{\sigma}q)\nabla_\mu \varphi_i(\vec{r}\sigma q) \\
&\qquad + \nabla_\mu \varphi_j(\vec{r}\bar{\sigma}'q)\vec{\nabla} \cdot \langle \sigma' | \vec{\sigma} | \sigma \rangle \varphi_i(\vec{r}\sigma q) \Big) \kappa^q_{ji}\,. && (9.106)
\end{aligned}
$$

One notes that most of these anomalous local densities are not used in current empirical parameterizations of nuclear EDFs (see section 4.2.2). In fact, only the local pairing density, $\tilde{\rho}_q$, is used. As discussed in section 5.3.8, the application of the DME to the anomalous part of the OBDM results in these local densities. Thus, these densities may be useful in future non-empirical construction of the particle-particle/pairing part of nuclear EDFs.

9.2.6 Relations among the densities

One can establish a number of relations among the various local and nonlocal densities defined in the previous section. We start with those relations which are important in the derivation of the DME of the scalar/vector components of the normal part of the OBDM. These are

$$
\left[\Big(\nabla^2 + \nabla'^2 \Big) \rho_q(\vec{r}, \vec{r}\,') \right] \Big|_{\vec{r}=\vec{r}\,'} = \nabla^2 \rho_q(\vec{r}) - 2\tau_q(\vec{r}) \qquad (9.107)
$$

$$\nabla^2 \rho_q(\vec{r}, \vec{r}\,')\Big|_{\vec{r}=\vec{r}\,'} = \frac{1}{2}\nabla^2\rho_q(\vec{r}) - \tau_q(\vec{r}) + i\vec{\nabla}\cdot\vec{j}_q(\vec{r}) \quad (9.108)$$

$$\nabla'^2 \rho_q(\vec{r}, \vec{r}\,')\Big|_{\vec{r}=\vec{r}\,'} = \frac{1}{2}\nabla^2\rho_q(\vec{r}) - \tau_q(\vec{r}) - i\vec{\nabla}\cdot\vec{j}(\vec{r}) \quad (9.109)$$

$$\begin{aligned}\left[\vec{\nabla}\rho_q(\vec{r}, \vec{r}\,')\right]\Big|_{\vec{r}=\vec{r}\,'} &= \left[\vec{\nabla}'\rho_q(\vec{r}, \vec{r}\,')\right]^*\Big|_{\vec{r}=\vec{r}\,'} \\ &= \frac{1}{2}\vec{\nabla}\rho_q(\vec{r}) + i\vec{j}_q(\vec{r}) \qquad (9.110)\end{aligned}$$

$$\left[\left(\nabla^2 + \nabla'^2\right) s_{\nu,q}(\vec{r}, \vec{r}\,')\right]\Big|_{\vec{r}=\vec{r}\,'} = \nabla^2 s_{\nu,q}(\vec{r}) - 2T_{\nu,q}(\vec{r}) \quad (9.111)$$

$$\begin{aligned}\left[\nabla_\mu s_{\nu,q}(\vec{r}, \vec{r}\,')\right]\Big|_{\vec{r}=\vec{r}\,'} &= \left[\nabla'_\mu s_{\nu,q}(\vec{r}, \vec{r}\,')\right]^*\Big|_{\vec{r}=\vec{r}\,'} \\ &= \frac{1}{2}\nabla_\mu s_{\nu,q}(\vec{r}) + iJ_{\mu\nu,q}(\vec{r}). \qquad (9.112)\end{aligned}$$

Most of these relations were initially given in Ref. [197]. Here, we extended the list by deriving additional relations which are found be useful in the derivation of the generalized PSA-DME, discussed in section 9.5.3. We illustrate the derivation of these relations by taking Eq. (9.107) as an example. Starting with the left hand side of Eq. (9.107)

$$\begin{aligned}\left[\left(\nabla^2 + \nabla'^2\right)\rho_q(\vec{r}, \vec{r}\,')\right]\Big|_{\vec{r}=\vec{r}\,'} &= \left[\left(\nabla^2 + \nabla'^2\right)\sum_{ji}\varphi_j^\dagger(\vec{r}\,'q)\,\varphi_i(\vec{r}q)\,\rho_{ij}^q\right]\Big|_{\vec{r}=\vec{r}\,'}, \\ &= \sum_{ji}\rho_{ij}^q\left[\varphi_i(\vec{r}q)\,\nabla^2\varphi_j^\dagger(\vec{r}q) + \varphi_j(\vec{r}q)\,\nabla^2\varphi_i^\dagger(\vec{r}q)\right], \\ &= \sum_{ji}\rho_{ij}^q\Big[\nabla^2\left(\varphi_i(\vec{r}q)\,\varphi_j^\dagger(\vec{r}q)\right) \\ &\qquad - 2\,\vec{\nabla}\varphi_j(\vec{r}q)\cdot\vec{\nabla}\varphi_i^\dagger(\vec{r}q)\Big], \\ &= \nabla^2\rho_q(\vec{r}) - 2\tau_q(\vec{r}), \qquad (9.113)\end{aligned}$$

where we used the definitions of $\rho_q(\vec{r})$ and $\tau_q(\vec{r})$ given in Eqs. (9.76) and (9.77). The same set of relations holds for the anomalous densities as differentiation is the only operation that is applied in the derivations. Hence, we avoid repeating these relations for the anomalous densities. However, under general circumstances discussed in [81], the nonlocal anomalous density, $\tilde{\rho}_q(\vec{r},\vec{r}')$ satisfies

$$\tilde{\rho}_q(\vec{r},\vec{r}') = \tilde{\rho}_q(\vec{r}',\vec{r}) , \tag{9.114}$$

which results in $\tilde{\vec{j}}_q(\vec{R}) = 0$. For the nonlocal anomalous spin density, we have

$$\tilde{\vec{s}}_q(\vec{r},\vec{r}') = -\tilde{\vec{s}}_q(\vec{r}',\vec{r}). \tag{9.115}$$

9.3 Local Gauge transformation of the OBDM and local densities

Neglecting relativistic effects, the nuclear EDF must be invariant under Galilean transformation, while the usual justification for the requirement of a locally gauge invariant EDF is the fact that the underlying nuclear interaction is expected to be gauge invariant. This seems to hold only for local interactions. Still, it is shown in Eq.(9.130) that Galilean transformation is a special kind of local gauge transformation. In addition, the locally gauge-invariant bilinear combination of densities, which is what we are interested in, do not depend on whether one invokes Galilean invariance or local gauge invariance. Thus for the sake of generality, we discuss the local gauge transformation of the normal and anomalous parts of the OBDM and densities. The ultimate objective is to obtain the bilinear combination of densities that are invariant with respect to local gauge transformation.

9.3.1 Local Gauge transformation in many-body physics

In many-body physics, one can formulate local gauge transformation in two equivalent ways (i) local gauge transformation of the many-body wave-function which is an intuitive generalization of the local gauge transformation of single-particle wave-functions especially in the case of Hartree-Fock approximation (ii) local gauge transformation in second quantization formalism which is very general and can be applied in any many-body approximation.

Conventional formulation

In the usual formulation, local gauge transformation is applied to the N-body Hartree-Fock wave-function $|\Phi\rangle$ in space, spin and isospin coordinate space

$$\Phi(x_1, x_2, ..., x_n, t) = \exp\left\{ i \sum_{j=1}^{A} \phi(x_j) \right\} \Phi(x_1, x_2, ..., x_n, t), \tag{9.116}$$

where $x_i = (\vec{r}_i, \sigma_i, q_i)$ and $\phi(x_j) = \phi(\vec{r}_j, t)$ is an arbitrary, differentiable real function of the position $\vec{r}$ and time t. In general $\phi(x_j)$ are independent of spin and isospin coordinates, and in the static picture, they do not depend on t.

Second quantization formulation

For generalization of local gauge transformation to other many-body approximations where there is no explicit conservation of particle number, one has to formulate local gauge transformation in second quantization. Since the state vectors in second quantization are elements of abstract Hilbert space or Fock space, local gauge transformation must be performed by an abstract unitary operator [198]. When the transformed-state vector is projected in to the N-particle subspace, the transformed wave-function in the subspace is equal to the projection of the original-state vector times the appropriate space and time dependent phase factors. In second quantization the state vector $|\Phi\rangle$, which is not necessarily an eigenstate of particle number, is represented in Fock space by the column vector

$$|\Phi\rangle = col\left\{|\Phi^0\rangle, |\Phi^1\rangle, ..., |\Phi^n\rangle, ...\right\}, \tag{9.117}$$

where $|\Phi^i\rangle$ refers to i-particle component of the state-vector. A local single-particle operator ϕ, which is assumed to be diagonal in isospin space, can be represented in second quantization as an operator in Fock space

$$\sum_{\sigma_1\sigma_2}\sum_{q}\int d\vec{r}\,\langle\vec{r}\sigma_1 q|\phi|\vec{r}\sigma_2 q\rangle\, a^\dagger(\vec{r}\sigma_1 q)\, a(\vec{r}\sigma_2 q)\,. \tag{9.118}$$

Defining the unitary operator U as

$$U = \exp\left\{i\sum_{\sigma_1\sigma_2}\sum_{q}\int d\vec{r}\,\langle\vec{r}\sigma_1 q|\phi|\vec{r}\sigma_2 q\rangle\, a^\dagger(\vec{r}\sigma_1 q)\, a(\vec{r}\sigma_2 q)\right\}, \tag{9.119}$$

the local gauge transformation of the state-vector is given by [199]

$$|\Phi\rangle' = U|\Phi\rangle. \tag{9.120}$$

One can easily verify that this gives back the previous formulation when applied to an N-particle Hartree-Fock wave-function. Once the unitary operator U is defined, local gauge transformation can be carried out by transforming the creation and annihilation operators

$$\begin{aligned} a'(\vec{r}\sigma q) &= Ua(\vec{r}\sigma q)U^\dagger = e^{-i\phi(\vec{r}\sigma q)}\, a(\vec{r}\sigma q) \\ a^{\dagger'}(\vec{r}\sigma q) &= Ua^\dagger(\vec{r}\sigma q)U^\dagger = e^{i\phi(\vec{r}\sigma q)} a^\dagger(\vec{r}\sigma q). \end{aligned} \tag{9.121}$$

9.3.2 Local Gauge transformation of normal densities

The local gauge transformation of the normal part of the OBDM is

$$\rho'_q(\vec{r}_1\sigma_1,\vec{r}_2\sigma_2) = \exp\left\{i\Big(\phi(\vec{r}_1)-\phi(\vec{r}_2)\Big)\right\}\rho_q(\vec{r}_1\sigma_1,\vec{r}_2\sigma_2). \tag{9.122}$$

When the various local densities involved in the EDF are calculated from the locally gauge-transformed density matrix Eq.(9.122), one obtains the following relations [200]

$$\begin{aligned}
\rho'_q(\vec{r}) &= \rho_q(\vec{r}) && (9.123)\\
\tau'_q(\vec{r}) &= \tau_q(\vec{r}) + 2\vec{j}_q(\vec{r})\cdot\vec{\nabla}\phi(\vec{r}) + \rho_q(\vec{r})\Big(\vec{\nabla}\phi(\vec{r})\Big)^2, && (9.124)\\
s'_{q,\nu}(\vec{r}) &= s_{q,\nu}(\vec{r}), && (9.125)\\
j'_{q,\nu}(\vec{r}) &= j_{q,\nu}(\vec{r}) + \rho_q(\vec{r})\nabla_\nu\phi(\vec{r}), && (9.126)\\
T'_{q,\nu}(\vec{r}) &= T_{q,\nu}(\vec{r}) + 2\sum_\mu J_{q,\nu\mu}(\vec{r})\nabla_\mu\phi(\vec{r}) + s_{q,\nu}(\vec{r})\Big(\vec{\nabla}\phi(\vec{r})\Big)^2, && (9.127)\\
J'_{q,\nu\mu}(\vec{r}) &= J_{q,\nu\mu}(\vec{r}) + s_{q,\mu}(\vec{r})\nabla_\nu\phi(\vec{r}), && (9.128)\\
F'_{q,\nu}(\vec{r}) &= F_{q,\nu}(\vec{r}) + \nabla_\nu\phi(\vec{r})\sum_\mu\nabla_\mu\phi(\vec{r})\,s_{q,\mu}(\vec{r}) + \sum_\mu\nabla_\mu\phi(\vec{r})\,J_{q,\nu\mu}(\vec{r})\\
&\quad + \nabla_\nu\phi(\vec{r})\sum_\mu J_{q,\mu\mu}(\vec{r}). && (9.129)
\end{aligned}$$

From the previous relationships, the only bilinear combinations of local densities which are invariant under local gauge transformation are

(i) $\rho_q(\vec{r})\tau_{q'}(\vec{r}) - \vec{j}_q(\vec{r})\cdot\vec{j}_{q'}(\vec{r})$

(ii) $\rho_q(\vec{r})\vec{\nabla}\cdot\vec{J}_{q'}(\vec{r}) + \vec{j}_q(\vec{r})\cdot\vec{\nabla}\times\vec{s}_{q'}(\vec{r})$,

(iii) $\vec{\nabla}\rho_q(\vec{r})\cdot\vec{J}_{q'}(\vec{r}) - \vec{s}_q(\vec{r})\cdot\vec{\nabla}\times\vec{j}_{q'}(\vec{r})$,

(iv)$\rho_q(\vec{r})\,\vec{J}_{q'}(\vec{r}) + \vec{s}_q(\vec{r})\times\vec{j}_{q'}(\vec{r})$

(v) $\vec{s}_q(\vec{r})\cdot\vec{T}_{q'}(\vec{r}) - \sum_{\nu\mu} J_{q.\nu\mu}(\vec{r})J_{q'.\nu\mu}(\vec{r})$

(vi) $\sum_{\mu} J_{q,\mu\mu}(\vec{r}) \sum_{\nu} J_{q',\nu\nu}(\vec{r}) + \sum_{\nu\mu} J_{q,\nu\mu}(\vec{r})\, J_{q',\mu\nu}(\vec{r}) - 2\vec{s}_q(\vec{r}) \cdot \vec{F}_{q'}(\vec{r})$.

Galilean invariance is a special case of the local gauge invariance for which the phase in Eq. (9.116) is given by

$$\phi(\vec{r}) = \frac{\vec{p} \cdot \vec{r}}{\hbar}, \tag{9.130}$$

where $\vec{p}$ is the linear momentum of the boost transformation [200]. Transformation properties of $\tau_q(\vec{r})$ and $\vec{j}_q(\vec{r})$ allow one to interpret $\vec{\nabla}\phi(\vec{r})$ as a velocity field,

$$\vec{v}(\vec{r}) = \frac{\hbar}{m}\vec{\nabla}\phi(\vec{r}), \tag{9.131}$$

which shows that the flow of matter obtained through the local gauge transformation is irrotational, $\vec{\nabla} \times \vec{v} = 0$ [200].

9.3.3 Local Gauge transformation of anomalous densities

The local gauge transformation of the anomalous part of the OBDM reads

$$\tilde{\rho}'_q(\vec{r}_1\sigma_1, \vec{r}_2\sigma_2) = \exp\left\{i\Big(\phi(\vec{r}_1) + \phi(\vec{r}_2)\Big)\right\} \tilde{\rho}_q(\vec{r}_1\sigma_1, \vec{r}_2\sigma_2). \tag{9.132}$$

The local gauge transformation of the various local anomalous densities are calculated from the locally gauge-transformed anomalous part of the OBDM as given in Eq.(9.132). Thus one obtains

$$\begin{aligned} \tilde{\rho}'_q(\vec{r}) &= e^{i2\phi(\vec{r})}\tilde{\rho}_q(\vec{r}) && (9.133) \\ \tilde{\tau}'_q(\vec{r}) &= e^{i2\phi(\vec{r})}\left[\tilde{\tau}_q(\vec{r}) + \vec{\nabla}\phi(\vec{r}) \cdot \left(\vec{\nabla}_1\tilde{\rho}_q(\vec{r}_1, \vec{r}_2) + \vec{\nabla}_2\tilde{\rho}_q(\vec{r}_1, \vec{r}_2)\right)\Big|_{\vec{r}_1=\vec{r}_2=\vec{r}}\right. \\ &\qquad \left. + \tilde{\rho}_q(\vec{r})\big(\vec{\nabla}\phi(\vec{r})\big)^2\right], && (9.134) \end{aligned}$$

$$\begin{aligned}
\tilde{s}'_{q,k}(\vec{r}) &= e^{i2\phi(\vec{r})}\tilde{s}_{q,k}(\vec{r}) \;=\; 0, && (9.135)\\
\tilde{\vec{j}}'_q(\vec{r}) &= e^{i2\phi(\vec{r})}\tilde{\vec{j}}_q(\vec{r}), && (9.136)\\
\tilde{\vec{T}}'_q(\vec{r}) &= e^{i2\phi(\vec{r})}\Big[\tilde{\vec{T}}_q(\vec{r}) + \vec{\nabla}\phi(\vec{r}) \cdot \Big(\vec{\nabla}_1\tilde{\vec{s}}_q(\vec{r}_1,\vec{r}_2) + \vec{\nabla}_2\tilde{\vec{s}}_q(\vec{r}_1,\vec{r}_2)\Big)\Big|_{\vec{r}_1=\vec{r}_2=\vec{r}} \\
&\quad + \tilde{\vec{s}}_q(\vec{r})\big(\vec{\nabla}\phi(\vec{r})\big)^2\Big], && (9.137)\\
\tilde{J}'_{q,kl}(\vec{r}) &= e^{i2\phi(\vec{r})}\tilde{J}_{q,kl}(\vec{r}). && (9.138)
\end{aligned}$$

The above relationships yield the following locally gauge invariant bilinear combination of densities in the pp-channel

(i) $\left|\tilde{\rho}_q(\vec{r})\right|^2$

(ii) $\left|\tilde{\vec{s}}_q(\vec{r})\right|^2$

(iii) $\tilde{\rho}_q(\vec{r})\big(\Delta\tilde{\rho}^*_q(\vec{r}) - 4\tilde{\tau}^*_q(\vec{r})\big)$

(iv) $\tilde{\vec{s}}_q(\vec{r}) \cdot \big(\Delta\tilde{\vec{s}}^*_q(\vec{r}) - 4\tilde{\vec{T}}^*_q(\vec{r})\big)$

(v) $\left|\tilde{\vec{j}}_q(\vec{r})\right|^2$

(vi) $\sum_{\nu\mu} \tilde{J}^*_{q,\nu\mu} J_{q,\nu\mu}$, noting that complex conjugates of (iii) and (iv) are also gauge invariant combinations. One can verify that starting from a local/semi-local interaction, such as the standard Skyrme given in Eq. (4.12), only the bilinear combination of normal and anomalous densities identified in this section occur in the HFB energy.

9.4 Densities in spherical systems

Under spherical symmetry, which also implies time-reversal invariance, the various densities defined in the previous section take simplified forms. In spherical symmetry, the HFB quasiparticle wave functions in the traditional representation take the form [81]

$$
\begin{aligned}
U_m^{nljq[k]}(\vec{r}q) &= \frac{U^q_{nlj}(rq)}{r} \sum_{m_l\sigma} Y_l^{m_l}(\hat{r})\, \langle l m_l \tfrac{1}{2}\sigma | jm\rangle\, |\sigma\rangle && (9.139)\\
V_m^{nljq[k]}(\vec{r}q) &= \frac{V^q_{nlj}(rq)}{r} \sum_{m_l\sigma} Y_l^{m_l}(\hat{r})\, 2\sigma\, \langle l m_l \tfrac{1}{2}\bar{\sigma} | jm\rangle\, |\sigma\rangle\ . && (9.140)
\end{aligned}
$$

9.4.1 Expression for the normal densities in spherical symmetry

Using the specific form of the quasiparticle wavefunctions given in Eqs.(9.139) and (9.140), the full density matrix reads

$$
\begin{aligned}
\rho_q(\vec{r}\sigma, \vec{r}'\sigma') &= \sum_{nljm} V_m^{nljq[k]}(\vec{r}\sigma q)\, V_m^{nljq[k]}(\vec{r}'\sigma' q)\\
&= \sum_{nljm} \frac{V^q_{nlj}(r')}{r'} \sum_{m_l'\sigma'} Y_l^{m_l'*}(\hat{r}')\, 2\sigma'\, \langle l m_l' \tfrac{1}{2}\bar{\sigma}' | jm\rangle\, \frac{V^q_{nlj}(r)}{r}\\
&\quad \times \sum_{m_l\sigma} Y_l^{m_l}(\hat{r})\, 2\sigma\, \langle l m_l \tfrac{1}{2}\bar{\sigma} | jm\rangle\,, && (9.141)
\end{aligned}
$$

where we have made use of the fact that the radial parts of the quasiparticle wave functions and Clebsch-Gordon coefficients are real. In the following sections, the most simplified forms of the various normal densities are given (for spherical symmetry).

Scalar part of the density matrix - matter density

The simplification of the nonlocal matter density proceeds by making use of the relations stated in appendix Eq.(9.15) and Eq.(9.43). Thus

$$
\rho_q(\vec{r}, \vec{r}') = \sum_{nlj} \frac{2j+1}{4\pi} \frac{V^q_{nlj}(r')}{r'} \frac{V^q_{nlj}(r)}{r} P_l(\hat{r}\cdot\hat{r}'), \qquad (9.142)
$$

where P_l is Legendre polynomial of order l. The above expression is manifestly symmetric in $\vec{r}$, $\vec{r}'$, viz. $\rho_q(\vec{r},\vec{r}') = \rho_q(\vec{r}',\vec{r})$. For the local part, one simply sets $\vec{r}' = \vec{r}$ in Eq.(9.142) to obtain

$$\rho_q(\vec{r}) = \sum_{nlj} \frac{2j+1}{4\pi} \left[\frac{V^q_{nlj}(r)}{r} \right]^2 . \tag{9.143}$$

To derive the local gradient and laplacian densities, one simply operates on Eq. (9.143) using the respective operators. Hence,

$$\vec{\nabla}\rho_q(\vec{r}) = \sum_{nlj} \frac{2j+1}{4\pi} \frac{\partial}{\partial r} \left[\frac{V^q_{nlj}(r)}{r} \right]^2 \hat{r} \tag{9.144}$$

$$\Delta\rho_q(\vec{r}) = \sum_{nlj} \frac{2j+1}{4\pi} \left(\frac{\partial^2}{\partial r^2} + \frac{2}{r} \right) \left[\frac{V^q_{nlj}(r)}{r} \right]^2 . \tag{9.145}$$

Kinetic density

For the kinetic density, one can proceed in two different ways: (i) Operating on the simplified form of the nonlocal matter density as given by Eq.(9.142) (ii) Operating on the quasiparticle wave functions (lower component) as given in (9.140) and employing angular momentum algebra. The first path is followed for the sake of simplicity. Starting with the nonlocal kinetic density,

$$\begin{aligned}
\tau_q(\vec{r},\vec{r}') &= \vec{\nabla}\cdot\vec{\nabla}'\rho_q(\vec{r},\vec{r}') \\
&= \sum_{nlj} \frac{2j+1}{4\pi} \Bigg[\left(\frac{V(r')}{r'} \right)' \hat{r}' \cdot \left(\frac{V(r)}{r} \right)' \hat{r}\, P_l(\hat{r}'\cdot\hat{r}) \\
&\qquad + \frac{V(r)}{r} P_l'(\hat{r}'\cdot\hat{r}) \left(\frac{V(r')}{r'} \right)' \sum_{ij} \frac{r_i' r_j'}{r'^2} \frac{\delta_{ij} r^2 - r_i r_j}{r^3} \\
&\qquad + \frac{V(r')}{r'} P_l'(\hat{r}'\cdot\hat{r}) \left(\frac{V(r)}{r} \right)' \frac{r_i r_j}{r^2} \frac{\delta_{ij} r'^2 - r_i' r_j'}{r'^3} \\
&\qquad + \frac{V(r')}{r'} \frac{V(r)}{r} P_l''(\hat{r}'\cdot\hat{r}) \sum_{ijk} \frac{r_k' r_j}{r r'} \frac{\delta_{ij} r'^2 - r_i' r_j'}{r'^3} \frac{\delta_{ik} r'^2 - r_i r_k}{r^3}
\end{aligned}$$

$$+ \frac{V(r')}{r'} \frac{V(r)}{r} P_l'(\hat{r}' \cdot \hat{r}) \sum_{ij} \frac{\delta_{ij} r'^2 - r_i' r_j'}{r'^3} \frac{\delta_{ij} r^2 - r_i r_j}{r^3} \Bigg] , \tag{9.146}$$

where P_l' and P_l'' denote first and second derivatives of the Legendre polynomials. Using this same notation and simplifying the above expression one obtains Even though the above expression looks complicated, it is handy to use when one wants to extract the local value. With the nonlocal kinetic density as given in Eq. (9.146) and setting $\vec{r}' = \vec{r}$, one can simplify the expression much further. Making use of the relations stated in Eq.(9.5) and Eq.(9.31), one obtains

$$\tau_q(r) = \sum_{nlj} \frac{2j+1}{4\pi r^2} \left[\left(V_{nlj}^{q\,\prime}(r) - \frac{V_{nlj}^q(r)}{r} \right)^2 + \frac{l(l+1)}{r^2} \left[V_{nlj}^q(r) \right]^2 \right] . \tag{9.147}$$

The vector part of the density matrix - Spin density

The nonlocal spin density is given by

$$\begin{aligned} \vec{s}_q(\vec{r}, \vec{r}') &= \sum_{\sigma\sigma'} \rho_q(\vec{r}\sigma, \vec{r}'\sigma') \, \langle \sigma' | \vec{\sigma} | \sigma \rangle \\ &= \sum_{nljm} \frac{V_{nlj}^q(r')}{r'} \frac{V_{nlj}^q(r)}{r} \sum_{m_l'\sigma'} Y_l^{m_l'*}(\hat{r}') \, \langle l m_l' \tfrac{1}{2} \sigma' | jm \rangle \sum_{m_l\sigma} Y_l^{m_l}(\hat{r}) \\ &\quad \times \langle l m_l \tfrac{1}{2} \sigma | jm \rangle \, 4\bar{\sigma}\bar{\sigma}' \, \langle \bar{\sigma}' | \vec{\sigma} | \bar{\sigma} \rangle \, . \end{aligned} \tag{9.148}$$

In the orthonormal coordinate system defined according to

$$\vec{e}_0 = \vec{e}_z \, , \quad \vec{e}_{\pm 1} = \mp \frac{1}{\sqrt{2}} \left(\vec{e}_x \pm i \vec{e}_y \right) \tag{9.149}$$

and using

$$\langle\bar{\sigma}'|\sigma_\mu|\bar{\sigma}\rangle = \sqrt{3}\,\langle\frac{1}{2}\sigma 1\mu|\frac{1}{2}\sigma'\rangle\,, \tag{9.150}$$

one can write the nonlocal spin density as

$$\begin{aligned} s_{q,\mu}(\vec{r},\vec{r}') &= \sqrt{6}\sum_{nljm}\frac{V^q_{nlj}(r')}{r'}\,\frac{V^q_{nlj}(r)}{r}\sum_{m_l\sigma m_l'\sigma'} Y_l^{m_l'*}(\hat{r}')\,Y_l^{m_l}(\hat{r})\,(2j+1) \\ &\quad\times(-1)^{2l+2m+3\sigma-2}\begin{pmatrix} l & \frac{1}{2} & j \\ m_l & \sigma & -m\end{pmatrix}\begin{pmatrix} l & \frac{1}{2} & j \\ m_l' & \sigma' & -m\end{pmatrix} \\ &\quad\times\begin{pmatrix} \frac{1}{2} & 1 & \frac{1}{2} \\ \bar{\sigma} & \mu & \sigma'\end{pmatrix}. \end{aligned} \tag{9.151}$$

Making use of the 3j-6j symbols relation stated in appendix 9.1.2, one obtains

$$\begin{aligned} s_{q,\mu}(\vec{r},\vec{r}') &= \sqrt{6}\sum_{nlj}(2j+1)\,\frac{V^q_{nlj}(r')}{r'}\,\frac{V^q_{nlj}(r)}{r}\sum_{m_lm_l'} Y_l^{m_l'*}(\hat{r}')\,Y_l^{m_l}(\hat{r})\,(-1)^{j+m_l'+1} \\ &\quad\times\begin{Bmatrix} l & l & 1 \\ \frac{1}{2} & \frac{1}{2} & j\end{Bmatrix}\begin{pmatrix} l & l & 1 \\ m_l & m_l' & \mu\end{pmatrix}. \end{aligned} \tag{9.152}$$

One can plug in the algebraic values for the 3j and 6j symbols in the above equation and do further simplification. To proceed further than that, it is imperative to choose a coordinate system in which one of the vectors ($\vec{r}$, $\vec{r}'$) is along the z−axis. Let $\vec{r}'$ be the one along the z-axis. This implies that $\theta' = 0$ and $\phi' = 0$. Thus, only $Y_l^{m_l'=0}$ contributes. Making use of the relations in Eq.(9.20)-Eq.(9.23) and simplifying,

$$\begin{aligned} s_{q,0}(\vec{r},\vec{r}') &= 0 \\ s_{q,1}(\vec{r},\vec{r}') &= i\sum_{nlj}(-1)^{2j+1}\,(2j+1)\,\frac{V^q_{nlj}(r')}{r'}\,\frac{V^q_{nlj}(r)}{r}\,Y_l^{-1}(\hat{r})\,Y_l^{0*}(\,\theta'=0\,,\,\phi'=0\,) \\ &\quad\times\frac{3/4+l(l+1)-j(j+1)}{\sqrt{2l(l+1)(2l+1)}} \end{aligned}$$

$$
\begin{aligned}
s_{q,-1}(\vec{r},\vec{r}') \;&=\; i \sum_{nlj} (-1)^{2j}\,(2j+1)\,\frac{V^q_{nlj}(r')}{r'}\,\frac{V^q_{nlj}(r)}{r}\,Y_l^1(\hat{r})\,Y_l^{0*}(\,\theta'=0\,,\,\phi'=0\,) \\
&\quad\times \frac{3/4+l(l+1)-j(j+1)}{\sqrt{2l(l+1)(2l+1)}}\,.
\end{aligned}
$$

One obtains the prefactor i after properly summing the exponents of -1 which takes the form $(-1)^a$ where $a = 2j + 3/2$ or $a = 2j + 1/2$. Writing the components in x, y, z coordinate space, one obtains

$$
\begin{aligned}
s_{q,z}(\vec{r},\vec{r}') \;&=\; 0 && (9.153)\\
s_{q,x}(\vec{r},\vec{r}') \;&=\; -i\sqrt{\frac{1}{4\pi}}\sum_{nlj}(2j+1)\,\frac{V^q_{nlj}(r')}{r'}\,\frac{V^q_{nlj}(r)}{r}\,P_l^1(\cos(\theta))\,Y_l^0(\,\theta'=0\,,\,\phi'=0\,) \\
&\quad\times\cos(\phi)\,\big(\,3/4+l(l+1)-j(j+1)\,\big)\,\frac{1}{l\sqrt{(l+1)(2l+1)}} && (9.154)\\
s_{q,y}(\vec{r},\vec{r}') \;&=\; -i\sqrt{\frac{1}{4\pi}}\sum_{nlj}(2j+1)\,\frac{V^q_{nlj}(r')}{r'}\,\frac{V^q_{nlj}(r)}{r}\,P_l^1(\cos(\theta))\,Y_l^0(\,\theta'=0\,,\,\phi'=0\,) \\
&\quad\times\sin(\phi)\,\big(\,3/4+l(l+1)-j(j+1)\,\big)\,\frac{1}{l\sqrt{(l+1)(2l+1)}}\,. && (9.155)
\end{aligned}
$$

The above result can be used to show that the nonlocal spin density is in the direction of $\vec{r}\times\vec{r}'$. This can also be shown to be true from a different perspective : using the properties of nonlocal spin density under time-reversal and symmetry arguments. In spherical systems, the general form of the nonlocal spin density can be constrained as follows. There are only three vectors available for the construction of any vector physical quantity. These are $\vec{r}, \vec{r}'$ and $\vec{r}\times\vec{r}'$. Thus

$$
\vec{s}(\vec{r},\vec{r}') \;=\; s_a(r,r',\theta)\,\vec{r} \;+\; s_b(r,r',\theta)\,\vec{r}' \;+\; s_c(r,r',\theta)\,\vec{r}\times\vec{r}'\,, \tag{9.156}
$$

where the $s_a(r,r',\theta)$, $s_b(r,r',\theta)$ and $s_c(r,r',\theta)$ are scalar functions dependent on the magnitudes of $\vec{r}$, $\vec{r}'$ and θ which is the angle between $\vec{r}$ and $\vec{r}'$. In spherical systems, the nonlocal spin density should satisfy

$$\vec{s}_q(\vec{r},\vec{r}\,') = \vec{s}_q(-\vec{r},-\vec{r}\,')\,. \tag{9.157}$$

This condition can be satisfied only by setting all except $s_c(r,r')$ to zero. Thus the nonlocal spin density is proportional to $\vec{r}\times\vec{r}\,'$. To further constrain the form, let us invoke the property of nonlocal spin density under time-reversal invariance. Under time reversal

$$\vec{s}_q^{\,T}(\vec{r},\vec{r}\,') = -\vec{s}_q^{\,*}(\vec{r},\vec{r}\,') = -\vec{s}_q(\vec{r}\,',\vec{r})\,, \tag{9.158}$$

from which one recovers that $\vec{s}_q(\vec{r}) = 0$. Using the above property, one can easily show that the nonlocal spin density has only an imaginary component. Thus

$$\vec{s}_q(\vec{r},\vec{r}\,') = i\,\vec{r}\times\vec{r}\,'\,s_q(r,r',\theta). \tag{9.159}$$

This result has been verified by the derivation in Eq.(9.153)

$$\begin{aligned} s_q(r,r',\theta) &= -\sqrt{\frac{1}{4\pi}}\sum_{nlj}\frac{V^q_{nlj}(r')}{r'^2}\,\frac{V^q_{nlj}(r)}{r^2}\,Y_l^0(0,0)\,\frac{P_l^1(\cos\theta)}{\sin\theta} \\ &\quad\times\frac{(2j+1)\left(3/4+l(l+1)-j(j+1)\right)}{l(l+1)\sqrt{2l+1}}\,. \end{aligned} \tag{9.160}$$

In ref. [170] a similar expression is given for the nonlocal spin density with $s_q(r,r',\theta)$ being

$$s_q(r,r',\theta) = \pm\frac{1}{2\pi}\sum_{nlj}\frac{V^q_{nlj}(r')}{r'^2}\,\frac{V^q_{nlj}(r)}{r^2}\,P_l'(\cos\theta)\,, \tag{9.161}$$

where ± is for $j = l \pm 1/2$, P_l' is the derivative of Legendre polynomial P_l and θ is the angle between $\vec{r}$ and $\vec{r}\,'$. One can show that Eq. (9.161) reduces to Eq. (9.160) by using the relations Eq.(9.46) given in the appendix. Obviously, in time-reversal invariant systems, the local part of the spin density is zero. I.e.

$$\vec{s}_q(\vec{r}) = 0 . \tag{9.162}$$

Spin-orbit density

Starting with the definition of the local spin-current tensor

$$J_{q,\mu\nu}(\vec{r}) = -\frac{i}{2}\left(\nabla_\mu - \nabla'_\mu\right) s_{q,\nu}(\vec{r},\vec{r}')\Big|_{\vec{r}=\vec{r}'} , \tag{9.163}$$

and making use of Eq.(9.159), we can write the local spin-orbit tensor as

$$J_{q,\mu\nu}(\vec{r}) = -r\, s_q(r) \sum_{\alpha} \epsilon_{\mu\nu\alpha} \frac{r_\alpha}{r} . \tag{9.164}$$

One can write $J_{q,\mu\nu}(\vec{r})$ as a sum of pseudoscalar, (antisymmetric) vector and (symmetric) traceless pseudotensor parts

$$J_{q,\mu\nu}(\vec{r}) = \frac{1}{3}\delta_{\mu\nu} J^{(0)}_q(\vec{r}) + \frac{1}{2}\sum_{k=x}^{z} \epsilon_{\mu\nu k} J^{(1)}_{q,k}(\vec{r}) + J^{(2)}_{q,\mu\nu}(\vec{r}) , \tag{9.165}$$

where the three components read

$$J^{(0)}_q(\vec{r}) = \sum_{\mu\nu} \delta_{\mu\nu} J_{q,\mu\nu}(\vec{r}) \tag{9.166}$$

$$J^{(1)}_{q,k}(\vec{r}) = \sum_{\mu\nu} \epsilon_{\mu\nu k} J_{q,\mu\nu}(\vec{r}) \tag{9.167}$$

$$J^{(2)}_{q,\mu\nu}(\vec{r}) = J_{q,\mu\nu}(\vec{r}) - \frac{1}{3}\delta_{\mu\nu} J^{(0)}_q(\vec{r}) - \frac{1}{2}\sum_{k=x}^{z} \epsilon_{\mu\nu k} J^{(1)}_{q,k}(\vec{r}) . \tag{9.168}$$

Combining the above results, it can easily be shown that both the pseudoscalar and the pseudotensor parts are zero i.e. $J^{(0)}(\vec{r}) = 0$ and $J^{(2)}(\vec{r}) = 0$. Thus one needs to simplify only the vector part. Even though one can perform a series of angular momentum coupling operations to obtain the most simplified form for the vector part of the local spin-current tensor in spherical systems, a simple physically motivated derivation is given in Ref. [201]. In spherical systems $\vec{J}_q(\vec{r})$ must be proportional to $\vec{r}$. Thus

$$\begin{aligned} \vec{J}_q(\vec{r}) &= \left(\frac{\vec{r}}{r} \cdot \vec{J}\right) \frac{\vec{r}}{r} \\ &= \frac{\vec{r}}{r^2} \langle \vec{l} \cdot \vec{\sigma} \rangle , \end{aligned} \tag{9.169}$$

resulting in

$$\vec{J}_q(\vec{r}) = \frac{\vec{r}}{4\pi r^4} \sum_{nlj} (2j+1) \left[j(j+1) - l(l+1) - \frac{3}{4} \right] \left(V^q_{nlj}(r) \right)^2 . \tag{9.170}$$

9.4.2 Expression for the anomalous densities in spherical symmetry

For the anomalous part, starting with the anomalous density matrix as defined in the traditional representation [81]

$$\begin{aligned} \tilde{\rho}_q(\vec{r}\sigma, \vec{r}'\sigma') &= -\sum_{nljm} 2\,\bar{\sigma}\, U^{nljq[k]}_m(\vec{r}\sigma)\, V^{nljq[k]\,*}_m(\vec{r}'\bar{\sigma}') \\ &= -\sum_{nljm} \frac{V^q_{nlj}(r')}{r'} \sum_{m_l'\sigma'} Y_l^{m_l'\,*}(\hat{r}')\, \langle l m_l' \tfrac{1}{2} \sigma' | jm \rangle\, 2\bar{\sigma}'\, \frac{U^q_{nlj}(r)}{r} \\ &\quad \times \sum_{m_l\sigma} Y_l^{m_l}(\hat{r})\, \langle l m_l \tfrac{1}{2} \sigma | jm \rangle\, 2\bar{\sigma} . \end{aligned} \tag{9.171}$$

For the following anomalous densities, we follow exactly the same mathematical steps as their normal counterparts. Thus only the results are stated. The two changes are (i) overall sign becomes opposite to that of the normal densities (ii) one of the lower part of the quasiparticle wavefunction is replaced with its upper part. Thus ringing the change in the respective densities, one obtains the following results.

pairing density

The nonlocal part of the pairing density reads

$$\tilde{\rho}_q(\vec{r},\vec{r}\,') \;=\; -\sum_{nlj} \frac{2j+1}{4\pi} \, \frac{V^q_{nlj}(r')}{r'} \, \frac{U^q_{nlj}(r)}{r} \, P_l(\hat{r}\cdot\hat{r}\,')\,, \tag{9.172}$$

while for the local part, one simply sets $\vec{r}\,' = \vec{r}$ in Eq.(9.172) to obtain

$$\tilde{\rho}_q(\vec{r}) \;=\; -\sum_{nlj} \frac{2j+1}{4\pi} \, \frac{V^q_{nlj}(r)\, U^q_{nlj}(r)}{r^2}\,. \tag{9.173}$$

The local pairing gradient and laplacian densities are given by

$$\vec{\nabla}\tilde{\rho}_q(\vec{r}) \;=\; -\sum_{nlj} \frac{2j+1}{4\pi} \, \frac{\partial}{\partial r} \, \frac{V^q_{nlj}(r)\, U^q_{nlj}(r)}{r^2} \, \hat{r} \tag{9.174}$$

$$\Delta\tilde{\rho}_q(\vec{r}) \;=\; -\sum_{nlj} \frac{2j+1}{4\pi} \left(\frac{\partial^2}{\partial r^2} + \frac{2}{r}\right) \frac{V^q_{nlj}(r)\, U^q_{nlj}(r)}{r^2}\,. \tag{9.175}$$

Pairing kinetic density

The local pairing kinetic density reads

$$\begin{aligned} \tilde{\tau}(r)_q \;=\; & -\sum_{nlj} \frac{2j+1}{4\pi r^2} \left[\left(V^{q\prime}_{nlj}(r) - \frac{V^q_{nlj}(r)}{r} \right) \left(U^{q\prime}_{nlj}(r) - \frac{U^q_{nlj}(r)}{r} \right) \right. \\ & \left. \times + \frac{l(l+1)}{r^2} \, V^q_{nlj}(r)\, U^q_{nlj}(r) \right]. \end{aligned} \tag{9.176}$$

Pairing spin-orbit density

The pairing spin-orbit density is given by

$$\tilde{\vec{J}}(\vec{r}) \;=\; -\frac{\vec{r}}{4\pi r^4} \sum_{nlj} (2j+1) \left[j(j+1) - l(l+1) - \frac{3}{4} \right] V^q_{nlj}(r)\, U^q_{nlj}(r)\,. \tag{9.177}$$

9.5 Details on the density matrix expansion

In this part of the appendix, we derive and discuss the generalized PSA-DME. First, we start with brief discussion of the Husimi distribution and the derivation of the quadrupolar deformation, $P_2^q(\vec{r})$. This is followed by few remarks and derivations related to the Wigner transform of the $\rho_q(\vec{r}_1, \vec{r}_2)$ up to $\hbar^2$. Subsequently, we derive the generalized PSA-DME, from which we recover all the special cases such as the PSA-DME discussed in section 5.3, the original DME of Ref. [170] and its subsequent generalizations [202]. Finally, we give the formal modified-Taylor series expansion, discussed in section 5.3.6, of all the local densities.

9.5.1 Husimi distribution and the local anisotropy $P_2^q(\vec{r})$

The Husimi distribution is one of the many quantum phase-space distribution functions. It possesses the key property of positive definiteness [[203],[169]] and is defined as

$$H_q(\vec{r}, \vec{p}) \equiv \frac{1}{N} \sum_i \left| \int \varphi_i(\vec{r}_1 q)\, e^{\frac{i}{\hbar}\vec{p}\cdot(\vec{r}-\vec{r}_1) - \frac{1}{2r_0^2}(\vec{r}-\vec{r}_1)^2}\, d\vec{r}_1 \right|^2 \rho^q_{ii}, \qquad (9.178)$$

where $N \equiv 1/(\pi^{3/4} r_0^{3/2})$ and r_0 is a chosen parameter. In the following, we use the HF single-particle wave functions. The occupation probability of a given spherical shell ρ^{qnjl} is one or zero, except for open-shell semi-magic nuclei where the so-called filling approximation provides the valence shell with a partial occupation. Modifying the derivation to include pairing (HFB) can be done through the proper formulation of the Wigner distribution as given in Ref. [204], as the Husimi distribution is a coarse-graining of the Wigner distribution using gaussian phase space factors[169].

To derive Eq. (5.15) for the quadrupolar local anisotropy of the momentum Fermi

surface $P_2^q(\vec{r})$ we start from the definition

$$P_2^q(\vec{r}) \equiv \frac{\int d\vec{p}\left[3(\vec{e}_r\cdot\vec{p})^2-\vec{p}^2\right]H_q(\vec{r},\vec{p})}{\int d\vec{p}\vec{p}^2H_q(\vec{r},\vec{p})}, \tag{9.179}$$

and make use of the relations

$$\int d\vec{p}\,\vec{p}^2\,e^{-\frac{i}{\hbar}\vec{p}\cdot(\vec{r}_1'-\vec{r}_1)} = (2\pi)^3\hbar^5\vec{\nabla}_1'\cdot\vec{\nabla}\,\delta(\vec{r}_1'-\vec{\nabla}_1), \tag{9.180}$$

$$e^{-\frac{1}{r_0^2}(\vec{r}_1-\vec{r}_1')^2} \approx \delta(\vec{r}_1-\vec{r}_1') + \mathcal{O}\big((k_F^q r_0)^2\big). \tag{9.181}$$

Through direct application of the above relations, one obtains

$$\begin{aligned}
\int d\vec{p}\,\vec{p}^2\,H_q(\vec{r},\vec{p}) &\approx (2\pi)^3\hbar^5\sum_i\left|\vec{\nabla}\varphi_i(\vec{r}q)\right|^2\rho_{ii}^q + \mathcal{O}\big((k_F^q r_0)^2\big),\\
\int d\vec{p}\,(\hat{r}\cdot\vec{p})^2 H_q(\vec{r},\vec{p}) &\approx (2\pi)^3\hbar^5\sum_i\left|(\hat{r}\cdot\vec{\nabla})\varphi_i(\vec{r}q)\right|^2\rho_{ii}^q + \mathcal{O}\big((k_F^q r_0)^2\big),
\end{aligned}$$

which, plugged into Eq.(9.179), gives

$$P_2^q(\vec{r}) = \left[\frac{3}{\tau_q(\vec{r})}\sum_i|(\vec{e}_r\cdot\vec{\nabla})\varphi_i(\vec{r}q)|^2\rho_{ii}^q - 1\right] + \mathcal{O}((k_F^q r_0)^2).$$

Further simplifications can be performed for spherical systems, using single-particle wave-functions essentially the same as the ones given in Eq. (9.140). However, note that we are working in the HF picture. Using the angular momentum relations in section 9.1.2, one obtains

$$\begin{aligned}
\sum_i\left|(\vec{e}_r\cdot\vec{\nabla})\varphi_i(\vec{r}q)\right|^2\rho_{ii}^q &= \sum_{nlj}\frac{2j+1}{4\pi}\left(\frac{\partial}{\partial r}\frac{V_{nlj}^q(r)}{r}\right)^2\rho^{qnjl}\\
\sum_i\left|\vec{\nabla}\varphi_i(\vec{r}q)\right|^2\rho_{ii}^q &= \sum_{nlj}\frac{2j+1}{4\pi}\left(\frac{\partial}{\partial r}\frac{V_{nlj}^q(r)}{r}\right)^2\rho^{qnjl}
\end{aligned}$$

$$+\sum_{nlj} F(l,j)\left(\frac{V^{q}_{nlj}(r)}{r^2}\right)^2 \rho^{qnjl},$$

where $F(l,j)$ is given in Eq. (9.1.3) and ρ^{qnjl} is the occupation probability of the (n,l,j) shell with q labeling the protons/neutrons. Plugging these intermediate results into Eq. (9.182) yields the expression of $P_2(\vec{r})$ as

$$P_2(\vec{r}) = \frac{1}{\tau_q(\vec{r})}\sum_{nlj}\frac{2j+1}{2\pi}\left[\left(\frac{\partial}{\partial r}\frac{V^{q}_{nlj}(r)}{r}\right)^2 - \frac{l(l+1)}{2r^2}\left(\frac{V^{q}_{nlj}(r)}{r}\right)^2\right]\rho^{qnjl} \quad (9.182)$$

where $\tau_q(\vec{r})$ is the kinetic density as defined in Eq. (9.77).

9.5.2 Wigner transform of the $\rho_q(\vec{r}_1,\vec{r}_2)$ up to $\hbar^2$

In the parameterized PSA-DME of $\vec{s}_q(\vec{r}_1,\vec{r}_2)$, we used the Wigner transform of $\rho_q(\vec{r}_1,\vec{r}_2)$ up to $\hbar^2$ to motivate the form of Eq. (5.41). In this section, we derive Eq. (5.40). We restrict the derivation to the HF approximation. Refer to [204] for a recent work on the formalism of the wigner distribution in systems with pairing (HFB). One can write the scalar part of the normal part of the OBDM as

$$\rho_q(\vec{r}_1,\vec{r}_2;\lambda_q) = \sum_i \varphi^{\dagger}_i(\vec{r}_2 q)\,\varphi_i(\vec{r}_1 q)\,\Theta(\lambda_q-\epsilon_i) = 2L^{-1}_{\beta\to\lambda_q}\left[\frac{C^{\beta}_q(\vec{r}_1,\vec{r}_2)}{\beta}\right], \quad (9.183)$$

where Θ is the unit step function, λ_q is the fermi energy, ϵ_i is the single-particle energy, $\beta = it$ and L^{-1} refers to the inverse Laplace tranform. $C^{\beta}_q(\vec{r}_1,\vec{r}_2)$ is the single-particle propagator which, in the HF approximation, reads

$$C^{\beta}_q(\vec{r}_1,\vec{r}_2) = \sum_i \varphi^{\dagger}_i(\vec{r}_2 q)\,\varphi_i(\vec{r}_1 q)\,e^{-\beta\epsilon_i}\,\Theta(\lambda_q-\epsilon_i)\,. \quad (9.184)$$

Since the Wigner transform of the right and left hand sides should be equal, one has

$$\rho_q(\vec{R},\vec{p}) = 2L^{-1}_{\beta\to\lambda_q}\left[\frac{C_q^\beta(\vec{R},\vec{p})}{\beta}\right]. \tag{9.185}$$

The derivation of the Wigner transform of the density matrix up to $\hbar^2$ can be obtained by working out the inverse Laplace transform up to $\hbar^2$ of the single particle propagator. It reads [38]

$$\begin{aligned} C_q^\beta(\vec{R},\vec{p}) &= e^{-\beta\left(\frac{p^2}{2m}+V_q(\vec{R})\right)}\left(1+\frac{\hbar^2\beta^2}{8m}\left(-\Delta V_q(\vec{R})+\frac{1}{3}\beta(\vec{\nabla}V_q(\vec{R}))^2\right.\right.\\ &\quad\left.\left.+\frac{\beta}{3m}(\vec{p}\cdot\vec{\nabla})^2V_q(\vec{R})\right)+\mathcal{O}(\hbar^4)\right). \end{aligned} \tag{9.186}$$

Defining the single-particle Hamiltonian $h^q = -\frac{\hbar^2}{2m}\Delta + V_q$ where V_q is the self-consistent HF potential, one can use the following relations

$$\begin{aligned} \int_{\gamma-i\infty}^{\gamma+i\infty} d\beta\, e^{\beta(\lambda_q-h^q_W)} &= \delta(\lambda_q-h^q_W),\\ \frac{\partial}{\partial\lambda_q}\int_{\gamma-i\infty}^{\gamma+i\infty} d\beta\, e^{\beta(\lambda_q-h^q_W)} &= \delta'(\lambda_q-h^q_W),\\ \frac{\partial^n}{\partial\lambda_q^n}\int_{\gamma-i\infty}^{\gamma+i\infty} d\beta\, e^{\beta(\lambda_q-h^q_W)} &= \frac{\partial^n}{\partial\lambda_q^n}\delta(\lambda_q-h^q_W), \end{aligned}$$

for integer n to obtain

$$\begin{aligned} L^{-1}_{\beta\to\lambda_q}\left[\frac{1}{\beta}e^{-\beta(\frac{p^2}{2m}+V_q(\vec{R}))}\right] &= \theta\left(\lambda_q-\frac{p^2}{2m}-V_q(\vec{R})\right),\\ L^{-1}_{\beta\to\lambda_q}\left[\frac{\hbar^2\beta}{8m}e^{-\beta(\frac{p^2}{2m}+V_q(\vec{R}))}\Delta V_q(\vec{R})\right] &= \frac{\hbar^2}{8m}\Delta V_q(\vec{R})\\ &\quad\times\delta'\left(\lambda_q-\frac{p^2}{2m}-V_q(\vec{R})\right),\\ L^{-1}_{\beta\to\lambda_q}\left[\frac{\hbar^2\beta^2}{24m}e^{-\beta(\frac{p^2}{2m}+V_q(\vec{R}))}(\vec{\nabla}V_q(\vec{R}))^2\right] &= -\frac{\hbar^2}{24m}(\vec{\nabla}V_q(\vec{R}))^2\\ &\quad\times\delta''\left(\lambda_q-\frac{p^2}{2m}-V_q(\vec{R})\right), \end{aligned}$$

$$L^{-1}_{\beta\rightarrow\lambda q}\left[\frac{\hbar^2\beta^2}{24m}e^{-\beta(\frac{p^2}{2m}+V_q(\vec{R}))}(\vec{p}\cdot\vec{\nabla})^2V_q(\vec{R})\right] = -\frac{\hbar^2}{24m}(\vec{p}\cdot\vec{\nabla})^2V_q(\vec{R}) \times\delta''\left(\lambda_q-\frac{p^2}{2m}-V_q(\vec{R})\right). \tag{9.187}$$

Plugging into Eq.(9.185), we obtain the Wigner transform of $\rho_q(\vec{r}_1,\vec{r}_2)$ up to $\hbar^2$

$$\begin{aligned}\rho_{WK,q}(\vec{R},\vec{p}) =&\Theta(\lambda_q-h^q_W)-\frac{\hbar^2}{8m}\Delta V_q\delta'(\lambda_q-h^q_W)\\ &+\frac{\hbar^2}{24m}\left[(\nabla V_q)^2+\frac{1}{m}(\vec{p}\cdot\nabla)^2V_q\right]\delta''(\lambda_q-h^q_W)+\mathcal{O}(\hbar^4)\,,\end{aligned} \tag{9.188}$$

where $h^q_W = H_q = \frac{p^2}{2m} - V_q(\vec{R})$ and the derivatives of the dirac-delta functions are performed with respect to λ_q. Even though it is not the main target of this section, one can calculate the inverse Wigner transform of Eq.(9.188) to obtain the density matrix up to order $\hbar^2$. This effectively gives the extended Thomas Fermi approximation to $\rho_q(\vec{r}_1,\vec{r}_2)$. We can call EFT-DME. The important relations one has to use are

$$\delta(\lambda_q-h^q_W) = \frac{m}{\hbar^2k_F}\delta(k-k_F) \text{ and } \frac{\partial}{\partial\lambda_q} = \frac{\partial k^q_F}{\partial\lambda_q}\frac{\partial}{\partial k^q_F}, \tag{9.189}$$

where $\lambda_q = \frac{\hbar^2k^{q\,2}_F}{2m} + V_q(\vec{R})$. Since the derivatives act on the dirac-delta functions, one has to perform integration by parts using the relation

$$\int dp\,\delta^n(\lambda_q-h^q_W)\,F(p,r,\lambda_q) = (-1)^n\frac{\partial^n}{\partial\lambda^n_q}F(p,r,\lambda_q)|_{p=p_F}, \tag{9.190}$$

where $F(p,r,\lambda_q)$ is any well behaved function and p_F is the value of p that satisfies the equation $\lambda_q - h^q_W = 0$. Applying these mathematical relations, one essentially obtains EFT-DME of $\rho_q(\vec{r}_1, \vec{r}_2)$

$$\begin{aligned} \rho_q(\vec{r}_1, \vec{r}_2) =& \frac{k_F^{q\,3}}{3\pi^2} \frac{3 j_1(k_F^q r)}{k_F^q r} + \frac{1}{12\pi^2} \Delta k_F^q \left[j_0(k_F^q r) - k_F^q r j_1(k_F^q r) \right] \\ &+ \frac{1}{24\pi^2} \frac{(\nabla k_F^q)^2}{k_F^q} \left[j_0(k_F^q r) - 4 k_F^q r j_1(k_F^q r) + k_F^{q\,2} r^2 j_2(k_F^q r) \right] \\ &- \frac{1}{24\pi^2} \frac{1}{k_F^q} \vec{\nabla} \left[k_F^q \vec{\nabla} k_F^q \cdot \frac{\vec{r}}{r} \right] \cdot \frac{\vec{r}}{r} \left[-3 k_F^q r j_1(k_F^q r) + k_F^{q\,2} r^2 j_2(k_F^q r) \right] + \mathcal{O}(\hbar^4) \,. \end{aligned} \tag{9.191}$$

In Ref. [173], the authors make angle-averaging (with respect to the orientation of $\vec{r}$) approximations, followed by the expansion of the Fermi momentum up to $\hbar^2$

$$k_F^q = \left(3\pi^2 \rho_q\right)^{1/3} + \frac{1}{72} \left(3\pi^2 \rho_q\right)^{-1/3} \left[\frac{(\nabla \rho_q)^2}{\rho_q^2} - 2 \frac{\Delta \rho_q}{\rho_q} \right], \tag{9.192}$$

and $2(\vec{\nabla} k_0^q)^2 \simeq k_0^q \Delta k_0^q$ to obtain

$$\begin{aligned} \breve{\rho}_{ETF,q}(\vec{R}, r) \;=\;& \rho_q(\vec{R}) \frac{3 j_1(k_F^q r)}{k_F^q r} + \frac{r^2}{72} \Delta \rho_q \left[j_0(k_F^q r) - 6 \frac{j_1(k_F^q r)}{k_F^q r} \right] \\ &- \frac{r^2}{216} \frac{(\nabla \rho_q)^2}{\rho_q} \left[4 j_0(k_F^q r) - 9 \frac{j_1(k_F^q r)}{k_F^q r} \right]. \end{aligned} \tag{9.193}$$

9.5.3 Generalized PSA-DME

In section 5.3, we discussed PSA-DME of the scalar and vector components of the normal part of the OBDM of time-reversal invariant systems. In that derivation, the chosen set of DME-coordinates $(\vec{R}, \vec{r})$ were integral parts of the derivation. In addition, we had a single nonlocality coordinate, namely, $\vec{r}$. Here, we give a generalized formulation of PSA-DME for time-reversal invariant systems where we relax these two constraints. This allows us to recover the DME of the nonlocal densities that occur in the HF energy of both NN and NNN interactions. It is to be noted that the three nonlocal densities that occur in the expression for the HF energy from the chiral EFT NNN interaction at N^{2}LO are of the form $\varsigma_q(\vec{r}_1, \vec{r}_1 + \vec{x}_2)$, $\varsigma_q(\vec{r}_1, \vec{r}_1 + \vec{x}_3)$ and $\varsigma_q(\vec{r}_1 + \vec{x}_2, \vec{r}_1 + \vec{x}_3)$, while for the HF energy from the two-nucleon interaction, the nonlocal densities are of the form $\varsigma_q(\vec{r}_1, \vec{r}_2)$. In this notation, the NNN case uses the coordinates defined in Eq. (7.22). Furthermore, ς_q can be either ρ_q or $\vec{s}_q$. As can be seen from the coordinate dependence, the nonlocal densities that occur in the NN case are particular cases of the ones that occur for the NNN. In fact, all the nonlocal coordinate dependencies can be generated from the general case $\varsigma(\vec{r}_1 + \vec{x}_2, \vec{r}_1 + \vec{x}_3)$. For instance, the usual DME-coordinates $(\vec{R}, \vec{r})$ used in the NN case is recovered for $\vec{x}_2 = -\vec{x}_3 = \vec{r}/2$ with $\vec{r}_1$ playing the role of the center of mass coordinates. Hence, we give the PSA-DME for $\rho_q(\vec{r}_1 + \vec{x}_2, \vec{r}_1 + \vec{x}_2)$ and $\vec{s}_q(\vec{r}_1 + \vec{x}_2, \vec{r}_1 + \vec{x}_2)$, which we call generalized PSA-DME, and generate more specific cases from it.

9.5.4 Generalized PSA-DME for the scalar part of the OBDM

In order to obtain the generalized PSA-DME for $\rho_q(\vec{r}_1 + \vec{x}_2, \vec{r}_1 + \vec{x}_2)$, we essentially follow the same set of steps as we did in section 5.3.3. One starts by extracting the exponential nonlocality operator before introducing a phase factor and performing a Taylor series expansion up to second order

$$\rho_q(\vec{r}_1 + \vec{x}_2, \vec{r}_1 + \vec{x}_3) = e^{i\vec{k}\cdot(\vec{x}_2 - \vec{x}_3)}\, e^{\vec{x}_2\cdot(\vec{\nabla}_2 - i\vec{k}) + \vec{x}_3\cdot(\vec{\nabla}_3 + i\vec{k})}\, \rho_q(\vec{r}_2, \vec{r}_3)\Big|_{\vec{r}_2 = \vec{r}_3 = \vec{r}_1} \tag{9.194}$$

$$\approx e^{i\vec{k}\cdot(\vec{x}_2 - \vec{x}_3)} \Bigg[1 + \vec{x}_2 \cdot (\vec{\nabla}_2 - i\vec{k}) + \vec{x}_3 \cdot (\vec{\nabla}_3 + i\vec{k}) + \frac{1}{2}\left(\vec{x}_2 \cdot (\vec{\nabla}_2 - i\vec{k}) + \vec{x}_3 \cdot (\vec{\nabla}_3 + i\vec{k}) \right)^2 \Bigg] \rho_q(\vec{r}_2, \vec{r}_3)\Big|_{\vec{r}_2 = \vec{r}_3 = \vec{r}_1} . \tag{9.195}$$

Note that for the PSA-DME developed in section 5.3.3, the next approximations involve angle averaging with respect to the orientation of the relative coordinate and averaging with respect to $\vec{k}$ over a Fermi sphere. For details of the logical arguments in favor of performing these approximations, refer to that section. Here also, we apply exactly the same approximations. First, We define a new coordinate system as given in Eq. (9.1)

$$\vec{x} = \vec{x}_2 - \vec{x}_3\,, \tag{9.196}$$

$$\vec{X} = (1-a)\,\vec{x}_2 + a\,\vec{x}_3\,, \tag{9.197}$$

where $a \in [0,\, 1]$. The essence of this parameter will be clear later in this section. Angle averaging with respect to the orientation of the relative coordinate, $\vec{x}$, entails performing $\frac{1}{4\pi}\int d\Omega_{\vec{x}}$ where $\Omega_{\vec{x}}$ denotes the orientation of $\vec{x}$. Let us apply these approximations to Eq. (9.195) term by term.

- The Leading term gets simplified as

$$\frac{3}{4\pi^3 k_F^{q\,3}} \int_{|\vec{k}|\le k_F^q} d\,\vec{k} \int \frac{d\Omega_{\vec{x}}}{4\pi}\, e^{i\vec{k}\cdot\vec{x}}\, \rho_q(\vec{r}_2,\vec{r}_3)\bigg|_{\vec{r}_2=\vec{r}_3=\vec{r}_1} = \Pi_0^{\rho}(k_F^q x)\,\rho_q(\vec{r}_1)\,, \tag{9.198}$$

where

$$\Pi_0^{\rho}(k_F^q x) = 3\,\frac{j_1(k_F^q x)}{k_F^q x}\,\rho(\vec{r}_1) = 3\,\frac{j_1(k_F^q|\vec{x}_2-\vec{x}_3|)}{k_F^q|\vec{x}_2-\vec{x}_3|}\,\rho(\vec{r}_1)\,. \tag{9.199}$$

- The linear (first-order correction) term has two origins. The first one is from $-i\vec{k}\cdot(\vec{x}_2-\vec{x}_3)$ and the second is from $\vec{x}_2\cdot\vec{\nabla}_2 + \vec{x}_3\cdot\vec{\nabla}_3$. Hence

$$\frac{3}{4\pi^3 k_F^{q\,3}} \int_{|\vec{k}|\le k_F^q} d\,\vec{k} \int \frac{d\Omega_{\vec{x}}}{4\pi}\, e^{i\vec{k}\cdot\vec{x}} \left[-i\vec{k}\cdot\vec{x}\right] \rho_q(\vec{r}_2,\vec{r}_3)\bigg|_{\vec{r}_2=\vec{r}_3=\vec{r}_1} = L_1(k_F^q x)\,\rho_q(\vec{r}_1), \tag{9.200}$$

where

$$L_1(k_F^q x) \;=\; -3\, j_0(k_F^q x) + 9\,\frac{j_1(k_F^q x)}{k_F^q x} \;=\; -3\, j_0(k_F^q|\vec{x}_2 - \vec{x}_3|) + 9\,\frac{j_1(k_F^q|\vec{x}_2 - \vec{x}_3|)}{k_F^q|\vec{x}_2 - \vec{x}_3|}\,. \tag{9.201}$$

For the simplification of the second linear term, first note that according to Eqs. (9.196)-(9.197), the operator in this term, viz, $\vec{x}_2 \cdot \vec{\nabla}_2 + \vec{x}_3 \cdot \vec{\nabla}_3$ simplifies to $\vec{x} \cdot (a\,\vec{\nabla}_2 - (1-a)\,\vec{\nabla}_3) \;+\; \vec{X} \cdot (\vec{\nabla}_2 + \vec{\nabla}_3)$. Let us designate

$$\vec{\nabla}_a \;\equiv\; a\,\vec{\nabla}_2 - (1-a)\,\vec{\nabla}_3\,. \tag{9.202}$$

Thus,

$$\begin{aligned}
\int \frac{d\Omega_{\vec{k}}}{4\pi} \int \frac{d\Omega_{\vec{x}}}{4\pi} e^{i\vec{k}\cdot\vec{x}} \Big(\vec{x}_2 \cdot \vec{\nabla}_2 + \vec{x}_3 \cdot \vec{\nabla}_3\Big) \;&=\; \int d\Omega_{\vec{k}} \int d\Omega_{\vec{x}} e^{i\vec{k}\cdot\vec{x}} \Big[\vec{x} \cdot \vec{\nabla}_a \\
&\qquad + \vec{X} \cdot (\vec{\nabla}_2 + \vec{\nabla}_3)\Big] \\
&=\; j_0(kx)\, \vec{X} \cdot (\vec{\nabla}_2 + \vec{\nabla}_3)\,,
\end{aligned}$$

which implies,

$$\begin{aligned}
\frac{3}{4\pi^3 k_F^{q3}} \int_{|\vec{k}| \le k_F^q} d\vec{k} \int \frac{d\Omega_{\vec{x}}}{4\pi}\, e^{i\vec{k}\cdot\vec{x}} \Big(\vec{x}_2 \cdot \vec{\nabla}_2 + \vec{x}_3 \cdot \vec{\nabla}_3\Big)\, \rho_q(\vec{r}_2, \vec{r}_3)\Big|_{\vec{r}_2=\vec{r}_3=\vec{r}_1} \\
= L_2(k_F^q x) \vec{X} \cdot \vec{\nabla}_1 \rho_q(\vec{r}_1)\,,
\end{aligned} \tag{9.203}$$

with

$$L_2(k_F^q x) \;=\; 3\,\frac{j_1(k_F^q x)}{k_F^q x} \;=\; 3\,\frac{j_1(k_F^q|\vec{x}_2 - \vec{x}_3|)}{k_F^q|\vec{x}_2 - \vec{x}_3|}\,. \tag{9.204}$$

- The second-order correction term is generated by the operator

$\left[\vec{x}_2 \cdot (\vec{\nabla}_2 - i\vec{k}) + \vec{x}_3 \cdot (\vec{\nabla}_3 + i\vec{k})\right]^2/2$, where we are not showing the phase factor explicitly. Using Eqs. (9.196)-(9.197), this operator reduces to $\left[\vec{x} \cdot (-i\vec{k} + \vec{\nabla}_a) + \vec{X} \cdot (\vec{\nabla}_2 + \vec{\nabla}_3)\right]^2/2$. The relations

$$\begin{aligned} \int \frac{d\Omega_{\vec{k}}}{4\pi} \int \frac{d\Omega_{\vec{x}}}{4\pi} e^{i\vec{k}\cdot\vec{x}} (\vec{x} \cdot \vec{k})(\vec{x} \cdot \vec{\nabla}_a) &= 0, \qquad (9.205) \\ \int \frac{d\Omega_{\vec{k}}}{4\pi} \int \frac{d\Omega_{\vec{x}}}{4\pi} e^{i\vec{k}\cdot\vec{x}} (\vec{x} \cdot \vec{k})(\vec{X} \cdot (\vec{\nabla}_2 + \vec{\nabla}_3)) &= 0, \qquad (9.206) \end{aligned}$$

and Eq. (9.5) can be used to simplify the second-order correction as

$$\begin{aligned} &= \frac{3}{4\pi^3 k_F^{q\,3}} \int_{|\vec{k}| \le k_F^q} d\vec{k} \int \frac{d\Omega_{\vec{x}}}{4\pi} e^{i\vec{k}\cdot\vec{x}} \, 1/2\left[\vec{x} \cdot (-i\vec{k} + \vec{\nabla}_a) + \vec{X} \cdot (\vec{\nabla}_2 + \vec{\nabla}_3)\right]^2 \\ &\quad \times \rho_q(\vec{r}_2, \vec{r}_3)\Big|_{\vec{r}_2 = \vec{r}_3 = \vec{r}_1}, \\ &= \frac{3}{2}\frac{j_1(k_F^q x)}{k_F^q x}\left[\vec{X} \cdot \vec{\nabla}_1\right]^2 \rho_q(\vec{r}_1) \; + \; L_1(k_F^q x)\, \vec{X} \cdot \vec{\nabla}_1 \rho_q(\vec{r}_1) \; + \; L_3(k_F^q x)\, \rho_q(\vec{r}_1) \\ &\quad + \frac{x^2}{2}\,\frac{j_1(k_F^q x)}{k_F^q x}\, \Delta_a\, \rho_q(\vec{r}_2, \vec{r}_3)\Big|_{\vec{r}_2 = \vec{r}_3 = \vec{r}_1}, \qquad (9.207) \end{aligned}$$

where

$$\begin{aligned} L_3(k_F^q x) &= \left(\frac{36 - 3(k_F^q x)^2}{2\, k_F^q x}\right) j_1(k_F^q x) \; - \; 6\, j_0(k_F^q x), \qquad (9.208) \\ \Delta_a &\equiv \vec{\nabla}_a \cdot \vec{\nabla}_a . \qquad (9.209) \end{aligned}$$

The last term involving Δ_a requires further simplification. Expanding the operator and using relation Eqs. (9.108)- (9.109) and the definition of kinetic density given in Eq. (9.77)

$$\begin{aligned}
\Delta_a\rho_q(\vec{r}_2,\vec{r}_3)\Big|_{\vec{r}_2=\vec{r}_3=\vec{r}_1} &= \Big(a\vec{\nabla}_2-(1-a)\vec{\nabla}_3\Big)^2\rho_q(\vec{r}_2,\vec{r}_3)\Big|_{\vec{r}_2=\vec{r}_3=\vec{r}_1}\\
&= \frac{a^2}{2}\Big(\Delta\rho_q(\vec{r}_1)-2\tau_q(\vec{r}_1)+i2\vec{\nabla}\cdot\vec{j}_q(\vec{r}_1)\Big)\\
&\quad+\frac{(1-a)^2}{2}\Big(\Delta\rho_q(\vec{r}_1)-2\tau_q(\vec{r}_1)-i2\vec{\nabla}\cdot\vec{j}_q(\vec{r}_1)\Big)\\
&\quad-2a(1-a)\tau_q(\vec{r}_1)\ ,\\
&= \frac{2a^2-2a+1}{2}\Delta\rho_q(\vec{r}_1)\ -\ \tau_q(\vec{r}_1)\ , \qquad (9.210)
\end{aligned}$$

where we used the fact that $\vec{j}_q(\vec{r}_1)\ =\ 0$ for time-reversal invariant systems.

Collecting all the contributions, the complete generalized PSA-DME for $\rho_q(\vec{r}_1+\vec{x}_2,\ \vec{r}_1+\vec{x}_3)$ in time-reversal invariant systems takes the form

$$\begin{aligned}
\rho_q(\vec{r}_1+\vec{x}_2,\ \vec{r}_1+\vec{x}_3) &= \Pi_0^\rho(k_F^q x)\Big[\rho_q(\vec{r}_1)\ +\ \Lambda_1(k_F^q x)\vec{X}\cdot\vec{\nabla}_1\rho_q(\vec{r}_1)\\
&\quad+\frac{1}{2}\,(\vec{X}\cdot\vec{\nabla}_1)^2\rho_q(\vec{r}_1)\Big]\\
&\quad+\frac{x^2}{6}\,\Pi_2^\rho(k_F^q x)\,\Big[(a^2-a+\frac{1}{2})\Delta\rho_q(\vec{r}_1)-\tau_q(\vec{r}_1)\\
&\quad+\frac{3}{5}k_F^{q2}\Lambda_2(k_F^q x)\rho_q(\vec{r}_1)\Big]\ , \qquad (9.211)
\end{aligned}$$

with

$$\begin{aligned}
\Pi_0^\rho(k_F^q x) &= 3\,\frac{j_1(k_F^q x)}{k_F^q x}\ =\ 3\,\frac{j_1(k_F^q|\vec{x}_2-\vec{x}_3|)}{k_F^q|\vec{x}_2-\vec{x}_3|}\ , \qquad (9.212)\\
\Pi_2^\rho(k_F^q x) &= 3\,\frac{j_1(k_F^q x)}{k_F^q x}\ =\ 3\,\frac{j_1(k_F^q|\vec{x}_2-\vec{x}_3|)}{k_F^q|\vec{x}_2-\vec{x}_3|}\ , \qquad (9.213)\\
\Lambda_1(k_F^q x) &= 1\ +\ \frac{L_1(k_F^q x)}{\Pi_0^\rho(k_F^q x)}\ \approx 1+\mathcal{O}((k_F^q r)^2)\ , \qquad (9.214)\\
\Lambda_2(k_F^q x) &= 1\ +\ \frac{L_1(k_F^q x)+L_2(k_F^q x)}{\Pi_2^\rho(k_F^q x)}\ \approx 1+\mathcal{O}((k_F^q r)^2)\ . \qquad (9.215)
\end{aligned}$$

As a can take any value between zero and one, it can be considered as an optimization parameter that is to be used to select the best DME-coordinates. Refer to the next section for some detail on related works.

Recovering previous DMEs of the scalar part of the OBDM

At this point, it should be emphasized that the approximations that are used up to now are exactly the same as the ones that are used in section 5.3.3 when we derived PSA-DME for $\rho_q(\vec{r}_1, \vec{r}_2)$ using $(\vec{R}, \vec{r})$ as the DME-coordinates. Hence, we can recover the PSA-DME of $\rho_q(\vec{R}+\vec{r}/2, \vec{R}-\vec{r}/2)$, i.e., Eq. (5.21) by setting $\vec{x}_2 = -\vec{x}_3 = \vec{r}/2$, $\vec{r}_1 = \vec{R}$ and $a = 1/2$. In this case, $\vec{X} = 0$, $\vec{x} = \vec{r}$ and Eq. (9.211) reduces to

$$\begin{aligned} \rho_q(\vec{R}+\frac{\vec{r}}{2}, \vec{R}-\frac{\vec{r}}{2}) &\simeq \Pi_0^\rho(k_F^q r)\,\rho_q(\vec{R}) + \frac{r^2}{6}\Pi_2^\rho(k_F^q r)\left[\frac{1}{4}\Delta\rho_q(\vec{R}) - \tau_q(\vec{R}) \right. \\ &\quad \left. + \frac{3}{5}k_F^{q\,2}\rho_q(\vec{R})\right], \end{aligned} \tag{9.216}$$

where $\Pi_0^\rho(k_F^q r)$ and $\Pi_2^\rho(k_F^q r)$ are as given in Eqs. (9.212) and (9.213), with $\vec{x}$ being replaced with $\vec{r}$. In obtaining Eq. (9.216), we considered only the leading order contribution to $\Lambda_2(k_F^q x)$. The only difference between that of Eq. (9.216) and the corresponding expression in Ref. [170] is the fact that $\Pi_2^\rho(k_F^q r) = 105\,j_3(k_F^q r)/(k_F^q r)^3$ in the original DME. As can be seen from the series expansion,

$$\frac{j_1(k_F^q r)}{2\,k_F^q r} \approx 1 + \mathcal{O}((k_F^q r)^2), \tag{9.217}$$

$$105\,\frac{j_3(k_F^q r)}{(k_F^q r)^3} \approx 1 + \mathcal{O}((k_F^q r)^2), \tag{9.218}$$

the two $\pi-$functions are similar in their leading order. Due to the $(k_F^q r)^2$ prefactor that we have in the second-order correction, the difference between the second-order correction terms of PSA-DME and the original DME appears in terms beyond $\mathcal{O}((k_F^q r)^2)$. As noted in Ref. [170], this difference in the higher-order terms should not be surprising due to the the ambiguity of DME correction terms beyond $\mathcal{O}((k_F^q r)^2)$. Hence, we have effectively recovered the DME of Ref. [170].

In Ref. [202], the authors generalize the original DME of [170] as

$$\begin{aligned}\rho_q(\vec{R}+b\,\vec{r},\vec{R}-(1-b)\,\vec{r}) \;\simeq\; & \Pi_0^\rho(k_F^q r)\,\rho_q(\vec{R}) + \frac{r^2}{6}\Pi_2^\rho(k_F^q r)\left[(b^2-b+1/2)\,\Delta\rho_q(\vec{R})\right. \\ & \left. -\,\tau_q(\vec{R}) + \frac{3}{5}k_F^{q\,2}\rho_q(\vec{R})\right], \qquad (9.219)\end{aligned}$$

with the same π−functions as given in Ref. [170]. Parameter $b = 1/2$ recovers the usual relative and center of mass coordinates. To obtain this expansion from our generalized PSA-DME, Eq. (9.211), one sets

$$\vec{r}_1 = \vec{R}\,,\ \vec{x}_2 = b\,\vec{r}\,,\ \text{and}\ \vec{x}_3 = -(1-b)\,\vec{r}\,, \qquad (9.220)$$

which implies $\vec{x} = \vec{r}$ and $\vec{X} = 0$. Hence, Eq. (9.211) reduces exactly to Eq. (9.219) with parameter a playing the role of parameter b. Optimizing parameter b, the authors of Ref. [202] note that $b = 0$ which amounts to expanding about one of the particles, instead of the center of mass, seems to give the best accuracy for molecular systems. This further enforces the view that optimization of parameter a can result in increased accuracy of the DME.

Further approximation with respect to $\vec{X}$

In the generalized PSA-DME of $\rho_q(\vec{r}_1+\vec{x}_2,\vec{r}_1+\vec{x}_3)$, our angle averaging with respect to the orientation of $\vec{x}$ is a well-supported step in that the scalar part of the OBDM is known to have a weak angular dependence on the orientation of the relative coordinate [176]. If we stretch the argument and assume that the dependence on the orientation of the other non-locality coordinate, $\vec{X}$, is weak, we can average over the orientation of $\vec{X}$. In this case, Eq. (9.211) reduces to

$$\rho_q(\vec{r}_1 + \vec{x}_2, \vec{r}_1 + \vec{x}_3) = \Pi_0^\rho(k_F^q x)\, \rho_q(\vec{r}_1) + \frac{x^2}{6}\Pi_2^\rho(k_F^q x)\left[(a^2 - a + \frac{1}{2} + \frac{X^2}{x^2})\,\Delta\rho_q(\vec{r}_1) - \tau_q(\vec{r}_1) + \frac{3}{5}k_F^{q\,2}\Lambda_2(k_F^q x)\,\rho_q(\vec{r}_1)\right], \qquad (9.221)$$

whose simplicity makes investigating its accuracy a worthy step. As mentioned in the previous section, parameter a may be optimized to reduce some of the inaccuracy that may result from averaging over the orientation of $\vec{X}$.

9.5.5 Generalized PSA-DME for the vector part of the OBDM

The generalized PSA-DME for the vector component of the OBDM involves a significantly less algebra than that of the scalar component as we stop at the linear order in the Taylor series expansion. It involves exactly the same approximations as the ones that we used in section 5.3.4. Extracting the non-locality operator and a phase space factor, followed by Taylor series expansion of the operator

$$\begin{aligned} s_{q,\nu}(\vec{r}_1 + \vec{x}_2, \vec{r}_1 + \vec{x}_3) &= e^{i\vec{k}\cdot(\vec{x}_2 - \vec{x}_3)}\, e^{\vec{x}_2\cdot(\vec{\nabla}_2 - i\vec{k}) + \vec{x}_3\cdot(\vec{\nabla}_3 + i\vec{k})}\, s_{q,\nu}(\vec{r}_2, \vec{r}_3)\Big|_{\vec{r}_2=\vec{r}_3=\vec{r}_1} \\ &\approx e^{i\vec{k}\cdot(\vec{x}_2 - \vec{x}_3)}\Big[1 + \vec{x}_2\cdot(\vec{\nabla}_2 - i\vec{k}) \\ &\qquad + \vec{x}_3\cdot(\vec{\nabla}_3 + i\vec{k})\Big]\, s_{q,\nu}(\vec{r}_2, \vec{r}_3)\Big|_{\vec{r}_2=\vec{r}_3=\vec{r}_1} \qquad (9.222) \end{aligned}$$

where we truncated the expansion at first order. Since $\vec{s}_q(\vec{r}_1) = 0$ for time-reversal invariant systems, the contribution from the leading term vanishes. Likewise, the contributions from the linear $i\vec{x}_{2/3}\cdot\vec{k}$ terms vanish. Using Eq. (9.112), the definition of the cartesian spin-orbit density, $J_{q,\mu\nu}$, given in Eq. (9.83), one writes Eq. (9.222) as

$$s_{q,\nu}(\vec{r}_1 + \vec{x}_2, \vec{r}_1 + \vec{x}_3) \approx i\, e^{i\vec{k}\cdot(\vec{x}_2 - \vec{x}_3)} \sum_{\mu} x_\mu\, J_{q,\mu\nu}(\vec{r}_1)\,. \qquad (9.223)$$

The final step involves performing the PSA over a deformed sphere that characterizes the local momentum distribution. Let us start from a spheroid in momentum space defined by the equation

$$\frac{k_x^2}{a(\vec{R})^2} + \frac{k_y^2}{a(\vec{R})^2} + \frac{k_z^2}{c(\vec{R})^2} = 1\,. \qquad (9.224)$$

For ease of notation, we write $a(\vec{R})$ as a and $c(\vec{R})$ as c in the following. We constrain the position-dependent quantities a and c by requiring that the spheroid has a given volume and quadrupole moment, viz,

$$\begin{aligned} V_q &\equiv \frac{4}{3}\pi^3 k_F^{q\,3} = \frac{4}{3}\pi^3 a^2 c\,, && (9.225)\\ P_2^q(\vec{R}) &= \frac{2\,(-a^2 + c^2)}{2\,a^2 + c^2}\,. && (9.226) \end{aligned}$$

The Π−function is obtained via the integration over the phase space of interest

$$\Pi_1^{\vec{s}} = \frac{3}{4\pi^3 k_F^{q\,3}} \int_{V_q} d\vec{k}\, e^{i\vec{r}\cdot\vec{k}}\,. \qquad (9.227)$$

Carrying out the integration over the volume V_q encompassed by the spheroid given in Eq. (9.224) can be done by using a stretched coordinate system from the transformation

$$\vec{k} \equiv (k_x, k_y, k_z) \to \vec{k}' \equiv (k_x, k_y, \frac{a}{c} k_z)\,, \qquad (9.228)$$

such that one finally obtains

$$s_{q,\nu}(\vec{r}_1 + \vec{x}_2, \vec{r}_1 + \vec{x}_3) \simeq i\,\Pi_1^{\vec{s}}(k_F^q x) \sum_\mu x_\mu J_{q,\mu\nu}(\vec{r}_1)\,, \tag{9.229}$$

where

$$\Pi_1^{\vec{s}}(\tilde{k}_F^q x) \equiv 3\,\frac{j_1(\tilde{k}_F^q x)}{\tilde{k}_F^q x} = 3\,\frac{j_1(\tilde{k}_F^q |\vec{x}_2 - \vec{x}_3|)}{\tilde{k}_F^q |\vec{x}_2 - \vec{x}_3|}\,, \tag{9.230}$$

and

$$\tilde{k}_F^q \equiv \left(\frac{2 + 2\,P_2^q(\vec{R})}{2 - P_2^q(\vec{R})}\right)^{1/3} k_F^q\,. \tag{9.231}$$

Setting $P_2^q(\vec{R}) = 0$, which consists of performing the PSA over INM phase-space, results in the same Π–function with $\tilde{k}_F^q$ replaced by k_F^q. For spherical systems, one can simplify the expression further by writing $J_{q,\mu\nu}(\vec{R})$ as a sum of pseudoscalar, vector and (antisymmetric) traceless tensor parts given in Eq. (9.165). Since in these systems, both the pseudoscalar and the tensor parts vanish, one obtains

$$\vec{s}_q\left(\vec{r}_1 + \vec{x}2, \vec{r}_1 + \vec{x}_3\right) \simeq -\frac{i}{2}\,\Pi_1^{\vec{s}}(\tilde{k}_F^q r)\,\vec{x} \times \vec{J}_q(\vec{r}_1)\,. \tag{9.232}$$

Hence, using Eq. (9.229), we have a DME for any type of nonlocal coordinate dependence. For example, $s(\vec{r}_1, \vec{r}_1 + \vec{x}_3)$ is obtained by simply setting $\vec{x}_2 = 0$, while setting $\vec{r}_1 = \vec{R}$ and $\vec{x}_2 = -\vec{x}_3 = \vec{r}/2$, Eq. (9.229) reduces to

$$\vec{s}_{q,\nu}\left(\vec{R} + \frac{\vec{r}}{2}, \vec{R} - \frac{\vec{r}}{2}\right) \simeq i\,\Pi_1^{\vec{s}}(k_F^q r) \sum_\mu r_\mu J_{q,\mu\nu}(\vec{R})\,, \tag{9.233}$$

where $\Pi_1^{\vec{s}}(k_F^q r)$ is as given in Eq. (9.230), with $\vec{x}$ replaced with $\vec{r}$. Due to the possible dependence of the accuracy of the DME on the specific coordinates used, one cannot claim or expect the same accuracy in expanding, for instance, $\vec{s}_q(\vec{r}_1, \vec{r}_1 + \vec{x}_2)$ and $\vec{s}_q(\vec{r}_1 + \vec{r}/2, \vec{r}_1 - \vec{r}/2)$.

9.5.6 Remarks on the generalized PSA-DME

As can be seen from Eqs. (9.212), (9.213) and (9.230), the final results of PSA-DME of $\rho_q(\vec{r}_1 + \vec{x}_2, \vec{r}_1 + \vec{x}_3)$ and $\vec{s}_q(\vec{r}_1 + \vec{x}_2, \vec{r}_1 + \vec{x}_3)$ are not separable in $\vec{x}_2$ and $\vec{x}_3$. In contrast, all nonlocal densities that involve only two of the coordinates such as $\rho_q(\vec{r}_1, \vec{r}_2)$, $\rho_q(\vec{r}_1, \vec{r}_1 + \vec{x}_2)$, ... led to a completely separable expansions. This can leave the perception that the objective of having a separable approximation, which is what the DME proposes to achieve, is not yet met.

However, $\rho_q(\vec{r}_1 + \vec{x}_2, \vec{r}_1 + \vec{x}_3)$ and $\vec{s}_q(\vec{r}_1 + \vec{x}_2, \vec{r}_1 + \vec{x}_3)$ appear in the HF energy from the chiral EFT NNN interaction at $\mathrm{N}^2\mathrm{LO}$ where $\vec{x}_2$ and $\vec{x}_3$ are part of the interaction form factors. Refer to section 7.1. In fact, the interaction does not depend on $\vec{r}_1$. Thus, all terms that depend solely on $\vec{x}_2$ and $\vec{x}_3$, whether they are separable in these two coordinates or not, can in principle be integrated out with the interaction form factors. The actual direct analytical integration of such terms is very difficult, if not impossible. Refer to section 9.11 for details on how we solve this problem. Leaving the technicalities for the relevant sections, it should be clear at this point that a local EDF will result from the application of the generalized PSA-DME of $\rho_q(\vec{r}_1 + \vec{x}_2, \vec{r}_1 + \vec{x}_3)$ and $\vec{s}_q(\vec{r}_1 + \vec{x}_2, \vec{r}_1 + \vec{x}_3)$ to the HF energy of the chiral EFT NNN interaction at $\mathrm{N}^2\mathrm{LO}$.

9.5.7 The modified-Taylor series expansion

As discussed in section 5.3.6, the modified-Taylor series approach provides a formal framework to extend the applicability of the density matrix expansion to non-time reversal invariant systems. It is obtained by replacing the coefficients of the Taylor series expansion of the densities with $\pi-$functions. The dimensionless variable Ω is

used to denote the possible argument of the $\pi-$functions. The modified Taylor series expansion of the densities that appear in the exact HF energy from a generic NN interaction reads

$$
\begin{aligned}
\rho_q(\vec{R} \pm \frac{\vec{r}}{2}) &\approx \pi_0^{\rho}(\Omega)\,\rho_q(\vec{R}) \pm \pi_1^{\rho}(\Omega)\,\frac{\vec{r}}{2} \cdot \vec{\nabla}_R \rho_q(\vec{R}) \\
&\quad + \frac{1}{2}\pi_2^{\rho}(\Omega) \left(\frac{\vec{r}}{2} \cdot \vec{\nabla}_R\right)^2 \rho_q(\vec{R})\,, \qquad (9.234) \\
\vec{s}_q(\vec{R} \pm \frac{\vec{r}}{2}) &\approx \pi_0^{\vec{s}}(\Omega)\,\vec{s}_q(\vec{R}) \pm \pi_1^{\vec{s}}(\Omega) \left(\frac{\vec{r}}{2} \cdot \vec{\nabla}_R\right)\vec{s}_q(\vec{R}) \\
&\quad + \frac{1}{2}\,\pi_2^{\vec{s}}(\Omega) \left(\frac{\vec{r}}{2} \cdot \vec{\nabla}_R\right)^2 \vec{s}_q(\vec{R})\,, \qquad (9.235) \\
\vec{j}_q(\vec{R} \pm \frac{\vec{r}}{2}) &= \pi_0^{\vec{j}}(\Omega)\,\vec{j}_q(\vec{R}) \pm \pi_1^{\vec{j}}(\Omega) \left(\frac{\vec{r}}{2} \cdot \vec{\nabla}_R\right)\vec{j}_q(\vec{R}) \\
&\quad + \frac{1}{2}\pi_2^{\vec{j}}(\Omega) \left(\frac{\vec{r}}{2} \cdot \vec{\nabla}_R\right)^2 \vec{j}_q(\vec{R})\,, \qquad (9.236) \\
\vec{J}_q(\vec{R} \pm \frac{\vec{r}}{2}) &\approx \pi_0^{\vec{J}}(\Omega)\,\vec{J}_q(\vec{R}) \pm \pi_1^{\vec{J}}(\Omega)\,\frac{\vec{r}}{2} \cdot \vec{\nabla}_R \vec{J}_q(\vec{R}) \\
&\quad + \frac{1}{2}\,\pi_2^{\vec{J}}(\Omega) \left(\frac{\vec{r}}{2} \cdot \vec{\nabla}_R\right)^2 \vec{J}_q(\vec{R})\,, \qquad (9.237) \\
\rho_q(\vec{R} \pm \frac{\vec{r}}{2}, \vec{R} \mp \frac{\vec{r}}{2}) &\approx \Pi_0^{\rho}(\Omega)\rho_q(\vec{R}) \pm \Pi_1^{\rho}(\Omega)\,\frac{\vec{r}}{2} \cdot \left(\vec{\nabla}_1 - \vec{\nabla}_2\right)\rho_q(\vec{r}_1, \vec{r}_2)\Big|_{\vec{r}_1=\vec{r}_2=\vec{R}} \\
&\quad + \frac{1}{2}\,\Pi_2^{\rho}(\Omega)\left[\left(\frac{\vec{r}}{2} \cdot \vec{\nabla}_1\right)^2 + \left(\frac{\vec{r}}{2} \cdot \vec{\nabla}_2\right)^2\right]\rho_q(\vec{r}_1, \vec{r}_2)\Big|_{\vec{r}_1=\vec{r}_2=\vec{R}} \\
&\quad - \Pi_3^{\rho}(\Omega) \left(\frac{\vec{r}}{2} \cdot \vec{\nabla}_1\right) \left(\frac{\vec{r}}{2} \cdot \vec{\nabla}_2\right) \rho_q(\vec{r}_1, \vec{r}_2)\Big|_{\vec{r}_1=\vec{r}_2=\vec{R}}\,, \qquad (9.238) \\
\vec{s}_q(\vec{R} \pm \frac{\vec{r}}{2}, \vec{R} \mp \frac{\vec{r}}{2}) &= \Pi_0^{\vec{s}}(\Omega)\vec{s}_q(\vec{R}) \pm \Pi_1^{\vec{s}}(\Omega)\,\frac{\vec{r}}{2} \cdot \left(\vec{\nabla}_1 - \vec{\nabla}_2\right)\vec{s}_q(\vec{r}_1, \vec{r}_2)\Big|_{\vec{r}_1=\vec{r}_2=\vec{R}} \\
&\quad + \frac{1}{2}\,\Pi_2^{\vec{s}}(\Omega)\left[\left(\frac{\vec{r}}{2} \cdot \vec{\nabla}_1\right)^2 + \left(\frac{\vec{r}}{2} \cdot \vec{\nabla}_2\right)^2\right]\vec{s}_q(\vec{r}_1, \vec{r}_2)\Big|_{\vec{r}_1=\vec{r}_2=\vec{R}} \\
&\quad - \Pi_3^{\vec{s}}(\Omega) \left(\frac{\vec{r}}{2} \cdot \vec{\nabla}_1\right) \left(\frac{\vec{r}}{2} \cdot \vec{\nabla}_2\right) \vec{s}_q(\vec{r}_1, \vec{r}_2)\Big|_{\vec{r}_1=\vec{r}_2=\vec{R}}\,, \qquad (9.239)
\end{aligned}
$$

and for the pairing densities

$$\begin{aligned}
\tilde{\rho}_q(\vec{R} \pm \frac{\vec{r}}{2}) &\approx \pi_0^{\tilde{\rho}}(\Omega)\,\tilde{\rho}_q(\vec{R}) \pm \pi_1^{\tilde{\rho}}(\Omega)\,\frac{\vec{r}}{2}\cdot\vec{\nabla}_R\tilde{\rho}_q(\vec{R}) \\
&\quad + \frac{1}{2}\pi_2^{\tilde{\rho}}(\Omega)\left(\frac{\vec{r}}{2}\cdot\vec{\nabla}_R\right)^2 \tilde{\rho}_q(\vec{R}), \qquad (9.240) \\
\tilde{\vec{s}}_q(\vec{R} \pm \frac{\vec{r}}{2}) &\approx \pi_0^{\tilde{\vec{s}}}(\Omega)\,\tilde{\vec{s}}_q(\vec{R}) \pm \pi_1^{\tilde{\vec{s}}}(\Omega)\left(\frac{\vec{r}}{2}\cdot\vec{\nabla}_R\right)\tilde{\vec{s}}_q(\vec{R}) \\
&\quad + \frac{1}{2}\,\pi_2^{\tilde{\vec{s}}}(\Omega)\left(\frac{\vec{r}}{2}\cdot\vec{\nabla}_R\right)^2 \tilde{\vec{s}}_q(\vec{R}), \qquad (9.241) \\
\tilde{\rho}_q(\vec{R} \pm \frac{\vec{r}}{2}, \vec{R} \mp \frac{\vec{r}}{2}) &\approx \Pi_0^{\tilde{\rho}}(\Omega)\tilde{\rho}_q(\vec{R}) \pm \Pi_1^{\tilde{\rho}}(\Omega)\,\frac{\vec{r}}{2}\cdot\left(\vec{\nabla}_1 - \vec{\nabla}_2\right)\tilde{\rho}_q(\vec{r}_1\,, \vec{r}_2)\Big|_{\vec{r}_1=\vec{r}_2=\vec{R}} \\
&\quad + \frac{1}{2}\,\Pi_2^{\tilde{\rho}}(\Omega)\left[\left(\frac{\vec{r}}{2}\cdot\vec{\nabla}_1\right)^2 + \left(\frac{\vec{r}}{2}\cdot\vec{\nabla}_2\right)^2\right]\tilde{\rho}_q(\vec{r}_1\,, \vec{r}_2)\Big|_{\vec{r}_1=\vec{r}_2=\vec{R}} \\
&\quad - \Pi_3^{\tilde{\rho}}(\Omega)\left(\frac{\vec{r}}{2}\cdot\vec{\nabla}_1\right)\left(\frac{\vec{r}}{2}\cdot\vec{\nabla}_2\right)\tilde{\rho}_q(\vec{r}_1\,, \vec{r}_2)\Big|_{\vec{r}_1=\vec{r}_2=\vec{R}}, \qquad (9.242) \\
\tilde{\vec{s}}_q(\vec{R} \pm \frac{\vec{r}}{2}, \vec{R} \mp \frac{\vec{r}}{2}) &\approx \Pi_0^{\tilde{\vec{s}}}(\Omega)\tilde{\vec{s}}_q(\vec{R}) \pm \Pi_1^{\tilde{\vec{s}}}(\Omega)\,\frac{\vec{r}}{2}\cdot\left(\vec{\nabla}_1 - \vec{\nabla}_2\right)\tilde{\vec{s}}_q(\vec{r}_1\,, \vec{r}_2)\Big|_{\vec{r}_1=\vec{r}_2=\vec{R}} \\
&\quad + \frac{1}{2}\,\Pi_2^{\tilde{\vec{s}}}(\Omega)\left[\left(\frac{\vec{r}}{2}\cdot\vec{\nabla}_1\right)^2 + \left(\frac{\vec{r}}{2}\cdot\vec{\nabla}_2\right)^2\right]\tilde{\vec{s}}_q(\vec{r}_1\,, \vec{r}_2)\Big|_{\vec{r}_1=\vec{r}_2=\vec{R}} \\
&\quad - \Pi_3^{\tilde{\vec{s}}}(\Omega)\left(\frac{\vec{r}}{2}\cdot\vec{\nabla}_1\right)\left(\frac{\vec{r}}{2}\cdot\vec{\nabla}_2\right)\tilde{\vec{s}}_q(\vec{r}_1\,, \vec{r}_2)\Big|_{\vec{r}_1=\vec{r}_2=\vec{R}}, \qquad (9.243)
\end{aligned}$$

At this point, the modified-Taylor series expansions of the densities can not be written in terms of the local densities defined in appendix 9.2.3 and 9.2.5. Implementing the steps explained in section 5.3.6, one obtains an equivalent expansion, this time with explicit local densities. These are

$$\begin{aligned}
\rho_q(\vec{R} \pm \frac{\vec{r}}{2}) &\approx \pi_0^{\rho}(\Omega)\,\rho_q(\vec{R}) \pm \pi_1^{\rho}(\Omega)\,\frac{\vec{r}}{2}\cdot\vec{\nabla}_R\,\rho_q(\vec{R}) \\
&\quad + \frac{1}{2}\,\pi_2^{\rho}(\Omega)\,(\frac{\vec{r}}{2}\cdot\vec{\nabla}_R)^2\,\rho_q(\vec{R}), \qquad (9.244) \\
\vec{s}_q(\vec{R} \pm \frac{\vec{r}}{2}) &\approx \pi_0^{\vec{s}}(\Omega)\,\vec{s}_q(\vec{R}) \pm \pi_1^{\vec{s}}(\Omega)\,\frac{\vec{r}}{2}\cdot\vec{\nabla}_R\vec{s}_q(\vec{R}) \\
&\quad + \frac{1}{2}\,\pi_2^{\vec{s}}(\Omega)\left(\frac{\vec{r}}{2}\cdot\vec{\nabla}_R\right)^2 \vec{s}_q(\vec{R}), \qquad (9.245)
\end{aligned}$$

$$\rho_q(\vec{R} \pm \frac{\vec{r}}{2}, \vec{R} \mp \frac{\vec{r}}{2}) \approx \Pi_0^{\rho}(\Omega)\,\rho_q(\vec{R}) \pm i\Pi_1^{\rho}(\Omega)\,\vec{r}\cdot\vec{j}_q(\vec{R}) + \frac{r^2}{24}\Pi_2^{\rho}(\Omega)\Big(\Delta\rho_q(\vec{R}) - 2\tau_q(\vec{R})\Big) - \frac{r^2}{12}\Pi_3^{\rho}(\Omega)\,\tau_q(\vec{R}), \tag{9.246}$$

$$s_{q,\nu}(\vec{R} \pm \frac{\vec{r}}{2}, \vec{R} \mp \frac{\vec{r}}{2}) \approx \Pi_0^{\vec{s}}(\Omega)\,s_{q,\nu}(\vec{R}) \pm i\Pi_1^{\vec{s}}(\Omega)\,r_\mu J_{q,\mu\nu}(\vec{R}) + \frac{r^2}{24}\Pi_2^{\vec{s}}(\Omega)\Big(\Delta s_{q,\nu}(\vec{R}) - 2T_{q,\nu}(\vec{R})\Big) - \frac{r^2}{12}\Pi_3^{\vec{s}}(\Omega)T_{q,\nu}(\vec{R}), \tag{9.247}$$

$$\vec{j}_q(\vec{R} \pm \frac{\vec{r}}{2}) \approx \pi_0^{\vec{j}}(\Omega)\,\vec{j}_q(\vec{R}) \pm \pi_1^{\vec{j}}(\Omega)\,\frac{\vec{r}}{2}\cdot\vec{\nabla}_R\vec{j}_q(\vec{R}) + \frac{1}{2}\pi_2^{\vec{j}}(\Omega)\left(\frac{\vec{r}}{2}\cdot\vec{\nabla}_R\right)^2\vec{j}_q(\vec{R}), \tag{9.248}$$

$$\vec{J}_q(\vec{R} \pm \frac{\vec{r}}{2}) \approx \pi_0^{\vec{J}}(\Omega)\,\vec{J}_q(\vec{R}) \pm \pi_1^{\vec{J}}(\Omega)\,\frac{\vec{r}}{2}\cdot(\vec{\nabla}_R)\vec{J}_q(\vec{R}) + \frac{1}{2}\pi_2^{\vec{J}}(\Omega)\left(\frac{\vec{r}}{2}\cdot\vec{\nabla}_R\right)^2\vec{J}_q(\vec{R}), \tag{9.249}$$

and for the pairing densities

$$\tilde{\rho}_q(\vec{R} \pm \frac{\vec{r}}{2}) \approx \pi_0^{\tilde{\rho}}(\Omega)\,\tilde{\rho}_q(\vec{R}) \pm \pi_1^{\tilde{\rho}}(\Omega)\,\frac{\vec{r}}{2}\cdot\vec{\nabla}_R\tilde{\rho}_q(\vec{R}) + \frac{1}{2}\pi_2^{\tilde{\rho}}(\Omega)\left(\frac{\vec{r}}{2}\cdot\vec{\nabla}_R\right)^2\tilde{\rho}_q(\vec{R}), \tag{9.250}$$

$$\tilde{\vec{s}}_q(\vec{R} \pm \frac{\vec{r}}{2}) \approx \pi_0^{\tilde{\vec{s}}}(\Omega)\,\tilde{\vec{s}}_q(\vec{R}) \pm \pi_1^{\tilde{\vec{s}}}(\Omega)\,\frac{\vec{r}}{2}\cdot\vec{\nabla}_R\,\tilde{\vec{s}}_q(\vec{R}) + \frac{1}{2}\pi_2^{\tilde{\vec{s}}}(\Omega)\left(\frac{\vec{r}}{2}\cdot\vec{\nabla}_R\right)^2\tilde{\vec{s}}_q(\vec{R}), \tag{9.251}$$

$$\tilde{\rho}_q(\vec{R} \pm \frac{\vec{r}}{2}, \vec{R} \mp \frac{\vec{r}}{2}) \approx \Pi_0^{\tilde{\rho}}(\Omega)\,\tilde{\rho}_q(\vec{R}) \pm i\Pi_1^{\tilde{\rho}}(\Omega)\,\vec{r}\cdot\tilde{\vec{j}}_q(\vec{R}) + \frac{r^2}{24}\Pi_2^{\tilde{\rho}}(\Omega)\Big(\Delta\tilde{\rho}_q(\vec{R}) - 2\tilde{\tau}_q(\vec{R})\Big) - \frac{r^2}{12}\Pi_3^{\tilde{\rho}}(\Omega)\,\tilde{\tau}_q(\vec{R}), \tag{9.252}$$

$$\tilde{s}_{q,\nu}(\vec{R} \pm \frac{\vec{r}}{2}, \vec{R} \mp \frac{\vec{r}}{2}) \approx \Pi_0^{\tilde{\vec{s}}}(\Omega)\,\tilde{s}_{q,\nu}(\vec{R}) \pm i\Pi_1^{\tilde{\vec{s}}}(\Omega)\,r_\mu J_{q,\mu\nu}(\vec{R}) + \frac{r^2}{24}\Pi_2^{\tilde{\vec{s}}}(\Omega)\Big(\Delta\tilde{s}_{q,\nu}(\vec{R}) - 2\tilde{T}_{q,\nu}(\vec{R})\Big) - \frac{r^2}{12}\Pi_3^{\vec{s}}(\Omega)\tilde{T}_{q,\nu}(\vec{R}), \tag{9.253}$$

9.6 Derivation of EDF from HF energy of local NN interaction

In this section, we give detailed derivation of the HF energy from a generic local two-nucleon interaction and the EDF that results after the application of the DME.

9.6.1 Central contribution

We demonstrate the derivation of the contribution to the HF energy from the central part of NN interaction by deriving the corresponding expression for the spin-triplet, isospin-triplet channel. Making use of the spin/isospin projection operators given in Table 1.2, the projection of a local central interaction in this channel reads

$$\hat{V}_C^{11} = \frac{1}{4}(1+\hat{P}_{12}^{\sigma})(1+\hat{P}_{12}^{\tau})\, V_C^{11}(r)\,. \tag{9.254}$$

Plugging this in Eq. (6.2), using the definition of the OBDM (Eq. (9.70)) and its scalar/isoscalar-vector/isovector decomposition, we obtain

$$\begin{aligned}
E_C^{NN}[11] = \; & \frac{1}{8}\int d\vec{r}_1\, d\vec{r}_2\, V_C^{11}(r)\Bigg[\rho_0(\,\vec{r}_1\,)\,\rho_0(\vec{r}_2) \;-\; \rho_0(\vec{r}_1,\vec{r}_2)\,\rho_0(\vec{r}_2,\vec{r}_1) \\
& + \sum_{\sigma_1\sigma_2}\Big(\frac{1}{2}\,\rho_0(\vec{r}_1)\,\delta_{\sigma_1\sigma_2} + \frac{1}{2}\vec{s_0}(\vec{r}_1).\vec{\sigma}_{\sigma_1\sigma_2}\Big) \\
& \times\Big(\frac{1}{2}\,\rho_0(\vec{r}_2)\,\delta_{\sigma_1\sigma_2} + \frac{1}{2}\vec{s_0}(\vec{r}_2).\vec{\sigma}_{\sigma_2\sigma_1}\Big) \\
& - \sum_{\sigma_1\sigma_2}\Big(\frac{1}{2}\,\rho_0(\vec{r}_1,\vec{r}_2)\,\delta_{\sigma_1\sigma_2} + \frac{1}{2}\vec{s_0}(\vec{r}_1,\vec{r}_2).\vec{\sigma}_{\sigma_1\sigma_2}\Big) \\
& \times\Big(\frac{1}{2}\,\rho_0(\vec{r}_2,\vec{r}_1)\,\delta_{\sigma_1\sigma_2} + \frac{1}{2}\vec{s_0}(\vec{r}_2,\vec{r}_1).\vec{\sigma}_{\sigma_2\sigma_1}\Big) \\
& + \sum_{q}\Big(\frac{1}{2}\,\rho_0(\vec{r}_1) + \frac{1}{2}(-1)^{\frac{1}{2}-q}\,\rho_1(\vec{r}_1)\Big)\Big(\frac{1}{2}\,\rho_0(\vec{r}_2) + \frac{1}{2}(-1)^{\frac{1}{2}-q}\,\rho_1(\vec{r}_2)\Big) \\
& - \sum_{q}\Big(\frac{1}{2}\,\rho_0(\vec{r}_1,\vec{r}_2) + \frac{1}{2}(-1)^{\frac{1}{2}-q}\,\rho_1(\vec{r}_1,\vec{r}_2)\Big)
\end{aligned}$$

$$
\begin{aligned}
&\times\Big(\frac{1}{2}\,\rho_0(\vec{r}_2,\vec{r}_1)+\frac{1}{2}(-1)^{\frac{1}{2}-q}\,\rho_1(\vec{r}_2,\vec{r}_1)\Big)\\
&+\frac{1}{16}\sum_q\sum_{\sigma_1\sigma_2}\Big(\rho_0(\vec{r}_1)\,\rho_0(\vec{r}_2)\,\delta_{\sigma_1\sigma_2}+\vec{s}_0(\vec{r}_1).\vec{\sigma}_{\sigma_1\sigma_2}\times\vec{s}_0(\vec{r}_2).\vec{\sigma}_{\sigma_2\sigma_1}\\
&+\rho_1(\vec{r}_1)\,\rho_1(\vec{r}_2)\,\delta_{\sigma_1\sigma_2}+\vec{s}_1(\vec{r}_1).\vec{\sigma}_{\sigma_1\sigma_2}\times\vec{s}_1(\vec{r}_2).\vec{\sigma}_{\sigma_2\sigma_1}\Big)\\
&-\frac{1}{16}\sum_q\sum_{\sigma_1\sigma_2}\Big(\rho_0(\vec{r}_1,\vec{r}_2)\,\rho_0(\vec{r}_2,\vec{r}_1)\,\delta_{\sigma_1\sigma_2}\\
&+\vec{s}_0(\vec{r}_1,\vec{r}_2).\vec{\sigma}_{\sigma_1\sigma_2}\times\vec{s}_0(\vec{r}_2,\vec{r}_1).\vec{\sigma}_{\sigma_2\sigma_1}\;+\;\rho_1(\vec{r}_1,\vec{r}_2)\,\rho_1(\vec{r}_2,\vec{r}_1)\,\delta_{\sigma_1\sigma_2}\\
&+\vec{s}_1(\vec{r}_1,\vec{r}_2).\vec{\sigma}_{\sigma_1\sigma_2}\times\vec{s}_1(\vec{r}_2,\vec{r}_1).\vec{\sigma}_{\sigma_2\sigma_1}\Big)\Big]\,. \qquad (9.255)
\end{aligned}
$$

To find the final, most simplified form of the above expression, we make repeated use of the relations listed in Eqs. (9.12)-(9.13) to obtain

$$
\begin{aligned}
E_C^{NN}[11] \;=\; &\frac{1}{8}\int d\vec{r}_1\,d\vec{r}_2\,V_C^{11}(r)\,\Big[\frac{9}{4}\,\rho_0(\vec{r}_1)\,\rho_0(\vec{r}_2)-\frac{9}{4}|\,\rho_0(\vec{r}_1,\vec{r}_2)\,|^2+\frac{3}{4}\,\rho_1(\vec{r}_1)\,\rho_1(\vec{r}_2)\\
&-\frac{3}{4}|\,\rho_1(\vec{r}_1,\vec{r}_2)\,|^2+\frac{3}{4}\vec{s}_0(\vec{r}_1).\vec{s}_0(\vec{r}_2)-\frac{3}{4}\vec{s}_0(\vec{r}_1,\vec{r}_2).\vec{s}_0(\vec{r}_2,\vec{r}_1)\\
&+\frac{1}{4}\vec{s}_1(\vec{r}_1).\vec{s}_1(\vec{r}_2)-\frac{1}{4}\vec{s}_1(\vec{r}_1,\vec{r}_2).\vec{s}_1(\vec{r}_2,\vec{r}_1)\Big]\,. \qquad (9.256)
\end{aligned}
$$

In terms of the proton and neutron densities

$$
\begin{aligned}
E_C^{NN}[11] \;=\; &\frac{1}{8}\sum_q\int d\vec{r}_1\,d\vec{r}_2\,V_C^{11}(r)\Big[3\,\rho_q(\vec{r}_1)\,\rho_q(\vec{r}_2)\;-\;3\,\rho_q(\vec{r}_1,\vec{r}_2)\,\rho_q(\vec{r}_2,\vec{r}_1)\\
&\qquad+\vec{s}_q(\vec{r}_1)\,\cdot\,\vec{s}_q(\vec{r}_2)\;-\;\vec{s}_q(\vec{r}_1,\vec{r}_2)\,\cdot\,\vec{s}_q(\vec{r}_2,\vec{r}_1)\Big] \qquad (9.257)\\
&+\frac{1}{8}\sum_q\int d\vec{r}_1\,d\vec{r}_2\,V_C^{11}(\vec{r})\Big[\frac{3}{2}\,\rho_q(\vec{r}_1)\,\rho_{\bar{q}}(\vec{r}_2)\;-\;\frac{3}{2}\,\rho_q(\vec{r}_1,\vec{r}_2)\,\rho_{\bar{q}}(\vec{r}_2,\,\vec{r}_1)\\
&\qquad+\frac{1}{2}\,\vec{s}_q(\vec{r}_1)\,\cdot\,\vec{s}_{\bar{q}}(\vec{r}_2)\;-\;\frac{1}{2}\,\vec{s}_q(\vec{r}_1,\vec{r}_2)\,\cdot\,\vec{s}_{\bar{q}}(\vec{r}_2,\vec{r}_1)\Big]\,. \qquad (9.258)
\end{aligned}
$$

Similar derivations can be done for the other three channels.

9.6.2 Spin-orbit contribution

For the spin-orbit interaction, we demonstrate the derivation for the spin-triplet, isospin-singlet channel. Starting with Eq. (6.2) and the projection of the spin-orbit part of the interaction in this channel, we can write the Hartree contribution as

$$\begin{aligned} E^{NN}_{LS,H}[10] &= -\frac{i}{4}\sum_q \int d\vec{r}_1\, d\vec{r}_2\, V^{10}_{LS}(r)\, \vec{r}\cdot \Big[\rho_q(\vec{r}_2)\, \vec{\nabla}_1 \times \vec{s}_{\bar{q}}(\vec{r}_1,\vec{r}_2^{\,\prime})|_{\vec{r}_2^{\,\prime}=\vec{r}_1} \\ &\qquad + \vec{s}_q(\vec{r}_1) \times \vec{\nabla}_2 \rho_{\bar{q}}(\vec{r}_2,\vec{r}_2^{\,\prime})|_{\vec{r}_2^{\,\prime}=\vec{r}_2}\Big] \\ &= -\frac{i}{4}\sum_q \int d\vec{r}_1\, d\vec{r}_2\, V^{10}_{LS}(r)\, \vec{r}\cdot \Big[\rho_q(\vec{r}_2)\, \big(\frac{1}{2}\vec{\nabla} \times \vec{s}_{\bar{q}}(\vec{r}_1) + i\,\vec{J}_{\bar{q}}(\vec{r}_1)\big) \\ &\qquad + \vec{s}_q(\vec{r}_1) \times \big(\frac{1}{2}\vec{\nabla}\rho_{\bar{q}}(\vec{r}_2) + i\vec{j}_{\bar{q}}(\vec{r}_2)\big)\Big] \\ &= \frac{1}{4}\sum_q \int d\vec{r}_1\, d\vec{r}_2\, V^{10}_{LS}(r)\, \vec{r}\cdot \Big[\vec{J}_q(\vec{r}_1)\, \rho_{\bar{q}}(\vec{r}_2) + \vec{r}\cdot \vec{s}_q(\vec{r}_1) \otimes \vec{j}_{\bar{q}}(\vec{r}_2) \\ &\qquad - \frac{i}{2}\vec{\nabla} \times \vec{s}_q(\vec{r}_1)\, \rho_{\bar{q}}(\vec{r}_2) + \frac{i}{2}\vec{\nabla}\rho_q(\vec{r}_2) \times \vec{s}_{\bar{q}}(\vec{r}_1)\Big]. \end{aligned} \tag{9.259}$$

Noting that

$$\int d\vec{r}_1\, d\vec{r}_2\, V_{LS}(r)\, \vec{r}\cdot \vec{\nabla} \otimes \left[\rho_q(\vec{r}_1)\, \vec{s}_{q/\bar{q}}(\vec{r}_2)\right] = 0\,, \tag{9.260}$$

where $\vec{\nabla} = \vec{\nabla}_1 - \vec{\nabla}_2$, the Hartree contribution from the spin-orbit interaction in the spin-triplet, isospin-singlet channel reads

$$E^{NN}_{LS,dir}[10] = \frac{1}{4}\sum_q \int d\vec{r}_1\, d\vec{r}_2\, V^{10}_{LS}(r)\, \vec{r}\cdot \Big[\vec{J}_q(\vec{r}_1)\, \rho_{\bar{q}}(\vec{r}_2) + \vec{s}_q(\vec{r}_1) \times \vec{j}_{\bar{q}}(\vec{r}_2)\Big]. \tag{9.261}$$

The Fock contribution in the spin-triplet, isospin singlet channel reads

$$E^{NN}_{LS,F}[10] = \frac{i}{8}\Big(V_5 - V_6 + V_7 - V_8\Big), \tag{9.262}$$

where expressing the V_i s in terms of the density matrix

$$\begin{aligned}
V_5 &= \sum_{\sigma_1\sigma_2\sigma_3}\sum_q \int d\vec{r}_1\, d\vec{r}_2\, V_{LS}^{10}(r)\, \vec{r}\times\vec{\nabla}_2\rho_q(\vec{r}_2\sigma_2,\vec{r}_1\sigma_1)\cdot\langle\sigma_1|\vec{\sigma}|\sigma_3\rangle\, \rho_{\bar{q}}(\vec{r}_1\sigma_3,\vec{r}_2\sigma_2)\\
V_6 &= \sum_{\sigma_1\sigma_2\sigma_3}\sum_q \int d\vec{r}_1\, d\vec{r}_2\, V_{LS}^{10}(r)\, \vec{r}\times\vec{\nabla}_1\rho_{\bar{q}}(\vec{r}_1\sigma_3,\vec{r}_2\sigma_2)\cdot\langle\sigma_1|\vec{\sigma}|\sigma_3\rangle\, \rho_q(\vec{r}_2\sigma_2,\vec{r}_1\sigma_1)\\
V_7 &= \sum_{\sigma_1\sigma_2\sigma_4}\sum_q \int d\vec{r}_1\, d\vec{r}_2\, V_{LS}^{10}(r)\, \vec{r}\times\vec{\nabla}_2\rho_q(\vec{r}_2\sigma_4,\vec{r}_1\sigma_1)\cdot\langle\sigma_2|\vec{\sigma}|\sigma_4\rangle\, \rho_{\bar{q}}(\vec{r}_1\sigma_1,\vec{r}_2\sigma_2)\\
V_8 &= \sum_{\sigma_1\sigma_2\sigma_4}\sum_q \int d\vec{r}_1\, d\vec{r}_2\, V_{LS}^{10}(r)\, \vec{r}\times\vec{\nabla}_1\rho_{\bar{q}}(\vec{r}_1\sigma_1,\vec{r}_2\sigma_2)\cdot\langle\sigma_2|\vec{\sigma}|\sigma_4\rangle\, \rho_q(\vec{r}_2\sigma_4,\vec{r}_1\sigma_1)\,.
\end{aligned} \tag{9.263}$$

The manipulation of the above four expressions involves repeated application of spin-traces. Finally, one obtains

$$\begin{aligned}
E_{LS,exc}^{NN}[10] &= \frac{i}{4}\sum_q \int d\vec{r}_1\, d\vec{r}_2\, V_{LS}^{10}(r)\Big[\vec{s}_q(\vec{r}_1,\vec{r}_2)\cdot\vec{r}\otimes\vec{\nabla}_2\rho_{\bar{q}}(\vec{r}_2,\vec{r}_1)\\
&\qquad + \rho_q(\vec{r}_1,\vec{r}_2)\,\vec{r}\otimes\vec{\nabla}_2\cdot\vec{s}_{\bar{q}}(\vec{r}_2,\vec{r}_1)\Big]\,.
\end{aligned} \tag{9.264}$$

Spin-orbit contribution in time-reversal invariant systems

To recover the expression given in [170] for the contribution from the Hartree-Fock energy in spin-orbit interaction, it suffices to show that $-\sum_q \int d\vec{r}_1\, d\vec{r}_2\, V_{LS}^{10}(r)\,\rho_q(\vec{r}_1,\vec{r}_2)\vec{r}\times\vec{\nabla}_2\cdot\vec{s}_{\bar{q}}(\vec{r}_1,\vec{r}_2)$ can be simplified as

$$\begin{aligned}
&= -\sum_q \int d\vec{r}_1\, d\vec{r}_2\, V_{LS}^{10}(r)\,\rho_q(\vec{r}_1,\vec{r}_2)\vec{r}\times\vec{\nabla}_2\cdot\vec{s}_{\bar{q}}(\vec{r}_1,\vec{r}_2)\\
&= \sum_q \int d\vec{r}_1\, d\vec{r}_2\, V_{LS}^{10}(r)\Big[\vec{s}_q(\vec{r}_1,\vec{r}_2)\cdot\vec{r}\times\vec{\nabla}_2\rho_{\bar{q}}(\vec{r}_1,\vec{r}_2)\\
&\qquad - \rho_{\bar{q}}(\vec{r}_1,\vec{r}_2)\,\vec{s}_q(\vec{r}_1,\vec{r}_2)\cdot\vec{\nabla}_2\times\vec{r}\Big]\\
&\qquad - \sum_q \int d\vec{r}_1\, d\vec{r}_2\, \frac{1}{r}\frac{dV_{LS}^{10}(r)}{dr}\,\rho_{\bar{q}}(\vec{r}_1,\vec{r}_2)\,\vec{s}_q(\vec{r}_1,\vec{r}_2)\cdot\vec{r}\times\vec{r}
\end{aligned}$$

$$= \sum_q \int d\vec{r}_1\, d\vec{r}_2\, V_{LS}^{10}(r)\ \vec{s}_q(\vec{r}_1, \vec{r}_2) \cdot \vec{r} \times \vec{\nabla}_2 \rho_{\bar{q}}(\vec{r}_1, \vec{r}_2)\,. \tag{9.265}$$

Thus taking the above result, adding it to the terms coming from the spin-triplet isospin-triplet one and assuming $V_{LS}^{10}(r) = V_{LS}^{11}(r)$ [1] one obtains

$$\begin{aligned} E_{LS}^{NN} &= \frac{1}{2} \int d\vec{r}_1\, d\vec{r}_2\, V_{LS}(r) \Big[\vec{r} \cdot \vec{J}(\vec{r}_1)\, \rho(\vec{r}_2) \\ &\qquad + i\, 2 \sum_q \vec{s}_q(\vec{r}_1, \vec{r}_2) \cdot \vec{r} \times \vec{\nabla}_2 \rho_q(\vec{r}_1, \vec{r}_2) \Big]\,, \end{aligned} \tag{9.266}$$

which is exactly the same expression as given in [170] for time-reversal invariant systems. Note that there is a factor of two difference between our expression and the expression in Ref. [170] which is due to a factor of two difference between the spin-orbit interaction used in our derivation and in Ref. [170].

9.6.3 Tensor contribution

The derivation of the Hartree contribution from the tensor part of the NN interaction is trivial due to the specific operator structure, viz,

$$\langle \sigma_1 \sigma_2 | \vec{\sigma}_1 \cdot \vec{e}_r\, \vec{\sigma}_2 \cdot \vec{e}_r | \sigma_3 \sigma_4 \rangle = \langle \sigma_1 | \vec{\sigma}_1 | \sigma_3 \rangle \cdot \vec{e}_r\, \langle \sigma_2 | \vec{\sigma}_2 | \sigma_4 \rangle \cdot \vec{e}_r\,, \tag{9.267}$$

$$\langle \sigma_1 \sigma_2 |\, \vec{\sigma}_1 \cdot \vec{\sigma}_2\, | \sigma_3 \sigma_4 \rangle = \langle \sigma_1 | \vec{\sigma}_1 | \sigma_3 \rangle \cdot \langle \sigma_2 | \vec{\sigma}_2 | \sigma_4 \rangle\,. \tag{9.268}$$

For example, in the spin-triplet, isospin-singlet channel,

$$E_{T,H}^{NN}[10] = \frac{1}{4} \sum_q \int d\vec{r}_1\, d\vec{r}_2\, V_T^{10}(r) \Big[3\, \vec{s}_q(\vec{r}_1) \cdot \hat{r}\, \vec{s}_{\bar{q}}(\vec{r}_2) \cdot \hat{r} - \vec{s}_q(\vec{r}_1) \cdot \vec{s}_{\bar{q}}(\vec{r}_2) \Big] \tag{9.269}$$

---

[1] This assumption is essential to obtain the form given in [170] as the authors use the same r dependence in both channels.

The derivation of the Fock contribution involves a significant number of spin-traces. Due to the similarity with the derivation given in section 9.6.1 for the central piece, we do not repeat the derivation.

9.6.4 Leading-order pairing contribution

Restricting the derivation to a central interaction and to the spin-singlet, isospin-triplet channel, the leading-order pairing contribution reads

$$\langle \Phi | \hat{V}_C^{01} | \Phi \rangle_{pair} = \frac{1}{2} \sum_q \sum_{ijkl} \kappa_{ij}^* \, \langle iqjq \, | \, \hat{V}_c^{01} \, | \, kqlq \rangle \, \kappa_{kl}. \tag{9.270}$$

Thus,

$$\begin{aligned} \langle \Phi | V_C^{01} | \Phi \rangle_{pair} &= \frac{1}{8} \sum_q \sum_{\sigma_1 \sigma_2} \int d\vec{r}_1 \, d\vec{r}_2 \, V_C^{01}(r) \\ &\times \left(\frac{1}{2\sigma_1} \tilde{\rho}^{q*} \left(\vec{r}_2 \sigma_2, \vec{r}_1 \bar{\sigma}_1 \right) \frac{1}{2\sigma_1} \tilde{\rho}^{q} \left(\vec{r}_2 \sigma_2, \vec{r}_1 \bar{\sigma}_1 \right) \right. \\ &- \frac{1}{2\sigma_1} \tilde{\rho}^{q*} \left(\vec{r}_2 \sigma_2, \vec{r}_1 \bar{\sigma}_1 \right) \frac{1}{2\sigma_2} \tilde{\rho}^{q} \left(\vec{r}_1 \sigma_1, \vec{r}_2 \bar{\sigma}_2 \right) \\ &- \frac{1}{2\sigma_1} \tilde{\rho}^{q*} \left(\vec{r}_2 \sigma_2, \vec{r}_1 \bar{\sigma}_1 \right) \frac{1}{2\sigma_2} \tilde{\rho}^{q} \left(\vec{r}_2 \sigma_1, \vec{r}_1 \bar{\sigma}_2 \right) \\ &\left. + \frac{1}{2\sigma_1} \tilde{\rho}^{q*} \left(\vec{r}_2 \sigma_2, \vec{r}_1 \bar{\sigma}_1 \right) \frac{1}{2\sigma_1} \tilde{\rho}^{q} \left(\vec{r}_1 \sigma_2, \vec{r}_2 \bar{\sigma}_1 \right) \right). \end{aligned} \tag{9.271}$$

After resolving into scalar/isoscalar, vector/isovector parts and simplifying one gets

$$\langle \Phi | V_C^{01} | \Phi \rangle_{pair} = \frac{1}{4} \sum_q \int d\vec{r}_1 \, d\vec{r}_2 \, V_C^{01}(r) \, | \tilde{\rho}_q(\vec{r}_1, \vec{r}_2) |^2 . \tag{9.272}$$

9.6.5 The resulting EDF: EDF-NN-DME

In section 5.3.6, we discussed the basic steps that are involved in the derivation of a local EDF from the exact HF energy of a generic NN interaction through the application of the modified-Taylor series (or any other DME). These steps are best exemplified by the simplifications that we carried out to obtain Eqs. (5.46) and (5.47). We apply essentially the same step on the exact HFB given in section 6.1 and arrive at a local EDF which we call EDF-NN-DME. It has three components: the particle-hole EDF (given in Eq. (4.11)), the particle-particle EDF (given in Eq. (6.35)) and the additional terms of the EDF (given in Eq. (6.36)). The couplings of the particle-hole part of the EDF, in terms of the notation defined in Table 1.2, are given by

$$
\begin{aligned}
A^{\rho\rho} &= \frac{1}{8}a_1^{C01}\big[(\pi_0^{\rho})^2 + (\Pi_0^{\rho})^2\big] + \frac{3}{8}a_1^{C11}\big[(\pi_0^{\rho})^2 - (\Pi_0^{\rho})^2\big] \\
A^{\rho\tau} &= \Big(-\frac{1}{16}a_2^{C01} + \frac{3}{16}a_2^{C11}\Big)\big[\Pi_0^{\rho}(\Pi_2^{\rho} + \Pi_3^{\rho})\big] \\
A^{\rho\Delta\rho} &= \Big(\frac{1}{32}a_2^{C01} + \frac{3}{32}a_2^{C11}\Big)\big[\pi_0^{\rho}\pi_2^{\rho}\big] + \Big(\frac{1}{32}a_2^{C01} - \frac{3}{32}a_2^{C11}\Big)\big[\Pi_0^{\rho}\Pi_2^{\rho}\big] \\
A^{\nabla\rho\nabla\rho} &= -\Big(\frac{1}{32}a_2^{C01} + \frac{3}{32}a_2^{C11}\Big)\big[(\pi_1^{\rho})^2\big] \\
A^{ss} &= -\frac{1}{8}a_1^{C01}\big[(\pi_0^{\vec{s}})^2 + (\Pi_0^{\vec{s}})^2\big] + \frac{1}{8}a_1^{C11}\big[(\pi_0^{\vec{s}})^2 - (\Pi_0^{\vec{s}})^2\big] \\
A^{\rho\nabla J} &= \frac{1}{4}a_2^{LS11}\big[\pi_0^{\rho}\pi_1^{\vec{J}} - \Pi_0^{\rho}\Pi_1^{\vec{s}}\big] \\
A^{\nabla\rho J} &= -\frac{1}{4}a_2^{LS11}\big[\pi_1^{\rho}\pi_0^{\vec{J}} - \Pi_0^{\rho}\Pi_1^{\vec{s}}\big] \\
A^{s\Delta s} &= -\frac{1}{32}a_2^{C01}\big[\pi_0^{\vec{s}}\pi_2^{\vec{s}} + \Pi_0^{\vec{s}}\Pi_2^{\vec{s}}\big] + \Big(\frac{1}{32}a_2^{C11} - \frac{1}{8}a_2^{T11}\Big)\big[\pi_0^{\vec{s}}\pi_2^{\vec{s}} - \Pi_0^{\vec{s}}\Pi_2^{\vec{s}}\big] \\
&\quad + \frac{3}{8}a_3^{T11}\big[2\pi_0^{\vec{s}}\pi_2^{\vec{s}} - \Pi_0^{\vec{s}}\Pi_2^{\vec{s}}\big] \\
A^{\nabla s\nabla s} &= -\frac{3}{2}a_3^{T11}\big[(\pi_1^{\vec{s}})^2\big] + \frac{3}{8}a_3^{T11}\big[\Pi_0^{\vec{s}}(\Pi_2^{\vec{s}} + \Pi_3^{\vec{s}})\big] \\
A^{\nabla s\circ\nabla s} &= \Big(\frac{1}{32}a_2^{C01} - \frac{1}{32}a_2^{C11} + \frac{1}{8}a_2^{T11}\Big)\big[(\pi_1^{\vec{s}})^2\big] \\
A^{JJ} &= \Big(-\frac{1}{16}a_2^{C01} - \frac{1}{16}a_2^{C11} + \frac{1}{4}a_2^{T11} - \frac{3}{4}a_3^{T11}\Big)\big[\Pi_0^{\vec{s}}(\Pi_2^{\vec{s}} + \Pi_3^{\vec{s}})\big] \\
A^{J\bar{J}} &= -\frac{3}{2}a_3^{T11}\big[\Pi_0^{\vec{s}}\Pi_2^{\vec{s}}\big] \\
B^{\rho\rho} &= \Big(\frac{3}{16}a_1^{C10} + \frac{1}{16}a_1^{C01}\Big)\big[(\pi_0^{\rho})^2 \\
&\quad + (\Pi_0^{\rho})^2\big] + \Big(\frac{3}{16}a_1^{C11} + \frac{1}{16}a_1^{C00}\Big)\big[(\pi_0^{\rho})^2 - (\Pi_0^{\rho})^2\big] \\
B^{\rho\tau} &= \Big(-\frac{3}{32}a_2^{C10} - \frac{1}{32}a_2^{C01} + \frac{3}{32}a_2^{C11} + \frac{1}{32}a_2^{C00}\Big)\big[\Pi_0^{\rho}(\Pi_2^{\rho} + \Pi_3^{\rho})\big]
\end{aligned}
$$

$$
\begin{aligned}
B^{\rho\Delta\rho} &= \Big(\frac{3}{64}a_2^{C10} + \frac{1}{64}a_2^{C01} + \frac{3}{64}a_2^{C11} + \frac{1}{64}a_2^{C00}\Big)\big[\,\pi_0^{\rho}\pi_2^{\rho}\,\big] \\
&\quad + \Big(\frac{3}{64}a_2^{C10} + \frac{1}{64}a_2^{C01} - \frac{3}{64}a_2^{C11} - \frac{1}{64}a_2^{C00}\Big)\big[\,\Pi_0^{\rho}\Pi_2^{\rho}\,\big] \\
B^{\nabla\rho\nabla\rho} &= -\Big(\frac{3}{64}a_2^{C10} + \frac{1}{64}a_2^{C01} + \frac{3}{64}a_2^{C11} + \frac{1}{64}a_2^{C00}\Big)\big[\,(\pi_1^{\rho})^2\,\big] \\
B^{ss} &= \Big(\frac{1}{16}a_1^{C10} - \frac{1}{16}a_1^{C01}\Big)\big[\,(\pi_0^{\vec{s}})^2 + (\Pi_0^{\vec{s}})^2\,\big] \\
&\quad + \Big(\frac{1}{16}a_1^{C11} - \frac{1}{16}a_1^{C00}\Big)\big[\,(\pi_0^{\vec{s}})^2 - (\Pi_0^{\vec{s}})^2\,\big] \\
B^{\rho\nabla J} &= \frac{1}{8}\,a_2^{LS10}\big[\,\pi_0^{\rho}\pi_1^{\vec{J}} - \Pi_0^{\rho}\Pi_1^{\vec{s}}\,\big] + \frac{1}{8}\,a_2^{LS11}\big[\,\pi_0^{\rho}\pi_1^{\vec{J}} + \Pi_0^{\rho}\Pi_1^{\vec{s}}\,\big] \\
B^{\nabla\rho J} &= -\frac{1}{8}\,a_2^{LS10}\big[\,\pi_1^{\rho}\pi_0^{\vec{J}} - \Pi_0^{\rho}\Pi_1^{\vec{s}}\,\big] - \frac{1}{8}\,a_2^{LS11}\big[\,\pi_1^{\rho}\pi_0^{\vec{J}} + \Pi_0^{\rho}\Pi_1^{\vec{s}}\,\big] \\
B^{s\Delta s} &= \Big(\frac{1}{64}\,a_2^{C10} - \frac{1}{64}\,a_2^{C01}\Big)\big[\,\pi_0^{\vec{s}}\pi_2^{\vec{s}} + \Pi_0^{\vec{s}}\Pi_2^{\vec{s}}\,\big] \\
&\quad + \Big(\frac{1}{64}\,a_2^{C11} - \frac{1}{64}\,a_2^{C00}\Big)\big[\,\pi_0^{\vec{s}}\pi_2^{\vec{s}} - \Pi_0^{\vec{s}}\Pi_2^{\vec{s}}\,\big] \\
&\quad + \Big(-\frac{1}{16}\,a_2^{T10} + \frac{3}{8}\,a_3^{T10} - \frac{1}{16}\,a_2^{T11} + \frac{3}{8}\,a_3^{T11}\Big)\big[\,\pi_0^{\vec{s}}\pi_2^{\vec{s}}\,\big] \\
&\quad + \Big(-\frac{3}{16}\,a_2^{T10} + \frac{3}{16}\,a_3^{T10} + \frac{3}{16}\,a_2^{T11} - \frac{3}{16}\,a_3^{T11}\Big)\big[\,\Pi_0^{\vec{s}}\Pi_2^{\vec{s}}\,\big] \\
B^{\nabla s\nabla s} &= -\Big(\frac{3}{4}a_3^{T10} + \frac{3}{4}a_3^{T11}\Big)\big[(\pi_1^{\vec{s}})^2\big] \\
&\quad + \Big(-\frac{3}{16}\,a_3^{T10} + \frac{3}{16}\,a_3^{T11}\Big)\,\big[\,\Pi_0^{\vec{s}}\,(\Pi_2^{\vec{s}} + \Pi_2^{\vec{s}})\,\big] \\
B^{\nabla s\circ\nabla s} &= \Big(-\frac{1}{64}\,a_2^{C10} + \frac{1}{64}\,a_2^{C01} - \frac{1}{64}\,a_2^{C11} + \frac{1}{64}\,a_2^{C00} \\
&\quad + \frac{1}{16}a_2^{T10} + \frac{1}{16}a_2^{T11}\Big)\big[(\pi_1^{\vec{s}})^2\big] \\
B^{JJ} &= \Big(\frac{1}{32}a_2^{C10} - \frac{1}{32}a_2^{C01} - \frac{1}{32}a_2^{C11} + \frac{1}{32}a_2^{C00} - \frac{1}{8}a_2^{T10} + \frac{3}{8}a_3^{T10} \\
&\quad + \frac{1}{8}a_2^{T11} - \frac{3}{8}a_3^{T11}\Big)\big[\,\Pi_0^{\vec{s}}\,(\Pi_2^{\vec{s}} + \Pi_3^{\vec{s}})\,\big] \\
B^{J\bar{J}} &= \Big(\frac{3}{4}\,a_3^{T10} - \frac{3}{4}\,a_3^{T11}\Big)\big[\,\Pi_0^{\vec{s}}\Pi_2^{\vec{s}}\,\big]\,,
\end{aligned}
$$

and for the particle-particle part of the EDF

$$
\begin{aligned}
A^{\tilde{\rho}\tilde{\rho}} &= \frac{1}{16}\,a_1^{C01}\big[\,\Pi_0^{\tilde{\rho}}\,\big]^2, \\
A^{\tilde{\rho}\tilde{\tau}} &= \frac{1}{128}\,a_2^{C01}\big[\,\Pi_0^{\tilde{\rho}}\Pi_2^{\tilde{\rho}}\,\big], \\
A^{\tilde{\vec{J}}\tilde{\vec{J}}} &= \frac{1}{4}a_2^{C11}\big[\,\Pi_0^{\tilde{\vec{s}}}\Pi_2^{\tilde{\vec{s}}}\,\big]\,.
\end{aligned}
\tag{9.273}
$$

In the EDF that results from the additional terms, given in Eq. (6.36), only the couplings from the Coulomb piece are unspecified. These are given by

$$
\begin{aligned}
C^{\rho\rho} &= a_1^C \left(\pi_0^\rho\right)^2 , \\
C^{\rho\Delta\rho} &= \frac{1}{2} a_2^C \left[\pi_0^\rho \pi_2^\rho \right] , \\
C^{\nabla\rho\nabla\rho} &= -\frac{1}{2} a_2^C \left[\left(\pi_1^\rho\right)^2 \right] ,
\end{aligned}
\tag{9.274}
$$

where in these equation a_i^C refers to using the Coulomb interaction to compute these couplings.

9.6.6 Analytical couplings from chiral EFT NN interaction at N^{2}LO

In this section, we derive the analytical couplings of the particle-hole EDF (given in Eq. (4.11)) for time-reversal invariant systems starting from the finite-range part of chiral EFT NN interaction at N^{2}LO (Eq. (6.5)). In line with the exact treatment of the direct part advocated in section 5.3.7, the contributions to the couplings that come from the Hartree part of the HF energy are not included. Furthermore, in conformance with the notation used in the NNN case, we use isoscalar/isovector notation instead of proton/neutron notation.

The starting point for the derivation is the expression for the couplings expressed as a functional of the $\pi-$functions. Note that the Fock contributions that we are interested in correspond to those terms that contain solely Π_i^ς, i.e. no π_i^ς, for any density ς. We illustrate the derivation taking the calculation of $A^{\rho\rho}$ as an example

$$
A^{\rho\rho} = \frac{\pi}{2} \int dr\, r^2 \left[V_C^{01}(r) \left(\Pi_0^\rho(k_F r)\right)^2 - 3\, V_C^{11}(r) \left(\Pi_0^\rho(k_F r)\right)^2 \Big) \right] , \tag{9.275}
$$

where the interaction vertices $V_C^{01}(r)$ and $V_C^{11}(r)$ are given by Eq. (6.10) and (6.11).

The starting chiral interaction is in momentum space and hence

$$\begin{aligned} A^{\rho\rho} &= \frac{1}{16\pi^2}\int dr\, r^2\, d\vec{q}\, e^{i\vec{q}\cdot\vec{r}} \Bigg[V_C^{01}(q) \left(\Pi_0^{\rho}(k_F r)\right)^2 \\ &\qquad - 3\, V_C^{11}(q) \left(\left(\Pi_0^{\rho}(k_F r)\right)^2 \Bigg) \Bigg] . \end{aligned} \tag{9.276}$$

The subsequent step requires specifying the $\pi-$functions which can be fixed according to any viable DME approach. In our case, we use PSA-DME with the $\pi-$functions given by Eqs. (5.22), (5.23) and (5.36). Next, we perform the integration with respect to r first. This is actually an important step to see that the integrals do not actually diverge. In contrast, in the NNN case, it is easier to perform the integrations first with respect to the momentum coordinates. Refer to appendix 9.11.4 for a related discussion. In performing the r integrals, we define

$$I_1(\bar{q}) \equiv \int r^4 dr\, j_0(\bar{q}r) \left(\Pi_0^{\rho}(r)\right)^2 , \tag{9.277}$$

$$I_2(\bar{q}) \equiv \int r^4 dr\, j_0(\bar{q}r)\, \Pi_0^{\rho}(r)\, \Pi_2^{\rho}(r) , \tag{9.278}$$

$$I_3(\bar{q}) \equiv \int r^2 dr\, j_0(\bar{q}r) \left(\Pi_1^{\vec{s}}(r)\right)^2 , \tag{9.279}$$

$$I_4(\bar{q}) \equiv \int r^4 dr\, j_0(\bar{q}r) \left(\Pi_1^{\vec{s}}(r)\right)^2 , \tag{9.280}$$

where $\bar{q} = q/k_F$. Upon inserting the PSA-DME $\pi-$functions, these integrals become

$$I_1(\bar{q}) = I_2(\bar{q}) = I_3(\bar{q}) = \frac{3\,\pi}{32}\left(\bar{q}^3 - 12\bar{q} + 16\right)\Theta(2-\bar{q}) , \tag{9.281}$$

$$I_4(\bar{q}) = \frac{9\pi}{8\bar{q}}\left(2-\bar{q}^2\right)\Theta(2-\bar{q}) , \tag{9.282}$$

where Θ denotes the unit step function. What remain are one-dimensional integrals with respect to the momentum coordinate, q. At this point, the couplings take the form

$$\begin{aligned}
C_t^{\rho\rho} &= -\frac{1}{\pi k_F^3}\int q^2 dq\,\Gamma_c^{xt}(q)\left[\,I_1(q/k_F) + \frac{6}{5}I_2(q/k_F)\right] && (9.283)\\
C_t^{\rho\tau} &= \frac{2}{\pi k_F^5}\int q^2 dq\,\Gamma_c^{xt}(q)\,I_2(q/k_F) && (9.284)\\
C_t^{\rho\Delta\rho} &= -\frac{1}{4}C_t^{\rho\tau} && (9.285)\\
C_t^{JJ} &= -\frac{1}{4\pi k_F^3}\int q^2 dq\,I_3(q/k_F)\left(1+\frac{2}{3}q\partial_q\right)\Gamma_T^{xt}(q)\\
&\quad - \frac{1}{6\pi k_F^5}\int q^2 dq\,\Gamma_S^{xt}(q)\,I_4(q/k_F)\,, && (9.286)
\end{aligned}$$

where

$$\begin{aligned}
\Gamma_i^{xt}(q) &= V_i^x(q) \qquad t=0 && (9.287)\\
&= W_i^x(q) \quad\; t=1
\end{aligned}$$

with $i \in \{C, S, T, LS\}$. These exchange-force form factors are given by

$$\begin{aligned}
V_C^x(q) &= V_C(q) + W_C(q) + 3V_S(q) + 3W_S(q)\\
&\quad + q^2V_T(q) + q^2W_T(q)\,, && (9.288)\\
W_C^x(q) &= W_C(q) + 3W_S(q) + q^2W_T(q)\,, && (9.289)\\
V_S^x(q) &= V_C(q) + W_C(q) - V_S(q) - W_S(q)\,, && (9.290)\\
W_S^x(q) &= W_C(q) - W_S(q)\,, && (9.291)\\
V_T^x(q) &= V_T(q) + W_T(q)\,, && (9.292)\\
W_T^x(q) &= -W_T(q)\,, && (9.293)
\end{aligned}$$

The remaining one-dimensional integrals are calculated after plugging the chiral EFT NN interaction form factors (at N^{2}LO) given in Ref. [12]. The complete expressions for the couplings are too lengthy to reproduce here. Consult the Mathematica files of Ref. [161]. Here, we list the contribution to the couplings from the LO finite-range piece. As given in Ref. [12], the only LO finite-range piece is a one-pion exchange term. Therefore we have

$$W_T^{(0)} = -\Big(\frac{g_A}{2f_\pi}\Big)^2 \frac{1}{q^2+m_\pi^2}\,, \tag{9.294}$$

where all other components (V_C, etc.) are zero. With $u \equiv k_F/m_\pi$, the non-zero couplings from the finite-range LO potential are:

$$\begin{aligned}
A^{\rho\rho}_{(0)} &= -\frac{g_A^2}{256 f_\pi^2 u^6}\Big\{\big(-21+498u^2+64u^4-16u^6\big)-12u\big(35+4u^2\big)\arctan(2u)\\
&\quad +\frac{3}{4u^2}\big(7+16u^2(8-9u^2)\big)\log(1+4u^2)\Big\}\,, && (9.295)\\
B^{\rho\rho}_{(0)} &= 2A^{\rho\rho}_{(0)} && (9.296)\\
A^{\rho\Delta\rho}_{(0)} &= -\frac{35 g_A^2}{3072 f_\pi^2 m_\pi^2 u^8}\Big\{\big(-3+72u^2+4u^4\big)-60\,u\arctan(2u)\\
&\quad +\frac{1}{4\,u^2}\big(3+54u^2-72u^4\big)\log(1+4u^2)\Big\} && (9.297)\\
B^{\rho\Delta\rho}_{(0)} &= 2A^{\rho\Delta\rho}_{(0)} && (9.298)\\
A^{\rho\tau}_{(0)} &= -4A^{\rho\Delta\rho}_{(0)} && (9.299)\\
B^{\rho\tau}_{(0)} &= 2A^{\rho\tau}_{(0)} && (9.300)\\
A^{J2}_{(0)} &= \frac{g_A^2}{48 f_\pi^2 m_\pi^2}\Big\{\frac{5+12u^2}{(1+4u^2)^2}+\frac{4}{u^2}\log(1+4u^2)\Big\} && (9.301)\\
B^{J2}_{(0)} &= 2A^{J2}_{(0)} && (9.302)
\end{aligned}$$

which can easily be put under the form of Eq. (6.39).

9.7 HFB equations from EDF-NN-DME

The general formalism of HFB equations is discussed in Ref. [81]. Just like HF equations, they are solved self-consistently. In coordinate space, HFB equations for general nonlocal "mean field", $h^q(\vec{r}\,\sigma,\vec{r}\,'\,\sigma')$, and pairing field, $\Delta^q(\vec{r}\,\sigma,\vec{r}\,'\,\sigma')$, take the form

$$\int \vec{r}\,' \sum_{\sigma'} \begin{pmatrix} h'^q(\vec{r}\,\sigma,\vec{r}\,'\,\sigma') & \Delta^q(\vec{r}\,\sigma,\vec{r}\,'\,\sigma') \\ -\Delta^{q*}(\vec{r}\,\sigma,\vec{r}\,'\,\sigma') & -h'^{q*}(\vec{r}\,\sigma,\vec{r}\,'\,\sigma') \end{pmatrix} \begin{bmatrix} U^q_\mu(\vec{r}\,'\,\sigma'\,q) \\ V^q_\mu(\vec{r}\,'\,\sigma'\,q) \end{bmatrix} = E^q_\mu \begin{bmatrix} U^q_\mu(\vec{r}\,\sigma\,q) \\ V^q_\mu(\vec{r}\,\sigma\,q) \end{bmatrix} \tag{9.303}$$

where $U^q_\mu(\vec{r}\,'\,\sigma'\,q)$ and $V^q_\mu(\vec{r}\,'\,\sigma'\,q)$ represent the upper and lower components of the quasi-particle wave functions. E^q_μ is the quasi-particle energy and $h'^q(\vec{r}\,\sigma,\vec{r}\,'\,\sigma')$ is defined as

$$h'^q(\vec{r}\,\sigma,\vec{r}\,'\,\sigma') \equiv h^q(\vec{r}\,\sigma,\vec{r}\,'\,\sigma') - \lambda^q\,\delta_{\sigma\sigma'}\,\delta(\vec{r}-\vec{r}\,')\,. \tag{9.304}$$

In Eq. (9.304), λ^q is the chemical potential which is calculated from particle number constraint at each stage of the self-consistent iteration [205]. In configuration space, the mean and pairing fields are given by

$$h^q_{ij} = \frac{\delta\mathcal{E}}{\delta\rho^q_{ji}}\,, \tag{9.305}$$

$$\Delta^q_{ij} = \frac{\delta\mathcal{E}}{\delta\kappa^{q*}_{ij}}\,. \tag{9.306}$$

Starting from a local HFB energy density, the mean and pairing fields become local in coordinate space. This is shown explicitly in the next sections where we derive $h^q(\vec{r}\,\sigma,\vec{r}\,'\,\sigma')$, and pairing field, $\Delta^q(\vec{r}\,\sigma,\vec{r}\,'\,\sigma')$ for EDF-NN-DME discussed in the previous section. These derivations involve just repeated applications of functional derivative which is briefly discussed in appendix 9.1.6.

9.7.1 The mean field from EDF-NN-DME

The derivation of $h^q(\vec{r}\sigma, \vec{r}'\sigma')$ in $(\vec{r}, \sigma, q)$ space proceeds by taking the functional derivative

$$h^q_{ji} \equiv \frac{\delta\big(\,\varepsilon^{\rho}_k \,+\, \varepsilon^{\rho\rho} \,+\, \varepsilon^{\rho\rho}_{coul+cm}\,\big)}{\delta\rho^q_{ij}}\,, \tag{9.307}$$

where from the coordinate representation of the mean field, one has the configuration representation

$$h^q_{ji} \,=\, \sum_{\sigma_1\sigma_2} \int d\vec{r}_1 d\vec{r}_2\, \varphi^*_j(\vec{r}_1\sigma_1 q)\, h^q(\vec{r}_1\sigma_1, \vec{r}_2\sigma_2)\, \varphi_i(\vec{r}_2\sigma_2 q)\,, \tag{9.308}$$

with $\varphi_i(\vec{r}\sigma q)$ denoting the spin up/down components of the basis $\varphi_i(\vec{r}q)$. Since the energy functional is quasi-local, it results in a local field of the form

$$h^q(\vec{r}_1\sigma_1, \vec{r}_2\sigma_2) \,\equiv\, \delta(\vec{r}_1 - \vec{r}_2)\, h^q(\vec{r}_1; \sigma_1, \sigma_2). \tag{9.309}$$

This field acts on the spin up and spin down components of the wave function through

$$\sum_{\sigma_2} h^q(\vec{r}_1; \sigma_1\sigma_2)\, \varphi_i(\vec{r}_1\sigma_2 q) \,=\, \Big[h^q\, \varphi_i\Big](\vec{r}_1\sigma_1 q)\,, \tag{9.310}$$

and it is given by

$$\begin{aligned} h^q\, \varphi_i(\vec{r}q) \;=\; & \Big[-\vec{\nabla}\cdot B_q(\vec{r})\, \vec{\nabla} \,+\, U_q(\vec{r}) \,+\, \vec{S}_q(\vec{r})\cdot\vec{\sigma} \,-\, \frac{i}{2}\,\big[\,\vec{A}_q(\vec{r})\cdot\vec{\nabla} \,+\, \vec{\nabla}\cdot\vec{A}_q(\vec{r})\,\big] \\ & -\vec{\nabla}\cdot\big[\,\vec{C}_q(\vec{r})\cdot\vec{\sigma}\,\big]\vec{\nabla} \,-\, \frac{i}{2}\,\big[\,\overline{W_q(\vec{r})} \otimes \overline{\nabla\sigma} \,+\, \overline{\nabla\sigma} \otimes \overline{W_q(\vec{r})}\,\big] \\ & -\frac{1}{2}\big[\,\vec{\nabla}\cdot\vec{D}_q(\vec{r})\vec{\sigma}\cdot\vec{\nabla} \,+\, \vec{\sigma}\cdot\vec{\nabla}\,\vec{D}_q(\vec{r})\cdot\vec{\nabla}\,\big]\Big]\, \varphi_i(\vec{r}q)\,, \end{aligned} \tag{9.311}$$

where a shorthand notation for the tensor product has been used $\overline{A} \otimes \overline{B} = \sum_{\nu\mu} A_{\nu\mu} B_{\nu\mu}$. The various components of the are given by

$$
\begin{aligned}
B_q(\vec{r}) &= \frac{(A-1)}{2Am}\hbar^2 + A^{\rho\tau}\rho_q(\vec{r}) + B^{\rho\tau}\rho_{\bar{q}}(\vec{r}), && (9.312)\\
U_q(\vec{r}) &= 2A^{\rho\rho}\rho_q(\vec{r}) + A^{\rho\tau}\tau_q(\vec{r}) + A^{\rho\Delta\rho}\Delta\rho_q(\vec{r}) + \Delta\left[A^{\rho\Delta\rho}\rho_q(\vec{r})\right]\\
&\quad -2\vec{\nabla}\cdot\left[A^{\nabla\rho\nabla\rho}\vec{\nabla}\rho_q\right] + A^{\rho\nabla J}\vec{\nabla}\cdot\vec{J}_q(\vec{r}) - \vec{\nabla}\cdot\left[A^{\nabla\rho J}\vec{J}_q(\vec{r})\right]\\
&\quad +2B^{\rho\rho}\rho_{\bar{q}}(\vec{r}) + B^{\rho\tau}\tau_{\bar{q}}(\vec{r}) + B^{\rho\Delta\rho}\Delta\rho_{\bar{q}}(\vec{r}) + \Delta\left[B^{\rho\Delta\rho}\rho_{\bar{q}}(\vec{r})\right]\\
&\quad -2\vec{\nabla}\cdot\left[B^{\nabla\rho\nabla\rho}\vec{\nabla}\rho_{\bar{q}}\right] + B^{\rho\nabla J}\vec{\nabla}\cdot\vec{J}_{\bar{q}}(\vec{r}) - \vec{\nabla}\cdot\left[B^{\nabla\rho J}\vec{J}_{\bar{q}}(\vec{r})\right]\\
&\quad +e^2\int d\vec{r}'\,\frac{\rho_p(\vec{r}')}{|\vec{r}-\vec{r}'|} - e^2\left(\frac{3}{\pi}\right)^{1/3}\rho_p^{1/3}(\vec{r}), && (9.313)\\
s_{q,\nu}(\vec{r}) &= 2A^{ss}s_{q,\nu}(\vec{r}) - 2\nabla_\nu\left[A^{\nabla s\nabla s}\vec{\nabla}\cdot\vec{s}_q(\vec{r})\right] - A^{JJ}T_{q,\nu}(\vec{r})\\
&\quad -2A^{J\bar{J}}F_{q,\nu}(\vec{r}) + A^{s\Delta s}\Delta s_{q,\nu}(\vec{r}) + \Delta\left[A^{s\Delta s}s_{q,v}(\vec{r})\right]\\
&\quad -2A^{\nabla s\circ\nabla s}\Delta s_{q,\nu}(\vec{r}) + \sum_{\alpha\beta}\epsilon_{\nu\alpha\beta}\nabla_\alpha\left[A^{\rho\nabla J}j_{q,\beta}(\vec{r})\right]\\
&\quad -\sum_{\alpha\beta}\epsilon_{\nu\alpha\beta}\left[A^{\nabla\rho J}\nabla_\alpha j_{q,\beta}(\vec{r})\right]\\
&\quad +2B^{ss}s_{\bar{q},\nu}(\vec{r}) - 2\nabla_\nu\left[B^{\nabla s\nabla s}\vec{\nabla}\cdot\vec{s}_{\bar{q}}(\vec{r})\right] - B^{JJ}T_{\bar{q},\nu}(\vec{r})\\
&\quad -2B^{J\bar{J}}F_{\bar{q},\nu}(\vec{r}) + B^{s\Delta s}\Delta s_{\bar{q},\nu}(\vec{r}) + \Delta\left[B^{s\Delta s}s_{\bar{q},v}(\vec{r})\right]\\
&\quad -2B^{\nabla s\circ\nabla s}\Delta s_{\bar{q},\nu}(\vec{r}) + \sum_{\alpha\beta}\epsilon_{\nu\alpha\beta}\nabla_\alpha\left[B^{\rho\nabla J}j_{\bar{q},\beta}(\vec{r})\right]\\
&\quad -\sum_{\alpha\beta}\epsilon_{\nu\alpha\beta}\left[B^{\nabla\rho J}\nabla_\alpha j_{\bar{q},\beta}(\vec{r})\right], && (9.314)\\
A_{q,\nu}(\vec{r}) &= -2A^{\rho\tau}j_{q,\nu}(\vec{r}) + \sum_{\alpha\beta}\epsilon_{\nu\alpha\beta}\left[A^{\rho\nabla J}\nabla_\alpha s_{q,\beta}(\vec{r})\right]\\
&\quad -\sum_{\alpha\beta}\epsilon_{\nu\alpha\beta}\nabla_\alpha\left[A^{\nabla\rho J}s_{q,\beta}(\vec{r})\right]\\
&\quad -2B^{\rho\tau}j_{\bar{q},\nu}(\vec{r}) + \sum_{\alpha\beta}\epsilon_{\nu\alpha\beta}\left[B^{\rho\nabla J}\nabla_\alpha s_{\bar{q},\beta}(\vec{r})\right]\\
&\quad -\sum_{\alpha\beta}\epsilon_{\nu\alpha\beta}\nabla_\alpha\left[B^{\nabla\rho J}s_{\bar{q},\beta}(\vec{r})\right]\\
&\quad -\frac{\hbar^2}{Am}\int d\vec{r}'\sum_{q'}j_{q',\nu}(\vec{r}'), && (9.315)
\end{aligned}
$$

$$
\begin{aligned}
C_{q,\nu}(\vec{r}) &= -A^{JJ} s_{q,\nu}(\vec{r}) - B^{JJ} s_{\bar{q},\nu}(\vec{r}) \,, && (9.316) \\
W_{q,\mu\nu} &= 2A^{JJ} J_{q,\mu\nu}(\vec{r}) - \sum_{\alpha} \epsilon_{\alpha\mu\nu} \nabla_{\alpha} \left[A^{\rho\nabla J} \rho_q(\vec{r})\right] \\
&\quad + \sum_{\alpha} \epsilon_{\alpha\mu\nu} \left[A^{\nabla\rho J} \nabla_{\alpha}\rho_q(\vec{r})\right] \\
&\quad + 2A^{J\bar{J}} \left[J_{q,\nu\mu}(\vec{r}) + \delta_{\nu\mu} \sum_{\alpha} J_{q,\alpha\alpha}\right] + 2B^{JJ} J_{\bar{q},\mu\nu}(\vec{r}) \\
&\quad - \sum_{\alpha} \epsilon_{\alpha\mu\nu} \nabla_{\alpha} \left[B^{\rho\nabla J} \rho_{\bar{q}}(\vec{r})\right] + \sum_{\alpha} \epsilon_{\alpha\mu\nu} \left[B^{\nabla\rho J} \nabla_{\alpha}\rho_{\bar{q}}(\vec{r})\right] \\
&\quad + 2B^{J\bar{J}} \left[J_{\bar{q},\nu\mu}(\vec{r}) + \delta_{\nu\mu} \sum_{\alpha} J_{\bar{q},\alpha\alpha}\right] , && (9.317) \\
D_{q,\nu}(\vec{r}) &= -2A^{J\bar{J}} s_{q,\nu}(\vec{r}) - 2B^{J\bar{J}} s_{\bar{q},\nu}(\vec{r}) \,. && (9.318)
\end{aligned}
$$

9.7.2 The Pairing field from EDF-NN-DME

The derivation of the pairing field proceeds by starting with the variational

$$\Delta^q_{ij} = \frac{\delta \varepsilon^{\kappa\kappa}}{\delta \kappa^{q*}_{ij}} . \tag{9.319}$$

The pairing field Δ^q in coordinate space is defined through [81]

$$\Delta^q_{ij} \equiv \sum_{\sigma_1\sigma_2} \int d\vec{r}_1 \, d\vec{r}_2 \, \varphi^*_i(\vec{r}_1\sigma_1 q) \, \varphi^*_j(\vec{r}_2\sigma_2 q) \, \Delta^q(\vec{r}_1\sigma_1, \vec{r}_2\sigma_2). \tag{9.320}$$

It is local

$$\Delta^q(\vec{r}_1\sigma_1, \vec{r}_2\sigma_2) = \delta(\vec{r}_1 - \vec{r}_2) \, \Delta^q(\vec{r}_1; \sigma_1, \sigma_2). \tag{9.321}$$

and has the structure

$$\Delta^q(\vec{r}; \sigma_1, \sigma_2) = \tilde{U}_q(\vec{r}; \sigma_1, \sigma_2) + \vec{\nabla} \cdot \tilde{D}_q(\vec{r}; \sigma_1, \sigma_2) \, \vec{\nabla} + \tilde{\vec{A}}_q(\vec{r}; \sigma_1, \sigma_2) \cdot \vec{\nabla}, \tag{9.322}$$

where the field components read

$$\begin{aligned}
\tilde{U}_q(\vec{r};\sigma_1,\sigma_2) &= 2\,A^{\tilde{\rho}\tilde{\rho}}\,\tilde{\rho}_q(\vec{r})\,\bar{\sigma}_1\delta_{\sigma_1\bar{\sigma}_2} + 2\,A^{\tilde{\rho}\tilde{\tau}}\left(\Delta\tilde{\rho}_q(\vec{r}) - 4\tau_q(\vec{r})\right)\bar{\sigma}_1\delta_{\sigma_1\bar{\sigma}_2} \\
&\quad + 2\,\Delta\big[A^{\tilde{\rho}\tilde{\tau}}\,\tilde{\rho}_q(\vec{r})\big]\,\bar{\sigma}_1\delta_{\sigma_1\bar{\sigma}_2} \\
&\quad + i\sum_{\nu\mu}\left(\bar{\sigma}_2\langle\sigma_2|\sigma_\nu|\sigma_1\rangle + \sigma_1\langle\bar{\sigma}_1|\sigma_\nu|\bar{\sigma}_2\rangle\right)\nabla_\mu\big[\,A^{\tilde{J}\tilde{J}}\,\tilde{J}_{q,\mu\nu}(\vec{r})\,\big]\,,
\end{aligned} \tag{9.323}$$

$$\tilde{D}_q(\vec{r};\sigma_1,\sigma_2) = 8\,A^{\tilde{\rho}\tilde{\tau}}\,\tilde{\rho}_q(\vec{r})\,\bar{\sigma}_1\,\delta_{\sigma_1\bar{\sigma}_2}\,, \tag{9.324}$$

$$\tilde{A}_{q,\mu}(\vec{r};\sigma_1,\sigma_2) = i\sum_{\nu}\left(\bar{\sigma}_2\langle\sigma_2|\sigma_\nu|\sigma_1\rangle + \sigma_1\langle\bar{\sigma}_1|\sigma_\nu|\sigma_2\rangle\right)A^{\tilde{J}\tilde{J}}\,\tilde{J}_{q,\mu\nu}(\vec{r})\,. \tag{9.325}$$

9.8 Numerical solution of EDF-HF equations in spherical systems

For the preliminary self-consistent tests of the DME discussed in section 5.4.6, we performed self-consistent calculation of the HF equations. This calculation was done with the assumption of spherical symmetry, which also implies time-reversal invariance. As the starting EDF, we took two different cases: (i) EDF-NN-DME with the Bogoliubov contributions turned off. This is what we call full-DME. (ii) In the second case, EDF-NN-DME is changed in such a way that the Hartree contributions to EDF-NN-DME are replaced with their exact counterparts, with the Bogoliubov contribution still turned off. This is what we call exchange-only-DME. Since the Bogoliubov contribution is turned off in both calculations, we refer to both calculations as EDF-HF calculation.

In both full-DME and exchange-only-DME, the spherical self-consistent HF equations take the form

$$h^q\varphi_i(\vec{r}q) = \epsilon_{iq}\varphi_i(\vec{r}q)\,, \tag{9.326}$$

where h^q is the single particle Hamiltonian given by

$$h^q = -\vec{\nabla} \cdot B_q(r) \vec{\nabla} + U_q(r) - i \vec{W}_q \cdot \vec{\nabla} \times \vec{\sigma} . \tag{9.327}$$

The only difference between the two is in the actual values of the field components: $B_q(\vec{r})$, $U_q(\vec{r})$ and $\vec{W}_q(\vec{r})$.

9.8.1 Full-DME in spherical systems

The components of h^q for the case of full-DME are given by

$$\begin{aligned}
B_q(\vec{r}) &= \frac{(A-1)}{2Am} \hbar^2 + A^{\rho\tau} \rho_q(\vec{r}) + B^{\rho\tau} \rho_{\bar{q}}(\vec{r}) , & (9.328) \\
U_q(\vec{r}) &= 2A^{\rho\rho} \rho_q(\vec{r}) + A^{\rho\tau} \tau_q(\vec{r}) + A^{\rho\Delta\rho} \Delta\rho_q(\vec{r}) + \Delta \left[A^{\rho\Delta\rho} \rho_q(\vec{r}) \right] \\
&\quad - 2\vec{\nabla} \cdot \left[A^{\nabla\rho\nabla\rho} \vec{\nabla} \rho_q \right] + A^{\rho\nabla J} \vec{\nabla} \cdot \vec{J}_q(\vec{r}) - \vec{\nabla} \cdot \left[A^{\nabla\rho J} \vec{J}_q(\vec{r}) \right] \\
&\quad + 2B^{\rho\rho} \rho_{\bar{q}}(\vec{r}) + B^{\rho\tau} \tau_{\bar{q}}(\vec{r}) + B^{\rho\Delta\rho} \Delta\rho_{\bar{q}}(\vec{r}) + \Delta \left[B^{\rho\Delta\rho} \rho_{\bar{q}}(\vec{r}) \right] \\
&\quad - 2\vec{\nabla} \cdot \left[B^{\nabla\rho\nabla\rho} \vec{\nabla} \rho_{\bar{q}} \right] + B^{\rho\nabla J} \vec{\nabla} \cdot \vec{J}_{\bar{q}}(\vec{r}) - \vec{\nabla} \cdot \left[B^{\nabla\rho J} \vec{J}_{\bar{q}}(\vec{r}) \right] \\
&\quad + e^2 \int d\vec{r}' \frac{\rho_p(\vec{r}')}{|\vec{r} - \vec{r}'|} - e^2 \left(\frac{3}{\pi}\right)^{1/3} \rho_p^{1/3}(\vec{r}) , & (9.329) \\
\vec{W}_q &= A^{JJ} \vec{J}_q(\vec{r}) - \vec{\nabla} \left[A^{\rho\nabla J} \rho_q(\vec{r}) \right] + A^{\nabla\rho J} \vec{\nabla} \rho_q(\vec{r}) - A^{J\bar{J}} \vec{J}_q(\vec{r}) \\
&\quad + B^{JJ} \vec{J}_{\bar{q}}(\vec{r}) - \vec{\nabla} \left[B^{\rho\nabla J} \rho_{\bar{q}}(\vec{r}) \right] + B^{\nabla\rho J} \vec{\nabla} \rho_{\bar{q}}(\vec{r}) - B^{J\bar{J}} \vec{J}_{\bar{q}}(\vec{r}) , \\
& & (9.330)
\end{aligned}$$

where $\vec{\nabla}$ and Δ operators that occur in the fields probe only the radial part as we are dealing with spherical systems. It should be noted that (i) all the local densities depend only on the magnitude of $\vec{r}$ (ii) all the derivative operators are not meant to act on the wave functions, they only act on the densities. All the couplings such as $A^{\rho\rho}$ and $B^{\rho\rho}$ are as defined in section 9.6.5.

9.8.2 Exchange-only-DME in spherical systems

In this case, the field components read

$$
\begin{aligned}
B_q(\vec{r}) &= \frac{(A-1)}{2Am}\hbar^2 + \breve{A}^{\rho\tau}\,\rho_q(\vec{r}) + \breve{B}^{\rho\tau}\,\rho_{\bar{q}}(\vec{r})\,, && (9.331)\\
U_q(\vec{r}) &= \int d\vec{r}\,'\left[2\,V_C^{qq,\rho\rho}(|\vec{r}-\vec{r}\,'|)\rho_q(\vec{r}\,') + 2\,V_C^{q\bar{q},\rho\rho}(|\vec{r}-\vec{r}\,'|)\rho_{\bar{q}}(\vec{r}\,')\right]\\
&\quad + \int d\vec{r}\,'\left[V_{LS}^{qq,\rho\rho}(|\vec{r}-\vec{r}\,'|)\big(\vec{r}\,'-\vec{r}\big)\cdot\vec{J}_q(\vec{r}\,')\right.\\
&\quad \left. + V_{LS}^{q\bar{q},\rho\rho}(|\vec{r}-\vec{r}\,'|)\big(\vec{r}\,'-\vec{r}\big)\cdot\vec{J}_{\bar{q}}(\vec{r}\,')\right]\\
&\quad + 2\,\breve{A}^{\rho\rho}\,\rho_q(\vec{r}) + \breve{A}^{\rho\tau}\,\tau_q(\vec{r}) + \breve{A}^{\rho\Delta\rho}\,\Delta\rho_q(\vec{r})\\
&\quad + \Delta\left[\breve{A}^{\rho\Delta\rho}\,\rho_q(\vec{r})\right] - 2\,\vec{\nabla}\cdot\left[\breve{A}^{\nabla\rho\nabla\rho}\vec{\nabla}\rho_q\right] + \breve{A}^{\rho\nabla J}\,\vec{\nabla}\cdot\vec{J}_q(\vec{r})\\
&\quad - \vec{\nabla}\cdot\left[\breve{A}^{\nabla\rho J}\,\vec{J}_q(\vec{r})\right] + 2\breve{B}^{\rho\rho}\,\rho_{\bar{q}}(\vec{r}) + \breve{B}^{\rho\tau}\,\tau_{\bar{q}}(\vec{r}) + \breve{B}^{\rho\Delta\rho}\,\Delta\rho_{\bar{q}}(\vec{r})\\
&\quad + \Delta\left[\breve{B}^{\rho\Delta\rho}\,\rho_{\bar{q}}(\vec{r})\right] - 2\vec{\nabla}\cdot\left[\breve{B}^{\nabla\rho\nabla\rho}\vec{\nabla}\rho_{\bar{q}}\right] + \breve{B}^{\rho\nabla J}\,\vec{\nabla}\cdot\vec{J}_{\bar{q}}(\vec{r})\\
&\quad - \vec{\nabla}\cdot\left[\breve{B}^{\nabla\rho J}\,\vec{J}_{\bar{q}}(\vec{r})\right] + e^2\int d\vec{r}\,'\,\frac{\rho_p(\vec{r}\,')}{|\vec{r}-\vec{r}\,'|} - e^2\Big(\frac{3}{\pi}\Big)^{\frac{1}{3}}\,\rho_p^{\frac{1}{3}}(\vec{r})\,, && (9.332)\\
\vec{W}_q &= \int d\vec{r}\,'\left[V_{LS}^{qq,\rho\rho}(|\vec{r}-\vec{r}\,'|)\rho_q(\vec{r}\,') + V_{LS}^{q\bar{q},\rho\rho}(|\vec{r}-\vec{r}\,'|)\rho_{\bar{q}}(\vec{r}\,')\right]\vec{r}\\
&\quad + \breve{A}^{JJ}\vec{J}_q(\vec{r}) - \vec{\nabla}\left[\breve{A}^{\rho\nabla J}\,\rho_q(\vec{r})\right] + \breve{A}^{\nabla\rho J}\,\vec{\nabla}\rho_q(\vec{r}) - \breve{A}^{J\bar{J}}\,\vec{J}_q(\vec{r})\\
&\quad + \breve{B}^{JJ}\vec{J}_{\bar{q}}(\vec{r}) - \vec{\nabla}\left[\breve{B}^{\rho\nabla J}\,\rho_{\bar{q}}(\vec{r})\right] + \breve{B}^{\nabla\rho J}\,\vec{\nabla}\rho_{\bar{q}}(\vec{r}) - \breve{B}^{J\bar{J}}\,\vec{J}_{\bar{q}}(\vec{r})\,. && (9.333)
\end{aligned}
$$

In this case, the couplings $\breve{A}_q^{\varsigma_1\varsigma_2}$ and $\breve{B}_q^{\varsigma\varsigma}$ (for any bilinear combination of local densities, $\varsigma_1\varsigma_2$) are obtained from the corresponding $A_q^{\varsigma\varsigma}$ and $B_q^{\varsigma\varsigma}$ couplings given in appendix 9.7 by setting Hartree contributions to zero. Note that, according to our notation, Hartree contributions are expressed exclusively in terms of π (the small letter $\pi-$functions) while the Fock ones are expressed in terms of Π (the capital letter $\pi-$functions).

For the numerical result reported in this work, we evaluate the 3D-integrals, which reduce to 2D for spherical systems, directly using Gauss-Legendre integration technique. An alternative is to solve the corresponding Helmholtz problem [206].

9.8.3 Harmonic Oscillator basis expansion method

In the numerical solution of the single particle HF equations, the spherical harmonic oscillator basis expansion method is used. Coupling the spin and angular momentum to a total angular momentum, the basis are given by

$$\phi_\mu(\vec{r},q) = \frac{R_{nl}(r)}{r}\,\Omega^{m}_{l1/2j}(\hat{r})\,\chi^{\tau}_{1/2}\,, \tag{9.334}$$

where

$$\begin{aligned} \mu &= (nljm\tau) \text{ refers to the single particle quantum numbers} \\ \Omega^{m}_{l1/2j}(\hat{r}) &= \sum_{m_l m_s} \langle l s m_l m_s | jm\rangle\, Y_l^{m_l}(\hat{r})\,\chi^{m_s}_{1/2}\,, \end{aligned} \tag{9.335}$$

with $R_{nl}(r)$ is defined in appendix 9.1.4. In the basis expansion method, one expands the HF single particle states,$|\varphi_\alpha\rangle$, in terms of the basis states, $|\phi_\mu\rangle$

$$|\varphi_\alpha\rangle = \sum_{\mu} C^{\alpha}_{\mu}\,|\phi_\mu\rangle\,, \tag{9.336}$$

where C^{α}_{μ} are the expansion coefficients. The basic steps in a single iteration of the HF self-consistent calculations is (i) the calculation of the matrix elements of the single particle hamiltonian (ii) the diagonalization of the hamiltonian matrix to identify the spectrum (iii) updating the single-particle fields or expansion coefficients using one of the available schemes to drive the calculation towards convergence. The form of the matrix elements for each of the three parts (the kinetic, central and spin-orbit parts) of the single particle hamiltonian listed in Eqs.(9.327) is given below. Of course, the calculation is performed self-consistently.

Matrix elements of the kinetic part

By the kinetic part, we are referring to the $\vec{\nabla} \cdot B_q(r)\vec{\nabla}$ term of the single particle field. The corresponding matrix elements read

$$\begin{aligned}\langle\phi_{\mu'}|\vec{\nabla} \cdot B_q(r)\vec{\nabla}|\phi_\mu\rangle &= \int dr\, r^2 \frac{R_{n'l'}}{r}\left(\frac{\partial}{\partial r}B_q(r)\frac{\partial}{\partial r}\frac{R_{nl}}{r} + B_q(r)\left(\frac{\partial^2}{\partial r^2}+\frac{2}{r}\right)\frac{R_{nl}}{r}\right) \\ &\quad \times \delta_{ll'}\,\delta_{jj'}\,\delta_{mm'}\,\delta_{\tau\tau'}\,, \qquad (9.337)\end{aligned}$$

where $\mu' = (n'l'j'm'\tau')$ and $\mu = (nljm\tau)$. One can be tempted to use the exact relation one has in spherical harmonic oscillator basis for kinetic energy operator $\hat{T} = -\hbar^2/2m\,\Delta$

$$\langle\phi_{\mu'}|\hat{T}|\phi_\mu\rangle = \frac{\hbar\omega}{2}\begin{cases}(2n+l-1/2) & \text{if } n=n', \\ \sqrt{N(N+l+1/2)} & \text{if } |n-n'| = 1 \text{ N} = \min(n,n'), \\ 0 & \text{if } |n'-n| > 1.\end{cases}$$

In order to make use of this relation, one writes $\langle\phi_{\mu'}|\vec{\nabla} \cdot B_q(r)\vec{\nabla}|\phi_\mu\rangle$ as

$$\langle\phi_{\mu'}|\vec{\nabla} \cdot B_q(r)\vec{\nabla}|\phi_\mu\rangle = \langle\phi_{\mu'}|\vec{\nabla}\left[B_q(r)\right] \cdot \vec{\nabla}|\phi_\mu\rangle + \langle\phi_{\mu'}|B_q(r)\Delta|\phi_\mu\rangle\,, \qquad (9.338)$$

where one can write $\langle\phi_{\mu'}|B_q(r)\Delta|\phi_\mu\rangle$ as

$$\begin{aligned}\langle\phi_{\mu'}|B_q(r)\Delta|\phi_\mu\rangle &= \sum_\nu \langle\phi_{\mu'}|B_q(r)|\phi_\nu\rangle\,\langle\phi_\nu|\Delta|\phi_\mu\rangle \\ &= -\frac{2m}{\hbar^2}\sum_\nu \langle\phi_{\mu'}|B_q(r)|\phi_\nu\rangle\,\langle\phi_\nu|\hat{T}|\phi_\mu\rangle\,. \qquad (9.339)\end{aligned}$$

Finally, using the exact kinetic relation in Eq.(9.339) and plugging in Eq.(9.338), one obtains a simplified formula for the matrix element. This is exact in the ideal case of both no truncation of the basis states and a box of infinite size. In practical calculations, one has to truncate the number of basis states and also use a finite-sized box. These truncations make the use of Eq.(9.339) numerically unstable and erroneous[2]. This is the case especially when the inverse-effective mass term, $B_q(r)$, is very different from 1 inside the nucleus. For cases where the inverse-effective mass remains more or less the same as the inverse bare nucleon mass, using Eq.(9.337) or Eqs.(9.338) and (9.339) give the same results for the matrix elements.

Matrix elements of the central potential part

The matrix element for the central potential part of the single particle field, $U_q(r)$, reads

$$\langle\phi_{\mu'}|U_q(r)|\phi_\mu\rangle = \int dr\, r^2 \frac{R_{n'l'}}{r} U_q(r) \frac{R_{nl}}{r} \delta_{ll'} \delta_{jj'} \delta_{mm'} \delta_{\tau\tau'}, \tag{9.340}$$

where again where $\mu' = (n'l'j'm'\tau')$ and $\mu = (nljm\tau)$.

Matrix elements of the spin-orbit part

The matrix element of the spin-orbit part of the single particle field, $i\vec{W} \cdot \vec{\nabla} \times \vec{\sigma}$, reads

$$\begin{aligned}\langle\phi_{\mu'}|i\vec{W}_q \cdot \vec{\nabla} \times \vec{\sigma}|\phi_\mu\rangle &= -\left(j(j+1) - l(l+1) - \frac{3}{4}\right) \int dr\, r \frac{R_{n'l'}}{r} |W_q(r)| \frac{R_{nl}}{r} \\ &\quad \times \delta_{ll'} \delta_{jj'} \delta_{mm'} \delta_{\tau\tau'},\end{aligned} \tag{9.341}$$

where again $\mu' = (n'l'j'm'\tau')$ and $\mu = (nljm\tau)$.

---

[2] This must be due to the practical violation of the completeness relation and the use of a finite box size. It can be shown numerically (by increasing the box size) that effect of the later is minimal.

9.8.4 Self-consistent iterations and convergence

As can be seen from the results of the matrix elements for the three parts of the single-particle fields, the hamiltonian couples basis states only within a single $l - j$ block. Hence, in the actual numerical solution of the HF equations, one diagonalizes each $l - j$ block independently. Of course, the other parts of the calculation will involve all the relevant $l - j$ blocks. To drive the calculation towards convergence, we implemented both Broyden's method [194] and Imaginary-time method in separate calculations. After convergence, the results of the two methods usually agree to three decimal points, and hence the results reported in section 5.4.6 have been obtained using both methods.

9.9 The HF energy of chiral EFT NNN interaction at N^{2}LO

Here, we give a few remarks on the symbolic derivation of the HF energy of chiral EFT NNN interaction at N^{2}LO and give the complete expression for non time-reversal invariant systems. The corresponding simplified expressions for INM, PNM and time-reversal invariant systems are also stated.

9.9.1 Remarks on the symbolic implementation

The details of the symbolic derivation of the HF energy from the chiral EFT is discussed in Ref. [156]. In addition to automating a tremendous amount of spin-isospin and other algebraic steps, we have demonstrated that the approach can be generalized to treat nonlocal interactions such as the quasi-local Skyrme interactions. There are several extensions of the symbolic derivation that can be made in the future: (i) One can envision expanding the work in such a way that first-order pairing correlations (due to the NNN interaction) are treated along with the HF part, viz, performing HFB (Hartree-Fock-Bogoliubov) calculations. Combining this extension with proton-neutron mixing, one can have a start- ing Skyrme-like functional that can be used to handle proton-neutron pairing correlations as discussed in Ref. [207]. (iv) Implementing a similar scheme to treat four-nucleon interactions can also be one area of extension.

9.9.2 HF energy from the E-term

Direct part

The direct part, which comes from the E-term, reads

$$\langle V_{3N}^{\mathrm{HF},E,dir} \rangle = \frac{1}{2} E \int d\vec{r}\, \rho_0(\vec{r})\, \rho_1^2(\vec{r}) \,. \tag{9.342}$$

Single-exchange part

The contribution from the single-exchange part, which originates from the E-term, reads

$$\begin{aligned} \langle V_{3N}^{\mathrm{HF},E,1x} \rangle &= -\frac{1}{8} E \int d\vec{r} \Big[3\,\rho_0^3(\vec{r}) + 3\,\rho_0(\vec{r})\,\rho_1^2(\vec{r}) + 3\,\rho_0(\vec{r})\,\vec{s}_0(\vec{r}) \cdot \vec{s}_0(\vec{r}) \\ &\quad - \rho_0(\vec{r})\,\vec{s}_1(\vec{r}) \cdot \vec{s}_1(\vec{r}) + 4\,\rho_1(\vec{r})\,\vec{s}_0(\vec{r}) \cdot \vec{s}_1(\vec{r}) \Big] \,. \end{aligned} \tag{9.343}$$

Double-exchange part

The contribution from double-exchange part of the E-term reads

$$\begin{aligned} \langle V_{3N}^{\mathrm{HF},E,2x} \rangle &= \frac{1}{16} E \int d\vec{r} \Big[3\,\rho_0^3(\vec{r}) + \rho_0(\vec{r})\,\rho_1^2(\vec{r}) + 9\,\rho_0(\vec{r})\,\vec{s}_0(\vec{r}) \cdot \vec{s}_0(\vec{r}) \\ &\quad + \rho_0(\vec{r})\,\vec{s}_1(\vec{r}) \cdot \vec{s}_1(\vec{r}) + 2\,\rho_1(\vec{r})\,\vec{s}_1(\vec{r}) \cdot \vec{s}_0(\vec{r}) \Big] \,. \end{aligned} \tag{9.344}$$

E-term contribution for specific systems

In symmetric INM, the HF energy from the E-term reduces to

$$\langle V_{3N}^{\mathrm{HF},E,\mathrm{INM}} \rangle = -\frac{3}{16} E \int d\vec{r} \rho_0^3(\vec{r}) \,. \tag{9.345}$$

In unpolarized PNM (pure neutron matter), the HF energy from the E-term vanishes

$$\langle V_{3N}^{\mathrm{HF},E,\mathrm{PNM}} \rangle = 0 \,, \tag{9.346}$$

which is due to Pauli exclusion principle. In time-reversal invariant systems, the HF energy contribution from the E-term takes the form

$$\langle V_{3N}^{\mathrm{HF},E,\mathrm{TRI}} \rangle = -\frac{3}{16} E \int d\vec{r} \left[\rho_0^3(\vec{r}) - \rho_0(\vec{r}) \rho_1^2(\vec{r}) \right] . \tag{9.347}$$

9.9.3 HF energy from the D-term

Direct part

The contribution from the direct part of the D-term reads

$$\begin{aligned} \langle V_{3N}^{\mathrm{HF},D,dir} \rangle = \; & \frac{-g_A}{4f_\pi^2} \frac{C_D}{f_\pi^2 \Lambda_x} \frac{1}{2} \int d\vec{r}_2 d\vec{r}_3 \int \frac{1}{(2\pi)^3} d\vec{q}_3 \, e^{i\vec{q}_3 \cdot (\vec{r}_3 - \vec{r}_2)} \frac{q_3^\beta q_3^\gamma}{q_3^2 + m_\pi^2} \\ & \times \rho_0(\vec{r}_2) \, s_1^\beta(\vec{r}_2) \, s_1^\gamma(\vec{r}_3) \,. \end{aligned} \tag{9.348}$$

In symmetric INM, there is no contribution from this term. Likewise, for time-reversal invariant systems where $\vec{s}_{0/1}(\vec{r}) = 0$, the contribution from this term vanishes.

Single-exchange part

The contribution from the single-exchange part of the D-term reads

$$
\begin{aligned}
\langle V_{3N}^{\mathrm{HF},D,1x} \rangle \quad = \quad & \frac{-g_A}{4f_\pi^2}\frac{C_D}{f_\pi^2\Lambda_x}\frac{1}{4}\int d\vec{r}_2 d\vec{r}_3 \int \frac{1}{(2\pi)^3} d\vec{q}_3\, e^{i\vec{q}_3\cdot(\vec{r}_3-\vec{r}_2)}\,\frac{q_3^\beta q_3^\gamma}{q_3^2+m_\pi^2} \\
& \times \Bigg[-\rho_0(\vec{r}_3,\vec{r}_2)s_1^\beta(\vec{r}_2)s_1^\gamma(\vec{r}_2,\vec{r}_3) \\
& - i\,\epsilon^{\alpha\mu\gamma}\, s_0^\alpha(\vec{r}_3,\vec{r}_2)s_1^\mu(\vec{r}_2,\vec{r}_3)s_1^\beta(\vec{r}_2) \\
& - \rho_1(\vec{r}_2,\vec{r}_3)\, s_0^\gamma(\vec{r}_3,\vec{r}_2)s_1^\beta(\vec{r}_2) \; - \; \rho_1(\vec{r}_3,\vec{r}_2)\, s_0^\gamma(\vec{r}_2,\vec{r}_3)s_1^\beta(\vec{r}_2) \\
& + i\,\epsilon^{\alpha\mu\gamma}\, s_0^\alpha(\vec{r}_2,\vec{r}_3)s_1^\mu(\vec{r}_3,\vec{r}_2)s_1^\beta(\vec{r}_2) \; - \; \rho_1(\vec{r}_2,\vec{r}_3)\, s_0^\gamma(\vec{r}_3,\vec{r}_2)s_1^\beta(\vec{r}_2) \\
& - \frac{1}{2}\,\rho_0(\vec{r}_2)s_1^\beta(\vec{r}_3,\vec{r}_2)s_1^\gamma(\vec{r}_2,\vec{r}_3) \; - \; \frac{1}{2}\,\delta_{\beta\gamma}\,\rho_0(\vec{r}_2)\rho_1(\vec{r}_3,\vec{r}_2)\rho_1(\vec{r}_2,\vec{r}_3) \\
& + \frac{1}{2}\,\epsilon^{\alpha\gamma\nu}\,\epsilon^{\omega\beta\nu}\,\rho_0(\vec{r}_2)s_1^\alpha(\vec{r}_3,\vec{r}_2)s_1^\omega(\vec{r}_2,\vec{r}_3) \\
& - \frac{3}{2}\,\rho_0(\vec{r}_2)s_0^\beta(\vec{r}_3,\vec{r}_2)s_0^\gamma(\vec{r}_2,\vec{r}_3) \\
& + \rho_0(\vec{r}_2)s_1^\beta(\vec{r}_3,\vec{r}_2)s_1^\gamma(\vec{r}_2,\vec{r}_3) \; - \; \frac{3}{2}\,\delta_{\beta\gamma}\,\rho_0(\vec{r}_2)\,\rho_0(\vec{r}_3,\vec{r}_2)\rho_0(\vec{r}_2,\vec{r}_3) \\
& + \delta_{\beta\gamma}\,\rho_0(\vec{r}_2)\rho_1(\vec{r}_3,\vec{r}_2)\rho_1(\vec{r}_2,\vec{r}_3) \\
& + \frac{3}{2}\,\epsilon^{\alpha\gamma\nu}\,\epsilon^{\omega\beta\nu}\,\rho_0(\vec{r}_2)\, s_0^\alpha(\vec{r}_3,\vec{r}_2)\, s_0^\omega(\vec{r}_2,\vec{r}_3) \\
& - \epsilon^{\alpha\gamma\nu}\,\epsilon^{\omega\beta\nu}\,\rho_0(\vec{r}_2)\, s_1^\alpha(\vec{r}_3,\vec{r}_2)s_1^\omega(\vec{r}_2,\vec{r}_3) \Bigg] . \qquad (9.349)
\end{aligned}
$$

For symmetric INM, the expression simplifies to

$$
\begin{aligned}
\langle V_{3N}^{\mathrm{HF},D,1x,\mathrm{INM}} \rangle \quad = \quad & \frac{-g_A}{4f_\pi^2}\frac{C_D}{f_\pi^2\Lambda_x}\frac{1}{4}\int d\vec{r}_2 d\vec{r}_3 \int \frac{1}{(2\pi)^3} d\vec{q}_3\, e^{i\vec{q}_3\cdot(\vec{r}_3-\vec{r}_2)}\,\frac{q_3^2}{q_3^2+m_\pi^2} \\
& \times \left[-\frac{3}{2}\,\rho_0(\vec{r}_2)\rho_0(\vec{r}_3,\vec{r}_2)\rho_0(\vec{r}_2,\vec{r}_3) \right] , \qquad (9.350)
\end{aligned}
$$

while for unpolarized PNM, one has

$$
\begin{aligned}
\langle V_{3N}^{\mathrm{HF},D,1x,\mathrm{PNM}} \rangle \quad = \quad & \frac{-g_A}{4f_\pi^2}\frac{C_D}{f_\pi^2\Lambda_x}\frac{1}{4}\int d\vec{r}_2 d\vec{r}_3 \int \frac{1}{(2\pi)^3} d\vec{q}_3\, e^{i\vec{q}_3\cdot(\vec{r}_3-\vec{r}_2)}\,\frac{q_3^2}{q_3^2+m_\pi^2} \\
& \times \left[-\frac{3}{2}\,\rho_n(\vec{r}_2)\rho_n(\vec{r}_3,\vec{r}_2)\rho_n(\vec{r}_2,\vec{r}_3) \right] . \qquad (9.351)
\end{aligned}
$$

In time-reversal invariant systems, using $\vec{s}_{0/1}(\vec{r}) = 0$, one obtains

$$
\begin{aligned}
\langle V_{3N}^{\mathrm{HF},D,1x,\mathrm{TRI}} \rangle \;=\; & \frac{-g_A}{4 f_\pi^2} \frac{C_D}{f_\pi^2 \Lambda_x} \frac{1}{4} \int d\vec{r}_2 d\vec{r}_3 \int \frac{1}{(2\pi)^3} d\vec{q}_3 \, e^{i\vec{q}_3 \cdot (\vec{r}_3 - \vec{r}_2)} \, \frac{q_3^\beta q_3^\gamma}{q_3^2 + m_\pi^2} \\
& \times \Bigg[- \frac{3}{2} \, \delta_{\beta\gamma} \, \rho_0(\vec{r}_2) \rho_0(\vec{r}_3, \vec{r}_2) \rho_0(\vec{r}_2, \vec{r}_3) \\
& + \frac{1}{2} \, \delta_{\beta\gamma} \, \rho_0(\vec{r}_2) \rho_1(\vec{r}_3, \vec{r}_2) \rho_1(\vec{r}_2, \vec{r}_3) \\
& + \frac{3}{2} \, \epsilon^{\alpha\gamma\nu} \, \epsilon^{\omega\beta\nu} \, \rho_0(\vec{r}_2) s_0^\alpha(\vec{r}_3, \vec{r}_2) s_0^\omega(\vec{r}_2, \vec{r}_3) \\
& - \frac{3}{2} \, \rho_0(\vec{r}_2) s_0^\beta(\vec{r}_3, \vec{r}_2) s_0^\gamma(\vec{r}_2, \vec{r}_3) \\
& - \frac{1}{2} \, \epsilon^{\alpha\gamma\nu} \, \epsilon^{\omega\beta\nu} \, \rho_0(\vec{r}_2) s_1^\alpha(\vec{r}_3, \vec{r}_2) s_1^\omega(\vec{r}_2, \vec{r}_3) \\
& + \frac{1}{2} \, \rho_0(\vec{r}_2) s_1^\beta(\vec{r}_3, \vec{r}_2) s_1^\gamma(\vec{r}_2, \vec{r}_3) \Bigg] . \qquad (9.352)
\end{aligned}
$$

Double-exchange part

The contribution from the double-exchange part of the D-term reads

$$
\begin{aligned}
\langle V_{3N}^{\mathrm{HF},D,2x} \rangle \;=\; & \frac{-g_A}{4 f_\pi^2} \frac{C_D}{f_\pi^2 \Lambda_x} \frac{1}{16} \int d\vec{r}_2 d\vec{r}_3 \int \frac{1}{(2\pi)^3} d\vec{q}_3 \, e^{i\vec{q}_3 \cdot (\vec{r}_3 - \vec{r}_2)} \, \frac{q_3^\beta q_3^\gamma}{q_3^2 + m_\pi^2} \\
& \times \Bigg[3 \, \delta_{\beta\gamma} \, \rho_0(\vec{r}_2) \rho_0(\vec{r}_2, \vec{r}_3) \rho_0(\vec{r}_3, \vec{r}_2) \\
& - \delta_{\beta\gamma} \, \rho_1(\vec{r}_2) \rho_0(\vec{r}_2, \vec{r}_3) \rho_1(\vec{r}_3, \vec{r}_2) \\
& + 3 \, \rho_0(\vec{r}_2) s_0^\beta(\vec{r}_2, \vec{r}_3) s_0^\gamma(\vec{r}_3, \vec{r}_2) \\
& - 3 \, \epsilon^{\alpha\gamma\nu} \, \epsilon^{\omega\beta\nu} \, \rho_0(\vec{r}_2) s_0^\alpha(\vec{r}_2, \vec{r}_3) s_0^\omega(\vec{r}_3, \vec{r}_2) \\
& - \rho_0(\vec{r}_2) s_1^\beta(\vec{r}_2, \vec{r}_3) s_1^\gamma(\vec{r}_3, \vec{r}_2) \\
& + \epsilon^{\alpha\gamma\nu} \, \epsilon^{\omega\beta\nu} \, \rho_0(\vec{r}_2) s_1^\alpha(\vec{r}_2, \vec{r}_3) s_1^\omega(\vec{r}_3, \vec{r}_2) \\
& + 6 \, \rho_0(\vec{r}_2, \vec{r}_3) s_0^\beta(\vec{r}_2) s_0^\gamma(\vec{r}_3, \vec{r}_2) \; - \; 3 \, \delta_{\beta\gamma} \, \rho_0(\vec{r}_2, \vec{r}_3) s_0^\beta(\vec{r}_2) s_0^\gamma(\vec{r}_3, \vec{r}_2) \\
& + 3 \, \delta_{\beta\gamma} \, \rho_0(\vec{r}_3, \vec{r}_2) s_0^\beta(\vec{r}_2) s_0^\gamma(\vec{r}_3, \vec{r}_2) \; - \; 2 \, \rho_1(\vec{r}_2, \vec{r}_3) s_0^\beta(\vec{r}_2) s_1^\gamma(\vec{r}_3, \vec{r}_2) \\
& + \delta_{\beta\gamma} \, \rho_1(\vec{r}_2, \vec{r}_3) s_0^\beta(\vec{r}_2) s_1^\gamma(\vec{r}_3, \vec{r}_2) \; - \; \delta_{\beta\gamma} \, \rho_1(\vec{r}_3, \vec{r}_2) s_0^\beta(\vec{r}_2) s_1^\gamma(\vec{r}_2, \vec{r}_3) \\
& - i3 \, \epsilon^{\mu_1 \beta\nu} \, \epsilon^{\mu_2 \mu_3 \mu_4} \, \epsilon^{\mu_4 \gamma\nu} \, s_0^{\mu_1}(\vec{r}_2) s_0^{\mu_2}(\vec{r}_3, \vec{r}_2) s_0^{\mu_3}(\vec{r}_2, \vec{r}_3)
\end{aligned}
$$

$$
\begin{aligned}
& - i3\, \epsilon^{\mu 1 \beta\nu}\, \epsilon^{\mu 2 \mu 3 \mu 4}\, \epsilon^{\mu 4 \gamma\nu}\, s_0^{\mu 1}(\vec{r}_2, \vec{r}_3) s_0^{\mu 2}(\vec{r}_2) s_0^{\mu 3}(\vec{r}_3, \vec{r}_2) \\
& + i6\, \epsilon^{\mu 1 \beta\nu}\, \epsilon^{\mu 2 \mu 3 \mu 4}\, \epsilon^{\mu 4 \gamma\nu}\, s_0^{\mu 1}(\vec{r}_2) s_0^{\mu 2}(\vec{r}_3, \vec{r}_2) s_0^{\mu 3}(\vec{r}_2, \vec{r}_3) \\
& + i\, \epsilon^{\mu 1 \beta\nu}\, \epsilon^{\mu 2 \mu 3 \mu 4}\, \epsilon^{\mu 4 \gamma\nu}\, s_0^{\mu 1}(\vec{r}_2) s_1^{\mu 2}(\vec{r}_3, \vec{r}_2) s_1^{\mu 3}(\vec{r}_2, \vec{r}_3) \\
& + i\, \epsilon^{\mu 1 \beta\nu}\, \epsilon^{\mu 2 \mu 3 \mu 4}\, \epsilon^{\mu 4 \gamma\nu}\, s_0^{\mu 1}(\vec{r}_2, \vec{r}_3) s_0^{\mu 2}(\vec{r}_2) s_0^{\mu 3}(\vec{r}_3, \vec{r}_2) \\
& - i2\, \epsilon^{\mu 1 \beta\nu}\, \epsilon^{\mu 2 \mu 3 \mu 4}\, \epsilon^{\mu 4 \gamma\nu}\, s_0^{\mu 1}(\vec{r}_2) s_1^{\mu 2}(\vec{r}_3, \vec{r}_2) s_1^{\mu 3}(\vec{r}_2, \vec{r}_3) \\
& + 3\, \delta_{\beta\gamma}\, \rho_1(\vec{r}_2) \rho_0(\vec{r}_3, \vec{r}_2) \rho_1(\vec{r}_2, \vec{r}_3) \\
& - \delta_{\beta\gamma}\, \rho_1(\vec{r}_2) \rho_1(\vec{r}_3, \vec{r}_2) \rho_0(\vec{r}_2, \vec{r}_3) \\
& - \rho_1(\vec{r}_2) s_0^{\beta}(\vec{r}_2, \vec{r}_3) s_1^{\gamma}(\vec{r}_3, \vec{r}_2) \\
& + \epsilon^{\alpha\gamma\nu}\, \epsilon^{\omega\beta\nu}\, \rho_1(\vec{r}_2) s_0^{\alpha}(\vec{r}_2, \vec{r}_3) s_1^{\omega}(\vec{r}_3, \vec{r}_2) \\
& + 3\, \rho_1(\vec{r}_2) s_0^{\beta}(\vec{r}_3, \vec{r}_2) s_1^{\gamma}(\vec{r}_2, \vec{r}_3) \\
& - 3\, \epsilon^{\alpha\gamma\nu}\, \epsilon^{\omega\beta\nu}\, \rho_1(\vec{r}_2) s_0^{\alpha}(\vec{r}_3, \vec{r}_2) s_1^{\omega}(\vec{r}_2, \vec{r}_3) \\
& - 2\, \rho_0(\vec{r}_2, \vec{r}_3) s_1^{\beta}(\vec{r}_2) s_2^{\gamma}(\vec{r}_3, \vec{r}_2) \;+\; \delta_{\beta\gamma}\, \rho_0(\vec{r}_2, \vec{r}_3) s_1^{\beta}(\vec{r}_2) s_1^{\gamma}(\vec{r}_3, \vec{r}_2) \\
& + 3\, \delta_{\beta\gamma}\, \rho_0(\vec{r}_3, \vec{r}_2) s_1^{\beta}(\vec{r}_2) s_1^{\gamma}(\vec{r}_3, \vec{r}_2) \;+\; 6\, \rho_1(\vec{r}_2, \vec{r}_3) s_1^{\beta}(\vec{r}_2) s_0^{\gamma}(\vec{r}_3, \vec{r}_2) \\
& - 3\, \delta_{\beta\gamma}\, \rho_1(\vec{r}_2, \vec{r}_3) s_1^{\beta}(\vec{r}_2) s_0^{\gamma}(\vec{r}_3, \vec{r}_2) \;-\; \delta_{\beta\gamma}\, \rho_1(\vec{r}_3, \vec{r}_2) s_1^{\beta}(\vec{r}_2) s_0^{\gamma}(\vec{r}_2, \vec{r}_3) \\
& + i\, \epsilon^{\mu 1 \beta\nu}\, \epsilon^{\mu 2 \mu 3 \mu 4}\, \epsilon^{\mu 4 \gamma\nu}\, s_1^{\mu 1}(\vec{r}_2) s_1^{\mu 2}(\vec{r}_3, \vec{r}_2) s_0^{\mu 3}(\vec{r}_2, \vec{r}_3) \\
& + i\, \epsilon^{\mu 1 \beta\nu}\, \epsilon^{\mu 2 \mu 3 \mu 4}\, \epsilon^{\mu 4 \gamma\nu}\, s_0^{\mu 1}(\vec{r}_2, \vec{r}_3) s_1^{\mu 2}(\vec{r}_2) s_1^{\mu 3}(\vec{r}_3, \vec{r}_2) \\
& - i2\, \epsilon^{\mu 1 \beta\nu}\, \epsilon^{\mu 2 \mu 3 \mu 4}\, \epsilon^{\mu 4 \gamma\nu}\, s_1^{\mu 1}(\vec{r}_2) s_1^{\mu 2}(\vec{r}_3, \vec{r}_2) s_0^{\mu 3}(\vec{r}_2, \vec{r}_3) \\
& - i3\, \epsilon^{\mu 1 \beta\nu}\, \epsilon^{\mu 2 \mu 3 \mu 4}\, \epsilon^{\mu 4 \gamma\nu}\, s_1^{\mu 1}(\vec{r}_2) s_0^{\mu 2}(\vec{r}_3, \vec{r}_2) s_1^{\mu 3}(\vec{r}_2, \vec{r}_3) \\
& - i3\, \epsilon^{\mu 1 \beta\nu}\, \epsilon^{\mu 2 \mu 3 \mu 4}\, \epsilon^{\mu 4 \gamma\nu}\, s_1^{\mu 1}(\vec{r}_2, \vec{r}_3) s_1^{\mu 2}(\vec{r}_2) s_0^{\mu 3}(\vec{r}_3, \vec{r}_2) \\
& + i6\, \epsilon^{\mu 1 \beta\nu}\, \epsilon^{\mu 2 \mu 3 \mu 4}\, \epsilon^{\mu 4 \gamma\nu}\, s_1^{\mu 1}(\vec{r}_2) s_0^{\mu 2}(\vec{r}_3, \vec{r}_2) s_1^{\mu 3}(\vec{r}_2, \vec{r}_3) \Big] .
\end{aligned}
\tag{9.353}
$$

In symmetric INM, the contribution reduces to

$$
\langle V_{3N}^{\mathrm{HF},D,2x,\mathrm{INM}} \rangle \;=\; \frac{-g_A}{4 f_\pi^2} \frac{C_D}{f_\pi^2 \Lambda_x} \frac{1}{16} \int d\vec{r}_2 d\vec{r}_3 \int \frac{1}{(2\pi)^3} d\vec{q}_3\, e^{i\vec{q}_3 \cdot (\vec{r}_3 - \vec{r}_2)} \frac{q_3^2}{q_3^2 + m_\pi^2}
$$

$$\times \left[3\,\rho_0(\vec{r}_2)\rho_0(\vec{r}_2,\vec{r}_3)\rho_0(\vec{r}_3,\vec{r}_2) \right], \tag{9.354}$$

while for unpolarized PNM, one has

$$\begin{aligned}
\langle V_{3N}^{\mathrm{HF},D,2x,\mathrm{PNM}} \rangle &= \frac{-g_A}{4f_\pi^2}\frac{C_D}{f_\pi^2\Lambda_x}\frac{1}{16}\int d\vec{r}_2 d\vec{r}_3 \int \frac{1}{(2\pi)^3} d\vec{q}_3\, e^{i\vec{q}_3\cdot(\vec{r}_3-\vec{r}_2)}\,\frac{q_3^2}{q_3^2+m_\pi^2} \\
&\quad \times \left[3\,\rho_n(\vec{r}_2)\rho_n(\vec{r}_2,\vec{r}_3)\rho_n(\vec{r}_3,\vec{r}_2) \right].
\end{aligned} \tag{9.355}$$

For time-reversal invariant systems, using the relations $\vec{s}_{0/1}(\vec{r}) = 0$ and $\rho_{0/1}(\vec{r}_2,\vec{r}_3) = \rho_{0/1}(\vec{r}_3,\vec{r}_2)$, one obtains

$$\begin{aligned}
\langle V_{3N}^{\mathrm{HF},D,2x,\mathrm{TRI}} \rangle &= \frac{-g_A}{4f_\pi^2}\frac{C_D}{f_\pi^2\Lambda_x}\frac{1}{16}\int d\vec{r}_2 d\vec{r}_3 \int \frac{1}{(2\pi)^3} d\vec{q}_3\, e^{i\vec{q}_3\cdot(\vec{r}_3-\vec{r}_2)}\,\frac{q_3^\beta q_3^\gamma}{q_3^2+m_\pi^2} \\
&\quad \times \Big[3\,\delta_{\beta\gamma}\,\rho_0(\vec{r}_2)\rho_0(\vec{r}_2,\vec{r}_3)\rho_0(\vec{r}_3,\vec{r}_2) \\
&\quad + \delta_{\beta\gamma}\,\rho_1(\vec{r}_2)\rho_0(\vec{r}_2,\vec{r}_3)\rho_1(\vec{r}_3,\vec{r}_2) \\
&\quad + 3\,\rho_0(\vec{r}_2)s_0^\beta(\vec{r}_2,\vec{r}_3)s_0^\gamma(\vec{r}_3,\vec{r}_2) \\
&\quad - 3\,\epsilon^{\alpha\gamma\nu}\,\epsilon^{\omega\beta\nu}\,\rho_0(\vec{r}_2)s_0^\alpha(\vec{r}_2,\vec{r}_3)s_0^\omega(\vec{r}_3,\vec{r}_2) \\
&\quad - \rho_0(\vec{r}_2)s_1^\beta(\vec{r}_2,\vec{r}_3)s_1^\gamma(\vec{r}_3,\vec{r}_2) \\
&\quad + \epsilon^{\alpha\gamma\nu}\,\epsilon^{\omega\beta\nu}\,\rho_0(\vec{r}_2)s_1^\alpha(\vec{r}_2,\vec{r}_3)s_1^\omega(\vec{r}_3,\vec{r}_2) \\
&\quad + 2\,\rho_1(\vec{r}_2)s_0^\beta(\vec{r}_2,\vec{r}_3)s_1^\gamma(\vec{r}_3,\vec{r}_2) \\
&\quad - 2\,\epsilon^{\alpha\gamma\nu}\,\epsilon^{\omega\beta\nu}\,\rho_1(\vec{r}_2)s_0^\alpha(\vec{r}_2,\vec{r}_3)s_1^\omega(\vec{r}_3,\vec{r}_2) \Big].
\end{aligned} \tag{9.356}$$

D-term contribution for specific systems

Combining the results obtained for the D-term, the contribution to the HF energy of symmetric INM reads

$$\begin{aligned}\langle V_{3N}^{\mathrm{HF},D,\mathrm{INM}}\rangle &= \frac{-g_A}{4f_\pi^2}\frac{C_D}{f_\pi^2\Lambda_x}\frac{1}{16}\int d\vec{r}_2 d\vec{r}_3 \int \frac{1}{(2\pi)^3} d\vec{q}_3\, e^{i\vec{q}_3\cdot(\vec{r}_3-\vec{r}_2)}\,\frac{q_3^2}{q_3^2+m_\pi^2} \\ &\quad\times\Big[-3\,\rho_0(\vec{r}_2)\rho_0(\vec{r}_2,\vec{r}_3)\rho_0(\vec{r}_3,\vec{r}_2)\Big]. \qquad (9.357)\end{aligned}$$

Combining the results obtained for the D-term, the contribution to the HF energy of unpolarized PNM reads

$$\begin{aligned}\langle V_{3N}^{\mathrm{HF},D,\mathrm{PNM}}\rangle &= \frac{-g_A}{4f_\pi^2}\frac{C_D}{f_\pi^2\Lambda_x}\frac{1}{16}\int d\vec{r}_2 d\vec{r}_3 \int \frac{1}{(2\pi)^3} d\vec{q}_3\, e^{i\vec{q}_3\cdot(\vec{r}_3-\vec{r}_2)}\,\frac{q_3^2}{q_3^2+m_\pi^2} \\ &\quad\times\Big[-3\,\rho_n(\vec{r}_2)\rho_n(\vec{r}_2,\vec{r}_3)\rho_n(\vec{r}_3,\vec{r}_2)\Big], \qquad (9.358)\end{aligned}$$

where $\rho_n(\vec{r})$ and $\rho_n(\vec{r},\vec{r}')$ refer to the local and non-local parts of neutron matter density. In time-reversal invariant systems, the HF energy contribution from the D-term takes the form

$$\begin{aligned}\langle V_{3N}^{\mathrm{HF},D,\mathrm{TRI}}\rangle &= \frac{-g_A}{4f_\pi^2}\frac{C_D}{f_\pi^2\Lambda_x}\frac{1}{16}\int d\vec{r}_2 d\vec{r}_3 \int \frac{1}{(2\pi)^3} d\vec{q}_3\, e^{i\vec{q}_3\cdot(\vec{r}_3-\vec{r}_2)}\,\frac{q_3^\beta q_3^\gamma}{q_3^2+m_\pi^2} \\ &\quad\times\Big[-3\,\delta_{\beta\gamma}\,\rho_0(\vec{r}_2)\rho_0(\vec{r}_2,\vec{r}_3)\rho_0(\vec{r}_3,\vec{r}_2) \\ &\quad+2\,\delta_{\beta\gamma}\,\rho_0(\vec{r}_2)\rho_1(\vec{r}_2,\vec{r}_3)\rho_1(\vec{r}_3,\vec{r}_2) \\ &\quad+\delta_{\beta\gamma}\,\rho_1(\vec{r}_2)\rho_0(\vec{r}_2,\vec{r}_3)\rho_1(\vec{r}_3,\vec{r}_2) \\ &\quad-3\,\rho_0(\vec{r}_2)s_0^\beta(\vec{r}_2,\vec{r}_3)s_0^\gamma(\vec{r}_3,\vec{r}_2) \\ &\quad+3\,\epsilon^{\alpha\gamma\nu}\,\epsilon^{\omega\beta\nu}\,\rho_0(\vec{r}_2)s_0^\alpha(\vec{r}_2,\vec{r}_3)s_0^\omega(\vec{r}_3,\vec{r}_2) \\ &\quad+\rho_0(\vec{r}_2)s_1^\beta(\vec{r}_2,\vec{r}_3)s_1^\gamma(\vec{r}_3,\vec{r}_2) \\ &\quad-\epsilon^{\alpha\gamma\nu}\,\epsilon^{\omega\beta\nu}\,\rho_0(\vec{r}_2)s_1^\alpha(\vec{r}_2,\vec{r}_3)s_1^\omega(\vec{r}_3,\vec{r}_2)\end{aligned}$$

$$
\begin{aligned}
&+ 2\,\rho_1(\vec{r}_2) s_0^{\beta}(\vec{r}_2, \vec{r}_3) s_1^{\gamma}(\vec{r}_3, \vec{r}_2) \\
&- 2\,\epsilon^{\alpha\gamma\nu}\,\epsilon^{\omega\beta\nu}\,\rho_1(\vec{r}_2) s_0^{\alpha}(\vec{r}_2, \vec{r}_3) s_1^{\omega}(\vec{r}_3, \vec{r}_2) \Big] .
\end{aligned}
\tag{9.359}
$$

9.9.4 HF energy from the C-term

The HF energy from the C-term of the chiral EFT N^{2}LO 3NF can be grouped into two groups: a D-like term and remaining terms (which we call R-part). This grouping originates from the operator structure of $F_{ijk}^{\alpha\beta}$ given in Eq.(2.20). The D-like term is associated with $\delta_{\alpha\beta}\left[-4\frac{c_1 m_\pi^2}{f_\pi^2} + 2\frac{c_3}{f_\pi^2}\vec{q}_i\cdot\vec{q}_j\right]$ whereas the R-part relates to $\frac{c_4}{f_\pi^2}\epsilon^{\alpha\beta\gamma}\tau_k^{\gamma}\,\vec{\sigma}_k\cdot(\vec{q}_i+\vec{q}_j)$. In the following, the HF energy from the various parts of the C-term are given.

Direct part

The contribution from the D-like piece of the direct part is

$$
\begin{aligned}
\langle V_{3N}^{\mathrm{HF},CD,dir}\rangle &= \left(\frac{g_A}{2f_\pi}\right)^2 \frac{1}{2} \int d\vec{r}_1 d\vec{r}_2 d\vec{r}_3 \int \frac{1}{(2\pi)^6} d\vec{q}_2 d\vec{q}_3\, e^{i\vec{q}_2\cdot(\vec{r}_2-\vec{r}_1)}\, e^{i\vec{q}_3\cdot(\vec{r}_3-\vec{r}_1)} \\
&\quad \times \frac{q_2^{\beta} q_3^{\gamma}}{(q_2^2+m_\pi^2)(q_3^2+m_\pi^2)} \left[-4\frac{c_1 m_\pi^2}{f_\pi^2} + 2\frac{c_3}{f_\pi^2}\vec{q}_2\cdot\vec{q}_3\right] \\
&\quad \times \rho_0(\vec{r}_1) s_1^{\beta}(\vec{r}_2) s_1^{\gamma}(\vec{r}_3) .
\end{aligned}
\tag{9.360}
$$

For both symmetric INM and time-reversal invariant systems, this contribution vanishes. The R-part contribution from the direct part vanishes

$$
\langle V_{3N}^{\mathrm{HF},CR,dir}\rangle = 0 . \tag{9.361}
$$

Hence, the direct part vanishes for spin-unpolarized INM/PNM and time-reversal invariant systems.

Single-exchange part

The contribution from the D-like piece of the single-exchange part reads

$$
\begin{aligned}
\langle V_{3N}^{\mathrm{HF,CD,1x}} \rangle \; = \; & \left(\frac{g_A}{2f_\pi}\right)^2 \frac{1}{4} \int d\vec{r}_1 d\vec{r}_2 d\vec{r}_3 \int \frac{1}{(2\pi)^6} d\vec{q}_2 d\vec{q}_3 \, e^{i\vec{q}_2\cdot(\vec{r}_2-\vec{r}_1)} \, e^{i\vec{q}_3\cdot(\vec{r}_3-\vec{r}_1)} \\
& \times \frac{q_2^\beta q_3^\gamma}{(q_2^2+m_\pi^2)(q_3^2+m_\pi^2)} \left[-4\frac{c_1 m_\pi^2}{f_\pi^2} + 2\frac{c_3}{f_\pi^2}\vec{q}_2\cdot\vec{q}_3\right] \\
& \times \Bigg[- \rho_0(\vec{r}_3,\vec{r}_1) \, s_1^\beta(\vec{r}_2) s_1^\gamma(\vec{r}_1,\vec{r}_3) \\
& -i\,\epsilon^{\mu\omega\gamma} \, s_1^\beta(\vec{r}_2) s_0^\mu(\vec{r}_3,\vec{r}_1) s_1^\omega(\vec{r}_1,\vec{r}_3) \\
& - \rho_1(\vec{r}_1,\vec{r}_3) \, s_1^\beta(\vec{r}_2) s_0^\gamma(\vec{r}_3,\vec{r}_1) \; - \; \rho_1(\vec{r}_3,\vec{r}_1) \, s_1^\beta(\vec{r}_2) s_0^\gamma(\vec{r}_1,\vec{r}_3) \\
& -i\,\epsilon^{\mu\omega\gamma} \, s_1^\beta(\vec{r}_2) s_0^\mu(\vec{r}_3,\vec{r}_1) s_1^\omega(\vec{r}_1,\vec{r}_3) \; - \; \rho_1(\vec{r}_1,\vec{r}_3) s_1^\beta(\vec{r}_2) s_0^\gamma(\vec{r}_3,\vec{r}_1) \\
& - \frac{1}{2}\,\rho_0(\vec{r}_1) s_1^\beta(\vec{r}_3,\vec{r}_2) s_1^\gamma(\vec{r}_2,\vec{r}_3) \; - \; \frac{1}{2}\,\delta_{\beta\gamma}\,\rho_0(\vec{r}_1)\rho_1(\vec{r}_3,\vec{r}_2)\rho_1(\vec{r}_2,\vec{r}_3) \\
& + \frac{1}{2}\,\epsilon^{\mu\beta\nu}\epsilon^{\omega\gamma\nu}\,\rho_0(\vec{r}_1) s_1^\mu(\vec{r}_3,\vec{r}_2) s_1^\omega(\vec{r}_2,\vec{r}_3) \\
& - \frac{3}{2}\,\rho_0(\vec{r}_1) s_0^\beta(\vec{r}_3,\vec{r}_2) s_0^\gamma(\vec{r}_2,\vec{r}_3) \\
& + \rho_0(\vec{r}_1) s_1^\beta(\vec{r}_3,\vec{r}_2) s_1^\gamma(\vec{r}_2,\vec{r}_3) \; - \; \frac{3}{2}\,\delta_{\beta\gamma}\,\rho_0(\vec{r}_1)\rho_0(\vec{r}_3,\vec{r}_2)\rho_0(\vec{r}_2,\vec{r}_3) \\
& + \delta_{\beta\gamma}\,\rho_0(\vec{r}_1)\rho_1(\vec{r}_3,\vec{r}_2)\rho_1(\vec{r}_2,\vec{r}_3) \\
& + \frac{3}{2}\,\epsilon^{\mu\beta\nu}\epsilon^{\omega\gamma\nu}\,\rho_0(\vec{r}_1) s_0^\mu(\vec{r}_3,\vec{r}_2) s_0^\omega(\vec{r}_2,\vec{r}_3) \\
& - \epsilon^{\mu\beta\nu}\epsilon^{\omega\gamma\nu}\,\rho_0(\vec{r}_1) s_1^\mu(\vec{r}_3,\vec{r}_2) s_1^\omega(\vec{r}_2,\vec{r}_3) \Bigg] \, .
\end{aligned}
\tag{9.362}
$$

For INM, this expression reduces to

$$
\begin{aligned}
\langle V_{3N}^{\mathrm{HF,CD,1x,INM}} \rangle \; = \; & \left(\frac{g_A}{2f_\pi}\right)^2 \frac{1}{4} \int d\vec{r}_1 d\vec{r}_2 d\vec{r}_3 \int \frac{1}{(2\pi)^6} d\vec{q}_2 d\vec{q}_3 \, e^{i\vec{q}_2\cdot(\vec{r}_2-\vec{r}_1)} \, e^{i\vec{q}_3\cdot(\vec{r}_3-\vec{r}_1)} \\
& \times \frac{q_2^\beta q_3^\gamma}{(q_2^2+m_\pi^2)(q_3^2+m_\pi^2)} \times \left[-4\frac{c_1 m_\pi^2}{f_\pi^2} + 2\frac{c_3}{f_\pi^2}\vec{q}_2\cdot\vec{q}_3\right] \\
& \times \left[- \frac{3}{2}\,\delta_{\beta\gamma}\,\rho_0(\vec{r}_1)\rho_0(\vec{r}_3,\vec{r}_2)\rho_0(\vec{r}_2,\vec{r}_3) \right] ,
\end{aligned}
\tag{9.363}
$$

while for unpolarized PNM, one has

$$\begin{aligned}
\langle V_{3N}^{\mathrm{HF,CD,1x,PNM}} \rangle &= \left(\frac{g_A}{2f_\pi}\right)^2 \frac{1}{4} \int d\vec{r}_1 d\vec{r}_2 d\vec{r}_3 \int \frac{1}{(2\pi)^6} d\vec{q}_2 d\vec{q}_3 \, e^{i\vec{q}_2\cdot(\vec{r}_2-\vec{r}_1)} \, e^{i\vec{q}_3\cdot(\vec{r}_3-\vec{r}_1)} \\
&\times \frac{q_2^\beta q_3^\gamma}{(q_2^2+m_\pi^2)(q_3^2+m_\pi^2)} \left[-4\frac{c_1 m_\pi^2}{f_\pi^2} + 2\frac{c_3}{f_\pi^2}\vec{q}_2\cdot\vec{q}_3\right] \\
&\times \left[-\frac{3}{2}\,\delta_{\beta\gamma}\,\rho_n(\vec{r}_1)\rho_n(\vec{r}_3,\vec{r}_2)\rho_n(\vec{r}_2,\vec{r}_3)\right]. \qquad (9.364)
\end{aligned}$$

For time-reversal invariant systems, it becomes

$$\begin{aligned}
\langle V_{3N}^{\mathrm{HF,CD,1x,TRI}} \rangle &= \left(\frac{g_A}{2f_\pi}\right)^2 \frac{1}{4} \int d\vec{r}_1 d\vec{r}_2 d\vec{r}_3 \int \frac{1}{(2\pi)^6} d\vec{q}_2 d\vec{q}_3 \, e^{i\vec{q}_2\cdot(\vec{r}_2-\vec{r}_1)} \, e^{i\vec{q}_3\cdot(\vec{r}_3-\vec{r}_1)} \\
&\times \frac{q_2^\beta q_3^\gamma}{(q_2^2+m_\pi^2)(q_3^2+m_\pi^2)} \left[-4\frac{c_1 m_\pi^2}{f_\pi^2} + 2\frac{c_3}{f_\pi^2}\vec{q}_2\cdot\vec{q}_3\right] \\
&\times \Bigg[-\frac{3}{2}\,\delta_{\beta\gamma}\,\rho_0(\vec{r}_1)\rho_0(\vec{r}_3,\vec{r}_2)\rho_0(\vec{r}_2,\vec{r}_3) \\
&+\frac{1}{2}\,\delta_{\beta\gamma}\,\rho_0(\vec{r}_1)\rho_1(\vec{r}_3,\vec{r}_2)\rho_1(\vec{r}_2,\vec{r}_3) \\
&+\frac{1}{2}\,\rho_0(\vec{r}_1)s_1^\beta(\vec{r}_3,\vec{r}_2)s_1^\gamma(\vec{r}_2,\vec{r}_3) - \frac{3}{2}\,\rho_0(\vec{r}_1)s_0^\beta(\vec{r}_3,\vec{r}_2)s_0^\gamma(\vec{r}_2,\vec{r}_3) \\
&+\frac{3}{2}\,\epsilon^{\mu\beta\nu}\epsilon^{\omega\gamma\nu}\,\rho_0(\vec{r}_1)s_0^\mu(\vec{r}_3,\vec{r}_2)s_0^\omega(\vec{r}_2,\vec{r}_3) \\
&-\frac{1}{2}\,\epsilon^{\mu\beta\nu}\epsilon^{\omega\gamma\nu}\,\rho_0(\vec{r}_1)s_1^\mu(\vec{r}_3,\vec{r}_2)s_1^\omega(\vec{r}_2,\vec{r}_3)\Bigg]. \qquad (9.365)
\end{aligned}$$

The contribution from the R-part of the single-exchange piece reads

$$\begin{aligned}
\langle V_{3N}^{\mathrm{HF,CR,1x}} \rangle &= \left(\frac{g_A}{2f_\pi}\right)^2 \frac{c_4}{f_\pi^2}\frac{i}{4} \int d\vec{r}_1 d\vec{r}_2 d\vec{r}_3 \int \frac{1}{(2\pi)^6} d\vec{q}_2 d\vec{q}_3 \, e^{i\vec{q}_2\cdot(\vec{r}_2-\vec{r}_1)} \, e^{i\vec{q}_3\cdot(\vec{r}_3-\vec{r}_1)} \\
&\times \frac{q_2^{\beta_1} q_2^{\beta_2} q_3^{\gamma_1} q_3^{\gamma_2}}{(q_2^2+m_\pi^2)(q_3^2+m_\pi^2)} \Bigg[2s_1^{\beta_1}(\vec{r}_2)\Bigg(-\delta_{\gamma_1\gamma_2}\,\epsilon^{\mu\omega\beta_2}\,s_1^\mu(\vec{r}_3,\vec{r}_1)s_0^\omega(\vec{r}_1,\vec{r}_3) \\
&+\delta_{\beta_2\gamma_2}\,\epsilon^{\mu\omega\gamma_1}\,s_1^\mu(\vec{r}_3,\vec{r}_1)s_0^\omega(\vec{r}_1,\vec{r}_3) + \epsilon^{\beta_2\gamma_2\nu}\,s_1^{\gamma_1}(\vec{r}_3,\vec{r}_1)s_0^\nu(\vec{r}_1,\vec{r}_3) \\
&+\delta_{\gamma_1\gamma_2}\,\epsilon^{\mu\omega\beta_2}\,s_0^\mu(\vec{r}_3,\vec{r}_1)s_1^\omega(\vec{r}_1,\vec{r}_3) - \delta_{\beta_2\gamma_2}\,\epsilon^{\mu\omega\gamma_1}\,s_0^\mu(\vec{r}_3,\vec{r}_1)s_1^\omega(\vec{r}_1,\vec{r}_3) \\
&-\epsilon^{\beta_2\gamma_2\nu}\,s_0^{\gamma_1}(\vec{r}_3,\vec{r}_1)s_1^\nu(\vec{r}_1,\vec{r}_3) + \epsilon^{\beta_2\gamma_2\nu}\,s_1^{\gamma_1}(\vec{r}_3,\vec{r}_1)s_0^\nu(\vec{r}_1,\vec{r}_3) \\
&-\epsilon^{\beta_2\gamma_2\nu}\,s_0^{\gamma_1}(\vec{r}_3,\vec{r}_1)s_1^\nu(\vec{r}_1,\vec{r}_3) - i\,\delta_{\gamma_1\gamma_2}\,\rho_0(\vec{r}_3,\vec{r}_1)s_1^{\beta_2}(\vec{r}_1,\vec{r}_3)
\end{aligned}$$

$$
\begin{aligned}
& - i\,\delta_{\beta_2\gamma_2}\,\rho_0(\vec{r}_3,\vec{r}_1)s_1^{\gamma_1}(\vec{r}_1,\vec{r}_3) \;+\; i\,\delta_{\gamma_1\gamma_2}\,\rho_1(\vec{r}_3,\vec{r}_1)s_0^{\beta_2}(\vec{r}_1,\vec{r}_3) \\
& - i\,\delta_{\beta_2\gamma_2}\,\rho_1(\vec{r}_3,\vec{r}_1)s_0^{\gamma_1}(\vec{r}_1,\vec{r}_3) \;-\; i\,\delta_{\gamma_1\gamma_2}\,\rho_0(\vec{r}_1,\vec{r}_3)s_1^{\beta_2}(\vec{r}_3,\vec{r}_1) \\
& - i\,\delta_{\beta_2\gamma_2}\,\rho_0(\vec{r}_1,\vec{r}_3)s_1^{\gamma_1}(\vec{r}_3,\vec{r}_1) \;+\; i\,\delta_{\gamma_1\gamma_2}\,\rho_1(\vec{r}_1,\vec{r}_3)s_0^{\beta_2}(\vec{r}_3,\vec{r}_1) \\
& - i\,\delta_{\beta_2\gamma_2}\,\rho_1(\vec{r}_1,\vec{r}_3)s_0^{\gamma_1}(\vec{r}_3,\vec{r}_1) \Bigg) \;-\; \epsilon^{\nu\gamma_1\beta_1}\, s_1^{\nu}(\vec{r}_1) \\
& \Bigg(- s_1^{\beta_2}(\vec{r}_3,\vec{r}_2)s_1^{\gamma_2}(\vec{r}_2,\vec{r}_3) \;+\; s_0^{\beta_2}(\vec{r}_3,\vec{r}_2)s_1^{\gamma_2}(\vec{r}_2,\vec{r}_3) \\
& - s_1^{\beta_2}(\vec{r}_2,\vec{r}_3)s_1^{\gamma_2}(\vec{r}_3,\vec{r}_2) \;-\; \delta_{\beta_2\gamma_2}\, s_1^{\nu}(\vec{r}_2,\vec{r}_3)s_1^{\nu}(\vec{r}_3,\vec{r}_2) \\
& + s_1^{\beta_2}(\vec{r}_2,\vec{r}_3)s_0^{\gamma_2}(\vec{r}_3,\vec{r}_2) \;-\; \delta_{\beta_2\gamma_2}\, s_0^{\nu}(\vec{r}_3,\vec{r}_2)s_1^{\nu}(\vec{r}_2,\vec{r}_3) \\
& + i\,\epsilon^{\mu\gamma_2\beta_2}\,\rho_0(\vec{r}_3,\vec{r}_2)s_1^{\mu}(\vec{r}_2,\vec{r}_3) \;-\; i\,\epsilon^{\mu\gamma_2\beta_2}\,\rho_1(\vec{r}_3,\vec{r}_2)s_0^{\mu}(\vec{r}_2,\vec{r}_3) \\
& + i\,\epsilon^{\mu\gamma_2\beta_2}\,\rho_0(\vec{r}_2,\vec{r}_3)s_1^{\mu}(\vec{r}_3,\vec{r}_2) \;-\; i\,\epsilon^{\mu\gamma_2\beta_2}\,\rho_1(\vec{r}_2,\vec{r}_3)s_0^{\mu}(\vec{r}_3,\vec{r}_2) \\
& - \delta_{\beta_2\gamma_2}\,\rho_0(\vec{r}_2,\vec{r}_3)\rho_1(\vec{r}_3,\vec{r}_2) \;+\; \delta_{\beta_2\gamma_2}\,\rho_0(\vec{r}_3,\vec{r}_2)\rho_1(\vec{r}_2,\vec{r}_3) \Bigg) \Bigg] \,.
\end{aligned}
\tag{9.366}
$$

The contribution of the R-part of the single-exchange piece vanishes for both spin-unpolarized INM/PNM and time-reversal invariant systems.

Double-exchange part

The contribution from the D-like piece of the double-exchange part reads

$$
\begin{aligned}
\langle V_{3N}^{\mathrm{HF,CD,2x}} \rangle \;=\; & \left(\frac{g_A}{2f_\pi}\right)^2 \frac{1}{16} \int d\vec{r}_1 d\vec{r}_2 d\vec{r}_3 \int \frac{1}{(2\pi)^6} d\vec{q}_2 d\vec{q}_3\, e^{i\vec{q}_2\cdot(\vec{r}_2-\vec{r}_1)}\, e^{i\vec{q}_3\cdot(\vec{r}_3-\vec{r}_1)} \\
& \times \frac{q_2^\beta q_3^\gamma}{(q_2^2+m_\pi^2)(q_3^2+m_\pi^2)} \left[-4\frac{c_1 m_\pi^2}{f_\pi^2} + 2\frac{c_3}{f_\pi^2}\vec{q}_2\cdot\vec{q}_3 \right] \\
& \times \Bigg[\; 3\delta_{\beta\gamma}\,\rho_0(\vec{r}_2,\vec{r}_1)\rho_0(\vec{r}_3,\vec{r}_2)\rho_0(\vec{r}_1,\vec{r}_3) \\
& - \delta_{\beta\gamma}\,\rho_0(\vec{r}_2,\vec{r}_1)\rho_1(\vec{r}_3,\vec{r}_2)\rho_1(\vec{r}_1,\vec{r}_3) \\
& + 3\,\rho_0(\vec{r}_2,\vec{r}_1)s_0^{\beta}(\vec{r}_3,\vec{r}_2)s_0^{\gamma}(\vec{r}_1,\vec{r}_3) \\
& - 3\epsilon^{\mu\beta\nu}\epsilon^{\omega\gamma\nu}\,\rho_0(\vec{r}_2,\vec{r}_1)s_0^{\mu}(\vec{r}_3,\vec{r}_2)s_0^{\omega}(\vec{r}_1,\vec{r}_3)
\end{aligned}
$$

$$
\begin{aligned}
&- \rho_0(\vec{r}_2, \vec{r}_1) s_1^\beta(\vec{r}_3, \vec{r}_2) s_1^\gamma(\vec{r}_1, \vec{r}_3) \\
&+ \epsilon^{\mu\beta\nu}\epsilon^{\omega\gamma\nu}\, \rho_0(\vec{r}_2, \vec{r}_1) s_1^\mu(\vec{r}_3, \vec{r}_2) s_1^\omega(\vec{r}_1, \vec{r}_3) \\
&+ 6\, \rho_0(\vec{r}_1, \vec{r}_3) s_0^\beta(\vec{r}_2, \vec{r}_1) s_0^\gamma(\vec{r}_3, \vec{r}_2) \\
&- 3\delta_{\beta\gamma}\, \rho_0(\vec{r}_1, \vec{r}_3) s_0^\beta(\vec{r}_2, \vec{r}_1) s_0^\gamma(\vec{r}_3, \vec{r}_2) \\
&+ 3\delta_{\beta\gamma}\, \rho_0(\vec{r}_3, \vec{r}_2) s_0^\beta(\vec{r}_2, \vec{r}_1) s_0^\gamma(\vec{r}_1, \vec{r}_3) \\
&- 2\, \rho_1(\vec{r}_1, \vec{r}_3) s_0^\beta(\vec{r}_2, \vec{r}_1) s_1^\gamma(\vec{r}_3, \vec{r}_2) \\
&+ \delta_{\beta\gamma}\, \rho_1(\vec{r}_1, \vec{r}_3) s_0^\beta(\vec{r}_2, \vec{r}_1) s_1^\gamma(\vec{r}_3, \vec{r}_2) \\
&- \delta_{\beta\gamma}\, \rho_1(\vec{r}_3, \vec{r}_2) s_0^\beta(\vec{r}_2, \vec{r}_1) s_1^\gamma(\vec{r}_1, \vec{r}_3) \\
&+ 3\delta_{\beta\gamma}\, \rho_0(\vec{r}_3, \vec{r}_2) \rho_1(\vec{r}_2, \vec{r}_1) \rho_1(\vec{r}_1, \vec{r}_3) \\
&- \delta_{\beta\gamma}\, \rho_0(\vec{r}_1, \vec{r}_3) \rho_1(\vec{r}_2, \vec{r}_1) \rho_1(\vec{r}_3, \vec{r}_2) \\
&+ 3\, \rho_1(\vec{r}_2, \vec{r}_1) s_0^\beta(\vec{r}_3, \vec{r}_2) s_1^\gamma(\vec{r}_1, \vec{r}_3) \\
&- 3\epsilon^{\mu\beta\nu}\epsilon^{\omega\gamma\nu}\, \rho_1(\vec{r}_2, \vec{r}_1) s_0^\mu(\vec{r}_3, \vec{r}_2) s_1^\omega(\vec{r}_1, \vec{r}_3) \\
&- \rho_1(\vec{r}_2, \vec{r}_1) s_1^\beta(\vec{r}_3, \vec{r}_2) s_0^\gamma(\vec{r}_1, \vec{r}_3) \\
&+ \epsilon^{\mu\beta\nu}\epsilon^{\omega\gamma\nu}\, \rho_1(\vec{r}_2, \vec{r}_1) s_1^\mu(\vec{r}_3, \vec{r}_2) s_0^\omega(\vec{r}_1, \vec{r}_3) \\
&- 2\, \rho_0(\vec{r}_1, \vec{r}_3) s_1^\beta(\vec{r}_2, \vec{r}_1) s_1^\gamma(\vec{r}_3, \vec{r}_2) \\
&+ \delta_{\beta\gamma}\, \rho_0(\vec{r}_1, \vec{r}_3) s_1^\beta(\vec{r}_2, \vec{r}_1) s_1^\gamma(\vec{r}_3, \vec{r}_2) \\
&+ 3\delta_{\beta\gamma}\, \rho_0(\vec{r}_3, \vec{r}_2) s_1^\beta(\vec{r}_2, \vec{r}_1) s_1^\gamma(\vec{r}_1, \vec{r}_3) \\
&+ 6\, \rho_1(\vec{r}_1, \vec{r}_3) s_1^\beta(\vec{r}_2, \vec{r}_1) s_0^\gamma(\vec{r}_3, \vec{r}_2) \\
&- 3\delta_{\beta\gamma}\, \rho_1(\vec{r}_1, \vec{r}_3) s_1^\beta(\vec{r}_2, \vec{r}_1) s_0^\gamma(\vec{r}_3, \vec{r}_2) \\
&- \delta_{\beta\gamma}\, \rho_1(\vec{r}_3, \vec{r}_2) s_1^\beta(\vec{r}_2, \vec{r}_1) s_0^\gamma(\vec{r}_1, \vec{r}_3) \\
&+ i3 \left[\, s_0^{\mu 1}(\vec{r}_1, \vec{r}_3) s_0^{\mu 2}(\vec{r}_2, \vec{r}_1) s_0^{\mu 3}(\vec{r}_3, \vec{r}_2) \right. \\
&- \frac{1}{3}\, s_1^{\mu 1}(\vec{r}_1, \vec{r}_3) s_0^{\mu 2}(\vec{r}_2, \vec{r}_1) s_1^{\mu 3}(\vec{r}_3, \vec{r}_2) \\
&+ s_1^{\mu 1}(\vec{r}_1, \vec{r}_3) s_1^{\mu 2}(\vec{r}_2, \vec{r}_1) s_0^{\mu 3}(\vec{r}_3, \vec{r}_2) \\
&\left. - \frac{1}{3}\, s_0^{\mu 1}(\vec{r}_1, \vec{r}_3) s_1^{\mu 2}(\vec{r}_2, \vec{r}_1) s_1^{\mu 3}(\vec{r}_3, \vec{r}_2) \,\right]
\end{aligned}
$$

$$\times \left[-\epsilon^{\mu_3\mu_1\mu_4}\epsilon^{\beta\mu_4\nu}\epsilon^{\gamma\mu_2\nu} + \epsilon^{\beta\mu_3\mu_4}\epsilon^{\mu_2\mu_4\nu}\epsilon^{\gamma\mu_1\nu} - \epsilon^{\beta\mu_3\mu_4}\epsilon^{\mu_4\mu_1\nu}\epsilon^{\gamma\mu_2\nu} \right.$$
$$\left. - \epsilon^{\gamma\mu_3\mu_4}\epsilon^{\mu_1\mu_4\nu}\epsilon^{\beta\mu_2\nu}\right]\Bigg] . \tag{9.367}$$

For symmetric INM, this reduces to

$$\begin{aligned}\langle V_{3N}^{\mathrm{HF,CD,2x,INM}}\rangle &= \left(\frac{g_A}{2f_\pi}\right)^2 \frac{1}{16}\int d\vec{r}_1 d\vec{r}_2 d\vec{r}_3 \int \frac{1}{(2\pi)^6} d\vec{q}_2 d\vec{q}_3\, e^{i\vec{q}_2\cdot(\vec{r}_2-\vec{r}_1)}\, e^{i\vec{q}_3\cdot(\vec{r}_3-\vec{r}_1)} \\ &\times \frac{q_2^\beta q_3^\gamma}{(q_2^2+m_\pi^2)(q_3^2+m_\pi^2)}\left[-4\frac{c_1 m_\pi^2}{f_\pi^2} + 2\frac{c_3}{f_\pi^2}\vec{q}_2\cdot\vec{q}_3\right] \\ &\times \left[\, 3\delta_{\beta\gamma}\, \rho_0(\vec{r}_1,\vec{r}_3)\rho_0(\vec{r}_2,\vec{r}_1)\rho_0(\vec{r}_3,\vec{r}_2)\right] ,\end{aligned} \tag{9.368}$$

while for unpolarized PNM, one has

$$\begin{aligned}\langle V_{3N}^{\mathrm{HF,CD,2x,PNM}}\rangle &= \left(\frac{g_A}{2f_\pi}\right)^2 \frac{1}{16}\int d\vec{r}_1 d\vec{r}_2 d\vec{r}_3 \int \frac{1}{(2\pi)^6} d\vec{q}_2 d\vec{q}_3\, e^{i\vec{q}_2\cdot(\vec{r}_2-\vec{r}_1)}\, e^{i\vec{q}_3\cdot(\vec{r}_3-\vec{r}_1)} \\ &\times \frac{q_2^\beta q_3^\gamma}{(q_2^2+m_\pi^2)(q_3^2+m_\pi^2)}\left[-4\frac{c_1 m_\pi^2}{f_\pi^2} + 2\frac{c_3}{f_\pi^2}\vec{q}_2\cdot\vec{q}_3\right] \\ &\times \left[\, 3\delta_{\beta\gamma}\, \rho_n(\vec{r}_1,\vec{r}_3)\rho_n(\vec{r}_2,\vec{r}_1)\rho_n(\vec{r}_3,\vec{r}_2)\right] .\end{aligned} \tag{9.369}$$

For time-reversal invariant systems, the expression given in Eq.(9.367) can be simplified only slightly. The reason is the phase factor $e^{i\vec{q}_2\cdot(\vec{r}_2-\vec{r}_1)}e^{i\vec{q}_3\cdot(\vec{r}_3-\vec{r}_1)}$ prevents one from treating $\vec{r}_1$ on equal footing as $\vec{r}_2$ and $\vec{r}_3$, i.e. even though one can interchange $\vec{r}_2$ and $\vec{r}_3$ and recover the same expression, the same can not be said of $\vec{r}_1$ and $\vec{r}_2$ or $\vec{r}_1$ and $\vec{r}_3$. This is further compounded by the fact that the HF energy of the C-term's double exchange involves invariably three non-local scalar/vector densities. Another simple interpretation of this is, most if not all of the available symmetries in the coordinates have already been utilized in Eqs. (7.13)-(7.15). Hence, the corresponding expression reads

$$\langle V_{3N}^{\mathrm{HF,CD,2x,TRI}}\rangle = \left(\frac{g_A}{2f_\pi}\right)^2 \frac{1}{16}\int d\vec{r}_1 d\vec{r}_2 d\vec{r}_3 \int \frac{1}{(2\pi)^6} d\vec{q}_2 d\vec{q}_3\, e^{i\vec{q}_2\cdot(\vec{r}_2-\vec{r}_1)}\, e^{i\vec{q}_3\cdot(\vec{r}_3-\vec{r}_1)}$$

$$\times \frac{q_2^\beta q_3^\gamma}{(q_2^2+m_\pi^2)(q_3^2+m_\pi^2)} \left[-4\frac{c_1 m_\pi^2}{f_\pi^2} + 2\frac{c_3}{f_\pi^2}\vec{q}_2 \cdot \vec{q}_3\right]$$

$$\times \Bigg[\; 3\delta_{\beta\gamma}\, \rho_0(\vec{r}_2,\vec{r}_1)\rho_0(\vec{r}_3,\vec{r}_2)\rho_0(\vec{r}_1,\vec{r}_3)$$

$$-\,\delta_{\beta\gamma}\, \rho_0(\vec{r}_2,\vec{r}_1)\rho_1(\vec{r}_3,\vec{r}_2)\rho_1(\vec{r}_1,\vec{r}_3)$$

$$+\,9\, \rho_0(\vec{r}_2,\vec{r}_1)s_0^\beta(\vec{r}_3,\vec{r}_2)s_0^\gamma(\vec{r}_1,\vec{r}_3)$$

$$-\,3\epsilon^{\mu\beta\nu}\epsilon^{\omega\gamma\nu}\, \rho_0(\vec{r}_2,\vec{r}_1)s_0^\mu(\vec{r}_3,\vec{r}_2)s_0^\omega(\vec{r}_1,\vec{r}_3)$$

$$-\,3\, \rho_0(\vec{r}_2,\vec{r}_1)s_1^\beta(\vec{r}_3,\vec{r}_2)s_1^\gamma(\vec{r}_1,\vec{r}_3)$$

$$+\,\epsilon^{\mu\beta\nu}\epsilon^{\omega\gamma\nu}\, \rho_0(\vec{r}_2,\vec{r}_1)s_1^\mu(\vec{r}_3,\vec{r}_2)s_1^\omega(\vec{r}_1,\vec{r}_3)$$

$$-\,3\delta_{\beta\gamma}\, \rho_0(\vec{r}_1,\vec{r}_3)s_0^\beta(\vec{r}_2,\vec{r}_1)s_0^\gamma(\vec{r}_3,\vec{r}_2)$$

$$+\,3\delta_{\beta\gamma}\, \rho_0(\vec{r}_3,\vec{r}_2)s_0^\beta(\vec{r}_2,\vec{r}_1)s_0^\gamma(\vec{r}_1,\vec{r}_3)$$

$$-\,2\, \rho_1(\vec{r}_1,\vec{r}_3)s_0^\beta(\vec{r}_2,\vec{r}_1)s_1^\gamma(\vec{r}_3,\vec{r}_2)$$

$$+\,\delta_{\beta\gamma}\, \rho_1(\vec{r}_1,\vec{r}_3)s_0^\beta(\vec{r}_2,\vec{r}_1)s_1^\gamma(\vec{r}_3,\vec{r}_2)$$

$$-\,\delta_{\beta\gamma}\, \rho_1(\vec{r}_3,\vec{r}_2)s_0^\beta(\vec{r}_2,\vec{r}_1)s_1^\gamma(\vec{r}_1,\vec{r}_3)$$

$$+\,3\delta_{\beta\gamma}\, \rho_0(\vec{r}_3,\vec{r}_2)\rho_1(\vec{r}_2,\vec{r}_1)\rho_1(\vec{r}_1,\vec{r}_3)$$

$$-\,\delta_{\beta\gamma}\, \rho_0(\vec{r}_1,\vec{r}_3)\rho_1(\vec{r}_2,\vec{r}_1)\rho_1(\vec{r}_3,\vec{r}_2)$$

$$+\,3\, \rho_1(\vec{r}_2,\vec{r}_1)s_0^\beta(\vec{r}_3,\vec{r}_2)s_1^\gamma(\vec{r}_1,\vec{r}_3)$$

$$-\,3\epsilon^{\mu\beta\nu}\epsilon^{\omega\gamma\nu}\, \rho_1(\vec{r}_2,\vec{r}_1)s_0^\mu(\vec{r}_3,\vec{r}_2)s_1^\omega(\vec{r}_1,\vec{r}_3)$$

$$-\,\rho_1(\vec{r}_2,\vec{r}_1)s_1^\beta(\vec{r}_3,\vec{r}_2)s_0^\gamma(\vec{r}_1,\vec{r}_3)$$

$$+\,\epsilon^{\mu\beta\nu}\epsilon^{\omega\gamma\nu}\, \rho_1(\vec{r}_2,\vec{r}_1)s_1^\mu(\vec{r}_3,\vec{r}_2)s_0^\omega(\vec{r}_1,\vec{r}_3)$$

$$+\,\delta_{\beta\gamma}\, \rho_0(\vec{r}_1,\vec{r}_3)s_1^\beta(\vec{r}_2,\vec{r}_1)s_1^\gamma(\vec{r}_3,\vec{r}_2)$$

$$+\,3\delta_{\beta\gamma}\, \rho_0(\vec{r}_3,\vec{r}_2)s_1^\beta(\vec{r}_2,\vec{r}_1)s_1^\gamma(\vec{r}_1,\vec{r}_3)$$

$$+\,6\, \rho_1(\vec{r}_1,\vec{r}_3)s_1^\beta(\vec{r}_2,\vec{r}_1)s_0^\gamma(\vec{r}_3,\vec{r}_2)$$

$$-\,3\delta_{\beta\gamma}\, \rho_1(\vec{r}_1,\vec{r}_3)s_1^\beta(\vec{r}_2,\vec{r}_1)s_0^\gamma(\vec{r}_3,\vec{r}_2)$$

$$-\,\delta_{\beta\gamma}\, \rho_1(\vec{r}_3,\vec{r}_2)s_1^\beta(\vec{r}_2,\vec{r}_1)s_0^\gamma(\vec{r}_1,\vec{r}_3)$$

$$
\begin{aligned}
&+ i3\,\Big(\, s_0^{\mu_1}(\vec{r}_1,\vec{r}_3) s_0^{\mu_2}(\vec{r}_2,\vec{r}_1) s_0^{\mu_3}(\vec{r}_3,\vec{r}_2) \\
&- \frac{1}{3}\, s_1^{\mu_1}(\vec{r}_1,\vec{r}_3) s_0^{\mu_2}(\vec{r}_2,\vec{r}_1) s_1^{\mu_3}(\vec{r}_3,\vec{r}_2) \\
&+ s_1^{\mu_1}(\vec{r}_1,\vec{r}_3) s_1^{\mu_2}(\vec{r}_2,\vec{r}_1) s_0^{\mu_3}(\vec{r}_3,\vec{r}_2) \\
&- \frac{1}{3}\, s_0^{\mu_1}(\vec{r}_1,\vec{r}_3) s_1^{\mu_2}(\vec{r}_2,\vec{r}_1) s_1^{\mu_3}(\vec{r}_3,\vec{r}_2) \Big) \\
&\times \Big[-\epsilon^{\mu_3\mu_1\mu_4}\epsilon^{\beta\mu_4\nu}\epsilon^{\gamma\mu_2\nu} + \epsilon^{\beta\mu_3\mu_4}\epsilon^{\mu_2\mu_4\nu}\epsilon^{\gamma\mu_1\nu} \\
&- \epsilon^{\beta\mu_3\mu_4}\epsilon^{\mu_4\mu_1\nu}\epsilon^{\gamma\mu_2\nu} - \epsilon^{\gamma\mu_3\mu_4}\epsilon^{\mu_1\mu_4\nu}\epsilon^{\beta\mu_2\nu} \Big] \Bigg] \,. \qquad (9.370)
\end{aligned}
$$

The contribution from the R-part of the double-exchange of the C-term is composed of

$$
\langle V_{3N}^{\mathrm{HF,CR,2x}} \rangle = \langle V_{3N}^{\mathrm{HF,CR1,2x}} \rangle + \langle V_{3N}^{\mathrm{HF,CR2,2x}} \rangle + \langle V_{3N}^{\mathrm{HF,CR3,2x}} \rangle + \langle V_{3N}^{\mathrm{HF,CR4,2x}} \rangle \qquad (9.371)
$$

where $\langle V_{3N}^{\mathrm{HF,CR1,2x}} \rangle$, $\langle V_{3N}^{\mathrm{HF,CR2,2x}} \rangle$, $\langle V_{3N}^{\mathrm{HF,CR3,2x}} \rangle$, and $\langle V_{3N}^{\mathrm{HF,CR4,2x}} \rangle$. Denoting

$$
\begin{aligned}
CR1 &\equiv \langle V_{3N}^{\mathrm{HF,CR1,2x}} \rangle , \\
CR2 &\equiv \langle V_{3N}^{\mathrm{HF,CR2,2x}} \rangle , \\
CR3 &\equiv \langle V_{3N}^{\mathrm{HF,CR3,2x}} \rangle , \\
CR4 &\equiv \langle V_{3N}^{\mathrm{HF,CR4,2x}} \rangle ,
\end{aligned}
$$

these are given by

$$
\begin{aligned}
CR1 \;=\;& \left(\frac{g_A}{2f_\pi}\right)^2 \frac{c_4}{f_\pi^2}\,\frac{i}{8} \int d\vec{r}_1 d\vec{r}_2 d\vec{r}_3 \int \frac{1}{(2\pi)^6} d\vec{q}_2 d\vec{q}_3\, e^{i\vec{q}_2\cdot(\vec{r}_2-\vec{r}_1)}\, e^{i\vec{q}_3\cdot(\vec{r}_3-\vec{r}_1)} \\
&\times \frac{q_2^{\beta_1} q_2^{\beta_2} q_3^{\gamma_1} q_3^{\gamma_2}}{(q_2^2+m_\pi^2)(q_3^2+m_\pi^2)} \\
&\times \Big[\epsilon^{\beta_1\gamma_1\mu_1} \left(-\delta_{\beta_2\gamma_2}\delta_{\mu_2\mu_3} + \delta_{\beta_2\mu_2}\delta_{\gamma_2\mu_3} + \delta_{\beta_2\mu_3}\delta_{\gamma_2\mu_2} \right)
\end{aligned}
$$

$$
\begin{aligned}
&\Bigg(s_1^{\mu_1}(\vec{r}_2,\vec{r}_1)s_1^{\mu_2}(\vec{r}_3,\vec{r}_2)s_0^{\mu_3}(\vec{r}_1,\vec{r}_3) \;-\; s_1^{\mu_1}(\vec{r}_2,\vec{r}_1)s_0^{\mu_2}(\vec{r}_3,\vec{r}_2)s_1^{\mu_3}(\vec{r}_1,\vec{r}_3) \Bigg) \\
&+ \epsilon^{\beta_1\gamma_1\mu_1}\,\delta_{\beta_2\gamma_2}\,s_1^{\mu_1}(\vec{r}_2,\vec{r}_1)\Bigg(\rho_1(\vec{r}_3,\vec{r}_2)\rho_0(\vec{r}_1,\vec{r}_3) - \rho_0(\vec{r}_3,\vec{r}_2)\rho_1(\vec{r}_1,\vec{r}_3) \Bigg) \\
&+ i\,\epsilon^{\beta_1\gamma_1\mu_1}\epsilon^{\beta_2\gamma_2\mu_2}\,\Bigg(s_1^{\mu_1}(\vec{r}_2,\vec{r}_1)s_1^{\mu_2}(\vec{r}_1,\vec{r}_3)\rho_0(\vec{r}_3,\vec{r}_2) \\
&- s_1^{\mu_1}(\vec{r}_2,\vec{r}_1)s_0^{\mu_2}(\vec{r}_1,\vec{r}_3)\rho_1(\vec{r}_3,\vec{r}_2) \;+\; s_1^{\mu_1}(\vec{r}_2,\vec{r}_1)s_1^{\mu_2}(\vec{r}_3,\vec{r}_2)\rho_0(\vec{r}_1,\vec{r}_3) \\
&- s_1^{\mu_1}(\vec{r}_2,\vec{r}_1)s_0^{\mu_2}(\vec{r}_3,\vec{r}_2)\rho_1(\vec{r}_1,\vec{r}_3) \Bigg)\Bigg] .
\end{aligned}
\tag{9.372}
$$

, we have

$$
\begin{aligned}
CR2 \;=\; & \left(\frac{g_A}{2f_\pi}\right)^2 \frac{c_4}{f_\pi^2}\,\frac{i}{8} \int d\vec{r}_1 d\vec{r}_2 d\vec{r}_3 \int \frac{1}{(2\pi)^6} d\vec{q}_2 d\vec{q}_3\, e^{i\vec{q}_2\cdot(\vec{r}_2-\vec{r}_1)}\, e^{i\vec{q}_3\cdot(\vec{r}_3-\vec{r}_1)} \\
& \times \frac{q_2^{\beta_1} q_2^{\beta_2} q_3^{\gamma_1} q_3^{\gamma_2}}{(q_2^2+m_\pi^2)(q_3^2+m_\pi^2)} \\
& \times \Bigg[\epsilon^{\beta_1\gamma_1\mu_1}\,\left(\delta_{\beta_2\gamma_2}\delta_{\mu_2\mu_3} - \delta_{\beta_2\mu_3}\delta_{\gamma_2\mu_2}\right)\, s_1^{\mu_1}(\vec{r}_3,\vec{r}_2)s_0^{\mu_2}(\vec{r}_2,\vec{r}_1)s_1^{\mu_3}(\vec{r}_1,\vec{r}_3) \\
& + \epsilon^{\beta_1\gamma_1\mu_1}\,\left(-\delta_{\beta_2\gamma_2}\delta_{\mu_2\mu_3} + \delta_{\beta_2\mu_2}\delta_{\gamma_2\mu_3} - \delta_{\beta_2\mu_3}\delta_{\gamma_2\mu_2}\right) \\
& \qquad\qquad \times s_1^{\mu_1}(\vec{r}_1,\vec{r}_3)s_0^{\mu_2}(\vec{r}_2,\vec{r}_1)s_1^{\mu_3}(\vec{r}_3,\vec{r}_2) \\
& + \epsilon^{\beta_1\gamma_1\mu_1}\,\left(-\delta_{\beta_2\gamma_2}\delta_{\mu_2\mu_3} + \delta_{\beta_2\mu_2}\delta_{\gamma_2\mu_3} + \delta_{\beta_2\mu_3}\delta_{\gamma_2\mu_2}\right) \\
& \qquad\qquad \times s_1^{\mu_1}(\vec{r}_3,\vec{r}_2)s_1^{\mu_2}(\vec{r}_2,\vec{r}_1)s_0^{\mu_3}(\vec{r}_1,\vec{r}_3) \\
& + \epsilon^{\beta_1\gamma_1\mu_1}\,\left(\delta_{\beta_2\gamma_2}\delta_{\mu_2\mu_3} - \delta_{\beta_2\mu_2}\delta_{\gamma_2\mu_3} + \delta_{\beta_2\mu_3}\delta_{\gamma_2\mu_2}\right) \\
& \qquad\qquad \times s_0^{\mu_1}(\vec{r}_1,\vec{r}_3)s_1^{\mu_2}(\vec{r}_2,\vec{r}_1)s_1^{\mu_3}(\vec{r}_3,\vec{r}_2) \\
& - \epsilon^{\beta_1\gamma_1\mu_1}\,\delta_{\beta_2\mu_2}\delta_{\gamma_2\mu_3}\, s_0^{\mu_1}(\vec{r}_3,\vec{r}_2)s_1^{\mu_2}(\vec{r}_2,\vec{r}_1)s_1^{\mu_3}(\vec{r}_1,\vec{r}_3) \\
& + i\,\epsilon^{\beta_1\gamma_1\nu}\epsilon^{\beta_2\gamma_2\nu}\,\rho_1(\vec{r}_3,\vec{r}_2)\Bigg(\rho_1(\vec{r}_2,\vec{r}_1)\rho_0(\vec{r}_1,\vec{r}_3) \;-\; \rho_0(\vec{r}_2,\vec{r}_1)\rho_1(\vec{r}_1,\vec{r}_3)\Bigg) \\
& + \epsilon^{\beta_1\gamma_1\mu_1}\delta_{\beta_2\gamma_2}\,\Bigg(s_1^{\mu_1}(\vec{r}_1,\vec{r}_3)\rho_0(\vec{r}_2,\vec{r}_1)\rho_1(\vec{r}_3,\vec{r}_2) \\
& \qquad\qquad - s_1^{\mu_1}(\vec{r}_3,\vec{r}_2)\rho_0(\vec{r}_2,\vec{r}_1)\rho_1(\vec{r}_1,\vec{r}_3) \\
& + s_1^{\mu_1}(\vec{r}_3,\vec{r}_2)\rho_1(\vec{r}_2,\vec{r}_1)\rho_0(\vec{r}_1,\vec{r}_3) \;-\; s_0^{\mu_1}(\vec{r}_1,\vec{r}_3)\rho_1(\vec{r}_2,\vec{r}_1)\rho_1(\vec{r}_3,\vec{r}_2)\Bigg) \\
& + i\,\epsilon^{\beta_1\gamma_1\mu_1}\,\left(\epsilon^{\beta_2\gamma_2\nu_2}\delta_{\mu_1\nu_1} + \epsilon^{\nu_1\beta_2\mu_1}\delta_{\gamma_2\nu_2} - \epsilon^{\nu_2\beta_2\mu_1}\delta_{\gamma_2\nu_1} - \epsilon^{\nu_1\gamma_2\mu_1}\delta_{\beta_2\nu_2}\right)
\end{aligned}
$$

$$
\begin{aligned}
&\times s_1^{\nu_1}(\vec{r}_3,\vec{r}_2)s_1^{\nu_2}(\vec{r}_1,\vec{r}_3)\rho_0(\vec{r}_2,\vec{r}_1)\\
&-i\,\epsilon^{\beta_1\gamma_1\mu_1}\epsilon^{\beta_2\gamma_2\mu_2}\,s_1^{\mu_1}(\vec{r}_3,\vec{r}_2)s_0^{\mu_2}(\vec{r}_1.\vec{r}_3)\rho_1(\vec{r}_2.\vec{r}_1)\\
&-i\,\epsilon^{\beta_1\gamma_1\nu}\epsilon^{\beta_2\mu_1\nu}\Bigg(-s_0^{\mu_1}(\vec{r}_3,\vec{r}_2)s_1^{\gamma_2}(\vec{r}_1,\vec{r}_3)\rho_1(\vec{r}_2,\vec{r}_1)\\
&+s_0^{\mu_1}(\vec{r}_1,\vec{r}_3)s_1^{\gamma_2}(\vec{r}_3,\vec{r}_2)\rho_1(\vec{r}_2,\vec{r}_1)\\
&-s_1^{\mu_1}(\vec{r}_3,\vec{r}_2)s_0^{\gamma_2}(\vec{r}_2,\vec{r}_1)\rho_1(\vec{r}_1,\vec{r}_3)\;+\;s_1^{\mu_1}(\vec{r}_2,\vec{r}_1)s_1^{\gamma_2}(\vec{r}_1,\vec{r}_3)\rho_0(\vec{r}_3,\vec{r}_2)\\
&-s_1^{\mu_1}(\vec{r}_2,\vec{r}_1)s_0^{\gamma_2}(\vec{r}_1,\vec{r}_3)\rho_1(\vec{r}_3,\vec{r}_2)\;+\;s_1^{\mu_1}(\vec{r}_3,\vec{r}_2)s_1^{\gamma_2}(\vec{r}_2,\vec{r}_1)\rho_0(\vec{r}_1,\vec{r}_3)\Bigg)\\
&-i\,\epsilon^{\beta_1\gamma_1\nu}\epsilon^{\gamma_2\mu_1\nu}\Bigg(s_1^{\mu_1}(\vec{r}_3,\vec{r}_2)s_0^{\beta_2}(\vec{r}_1,\vec{r}_3)\rho_1(\vec{r}_2,\vec{r}_1)\\
&+s_1^{\mu_1}(\vec{r}_1,\vec{r}_3)s_0^{\beta_2}(\vec{r}_2,\vec{r}_1)\rho_1(\vec{r}_3,\vec{r}_2)\\
&+s_0^{\mu_1}(\vec{r}_1,\vec{r}_2)s_1^{\beta_2}(\vec{r}_3,\vec{r}_2)\rho_1(\vec{r}_1,\vec{r}_3)\;-\;s_0^{\mu_1}(\vec{r}_1,\vec{r}_3)s_1^{\beta_2}(\vec{r}_2,\vec{r}_1)\rho_1(\vec{r}_3,\vec{r}_2)\\
&-s_1^{\mu_1}(\vec{r}_2,\vec{r}_1)s_1^{\beta_2}(\vec{r}_3,\vec{r}_2)\rho_0(\vec{r}_1,\vec{r}_3)\Bigg)\Bigg]\,.
\end{aligned}
\tag{9.373}
$$

$$
\begin{aligned}
CR3\;=\;&\left(\frac{g_A}{2f_\pi}\right)^2\frac{c_4}{f_\pi^2}\frac{i}{8}\int d\vec{r}_1d\vec{r}_2d\vec{r}_3\int\frac{1}{(2\pi)^6}d\vec{q}_2d\vec{q}_3\,e^{i\vec{q}_2\cdot(\vec{r}_2-\vec{r}_1)}\,e^{i\vec{q}_3\cdot(\vec{r}_3-\vec{r}_1)}\\
&\times\frac{q_2^{\beta_1}q_2^{\beta_2}q_3^{\gamma_1}q_3^{\gamma_2}}{(q_2^2+m_\pi^2)(q_3^2+m_\pi^2)}\\
&\times\Bigg[\epsilon^{\beta_1\gamma_1\mu_1}\left(\delta_{\beta_2\gamma_2}\delta_{\mu_2\mu_3}-\delta_{\beta_2\mu_2}\delta_{\gamma_2\mu_3}-\delta_{\beta_2\mu_3}\delta_{\gamma_2\mu_2}\right)\\
&\times\Bigg(s_0^{\mu_1}(\vec{r}_2,\vec{r}_1)s_1^{\mu_2}(\vec{r}_3,\vec{r}_2)s_1^{\mu_3}(\vec{r}_1,\vec{r}_3)\\
&-3\,s_0^{\mu_1}(\vec{r}_2,\vec{r}_1)s_0^{\mu_2}(\vec{r}_3,\vec{r}_2)s_0^{\mu_3}(\vec{r}_1,\vec{r}_3)\;+\;2\,s_1^{\mu_1}(\vec{r}_2,\vec{r}_1)s_1^{\mu_2}(\vec{r}_3,\vec{r}_2)s_0^{\mu_3}(\vec{r}_1,\vec{r}_3)\Bigg)\\
&+\epsilon^{\beta_1\gamma_1\mu_1}\,\delta_{\beta_2\gamma_2}\,s_0^{\mu_1}(\vec{r}_2,\vec{r}_1)\Bigg(3\rho_0(\vec{r}_3,\vec{r}_2)\rho_0(\vec{r}_1,\vec{r}_3)-\rho_1(\vec{r}_3,\vec{r}_2)\rho_1(\vec{r}_1,\vec{r}_3)\Bigg)\\
&-\epsilon^{\beta_1\gamma_1\mu_1}\,\delta_{\beta_2\gamma_2}\,s_1^{\mu_1}(\vec{r}_2,\vec{r}_1)2\rho_1(\vec{r}_3,\vec{r}_2)\rho_0(\vec{r}_1,\vec{r}_3)\\
&+i\,\epsilon^{\beta_1\gamma_1\mu_1}\epsilon^{\beta_2\gamma_2\mu_2}\Bigg(-3\,s_0^{\mu_1}(\vec{r}_2,\vec{r}_1)s_0^{\mu_2}(\vec{r}_1,\vec{r}_3)\rho_0(\vec{r}_3,\vec{r}_2)\\
&+s_0^{\mu_1}(\vec{r}_2,\vec{r}_1)s_1^{\mu_2}(\vec{r}_1,\vec{r}_3)\rho_1(\vec{r}_3,\vec{r}_2)\\
&+3\,s_0^{\mu_1}(\vec{r}_2,\vec{r}_1)s_0^{\mu_2}(\vec{r}_3,\vec{r}_2)\rho_0(\vec{r}_1,\vec{r}_3)\;-\;s_0^{\mu_1}(\vec{r}_2,\vec{r}_1)s_1^{\mu_2}(\vec{r}_3,\vec{r}_2)\rho_1(\vec{r}_1,\vec{r}_3)
\end{aligned}
$$

$$+\,2\,s_1^{\mu_1}(\vec r_2,\vec r_1)s_0^{\mu_2}(\vec r_1,\vec r_3)\rho_1(\vec r_3,\vec r_2)\;-\;2\,s_1^{\mu_1}(\vec r_2,\vec r_1)s_1^{\mu_2}(\vec r_3,\vec r_2)\rho_0(\vec r_1,\vec r_3)\Bigg)\Bigg]\,. \tag{9.374}$$

$$\begin{aligned}
CR4 \;=\;& \left(\frac{g_A}{2f_\pi}\right)^2 \frac{c_4}{f_\pi^2}\,\frac{i}{8}\int d\vec r_1 d\vec r_2 d\vec r_3 \int \frac{1}{(2\pi)^6} d\vec q_2 d\vec q_3\, e^{i\vec q_2\cdot(\vec r_2-\vec r_1)}\, e^{i\vec q_3\cdot(\vec r_3-\vec r_1)} \\
&\times \frac{q_2^{\beta_1} q_2^{\beta_2} q_3^{\gamma_1} q_3^{\gamma_2}}{(q_2^2+m_\pi^2)(q_3^2+m_\pi^2)} \\
&\Big[\;\epsilon^{\beta_1\gamma_1\mu_1}\left(-\delta_{\beta_2\gamma_2}\delta_{\mu_2\mu_3}+\delta_{\beta_2\mu_2}\delta_{\gamma_2\mu_3}+\delta_{\beta_2\mu_3}\delta_{\gamma_2\mu_2}\right) \\
&\qquad\times\Bigg(\,3\,s_0^{\mu_1}(\vec r_3,\vec r_2)s_0^{\mu_2}(\vec r_2,\vec r_1)s_0^{\mu_3}(\vec r_1,\vec r_3) \\
&-\,s_1^{\mu_1}(\vec r_3,\vec r_2)s_0^{\mu_2}(\vec r_2,\vec r_1)s_1^{\mu_3}(\vec r_1,\vec r_3)\;-\;2\,s_1^{\mu_1}(\vec r_3,\vec r_2)s_1^{\mu_2}(\vec r_2,\vec r_1)s_0^{\mu_3}(\vec r_1,\vec r_3)\,\Bigg) \\
&+\,\epsilon^{\beta_1\gamma_1\mu_1}\left(\delta_{\beta_2\gamma_2}\delta_{\mu_2\mu_3}-\delta_{\beta_2\mu_2}\delta_{\gamma_2\mu_3}+\delta_{\beta_2\mu_3}\delta_{\gamma_2\mu_2}\right) \\
&\qquad\times\Bigg(\,3\,s_0^{\mu_1}(\vec r_1,\vec r_3)s_0^{\mu_2}(\vec r_2,\vec r_1)s_0^{\mu_3}(\vec r_3,\vec r_2) \\
&-\,s_1^{\mu_1}(\vec r_1,\vec r_3)s_0^{\mu_2}(\vec r_2,\vec r_1)s_1^{\mu_3}(\vec r_3,\vec r_2)\;-\;2\,s_0^{\mu_1}(\vec r_1,\vec r_3)s_1^{\mu_2}(\vec r_2,\vec r_1)s_1^{\mu_3}(\vec r_3,\vec r_2)\,\Bigg) \\
&+\,\epsilon^{\beta_1\gamma_1\mu_1}\delta_{\beta_2\gamma_2}\Bigg(-\,3\,s_0^{\mu_1}(\vec r_1,\vec r_3)\rho_0(\vec r_2,\vec r_1)\rho_0(\vec r_3,\vec r_2) \\
&+\,3\,s_0^{\mu_1}(\vec r_3,\vec r_2)\rho_0(\vec r_2,\vec r_1)\rho_0(\vec r_1,\vec r_3) \\
&+\,s_1^{\mu_1}(\vec r_1,\vec r_3)\rho_0(\vec r_2,\vec r_1)\rho_1(\vec r_3,\vec r_2)\;-\;s_1^{\mu_1}(\vec r_3,\vec r_2)\rho_0(\vec r_2,\vec r_1)\rho_1(\vec r_1,\vec r_3) \\
&-\,2\,s_1^{\mu_1}(\vec r_3,\vec r_2)\rho_1(\vec r_2,\vec r_1)\rho_0(\vec r_1,\vec r_3)\;+\;2\,s_0^{\mu_1}(\vec r_1,\vec r_3)\rho_1(\vec r_2,\vec r_1)\rho_1(\vec r_3,\vec r_2)\,\Bigg) \\
&+\,i\,\epsilon^{\beta_1\gamma_1\nu}\epsilon^{\beta_2\gamma_2\nu}\Bigg(\,3\rho_0(\vec r_2,\vec r_1)\rho_0(\vec r_1,\vec r_3)\rho_0(\vec r_3,\vec r_2) \\
&-\,2\,\rho_0(\vec r_1,\vec r_3)\rho_1(\vec r_3,\vec r_2)\rho_1(\vec r_2,\vec r_1) \\
&-\,\rho_0(\vec r_2,\vec r_1)\rho_1(\vec r_3,\vec r_2)\rho_1(\vec r_1,\vec r_3)\,\Bigg) \\
&+\,i\epsilon^{\beta_1\gamma_1\mu_1}\epsilon^{\beta_2\gamma_2\mu_2}\Bigg(\,s_1^{\mu_1}(\vec r_3,\vec r_2)s_1^{\mu_2}(\vec r_1,\vec r_3)\rho_0(\vec r_2,\vec r_1) \\
&-\,3\,s_0^{\mu_1}(\vec r_3,\vec r_2)s_0^{\mu_2}(\vec r_1,\vec r_3)\rho_0(\vec r_2,\vec r_1)
\end{aligned}$$

$$
\begin{aligned}
&+ 2\, s_1^{\mu_1}(\vec{r}_3,\vec{r}_2) s_0^{\mu_2}(\vec{r}_1,\vec{r}_3)\rho_1(\vec{r}_2,\vec{r}_1) \Big) \\
&- i\,\epsilon^{\beta_1\gamma_1\nu}\epsilon^{\beta_2\mu_1\nu} \Big(- s_1^{\mu_1}(\vec{r}_1,\vec{r}_3) s_1^{\gamma_2}(\vec{r}_3,\vec{r}_2)\rho_0(\vec{r}_2,\vec{r}_1) \\
&+ 3\, s_0^{\mu_1}(\vec{r}_1,\vec{r}_3) s_0^{\gamma_2}(\vec{r}_3,\vec{r}_2)\rho_0(\vec{r}_2,\vec{r}_1) \\
&- 2\, s_0^{\mu_1}(\vec{r}_1,\vec{r}_3) s_1^{\gamma_2}(\vec{r}_3,\vec{r}_2)\rho_1(\vec{r}_2,\vec{r}_1) \\
&- 3\, s_0^{\mu_1}(\vec{r}_1,\vec{r}_3) s_0^{\gamma_2}(\vec{r}_2,\vec{r}_1)\rho_0(\vec{r}_3,\vec{r}_2) \\
&+ s_1^{\mu_1}(\vec{r}_1,\vec{r}_3) s_0^{\gamma_2}(\vec{r}_2,\vec{r}_1)\rho_1(\vec{r}_3,\vec{r}_2) \\
&+ 3\, s_0^{\mu_1}(\vec{r}_3,\vec{r}_2) s_0^{\gamma_2}(\vec{r}_2,\vec{r}_1)\rho_0(\vec{r}_1,\vec{r}_3) \\
&- s_1^{\mu_1}(\vec{r}_3,\vec{r}_2) s_0^{\gamma_2}(\vec{r}_2,\vec{r}_1)\rho_1(\vec{r}_1,\vec{r}_3) \\
&- 2\, s_1^{\mu_1}(\vec{r}_3,\vec{r}_2) s_1^{\gamma_2}(\vec{r}_2,\vec{r}_1)\rho_0(\vec{r}_1,\vec{r}_3) \Big) \\
&- i\,\epsilon^{\beta_1\gamma_1\nu}\epsilon^{\gamma_2\mu_1\nu} \Big(- s_1^{\mu_1}(\vec{r}_3,\vec{r}_2) s_1^{\beta_2}(\vec{r}_1,\vec{r}_3)\rho_0(\vec{r}_2,\vec{r}_1) \\
&+ 3\, s_0^{\mu_1}(\vec{r}_3,\vec{r}_2) s_0^{\beta_2}(\vec{r}_1,\vec{r}_3)\rho_0(\vec{r}_2,\vec{r}_1) \\
&- 2\, s_1^{\mu_1}(\vec{r}_3,\vec{r}_2) s_0^{\beta_2}(\vec{r}_1,\vec{r}_3)\rho_1(\vec{r}_2,\vec{r}_1) \\
&- 3\, s_0^{\mu_1}(\vec{r}_2,\vec{r}_1) s_0^{\beta_2}(\vec{r}_1,\vec{r}_3)\rho_0(\vec{r}_3,\vec{r}_2) \\
&+ s_0^{\mu_1}(\vec{r}_2,\vec{r}_1) s_1^{\beta_2}(\vec{r}_1,\vec{r}_3)\rho_1(\vec{r}_3,\vec{r}_2) \\
&- 3\, s_0^{\mu_1}(\vec{r}_2,\vec{r}_1) s_0^{\beta_2}(\vec{r}_3,\vec{r}_2)\rho_0(\vec{r}_1,\vec{r}_3) \\
&+ s_0^{\mu_1}(\vec{r}_2,\vec{r}_1) s_1^{\beta_2}(\vec{r}_3,\vec{r}_2)\rho_1(\vec{r}_1,\vec{r}_3) \\
&+ 2\, s_1^{\mu_1}(\vec{r}_2,\vec{r}_1) s_0^{\beta_2}(\vec{r}_1,\vec{r}_3)\rho_1(\vec{r}_3,\vec{r}_2) \\
&+ 2\, s_0^{\mu_1}(\vec{r}_1,\vec{r}_3) s_1^{\beta_2}(\vec{r}_2,\vec{r}_1)\rho_1(\vec{r}_3,\vec{r}_2) \\
&+ 2\, s_1^{\mu_1}(\vec{r}_2,\vec{r}_1) s_1^{\beta_2}(\vec{r}_3,\vec{r}_2)\rho_0(\vec{r}_1,\vec{r}_3) \Big) \Big] . \qquad (9.375)
\end{aligned}
$$

For symmetric INM, this reduces to

$$
\langle V_{3N}^{\mathrm{HF,CR,2x,INM}} \rangle = -\left(\frac{g_A}{2f_\pi}\right)^2 \frac{c_4}{f_\pi^2}\,\frac{3}{8} \int d\vec{r}_1 d\vec{r}_2 d\vec{r}_3 \int \frac{1}{(2\pi)^6} d\vec{q}_2 d\vec{q}_3
$$

$$
\begin{aligned}
&\times e^{i\vec{q}_2\cdot(\vec{r}_2-\vec{r}_1)}\, e^{i\vec{q}_3\cdot(\vec{r}_3-\vec{r}_1)}\, \frac{q_2^{\beta_1} q_2^{\beta_2} q_3^{\gamma_1} q_3^{\gamma_2}}{(q_2^2+m_\pi^2)(q_3^2+m_\pi^2)} \\
&\times \left[\epsilon^{\beta_1\gamma_1\nu}\, \epsilon^{\beta_2\gamma_2\nu}\, \rho_0(\vec{r}_1,\vec{r}_3)\rho_0(\vec{r}_2,\vec{r}_1)\rho_0(\vec{r}_3,\vec{r}_2) \right],
\end{aligned}
\tag{9.376}
$$

while for unpolarized PNM, one has

$$
\begin{aligned}
\langle V_{3N}^{\mathrm{HF,CR,2x,PNM}} \rangle &= -\left(\frac{g_A}{2f_\pi}\right)^2 \frac{c_4}{f_\pi^2} \frac{3}{8} \int d\vec{r}_1 d\vec{r}_2 d\vec{r}_3 \int \frac{1}{(2\pi)^6} d\vec{q}_2 d\vec{q}_3 \\
&\quad \times e^{i\vec{q}_2\cdot(\vec{r}_2-\vec{r}_1)}\, e^{i\vec{q}_3\cdot(\vec{r}_3-\vec{r}_1)}\, \frac{q_2^{\beta_1} q_2^{\beta_2} q_3^{\gamma_1} q_3^{\gamma_2}}{(q_2^2+m_\pi^2)(q_3^2+m_\pi^2)} \\
&\quad \times \left[i3\, \epsilon^{\beta_1\gamma_1\nu}\, \epsilon^{\beta_2\gamma_2\nu}\, \rho_n(\vec{r}_1,\vec{r}_3)\rho_n(\vec{r}_2,\vec{r}_1)\rho_n(\vec{r}_3,\vec{r}_2) \right].
\end{aligned}
\tag{9.377}
$$

For time-reversal invariant systems, there is no appreciable reduction in the size of the expressions. Thus, we avoid repeating the expressions.

C-term contribution for specific systems

Combining the expressions for the direct, single and double-exchanges for the case of symmetric INM, the contribution of the C-term to the HF energy of symmetric INM becomes

$$
\begin{aligned}
\langle V_{3N}^{\mathrm{HF,C,INM}} \rangle &= \left(\frac{g_A}{2f_\pi}\right)^2 \frac{1}{16} \int d\vec{r}_1 d\vec{r}_2 d\vec{r}_3 \int \frac{1}{(2\pi)^6} d\vec{q}_2 d\vec{q}_3\, e^{i\vec{q}_2\cdot(\vec{r}_2-\vec{r}_1)}\, e^{i\vec{q}_3\cdot(\vec{r}_3-\vec{r}_1)} \\
&\quad \times \frac{q_2^{\beta_1} q_3^{\gamma_1}}{(q_2^2+m_\pi^2)(q_3^2+m_\pi^2)} \left[\left(-4\frac{c_1 m_\pi^2}{f_\pi^2} + 2\frac{c_3}{f_\pi^2} \vec{q}_2\cdot\vec{q}_3 \right) \right. \\
&\quad \times \Big(-6\, \delta_{\beta_1\gamma_1}\, \rho_0(\vec{r}_1)\rho_0(\vec{r}_3,\vec{r}_2)\rho_0(\vec{r}_2,\vec{r}_3) \\
&\qquad + 3\, \delta_{\beta_1\gamma_1}\, \rho_0(\vec{r}_1,\vec{r}_3)\rho_0(\vec{r}_2,\vec{r}_1)\rho_0(\vec{r}_3,\vec{r}_2) \Big) \\
&\quad \left. - 6\frac{c_4}{f_\pi^2}\, \epsilon^{\beta_1\gamma_1\nu} \epsilon^{\beta_2\gamma_2\nu}\, q_2^{\beta_2} q_3^{\gamma_2}\, \rho_0(\vec{r}_1,\vec{r}_3)\rho_0(\vec{r}_2,\vec{r}_1)\rho_0(\vec{r}_3,\vec{r}_2) \right].
\end{aligned}
\tag{9.378}
$$

The contribution of the C-term to the HF energy of unpolarized PNM becomes

$$
\begin{aligned}
\langle V_{3N}^{\mathrm{HF,C,PNM}} \rangle \;=\;& \left(\frac{g_A}{2f_\pi}\right)^2 \frac{1}{16} \int d\vec{r}_1 d\vec{r}_2 d\vec{r}_3 \int \frac{1}{(2\pi)^6} d\vec{q}_2 d\vec{q}_3\, e^{i\vec{q}_2\cdot(\vec{r}_2-\vec{r}_1)}\, e^{i\vec{q}_3\cdot(\vec{r}_3-\vec{r}_1)} \\
&\times \frac{q_2^{\beta_1} q_3^{\gamma_1}}{(q_2^2+m_\pi^2)(q_3^2+m_\pi^2)} \Bigg[\left(-4\frac{c_1 m_\pi^2}{f_\pi^2} + 2\frac{c_3}{f_\pi^2}\vec{q}_2\cdot\vec{q}_3\right) \\
&\times \Bigg(-6\,\delta_{\beta_1\gamma_1}\, \rho_n(\vec{r}_1)\rho_n(\vec{r}_3,\vec{r}_2)\rho_n(\vec{r}_2,\vec{r}_3) \\
&\qquad + 3\,\delta_{\beta_1\gamma_1}\, \rho_n(\vec{r}_1,\vec{r}_3)\rho_n(\vec{r}_2,\vec{r}_1)\rho_n(\vec{r}_3,\vec{r}_2) \Bigg) \\
&- 6\frac{c_4}{f_\pi^2}\, \epsilon^{\beta_1\gamma_1\nu}\epsilon^{\beta_2\gamma_2\nu}\, q_2^{\beta_2} q_3^{\gamma_2}\, \rho_n(\vec{r}_1,\vec{r}_3)\rho_n(\vec{r}_2,\vec{r}_1)\rho_n(\vec{r}_3,\vec{r}_2) \Bigg]. \qquad (9.379)
\end{aligned}
$$

For time-reversal invariant systems, the HF energy contribution from the C-term is given by the sum of the direct, single and double-exchanges. Since there is no appreciable reduction in the complexity of the expressions even after the assumption of time-reversal invariance, the expressions are not reproduced here.

9.10 Symbolic derivation of EDF-NNN-DME for time-reversal invariance

In this section, we discuss some of the ingredients of the symbolic derivation of EDF-NNN-DME, i.e. the EDF that we obtain after the application of the DME to the HF energy from chiral EFT NNN interaction at N^{2}LO. The derivation is performed for time-reversal invariant systems. This should be kept in mind in subsequent discussions. In the final step which involves angular integrations, we assume spherical symmetry, which also implies time-reversal invariance. The symbolic steps required to relax this assumption and treat deformed time-reversal invariant systems is discussed in appendix 9.10.5. For the complete detail of the symbolic derivation, refer to Ref. [161].

9.10.1 Generic DME ansatz

In section 7.2.4, we discussed the merits of the symbolic derivation of EDF-NNN-DME starting from a generic DME ansatz. Here, we develop the generic ansatz for the basic nonlocal densities $\varsigma^{\mu 1}(\vec{r}_1, \vec{r}_1 + \vec{x}_3)$, $\varsigma^{\mu 2}(\vec{r}_1 + \vec{x}_2, \vec{r}_1)$ and $\varsigma^{\mu 3}(\vec{r}_1 + \vec{x}_3, \vec{r}_1 + \vec{x}_2)$. These non-local densities can be scalar/vector, isoscalar/isovector. The basic objective of the DME ansatz is to approximate each of these non-local densities in terms of local densities, dependent on $\vec{r}_1$, and $\pi-$functions which can depend on $\vec{x}_2$ and/or $\vec{x}_3$.

In developing the DME ansatz for these nonlocal densities, we follow the same scheme as in section 5.3.6 where we relied on short-range/Taylor series expansion of the nonlocal densities. However, the formal expansion that is given in appendix 9.5.7 in relation to the application of the DME to the HF energy from NN interactions cannot be used. With the aim of implementing the symbolic machinery in the most general way, the DME ansatz we need at this point should be general and complex enough so that it can be adopted to different special cases. For instance, for the analytical coupling calculation discussed in section 9.11, we adopted the generalized PSA-DME. This will have the benefit of minimizing the effort required to implement a different approximation of the nonlocal densities and obtain a new EDF (perhaps both in form and couplings).

Imagine one wants to build an expansion scheme for $\varsigma^{\mu 1}(\vec{r}_1, \vec{r}_1 + \vec{x}_3)$. In this case, we have a single nonlocality coordinate, $\vec{x}_3$. The simplest route to a possible ansatz is one that applies Taylor series to the density about $\vec{r}_1$

$$\varsigma^{\mu 1}(\vec{r}_1, \vec{r}_1 + \vec{x}_3) \sim \varsigma^{\mu 1}(\vec{r}_1) + \vec{x}_3 \cdot \vec{\nabla}' \varsigma^{\mu 1}(\vec{r}_1, \vec{r}')\Big|_{\vec{r}'=\vec{r}_1} + \frac{1}{2}\left(\vec{x}_3 \cdot \vec{\nabla}'\right)^2 \varsigma^{\mu 1}(\vec{r}_1)\Big|_{\vec{r}'=\vec{r}_1} , \tag{9.380}$$

where we truncated the expansion at second order, and hence we generalize it to

$$\begin{aligned} \varsigma^{\mu_1}(\vec{r}_1, \vec{r}_1 + \vec{x}_3) \;\simeq\;& \Pi^{\varsigma_1,0}(\Omega)\,\varsigma^{\mu_1}(\vec{r}_1) + \Pi^{\varsigma_1,1}(\Omega)\,\vec{x}_3 \cdot \vec{\nabla}'\varsigma^{\mu_1}(\vec{r}_1, \vec{r}\,')\Big|_{\vec{r}\,'=\vec{r}_1} \\ &+ \frac{1}{2}\Pi^{\varsigma_1,2}(\Omega)\left(\vec{x}_3 \cdot \vec{\nabla}'\right)^2 \varsigma^{\mu_1}(\vec{r}_1)\Big|_{\vec{r}\,'=\vec{r}_1} \;. \end{aligned} \tag{9.381}$$

Needless to say, the π–functions and Ω in Eqs. (9.381) are to be fixed by the choosen analytical/parameterized DME scheme. But, this route does not lead to the most general form of the ansatz. Rather, we follow a circuitous way which leads to a general ansatz with which Eq. (9.381), for example, can be recovered as a special case. Note that if we write $\varsigma^{\mu_1}(\vec{r}_1, \vec{r}_1 + \vec{x}_3)$ as $\varsigma^{\mu_1}(\vec{R} + \vec{r}/2, \vec{R} - \vec{R}/2)$, where $\vec{R} = \vec{r} + 1/2\vec{x}_3$ and $\vec{r} = -\vec{x}_3$, we can apply the DME derived in section 5.3. In order to arrive at a final expression which is separable in $\vec{r}_1$ and $\vec{x}_3$, we perform a short-range expansion (Taylor series) and truncate beyond second-order terms. Performing these set of steps yields

$$\begin{aligned} \varsigma^{\mu_1}(\vec{r}_1, \vec{r}_1 + \vec{x}_3) \;\simeq\;& \Pi_0^{\mu_1}(kx_3)\Big[\pi_0^{\mu_1,0}(kx_3)\varsigma^{\mu_1}(\vec{r}_1) + \frac{1}{2}\,\pi_1^{\mu_1,0}(kx_3)\vec{x}_3 \cdot \vec{\nabla}\varsigma^{\mu_1}(\vec{r}_1) \\ &\qquad + \frac{1}{8}\,\pi_2^{\mu_1,0}(kx_3)\left(\vec{x}_3 \cdot \vec{\nabla}\right)^2 \varsigma^{\mu_1}(\vec{r}_1)\Big] \\ &- \; i\,\Pi_1^{\mu_1}(kx_3)\,x_3^{\nu_1}\Big[\pi_0^{\mu_1,1}(kx_3)\varsigma_1^{\mu_1,\nu_1}(\vec{r}_1) \\ &\qquad + \frac{1}{2}\,\pi_1^{\mu_1,1}(kx_3)\vec{x}_3 \cdot \vec{\nabla}\varsigma_1^{\mu_1,\nu_1}(\vec{r}_1) \\ &\qquad + \frac{1}{8}\,\pi_2^{\mu_1,1}(kx_3)\left(\vec{x}_3 \cdot \vec{\nabla}\right)^2 \varsigma_1^{\mu_1,\nu_1}(\vec{r}_1)\Big] \\ &+ \; \frac{1}{24}\,\Pi_2^{\mu_1}(kx_3)x_3^2\varsigma_2^{\mu_1}(\vec{r}_1)\,, \end{aligned} \tag{9.382}$$

and the same form holds for $\varsigma^{\mu_1}(\vec{r}_1, \vec{r}_1 + \vec{x}_2)$ after replacing $\vec{x}_3$ with $\vec{x}_2$. While

$$\varsigma^{\mu_2}(\vec{r}_1 + \vec{x}_2, \vec{r}_1) \;=\; \varsigma^{\mu_2 *}(\vec{r}_1, \vec{r}_1 + \vec{x}_2)\;,$$

$$\varsigma^{\mu 2}(\vec{r}_1 + \vec{x}_3, \vec{r}_1) \;=\; \varsigma^{\mu 2\,*}(\vec{r}_1, \vec{r}_1 + \vec{x}_3) \;, \tag{9.383}$$

by time-reversal invariance. Hence, the corresponding ansatz is the same as the one in Eq.(9.382) as all quantities are real for the case of time-reversal invariant systems. $\varsigma^{\mu 3}(\vec{r}_1 + \vec{x}_3, \vec{r}_1 + \vec{x}_2)$ has two nonlocality coordinates. Still, the set of steps applied to arrive at Eq. (9.382) can be applied to obtain

$$\begin{aligned}
\varsigma^{\mu 3}(\vec{r}_1 + \vec{x}_3, \vec{r}_1 + \vec{x}_2) \;\simeq\;& \Pi^{\mu 3}_{0,fr}(k, \vec{x}_2, \vec{x}_3)\left[\varsigma^{\mu 3}(\vec{r}_1) + \frac{1}{2}\left(\vec{x}_2 + \vec{x}_3\right)\cdot\vec{\nabla}\varsigma^{\mu 3}(\vec{r}_1)\right.\\
&\left. + \frac{1}{8}\left(\left(\vec{x}_2 + \vec{x}_3\right)\cdot\vec{\nabla}\right)^2 \varsigma^{\mu 3}(\vec{r}_1)\right]\\
-\;& i\,\Pi^{\mu 3}_{1,fr}(k, \vec{x}_2, \vec{x}_3)\left(x_2^{\nu 1} - x_3^{\nu 1}\right)\\
&\times\left[\varsigma_1^{\mu 3,\nu 1}(\vec{r}_1) + \frac{1}{2}\left(\vec{x}_2 + \vec{x}_3\right)\cdot\vec{\nabla}\varsigma_1^{\mu 3,\nu 1}(\vec{r}_1)\right.\\
&\left. + \frac{1}{8}\left(\left(\vec{x}_2 + \vec{x}_3\right)\cdot\vec{\nabla}\right)^2 \varsigma_1^{\mu 3,\nu 1}(\vec{r}_1)\right]\\
+\;& \frac{1}{24}\,\Pi^{\mu 2}_{2,fr}(k, \vec{x}_2, \vec{x}_3)\left(x_2^2 + x_3^2 - 2\vec{x}_2\cdot\vec{x}_3\right)\varsigma_2^{\mu 3}(\vec{r}_1)\,.
\end{aligned} \tag{9.384}$$

Unlike the $\pi-$functions discussed so far, $\Pi^{\mu 3}_{i,fr}$ are not manifestly separable in $\vec{x}_2$ and $\vec{x}_3$ and in fact depend on the relative orientation of the two vectors. This has an important implication for the analytical calculation of the couplings. Refer to section 9.11.

Key points on the DME ansatz

One notes that in the generic DME expansions given in Eqs.(9.382)-(9.384), each nonlocal density can be either $\rho_{0/1}$ or $\vec{s}_{0/1}$. To recap the notations used in the Eq.(9.382)-(9.384), for example, $\varsigma_1^{\mu 1,\nu 1}$ refers to the local cartesian tensor spin-current density that results at first order gradient with respect to the relative gradient operator. To elaborate on this point, consider the ansatz as applied to $\rho_0(\vec{r}_1, \vec{r}_1 + \vec{x}_3)$. The resulting expansion reads

$$
\begin{aligned}
\rho_0(\vec{r}_1, \vec{r}_1 + \vec{x}_3) \;\; \simeq \;\; & \Pi_0^{\rho}(kx_3)\Bigg[\pi_0^{\rho}(kx_3)\rho_0(\vec{r}_1) + \frac{1}{2}\,\pi_1^{\rho}(kx_3)\vec{x}_3 \cdot \vec{\nabla}\rho_0(\vec{r}_1) \\
& \qquad + \frac{1}{8}\,\pi_2^{\rho}(kx_3)\left(\vec{x}_3 \cdot \vec{\nabla}\right)^2 \rho_0(\vec{r}_1)\Bigg] \\
- \;\; & i\,\Pi_1^{\rho}(kx_3)\, x_3^{\nu 1}\Bigg[\pi_0^{\vec{j}}(kx_3) j_1^{\nu 1}(\vec{r}_1) + \frac{1}{2}\,\pi_1^{\vec{j}}(kx_3)\vec{x}_3 \cdot \vec{\nabla} j^{\nu 1}(\vec{r}_1) \\
& \qquad + \frac{1}{8}\,\pi_2^{\vec{j}}(kx_3)\left(\vec{x}_3 \cdot \vec{\nabla}\right)^2 j_1^{\nu 1}(\vec{r}_1)\Bigg] \\
+ \;\; & \frac{1}{24}\,\Pi_2^{\rho}(kx_3) x_3^2\, \varsigma_2^{\mu 1}(\vec{r}_1)\,. \qquad (9.385)
\end{aligned}
$$

Hence, in the case where $\varsigma^{\mu 1} = \rho_{0/1}$, then $\varsigma_1^{\mu 1, \nu 1} = j_{0/1}^{\nu 1}$, i.e. the current density. Since we are dealing with time-reversal invariant systems, $\vec{j}_{0/1} = \vec{0}$. However, we did not set it to zero in Eqs. (9.382)-(9.383) as we wrote the equation to hold for both scalar and vector densities, and when $\varsigma^{\mu 1} = \vec{s}_{0/1}$, then $\varsigma_1^{\mu 1, \nu 1} = J_{0/1, \mu_1 \nu_1}$, i.e. cartesian tensor spin-current density. As to $\varsigma_2^{\mu 1}$ in Eq .(9.385) and in general, it refers to a second order correction term in the expansion. It is analogous[3] to $\frac{1}{4}\Delta\rho - \tau + 3/5\, k_F^2\, \rho$ of the DME discussed in section 5.3.3. Obviously, $\varsigma_2^{\mu 1} = 0$ in the case where $\varsigma^{\mu 1} = \vec{s}_{0/1}$. The same notation applies to $\varsigma^{\mu 2}$ and $\varsigma^{\mu 3}$.

Even though all notations and conventions have been explicitly given in Table 1.2, we recap the ones used for the $\pi-$functions. Taking $\varsigma^{\mu 1}$ as an example, $\pi_0^{\mu 1, 0}, \pi_1^{\mu 1, 0}, \pi_2^{\mu 1, 0}$ refer to the $\pi-$functions of the local part of the non-local density $\varsigma^{\mu 1}$ and $\pi_0^{\mu 1, 1}, \pi_1^{\mu 1, 1}, \pi_2^{\mu 1, 1}$ refer to the zeroth, first and second $\pi-$functions for the local density that appears at first order with respect to the relative gradient operator. Hence, these $\pi-$functions are equal to $\pi_0^{\rho}, \pi_1^{\rho}, \pi_2^{\rho}, \pi_0^{\vec{j}}, \pi_1^{\vec{j}}, \pi_2^{\vec{j}}$ or $\pi_0^{\vec{s}}, \pi_1^{\vec{s}}, \pi_2^{\vec{s}}, \pi_0^{J}, \pi_1^{J}, \pi_2^{J}$ when $\varsigma^{\mu 1} = \rho_{0/1}$ or $\varsigma^{\mu 2} = \vec{s}_{0/1}$ respectively. The example given in Eq.(9.385) illustrates this statement explicitly. Since we are dealing with time-reversal invariant systems, $\pi_0^{\vec{s}}, \pi_1^{\vec{s}}, \pi_2^{\vec{s}}, \pi_0^{\vec{j}}, \pi_1^{\vec{j}}, \pi_2^{\vec{j}}$ are irrelevant. $\Pi_0^{\mu_i}$ and $\Pi_1^{\mu_i}$ can be seen as some common prefactors while $\Pi_2^{\mu_i}$ is the $\pi-$function of the second order correction.

---

[3] It does not mean they are the same.

Comments on the DME ansatz

The following comments are at play concerning the DME ansatz: (i) The ansatz is designed to be a general template on which all the known (and perhaps future) analytical/parameterized DMEs can be mapped. This can be done by setting the various $\pi-$functions to the values dictated by the analytical/parameterized DME at hand. This allows for a minimal effort to adopt the symbolic machinery to specific cases. (ii) As mentioned at the beginning of this section, any discrepancy between the EDF that results after the application of the DME, and the exact NNN HF energy is solely due to the DME ansatz of the nonlocal densities and the $\pi-$functions. This is a trivial statement in the case of two-body interactions. However, it is not so for three-body interactions as unless one makes a convenient coordinate choice, it is not trivial to treat even the non-DME part exactly. Thus, by improving the $\pi-$functions, one can hope to get better and better accuracy.

9.10.2 The G-tensors and their analytical forms

In sections 7.2.1- 7.2.1, we identified the three generic forms (Eqs. (9.406)-(7.2.1)) of the terms that occur in the HF energy from the chiral EFT NNN interaction at N^{2}LO. We refer to the interaction form factors that enter these equations as G-tensors. They are of the form

$$G^{\beta_1\gamma_1\beta_2\gamma_2}(x_2, x_3, q_2, q_3, \omega) \equiv \int d\Omega_{q_2} d\Omega_{q_3}\, e^{i\vec{q}_2\cdot\vec{x}_2} e^{i\vec{q}_3\cdot\vec{x}_3} \frac{q_2^{\beta_1} q_3^{\gamma_1} q_2^{\beta_2} q_3^{\gamma_2}}{(q_2^2+m_\pi^2)(q_3^2+m_\pi^2)}, \tag{9.386}$$

$$G^{\beta\gamma}(x_2, x_3, q_2, q_3, \omega) \equiv \int d\Omega_{q_2} d\Omega_{q_3}\, e^{i\vec{q}_2\cdot\vec{x}_2} e^{i\vec{q}_3\cdot\vec{x}_3} \frac{q_2^\beta q_3^\gamma}{(q_2^2+m_\pi^2)(q_3^2+m_\pi^2)}, \tag{9.387}$$

$$\bar{G}^{\beta\gamma}(\vec{x}_3, q_3) \equiv \int d\Omega_{q_3}\, e^{i\vec{q}_3\cdot\vec{x}_3} \frac{q_3^\beta q_3^\gamma}{q_3^2+m_\pi^2}, \tag{9.388}$$

where $d\Omega_{q_2}$ and $d\Omega_{q_3}$ refer to the differential solid angles of the two vectors, and ω is the angle between $\vec{x}_2$ and $\vec{x}_3$. In the following, we derive the analytical forms of these tensors. Indices $\beta_1, \gamma_1, \beta_2, \gamma_2$ can take values $\{1, 2, 3\}$ corresponding to the cartesian labels $\{x, y, z\}$. To obtain the analytical form for $G^{\beta_1\gamma_1\beta_2\gamma_2}(x_2, x_3, q_2, q_3, \omega)$, we define

$$F^{\beta\gamma}(\vec{x}, q) \equiv \int d\Omega_q e^{i\vec{q}.\vec{x}} \frac{q^\beta q^\gamma}{q^2+m_\pi^2}. \tag{9.389}$$

In the case where the vector $\vec{x}$ is along the $\hat{z}$ direction, we denote the $F^{\beta\gamma}(\vec{x}, q)$ tensor as $F_z^{\beta\gamma}(\vec{x}, q)$, which equals

$$F_z^{\beta\gamma}(\vec{x}, q) = \delta_{\beta\gamma} \int d\Omega_q e^{i\vec{q}.\vec{x}} \frac{q^\beta q^\beta}{q^2+m_\pi^2}. \tag{9.390}$$

Denoting $F_z^{11} \equiv F_z^{\mathrm{xx}}, F_z^{22} \equiv F_z^{\mathrm{yy}}, F_z^{33} \equiv F_z^{\mathrm{zz}}$, we obtain

$$F_z^{xx}(x, q) = -4\pi \frac{q^2}{q^2+m_\pi^2} \frac{j_1(qx)}{(qx)}, \tag{9.391}$$

$$F_z^{yy}(x, q) = -4\pi \frac{q^2}{q^2+m_\pi^2} \frac{j_1(qx)}{(qx)}, \tag{9.392}$$

$$F_z^{zz}(x, q) = \frac{q^2}{q^2+m_\pi^2} \left(2\pi\, j_0(qx) - 4\pi \frac{j_1(qx)}{(qx)}\right). \tag{9.393}$$

Next, we need to define a convenient coordinate system. If one could define both $\hat{x}_2$ and $\hat{x}_3$ to be along the $\hat{z}$ direction of the coordinate system, the G-tensor could be calculated very easily. But in the actual case, one cannot, in general, define both $\hat{x}_2$ and $\hat{x}_3$ to be along the $\hat{z}$ direction. Let $\vec{x}_2$ be such that it is along the $\hat{z}$ direction and

$\hat{x}_3$ be in the $x-z$ plane, with angle ω between $\hat{x}_2$ and $\hat{x}_3$. Next, write

$$\begin{aligned} G^{\beta_1\gamma_1\beta_2\gamma_2}(x_2,x_3,q_2,q_3,\omega) &= F^{\beta_1\beta_2}(\vec{x}_2,q_2)\,F^{\gamma_1\gamma_2}(\vec{x}_3,q_3) \\ &= \delta_{\beta_1\beta_2}\,F_z^{\beta_1\beta_1}(x_2,q_2)\,F^{\gamma_1\gamma_2}(x_3,q_3,\omega)\,, \quad (9.394) \end{aligned}$$

where due to the specific coordinate system chosen, the G-tensor will be nonzero only when $\beta_1 = \beta_2$. The same cannot be said about γ_1 and γ_2. In the next step, we concentrate on $F^{\gamma_1\gamma_2}(x_3,q_3,\omega)$. One can calculate this quantity by performing a few steps involving rotation of the coordinate system. Hence, rotate the coordinate system with respect to the y-axis such that $\hat{x}_3$ aligns with the new $\hat{z}'$ axis. The rotation matrix for this operation reads

$$R(\omega) = \begin{pmatrix} \cos(\omega) & 0 & -\sin(\omega) \\ 0 & 1 & 0 \\ \sin(\omega) & 0 & \cos(\omega) \end{pmatrix}.$$

The transformation of the various terms of $F^{\gamma_1\gamma_2}$ is (obviously only the vectors get affected)

$$\begin{aligned} e^{i\vec{q}_3\cdot\vec{x}_3} &\Rightarrow e^{i\vec{q}_3'\cdot\vec{x}_3'} \\ \vec{q} &\Rightarrow R^{-1}\vec{q}_3'\,, \end{aligned} \quad (9.395)$$

where we have left out other trivial terms. Using these intermediate results

$$F^{\gamma_1\gamma_2}(x_3,q_3,\omega) = \delta_{\mu_1\mu_2}\,R^{-1}_{\mu_1\gamma_1}(\omega)\,R^{-1}_{\mu_2\gamma_2}(\omega)\,F_z^{\mu_1\mu_2}(x_3,q_3)\,. \quad (9.396)$$

Plugging this result into Eq. (9.394), one obtains the analytical form

$$G^{\beta_1\gamma_1\beta_2\gamma_2}(x_2, x_3, q_2, q_3, \omega) = \delta_{\beta_1\beta_2} R^{-1}_{\mu\gamma_1}(\omega) R^{-1}_{\mu\gamma_2}(\omega) F_z^{\beta_1\beta_1}(x_2, q_2) F_z^{\mu\mu}(x_3, q_3) . \tag{9.397}$$

To calculate the related but different G tensor, $G^{\beta\gamma}(x_2, x_3, q_2, q_3, \omega)$, we define

$$F^{\beta}(\vec{x}, q) = \int d\Omega_q e^{i\vec{q}.\vec{x}} \frac{q^\beta}{q^2 + m_\pi^2} . \tag{9.398}$$

We represent the case where the vector $\vec{x}$ is along the z axis by $F_z^\beta(\vec{x}, q)$

$$F_z^\beta(\vec{x}, q) = \delta_{3\beta} \int d\Omega_q e^{i\vec{q}.\vec{x}} \frac{q^\beta}{q^2 + m_\pi^2} , \tag{9.399}$$

where $\delta_{3\beta} \equiv \delta_{z\beta}$ and representing $F_z^1 \equiv F_z^{\mathrm{x}}, F_z^2 \equiv F_z^{\mathrm{y}}, F_z^3 \equiv F_z^{\mathrm{z}}$, we obtain

$$F_z^x(x, q) = 0 , \tag{9.400}$$

$$F_z^y(x, q) = 0 , \tag{9.401}$$

$$F_z^z(x, q) = i\, 4\pi \frac{q}{q^2 + m_\pi^2} j_1(qx) . \tag{9.402}$$

$$\tag{9.403}$$

Plugging this result

$$G^{\beta\gamma}(x_2, x_3, q_2, q_3, \omega) = \delta_{3\beta}\, \delta_{3\mu}\, R^{-1}_{\mu\gamma}(\omega) F_z^\beta(x_2, q_2) F_z^\mu(x_3, q_3). \tag{9.404}$$

Finally, we have a trivial tensor $\bar{G}$ defined in Eq.(9.388) is given by

$$\bar{G}^{\beta\gamma}(\vec{x}, q) \equiv F^{\beta\gamma}(\vec{x}, q) . \tag{9.405}$$

9.10.3 Sample DME simplification

After the specification of the DME ansatz and the analytical calculation of the G-tensors, the next logical step is to plug them into the respective exact HF energy terms to obtain the EDF. We discuss the DME simpification by considering a term that has the form of Generic-Form-1. Consider

$$\begin{aligned}\langle V_{3N}^{\mathrm{HF},G1,\rho_0\rho_0\rho_0}\rangle &= \int d\vec{r}_1 d\vec{r}_2 d\vec{r}_3\, dq_2\, dq_3\, q_2^2\, q_3^2\, G^{\beta_1\gamma_1\beta_2\gamma_2}(x_2, x_3, q_2, q_3, \omega) \\ &\quad \times \delta_{\beta_1\gamma_1}\, \delta_{\beta_2\gamma_2}\, \rho_0(\vec{r}_1, \vec{r}_3)\rho_0(\vec{r}_2, \vec{r}_1)\rho_0(\vec{r}_3, \vec{r}_2)\,, \qquad (9.406)\end{aligned}$$

where we recap that ω is the angle between $\vec{x}_2$ and $\vec{x}_3$. According to the description given in section 7.2.1, this means, Eq. (9.406) corresponds to a case of Eq. (7.2.1) where $c_1 = 0$, $c_2 = 0$ $c_3 = 1$ and

$$\begin{aligned}\varsigma^{\mu_1}(\vec{r}_1, \vec{r}_3) &= \rho_0(\vec{r}_1, \vec{r}_3)\,, \\ \varsigma^{\mu_2}(\vec{r}_3, \vec{r}_1) &= \rho_0(\vec{r}_3, \vec{r}_1)\,, \\ \varsigma^{\mu_3}(\vec{r}_2, \vec{r}_1) &= \rho_0(\vec{r}_2, \vec{r}_1)\,, \\ T^{\mu_1\mu_2\mu_3}_{\beta_1\gamma_1\beta_2\gamma_2} &= \delta_{\beta_1\gamma_1}\, \delta_{\beta_2\gamma_2}\,, \qquad (9.407)\end{aligned}$$

where due to there being only scalar densities, the tensor $T^{\mu_1\mu_2\mu_3}_{\beta_1\gamma_1\beta_2\gamma_2}$ is independent of $\{\mu_1, \mu_2, \mu_3\}$. Refer to section 7.2.1 for the explanation of this notation. Plugging the DME ansatz discussed in the previous section, and noting that $\vec{j}_q(\vec{r}_1) = 0$ for time-reversal invariant systems, one obtains

$$\begin{aligned}\langle V_{3N}^{\mathrm{HF},G1,\rho_0\rho_0\rho_0}\rangle &\simeq \int d\vec{r}_1 d\vec{x}_2 d\vec{x}_3\, dq_2\, dq_3\, q_2^2 q_3^2\, G^{\beta_1\gamma_1\beta_2\gamma_2}(x_2, x_3, q_2, q_3, \omega)\, \delta_{\beta_1\gamma_1}\, \delta_{\beta_2\gamma_2} \\ &\quad \times \Bigg(\Pi_0^{\rho}(kx_2)\bigg[\pi_0^{\rho}(kx_2)\rho_0(\vec{r}_1) + \frac{1}{2}\,\pi_1^{\rho}(kx_2)\vec{x}_3 \cdot \vec{\nabla}\rho_0(\vec{r}_1) \\ &\qquad + \frac{1}{8}\,\pi_2^{\rho}(kx_2)\Big(\vec{x}_2 \cdot \vec{\nabla}\Big)^2 \rho_0(\vec{r}_1)\bigg]\end{aligned}$$

$$
\begin{aligned}
&\qquad +\frac{1}{24}\,\Pi_2^{\mu 1}(kx_2)\,x_2^2\,\varsigma_0^2(\vec{r}_1)\biggr) \\
\times\quad &\biggl(\Pi_0^{\rho}(kx_3)\biggl[\pi_0^{\rho}(kx_3)\rho_0(\vec{r}_1)+\frac{1}{2}\,\pi_1^{\rho}(kx_3)\vec{x}_3\cdot\vec{\nabla}\rho_0(\vec{r}_1) \\
&\qquad +\frac{1}{8}\,\pi_2^{\rho}(kx_3)\Bigl(\vec{x}_3\cdot\vec{\nabla}\Bigr)^2\rho_0(\vec{r}_1)\biggr] \\
&\qquad +\frac{1}{24}\,\Pi_2^{\mu 1}(kx_3)\,x_3^2\,\varsigma_0^2(\vec{r}_1)\biggr) \\
\times\quad &\biggl(\Pi_{0,fr}^{\rho}(k,\vec{x}_2,\vec{x}_3)\biggl(\rho_0(\vec{r}_1)\,+\,\frac{1}{2}\,(\vec{x}_2+\vec{x}_3)\cdot\vec{\nabla}\rho_0(\vec{r}_1) \\
&\qquad +\frac{1}{8}\,\bigl((\vec{x}_2+\vec{x}_3)\cdot\vec{\nabla}\bigr)^2\rho_0(\vec{r}_1)\biggr) \\
&\qquad +\frac{1}{24}\Pi_{2,fr}^{\rho}(k,\vec{x}_2,\vec{x}_3)\,(x_2^2+x_3^2-2\vec{x}_2\cdot\vec{x}_3)\,\varsigma_0^2(\vec{r}_1)\biggr)\,,
\end{aligned}
\tag{9.408}
$$

where $\varsigma_0^2(\vec{r}_1)$ is the second-order correction density in the DME of the scalar density with the given coordinates. For instance, the generalized PSA-DME discussed in appendix 9.5.3 sets this correction density as

$$
\varsigma_0^2(\vec{r}_1) \;=\; \frac{1}{2}\,\Delta\rho_0(\vec{r}_1)-\tau_0(\vec{r}_1)+\frac{3}{5}\,k_F^2\rho_0(\vec{r}_1)\,. \tag{9.409}
$$

The expressions given in appendix 9.9 show that we already have a very large number of terms in the exact HF energy, even for time-reversal invariant systems. The application of the DME increases the number of terms by at least an order of magnitude, further ruling out any hope for manual simplification. The next step in the symbolic simplification involves angular integrations with respect to the orientation of $\vec{x}_2$ and $\vec{x}_3$.

Angular integrations for spherical systems

From our sample DME simplification given in Eq. (9.408), it can be seen that we can perform the angular integrations with respect to the orientations of $\vec{x}_2$ and $\vec{x}_3$

if we solve one remaining problem. I.e. obtain a separable expression for the $\Pi^{\rho}_{i,fr}$ $\pi-$functions that couple $\vec{x}_2$ and $\vec{x}_3$. This holds for all $\Pi^{\mu i}_{j,fr}$ $\pi-$functions used in the DME ansatz of $\varsigma^{\mu i}(\vec{r}_1 + \vec{x}_2, \vec{r}_1 + \vec{x}_2)$, given in Eq. (9.384). Within the symbolic approach, we solve this problem by expanding these problematic $\pi-$functions as

$$\Pi^{\varsigma}_{i,fr}(k, \vec{x}_2, \vec{x}_3) \approx \sum_{n=0}^{nmax} \left[\sum_{m=0}^{mmax(n)} f^{\varsigma,i}_{n\,m}(kx_2)\, g^{\varsigma,i}_{n\,m}(kx_3) \right] (\hat{x}_2 \cdot \hat{x}_3)^n , \qquad (9.410)$$

where $f^{\varsigma,i}_{n\,m}(kx_2)$ and $g^{\varsigma,i}_{n\,m}(kx_3)$ are unspecified scalar functions and the number of terms in the inner summation depends on the value of n, expressed as $(m_{max}(n))$. Note that the angular integrations (with respect to $\vec{x}_2$ and $\vec{x}_3$) do not require the values of $f^{\varsigma,i}_{n\,m}(kx_2)$ and $g^{\varsigma,i}_{n\,m}(kx_3)$ to be specified. In addition, the special symbolic technique that we developed, Ref. [161], helped us avoid specifying $m_{max}(n)$ which is not known anyways. As to n_{max}, we found that $n_{max} = 5$ suffices in the practical implementation [161]. In section 9.11.3, we discuss how these scalar functions are obtained for $\Pi^{\varsigma}_{i,fr}$ derived from the generalized PSA-DME. In addition, we show that at $n_{max} \geq 5$, Eq. (9.410) becomes practically exact for these $\pi-$functions. Actually, one can increase n_{max} for any $\Pi^{\varsigma}_{i,fr}$ if there is a need. The only problem with increasing n_{max} to a much higher value is the rapid increase in the time-complexity of the symbolic computation. Similar to the application of the DME (ansatz) to the exact HF energy, the expansion of $\Pi^{\varsigma}_{i,fr}$ introduces yet another increase in the number of terms to simplify.

With this expansion at hand, we are able to perform the angular integrations with respect to $\vec{x}_2$ and $\vec{x}_3$. At this point, due to the complexity of the problem, we introduce the assumption of spherical symmetry. This implies that all the local densities depend only on the magnitude of the radial vector. In other words, we now have only three independent directions: $\vec{x}_2$, $\vec{x}_3$ and $\vec{r}_1$. Appendix 9.10.5 discusses how we can relax this assumption. The generic form of the required angular integrations for the case of spherical symmetry read

$$\int d\Omega_{x_2} d\Omega_{x_3} \left(\hat{x}_3 \cdot \vec{\nabla}\right)^l \left(\hat{x}_2 \cdot \hat{x}_3\right)^m |\hat{x}_2 \otimes \hat{x}_3|^n \left(\hat{x}_2 \cdot \vec{\nabla}\right)^p \left(\hat{x}_2 \otimes \hat{r}_1\right)^{n_1}_{\mu_1}$$
$$\left(\hat{x}_2 \otimes \hat{r}_1\right)^{n_2}_{\mu_2} \left(\hat{x}_3 \otimes \hat{r}_1\right)^{n_3}_{\mu_3} \left(\hat{x}_3 \otimes \hat{r}_1\right)^{n_4}_{\mu_4}, \tag{9.411}$$

where l, m, n and p are integers. The maximum power of gradient in the DME ansatz for any density is fixed at two, hence, $l \epsilon \{0,1,2\}$ and also $p \epsilon \{0,1,2\}$. Due to the specific form of the ansatz, $m \epsilon \{0,1,2,3,4,5,6,7,8,9,10\}$ and $n \epsilon \{0,1,2\}$. The exponents $n_1, n_2, n_3, n_4 \epsilon \{0,1\}$. Even though the generic angular dependence given in Eq. (9.411) is very complex, all these terms do not occur at the same time.

The origin of the various angular dependencies is (i) $\hat{x}_3.\vec{\nabla}$ and $\hat{x}_2.\vec{\nabla}$ are due to the DME ansatz, (ii) $\hat{x}_2.\hat{x}_3$ originates from the DME ansatz (Eqs. (9.382)-(9.384)), the rotation matrix of the G tensors (Eq. (9.10.2)) and the expansion of $\Pi^{\mu_i}_{j,fr}$ (Eq. (9.410)) (iii) $|\hat{x}_2 \otimes \hat{x}_3|$ comes from the rotation matrix in the G tensors and (iv) $\left(\hat{x}_2 \otimes \hat{r}_1\right)^{n_i}_{\mu_i}$ where $i \epsilon \{1,2,3,4\}$ originate from the directional coupling in the DME of the vector density, $\vec{s}_{0/1}$. Remember that in spherical symmetry, only the vector component of the cartesian spin-current tensor density is nonzero. The exponents n_1, n_2, n_3 and n_4 can not be one at the same time i.e, at most only three of the exponents can be one at the same time. This is due to the fact that only three local/non-local densities (be it vector/scalar) densities appear in all terms of the exact 3NF HF energy.

Due to the huge number of terms generated by the DME expansion, direct multi-dimensional (four dimensions) angular integrations is both impossible and not required. Rather we developed a Mathematica rule-based technique to replace the multi-dimensional integrals with four independent single dimensional integrals. The merit of this technique is that one can calculate the single dimensional integrals once and use their stored values in the whole computation. The angular integrations is followed by several symbolic manipulation techniques to obtain the final EDF. The details of these techniques can be found in Ref. [161]. We remark that the symbolic automation enabled us to keep all higher-order terms in the final EDF (up to sixth order) for whenever necessary.

9.10.4 Contributions to EDF-NNN-DME

In the following, we list the EDF, truncated at fourth-order, that results from the application of the DME on specific contributions to the HF energy (of time-reversal invariant systems) from chiral EFT NNN interaction at N^{2}LO. Due to the assumption of spherical symmetry that we imposed in the previous angular integration step, the given expressions hold only for spherical systems. The actual values of the couplings as a functional of the $\pi-$functions is found in the Mathematica files of Ref. [161]. First let us define the auxiliary quantity $\varsigma^1_{0/1}(\vec{r})$ as

$$\varsigma^1_{0/1}(\vec{r}) \;=\; \hat{r}\cdot\vec{\nabla}\rho_{0/1}(\vec{r})\,. \tag{9.412}$$

Also note that $\varsigma^2_{0/1}(\vec{r})$ stands for the second-order correction density which in the case of generalized PSA-DME reads

$$\varsigma^2_{0/1}(\vec{r}) \;=\; \frac{1}{2}\,\Delta\rho_{0/1}(\vec{r}) \;-\; \tau_{0/1}(\vec{r}) \;+\; \frac{3}{5}\,k_F^2\,\rho_{0/1}(\vec{r})\,. \tag{9.413}$$

Fourth order EDF from the D-term

$$\begin{aligned}
\mathcal{E}^D \;=\; \int d\vec{r}\Big\{ & C_1^{\rho_0^3}\,\rho_0^3(\vec{r}) \;+\; C_1^{\rho_0\rho_1^2}\,\rho_0(\vec{r})\,\rho_1^2(\vec{r}) \;+\; C_1^{\rho_0^2\varsigma_0^2}\,\rho_0^2(\vec{r})\,\varsigma_0^2(\vec{r}) \\
& +C_1^{\rho_1^2\varsigma_0^2}\,\rho_1^2(\vec{r})\,\varsigma_0^2(\vec{r}) \;+\; C_1^{\rho_0\rho_1\varsigma_1^2}\,\rho_0(\vec{r})\,\rho_1(\vec{r})\,\varsigma_1^2(\vec{r}) \\
& +C_1^{\rho_0 J_0^2}\,\rho_0(\vec{r})\,\vec{J}_0(\vec{r})\cdot\vec{J}_0(\vec{r}) \;+\; C_1^{\rho_1 J_0 J_1}\,\rho_1(\vec{r})\,\vec{J}_0(\vec{r})\cdot\vec{J}_1(\vec{r})
\end{aligned}$$

$$
\begin{aligned}
&+\mathcal{C}_1^{\rho_0 J_1^2}\,\rho_0(\vec{r})\,\vec{J}_1(\vec{r})\cdot\vec{J}_1(\vec{r}) + \mathcal{C}_1^{\rho_0 \nabla J_0 \nabla J_0}\,\rho_0(\vec{r})\,\left[\vec{\nabla}\cdot\vec{J}_0(\vec{r})\right]^2 \\
&+\mathcal{C}_1^{\rho_0 J_0 \Delta J_0}\,\rho_0(\vec{r})\,\vec{J}_0(\vec{r})\cdot\Delta\vec{J}_0(\vec{r}) + \mathcal{C}_1^{\rho_1 J_1 \Delta J_0}\,\rho_1(\vec{r})\,\vec{J}_1(\vec{r})\cdot\Delta\vec{J}_0(\vec{r}) \\
&+\mathcal{C}_1^{\rho_1 \nabla J_0 \nabla J_1}\,\rho_1(\vec{r})\,\vec{\nabla}\cdot\vec{J}_0(\vec{r})\,\vec{\nabla}\cdot\vec{J}_1(\vec{r}) + \mathcal{C}_1^{\rho_0 \nabla J_1 \nabla J_1}\,\rho_0(\vec{r})\,\left[\vec{\nabla}\cdot\vec{J}_1(\vec{r})\right]^2 \\
&+\mathcal{C}_1^{\rho_1 J_0 \Delta J_1}\,\rho_1(\vec{r})\,\vec{J}_0(\vec{r})\cdot\Delta\vec{J}_1(\vec{r}) + \mathcal{C}_1^{\rho_0 J_1 \Delta J_1}\,\rho_0(\vec{r})\,\vec{J}_1(\vec{r})\cdot\Delta\vec{J}_1(\vec{r})\Big\}\,.
\end{aligned}
\tag{9.414}
$$

Fourth order EDF from the single-exchange piece of the D-like part of the C-term

$$
\begin{aligned}
\mathcal{E}^{CD,1x} = \int d\vec{r}\Big\{ &\mathcal{C}_2^{\rho_0^3}\,\rho_0^3(\vec{r}) + \mathcal{C}_2^{\rho_0\rho_1^2}\,\rho_0(\vec{r})\,\rho_1^2(\vec{r}) + \mathcal{C}_2^{\rho_0\rho_1\varsigma_1^1}\,\rho_0(\vec{r})\,\rho_1(\vec{r})\,\varsigma_1^1(\vec{r}) \\
&+\mathcal{C}_2^{\rho_0 \nabla\rho_0 \cdot \nabla\rho_0}\,\rho_0(\vec{r})\,\vec{\nabla}\rho_0(\vec{r})\cdot\vec{\nabla}\rho_0(\vec{r}) \\
&+\mathcal{C}_2^{\rho_0 \nabla\rho_1 \cdot \nabla\rho_1}\,\rho_0(\vec{r})\,\vec{\nabla}\rho_1(\vec{r})\cdot\vec{\nabla}\rho_1(\vec{r}) \\
&+\mathcal{C}_2^{\rho_0^2 \Delta\rho_0}\,\rho_0^2(\vec{r})\,\Delta\rho_0(\vec{r}) + \mathcal{C}_2^{\rho_0\rho_1\Delta\rho_1}\,\rho_0(\vec{r})\,\rho_1(\vec{r})\,\Delta\rho_1(\vec{r}) \\
&+\mathcal{C}_2^{\rho_0^2\varsigma_0^2}\,\rho_0^2(\vec{r})\,\varsigma_0^2(\vec{r}) + \mathcal{C}_2^{\rho_0\rho_1\varsigma_1^2}\,\rho_0(\vec{r})\,\rho_1(\vec{r})\,\varsigma_1^2(\vec{r}) \\
&+\mathcal{C}_2^{\rho_0^2\varsigma_0^1}\,\rho_0^2(\vec{r})\,\varsigma_0^1(\vec{r}) + \mathcal{C}_2^{\rho_0 J_0^2}\,\rho_0(\vec{r})\,\vec{J}_0(\vec{r})\cdot\vec{J}_0(\vec{r}) \\
&+\mathcal{C}_2^{\rho_0 J_1^2}\,\rho_0(\vec{r})\,\vec{J}_1(\vec{r})\cdot\vec{J}_1(\vec{r}) + \mathcal{C}_2^{\rho_0 \nabla J_0 \nabla J_0}\,\rho_0(\vec{r})\,\left[\vec{\nabla}\cdot\vec{J}_0(\vec{r})\right]^2 \\
&+\mathcal{C}_2^{\rho_0 J_0 \Delta J_0}\,\rho_0(\vec{r})\,\vec{J}_0(\vec{r})\cdot\Delta\vec{J}_0(\vec{r}) + \mathcal{C}_2^{\rho_0 \nabla J_1 \nabla J_1}\,\rho_0(\vec{r})\,\left[\vec{\nabla}\cdot\vec{J}_1(\vec{r})\right]^2 \\
&+\mathcal{C}_2^{\rho_0 J_1 \Delta J_1}\,\rho_0(\vec{r})\,\vec{J}_1(\vec{r})\cdot\Delta\vec{J}_1(\vec{r})\Big\}\,.
\end{aligned}
\tag{9.415}
$$

Fourth order EDF from the double-exchange piece of the D-like part of the C-term

$$
\begin{aligned}
\mathcal{E}^{CD,2x} = \int d\vec{r}\Big\{ &\mathcal{C}_3^{\rho_0^3}\,\rho_0^3(\vec{r}) + \mathcal{C}_3^{\rho_0\rho_1^2}\,\rho_0(\vec{r})\,\rho_1^2(\vec{r}) + \mathcal{C}_3^{\rho_0\rho_1\varsigma_1^1}\,\rho_0(\vec{r})\,\rho_1(\vec{r})\,\varsigma_1^1(\vec{r}) \\
&+\mathcal{C}_3^{\rho_0^2\Delta\rho_0}\,\rho_0^2(\vec{r})\,\Delta\rho_0(\vec{r}) + \mathcal{C}_3^{\rho_1^2\Delta\rho_0}\,\rho_1^2(\vec{r})\,\Delta\rho_0(\vec{r})
\end{aligned}
$$

$$
\begin{aligned}
&+\mathcal{C}_3^{\rho_0\rho_1\Delta\rho_1}\,\rho_0(\vec r)\,\rho_1(\vec r)\,\Delta\rho_1(\vec r) \;+\; \mathcal{C}_3^{\rho_0^2\varsigma_0^2}\,\rho_0^2(\vec r)\,\varsigma_0^2(\vec r)\\
&+\mathcal{C}_3^{\rho_1^2\varsigma_0^2}\,\rho_1^2(\vec r)\,\varsigma_0^2(\vec r) \;+\; \mathcal{C}_3^{\rho_0\rho_1\varsigma_1^2}\,\rho_0(\vec r)\,\rho_1(\vec r)\,\varsigma_1^2(\vec r)\\
&+\mathcal{C}_3^{\rho_0^2\varsigma_0^1}\,\rho_0^2(\vec r)\,\varsigma_0^1(\vec r) \;+\; \mathcal{C}_3^{\rho_1^2\varsigma_0^1}\,\rho_1^2(\vec r)\,\varsigma_0^1(\vec r)\\
&+\mathcal{C}_3^{\rho_0 J_0^2}\,\rho_0(\vec r)\,\vec J_0(\vec r)\cdot\vec J_0(\vec r) \;+\; \mathcal{C}_3^{\rho_1 J_0 J_1}\,\rho_1(\vec r)\,\vec J_0(\vec r)\cdot\vec J_1(\vec r)\\
&+\mathcal{C}_3^{\rho_0 J_1^2}\,\rho_0(\vec r)\,\vec J_1(\vec r)\cdot\vec J_1(\vec r) \;+\; \mathcal{C}_3^{\Delta\rho_0 J_0^2}\,\Delta\rho_0(\vec r)\,\vec J_0(\vec r)\cdot\vec J_0(\vec r)\\
&+\mathcal{C}_3^{\varsigma_0^2 J_0^2}\,\varsigma_0^2(\vec r)\,\vec J_0(\vec r)\cdot\vec J_0(\vec r) \;+\; \mathcal{C}_3^{\varsigma_0^1 J_0^2}\,\varsigma_0^1(\vec r)\,\vec J_0(\vec r)\cdot\vec J_0(\vec r)\\
&+\mathcal{C}_3^{\nabla\rho_0 J_0\nabla J_0}\,\vec\nabla\rho_0(\vec r)\cdot\vec J_0(\vec r)\,\vec\nabla\cdot\vec J_0(\vec r)\\
&+\mathcal{C}_3^{\rho_0\nabla J_0\nabla J_0}\,\rho_0(\vec r)\,\big[\vec\nabla\cdot\vec J_0(\vec r)\big]^2\\
&+\mathcal{C}_3^{\rho_0 J_0\Delta J_0}\,\rho_0(\vec r)\,\vec J_0(\vec r)\cdot\Delta\vec J_0(\vec r) \;+\; \mathcal{C}_3^{\varsigma_1^1 J_0 J_1}\,\varsigma_1^1(\vec r)\,\vec J_0(\vec r)\cdot\vec J_1(\vec r)\\
&+\mathcal{C}_3^{\Delta\rho_1 J_0 J_1}\,\Delta\rho_1(\vec r)\,\vec J_0(\vec r)\cdot\vec J_1(\vec r) \;+\; \mathcal{C}_3^{\varsigma_1^2 J_0 J_1}\,\varsigma_1^2(\vec r)\,\vec J_0(\vec r)\cdot\vec J_1(\vec r)\\
&+\mathcal{C}_3^{\nabla\rho_1 J_1\nabla J_0}\,\vec\nabla\rho_1(\vec r)\cdot\vec J_1(\vec r)\,\vec\nabla\cdot\vec J_0(\vec r)\\
&+\mathcal{C}_3^{\rho_1 J_1\Delta J_0}\,\rho_1(\vec r)\,\vec J_1(\vec r)\cdot\Delta\vec J_0(\vec r)\\
&+\mathcal{C}_3^{\Delta\rho_0 J_1^2}\,\Delta\rho_0(\vec r)\,\vec J_1(\vec r)\cdot\vec J_1(\vec r) \;+\; \mathcal{C}_3^{\varsigma_0^2 J_1^2}\,\varsigma_0^2(\vec r)\,\vec J_1(\vec r)\cdot\vec J_1(\vec r)\\
&+\mathcal{C}_3^{\varsigma_0^1 J_1^2}\,\varsigma_0^1(\vec r)\,\vec J_1(\vec r)\cdot\vec J_1(\vec r) \;+\; \mathcal{C}_3^{\nabla\rho_1 J_0\nabla J_1}\,\vec\nabla\rho_1(\vec r)\cdot\vec J_0(\vec r)\,\vec\nabla\cdot\vec J_1(\vec r)\\
&+\mathcal{C}_3^{\rho_1\nabla J_0\nabla J_1}\,\rho_1(\vec r)\,\vec\nabla\cdot\vec J_0(\vec r)\,\vec\nabla\cdot\vec J_1(\vec r)\\
&+\mathcal{C}_3^{\nabla\rho_0 J_1\nabla J_1}\,\vec\nabla\rho_0(\vec r)\cdot\vec J_1(\vec r)\,\vec\nabla\cdot\vec J_1(\vec r)\\
&+\mathcal{C}_3^{\rho_0\nabla J_1\nabla J_1}\,\rho_0(\vec r)\,\big[\vec\nabla\cdot\vec J_1(\vec r)\big]^2 \;+\; \mathcal{C}_3^{\rho_1 J_0\Delta J_1}\,\rho_1(\vec r)\,\vec J_0(\vec r)\cdot\Delta\vec J_1(\vec r)\\
&+\mathcal{C}_3^{\rho_0 J_1\Delta J_1}\,\rho_0(\vec r)\,\vec J_1(\vec r)\cdot\Delta\vec J_1(\vec r)\Big\}\,.
\end{aligned}
\tag{9.416}
$$

Fourth order EDF from the R1-double-exchange piece of the C-term

$$
\begin{aligned}
\mathcal{E}^{CR1,2x} \;=\; \int d\vec r\Big\{ &\mathcal{C}_4^{\rho_1 J_0 J_1}\,\rho_1(\vec r)\,\vec J_0(\vec r)\cdot\vec J_1(\vec r) \;+\; \mathcal{C}_4^{\rho_0 J_1^2}\,\rho_0(\vec r)\,\vec J_1(\vec r)\cdot\vec J_1(\vec r)\\
&+\mathcal{C}_4^{J_1^2\nabla J_0}\,\vec J_1(\vec r)\cdot\vec J_1(\vec r)\,\vec\nabla\cdot\vec J_0(\vec r)\\
&+\mathcal{C}_4^{J_0 J_1\nabla J_1}\,\vec J_0(\vec r)\cdot\vec J_1(\vec r)\,\vec\nabla\cdot\vec J_1(\vec r)
\end{aligned}
$$

$$\begin{aligned}
&+ C_4^{\varsigma_1^1 J_0 J_1}\, \varsigma_1^1(\vec{r})\, \vec{J}_0(\vec{r}) \cdot \vec{J}_1(\vec{r}) + C_4^{\Delta\rho_1 J_0 J_1}\, \Delta\rho_1(\vec{r})\, \vec{J}_0(\vec{r}) \cdot \vec{J}_1(\vec{r}) \\
&+ C_4^{\varsigma_1^2 J_0 J_1}\, \varsigma_1^2(\vec{r})\, \vec{J}_0(\vec{r}) \cdot \vec{J}_1(\vec{r}) \\
&+ C_4^{\nabla\rho_1 J_1 \nabla J_0}\, \vec{\nabla}\rho_1(\vec{r}) \cdot \vec{J}_1(\vec{r})\, \vec{\nabla} \cdot \vec{J}_0(\vec{r}) \\
&+ C_4^{\rho_1 J_1 \Delta J_0}\, \rho_1(\vec{r})\, \vec{J}_1(\vec{r}) \cdot \Delta\vec{J}_0(\vec{r}) + C_4^{\Delta\rho_0 J_1^2}\, \Delta\rho_0(\vec{r})\, \vec{J}_1(\vec{r}) \cdot \vec{J}_1(\vec{r}) \\
&+ C_4^{\varsigma_0^2 J_1^2}\, \varsigma_0^2(\vec{r})\, \vec{J}_1(\vec{r}) \cdot \vec{J}_1(\vec{r}) + C_4^{\varsigma_0^1 J_1^2}\, \varsigma_0^1(\vec{r})\, \vec{J}_1(\vec{r}) \cdot \vec{J}_1(\vec{r}) \\
&+ C_4^{\nabla\rho_1 J_0 \nabla J_1}\, \vec{\nabla}\rho_1(\vec{r}) \cdot \vec{J}_0(\vec{r})\, \vec{\nabla} \cdot \vec{J}_1(\vec{r}) \\
&+ C_4^{\rho_1 \nabla J_0 \nabla J_1}\, \rho_1(\vec{r})\, \vec{\nabla} \cdot \vec{J}_0(\vec{r})\, \vec{\nabla} \cdot \vec{J}_1(\vec{r}) \\
&+ C_4^{\nabla\rho_0 J_1 \nabla J_1}\, \vec{\nabla}\rho_0(\vec{r}) \cdot \vec{J}_1(\vec{r})\, \vec{\nabla} \cdot \vec{J}_1(\vec{r}) \\
&+ C_4^{\rho_0 \nabla J_1 \nabla J_1}\, \rho_0(\vec{r}) \left[\vec{\nabla} \cdot \vec{J}_1(\vec{r})\right]^2 \\
&+ C_4^{\rho_1 J_0 \Delta J_1}\, \rho_1(\vec{r})\, \vec{J}_0(\vec{r}) \cdot \Delta\vec{J}_1(\vec{r}) \\
&+ C_4^{\rho_0 J_1 \Delta J_1}\, \rho_0(\vec{r})\, \vec{J}_1(\vec{r}) \cdot \Delta\vec{J}_1(\vec{r}) \Big\}\,. \qquad (9.417)
\end{aligned}$$

Fourth order EDF from the R2-double-exchange piece of the C-term

$$\begin{aligned}
\mathcal{E}^{CR2,2x} = \int d\vec{r} \Big\{ & C_5^{\rho_1^2 \varsigma_0^2}\, \rho_1^2(\vec{r})\, \varsigma_0^2(\vec{r}) + C_5^{\rho_0 \rho_1 \varsigma_1^2}\, \rho_0(\vec{r})\, \rho_1(\vec{r})\, \varsigma_1^2(\vec{r}) \\
&+ C_5^{\rho_1 J_0 J_1}\, \rho_1(\vec{r})\, \vec{J}_0(\vec{r}) \cdot \vec{J}_1(\vec{r}) + C_5^{\rho_0 J_1^2}\, \rho_0(\vec{r})\, \vec{J}_1(\vec{r}) \cdot \vec{J}_1(\vec{r}) \\
&+ C_5^{J_1^2 \nabla J_0}\, \vec{J}_1(\vec{r}) \cdot \vec{J}_1(\vec{r})\, \vec{\nabla} \cdot \vec{J}_0(\vec{r}) + C_5^{J_0 J_1 \nabla J_1}\, \vec{J}_0(\vec{r}) \cdot \vec{J}_1(\vec{r})\, \vec{\nabla} \cdot \vec{J}_1(\vec{r}) \\
&+ C_5^{\varsigma_1^1 J_0 J_1}\, \varsigma_1^1(\vec{r})\, \vec{J}_0(\vec{r}) \cdot \vec{J}_1(\vec{r}) + C_5^{\Delta\rho_1 J_0 J_1}\, \Delta\rho_1(\vec{r})\, \vec{J}_0(\vec{r}) \cdot \vec{J}_1(\vec{r}) \\
&+ C_5^{\varsigma_1^2 J_0 J_1}\, \varsigma_1^2(\vec{r})\, \vec{J}_0(\vec{r}) \cdot \vec{J}_1(\vec{r}) + C_5^{\nabla\rho_1 J_1 \nabla J_0}\, \vec{\nabla}\rho_1(\vec{r}) \cdot \vec{J}_1(\vec{r})\, \vec{\nabla} \cdot \vec{J}_0(\vec{r}) \\
&+ C_5^{\rho_1 J_1 \Delta J_0}\, \rho_1(\vec{r})\, \vec{J}_1(\vec{r}) \cdot \Delta\vec{J}_0(\vec{r}) + C_5^{\Delta\rho_0 J_1^2}\, \Delta\rho_0(\vec{r})\, \vec{J}_1(\vec{r}) \cdot \vec{J}_1(\vec{r}) \\
&+ C_5^{\varsigma_0^2 J_1^2}\, \varsigma_0^2(\vec{r})\, \vec{J}_1(\vec{r}) \cdot \vec{J}_1(\vec{r}) + C_5^{\varsigma_0^1 J_1^2}\, \varsigma_0^1(\vec{r})\, \vec{J}_1(\vec{r}) \cdot \vec{J}_1(\vec{r}) \\
&+ C_5^{\nabla\rho_1 J_0 \nabla J_1}\, \vec{\nabla}\rho_1(\vec{r}) \cdot \vec{J}_0(\vec{r})\, \vec{\nabla} \cdot \vec{J}_1(\vec{r}) \\
&+ C_5^{\rho_1 \nabla J_0 \nabla J_1}\, \rho_1(\vec{r})\, \vec{\nabla} \cdot \vec{J}_0(\vec{r})\, \vec{\nabla} \cdot \vec{J}_1(\vec{r}) \\
&+ C_5^{\nabla\rho_0 J_1 \nabla J_1}\, \vec{\nabla}\rho_0(\vec{r}) \cdot \vec{J}_1(\vec{r})\, \vec{\nabla} \cdot \vec{J}_1(\vec{r})
\end{aligned}$$

$$
\begin{aligned}
&+\mathcal{C}_5^{\rho_0{}^{\nabla J_1}{}^{\nabla J_1}}\,\rho_0(\vec{r})\,\left[\vec{\nabla}\cdot\vec{J}_1(\vec{r})\right]^2\\
&+\mathcal{C}_5^{\rho_1{}^{J_0}{}^{\Delta J_1}}\,\rho_1(\vec{r})\,\vec{J}_0(\vec{r})\cdot\Delta\vec{J}_1(\vec{r})\\
&+\mathcal{C}_5^{\rho_0{}^{J_1}{}^{\Delta J_1}}\,\rho_0(\vec{r})\,\vec{J}_1(\vec{r})\cdot\Delta\vec{J}_1(\vec{r})\Big\}\,. \qquad (9.418)
\end{aligned}
$$

Fourth order EDF from the R3-double-exchange piece of the C-term

$$
\begin{aligned}
\mathcal{E}^{CR3,2x} \;=\; \int d\vec{r}\Big\{ &\mathcal{C}_6^{\rho_0 J_0^2}\,\rho_0(\vec{r})\,\vec{J}_0(\vec{r})\cdot\vec{J}_0(\vec{r}) + \mathcal{C}_6^{\rho_1 J_0 J_1}\,\rho_1(\vec{r})\,\vec{J}_0(\vec{r})\cdot\vec{J}_1(\vec{r})\\
&+\mathcal{C}_6^{\rho_0 J_1^2}\,\rho_0(\vec{r})\,\vec{J}_1(\vec{r})\cdot\vec{J}_1(\vec{r}) + \mathcal{C}_6^{J_0^2 \nabla J_0}\,\vec{J}_0(\vec{r})\cdot\vec{J}_0(\vec{r})\,\vec{\nabla}\cdot\vec{J}_0(\vec{r})\\
&+\mathcal{C}_6^{J_1^2 \nabla J_0}\,\vec{J}_1(\vec{r})\cdot\vec{J}_1(\vec{r})\,\vec{\nabla}\cdot\vec{J}_0(\vec{r}) + \mathcal{C}_6^{J_0 J_1 \nabla J_1}\,\vec{J}_0(\vec{r})\,\vec{J}_1(\vec{r})\,\vec{\nabla}\cdot\vec{J}_1(\vec{r})\\
&+\mathcal{C}_6^{\Delta\rho_0 J_0^2}\,\Delta\rho_0(\vec{r})\,\vec{J}_0(\vec{r})\cdot\vec{J}_0(\vec{r}) + \mathcal{C}_6^{\varsigma_0^2 J_0^2}\,\varsigma_0^2(\vec{r})\,\vec{J}_0(\vec{r})\cdot\vec{J}_0(\vec{r})\\
&+\mathcal{C}_6^{\varsigma_0^1 J_0^2}\,\varsigma_0^1(\vec{r})\,\vec{J}_0(\vec{r})\cdot\vec{J}_0(\vec{r}) + \mathcal{C}_6^{\nabla\rho_0 J_0 \nabla J_0}\,\vec{\nabla}\rho_0(\vec{r})\,\vec{J}_0(\vec{r})\,\vec{\nabla}\cdot\vec{J}_0(\vec{r})\\
&+\mathcal{C}_6^{\rho_0 \nabla J_0 \nabla J_0}\,\rho_0(\vec{r})\,\left[\vec{\nabla}\cdot\vec{J}_0(\vec{r})\right]^2 + \mathcal{C}_6^{\rho_0 J_0 \Delta J_0}\,\rho_0(\vec{r})\,\vec{J}_0(\vec{r})\cdot\Delta\vec{J}_0(\vec{r})\\
&+\mathcal{C}_6^{\varsigma_1^1 J_0 J_1}\,\varsigma_1^1(\vec{r})\,\vec{J}_0(\vec{r})\cdot\vec{J}_1(\vec{r}) + \mathcal{C}_6^{\Delta\rho_1 J_0 J_1}\,\Delta\rho_1(\vec{r})\,\vec{J}_0(\vec{r})\cdot\vec{J}_1(\vec{r})\\
&+\mathcal{C}_6^{\varsigma_1^2 J_0 J_1}\,\varsigma_1^2(\vec{r})\,\vec{J}_0(\vec{r})\cdot\vec{J}_1(\vec{r}) + \mathcal{C}_6^{\nabla\rho_1 J_1 \nabla J_0}\,\vec{\nabla}\rho_1(\vec{r})\cdot\vec{J}_1(\vec{r})\,\vec{\nabla}\cdot\vec{J}_0(\vec{r})\\
&+\mathcal{C}_6^{\rho_1 J_1 \Delta J_0}\,\rho_1(\vec{r})\,\vec{J}_1(\vec{r})\cdot\Delta\vec{J}_0(\vec{r}) + \mathcal{C}_6^{\varsigma_0^2 J_1^2}\,\varsigma_0^2(\vec{r})\,\vec{J}_1(\vec{r})\cdot\vec{J}_1(\vec{r})\\
&+\mathcal{C}_6^{\nabla\rho_1 J_0 \nabla J_1}\,\vec{\nabla}\rho_1(\vec{r})\cdot\vec{J}_0(\vec{r})\,\vec{\nabla}\cdot\vec{J}_1(\vec{r})\\
&+\mathcal{C}_6^{\rho_1 \nabla J_0 \nabla J_1}\,\rho_1(\vec{r})\,\vec{\nabla}\cdot\vec{J}_0(\vec{r})\,\vec{\nabla}\cdot\vec{J}_1(\vec{r})\\
&+\mathcal{C}_6^{\rho_0 \nabla J_1 \nabla J_1}\,\rho_0(\vec{r})\,\left[\vec{\nabla}\cdot\vec{J}_1(\vec{r})\right]^2\\
&+\mathcal{C}_6^{\rho_1 J_0 \Delta J_1}\,\rho_1(\vec{r})\,\vec{J}_0(\vec{r})\cdot\Delta\vec{J}_1(\vec{r})\\
&+\mathcal{C}_6^{\rho_0 J_1 \Delta J_1}\,\rho_0(\vec{r})\,\vec{J}_1(\vec{r})\cdot\Delta\vec{J}_1(\vec{r})\Big\}\,. \qquad (9.419)
\end{aligned}
$$

Fourth order EDF from the R4-double-exchange piece of the C-term

$$
\mathcal{E}^{CR4,2x} \;=\; \int d\vec{r}\Big\{ \mathcal{C}_7^{\rho_0^3}\,\rho_0^3(\vec{r}) + \mathcal{C}_7^{\rho_0\rho_1^2}\,\rho_0(\vec{r})\,\rho_1^2(\vec{r})
$$

$$
\begin{aligned}
&+\mathcal{C}_7^{\rho_0\rho_1\varsigma_1^1}\,\rho_0(\vec{r})\,\rho_1(\vec{r})\,\varsigma_1^1(\vec{r}) \;+\; \mathcal{C}_7^{\rho_0^2\Delta\rho_0}\,\rho_0^2(\vec{r})\,\Delta\rho_0(\vec{r})\\
&+\mathcal{C}_7^{\rho_0\rho_1\Delta\rho_1}\,\rho_0(\vec{r})\,\rho_1(\vec{r})\,\Delta\rho_1(\vec{r}) \;+\; \mathcal{C}_7^{\rho_0^2\varsigma_0^2}\,\rho_0^2(\vec{r})\,\varsigma_0^2(\vec{r})\\
&+\mathcal{C}_7^{\rho_1^2\varsigma_0^2}\,\rho_1^2(\vec{r})\,\varsigma_0^2(\vec{r}) \;+\; \mathcal{C}_7^{\rho_0\rho_1\varsigma_1^2}\,\rho_0(\vec{r})\,\rho_1(\vec{r})\,\varsigma_1^2(\vec{r})\\
&+\mathcal{C}_7^{\rho_0^2\varsigma_0^1}\,\rho_0^2(\vec{r})\,\varsigma_0^1(\vec{r}) \;+\; \mathcal{C}_7^{\rho_0 J_0^2}\,\rho_0(\vec{r})\,\vec{J}_0(\vec{r})\cdot\vec{J}_0(\vec{r})\\
&+\mathcal{C}_7^{\rho_1 J_0 J_1}\,\rho_1(\vec{r})\,\vec{J}_0(\vec{r})\cdot\vec{J}_1(\vec{r}) \;+\; \mathcal{C}_7^{\rho_0 J_1^2}\,\rho_0(\vec{r})\,\vec{J}_1(\vec{r})\cdot\vec{J}_1(\vec{r})\\
&+\mathcal{C}_7^{J_0^2\nabla J_0}\,\vec{J}_0(\vec{r})\cdot\vec{J}_0(\vec{r})\,\vec{\nabla}\cdot\vec{J}_0(\vec{r}) \;+\; \mathcal{C}_7^{J_1^2\nabla J_0}\,\vec{J}_1(\vec{r})\cdot\vec{J}_1(\vec{r})\,\vec{\nabla}\cdot\vec{J}_0(\vec{r})\\
&+\mathcal{C}_7^{J_0 J_1\nabla J_1}\,\vec{J}_0(\vec{r})\,\vec{J}_1(\vec{r})\,\vec{\nabla}\cdot\vec{J}_1(\vec{r}) \;+\; \mathcal{C}_7^{\Delta\rho_0 J_0^2}\,\Delta\rho_0(\vec{r})\,\vec{J}_0(\vec{r})\cdot\vec{J}_0(\vec{r})\\
&+\mathcal{C}_7^{\varsigma_0^2 J_0^2}\,\varsigma_0^2(\vec{r})\,\vec{J}_0(\vec{r})\cdot\vec{J}_0(\vec{r}) \;+\; \mathcal{C}_7^{\varsigma_0^1 J_0^2}\,\varsigma_0^1(\vec{r})\,\vec{J}_0(\vec{r})\cdot\vec{J}_0(\vec{r})\\
&+\mathcal{C}_7^{\nabla\rho_0 J_0\nabla J_0}\,\vec{\nabla}\rho_0(\vec{r})\,\vec{J}_0(\vec{r})\,\vec{\nabla}\cdot\vec{J}_0(\vec{r})\\
&+\mathcal{C}_7^{\rho_0\nabla J_0\nabla J_0}\,\rho_0(\vec{r})\,\left[\vec{\nabla}\cdot\vec{J}_0(\vec{r})\right]^2\\
&+\mathcal{C}_7^{\rho_0 J_0\Delta J_0}\,\rho_0(\vec{r})\,\vec{J}_0(\vec{r})\cdot\Delta\vec{J}_0(\vec{r}) \;+\; \mathcal{C}_7^{\varsigma_1^1 J_0 J_1}\,\varsigma_1^1(\vec{r})\,\vec{J}_0(\vec{r})\cdot\vec{J}_1(\vec{r})\\
&+\mathcal{C}_7^{\Delta\rho_1 J_0 J_1}\,\Delta\rho_1(\vec{r})\,\vec{J}_0(\vec{r})\cdot\vec{J}_1(\vec{r}) \;+\; \mathcal{C}_7^{\varsigma_1^2 J_0 J_1}\,\varsigma_1^2(\vec{r})\,\vec{J}_0(\vec{r})\cdot\vec{J}_1(\vec{r})\\
&+\mathcal{C}_7^{\nabla\rho_1 J_1\nabla J_0}\,\vec{\nabla}\rho_1(\vec{r})\cdot\vec{J}_1(\vec{r})\,\vec{\nabla}\cdot\vec{J}_0(\vec{r})\\
&+\mathcal{C}_7^{\rho_1 J_1\Delta J_0}\,\rho_1(\vec{r})\,\vec{J}_1(\vec{r})\cdot\Delta\vec{J}_0(\vec{r})\\
&+\mathcal{C}_7^{\varsigma_0^2 J_1^2}\,\varsigma_0^2(\vec{r})\,\vec{J}_1(\vec{r})\cdot\vec{J}_1(\vec{r}) \;+\; \mathcal{C}_7^{\nabla\rho_1 J_0\nabla J_1}\,\vec{\nabla}\rho_1(\vec{r})\cdot\vec{J}_0(\vec{r})\,\vec{\nabla}\cdot\vec{J}_1(\vec{r})\\
&+\mathcal{C}_7^{\rho_1\nabla J_0\nabla J_1}\,\rho_1(\vec{r})\,\vec{\nabla}\cdot\vec{J}_0(\vec{r})\,\vec{\nabla}\cdot\vec{J}_1(\vec{r})\\
&+\mathcal{C}_7^{\rho_0\nabla J_1\nabla J_1}\,\rho_0(\vec{r})\,\left[\vec{\nabla}\cdot\vec{J}_1(\vec{r})\right]^2\\
&+\mathcal{C}_7^{\rho_1 J_0\Delta J_1}\,\rho_1(\vec{r})\,\vec{J}_0(\vec{r})\cdot\Delta\vec{J}_1(\vec{r})\\
&+\mathcal{C}_7^{\rho_0 J_1\Delta J_1}\,\rho_0(\vec{r})\,\vec{J}_1(\vec{r})\cdot\Delta\vec{J}_1(\vec{r})\,\Bigg\}\,.
\end{aligned}
\tag{9.420}
$$

9.10.5 Extension to deformed time-reversal invariant systems

The assumption of spherical symmetry was used to obtain the generic form of the angular integrations in Eq. (9.411). This can be relaxed to treat deformed time-reversal invariant systems, though with a significant increase in the time-complexity of the symbolic computation. In deformed systems, all local densities denoted here by, $\varsigma(\vec{r}_1)$, depend on the orientation of $\vec{r}_1$. Hence, they come with their own direction, increasing the number of available vector directions to a much higher value than the three that we have in spherical systems ($\vec{x}_2$, $\vec{x}_3$ and $\vec{r}_1$). This entails changing the angular integration technique discussed in appendix 9.10.3 with symbolic tensor manipulation. To illustrate the difference between the two-techniques, consider a schematic example, perhaps misleading due to its simplicity,

$$T = \int d\Omega_2 \, (\hat{x}_2 \cdot \hat{r}_1) \, (\hat{x}_2 \cdot \vec{\nabla}) \, . \tag{9.421}$$

Note that $\vec{\nabla}$ is acting on some unspecified local density which depends on $\vec{r}_1$. In the case of spherical symmetry, the action of $\vec{\nabla}$ results in a gradient density that is along $\hat{r}_1$. Hence, T is written as

$$T = \int d\theta_2 \, d\phi_2 \, |\vec{\nabla}| \cos^2(\theta_2) \sin(\theta_2) \, , \tag{9.422}$$

which is directly integrable. In deformed systems, one can no longer assume that the direction of the local densities is along $\hat{r}_1$. Hence, one spells out Eq. (9.421) as

$$T = \sum_{ij} \hat{r}_{1,i} \, \vec{\nabla}_j \int d\Omega_2 \, \hat{x}_{2,i} \, \hat{x}_{2,j} \, , \tag{9.423}$$

where i and j label the cartesian coordinates of the labels. A symbolic algorithm, a la the one developed for the angular integrations in appendix 9.10.3 needs to be developed that not only does the integration but also groups the tensor components so that a manifestly scalar EDF results. For details, refer to Ref. [162].

9.11 Analytical couplings for the EDF from chiral EFT NNN interaction at N^{2}LO

9.11.1 Functional form of the couplings

The main objective of this section is to motivate the analytical calculation of the couplings of the EDFs given in appendix 9.10.4, $C_i^{\varsigma_1\varsigma_2\varsigma_3}$, by isolating the forms and types of integrals required. Note that at this stage, all required angular integrations, viz, $\int d\Omega_{q_2}$, $\int d\Omega_{q_3}$, $\int d\Omega_{x_2}$ and $\int d\Omega_{x_3}$ have been carried out. Of course, $\int d\Omega_{r_1}$ is left intact as $\vec{r}_1$ is the coordinate of the local EDF. To recap, we performed $\int d\Omega_{q_2}$ and $\int d\Omega_{q_3}$ in appendix 9.10.2 where the G-tensors are discussed, while $\int d\Omega_{x_2}$ and $\int d\Omega_{x_3}$ are handled in appendix 9.10.3. Thus, the remaining integrals are $\int dq_2\, q_2^2$, $\int dq_3\, q_3^2$, $\int dx_2\, x_2^2$ and $\int dx_3\, x_3^2$. For the sake of notational simplicity, we use $\Pi^{\mu_i}_{j,fr}$ as it is rather than their separable expansion discussed in appendix 9.10.3. In the actual analytical calculation, the expansion is used. Refer to appendix 9.11.3 for details. After dropping all pre-factors, the couplings take the following general forms.

Couplings from Generic-Form-1

All the couplings that originate from Generic-Form-1 7.2.1 take the form

$$\begin{aligned} C^{\varsigma^{1}\varsigma^{2}\varsigma^{3}}(k) \quad \propto \quad & \int dx_2\, dx_3\, dq_2\, dq_3\, x_2^2\, x_3^2\, q_2^2\, q_3^2 \Big[x_2^p x_3^q \; F_z^{\beta}(x_2, q_2)\, F_z^{\gamma}(x_3, q_3) \\ & \times \Pi_r^{\varsigma_1}(kx_3)\, \pi_s^{\varsigma_1,0/1}(kx_3) \\ & \times \Pi_t^{\varsigma_2}(kx_2)\, \pi_u^{\varsigma_2,0/1}(kx_2)\, \Pi^{\varsigma_3}_{v,fr}(\vec{x}_2, \vec{x}_3, k) \Big], \end{aligned} \qquad (9.424)$$

or

$$C^{\varsigma^{1}\varsigma^{2}\varsigma^{3}}(k) \quad \propto \quad \int dx_2\, dx_3\, dq_2\, dq_3\, x_2^2\, x_3^2\, q_2^2\, q_3^2 \left[x_2^p x_3^q \; F_z^{\beta\beta}(x_2, q_2)\, F_z^{\gamma\gamma}(x_3, q_3) \right.$$

$$
\begin{aligned}
&\times \Pi_r^{\varsigma 1}(kx_3)\, \pi_s^{\varsigma 1,0/1}(kx_3) \\
&\times \Pi_t^{\varsigma 2}(kx_2)\, \pi_u^{\varsigma 2,0/1}(kx_2)\, \Pi^{\varsigma 3}_{v,fr}(\vec{x}_2, \vec{x}_3, k) \Big] , \qquad (9.425)
\end{aligned}
$$

where $p, q, r, s, t, u, v, \beta, \gamma$ take only integer values, $F_z^{\beta\beta}, F_z^{\gamma\gamma}$ are given in Eqs.(9.391)-(9.393) and $F_z^{\beta}, F_z^{\gamma}$ are as defined in Eqs.(9.400)-(9.402). In fact, $r, s, t, u, v \in \{0, 1, 2\}$, $\beta, \gamma \in \{1, 2, 3\}$, while $p, q \in \{0, 1, 2, 3, 4\}$.

Couplings from Generic-Form-2

All the couplings that originate from Generic-Form-2 7.2.1 take the form

$$
\begin{aligned}
C^{\varsigma^1 \varsigma^2 \varsigma^3}(k) \quad \propto \quad & \int dx_2\, dx_3\, dq_2\, dq_3\, x_2^2\, x_3^2\, q_2^2\, q_3^2 \Big[x_2^p x_3^q \; F_z^{\beta}(x_2, q_2)\, F_z^{\gamma}(x_3, q_3) \\
& \times \Pi^{\varsigma 3}_{u,fr}(x_2, x_3, k)\, \Pi^{\varsigma 3}_{v,fr}(\vec{x}_2, \vec{x}_3, k) \Big] , \qquad (9.426)
\end{aligned}
$$

or

$$
\begin{aligned}
C^{\varsigma^1 \varsigma^2 \varsigma^3}(k) \quad \propto \quad & \int dx_2\, dx_3\, dq_2\, dq_3\, x_2^2\, x_3^2\, q_2^2\, q_3^2 \Big[x_2^p x_3^q \; F_z^{\beta\beta}(x_2, q_2)\, F_z^{\gamma\gamma}(x_3, q_3) \\
& \times \Pi^{\varsigma 3}_{u,fr}(x_2, x_3, k)\, \Pi^{\varsigma 3}_{v,fr}(\vec{x}_2, \vec{x}_3, k) \Big] , \qquad (9.427)
\end{aligned}
$$

where all the specifications given at the end of Eq. (9.424) regarding the indices and functions hold.

Couplings from Generic-Form-3

All the couplings that originate from Generic-Form-3 7.2.1 take the form

$$
\begin{aligned}
C^{\varsigma^1 \varsigma^2 \varsigma^3} \quad \propto \quad & \int dx_3\, dq_3\, x_3^2\, q_3^2 \Big[x_3^p \; F_z^{\beta\beta}(x_3, q_3) \\
& \times \Pi_r^{\varsigma 2}(kx_3)\, \pi_s^{\varsigma 2,0/1}(kx_3)\, \Pi_t^{\varsigma 3}(kx_3)\, \pi_u^{\varsigma 3,0/1}(kx_3) \Big] , \qquad (9.428)
\end{aligned}
$$

where again all the specifications given at the end of Eq.(9.424) regarding the indices hold and $F^{\beta\beta}$ is defined in Eqs.(9.391)-(9.393).

9.11.2 Matching generalized PSA-DME against the DME-ansatz

At this point, we have the expressions for the couplings expressed as a functional of the $\pi-$functions of the DME ansatz discussed in appendix 9.10.1. In line with the view that the DME ansatz is just a general symbolic template for an anlytical/parameterized DME, we fix the $\pi-$functions of the DME ansatz with the generalized PSA-DME of appendix 9.5.3 (also discussed in sections 7.2.3) for the analytical calculation of the couplings.

Adopting and matching the DME ansatz, Eq. (9.382), for $\rho_q(\vec{r}_1, \vec{r}_1 + \vec{x}_2)$ with its generalized PSA-DME expansion, Eq. (9.211), the $\pi-$functions for this density read

$$\begin{aligned}
\Pi_0^\rho(k_F x_2) &= 3\,\frac{j_1(k_F x_2)}{k_F x_2}\,, \\
\Pi_2^\rho(k_F x_2) &= 3\,\frac{j_1(k_F x_2)}{k_F x_2}\,, \\
\pi_0^\rho(k_F x_2) &= 1\,, \qquad \pi_1^\rho(k_F x_2) = 0\,, \qquad \pi_1^\rho(k_F x_2) = 0\,,
\end{aligned} \tag{9.429}$$

where we set $k = k_F$. Similar $\pi-$functions hold for $\rho_q(\vec{r}_1 + \vec{x}_2, \vec{r}_1)$ due to the assumption of time-reversal invariance, while for $\rho_q(\vec{r}_1, \vec{r}_1 + \vec{x}_3)$ and $\rho_q(\vec{r}_1 + \vec{x}_3, \vec{r}_1)$ one simply replaces x_2 with x_3. We leave the $\pi-$functions multiplying the time-odd densities unspecified. As to $\rho_q(\vec{r}_1 + \vec{x}_2, \vec{r}_1 + \vec{x}_3)$, following the same set of steps

$$\begin{aligned}
\Pi_{0,fr}^\rho(k_F, \vec{x}_2, \vec{x}_3) &= 3\,\frac{j_1(k_F|\vec{x}_2 - \vec{x}_3|)}{k_F|\vec{x}_2 - \vec{x}_3|}\,, \\
\Pi_{2,fr}^\rho(k_F, \vec{x}_2, \vec{x}_3) &= 3\,\frac{j_1(k_F|\vec{x}_2 - \vec{x}_3|)}{k_F|\vec{x}_2 - \vec{x}_3|}\,,
\end{aligned} \tag{9.430}$$

where again time-reversal invariance implies the same set of $\pi-$functions for $\rho_q(\vec{r}_1 + \vec{x}_3, \vec{r}_1 + \vec{x}_2)$.

The $\pi-$functions for $\vec{s}_q(\vec{r}_1, \vec{r}_1 + \vec{x}_2)$ read

$$\begin{aligned} \Pi_1^{\vec{s}}(k_F x_2) &= 3\,\frac{j_1(k_F x_2)}{k_F x_2}\,, \\ \pi_0^J(k_F x_2) &= 1\,, \qquad \pi_1^J(k_F x_2) = 0\,, \qquad \pi_1^J(k_F x_2) = 0\,. \end{aligned} \tag{9.431}$$

Similar $\pi-$functions hold for $\vec{s}_q(\vec{r}_1 + \vec{x}_2, \vec{r}_1)$, while for $\vec{s}_q(\vec{r}_1, \vec{r}_1 + \vec{x}_3)$ and $\vec{s}_q(\vec{r}_1 + \vec{x}_3, \vec{r}_1)$, one simply replaces x_2 with x_3. Again, we leave the $\pi-$functions multiplying the time-odd densities unspecified. As to $\vec{s}_q(\vec{r}_1 + \vec{x}_2, \vec{r}_1 + \vec{x}_3)$, following the same set of steps

$$\Pi_{1,fr}^{\vec{s}}(k_F, \vec{x}_2, \vec{x}_3) = 3\,\frac{j_1(k_F|\vec{x}_2 - \vec{x}_3|)}{k_F|\vec{x}_2 - \vec{x}_3|}\,, \tag{9.432}$$

where again time-reversal invariance implies the same $\pi-$functions for $\vec{s}_q(\vec{r}_1 + \vec{x}_3, \vec{r}_1 + \vec{x}_2)$.

9.11.3 Application of Gegenbaur's addition theorem

In appendix 9.10.3, we discussed the need for the separable expansion and its formal solution of $\Pi_{i,fr}^{c}(k, \vec{x}_2, \vec{x}_3)$. With the generalized PSA-DME used to fix the $\pi-$functions of the DME ansatz, one can apply Gegenbaur's addition theorem, which is discussed in appendix 9.1.5 to the as of yet non-separable $\pi-$functions given in the Eqs. (9.212), (9.213) and (9.230) : $\Pi_{0,fr}^{\rho}$, $\Pi_{2,fr}^{\rho}$ and $\Pi_{1,fr}^{\vec{s}}$. In this case, the non-separability is due to the appearance of the following function in these $\pi-$functions

$$f(k, \vec{x}_2, \vec{x}_3) = \frac{j_1(k|\vec{x}_3 - \vec{x}_2|)}{k|\vec{x}_3 - \vec{x}_2|}\,, \tag{9.433}$$

whose Gegenbaur expansion is obtained by using Eqs. (9.59) and (9.50). It reads

$$\begin{aligned} f(k,\vec{x}_2,\vec{x}_3) &= \sqrt{\frac{\pi}{2}}\frac{J_{3/2}(k|\vec{x}_3-\vec{x}_2|)}{(k|\vec{x}_3-\vec{x}_2|)^{3/2}}\,, \\ &= \sqrt{\frac{144}{\pi}}\frac{\Gamma(3/2)}{k^2\,x_3\,x_2}\sum_{\mu=0}^{\infty}(\mu+\frac{3}{2})\,j_{\mu+1}(kx_2)\,j_{\mu+1}(kx_3)\,C_\mu^{3/2}(\cos(\theta))\,, \end{aligned} \tag{9.434}$$

where θ is the angle between $\vec{x}_2$ and $\vec{x}_3$. A simple re-organization of the terms is needed to recast Eq. (9.434) in to the form of Eq. (9.410). There are several interesting characteristics of this expansion that make it highly applicable to this work: (i) It converges very fast, (ii) In combination with the symbolic integration technique mentioned in the next section (appendix 9.11.4), it makes the analytical computation of the couplings possible (iii) the validity of truncating the expansion at some value of μ can readily be tested with Mathematica. Our numerical experiments show that $\mu \geq 5$ suffices for a practically perfect reproduction of the exact quantity. Furthermore, these numerical experiments show that the accuracy increases progressively as the value at which μ is truncated increases. This, seemingly trivial statement, is not obvious just from the expansion formula given in Eq. (9.434). In the following we test the accuracy of truncating the expansion at $\mu = 5$. For this, let us define $f_5(k,\vec{x}_2,\vec{x}_3)$ as

$$f_5(k,\vec{x}_2,\vec{x}_3) = \sqrt{\frac{144}{\pi}}\frac{\Gamma(3/2)}{k^2\,x_3\,x_2}\sum_{\mu=0}^{5}(\mu+\frac{3}{2})\,j_{\mu+1}(kx_2)\,j_{\mu+1}(kx_3)\,C_\mu^{3/2}(\cos(\theta))\,, \tag{9.435}$$

and the ratio function $R_5(k,x_2,x_3,\theta)$ as

$$R_5(k,x_2,x_3,\theta) = \frac{f(k,\vec{x}_2,\vec{x}_3)}{f_5(k,\vec{x}_2,\vec{x}_3)}\,. \tag{9.436}$$

We plot $R_5(k, x_2, x_3, \theta)$ in Fig. 9.1, after absorbing the k dependence into $X_2 = k\,x_2$ and $X_3 = k\,x_3$. First, note that the region of interest for this work is set

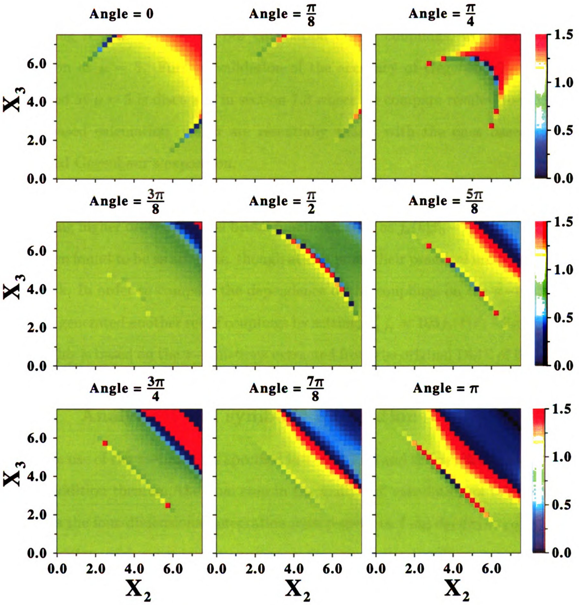

Figure 9.1: (Color online) $R_5(k, x_2, x_3, \theta)$ for a set of angles.

by the range of nuclear interactions as $\vec{x}_2$ and $\vec{x}_3$ are relative coordinates and the k parameter, viz, the DME length scale. Setting $k = k_F \approx 1.42$fm close to the saturation density of INM, and the a maximum range of about 5fm for the nuclear-interaction range dependent pieces ,viz, x_2 and x_3, the region of interest becomes

$X_2 \leq 7.5$ and $X_3 \leq 7.5$. As can be seen from the plot, Fig. 7.3, $R_5(k, x_2, x_3, \theta)$ is close to one for most, if not all, of the region of interest. In fact, investigation of the actual numerical values shows that $R_5(k, x_2, x_3, \theta) \geq 0.995$ for most of the physically interesting region. Hence, for our calculation of the couplings, we truncated the expansion at $\mu = 5$. Further validation of the accuracy of Gegenbaur's expansion truncated at $\mu = 5$ is discussed in section 7.3 where we compare results from Monte-Carlo based calculation, which are essentially exact, with the ones based on the truncated Gegenbaur's expansion.

Finally, it should be mentioned that, the Gegenbaur expansion of expressions containing higher order spherical bessel functions, such as $j_3(k|\vec{x}_3 - \vec{x}_2|)/(k|\vec{x}_3 - \vec{x}_2|)^3$, have been found to be as accurate, though at this point their practical use is limited for this work. In order to compare the dependence of the couplings on the π−functions, we have generated another set of couplings by setting $\Pi^{\rho}_{2,fr} = 105 j_3(k|\vec{x}_3 - \vec{x}_2|)/(k|\vec{x}_3 - \vec{x}_2|)^3$. This is based on the π−functions extracted from the original DME of Ref. [170].

9.11.4 Analytical and symbolic integration

With the use of the π−functions specified in Eqs. 9.11.2 and the application of Gegenbaur's addition theorem, the final step in the analytical calculation of the couplings $C_i^{\varsigma_1\varsigma_2\varsigma_3}$ is the four-dimensional integration with respect to $\int dq_2\, dq_3\, dx_2\, dx_3\, q_2^2\, q_3^2\, x_2^2\, x_3^2$. At this point, each term in the expression for any of the couplings is separable in (q_2, x_2) and (q_3, x_3). This can be seen from the form of the generic couplings given in Eqs. (9.424)-(9.428) and the expansion discussed in appendix 9.11.3.

We first perform the analytical integrations with respect to q_2 and q_3. Note that we have already absorbed all q_2 and q_3 dependencies into the G-tensors. Hence, the only integrals that we need to integrate out the q_2 and q_3 dependencies from the are

$$\int_0^{\infty} dq \, \frac{q^4}{q^2 + m^2} \, j_0(qx) \;=\; -\pi \, \frac{\delta(x)}{x^2} \;-\; \pi \, m^2 \, \frac{e^{-mx}}{2x} \, , \tag{9.437}$$

$$
\begin{aligned}
\int_0^\infty dq \, \frac{q^4}{q^2+m^2} \, \frac{j_1(qx)}{qx} &= -\pi \, \frac{\delta(x)}{x^2} + \pi \, m \, \frac{e^{-mx}}{2x^2} + \pi \, m \, \frac{e^{-mx}}{2x^3} \, , && (9.438) \\
\int_0^\infty dq \, \frac{q^3}{q^2+m^2} \, j_1(qx) &= -\pi \, \frac{\delta(x)}{x} + \pi \, m \, \frac{e^{-mx}}{2x} + \pi \, \frac{e^{-mx}}{2x^2} \, , && (9.439)
\end{aligned}
$$

where q stands for either q_2 or q_3. These integrals can be obtained by following the steps: (i) Rewrite the fractional prefactors, for instance, $q^4/(q^2+m^2)$ as $q^2 - m^2/(q^2+m^2)$ and (ii) Express the integral of the non-fractional piece in terms of $\delta(x)$ whereas that of the other piece can be found by standard contour integration.

The subsequent integrations are with respect to x_2 and x_3. Even though each relevant term is separable in x_2 and x_3 and thus the integrals calculable separately, the required integrals are much more complex. In general, we need to obtain

$$
\int_0^\infty e^{-x/u} x^n j_\nu(x) j_\mu(x) dx \, , \tag{9.440}
$$

where $\nu \geq 0$, $\mu \geq 0$, whereas $u > 0$ is a real parameter and n is an integer. Convergence of the integral requires that $n+\nu+\mu \geq 0$. Note that in our problem, $u = k_F/m_\pi$. The application of Gegenbaur's expansion introduces higher order spherical Bessel functions. I.e. if the expansion is truncated at $\mu = 5$, up to sixth-order ($j_6(x)$) spherical Bessel functions are introduced. However, we are not aware of any analytical or symbolic integration technique that works for any values of the indices: $\{n, \nu, \mu\}$ which satisfy the convergence criterion. Furthermore, we need to perform calculation of hundreds these integrals. In Ref. [157], we discuss how we solve this problem with the Mathematica package that we developed. In the package, we designed and implemented a symbolic integration algorithm that can calculate these integrals for any values of $\{n, \nu, \mu\}$, which satisfy the convergence criterion, and gives the exact analytical expression.

In principle, we have analytical expressions for the couplings at this point. However, the actual Mathematica implementation of the DME starting from the exact

HF energy from the chiral EFT NNN interaction at N^2LO has not been discussed. In Ref. [161], we give a detailed presentation of the symbolic implementation. We remark that the implementation is done in such a way that it can be adapted to deformed time-reversal invariant systems as discussed in appendix 9.10.5 with only a modest amount of change. The implementation for deformed time-reversal invariant systems will be the subject of a subsequent publication [162]. A detailed analysis and discussion of these couplings can be found in Ref. [160]. Finally, the lengths of the coupling expressions prevent us from reproducing even a single coupling in here. Consult the Mathematica files of Ref. [161].

BIBLIOGRAPHY

[1] W. Zuo, I. Bombaci and U. Lombardo. Phys. Rev. C 60 (1999) 024605.

[2] A. Lejeune, U. Lombardo and W. Zuo. Phys. Lett. B 477 (2000) 45.

[3] W. Zuo, A. Lejeune, U. Lombardo and J. F. Mathiot. Nucl. Phys. A 706 (2002) 418-430.

[4] W. Zuo, A. Lejeune, U. Lombardo and J. F. Mathiot. Eur. Phys. J. A 14 (2002) 469-475.

[5] F. Coester, S. Cohen, B. Day and C. M. Vincent. Phys. Rev. C 1 (1970) 769-776.

[6] R. Brockmann and R. Machleidt. Nuclear Matter. Phys. Rev. C 42 (1990) 1965-1980.

[7] R. Brockmann and R. Machleidt. Finite nuclei. Phys. Rev. C 42 (1990) 1981-1988.

[8] A. Nogga, S. K. Bogner and A. Schwenk. Phys. Rev. C 70 (2004) 061002.

[9] S. Weinberg. Nucl. Phys. B 363 (1991) 3-18.

[10] C. Ordonez, L. Ray and U. van Kolk. Phys. Rev. C 53 (1996) 2086-2105.

[11] U. van Kolk. Prog. Part. Nucl. Phys. 43 (1999) 337-418.

[12] E. Epelbaum, W. Glockle and U.-G. Meijner. The two-nucleon system. Nucl. Phys. A 671 (2000) 295-331.

[13] T. T. S. Kuo and E. Osnes. Springer Lect. Notes. Phys. 364 (1990) 100170.

[14] K. Suzuki and S. Y. Lee. Prog. Theor. Phys. 64 (1980) 2091-2106.

[15] S. K. Bogner, A. Schwenk, T. T. S. Kuo and G. E. Brown. ArXiv:0111042[nucl-th].

[16] R. B. Wiringa, V. G. J. Stoks and R. Schiavilla. Phys. Rev. C 51 (1995) 38-51.

[17] R. B. Wiringa, R. A. Smith and T. L. Ainsworth. Phys. Rev. C 29 (1984) 1207-1221.

[18] I. E. Lagaris and V. R. Pandharipande. Nucl. Phys. A 359 (1981) 331-348.

[19] R. Machleidt. (Wiley, New York, NY, 1986), pp. 71-173.

[20] R. Machleidt. vol. 19 (Plenum, New York, 1989).

[21] R. Machleidt, K. Holinde and C. Elster. Phys. Rept. 149 (1987) 1-89.

[22] R. Machleidt. Nucl. Phys. A 790 17-23, 2007.

[23] S. C. Pieper and R. B. Wiringa. Annu. Rev. Nucl. Part. Sci. 51, 53 (2001) and references therein.

[24] R. Roth, J. R. Gour and P. Piecuch. Phys. Rev. C 79 (2009) 054325.

[25] R. Roth, J. R. Gour and P. Piecuch. Phys. Lett. B 679 (2009) 334-339.

[26] M. Bender, P.-H. Heenen, P.-G. Reinhard. Rev. Mod. Phys. 75 (2003) 121 and references therein

[27] S.K. Bogner, R.J. Furnstahl, A. Schwenk. ArXiv:0912.3688[nucl-th] and references therein.

[28] S.K. Bogner, R.J. Furnstahl, A. Nogga, A. Schwenk. ArXiv:0903.3366[nucl-th].

[29] R. Roth, P. Papakonstantinou, N. Paar, H. Hergert, T. Nek, and H. Feldmeier. Phys. Rev. C 73, 044312 (2006).

[30] N.M. Hugenholtz. Physica 23 (1957) 533.

[31] T. Lesinski, K. Bennaceur, T. Duguet, and J. Meyer. Phys. Rev. C74, 044315 (2006).

[32] T. Lesinski, M. Bender, K. Bennaceur, T. Duguet, and J. Meyer. Phys. Rev. C76, 014312 (2007).

[33] J. Margueron, H. Sagawa, and K. Hagino, Phys. Rev. C77, 054309 (2008).

[34] T. Niksic, D. Vretenar, and P. Ring. Phys. Rev. C78, 034318 (2008).

[35] B. G. Carlsson, J. Dobaczewski, and M. Kortelainen. Phys. Rev. C78, 044326 (2009).

[36] S. Goriely, S. Hilaire, M. Girod, and S. Peru. Phys. Rev. Lett. 102, 242501 (2009).

[37] H. Yukawa. Proc. Phys. Math. Soc. Japan 17, 48 (1935).

[38] Peter Ring, Peter Schuck. The nuclear many-body problem. (Springer, 2004).

[39] G. Q. Li and R. Machleidt. Phys. Rev. C 58 (1998) 1393-1402.

[40] V. G. J. Stoks, P. C. van Campen, T. A. Rijken and J. J. De Swart. Phys. Rev. Lett. 61 (1988) 1702-1705.

[41] G. Q. Li and R. Machleidt. Phys. Rev. C 58 (1998) 3153-3162.

[42] E. M. Henley and G. A. Miller. (North-Holland, Amsterdam, 1979), pp. 405-434.

[43] S. Okubo and R. E. Marshak. Ann. Phys. 4 (1958) 166-179.

[44] H. Wita la, W. Glockle, D. Huber, J. Golak and H. Kamada. Phys. Rev. Lett. 81 (1998) 1183-1186.

[45] S. Nemoto, K. Chmielewski, S. Oryu and P. U. Sauer. Phys. Rev. C 58 (1998) 2599-2602.

[46] S. Kistryn et al. Phys. Rev. C 72 (2005) 044006.

[47] A. Nogga, H. Kamada and W. Glockle. Phys. Rev. Lett. 85 (2000) 944-947.

[48] A. Faessler, S. Krewald and G. J. Wagner. Phys. Rev. C 11 (1975) 2069-2072.

[49] J. Fujita and H. Miyazawa. Prog. Theor. Phys. 17 (1957) 360-365.

[50] B. Loiseau and Y. Nogami. Nucl. Phys. B2 (1967) 470-478.

[51] B. S. Pudliner, V. R. Pandharipande, J. Carlson, S. C. Pieper and R. B. Wiringa. Phys. Rev. C 56 (1997) 1720-1750.

[52] H. T. Coelho, T. K. Das and M. R. Robilotta. Phys. Rev. C 28 (1983) 1812-1828.

[53] S. C. Pieper, V. R. Pandharipande, R. B. Wiringa and J. Carlson. Phys. Rev. C 64 (2001) 014001.

[54] S. A. Coon and H. K. Han. Few Body Syst. 30 (2001) 131-141.

[55] R. Bieber et al. Phys. Rev. Lett. 84 (2000) 606-609.

[56] K. Ermisch et al. Phys. Rev. C 68 (2003) 051001.

[57] N. Kalantar-Nayestanaki and E. Epelbaum. ArXiv:0703089[nucl-th].

[58] D. R. Entem and R. Machleidt. Phys. Rev. C 68 (2003) 041001. arXiv:0304018[nucl-th]

[59] E. Epelbaum, W. Glockle and U.-G. Meissner. Nucl. Phys. A747 (2005) 362-424.

[60] E. Epelbaum, H. Krebs, D. Lee, U. -G. Meissner. Eur. Phys. J. A 41, (2009), 125-139.

[61] M. C. M. Rentmeester, R. G. E. Timmermans and J. J. de Swart. Phys. Rev. C 67, (2003) 044001.

[62] D. R. Entem and R. Machleidt. Phys. Rev. C 66 (2002) 014002.

[63] E. Epelbaum, W. Glockle and U.-G. Meijner. Eur. Phys. J. A 19 (2004) 125-137.

[64] E. Epelbaum, W. Glockle and U.-G. Meijner. Eur. Phys. J. A 19 (2004) 401-412.

[65] E. Epelbaum. Eur. Phys. J. A 34 (2007) 197-214.

[66] J. Fujita and H. Miyazawa. Prog. Theor. Phys. 17 (1957) 360-365.

[67] E. Epelbaum, H. Krebs and U.-G. Meijner. ArXiv:0712.1969[nucl-th].

[68] E. Epelbaum, H. Krebs and U.-G. Meijner. ArXiv:0801.1299[nucl-th].

[69] E. Epelbaum et al. Phys. Rev. C 66 (2002) 064001.

[70] B. D. Day. Rev. Mod. Phys. 39 (1967) 719-744.

[71] M. Gell-Mann and F. E. Low. Phys. Rev. 84 (1951) 350-354.

[72] A. Fetter and J. D. Walecka. Quantum Theory of Many-Particle Systems (McGraw-Hill, New-York, 1971).

[73] K. A. Brueckner. Phys. Rev. 100 (1955) 36-45.

[74] K. A. Brueckner. Phys. Rev. 100 (1955) 36-45.

[75] K. A. Brueckner, C. A. Levinson and H. M. Mahmoud. Phys. Rev. 95 (1954) 217-228.

[76] K. A. Brueckner and C. A. Levinson. Phys. Rev. 97 (1954) 1344-1352.

[77] [178] K. A. Brueckner, J. L. Gammel and H. Weitzner. Phys. Rev. 110 (1958) 431-445.

[78] [179] K. A. Brueckner, A. M. Lockett and M. Rotenberg. Phys. Rev. 121 (1958) 255-269.

[79] J. Goldstone. Proc. R. Soc. London Ser. A 239 (1957) 267-279.

[80] B. H. Brandow. Rev. Mod. Phys. 39 (1967) 771-828.

[81] V. Rotival. PhD thesis. 2009.

[82] H. Q. Song, M. Baldo, G. Giansiracusa and U. Lombardo. Phys. Rev. Lett. 81 (1998) 1582-1587.

[83] B. H. Brandow. Phys. Rev. 152 (1966) 863-882.

[84] R. L. Becker, A. D. Mackellar and B. M. Morris. Phys. Rev. 172 (1968) 1264-1290.

[85] S. Kohler and R. J. McCarthy. Nucl. Phys. A106 (1968) 313-322.

[86] R. K. Tripathi, A. Faessler and A. D. MacKellar. Phys. Rev. C 8 (1979) 129-134.

[87] R. D. Mattuck. A guide to Feynman Diagrams in the Many-Body problem. 1975.

[88] R. G. Paar and W. Yang. Density Functional Theory of Atoms and Molecules (Oxford University Press, Oxford, 1989).

[89] J. Perdew and S. Kurth. Density functionals for non-relativistic coulomb systems in the new century, A Primer in Density Functional Theory, pp. 155, Springer, 2003.

[90] R. M. Dreizler and E. K. U. Gross. Density Functional Theory (Springer, Berlin, 1990)

[91] W. Kohn: Nobel Lecture. Rev. Mod. Phys. 71 (1999) 1253-1266.

[92] M. Head-Gordon and E. Artacho, Phys. Today 61 (2008), 0809.2041.

[93] W. Kutzelnigg, J. Mol. Struct. 768 (2006) 163.

[94] J.E. Drut, R.J. Furnstahl, L. Platter. ArXiv:0906.1463v2[nucl-th].

[95] P. Hohenberg and W. Kohn. Phys. Rev. 136 (1964) B864-B871.

[96] W. Kohn and L. J. Sham. Phys. Rev. 137 (1964) A1697-A1705.

[97] W. Kohn and L. Sham. Phys. Rev. 140 (1965) A1133-A1138.

[98] J. Engel, Phys. Rev. C75 (2007) 014306.

[99] B.G. Giraud, B.K. Jennings and B.R. Barrett, Phys. Rev. A78 (2008) 032507.

[100] N. Barnea, Phys. Rev. C76 (2007) 067302.

[101] B.G. Giraud, Phys. Rev. C77 (2008) 014311.

[102] B.G. Giraud, Phys. Rev. C78 (2008) 014307.

[103] J. Messud, M. Bender and E. Suraud, (2009), ArXiv:0904.0162[nucl-th].

[104] L. N. Oliveira, E. K. Gross and W. Kohn. Phys. Rev. Lett. 60 (1988) 2430-2433.

[105] D. Lacroix, T. Duguet, M. Bender. Phys. Rev. C 79:044318, 2009.

[106] J. R. Stone, P.-G. Reinhard. Prog. Part. Nucl. Phys. 58:587-657, 2007 and references therein.

[107] B. Gebremariam, T. Duguet and S. K. Bogner. ArXiv:0910.4979v1 [nucl-th].

[108] T. H. R. Skyrme. Phil. Mag. 1 (1956) 1043-1054.

[109] M. Kortelainen, J. Dobaczewski, K. Mizuyama, J. Toivanen. Phys. Rev. C 77:064307, 2008.

[110] T. Lesinski, T. Duguet, K. Bennaceur, and J. Meyer, Eur. Phys. J. A40, 121 (2009).

[111] J. E. Drut, R. J. Furnstahl, and L. Platter (2009), Arxiv:0906.1463 [nucl-th].

[112] T. Duguet and T. Lesinski, AIP Conf. Proc. 1165, 243 (2009).

[113] S. K. Bogner, R. J. Furnstahl, and L. Platter, Eur. Phys. J. A39, 219 (2009).

[114] N. Kaiser, Phys. Rev. C68, 014323 (2003).

[115] S. Hirata, S. Ivanov, I. Grabowski, R.J. Bartlett, K. Burke and J. Talman. J. Chem. Phys. 115, (2001), 1635.

[116] R.J. Bartlett , I.Grabowski, S.Hirata and S.Ivanov. J. Chem. Phys. 122, (2005), 034104.

[117] D. J. Dean and M. Hjorth-Jensen. Rev. Mod. Phys. 75 (2003) 607-656.

[118] J. Terasaki, R. Wyss and P. H. Heenen. Phys. Lett. B 437 (1998) 1-6.

[119] A. L. Goodman. Phys. Rev. C 60 (1999) 014311.

[120] J. R. Stone, J. C. Miller, R. Koncewicz, P. D. Stevenson and M. R. Strayer. Phys. Rev. C 68 (2003) 034324.

[121] M. Samyn, S. Goriely and J. M. Pearson. Nucl. Phys. A 725 (2002) 69-81.

[122] S. Goriely, M. Samyn, M. Bender and J. M. Pearson. Phys. Rev. C 68 (2003) 054325.

[123] M. Samyn, S. Goriely, M. Bender and J. M. Pearson. Phys. Rev. C 70 (2004) 044309.

[124] J. A. Sheikh and P. Ring. Nucl. Phys. A 665 (2000) 71-91.

[125] J. L. Egido and P. Ring. Nucl. Phys. A383 (1982) 189-204.

[126] J. Dobaczewski and J. Dudek. Acta Phys. Pol. B 27 (1996) 45-58.

[127] F. Tondeur. Nucl. Phys. A315 (1979) 353-369.

[128] S. J. Krieger, P. Bonche, H. Flocard, P. Quentin and M. S. Weiss. Nucl. Phys. A517 (1990) 275-286.

[129] G. F. Bertsch and H. Esbensen. Ann. Phys. (NY) 209 (1991) 327-363.

[130] N. Tajima, P. Bonche, H. Flocard, P.-H. Heenen and M. S. Weiss. Nucl. Phys. A551 (1993) 434-450.

[131] J. Terasaki, P.-H. Heenen, P. Bonche, J. Dobaczewski and H. Flocard. Nucl. Phys. A593 (1995) 1-20.

[132] M. Honma, T. Otsuka, B. A. Brown and T. Mizusaki. Phys. Rev. C 65 (2002) 061301.

[133] M. Honma, T. Otsuka, B. A. Brown and T. Mizusaki. Phys. Rev. C 69 (2004) 034335.

[134] A. F. Lisetskiy, B. A. Brown, M. Horoi and H. Grawe. Phys. Rev. C 70 (2004) 044314.

[135] E. Chabanat, J. Meyer, P. Bonche, R. Schaefer and P. Haensel. Nucl. Phys. A627 (1997) 710-746.

[136] J. C. Slater. Phys. Rev. 85 (1951) 385-390.

[137] J. S. Bell and T. H. R. Skyrme. Phil. Mag. 1 (1956) 1055-1068.

[138] T. H. R. Skyrme. Phys. 9 (1959) 615-634.

[139] T. H. R. Skyrme. Nucl. Phys. 9 (1959) 635-640.

[140] E. Perlinska, S. G. Rohozinski, J. Dobaczewski and W. Nazarewicz. Phys. Rev. C 69 (2004) 014316.

[141] J. R. Stone, J. C. Miller, R. Koncewicz, P. D. Stevenson and M. R. Strayer. Phys. Rev. C 68 (2003) 034324.

[142] T. Lesinski, M. Bender, K. Bennaceur, T. Duguet and J. Meyer. Phys. Rev. C 76 (2007) 014312.

[143] T. Lesinski, K. Bennaceur, T. Duguet and J. Meyer. Phys. Rev. C 74 (2006) 044315.

[144] T. Lesinski. Priv. comm.

[145] E. Chabanat, P. Bonche, P. Haensel, J. Meyer and R. Schaefer. Nucl. Phys. A635 (1998) 231-256.

[146] M. Beiner, H. Flocard, N. Van Giai and P. Quentin. Phys. A238 (1975) 29-69.

[147] F. Tondeur, M. Brack, M. Farine and J. M. Pearson. Nucl. Phys. A420 (1984) 297-319.

[148] S. Kohler. Nucl. Phys. A258 (1976) 301-316.

[149] F. Tondeur. Nucl. Phys. A315 (1979) 353-369.

[150] J. Dobaczewski and W. Nazarewicz. Prog. Theor. Phys. Suppl. 146 (2002) 70-83.

[151] S. Wolfram. *The Mathematica Book.* Wolfram Media/Cambridge University Press, Cambridge, 1996.

[152] M. Abramowitz and I. A. Stegun. *Handbook of Mathematical Functions with Formulas, Graphs, and Mathematical Tables.* Applied Mathematics Series. vol. 55, National Bureau of Standards, Washington, D.C. (1964).

[153] B. Gebremariam, T. Duguet and S. K. Bogner. ArXiv:1003.5210v1 [nucl-th].

[154] N. Kaiser. Phys. Rev. C68, 014323 (2003).

[155] J. C. Slater. Phys. Rev. 81 (1951) 385.

[156] B. Gebremariam, S. K. Bogner, T. Duguet. ArXiv:0912.3086[physics.comp-ph].

[157] B. Gebremariam, S. K. Bogner, T. Duguet. ArXiv:0910.4993v2 [physics.comp-ph].

[158] M. Bender, K. Bennaceur, T. Duguet, P.-H. Heenen, T. Lesinski, J. Meyer. Phys. Rev. C 80:064302, 2009.

[159] T. Lesinski, M. Bender, K. Bennaceur, T. Duguet, J. Meyer. Phys. Rev. C 76, 014312, 2007.

[160] B. Gebremariam, S. K. Bogner, T. Duguet. In preparation.

[161] B. Gebremariam, S. K. Bogner, T. Duguet. In preparation.

[162] B. Gebremariam, S. K. Bogner, T. Duguet. In preparation.

[163] R. J. Furnstahl, James C. Hackworth. Phys. Rev. C 56 2875, 1997.

[164] M. V. Stoitsov et. al. In preparation.

[165] D. Rozpedzik, J. Golak, R. Skibinski, H. Witala, W. Gloeckle, E. Epelbaum, A. Nogga, H. Kamada. Acta Phys. Polon. B37 (2006) 2889-2904.

[166] V. Rotival et. al. In preparation.

[167] S. A. Moskzowksi. Phys. Rev. C 2, 402 (1970).

[168] J. Dobaczewski. Interactions, Symmetry breaking and Effective fields from quarks to nuclie. 2003.

[169] H.W.Lee, Phys. Rep. 259, 147 (1995).

[170] J.W. Negele and D. Vautherin. Phys. Rev. C 5, 1472, 1972.

[171] X. Campi and A. Bouyssy. Phys. Lett. 73B, 263, 1973.

[172] J. Meyer and J. Bartel and M. Barack and P. Quentin and S. Aicher. Phys. Lett. B. 172, 122-128, 1986.

[173] Soubbotin, V. B. and Vinas, X. ArXiv:9902039[nucl-th], 1999.

[174] F. G. Perey and D. S. Saxon. Phys. Lett., 10, "107", 1964.

[175] E. Wigner. Phys. Rev. 40, 749 (1932).

[176] J. Martorell and E. Moya De Guerra. Ann. Phys., 158, 1-30, 1984.

[177] M. Durand, V.S.Ramamurthy and P. Schuck. Phys. Lett, 113B, 116-118, 1982.

[178] A. Bulgac, Jeffrey M. Thompson. Phys. Lett. B, 383, 127-132, 1996.

[179] M. Casas, J. Martorell and E. Moya De Guerra. Phys. Lett. 167B, 263-267, 1986.

[180] M. Prakash a, S. Shlomo and V.M.Kolomietz. Nucl. Phys., A370, 30-46, 1981.

[181] T. Lesinski. Unpublished.

[182] R. M. Koehl, Gregory K. Odom and Gustavo E. Scuseria. Mole. Phys., 87, 835, 1995.

[183] J.W. Negele and D. Vautherin. Phys. Rev. C 11, 1031, 1975.

[184] D. Sprung, M. Vallieres, X. Campi, and C.-M. Ko. Nucl. Phys. A253, 1, 1975.

[185] R. K. Bhaduri and D. W. L. Sprung, Nucl. Phys. A 297, 365 (1978).

[186] K. Hagino, H. Sagawa, P. Schuck. ArXiv:0912.4792v1 [nucl-th].

[187] N. Pillet, N. Sandulescu, P. Schuck. ArXiv:0701086v1[nucl-th].

[188] A. B. Pippard. Proc. Roy. Soc. A 216, 547 (1953).

[189] W. Satula. Phys. Scripta T125 (2006) 82-86.

[190] S.S. Pankratov, E.E. Saperstein, M.V. Zverev, M. Baldo, U. Lombardo. Phys. Rev. C 79: 024309, 2009.

[191] Ricardo A. Broglia and Aage Winther. Phys. Lett. B. 124, 11-13, 1983.

[192] G.P.Lepage. ArXiv:9706029v1[nucl-th], 1997.

[193] D. M. Brink and E. Boeker. Nucl. Phys. A 91 (1967).

[194] . C. G. Broyden. AMS 19 (92): 577593, 1965.

[195] G. N. Watson. A Treatise on the Theory of Bessel Functions, 2nd ed. 1966.

[196] M. Bender and P.-H. Heenen and P.-G. Reinhard. Rev. Mod. Phys. 75, 121, 2003.

[197] Y. Engel, D. Brink, K. Goeke, S. Krieger, and D. Vautherin. Nucl. Phys. A249, 215 (1975).

[198] K. O. Friedrich. Mathematical Aspects of the Quantum Theory of Fields, 1953.

[199] Donald H. Kobe. Phys. Rev. A, 19, 1878-1885, 1979.

[200] J. Dobaczewski and J. Dudek. Phys. Rev. C 52, 1827, 1995.

[201] D. Vautherin and D. M. Brink. Phys. Rev. C5, 626, 1972.

[202] R. M. Koehl, Gregory K. Odom and Gustavo E. Scuseria. Mole. Phys., 87, 835, 1995.

[203] K. Husimi, Prog. Phys. Math. Soc. Japan 22, 264 (1940).

[204] M.H.S. Amin, E.V. Bezuglyi, A.S. Kijko, A.N. Omelyanchouk. ArXiv:0404401[cond-mat].

[205] J. Dobaczewski and H. Flocard and J. Treiner. Nucl. Phys. A422, 103, 1984.

[206] S. Levit, J. W. Negele, and Z. Paltiel. Phys. Rev. C 22, 19791995, 1980.

[207] E. Perlinska and S. G. Rohozinski and J. Dobaczewski and W. Nazarewicz. Phys. Rev. C 69, 014316, 2004.

[208] Brandon P. van Zyl. Phys. Rev. A. 68. 033601, 2003.

MICHIGAN STATE UNIVERSITY LI
3 1293 03063 521